

Alan N. Gent

Engineering with Rubber

How to Design Rubber Components



3rd Edition

HANSER

@seismicisolation

Gent
Engineering with Rubber

Alan N. Gent

Engineering with Rubber

How to Design Rubber Components

3rd Edition

Hanser Publishers, Munich

HANSER
Hanser Publications, Cincinnati

@seismicisolation


The Editor:

Dr. Alan N. Gent, 4498 Cobblestone Trail, Ravenna, OH 44266-8249, USA

Distributed in North and South America by:

Hanser Publications
6915 Valley Avenue, Cincinnati, Ohio 45244-3029, USA
Fax: (513) 527-8801
Phone: (513) 527-8977
www.hanserpublications.com

Distributed in all other countries by

Carl Hanser Verlag
Postfach 86 04 20, 81631 München, Germany
Fax: +49 (89) 98 48 09
www.hanser.de

The use of general descriptive names, trademarks, etc., in this publication, even if the former are not especially identified, is not to be taken as a sign that such names, as understood by the Trade Marks and Merchandise Marks Act, may accordingly be used freely by anyone.

While the advice and information in this book are believed to be true and accurate at the date of going to press, neither the authors nor the editors nor the publisher can accept any legal responsibility for any errors or omissions that may be made. The publisher makes no warranty, express or implied, with respect to the material contained herein.

Library of Congress Cataloging-in-Publication Data

Engineering with rubber : how to design rubber components / [edited by] Alan N. Gent. -- 3rd ed.

p. cm.

Includes bibliographical references and index.

ISBN 978-3-446-42764-8 (hardcover) -- ISBN 978-1-56990-508-1 (hardcover) 1. Rubber. 2. Engineering design. I. Gent, Alan N.

TA455.R8E54 2012

620.1'94--dc23

2011045185

Bibliografische Information Der Deutschen Bibliothek

Die Deutsche Bibliothek verzeichnet diese Publikation in der Deutschen Nationalbibliografie;
detaillierte bibliografische Daten sind im Internet über <<http://dnb.d-nb.de>> abrufbar.

ISBN 978-3-446-42764-8

E-Book-ISBN 978-3-446-42871-3

All rights reserved. No part of this book may be reproduced or transmitted in any form or by any means, electronic or mechanical, including photocopying or by any information storage and retrieval system, without permission in writing from the publisher.

© Carl Hanser Verlag, Munich 2012

Production Management: Steffen Jörg

Coverconcept: Marc Müller-Bremer, www.rebranding.de, München

Coverdesign: Stephan Rönigk

Typeset: Manuela Treindl, Fürth

Printed and bound by Kösel, Krugzell

Printed in Germany

Contents

Preface to Third Edition	XV
Authors	XVII
1 Introduction	1
1.1 Rubber in Engineering	1
1.2 Elastomers	2
1.3 Dynamic Application	3
1.4 General Design Principles	3
1.5 Thermal Expansivity, Pressure, and Swelling	4
1.6 Specific Applications and Operating Principles	5
1.7 Seal Life	8
1.8 Seal Friction	8
Acknowledgments	9
References	9
2 Materials and Compounds	11
2.1 Introduction	11
2.2 Elastomer Types	12
2.2.1 General Purpose	12
2.2.1.1 Styrene-Butadiene Rubber (SBR)	12
2.2.1.2 Polyisoprene (NR, IR)	13
2.2.1.3 Polybutadiene (BR)	14
2.2.2 Specialty Elastomers	14
2.2.2.1 Polychloroprene (CR)	14
2.2.2.2 Acrylonitrile-Butadiene Rubber (NBR)	15
2.2.2.3 Hydrogenated Nitrile Rubber (HNBR)	15
2.2.2.4 Butyl Rubber (IIR)	15
2.2.2.5 Ethylene-Propylene Rubber (EPR, EPDM)	15
2.2.2.6 Silicone Rubber (MQ, VMQ, PMQ, PVMQ)	16
2.2.2.7 Polysulfide Rubber (T)	16
2.2.2.8 Chlorosulfonated Polyethylene (CSM)	16

2.2.2.9	Chlorinated Polyethylene (CM)	16
2.2.2.10	Ethylene-Methyl Acrylate Rubber (AEM)	17
2.2.2.11	Acrylic Rubber (ACM).....	17
2.2.2.12	Fluorocarbon Rubbers	17
2.2.2.13	Epichlorohydrin Rubber (CO, ECO).....	17
2.2.2.14	Urethane Rubber	17
2.3	Compounding	18
2.3.1	Vulcanization and Curing.....	18
2.3.1.1	Sulfur Curing.....	18
2.3.1.2	Determination of Crosslink Density.....	21
2.3.1.3	Influence of Crosslink Density.....	22
2.3.1.4	Other Cure Systems.....	23
2.3.2	Reinforcement	23
2.3.3	Anti-Degradants	25
2.3.3.1	Ozone Attack.....	26
2.3.3.2	Oxidation	26
2.3.4	Process Aids	28
2.3.5	Extenders.....	29
2.3.6	Tackifiers.....	29
2.4	Typical Rubber Compositions.....	30
Acknowledgment	34
References	34
Problems for Chapter 2	35
Answers to Problems for Chapter 2	35
3	Elasticity	37
3.1	Introduction.....	37
3.2	Elastic Properties at Small Strains	38
3.2.1	Elastic Constants.....	38
3.2.2	Relation Between Shear Modulus G and Composition	41
3.2.3	Stiffness of Components	44
3.2.3.1	Choice of Shear Modulus	44
3.2.3.2	Shear Deformations of Bonded Blocks and Hollow Cylindrical Tubes.....	45
3.2.3.3	Small Compressions or Extensions of Bonded Blocks.	47
3.2.3.4	Compression of Blocks Between Frictional Surfaces..	50
3.2.3.5	Maximum Allowable Loads in Tension and Compression	52
3.2.3.6	Indentation of Rubber Blocks by Rigid Indentors.....	53
3.2.3.7	Compression of O-rings	55
3.2.3.8	Protrusion of Rubber Through a Hole or Slit	55

3.3	Large Deformations	56
3.3.1	General Theory of Large Elastic Deformations.....	56
3.3.2	Forms for W Valid at Large Strains	58
3.3.3	Stress-Strain Relations in Selected Cases	59
3.3.3.1	Simple Extension	59
3.3.3.2	Equibiaxial Stretching	61
3.3.3.3	Constrained Tension (Pure Shear)	61
3.3.4	Determining the Strain Energy Function W	63
3.3.4.1	Elastic Behavior of Filled Rubber Vulcanizates.....	65
3.3.4.2	Does Any Strain Energy Function Apply?.....	67
3.3.5	Other Stress-Strain Relations Valid at Large Strains	67
3.3.5.1	Simple Shear	67
3.3.5.2	Torsion.....	70
3.3.5.3	Instability in Torsion.....	72
3.3.5.4	Inflation of a Thin-Walled Tube [58].....	73
3.3.5.5	Inflation of a Spherical Shell (Balloon)	74
3.3.5.6	Inflation of a Spherical Cavity; Explosive Decompression	76
3.3.5.7	Surface Creasing in Compression.....	77
3.4	Molecular Theory of Rubber Elasticity	78
3.4.1	Elastic Behavior of a Molecular Network	78
3.4.3	Effective Density of Network Strands	81
3.4.4	The Second Term in the Strain Energy Function.....	82
3.4.5	Concluding Remarks on Molecular Theories	83
	Acknowledgments	84
	References	84
	Problems for Chapter 3	87
	Answers to Selected Problems for Chapter 3	88
4	Dynamic Mechanical Properties	89
4.1	Introduction.....	89
4.2	Stress Waves in Rubbery Solids, Transit Times, and Speeds of Retraction	90
4.3	Viscoelasticity.....	92
4.4	Dynamic Experiments	96
4.5	Energy Considerations	100
4.6	Motion of a Suspended Mass	102
4.7	Experimental Techniques	106
4.7.1	Forced Nonresonance Vibration	106
4.7.2	Forced Resonance Vibration	106
4.7.3	Free Vibration Methods.....	107

4.7.4	Rebound Resilience	107
4.7.5	Effect of Static and Dynamic Strain Levels	108
4.8	Application of Dynamic Mechanical Measurements	108
4.8.1	Heat Generation in Rubber Components	108
4.8.2	Vibration Isolation	109
4.8.3	Shock Absorbers	109
4.9	Effects of Temperature and Frequency	110
4.10	Thixotropic Effects in Filled Rubber Compounds	114
	Acknowledgments	116
	References	116
	Problems for Chapter 4	116
	Answers to Problems for Chapter 4	117
5	Strength	119
5.1	Introduction	119
5.2	Fracture Mechanics	119
5.2.1	Analysis of the Test Pieces	122
5.2.2	The Strain Energy Concentration at a Crack Tip	123
5.3	Tear Behavior	125
5.4	Crack Growth under Repeated Loading	131
5.4.1	The Fatigue Limit and the Effect of Ozone	132
5.4.2	Physical Interpretation of G_0	133
5.4.3	Effects of Type of Elastomer and Filler	135
5.4.4	Effect of Oxygen	135
5.4.5	Effects of Frequency and Temperature	137
5.4.6	Nonrelaxing Effects	137
5.4.7	Time-Dependent Failure	138
5.5	Ozone Attack	138
5.6	Tensile Strength	142
5.7	Crack Growth in Shear and Compression	144
5.8	Cavitation and Related Failures	147
5.9	Conclusions	148
	References	149
	Problems for Chapter 5	152
	Answers to Problems for Chapter 5	153
6	Mechanical Fatigue	159
6.1	Introduction	159
6.2	Application of Fracture Mechanics to Mechanical Fatigue of Rubber	161
6.3	Initiation and Propagation of Cracks	163
6.3.1	Fatigue Crack Initiation	163

6.3.2	Fatigue Life and Crack Growth	164
6.3.3	Fatigue Crack Propagation: The Fatigue Crack Growth Characteristic	166
6.3.4	Fatigue Life Determinations from the Crack Growth Characteristics.....	168
6.4	Fatigue Crack Growth Test Methodology	170
6.4.1	Experimental Determination of Dynamic Tearing Energies for Fatigue Crack Propagation.....	170
6.4.2	Kinetics of Crack Growth	171
6.4.3	Effects of Test Variables on Fatigue Crack Growth Characteristics and Dynamic Fatigue Life.....	172
6.4.3.1	Waveform	172
6.4.3.2	Frequency	172
6.4.3.3	Temperature	172
6.4.3.4	Static Strain/Stress	174
6.5	Material Variables and Their Effect on Fatigue Crack Growth	176
6.5.1	Reinforcing Fillers and Compound Modulus.....	176
6.5.2	Elastomer Type	178
6.5.3	Vulcanizing System	179
6.5.3	Fatigue of Double Network Elastomers and Blends.....	181
6.6	Fatigue and Crack Growth of Rubber under Biaxial Stresses and Multiaxial Loading.....	182
6.7	Fatigue in Rubber Composites	184
6.7.1	Effect of Wires, Cords, and Their Spacing on Fatigue Crack Propagation.....	185
6.7.2	Effect of Minimum Strain or Stress	185
6.7.3	Comparison of S-N Curve and Fatigue Crack Propagation Constants for Rubber-Wire Composites [53].....	187
6.7.4	Fatigue of Two-Ply Rubber-Cord Laminates	188
6.8	Fatigue Cracking of Rubber in Compression and Shear Applications .	189
6.8.1	Crack Growth in Compression	189
6.8.2	Crack Growth in Shear	192
6.9	Environmental Effects.....	193
6.10	Modeling and Life Predictions of Elastomeric Components	194
6.11	Fatigue Crack Propagation of Thermoplastic Elastomers.....	194
6.12	Durability of Thermoplastic Elastomers	195
6.13	Summary	197
	Acknowledgments	198
	References	198
	Problems for Chapter 6	200
	Answers to Problems for Chapter 6	201

7 Durability.....	205
7.1 Introduction.....	205
7.2 Creep, Stress Relaxation, and Set	207
7.2.1 Creep.....	208
7.2.2 Stress Relaxation.....	208
7.2.3 Physical Relaxation.....	209
7.2.4 Chemical Relaxation.....	211
7.2.5 Compression Set and Recovery.....	211
7.2.6 Case History Study	213
7.3 Longevity of Elastomers in Air.....	214
7.3.1 Durability at Ambient Temperatures	214
7.3.2 Sunlight and Weathering	215
7.3.3 Ozone Cracking	215
7.3.4 Structural Bearings: Case Histories.....	216
7.3.4.1 Natural Rubber Pads for a Rail Viaduct after 100 Years of Service	216
7.3.4.2 Laminated Bridge Bearings after 20 Years of Service	217
7.4 Effect of Low Temperatures.....	220
7.4.1 Glass Transition.....	220
7.4.2 Crystallization	221
7.5 Effect of Elevated Temperatures.....	222
7.6 Effect of Fluid Environments	224
7.6.1 Aqueous Liquids	229
7.6.2 Hydrocarbon Liquids	232
7.6.3 Hydrocarbon and Other Gases	235
7.6.3.1 Pressurized CO ₂ for Assessing Interface Quality in Bonded Rubber/Rubber Systems	240
7.6.4 Effects of Temperature and Chemical Fluid Attack.....	240
7.6.5 Effect of Radiation.....	242
7.7 Durability of Rubber-Metal Bonds.....	243
7.7.1 Adhesion Tests.....	243
7.7.2 Rubber-Metal Adhesive Systems	245
7.7.3 Durability in Salt Water: Role of Electrochemical Potentials ..	246
7.8 Life Prediction Methodology.....	248
Acknowledgment	251
References	251
Problems for Chapter 7	253
Answers to Problems for Chapter 7	256

8 Design of Components	259
8.1 Introduction.....	259
8.2 Shear and Compression Bearings	261
8.2.1 Planar Sandwich Forms	261
8.2.2 Laminate Bearings	267
8.2.3 Tube Form Bearings and Mountings.....	269
8.2.4 Effective Shape Factors	274
8.3 Vibration and Noise Control.....	275
8.3.1 Vibration Background Information	276
8.3.2 Design Requirements.....	278
8.3.3 Sample Problems.....	278
8.4 Practical Design Guidelines	287
8.5 Summary and Acknowledgments	288
Nomenclature	289
References	290
Problems for Chapter 8	290
Answers to Problems for Chapter 8	291
 9a Finite Element Analysis.....	295
9a.1 Introduction.....	295
9a.2 Material Specification.....	297
9a.2.1 Metal.....	297
9a.2.2 Elastomers.....	298
9a.2.2.1 Linear.....	298
9a.2.2.2 Non-Linear	303
9a.2.2.2.1 Non-Linear Characteristics	303
9a.2.2.2.2 Non-Linear Material Models	303
9a.2.2.2.3 Obtaining Material Data.....	304
9a.2.2.2.4 Obtaining the Coefficients.....	309
9a.2.2.2.5 Mooney-Rivlin Material Coefficients	310
9a.2.3 Elastomer Material Model Correlation	311
9a.2.3.1 ASTM 412 Tensile Correlation.....	311
9a.2.3.2 Pure Shear Correlation.....	312
9a.2.3.3 Bi-Axial Correlation.....	312
9a.2.3.4 Simple Shear Correlation.....	312
9a.3 Terminology and Verification	313
9a.3.1 Terminology	313
9a.3.2 Types of FEA Models	314
9a.3.3 Model Building.....	315
9a.3.4 Boundary Conditions	317
9a.3.5 Solution	318

9a.3.5.1 Tangent Stiffness	318
9a.3.5.2 Newton-Raphson.....	319
9a.3.5.3 Non-Linear Material Behavior	319
9a.3.5.4 Viscoelasticity (See Chapter 4).....	319
9a.3.5.5 Model Verification	320
9a.3.6 Results	320
9a.3.7 Linear Verification	322
9a.3.8 Classical Verification – Non-Linear.....	323
9a.4 Example Applications	325
9a.4.1 Positive Drive Timing Belt	325
9a.4.2 Dock Fender	326
9a.4.3 Rubber Boot	329
9a.4.4 Bumper Design	331
9a.4.5 Laminated Bearing	333
9a.4.6 Down Hole Packer	335
9a.4.7 Bonded Sandwich Mount	337
9a.4.8 O-Ring.....	339
9a.4.9 Elastomer Hose Model.....	339
9a.4.10 Sample Belt	340
References	342
 9b Developments in Finite Element Analysis	 345
9b.1 Introduction	345
9b.2 Material Models	345
9b.2.1 Hyperelastic Models.....	346
9b.2.2 Compressibility	350
9b.2.3 Deviations from Hyperelasticity	351
9b.2.3.1 Viscoelasticity.....	351
9b.2.3.2 Stress-Softening	352
9b.3 FEA Modelling Techniques	353
9b.3.1 Pre- and Post-Processing.....	353
9b.3.2 Choice of Elements	354
9b.3.3 Convergence	355
9b.3.4 Fracture Mechanics	356
9b.4 Verification	356
9b.4.1 Stresses and Strains	357
9b.4.2 Tearing Energy.....	358
9b.5 Applications	359
9b.5.1 Load Deflection	359
9b.5.2 Failure	360
References	362

10 Tests and Specifications	365
10.1 Introduction	365
10.1.1 Standard Test Methods	365
10.1.2 Purpose of Testing	366
10.1.3 Test Piece Preparation	366
10.1.4 Time Between Vulcanization and Testing	367
10.1.5 Scope of This Chapter	367
10.2 Measurement of Design Parameters	367
10.2.1 Young's Modulus	368
10.2.2 Shear Modulus	370
10.2.3 Creep and Stress Relaxation	372
10.2.3.1 Creep	373
10.2.3.2 Stress Relaxation	374
10.3 Quality Control Tests	374
10.3.1 Hardness	375
10.3.1.1 Durometer	375
10.3.1.2 International Rubber Hardness Tester	376
10.3.2 Tensile Properties	378
10.3.3 Compression Set	380
10.3.4 Accelerated Aging	381
10.3.4.1 Aging in an Air Oven	381
10.3.4.2 Ozone Cracking	382
10.3.5 Liquid Resistance	384
10.3.5.1 Factors in Swelling	384
10.3.5.2 Swelling Tests	385
10.3.6 Adhesion to Substrates	385
10.3.7 Processability	388
10.4 Dynamic Properties	390
10.4.1 Resilience	392
10.4.2 Yerzley Oscillograph	393
10.4.3 Resonant Beam	394
10.4.4 Servohydraulic Testers	395
10.4.5 Electrodynamic Testers	396
10.4.6 Preferred Test Conditions	397
10.5 Tests for Tires	397
10.5.1 Bead Unseating Resistance	398
10.5.2 Tire Strength	399
10.5.3 Tire Endurance	400
10.5.4 High Speed Performance	400
10.6 Specifications	401
10.6.1 Classification System	401

10.6.1.1 Type	402
10.6.1.2 Class	403
10.6.1.3 Further Description	403
10.6.2 Tolerances	406
10.6.2.1 Molded Products	406
10.6.2.2 Extruded Products	408
10.6.2.3 Load-Deflection Characteristics	408
10.6.3 Rubber Bridge Bearings	409
10.6.3.1 Function	409
10.6.3.2 Design Code	410
10.6.3.3 Materials Specification	411
10.6.4 Pipe Sealing Rings	413
10.6.4.1 Function	413
10.6.4.2 Materials	413
10.6.4.3 Tensile Properties	413
10.6.4.4 Compression Set	414
10.6.4.5 Low Temperature Flexibility	414
10.6.4.6 Oven Aging	415
10.6.4.7 Oil Resistance	415
10.6.4.8 Closing Remarks	415
References	416
Problems for Chapter 10	419
Answers to Problems for Chapter 10	420
Appendix: Tables of Physical Constants	423
Index	427

Preface to Third Edition

The two former editions of “Engineering with rubber” have served as handbooks and teaching texts in a rather specialized branch of materials science and engineering – the design, testing and use of engineered products incorporating rubber – for two generations of students, engineers and scientists who have encountered this unusual and fascinating branch of engineering technology. During this period, applications of rubber in engineering have increased significantly, notably in seals (for example in oil wells and transmission lines) and in flexible mountings to protect buildings against earthquake shocks. However, the second edition of the book has become out-of-print, and some of the material in it, particularly the references, has become out-dated.

This third edition includes revised versions of most of the previous chapters and also contains a new chapter reviewing recent developments in the use of finite-element programs, an important advance in methods of designing rubber products. We hope that the book will continue to help scientists and engineers as they study and apply the basic principles governing the use of rubber components in engineering applications.

Alan N. Gent
The University of Akron
August 1, 2011

Authors

Campion, Robert,
Materials Engineering Research Laboratory (MERL Ltd.),
Wilbury Way, Hitchin, Hertfordshire, SG4 0TW, England

Ellul, Maria D.,
ExxonMobil Chemical Company,
388 S. Main Street, Akron, Ohio 44311-1059, USA

Finney, Robert H.,
HLA Engineers, Inc.,
5619 Dyer Street, Suite 110, Dallas, Texas, 75206, USA

Gent, Alan N.,
College of Polymer Science and Polymer Engineering,
The University of Akron,
Akron, Ohio 44325-3909, USA

Hamed, G. R.,
Department of Polymer Science, The University of Akron,
Akron, Ohio 44325-3909, USA

Hertz, Daniel L., Jr.,
Seals Eastern, Inc.,
Red Bank, New Jersey 07701, USA

James, Frank O.,
Mechanical Products Division, Lord Corporation,
Erie, Pennsylvania 16514-0039, USA

Lake, Graham J.,
University of East London,
Dagenham, RM8 2AS, U.K.

Miller, Thomas S.,
Mechanical Products Division, Lord Corporation,
Erie, Pennsylvania 16514-0039, USA

Scott, Kenneth W. (deceased)

Sheridan, Patrick M.,
Mechanical Products Division, Lord Corporation,
Erie, Pennsylvania 16514-0039, USA

Sommer, John G.,
5939 Bradford Way,
Hudson, OH 44236, USA

Stevenson, Andrew,
Materials Engineering Research Laboratory (MERL Ltd.),
Wilbury Way, Hitchin, Hertfordshire, SG4 0TW, England

Thomas, Alan G.,
Queen Mary and Westfield College,
University of London, E1 4NS, U.K.

Yeoh, Oon Hock,
Freudenberg-NOK General Partnership,
Plymouth, MI 48170, USA

1

Introduction

Daniel L. Hertz, Jr.

■ 1.1 Rubber in Engineering

Elastomers (natural and synthetic rubber) are amorphous polymers to which various ingredients are added, creating what the rubber chemist refers to as a compound. After heating and reaction (vulcanization), these materials become “rubber”. While they are elastic and rubbery, they also dissipate energy because of their viscoelastic nature. Their strength is high, especially under shear and compressive deformations. But, as with any mechanically loaded component, failure can occur as a result of fatigue. Thus the long-term durability of rubber has to be predictable. Simple design criteria should be made available. Computer-aided design and analysis would be desirable. Specifications are required to control product quality. Physical constants, as with any engineering material, should be readily available. These are the reasons for this book: *Engineering Design of Rubber Components*.

The next question is: Which are the necessary chapters to read? Answer: All of them – sooner (the reason you probably bought the book) or later (the reason you are re-reading the book), when you have problems. Many failures of rubber components are due to a basic lack of understanding of the nature of rubber.

Rubber is an engineering material. Consider now the process of designing a long-lived rubber component. To be successful, we must understand:

- Polymers and the rubbery state
- General design principles

This is not as daunting a task as it appears. Chapters 2 to 4 provide a background for polymers and the rubbery state, and Chapters 5 to 10 give some general design principles. Without attempting to preempt the authors, let me present a sometimes overly simplistic view as I might use in addressing a fellow engineer.

■ 1.2 Elastomers

Through polymerization, a long-chain molecule is created (the primary structure of any polymeric material) from simple molecules, known as monomers. Polymer molecules can be either amorphous rubbery, amorphous glassy, or crystalline materials. Elastomers are typically amorphous polymers with their molecules in random motion. Thus, they are essentially viscous liquids. By bonding (crosslinking) the long molecules together at relatively large distances, a flexible molecular network is created with the component molecular strands still in rapid motion. But the material has now a fixed shape and size – it has become a soft elastic solid.

As an engineered product, the material at some point will be subject to an external force. When a solid body is deformed, an internal reactive force called stress, acting across a unit area, tends to resist this deformation. The measure of deformation is called strain. Consider now Fig. 1.1, a tensile stress–strain diagram for three physical states of a polymer: glassy, crystalline, and rubbery. Glassy polymers are hard and brittle. The failure (rupture) point (X) is shown in Fig. 1.1. Crystalline polymers go through a succession of changes: elastic deformation, yield, plastic flow, necking, strain hardening, and fracture.

Rubber is unique in being soft, highly extensible, and highly elastic. Considering rubber as an engineering material, we can employ the term shear modulus $G = N k T$, where N is the number of molecular network chains in a unit volume, k is Boltzmann's constant, and T is temperature in Kelvin. Many rubbery materials have a similar modulus G or hardness at equivalent temperatures above their glass transition temperature.

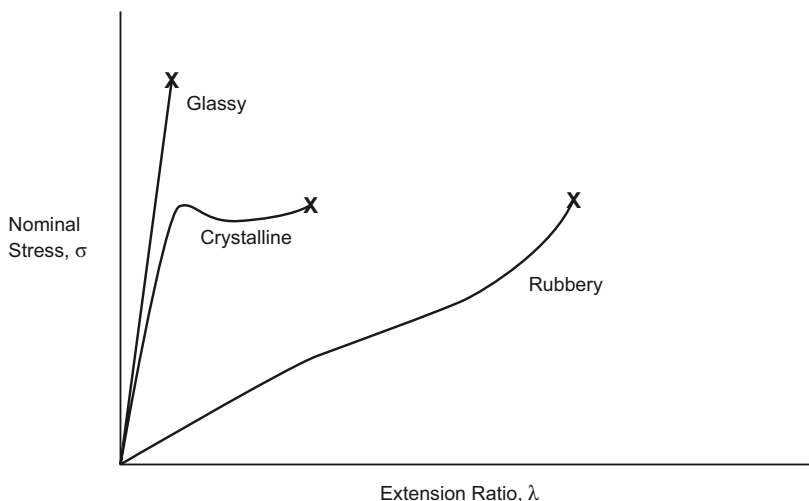


FIGURE 1.1 Tensile stress–strain diagrams for polymers in three physical states; X denotes rupture

It is not inappropriate to look on rubber as a thermodynamic “system”. In a static sense, we have an engineering material that has a broad response to external influences such as temperature and pressure. (Of course, there is no such condition as a static application of rubber.)

■ 1.3 Dynamic Application

There are two basic mechanical properties of any material: elastic modulus (stiffness) and damping (ability to dissipate energy). Typically, some energy is lost (converted to heat) in any deformation. Viscoelastic response was originally modelled by a combination of a spring (elastic component) and dashpot (viscous response). For the spring, stress is directly proportional to strain (Hooke’s law), and for the dashpot, the rate of strain is proportional to the stress applied. Of course, it is not that simple; a dashpot’s resistance depends on both time and viscosity. Consider a common example: a car shock absorber is stiff on a very cold day (high viscosity) and gives poor damping on a “washboard” road, at high frequency. The rate at which a deformed elastomer returns to its original state after release is a function of its internal friction coefficient. This value ranges over many orders of magnitude. In butyl rubber, for example, it is very high, while for dimethyl silicone it is very low. The time-temperature dependence of elastomers is of major importance, as discussed later.

■ 1.4 General Design Principles

Rubber is an engineering material: this is a fundamental point. To design adequately, basic mechanical properties must be appreciated.

Elastomers, as previously noted, are amorphous solids and behave isotropically (that is, the properties are independent of direction). The three elementary types of strain are simple tension, simple shear, and uniform (hydrostatic) compression. The elastic behavior for these cases is defined by coefficients: Young’s modulus E (tension), rigidity modulus G (shear), bulk modulus K (compression), and Poisson’s ratio ν (see Chapter 3). Poisson’s ratio, defined as the ratio of relative lateral contraction to longitudinal extension under a simple tension stress, would be 0.5 for a totally incompressible solid. For elastomers, ν is 0.499 + (for steel, ν is approximately 0.3). For an isotropic incompressible material, $E = 3 G$.

The essential incompressibility of rubber has many consequences in design, manufacturing, and application.

■ 1.5 Thermal Expansivity, Pressure, and Swelling

The coefficient of thermal expansion of rubber is approximately $4.8 \times 10^{-4}/\text{K}$, similar to a hydrocarbon liquid. Addition of fillers reduces the value slightly. Comparing this expansivity to steel ($3.5 \times 10^{-5}/\text{K}$), a tenfold difference, one begins to understand that built-in interfacial strains may occur in a bonded rubber-metal or composite structure.

The high coefficient of expansion coupled with the high bulk modulus means that a potential exists for substantial thermal pressure if the elastomer is confined and subsequently heated. This is also the molding environment, with thermal pressure a necessity for replicating mold contours and surface finishes. The molding procedure of “bumping” vents excess rubber created by this thermal expansion. If not relieved, the thermal pressure could exceed the press clamping force. This can make the mold open at the parting line, creating a condition referred to as “back-rind”. Beerbower [1] has calculated these pressures using the ratio γ of thermal expansion at constant pressure to compressibility at constant temperature. This value is available from the *Polymer Handbook* [2]. It is reasonable to use a value for γ of 1.13 for saturated backbone hydrocarbon elastomers (identified according to the American Society for Testing and Materials by ASTM D 1418 designation “M”; e.g., EPDM) and 1.22 for unsaturated elastomers (ASTM D 1418 designation “R”; e.g., NBR, SBR, NR). Using Beerbower’s equation:

$$P (\text{MPa}) = 0.1 + 298 \gamma \ln \frac{T}{298} \quad (1.1)$$

it is possible to predict the pressure developed. For example, if an EPDM seal is completely confined at 25°C (298 K), and the temperature is increased to 150°C (423 K), the potential thermal pressure is 118 MPa (17,100 psi).

Thermal pressure and osmotic swelling pressure can be additive, but the terms should not be confused. Rubber components are often exposed to a liquid that has some degree of thermodynamic compatibility (partial solubility). When two liquids are mixed together they can be (a) totally miscible (soluble), (b) partially miscible, or (c) totally immiscible. We would avoid an elastomer selection based on (a) unless we are making a rubber solution. We prefer (c), but it is often difficult (high cost) or impossible. We must therefore learn to design with (b), partial miscibility. Going back to our design application, the rubber component can swell and the osmotic swelling pressure (3–500 psi) can be roughly calculated by referring to a physical chemistry textbook. Suppose the now-swollen rubber completely fills the available volume. Increasing temperature will then create a thermal pressure due to the confinement of the elastomer.

■ 1.6 Specific Applications and Operating Principles

Consider three specific applications of elastomers:

- Seals
- Vibration and shock absorption
- Load-bearing applications (bridge and building bearing pads)

The dynamic response is important in each case. We will concentrate on seals. These might be O-rings or shaft seals. Each design creates a range of challenges extending beyond the selection of the suitable elastomer. An O-ring, for example, consists of a toroidal rubber seal, with sealing being effected by deflection of the seal cross section. This creates an initial seal contact stress. Lindley's paper is an excellent reference [3]. The average design limits for rubber deformation are typically 15% in compression and 50% in shear. Although these limits appear to be conservative, consider them from another aspect. Ferry [4] makes the following comments:

In considering the effectiveness of an elastomeric seal, two useful questions are:

1. After a sudden stress due to a change in articulation of the structure or a burst of pressure, how long will it take for the elastomer to adjust its shape to maintain the seal?
2. If there are oscillating stresses, will there be sufficient time in the period of oscillation for the elastomer to adjust its shape to maintain the seal?

Prof. Ferry's two questions are of course applicable to any seal, but they are particularly relevant to O-rings and lip-type shaft seals. (Points 1–3 and the two paragraphs that follow are quoted from Ferry's memorandum [4].)

1. Response to a sudden, transient shear stress is described by the creep compliance $J(t)$ or ratio of time-dependent strain to the applied stress. It depends on the time t elapsed since imposition of stress as shown in Fig. 1.2 for a crosslinked elastomer. At short times, the shape change will be incomplete. For purposes of illustration, we will assume that accomplishment of 90% of the final shape change is satisfactory and indicate the corresponding time $t_{0.9}$ as shown in Fig. 1.2. It may be anywhere from milliseconds to hours, depending highly on temperature as well as the chemical nature of the elastomer and the degree of cross-linking.
2. Response in shape change to an oscillating stress can be described by the storage shear compliance J' , but a more familiar property is the storage shear modulus G' , or the ratio of the elastic (in-phase) component of stress to the oscillating strain (see Chapter 4). It varies with frequency, as shown in Fig. 1.3 for a crosslinked elastomer. At high frequencies the elastomer will appear to be stiff and the shape changes will be incomplete. Similarly, we assume that an increase in stiffness of 10% will be acceptable and indicate the corresponding frequency $f_{1.1}$ as shown.

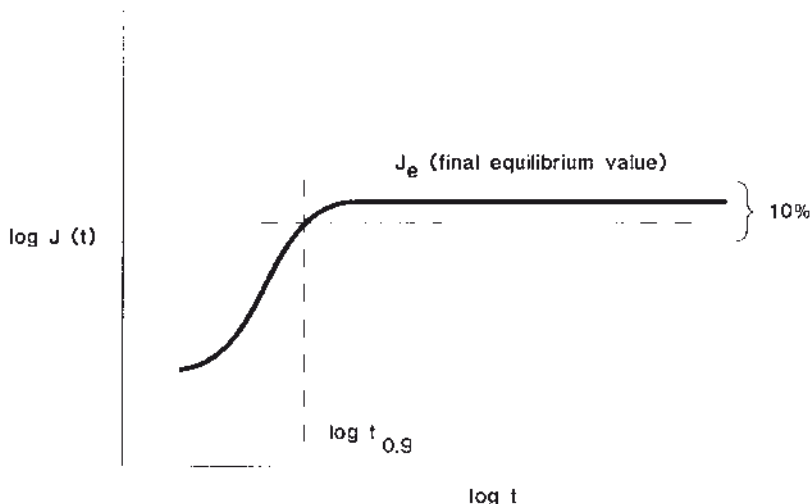


FIGURE 1.2 Schematic diagram showing response (compliance J) as a function of time.

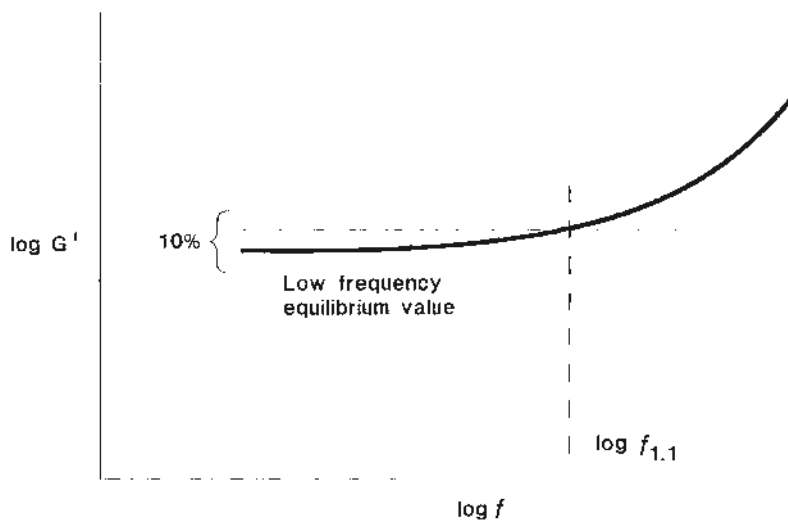


FIGURE 1.3 Schematic diagram showing real part G' of dynamic shear modulus as a function of frequency f

3. Interrelation of $t_{0.9}$ and $f_{1.1}$ and their determination. For practical purposes, only one of the experiments of Figs. 1.2 and 1.3 needs to be performed to characterize the material. It can be estimated that

$$f_{1.1} \text{ (Hz)} \cong \frac{0.2}{t_{0.9}} \text{ (second)} \quad (1.2)$$

so one can be estimated from the other. If the elastomer is any good at all, $t_{0.9}$ should be very small and the experiment of Fig. 1.2 is not practical. The usual test would therefore be of the dynamic shear storage modulus G' (or the corresponding Young's modulus, $E' = 3 G'$). The test usually needs to be performed at only one temperature, T_0 , since values at any other temperature can be calculated from the shift factor a_T (as discussed in Chapter 4). The temperature dependence of a_T depends primarily on the chemical nature of the elastomer. Data are available in the literature for many elastomers.

The examples given in Table 1.1 for cured 1,4-polybutadiene and butyl rubber were evaluated by the procedure illustrated in Fig. 1.2 with the use of Eq. (1.2) to obtain $t_{0.9}$, at 25 °C. The values at -25 °C were obtained from Eq. (1.2) with values of $\log a_T$ taken from the literature: 1.32 for polybutadiene, and 2.98 for butyl rubber.

According to these estimations, the response to transient stress would be very rapid for polybutadiene at both temperatures, and a frequency of 13 Hz could be tolerated even at -25 °C without exceeding a 10% rise in G' . For butyl rubber, well known to have slower responses, the response appears barely satisfactory at 25 °C, but at -25 °C a 40-second requirement for a transient stress and a maximum frequency of 0.005 Hz for oscillatory stress would probably be unacceptable.

Thus, the key to leak-free sealing is a rapid recovery of the seal deformation. Having determined the natural recovery time, we convert the imposed (disturbing) frequency f into a real time interval $t = 1/2 \cdot \pi \cdot f$. If the ratio of recovery time to real time exceeds 1, then the seal will leak. If it is about 1, the seal might leak. And if it is less than 1, the seal should not leak.

TABLE 1.1 Characteristic Response Times and Frequencies

	1,4-Polybutadiene		Butyl rubber	
	25 °C	-25 °C	25 °C	-25 °C
$t_{0.9}$ (s)	0.0008	0.015	0.04	40
$F_{1.1}$ (Hz)	250	13	5	0.005

■ 1.7 Seal Life

Seal life in dynamic applications is strongly dependent on the development of a hydrodynamic film between the rubber surface and the sealing surface. The ability of a lubricant to wet these surfaces is a function of their surface chemistry. The long life of a rubber marine “cutless” bearing is enhanced by the use of nitrile rubber, probably because the polar aspect of the nitrile groups creates a high energy, easily wetted surface. Conversely, the low abrasion resistance of a silicone rubber shaft seal is probably due, in part, to the low energy surface of silicone rubber, which tends to discourage “wetting” of the elastomer by the lubricant.

■ 1.8 Seal Friction

Roberts [5] notes that the coefficient of friction of rubber ranges from 0.001 to 10, depending on the interface conditions. In the case of a shaft seal or O-ring, a typical hydrodynamic film thickness is about 150 nm. Shearing of this film is the prime cause of dynamic or running friction, so that the dynamic coefficient of friction is a function of lubricant viscosity and sliding velocity. The coefficient generally starts high, because seal contact stress breaks down the hydrodynamic film. It decreases to a minimum value as the sliding velocity is increased, and then increases again. Thus, running friction can be minimized by optimizing viscosity and velocity effects. Seal friction will create a heat build-up, often causing premature failure due to excessive heat aging of the elastomer. Earlier nitrile seal formulations often included a high percentage of graphite as a filler. One might assume that graphite was used to reduce friction. In actuality, it served to increase the thermal conductivity, thus carrying heat away from the rubbing surface. Graphite is no more than a bulk filler (increasing hardness only), offering little or no reinforcing capabilities on its own. Today’s trend is to utilize finer-particle, reinforcing furnace-type carbon blacks. Concurrent with this change, engine oil temperatures have increased with smaller engines operating at higher rpm’s. This combination of more severe operating conditions and changing seal requirements has forced seal manufacturers to use more temperature-resistant elastomers. A conventional nitrile (NBR) elastomer might be capable of meeting the static heat-aging requirements at oil operating temperatures (now 135–150 °C). But the additional thermal load created by seal friction can raise this value to 175–200 °C at the seal contact area, a temperature in excess of the capabilities of nitrile rubber. Finite element modelling (FEM) of heat transfer in rubber products is increasingly needed in the design stage, using a specific heat value of the rubber compound, to maximize service life.

■ Acknowledgments

Acknowledgments are extended to the Education Committee of the Rubber Division of the American Chemical Society, who determined the need for this handbook; to Dr. Alan N. Gent, who accepted the challenge of becoming the editor of this very necessary publication; and to our “Distinguished Advisers” of the Education Committee, J. D. Ferry, R. Pariser, and T. L. Smith for their encouragement.

■ References

- [1] A. Beerbower, “Thermodynamics of Geothermal Seals”, ASTM E 45.10.02 Materials Task Group, May 19, 1980.
- [2] “Thermal Pressure Coefficients”, in J. Brandrup and E. H. Immergut (Eds.), Polymer Handbook, 2nd ed., Wiley, New York, 1975.
- [3] P. B. Lindley, “Compression Characteristics of Laterally Unrestrained Rubber O-Rings”, *J. Inst. Rubber Ind.*, July/August 1967.
- [4] J. D. Ferry, private memorandum, Nov. 14, 1986.
- [5] A. D. Roberts, *Tribology Int.*, **4**, 115–120 (1977).

2

Materials and Compounds

G. R. Hamed

■ 2.1 Introduction

Rubbers can be divided broadly into two types: thermosets and thermoplastics. Thermosets are three-dimensional molecular networks, with the long molecules held together by chemical bonds. They imbibe solvent and swell, but do not dissolve; furthermore, they cannot be reprocessed simply by heating. The molecules of thermoplastic rubbers, on the other hand, are not connected by primary chemical bonds. Instead, they are joined by the physical aggregation of parts of the molecules into hard domains. Hence, thermoplastic rubbers dissolve in suitable solvents and soften on heating, so that they can be processed repeatedly. In many cases thermoplastic and thermoset rubbers may be used interchangeably. However, in demanding uses, such as in tires, engine mounts and springs, thermoset elastomers are used exclusively because of their better elasticity, resistance to set, and durability. The reader is referred to other sources for data on thermoplastic elastomers and their mechanical properties (1–3). This chapter deals only with thermoset rubbery materials and their formulation.

The addition of various chemicals to raw rubber in order to impart desirable properties is termed rubber compounding or formulation. Typical ingredients include: crosslinking agents (also called curatives), reinforcements, anti-degradants, process aids, extenders, and specialty additives, such as tackifiers, blowing agents, and colorants. Because thermoplastic rubbers contain hard domains which interconnect the molecules and impart strength and elasticity, they do not require crosslinking agents or reinforcing fillers. However, the selection of appropriate curatives and fillers is critical to the performance of thermoset elastomers. We begin by describing the types of elastomers commercially available and then discuss fundamentals of their compounding.

■ 2.2 Elastomer Types

2.2.1 General Purpose

General purpose elastomers are hydrocarbon polymers. They include styrene-butadiene rubber (SBR), butadiene rubber (BR), and polyisoprene – both natural rubber (NR) and synthetic (IR). These “diene” rubbers contain substantial chemical unsaturation in their backbones, causing them to be rather susceptible to attack by oxygen, and especially by ozone. Additionally, they are readily swollen by hydrocarbon fluids. The primary application of these elastomers is in automobile and truck tires.

2.2.1.1 Styrene-Butadiene Rubber (SBR)

SBR denotes a copolymer of styrene and butadiene, typically containing about 23% styrene, with a T_g of approximately $-55\text{ }^\circ\text{C}$. It is the most widely used synthetic elastomer, with the largest volume production. It is synthesized via free-radical polymerization as an emulsion in water, or anionically in solution. In emulsion polymerization, the emulsifier is usually a fatty acid or a rosin acid. The former gives a faster curing rubber with less tack and less staining. The molecular weight is controlled (to prevent gelation) by mercaptan chain transfer agents. When polymerization is complete, coagulation of the emulsion is carried out with salt, dilute sulfuric acid, or an alum solution. Alum coagulation results in a rubber with the highest electrical resistivity.

When emulsion polymerization is carried out at an elevated temperature ($\sim 50\text{ }^\circ\text{C}$), the rate of radical generation and chain transfer is high, and the polymer formed is highly branched. To overcome this, polymerization is carried out at low temperature ($\sim 5\text{ }^\circ\text{C}$), producing “cold” emulsion SBR, with less branching and giving stronger vulcanizates.

A common initiator for anionic polymerization is butyl lithium. The vinyl butadiene content, and hence T_g , of SBRs polymerized in solution are increased by increasing solvent polarity. In comparison with emulsion polymers, the molecular weight distribution of anionically prepared SBR is narrow, and, because the chain ends are “living”, i.e., they remain reactive after polymerization, the molecules can be functionalized or coupled. For example, the SBR macromolecules can be amine-terminated to provide increased interaction with carbon black, or coupled with SnCl_4 to give star-shaped macromolecules that break upon mastication in the presence of stearic acid to yield a material with lower viscosity. Solution SBR is also purer than emulsion SBR, because of the absence of emulsion residues. But compared at similar number-average molecular weights, emulsion SBRs are more extensible in the uncured (so-called green) state than anionic SBRs.

2.2.1.2 Polyisoprene (NR, IR)

Natural Rubber (NR): Natural rubber is produced from the latex of the Hevea brasiliensis tree. Before coagulation, the latex is stabilized with preservatives (e.g., ammonia, formaldehyde, sodium sulfite) and hydroxylamine may be added to produce technically-specified, constant-viscosity grades of NR. The T_g of NR is about -70°C and its structure is thought to be completely *cis*-1,4-polyisoprene, except for the chain ends. NR contains small amounts of fatty acids and proteinaceous residues that promote sulfur vulcanization. Because NR macromolecules are configured identically (stereoregular), they spontaneously pack together as crystallites on standing at low temperature, at a maximum rate at temperatures around -25°C . NR also crystallizes upon straining. In fact, strain-induced crystallization imparts outstanding green strength and tack, and gives vulcanizates with high resistance to cut growth at severe deformations.

NR macromolecules are susceptible to fracture on shearing. High shearing stresses and oxygen promote the rate of molecular chain scission.

Several modified natural rubbers are available commercially. Some examples are:

- a) Deproteinized, to reduce water absorption, e.g., in electrical applications where maximum resistivity is required. Reduced water absorption has important benefits for engineering applications, giving better control of modulus and lower creep and stress relaxation.
- b) Skim rubber, a high-protein, fast curing product used in cellular foams and pressure sensitive adhesives.
- c) Superior processing, in which ordinary and vulcanized lattices are blended in about an 80:20 ratio before coagulation. Unfilled or lightly filled compounds made with superior processing NR give smoother extrudates with better dimensional control compared to those prepared from regular NR because of reduced die swell.
- d) Isomerized, prepared by milling NR with butadiene sulfone, resulting in *cis/trans* isomerization which inhibits crystallization. Unfortunately, inhibition of crystallization reduces the high strength and fatigue resistance characteristics of NR because these desirable properties are derived from the ability of NR to crystallize on stretching.
- e) Epoxidized, an oil resistant rubber, which retains the ability to strain crystallize.

Synthetic polyisoprene (IR): IR is produced both anionically and by Ziegler-Natta polymerization. The former material has up to 95% *cis*-1,4 microstructure, while the latter may be as much as 98% stereoregular. Even though the difference in stereoregularity is small, Ziegler-Natta IR is substantially more crystallizable. However, both types of IR have less green strength and tack than NR. IR compounds have lower modulus and higher breaking elongation than similarly formulated NR

compositions. This is due, at least in part, to less strain-induced crystallization with IR, especially at high rates of deformation.

2.2.1.3 Polybutadiene (BR)

Like polyisoprene, polybutadiene (BR) can be synthesized anionically or via Ziegler-Natta catalysis. Cold emulsion BR produced by free-radical polymerization is also available. Anionic BR, prepared in hydrocarbon solvent, contains about 90% 1,4 structure and 10% 1,2 (i.e., vinyl). The vinyl content can be increased by adding an amine or ether as co-solvent during polymerization. The 1,4 structure is an approximately equal mix of *cis* and *trans*. Because it consists of mixed isomers, anionically-prepared BR does not crystallize. Emulsion BR has a mostly *trans* microstructure and also does not crystallize. On the other hand, the Ziegler-Natta product has a very high *cis* content and can crystallize. The T_g of low-vinyl BRs is about $-100\text{ }^\circ\text{C}$, among the lowest of all rubbers, while that of high-vinyl BRs can reach $0\text{ }^\circ\text{C}$. Low-vinyl BRs are highly resilient and are often blended with SBR, NR, and IR to make tire treads with good abrasion resistance. Unlike NR, BR is resistant to chain scission during mastication.

2.2.2 Specialty Elastomers

In many applications, general purpose elastomers are unsuitable due to their insufficient resistance to swelling, aging, and/or elevated temperatures. Specialty elastomers have been developed to meet these needs.

2.2.2.1 Polychloroprene (CR)

Polychloroprene is an emulsion polymer of 2-chlorobutadiene and has a T_g of about $-50\text{ }^\circ\text{C}$. The electron-withdrawing chlorine atom deactivates the double bond towards attack by oxygen and ozone and imparts polarity to the rubber, making it resistant to swelling by hydrocarbons. Compared to general-purpose elastomers, CR has superior weatherability, heat resistance, flame resistance, and adhesion to polar substrates, such as metals. In addition, CR has lower permeability to air and water vapor.

The micro-structure of CR is mostly *trans*-1,4 and homopolymer grades crystallize upon standing or straining, even though they are not as stereoregular as NR. Apparently, C-Cl dipoles enhance interchain interaction and promote crystallization. Copolymer grades of CR crystallize less or not at all. Applications include wire, cable, hose, and some mechanical goods.

2.2.2.2 Acrylonitrile-Butadiene Rubber (NBR)

NBR, also termed nitrile rubber, is an emulsion copolymer of acrylonitrile and butadiene. Acrylonitrile contents vary from 18 to 50%. Unlike CR, polarity in NBR is introduced by copolymerization with the polar monomer, acrylonitrile, which imparts excellent fuel and oil resistance. With increased acrylonitrile content, there is an increase in T_g , reduction in resilience, lower die swell, decreased gas permeability, increased heat resistance, and increased strength. Because of unsaturation in the butadiene portion, NBR is still rather susceptible to attack by oxygen and ozone. Aging behavior can be improved by blending with small amounts of polyvinyl chloride. Nitrile rubber is widely used for fuel and oil hoses, and seals.

2.2.2.3 Hydrogenated Nitrile Rubber (HNBR)

Nitrile rubber can be hydrogenated to eliminate most of the unsaturation and hence greatly improve aging and heat resistance. Fuel resistance is maintained. HNBR is used especially in oil field applications, where resistance to hydrocarbons at elevated temperatures is required.

2.2.2.4 Butyl Rubber (IIR)

Butyl rubber is a copolymer of isobutylene with a small percentage of isoprene to provide sites for curing. IIR has unusually low resilience for an elastomer with such a low T_g (about -70 °C). Because IIR is largely saturated, it has excellent aging stability. Another outstanding feature of butyl rubber is its low permeability to gases. Thus, it is widely used in inner tubes and tire innerliners. Brominated (BIIR) and chlorinated (CIIR) modifications of IIR are also available. They have enhanced cure compatibility with the general purpose diene elastomers.

2.2.2.5 Ethylene-Propylene Rubber (EPR, EPDM)

The commercial rubbers with the lowest density are ethylene-propylene (EPR) copolymers made by Ziegler-Natta and metallocene polymerization. To introduce unsaturated cure sites, a non-conjugated diene termonomer, such as 1,4 hexadiene, ethylidene norbornene, or dicyclopentadiene, is employed. EPDM (ethylene-propylene diene monomer) has a small number of double bonds, external to the backbone, introduced in this way. The ratio of ethylene to propylene in commercial grades varies from 50/50 to 75/25, and a typical T_g is -60 °C. EPRs and EPDMs have excellent resistance to weathering and good heat stability. They can be made partially crystalline to give high green strength, but they possess poor building tack. Applications include roofing, seals, gaskets, and hose.

2.2.2.6 Silicone Rubber (MQ, VMO, PMQ, PVMQ)

Unlike the previously discussed elastomers which have carbon-carbon backbones, silicone rubbers contain very flexible siloxane backbones, and have very low glass transition temperatures. The most common silicone elastomer is polydimethyl siloxane (MQ) with methyl substituent groups on the polymer chain. It has a T_g of -127 °C. Other members of the silicone rubber family have vinyl and phenyl substituent groups in addition to methyl, as denoted by the additional letters in their reference letters. Silicone rubbers have both excellent high temperature resistance and low temperature flexibility. In addition, they possess good biocompatibility and thus are used in implants and prostheses. Other uses include gaskets, seals, and O-rings.

2.2.2.7 Polysulfide Rubber (T)

Polysulfide rubbers contain a substantial proportion of sulfur in their structure. For example, the polysulfide rubber made by reacting dichloroethane with sodium tetrasulfide contains about 80% by weight of sulfur. This results in high density (1.34 g/cm³) and outstanding resistance to ketones, esters, and most solvents. Major uses of polysulfide rubbers include permanent putties for fuel tank sealants, fuel hose liners, and gaskets.

2.2.2.8 Chlorosulfonated Polyethylene (CSM)

When polyethylene is chlorosulfonated, its crystallinity is disrupted and a chemically stable elastomer results. Commercial grades contain 25–45% chlorine and 1–1.4% sulfur. These elastomers have excellent weatherability and good flame resistance. Oil resistance increases with increasing chlorine content, while low-temperature flexibility and heat-aging resistance are improved when the chlorine content is low.

2.2.2.9 Chlorinated Polyethylene (CM)

Another modification of polyethylene to produce an elastomer is simple chlorination (25–42%, typically about 36%). CMs are less expensive than CSMs and provide vulcanizates with lower compression set. Increased chlorine content improves oil, fuel, and flame resistance, but results in poorer heat resistance. CM has excellent weatherability and heat resistance to 150–175 °C, even when immersed in many types of oil. Hose and wire and cable coverings are typical applications.

2.2.2.10 Ethylene-Methyl Acrylate Rubber (AEM)

This elastomer is a terpolymer of ethylene, methyl acrylate, and a small amount of carboxylic monomer as a cure site. Amines and peroxides are used as curatives. AEM has heat resistance between that of CSM and MQ elastomers. It is resistant to aliphatics, but has poor resistance to strong acids and other hydrolyzing agents. Weathering and heat aging resistance are good up to 150 °C. Example applications are power steering hose, spark plug boots, and transmission seals.

2.2.2.11 Acrylic Rubber (ACM)

ACMs are copolymers of a dominant acrylate monomer (ethyl or butyl) and a cure site monomer, such as 2-chloroethyl vinyl ether. Butyl acrylate results in a lower T_g , but poorer oil resistance compared to ethyl acrylate. Copolymerization with acrylonitrile improves oil resistance. Although acrylate rubbers have good heat resistance, they have poor resistance to alkali and acids. Applications include gaskets, O-rings, oil hose, and transmission seals.

2.2.2.12 Fluorocarbon Rubbers

Fluorocarbon rubbers are made in emulsion and are among the most inert and expensive elastomers. A typical one is made by copolymerizing the fluorinated analogs of ethylene and propylene. This rubber has a density of 1.85 g/cm³ and has a service temperature exceeding 250 °C. It is little affected by immersion in acids, bases, or aromatic solvents; however, ketones and acetates attack the material. There are many aircraft applications for fluorocarbon rubbers, including O-rings, seals, and gaskets.

2.2.2.13 Epichlorohydrin Rubber (CO, ECO)

Two common types are polyepichlorohydrin (CO) and copolymers with ethylene oxide (ECO), which exhibit a lower T_g . Epichlorohydrin rubbers are quite resistant to aliphatic and aromatic fluids, and have good building tack. Other notable properties include good ozone resistance, low gas permeability (about one third that of butyl rubber), and heat resistance up to 150 °C. Applications include wire and cable jackets, hose and belting, and packings.

2.2.2.14 Urethane Rubber

Polyester and polyether type millable urethane rubbers are available. The latter have better hydrolytic stability, but somewhat worse mechanical properties. Urethane rubbers can be cured with sulfur or peroxide and vulcanizates have excellent resistance to weathering, abrasion, and swelling by oil. Some applications are industrial rolls, caster wheels, gaskets, shoe soles, and conveyor belts.

■ 2.3 Compounding

None of the elastomers discussed in the previous section have useful properties until they have been properly formulated. Although some of the science of compounding is understood, much art still remains in preparing technical rubber compositions. In this section, the science and technology of the various ingredients used in rubber are discussed.

2.3.1 Vulcanization and Curing

An elastomer, as synthesized, is basically a high molecular weight liquid with low elasticity and strength. Although the molecules are entangled, they can readily disentangle upon stressing, leading to viscous flow. Vulcanization or curing is the process in which the chains are chemically linked together to form a network, thereby transforming the material from a viscous liquid to a tough elastic solid. Strength and modulus increase, while set and hysteresis decrease. Various curing systems are used to vulcanize different types of elastomers, but complete coverage is beyond the scope of this chapter. Rather, discussion here is primarily on the curing of general purpose diene elastomers with sulfur, with only brief mention of other cure systems.

2.3.1.1 Sulfur Curing

The most widely used vulcanizing agent is sulfur. In order to use sulfur for crosslinking, an elastomer must contain double bonds with *allylic* hydrogens. General purpose diene elastomers such as BR, SBR, NR and IR meet this basic requirement.

Two forms of sulfur are used in vulcanization: soluble (rhombic crystals of S_8 rings) and insoluble (amorphous, polymeric sulfur). Sometimes, in compounds containing high levels of sulfur, insoluble sulfur is used to prevent sulfur blooming, a process in which the sulfur migrates to the surface of a compound and crystallizes there. Blooming can occur when large amounts of soluble sulfur are used, because at high mixing temperatures, the solubility of S_8 is high, enabling large amounts to dissolve, but upon cooling the solubility decreases. When the solubility limit is reached, excess sulfur blooms to the surface. Sulfur bloom reduces the “tack” of a rubber compound, a necessary property if layers of rubber are to be plied-up to make a composite structure such as a tire. Insoluble sulfur does not bloom because it disperses in rubber as discrete particles, which cannot readily diffuse through the rubber. However, above 120 °C insoluble sulfur transforms into soluble sulfur.

Thus, mixing temperatures must be kept below 120 °C in order to take advantage of the bloom resistance of insoluble sulfur.

Crosslinking with sulfur alone is quite inefficient and requires curing times of several hours. For every crosslink, 40–55 sulfur atoms are combined with the rubber. The structure contains polysulfide linkages, dangling sulfur fragments, and cyclic sulfides. Much of the sulfur is not involved in crosslinks between chains. Moreover, such networks are unstable and have poor aging resistance.

In order to increase the rate and efficiency of sulfur crosslinking, accelerators are normally added. These are organic bases and can be divided into five major categories: guanidines, thiazoles, dithiocarbamates, xanthates, and thiurams. Of these, the guanidine-type accelerators, such as diphenyl guanidine (DPG), give the lowest rate of vulcanization as well as a relatively slow onset of vulcanization. Delayed onset of vulcanization is a desirable feature of rubber compounds. It allows shaping processes to be carried out before vulcanization starts and the material becomes set in its final shape. Premature vulcanization is known as “scorch”.

Guanidines are seldom used alone, but rather are combined with another type of accelerator. The accelerators that increase the rate of curing the most are the xanthate types. These ultra-accelerators cause crosslinking so readily that they are seldom used in solid rubber because curing would be initiated just from the heat generated while mixing. Rather, xanthates are used mainly for crosslinking rubber as a latex.

The accelerators with the widest application are the thiazoles, a subcategory of which is the delayed-action sulfenamides. Compounds containing sulfenamides may be sheared for long times without premature vulcanization (scorch). This is particularly important in the tire industry, where a compound may be mixed, repeatedly milled, and then calendered or extruded before being fabricated into a tire.

Thiurams and dithiocarbamates are considered ultra-accelerators, although they are not as active as the xanthates. Because these accelerators have a short scorch time, care must be taken to keep processing temperatures low. Some compounds with ultra-accelerators may begin curing within one day at room temperature, so they must be processed soon after mixing. Crosslinking is efficient when ultra-accelerators are used, and especially when the ratio of accelerator to sulfur is high, so that only low levels of sulfur are required for proper vulcanization.

Often, a combination of accelerators is used to obtain the desired scorch resistance and cure rate. Generally, if two accelerators of the same type are combined, cure characteristics are approximately the average of those for each accelerator alone. However, there is no general rule when combining accelerators of different types. Moreover, the type of accelerator is much more important than the level of accelerator in controlling scorch time. Although increased levels of accelerator increase the

degree of crosslinking attained, there generally is only a small effect of accelerator concentration on scorch time.

Accelerated sulfur curing is more efficient when the activators zinc oxide and stearic acid are added. It is thought that these additives combine to create soluble zinc ions that activate intermediate reactions involved in crosslink formation.

One instrument used to determine the kinetics of crosslinking is the oscillating disc rheometer (ODR). An oscillating rotor is surrounded by a test compound, which is enclosed in a heated chamber. The torque required to oscillate the rotor is monitored as a function of time. Another instrument to follow curing is the rotor-less moving-die rheometer (MDR), which uses thinner samples, and hence has faster thermal response than the ODR. Examples of curemeter responses are shown in Figure 2.1. Initially, there is a sudden increase in torque as the chamber is closed. Then, as the rubber is heated, its viscosity decreases causing a decrease in torque. Eventually, the rubber compound begins to vulcanize and transform into an elastic solid, and the torque rises. Molecular chain scission also may be occurring; however, an increasing torque indicates that crosslinking is dominant. If the torque reaches a plateau, this indicates completion of curing and the formation of a stable network. If chain scission and/or crosslink breakage become dominant during prolonged heating, the torque passes through a maximum and then decreases. This is termed reversion. Some NR compounds, particularly at high curing temperatures, exhibit reversion. On the other hand, some compounds show a slowly increasing torque at long cure times, termed creeping cure. This behavior is often shown by compounds which initially form many polysulfidic linkages. With extended cure times, these linkages may break down and reform into new crosslinks of lower sulfur rank, thereby increasing the total number of crosslinks.

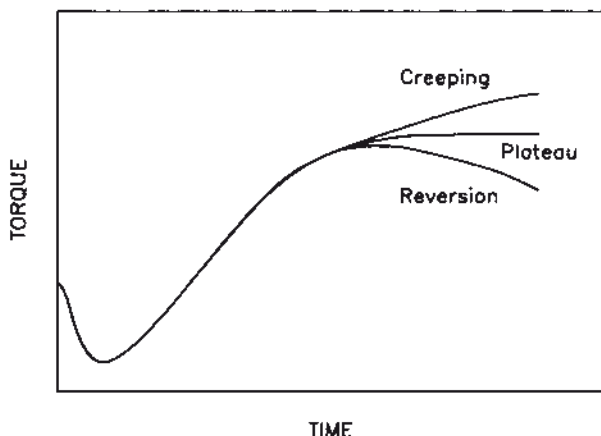


FIGURE 2.1 Three types of response from an oscillating disk rheometer

It can be seen from this short survey that the rubber chemist has many options in designing the sulfur cure system for a particular application. Indeed, it is this ability to fine-tune curing characteristics as well as the final properties that makes sulfur the generally preferred vulcanizing agent. Its versatility allows the compound to be designed in a cost-effective manner for ease of manufacture as well as for obtaining the desired properties.

2.3.1.2 Determination of Crosslink Density

The crosslink density of an elastomer can be determined from swelling or mechanical measurements. An elastomer crosslinked above its gel point will imbibe a solvent and swell, sometimes highly, but it will not dissolve. Swelling continues until the retractive forces in the extended molecular strands in the network balance the forces tending to swell the network. For unfilled elastomers, the Flory-Rehner equation is widely used to relate the amount of swelling to the crosslink density:

$$N' = -\frac{1}{2 V_s} \frac{\ln(1-v_r) + v_r + \chi v_r^2}{v_r^{1/3} - v_r / 2} \quad (2.1)$$

where N' is the number of moles of crosslinks per unit volume, V_s is the molar volume of the swelling solvent, v_r is the volume fraction of rubber in the swollen gel, and χ is the polymer-solvent interaction parameter.

For vulcanizates containing reinforcing filler such as carbon black, v_r for use in the Flory-Rehner equation may be obtained from the following expression derived by Kraus:

$$\frac{v_r}{v_{rf}} = 1 - \left[3c \left(1 - v_r^{1/3} \right) + v_r - 1 \right] \frac{\phi}{1 - \phi} \quad (2.2)$$

where v_{rf} is the volume fraction of filled rubber in the swollen gel, ϕ is the volume fraction of filler in the unswollen filled rubber, and c is the filler-rubber interaction parameter.

Crosslink densities of unfilled rubbers have also been determined from equilibrium stress-strain measurements using the Mooney-Rivlin equation:

$$\frac{\sigma}{2(\lambda - \lambda^{-2})} = C_1 + \frac{C_2}{\lambda} \quad (2.3)$$

where σ is the engineering stress, λ is the extension ratio, and C_1, C_2 are elastic constants. On plotting $\sigma / 2 (\lambda - \lambda^{-2})$ vs. $1/\lambda$ and extrapolating to $1/\lambda = 0$, a value of C_1 can be obtained from the intercept. From the theory of rubber elasticity,

$C_1 = N' R T$, where N' is the crosslink density, R is the gas constant, and T is the absolute temperature (see Chapter 3). To assure near equilibrium response, stress-strain measurements should be carried out at a low strain rate.

2.3.1.3 Influence of Crosslink Density

Mechanical properties of an elastomer depend strongly on crosslink density. Modulus and hardness increase monotonically with increasing crosslink density, and the material becomes more elastic, or stated alternatively, less hysteretic. Fracture properties, such as tear and tensile strength, pass through a maximum as crosslinking is increased. To understand this behavior, it is helpful first to consider fracture of an uncrosslinked elastomer, and then to discuss changes in the mechanism of fracture as crosslinks are introduced.

When an uncrosslinked elastomer is stressed, chains may readily slide past one another and disentangle. At slow rates, fracture occurs at low stresses by viscous flow without breaking chemical bonds. The effect of a few crosslinks is to increase the molecular weight, creating branched molecules and a broader molecular weight distribution. It is more difficult for these branched molecules to disentangle and hence strength increases. As crosslinking is increased further, the gel point is eventually reached when a three-dimensional network forms. Some chains may not be attached to the network (soluble sol phase), but the whole composition will no longer dissolve in a solvent. A gel cannot be fractured without breaking chemical bonds. Thus, strength is higher at the gel point, since chemical bonds must be ruptured to create fracture surface. However, strength does not increase indefinitely with more crosslinking.

When an elastomer is deformed by an external force, part of the input energy is stored elastically in the chains and is available (will be released upon crack growth) as a driving force for fracture. The remainder of the energy is dissipated through molecular motions into heat, and in this manner is made unavailable to break chains. At high crosslink levels, chain motions become restricted, and the “tight” network is incapable of dissipating much energy. This results in relatively easy, brittle fracture at low elongation. Elastomers have an optimum crosslink density range for practical use. Crosslink levels must be high enough to prevent failure by viscous flow, but low enough to avoid brittle failure.

Both the level and type of crosslinking are important. When curing with sulfur, the type of crosslinks depends on: (1) sulfur level, (2) accelerator type, (3) accelerator/sulfur ratio, and (4) cure time. Generally, high accelerator/sulfur ratio and longer cure time increase the number of monosulfidic linkages at the expense of polysulfidic ones. Vulcanizates containing predominately monosulfidic crosslinks have better heat stability, set resistance, and reversion resistance than those with

polysulfidic links. This is attributed to greater stability of C-S bonds compared to S-S bonds. On the other hand, compounds containing a high proportion of polysulfidic crosslinks possess greater tensile strength and fatigue cracking resistance compared to compositions with monosulfidic links. This is thought to be due to the ability of S-S bonds in polysulfidic linkages to break reversibly, thereby relieving locally high stresses that could initiate failure.

2.3.1.4 Other Cure Systems

Peroxides are another type of curing agent for elastomers. Unlike sulfur vulcanization, carbon-carbon double bonds are not required for peroxide curing and thus peroxides may be used to crosslink saturated elastomers, e.g., ethylene-propylene copolymers, chlorinated polyethylene, chlorosulfonated polyethylene, and silicone rubber. In addition, peroxides readily crosslink diene elastomers. Peroxide curing takes place via a free-radical mechanism and leads to carbon-carbon crosslinks, which are quite stable. The crosslinked materials show good aging resistance and low compression set.

Some elastomers, particularly polychloroprene, can be crosslinked with metal oxides, ZnO and MgO. It has been proposed that the crosslinking occurs via allylic chlorines on the polymer molecules. Generally, mixtures of ZnO and MgO are used because ZnO by itself is too scorchy and MgO alone is inefficient.

Butyl rubber cannot be cured with peroxides and sulfur vulcanization is often inefficient. Instead, polymethylol phenolic resins with metallic chlorides are often used. They give crosslinked materials with excellent resistance to high temperatures.

2.3.2 Reinforcement

Particulate fillers can increase the strength of an amorphous rubber more than 10-fold. In order for a filler to cause significant reinforcement, it must possess high specific surface area, i.e., the particles must be small, less than about 1 μm in size. Small particles have large surface areas to interact with the rubber and close particle-to-particle spacing in the compound. Two types of fillers that are most effective for reinforcing rubber are carbon black and silica. They can be produced with a primary particle size as small as 100 Å, corresponding to a surface area of a few hundred m^2 per gram of filler.

Two other important characteristics of fillers are structure and surface chemistry. Structure relates to irregularity in shape of filler aggregates (Figure 2.2), determined by the extent and manner of clustering of primary particles. A filler aggregate with high structure has a large void volume within the space it pervades, in which

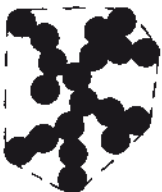


FIGURE 2.2 Schematic of a carbon black aggregate consisting of fused primary particles. The dotted line (a surface in 3D) depicts the volume pervaded by the aggregate. The larger the ratio of pervaded to actual volume, the higher the “structure”

rubber molecules may become “occluded”. The combination of occluded rubber and filler then becomes the reinforcing entity, so that the effective volume fraction of filler is increased. (Aggregates are not broken down into primary particles upon mixing with rubber.) Generally, reinforcement is enhanced by high structure and strong bonding between filler and rubber. Silica fillers are often treated with silane coupling agents to bond them chemically to rubber, or the coupling agents may be added directly to the rubber compound.

During shear mixing, rubber and carbon black become chemically linked. This has been demonstrated by attempting to dissolve filled, uncrosslinked compounds in good solvents. Only a portion of the rubber dissolves, leaving a “carbon gel” containing all of the carbon black and the remainder of the rubber which is strongly bound to the filler, and termed “bound rubber”. The interactions between rubber and carbon black include a spectrum of strengths, with some chains chemically attached to the black and others having physical bonds of varying magnitude. The importance of bonding between rubber and carbon black is illustrated by exposing carbon black to extreme heating (graphitization) in an inert atmosphere before mixing into rubber. Graphitization removes active functional sites on the black, decreases the amount of bound rubber, and reduces the reinforcing effect, as shown in Fig. 2.3. Compared to the vulcanizate reinforced with normal furnace black, the vulcanizate containing graphitized black has lower modulus, higher ultimate elongation, and reduced strength. However, the rubber filled with graphitized-black is much stronger than a simple unfilled (gum) vulcanizate or one filled with an equal volume fraction of larger-sized particles (e.g., clay).

Before addition to rubber, carbon black aggregates are “clumped” together as so-called agglomerates. In order to provide the greatest reinforcement, these black agglomerates must be broken down into aggregates and thoroughly dispersed in the rubber. This requires mixing at high shear stress. The viscosity of the rubber must not be too low, or the shear stresses will be insufficient to break apart the filler agglomerates. Thus, when oil is to be added to a stock, it should be added toward the end of the mixing cycle, after the carbon black has already been well dispersed.

Besides enhancing strength, carbon black also improves processability by greatly reducing melt elasticity. This allows shaping operations, such as extrusion and calendering, to occur with less shrinkage and melt distortion.

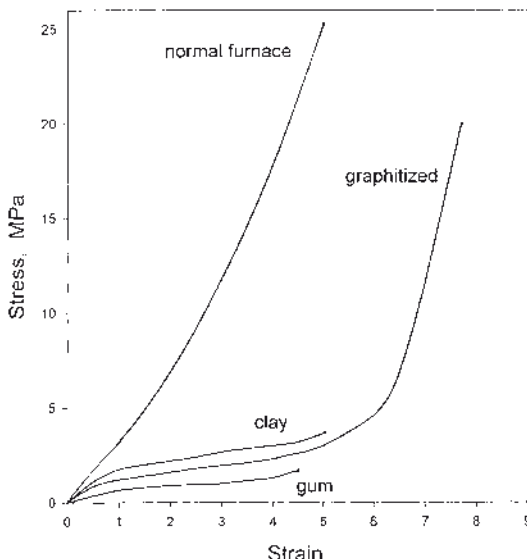


FIGURE 2.3 Typical stress-strain curves for an unfilled (gum) vulcanizate and vulcanizates filled with normal furnace black, graphitized black, and a filler consisting of micron-sized particles (e.g., clay)

Carbon black is most effective for strengthening non-crystallizing elastomers such as SBR. Strain-crystallizing elastomers such as NR already have a self-reinforcing mechanism. Indeed, unfilled and black-filled NR vulcanizates have comparable tensile strengths, although the latter have improved resistance to tearing and abrasion.

2.3.3 Anti-Degradants

Oxygen and ozone can react with elastomers and alter network structure by causing chain scission and/or crosslinking. Antioxidants and antiozonants, which can function chemically or physically, have been developed to inhibit the action of these reactive components of air.

Chemical protectants are capable of reacting with the degradant or interfering with the chain of reactions that otherwise would culminate in degradation of the rubber. The most common types are aromatic amines, phenolics, and phosphites. The first type is staining, while the other two are not. Physical protectants function by migrating, i.e., blooming, to the rubber surface and providing a barrier to attack by degradants. Microcrystalline waxes, which are mixtures of alkanes, isoalkanes, and cyclo-aliphatic hydrocarbons, are commonly used. The rate and extent of blooming are important and depend on the level of compatibility with the elastomer.

2.3.3.1 Ozone Attack

Ozone, even when present in the atmosphere at a few parts per hundred million, readily cleaves carbon-carbon double bonds in elastomers. As a result, an unsaturated rubber, exposed to ozone in the strained state, quickly develops surface cracks. The severity of cracking increases rapidly with the applied strain above a small threshold level, of the order of 10%. Para-phenylenediamines (PPDs) are effective in reducing ozone cracking in diene rubbers and there is good evidence that they react directly with ozone, competing with the ozone-rubber reaction. However, there are no additives that enable unsaturated elastomers to resist ozone as well as saturated ones.

2.3.3.2 Oxidation

In general, the reaction of oxygen with elastomers causes both chain scission and crosslinking. If chain scission dominates during aging, the elastomer softens and eventually may become sticky. This is the usual behavior of unfilled NR and IIR vulcanizates. However, most technical elastomer compounds eventually harden and embrittle during oxidation – a consequence of the dominance of crosslinking reactions. For some compounds, in the early stages of oxidation, there is a fortuitous equality in the extent of chain scission and crosslinking, such that modulus does not change. Nonetheless, the altered network now contains increased chain-end defects, and the strength and elongation are reduced.

Only one to two percent of reacted oxygen is normally sufficient to cause severe deterioration of an elastomer. The principal mechanism of oxygen attack involves an autocatalytic free radical reaction. The first step is creation of macroradicals, as a result of hydrogen abstraction from rubber chains by a proton acceptor. Oxidation continues by reaction of macroradicals with oxygen and the subsequent formation of peroxy radicals and hydroperoxides (which are readily detected by infrared spectroscopy). Oxidation is accelerated by heat, exposure to ultraviolet light, and the presence of some metals, notably copper, cobalt, and manganese. Also, stress hastens oxidation. For sulfur-cured vulcanizates, the oxidation rate increases as sulfur content increases. It is believed that the allylic crosslink site is particularly susceptible to oxidation.

Antioxidants are employed to slow oxidation. They fall into two classes, with different functions. The first type, called preventive antioxidants, reacts with hydroperoxides to form harmless, non-radical products. In the process the antioxidant is oxidized. The second type, chain-breaking antioxidants, destroys peroxy radicals that would otherwise propagate. Chain breaking antioxidants are aromatic and contain labile protons, which are “donated” to the peroxy radicals. This occurs readily because the resulting antioxidant radical is highly resonance stabilized. A listing of some

TABLE 2.1 Some Amine Antioxidants and Their Common Abbreviations

Phenyl- α -naphthylamine (PAN)
N-isopropyl-N'-phenyl-p-phenylenediamine (IPPD)
N-(1,3 dimethyl butyl)-N'-phenyl-p-phenylenediamine (6PPD)
N,N'-diphenyl-p-phenylenediamine (DPPD)
poly-1,2-dihydro-2,2,4-trimethylquinoline (TMQ)

common amine antioxidants, which are quite effective in diene elastomers, is given in Table 2.1.

It is common to use accelerated aging tests to determine the resistance of a vulcanizate to oxidation. However, caution should be used in attempting to infer long-term aging performance from short-term tests carried out at temperatures much higher than service temperature. The reason is well illustrated in Fig. 2.4. A black-filled NR vulcanizate was oxidized at various temperatures, while the degree of oxidation was determined directly by the quantity of oxygen absorbed. Stress-strain measurements were carried out on the aged samples. Stiffness at room temperature is plotted schematically against oxygen uptake at various temperatures in Fig. 2.4. It is noteworthy that, when aged at 50 °C, the vulcanizate stiffened, whereas when aged at 110 °C, it softened. Clearly, in this case, relative rates of chain scission and crosslinking depend on aging temperature.

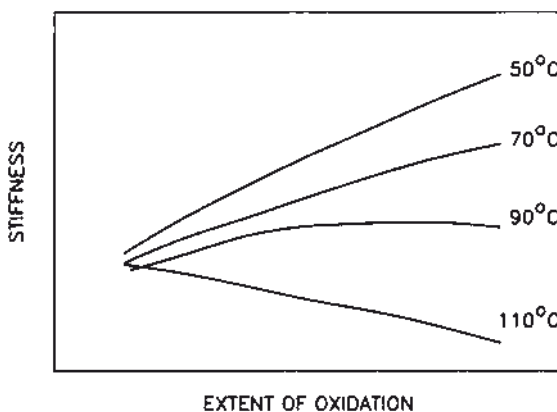


FIGURE 2.4 Stiffness of an NR vulcanizate determined at room temperature after oxidative aging at the temperatures indicated

A convenient way to determine separately the extents of chain scission and cross-linking during aging is to carry out two types of stress relaxation test: continuous stress relaxation (CSR) and intermittent stress measurement (ISM). The procedures are as follows:

A sample of the rubber to be aged is stretched to a given low extension ratio, λ . The stress is allowed to decay to an equilibrium value, $\sigma(0)$. Then, while maintaining the extension, the sample is placed in an aging chamber and stress, $\sigma_c(t)$, is monitored continuously as a function of aging time, t . This is the CSR experiment. Newly-formed network chains due to additional crosslinking are non-load bearing since they are introduced in the strained state. Only scission of the original network chains causes $\sigma_c(t)$ to be reduced. In ISM testing, on the other hand, a sample is aged in the unstretched state, then periodically, the equilibrium stress, $\sigma_i(t)$, required to impose the extension ratio, λ , is determined. In this case, the measured stress depends on the net difference between crosslinking and chain scission.

Now, based on rubber elasticity theory, it is assumed that the stress $\sigma(t)$ is directly proportional to network chain density, $N(t)$, thus

$$\frac{\sigma(t)}{\sigma(0)} = \frac{N(t)}{N(0)} \quad (2.4)$$

where $N(0)$ is the network chain density at the start of aging. Furthermore,

$$N_c(t) = N(0) - N_s(t) \quad (2.5)$$

and

$$N_i(t) = N(0) + N_x(t) - N_s(t) \quad (2.6)$$

where $N_c(t)$, $N_s(t)$ and $N_x(t)$ are, respectively, the number of molecular chains remaining after aging time t , the number of chain scissions that occurred and the number of new crosslinks introduced per unit volume. $N_c(t)$, is determined from Eq. (2.4) and the results of CSR, and $N_i(t)$ likewise from ISM. Thus, the number of chain scissions $N_s(t)$ is obtained directly from CSM, and the number of new crosslinks, $N_x(t)$, is obtained from $N_s(t)$ when combined with the results of ISM.

2.3.4 Process Aids

Process aids are additives that lower viscosity and thus enable a rubber compound to be fabricated with less energy. They also increase melt stability so that the rate of processing can be increased. There are two general kinds of process aids: chemical peptizers and physical plasticizers. Chemical peptizers, typically added at 1 to 3 parts by weight per hundred parts of elastomer (phr), reduce molecular weight by increasing oxidative chain scission. Examples include sulfonic acids and pentachlorothiophenol, which are commonly used in NR. Excess peptizer must be avoided, because it will result in reduced vulcanizate strength. Physical plasticizers soften a compound by reducing entanglements and decreasing internal friction.

The entanglement plateau modulus (indicative of entanglement density) depends on the concentration of rubber in a rubber/plasticizer mixture to a power of 2.0 to 2.3. An additional benefit of physical plasticization may be improvement in low temperature flexibility. Plasticizers should have good compatibility, which can become a problem especially at low temperatures, where a poorly compatible plasticizer may “bleed” from the compound. Common plasticizers include, e.g., oils, fatty acids, esters, pine tar, liquid polymers, and rosin.

2.3.5 Extenders

Extenders are added to rubber compositions to reduce cost. Usually, this results in a decrease in physical properties, which limits the amount of extender that can be used. Oil extension of rubber, especially in tire treads, is widely practiced. Oil levels of 30 to 40 phr are typical. Oil addition permits the use of elastomers with higher molecular weight and addition of greater amounts of filler than would be possible otherwise. This compensates for the dilution of network chains, so that good physical properties are obtainable even at rather high oil levels.

Other types of extenders are particulate solids, whose primary particle size is greater than about 1 μm . These stiffen rubber compositions, but either have little influence on strength or diminish it. Examples include clay, calcium carbonate, and ground coal.

Resins are hard brittle solids which can dissolve in rubber at processing temperatures, but may separate out as another phase in the vulcanized material and stiffen it. Some are two-component systems, which react chemically at vulcanization temperatures. A phenolic resin which reacts with a formaldehyde donor is an example.

2.3.6 Tackifiers

Tack is the ability of two materials to resist separation after contacting them for a short time under light pressure. Tackifiers are a class of resins that are added to elastomers to improve tack. Several types are available:

1. Rosin derivatives, which are chemical mixtures of abietic and related acids that are usually esterified by polyhydric alcohols then hydrogenated, dimerized, or disproportionated to improve aging and heat stability.
2. Coumarone-indene resins consisting of indene, coumarone, styrene, methyl styrene, methyl indene, etc., obtained from coal coke oven light oils.
3. Aliphatic petroleum resins made from unsaturates obtained while cracking crude oil.

4. Terpene oligomers of alpha or beta-pinene obtained from pine tree stumps.
5. Alkyl modified phenol-formaldehyde resins.

Tackifiers generally have molecular weights in the 500–2000 range. Ring and ball softening points vary from 50 to 150 °C and tackifiers often have limited compatibility with the elastomer to which they are added – they are less compatible than a plasticizer, but more compatible than a filler. The function of tackifiers, typically added in the range 1–10 phr, is two-fold: to increase initial tack and to prevent tack degradation which can occur after a stock has been processed. In NR stocks, the latter function is the more important one, whereas, for SBR and NR/SBR blends, the tackifier serves both functions.

A tackifier must possess proper compatibility with the rubber. This is dependent on chemical composition and molecular weight. For modified phenolics, the para-alkyl group must be large, t-butyl or greater, in order to improve compatibility with a non-polar hydrocarbon elastomer. When the alkyl group is t-octyl, the most effective tackifying action occurs at a molecular weight of about 2000.

■ 2.4 Typical Rubber Compositions

This chapter concludes with a few typical rubber formulations and some physical properties of the vulcanizates obtained from them, taken in part from the Vanderbilt Rubber Handbook, edited by R. F. Ohm (R. T. Vanderbilt Co., Inc., 1990).

TABLE 2.2 An Unfilled Natural Rubber Formulation

Ingredient	Amount (phr*)
Natural rubber	100
Process oil	2
Stearic acid	2
Zinc oxide	5
Antioxidant: 6PPD	1
Sulfur	2.75
Cure accelerator: benzothiazyl disulfide	1
Cure accelerator: tetramethyl thiuram disulfide	0.1

* Parts by weight per 100 parts by weight of rubber

Cure: 10 minutes at 150 °C

Shore A hardness	39
Tensile strength (MPa)	24
Breaking elongation (%)	750

TABLE 2.3 Carbon Black Filled Natural Rubber Formulations for General-Purpose Engineering Use

Ingredient	Amount (phr*)
Natural rubber	100
Process oil	5
Stearic acid	2
Zinc oxide	5
N-550 carbon black	25, 50, 75
Phenylamine antioxidant	1.5
Sulfur	2.5
Cure accelerator: benzothiazyl disulfide	1.0
Cure accelerator: tetramethyl thiuram disulfide	0.1

* Parts by weight per 100 parts by weight of rubber

Cure: 20 minutes at 150 °C

	N550 carbon black (phr)		
	25	50	75
Shore A hardness	51	62	72
300% modulus (MPa)	7	9	11
Tensile strength (MPa)	22	24	25
Breaking Elongation (%)	700	600	550

TABLE 2.4 A Typical Styrene-Butadiene Rubber (SBR) Formulation

Ingredient	Amount (phr*)
SBR-1500	100
Process oil	4
Stearic acid	2
Zinc oxide	5
Antioxidant: DPPD	1.5
N-330 carbon black	50
Sulfur	2
Cure accelerator: benzothiazyl disulfide	2
Cure accelerator: tetramethyl thiuram disulfide	0.15

* Parts by weight per 100 parts by weight of rubber

Cure: 25 minutes at 150 °C

Shore A hardness	65
300% modulus (MPa)	13.5
Tensile strength (MPa)	25
Breaking elongation (%)	500

TABLE 2.5 A Butyl Rubber Formulation

Ingredient	Amount (phr*)
Butyl 268	100
Process oil	2
Stearic acid	1
Zinc oxide	5
N-330 carbon black	50
Sulfur	2
Cure accelerator: tetramethyl thiuram disulfide	1
Cure accelerator: mercaptobenzothiazole	0.5

* Parts by weight per 100 parts by weight of rubber

Cure: 20 minutes at 171 °C

Shore A hardness	62
300% modulus (MPa)	8.5
Tensile Strength (MPa)	16.3
Breaking elongation (%)	530

TABLE 2.6 Polychloroprene Formulations for General-Purpose Engineering Use

Ingredient	Amount (phr*)
Polychloroprene (Neoprene W)	100
Process aid	5
N550 carbon black	25, 50, 75
Stearic acid	2
Zinc oxide	5
Magnesium oxide	4
Antioxidant: octylated diphenylamine	2
Cure accelerator: activated thiadiazine	1

* Parts by weight per 100 parts by weight of rubber

Cure: 20 minutes at 150 °C

	N550 carbon black (phr)		
	25	50	75
Shore A hardness	53	64	78
300% modulus (MPa)	9	11	14
Tensile strength (MPa)	20	21	24
Breaking elongation (%)	400	350	300

TABLE 2.7 An Acrylonitrile-Butadiene Rubber (NBR) Formulation

Ingredient	Amount (phr*)
NBR (Chemigum N689B)	100
Process aid	2
N330 carbon black	50
Zinc oxide	5
Stearic acid	1.5
Sulfur	1.75
Antioxidant: octylated diphenylamines	1.5
Plasticizer: dibutyl phthalate	12.5
Coumarone-indene resin	12.5
Cure accelerator: benzothiazyl disulfide	1.5

* Parts by weight per 100 parts by weight of rubber

Cure: 35 minutes at 150 °C

Shore A hardness	59
300% modulus (MPa)	9.2
Tensile strength (MPa)	18.5
Breaking elongation (%)	510

TABLE 2.8 An Ethylene-Propylene Diene Monomer (EPDM) Formulation

Ingredient	Amount (phr*)
EPDM (Nordel 2744)	100
Extender: paraffinic process oil	90
N-550 carbon black	100
Zinc oxide	5
Stearic acid	1
Sulfur	2
Cure accelerator: mercaptobenzothiazole	1.0
Cure accelerator: tetramethylthiuram monosulfide	1.5

* Parts by weight per 100 parts by weight of rubber

Cure: 20 minutes at 166 °C

Shore A hardness	64
300% modulus (MPa)	6.8
Tensile strength (MPa)	15.5
Breaking elongation (%)	410

■ Acknowledgment

This chapter was prepared with support from the D'lanni Research Endowment Fund.

■ References

- [1] Legge, N. R., Holden, G., and Schroeder, H. E., Thermoplastic Elastomers: a Comprehensive Review, Carl Hanser Verlag, Munich, 1987.
- [2] Coran, A., Thermoplastic Rubber-Plastic Blends, Chapter 8 in Handbook of Elastomers, ed. by Bhowmick, A. K., and Stephens, H. L., M. Dekker, New York, 1988.
- [3] Abdou-Sabet, S., Puydak, R. C., and Rader, C. P., Dynamically vulcanized thermoplastic elastomers, *Rubber, Chem. Technol.*, **69** (1996) p. 476–494
- [4] Tam, E., Thermoplastic Elastomers, John Wiley & Sons, London, 2010
- [5] “Blue Book: Materials, Compounding Ingredients, Machinery and Services for the Rubber Industry”, Lippincott and Petro Inc., published yearly.
- [6] Long, H. (Ed.), “Basic Compounding and Processing of Rubber”, A.C.S. Rubber Division, 1985
- [7] Morton, M. (Ed.), “Rubber Technology”, 3rd ed., Van Nostrand Reinhold Co., 1987
- [8] Whelan, A., and Lee, K., S. (Eds.), “Developments in Rubber Technology-4”, Elsevier Applied Science, 1987
- [9] Dick, J. S., “Compounding Materials for the Polymer Industries”, Noyes Publications, 1987
- [10] Brydson, J. A., “Rubbery Materials and Their Compounds”, Elsevier Applied Science, 1988
- [11] Roberts, A. D. (Ed.), “Natural Rubber Science and Technology”, Oxford Science Publications, 1988
- [12] Hofmann, W., “Rubber Technology Handbook”, Hanser Publishers, 1989
- [13] Franta, I. (Ed.), “Elastomers and Rubber Compounding Materials”, Elsevier, 1989
- [14] Ohm, R. F. (Ed.), “Vanderbilt Rubber Handbook”, R.T. Vanderbilt Co., Inc., 1990
- [15] Hepburn, C., “Rubber Compounding Ingredients – Need, Theory and Innovation. Part I. Vulcanizing Systems, Antidegradants and Particulate Fillers for General Purpose Rubbers”, Rapra Review Report No. 79, Rapra Technologies Ltd., 1994
- [16] Mark, J. E., Erman, B., and Eirich, F. R. (Eds.), “Science and Technology of Rubber”, 2nd ed., Academic Press, Inc., 1994
- [17] Ciesielski, A., “An Introduction to Rubber Technology”, Rapra Technology Ltd., 1998
- [18] Ciullo, P. A., and Hewitt, N., “The Rubber Formulary”, ChemTec Publishing, 1999
- [19] Rogers, B. (Ed.), “Rubber Compounding: Chemistry and Applications“, CRC Press, 2004

■ Problems for Chapter 2

1. Polychloroprene, though containing more unsaturation, has higher resistance to ozone than nitrile rubber. Furthermore, nitrile rubber cures readily with sulfur, while polychloroprene does not. Explain.
2. Homopolymerization of ethylene or propylene results in a hard plastic, while a 50/50 copolymer is an elastomer. Why?
3. What are the two types of sulfur used as a curative for rubber? Which one is resistant to blooming? Why?
4. 1,2 polybutadiene and 1,4 polybutadiene have the same number of double bonds, but the former cures less effectively with sulfur. Explain.
5. Why does the stiffness of a black-filled vulcanizate increase with increasing black structure (at fixed specific surface area)?
6. Distinguish between preventive and chain-breaking antioxidants.
7. A vulcanizate is subjected to oxidative aging. The change in stress with time in both CSR and ISM experiments is the same. What does this signify?

■ Answers to Problems for Chapter 2

1. NBR is a copolymer of butadiene and acrylonitrile. As with BR, unprotected double bonds in the butadiene portion are readily cleaved by ozone and can undergo crosslinking via sulfur. The double bonds in CR are protected by a polar, electron-withdrawing chlorine group. This reduces reactivity of the double bonds towards ozone and towards the curing reaction with sulfur.
2. Homopolymers of ethylene and propylene have low glass transition temperatures, but they have regular structures and are crystalline solids at room temperature. Copolymerization creates molecular chains with an irregular microstructure that cannot fit together into a crystal lattice. Hence, the copolymer is an amorphous rubbery material with low T_g .
3. Crystalline soluble sulfur and amorphous insoluble sulfur are the two types. The latter does not bloom because it remains as discrete particles when mixed into rubber.
4. Accelerated sulfur vulcanization occurs through allylic hydrogens. Each monomer unit of 1,2-BR has one allylic hydrogen, while a 1,4 unit has four allylic hydrogens, with less steric hindrance.

5. Carbon black with increased structure can occlude more rubber. This effectively increases the volume fraction of filler by shielding a portion of the rubber from stress.
6. Two principal intermediates in the reactions leading to oxidative degradation of rubber are hydroperoxides and peroxy radicals. Preventive antioxidants react with the first, and chain-breaking ones with the second.
7. Continuous stress relaxation (CSR) is sensitive only to chain scission, while ISM indicates the net difference between scission and crosslinking. Thus, if CSR and ISM give the same results, the vulcanize must degrade by chain scission only.

3

Elasticity

Alan N. Gent

■ 3.1 Introduction

Rubber consists of long flexible molecules that are in continuous Brownian motion at normal temperatures due to thermal agitation. As a result, the molecules take up a variety of random configurations like a basketful of snakes. When the molecules are straightened out by an applied force and released, they spring back to random shapes as fast as their thermal motion allows. This is the origin of the unique ability of rubber to undergo large elastic deformations and recover completely – rubber molecules are highly flexible and therefore highly extensible, but in the absence of an external force they adopt rather compact, random configurations.

To give rubber a permanent shape, the molecules are tied together by a few chemical bonds, in a process known as “crosslinking” or “vulcanization”. Molecular sequences or strands between sites of interlinking still move about and change their shapes, but they are now subject to the restriction that the crosslinks remain in more or less stationary positions. Before crosslinking, rubber is basically a very viscous, elastic liquid and after crosslinking it is a soft, highly elastic solid. We will discuss quantitative relationships between the structure of a rubber vulcanizate and its elastic properties in Section 3.4.

In this chapter we neglect the effects of internal viscosity and ignore any delay in reaching equilibrium. The response is usually so rapid at normal temperatures that rubbery materials can be treated as simple elastic solids. But at high rates of straining and at low temperatures, the delay in response becomes important. The visco-elastic properties of rubber are described in Chapter 4.

Although rubber has the unique ability to undergo large elastic deformations, in practice many rubber springs are subjected only to relatively small strains, less than about 50% in extension or compression, or 100% in simple shear. An approximation for the corresponding stresses is then given by conventional elastic analysis, assuming simple linear stress-strain relationships because, like all solids, rubber behaves as a linearly-elastic substance at small strains. Thus, we can treat many common rubber design problems knowing only the value of the modulus of elasticity. Several examples are discussed in Section 3.2.

But some features of the behavior of rubber can be understood only in terms of its response to large deformations. We therefore need to know how to characterize the elastic behavior of highly extensible, nonlinearly-elastic materials. A simple modulus of elasticity is no longer sufficient. The theory of large elastic deformations is described in Section 3.3. Some important consequences of permitting the deformations to be large are also described.

Finally, it should be noted that rubber compounds are usually “reinforced” by adding substantial amounts of a particulate filler, usually carbon black. The resulting material is stiffer and stronger than the unfilled material but the stiffness is now rather ill-defined, being reduced by applying a pre-stretch, and recovering to the original state only slowly after release. These features makes predicting the elastic response an uncertain matter, because the stresses depend on the history of deformation and the temperature and time allowed for recovery. Attempts to deal with this complex situation are described in Section 3.2.2.

■ 3.2 Elastic Properties at Small Strains

3.2.1 Elastic Constants

Elastic materials that are isotropic in their undeformed state can be characterized by two fundamental elastic constants. The first deals with their resistance to compression in volume under a hydrostatic pressure. Termed the modulus K of bulk compression, it is defined by a linear relation between the applied pressure P and the consequent shrinkage $-\Delta V$ of the original volume V_0 (Fig. 3.1a).

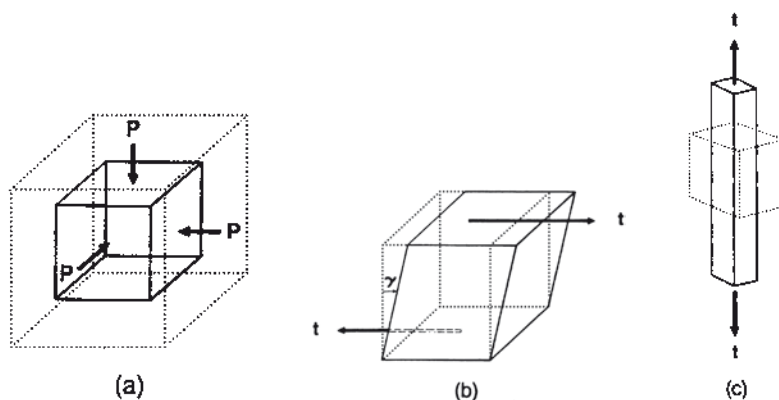


FIGURE 3.1 (a) Bulk compression, (b) simple shear, (c) simple extension

$$P = K \left(\frac{-\Delta V}{V_0} \right) \quad (3.1)$$

The second constant describes the response to a shear stress t (Figure 3.1b). Termed the shear modulus G , it is defined by the relation:

$$G = t / \gamma \quad (3.2)$$

where γ is the amount of shear, defined as the ratio of the lateral displacement d to the height h of the sheared block.

Other commonly-used elastic constants can be derived from these two. The tensile modulus E (Young's modulus of elasticity), defined by the ratio of a simple tensile stress t to the corresponding fractional tensile elongation ε (Figure 3.1c), is given by

$$E = \frac{t}{\varepsilon} = \frac{(9 K G)}{(3 K + G)} \quad (3.3)$$

and Poisson's ratio ν , defined by the ratio of lateral contraction strain ε_w to longitudinal tension strain ε_l for a bar subjected to a simple tensile stress (Figure 3.1c), is given by

$$\nu = \frac{(1/2)(3 K - 2 G)}{(3 K + G)} \quad (3.4)$$

Rubbery solids have high values of bulk compression modulus K , comparable to that of simple liquids, of the order of 1.5–2 GPa (1 GPa = 10^9 N/m²). On the other hand, the shear modulus G is typically rather low, only about 0.5 to 2 MPa, i.e., two to three orders of magnitude smaller than K . Thus, Poisson's ratio ν is close to one-half (typically 0.499) and the tensile modulus E of elasticity is given almost exactly by $3 G$. If we consider rubber to be completely incompressible in bulk – a reasonable approximation for most purposes – then $\nu = 1/2$ and the elastic behavior at small strains can be described by a single elastic constant: G . (Note that when a rubber block is “compressed”, its volume does not decrease significantly unless the pressure is extremely high. Instead, the block bulges laterally and the rubber volume remains virtually unchanged. But accurate measurements of bulging can be used to determine the actual change in volume change and hence the value of Poisson's ratio [1]).

Poisson's ratio ν of lateral to longitudinal strains is only constant at small strains. It becomes a function of the strains themselves when they are no longer small. Hence, at large strains the concept of a single value for the strain ratio is invalid and Poisson's ratio no longer serves a useful function in calculating stress and strain.

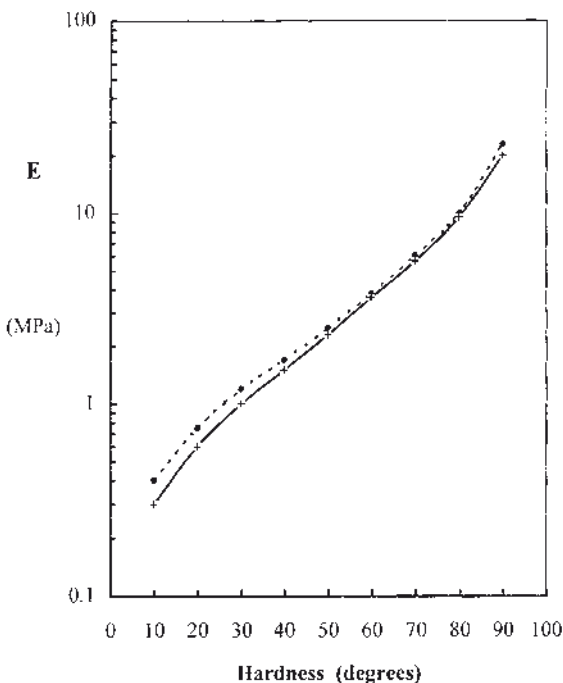


FIGURE 3.2 Relation between indentation hardness and tensile modulus E ;
 full line: International Rubber Hardness,
 broken line: Shore A hardness

A quick estimate of the elastic modulus of rubber is often achieved by indenting a rubber sample with a rigid indenter of prescribed size and shape (a flat-ended cylinder, a truncated cone, or a sphere) under specified loading conditions. Various nonlinear scales are employed to derive a value of “rubber hardness” from such measurements [2, 3]. Hardness values range from zero degrees when the material has no resistance to indentation (modulus is zero) up to 100 hardness degrees when the modulus is infinitely high. Corresponding values of shear modulus G for two common hardness scales: Shore A, using a truncated conical indenter, and the International Rubber Hardness scale (IRHD), using a spherical indenter, are compared in Table 3.1 and Fig. 3.2. The IRHD hardness scale has been chosen so that the results agree quite closely.

Note, however, that rubbery solids show creep and stress relaxation to various extents. The estimated value of E therefore depends on the time under load. It is customary to fix this at a convenient value, for example, 10 s. Soft compounds are typically more elastic and show less creep, so that the estimated value of E is better defined in these cases. However, in general, indentation hardness provides only an approximate estimate of E within an “error” range of about $\pm 10\%$.

TABLE 3.1 Relation Between Indentation Hardness and Elastic (Young) Modulus E

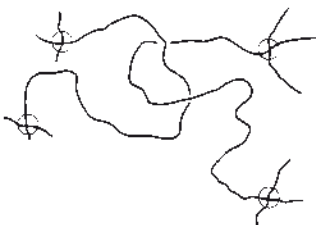
Hardness (Degrees)	E (Shore) (MPa)	E (IRHD) (MPa)
10	0.4	0.3
20	0.7	0.6
30	1.2	1.0
40	1.7	1.5
50	2.5	2.3
60	3.8	3.6
70	6	5.5
80	10	9.5
90	23	20

3.2.2 Relation Between Shear Modulus G and Composition

For an unfilled rubber compound, the shear modulus G is directly related to the molecular structure. A network of elastic strands is created by interlinking the original long molecules, with a density N per unit volume of material (see Section 3.4 below), and the modulus G is predicted to be proportional to N :

$$G = N k T \quad (3.5)$$

where k is Boltzmann's constant and T is absolute temperature. Actually, network strands are formed both by crosslinking and by molecular entanglement (Fig. 3.3). The greater the degree of crosslinking, the greater the elastic modulus becomes, because the number of elastic elements (i.e., portions of molecules between crosslinks) increases in direct proportion to the number of crosslinks. However, even though the original rubber molecules are very long (typically 10,000–50,000 main-chain atoms), there are practical reasons for restricting the degree of crosslinking to a rather narrow range, typically with one crosslink site for every 100 to 1000 main-chain atoms, on average. If there are more crosslinks than this, the molecular strands between crosslink sites are too short to stretch much and the material is rather inextensible and brittle, eventually becoming a hard thermoset resin when the molecules are crosslinked frequently.

**FIGURE 3.3** Sketch of a molecular entanglement

On the other hand, long elastomeric molecules tend to entangle with each other, forming temporary physical crosslinks at a spacing characteristic of the particular molecular structure. This spacing ranges from about 250 main-chain atoms for an ethylene-propylene copolymer (EPR) to about 1000 main-chain atoms for a substituted diene elastomer, such as natural rubber (NR) or a butadiene-styrene copolymer (SBR) [4]. (It appears to depend on the local stiffness of the molecules. Flexible chains entangle more frequently, and vice-versa.). Thus, even if one wished to make a soft, highly-extensible elastic solid by introducing only a few crosslinks per original molecule, the presence of natural entanglements at their characteristic density would cause the number of effective crosslinks to be at least this large, and the elastic modulus would thus be higher than expected. Thus, as a result of the tendency of long linear molecules to entangle with each other, it is not a simple matter to make soft vulcanizates, especially with densely entangled polymers such as EPR and EPDM. One method is to dilute the rubber molecules before crosslinking takes place by adding a substantial amount of a non-volatile compatible liquid (a process known as oil-extension or plasticization). By reducing the packing density of rubber molecules, the number of molecular entanglements per molecule is reduced.

An alternative way to link flexible molecules together is by a physical aggregation of segments from different molecules. For example, in molecules composed of long sequences of incompatible species (e.g., isoprene and styrene), the polystyrene sequences are not compatible with polyisoprene and separate out into polystyrene domains, about 10–30 nm in diameter. Sometimes the domains are formed by sequences of a crystalline polymer (e.g., polyethylene). In all such “thermoplastic” elastomers the domains act like large polyfunctional crosslinks, because long flexible elastomeric sequences are linked together by them [5]. However, the crystalline or plastic domains are held together only by van der Waals forces of attraction, and they yield and flow under high stresses or at high temperatures.

Such materials have marked advantages and equally pronounced disadvantages compared to chemically crosslinked rubber. They can be shaped without chemical reaction, simply by molding at high temperatures when the “rigid” sequences become mobile and take up different arrangements. And they can be re-used by re-molding. On the other hand, the rigid domains do not have the inherent coherence of chemical crosslinks and therefore thermoplastic elastomers tend to yield and flow under high stresses, especially at elevated temperatures.

In practice, rubbery materials are generally formulated to include large amounts, typically about 30% by volume, of particulate fillers, commonly carbon black. This has two effects. First, the material is considerably stiffer than expected from the molecular structure – from 2 to 10 times stiffer, depending on the type and amount of filler added. Second, the material becomes somewhat thixotropic, i.e., the elastic modulus is reduced after straining and the more so, the greater the previous strain [6].

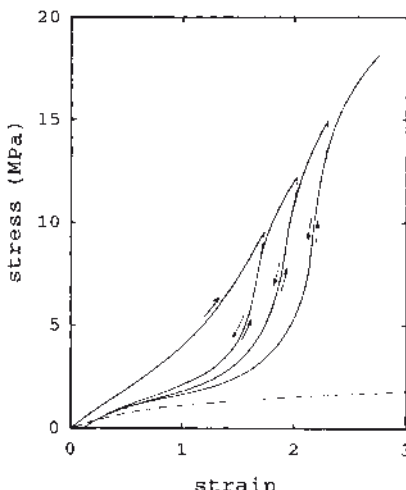


FIGURE 3.4 Stress softening of a relatively highly filled rubber compound (60 parts by weight of HAF carbon black per 100 parts by weight of natural rubber, hardness approx. 75 IRHD)

This phenomenon probably reflects a breakdown of weak bonds between rubber molecules and filler particles, and at very small strains, between filler particles themselves. Typical thixotropic behavior is shown in Fig. 3.4 for a rather highly filled compound. For comparison, the elastic behavior of the corresponding unfilled material is also shown as a broken line.

Thus, filled compounds have a somewhat ill-defined modulus of elasticity. It depends on the degree to which they have been strained previously. For precise use, components are often prestrained to a specified extent, greater than the one likely to be reached in practice, to make their elastic behavior more consistent. This practice is unnecessary for unfilled and lightly filled compounds, because they do not show a significant degree of "stress softening". It should also be noted that the original hard state is slowly recovered, taking months at room temperature and more than one day at 100 °C [7].

Attempts have been made to describe stress-softening in terms of fracture of the rubber molecules, or their detachment from particles of carbon black, to an increasing extent at higher applied loads [8, 9, 10]. In other words, stress-softening is regarded as a cumulative internal fracture process. An alternative view is that stress-softening is due primarily to slow visco-elastic relaxation processes in the neighborhood of filler particles [11]. Although stress-softening is known to be strongly affected by the rate of stretching or the time allowed for relaxation, it is still not known whether this time-dependence is a consequence of the principal mechanism of softening or merely an added complexity. An example of the time-dependence is shown in Fig. 3.5.

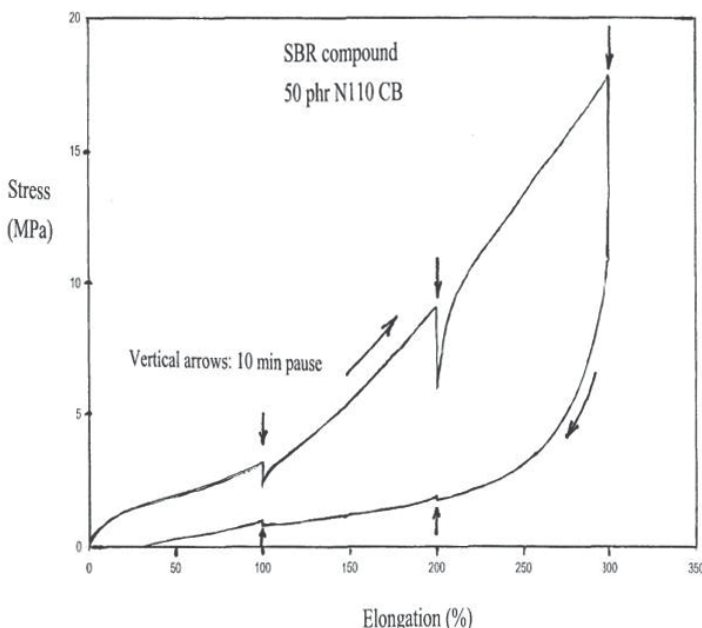


FIGURE 3.5 Stress softening of a carbon-black-filled rubber compound with pauses for 10 minutes of stress relaxation at increments of 100% strain

When stretching was interrupted for 10 minutes at various points on the loading curve, the stress relaxed markedly on each occasion, by about 30%. When stretching was resumed, the stress rose rapidly to the same level as if the original stretching had continued without pause, and then continued to increase on further stretching as if no interruption had taken place. These observations confirm that softening is a strong function of time under load, but they also suggest that the "damage" consists of the replacement of one transitory network by another, formed in the stretched state. Thus, stretching appears to take place by a ratcheting mechanism in which the original carbon black structure rearranges continuously to minimize internal stresses at the current state of strain. It should be noted, however, that little recovery, if any, occurred during retraction.

3.2.3 Stiffness of Components

3.2.3.1 Choice of Shear Modulus

By varying the degree of crosslinking and by dilution with oil, the shear modulus G of practical rubber compounds can be varied over a rather wide range, from about 0.2 to 0.8 MN/m². Stiffening by fillers increases the upper limit to about

2–5 MN/m², but fillers that have a particularly pronounced stiffening action also give rise to stress-softening effects such as those shown in Figs. 3.4 and 3.5, so that the modulus becomes a somewhat uncertain quantity. Nevertheless, the practical advantages obtained by adding a reinforcing filler – notably, improved resistance to abrasion and enhanced strength – are so marked that it is usual to add about 20–30% by volume to the mix formulation. This has important consequences in specifying the stiffness of rubber components. Whereas the modulus of soft rubber, and hence the stiffness of components, can be specified to within about 10%, or even closer, the stiffness of components made from filled, relatively hard rubber compounds ($G \geq 1$ MPa) can be specified only to within about 25%. When a more precise control over the stiffness of a component is required, the compound is usually reinforced with lower amounts of a large-particle carbon black, having a lower stiffening effect, but giving a product with a better defined modulus, i.e., one which is less sensitive to pre-strains.

Approximate values of stiffness for simple rubber springs can be calculated using elementary elasticity theory: see Chapter 8. Many others can be treated using finite element analysis (FEA): see Chapter 9. Some common rubber components are discussed in the following.

3.2.3.2 Shear Deformations of Bonded Blocks and Hollow Cylindrical Tubes

A rubber block under a simple shear stress, as shown in Fig. 3.1b, takes up a simple shear deformation only if certain conditions are met. The height h of the block must be smaller than the length l or the diameter d ; otherwise, the deformation contains a significant extra component due to bending [12]. (Indeed, if the height is much larger – say, more than three times l or d – then the deformation is largely due to stretching [12].) The effective shear modulus G_e , when the height h is comparable to or smaller than l or d , is given for rectangular blocks by

$$G_e = \frac{G}{\left[1 + \left(3 h^2 / l^2\right)\right]} \quad (3.6)$$

or for cylindrical ones by

$$G_e = \frac{G}{\left[1 + \left(4 h^2 / 9 d^2\right)\right]} \quad (3.7)$$

when the height h is not too large relative to l or d : less than say, 3 l or 3 d . And, of course, these results are only valid for small displacements, less than about 25% of h . Stress-strain relations for large shear strains are discussed in Section 3.3.

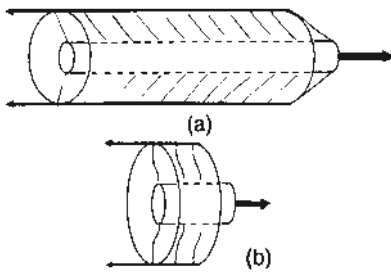


FIGURE 3.6 (a) Long bonded rubber annulus – shear deformation
 (b) Short bonded rubber annulus – bending deformation

The behavior of hollow rubber tubes under small shear deformations is similar to that of rubber blocks. A tube spring consists typically of a rubber tube bonded on its inner and outer curved surface to rigid (usually steel) tubes (Fig. 3.6). The length of the rubber tube is denoted l and the inner and outer radii are denoted a_1 and a_2 . When the length l is long compared to the wall thickness ($a_2 - a_1$), then an axial deformation (Fig. 3.6a) is mainly due to simple shear and the axial stiffness is given by:

$$\frac{F}{d} = \frac{2 \pi G l}{\ln\left(\frac{a_2}{a_1}\right)} \quad (3.8)$$

where d is the axial displacement under an axial force F . When the length l is comparable to, or smaller than, $(a_2 - a_1)$, then the axial stiffness is less than predicted by Eq. (3.8) because, again, a significant additional contribution to the displacement arises from bending. And for thin disks, resembling membranes, the stiffness is smaller still, because the principal mode of axial displacement then becomes stretching [13].

When the outer cylinder is rotated about its axis with respect to the inner cylinder, the rubber tube between them is subjected to a torsional shearing deformation. For small rotations the torque M is related to the rotation angle θ as follows:

$$\frac{M}{\theta} = \frac{4 \pi G l}{(a_1^{-2} - a_2^{-2})} \quad (3.9)$$

When the inner cylinder is displaced in a radial direction towards the outer cylinder, the corresponding stiffness is again an increasing function of the length l and a decreasing function of the rubber thickness ($a_2 - a_1$), as described in [13, 14].

When a solid disk or a rectangular block is subjected to torsion about its axis, the rubber is subjected to non-uniform shear strains. Some relations for the applied torque M as a function of the angle θ of rotation are:

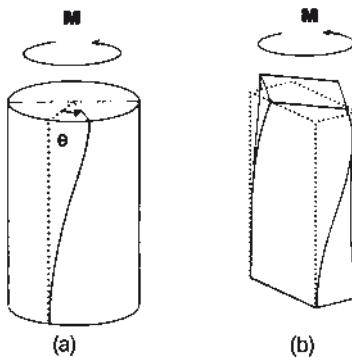


FIGURE 3.7 Torsion of (a) a cylinder and (b) a rectangular bar

(a) Torsion of a cylindrical disk of radius a and length l (Fig. 3.7a):

$$\frac{M}{\theta} = \frac{\pi a^4 G}{2 l} \quad (3.10)$$

(b) Torsion of a thin strip of rectangular cross-section, of width w and thickness t (Fig. 3.7b):

$$\frac{M}{\theta} = \frac{C w t^3 G}{l} \quad (3.11)$$

In Eq. (3.11), C is a constant, given by $[1 - (0.63 \cdot t/w)]/3$ for strips having a thickness t less than about $w/3$ [15].

3.2.3.3 Small Compressions or Extensions of Bonded Blocks

One particularly important deformation will now be discussed: the compression or extension of a thin rubber block, bonded between rigid plates. Consider a cylindrical block of radius a and thickness h (Fig. 3.8) of an incompressible material.

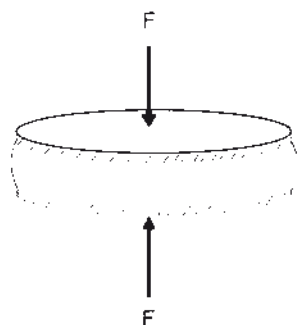


FIGURE 3.8 Compression of a bonded block

The deformation can be considered to take place in two stages: a simple compression or extension strain of amount ε , requiring a uniform compressive or tensile stress $t_1 = 3 G \varepsilon$ (Eq. (3.3)), and a distributed shear deformation that restores points in the planes of the bonded surfaces to their original positions in these planes [16–18]. The corresponding shear stress t_2 acting at the bonded surfaces at a radial distance r from the cylinder axis is given by

$$t_2 = 3 G \left(\frac{r}{h} \right) \varepsilon \quad (3.12)$$

increasing linearly with r . This shear stress is associated with a corresponding normal stress or pressure P , related to the shear stress t_2 by

$$t_2 = \left(\frac{h}{2} \right) \left(\frac{\partial P}{\partial r} \right) \quad (3.13)$$

Upon integrating, P is obtained as a function of the distance r from the center:

$$P = 3 G \varepsilon \left(\frac{a^2}{h^2} \right) \left[1 - \left(\frac{r^2}{a^2} \right) \right] \quad (3.14)$$

These stress distributions are shown schematically in Fig. 3.9. Although they will be incorrect at the edges of the block because the assumption of a simple shear deformation cannot be valid at this singular line, experiments show that they provide satisfactory approximations over the major part of the bonded surfaces [19].

By integrating the normal stresses ($P + t_1$) acting over the bonded surface, the total compressive force F is obtained as:

$$F = 3 \pi a^2 G \varepsilon \left[1 + \left(\frac{a^2}{2 h^2} \right) \right] \quad (3.15)$$

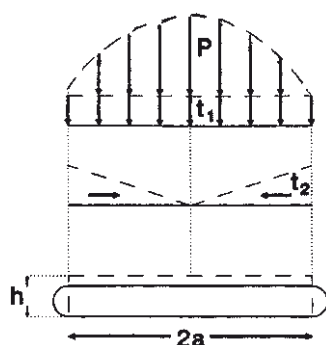


FIGURE 3.9 Stress distributions for a bonded block in compression

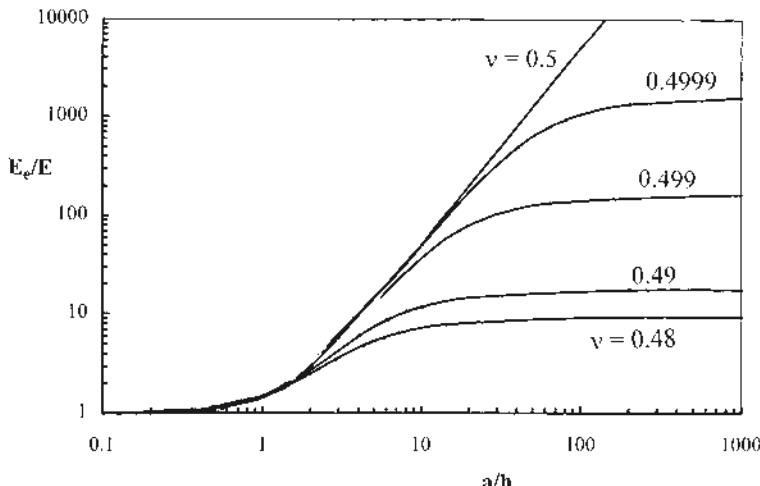


FIGURE 3.10 Effective modulus E_e of a bonded rubber disk, radius a and thickness h , for various values of Poisson's ratio ν

Equation (3.15) shows that the effect of constraints at the bonded surfaces is to increase the effective compression modulus from E ($= 3G$) by a factor of $[1 + (a^2/2 h^2)]$. Thus, for thin blocks of large radius, when a is much greater than h , the effective value of Young's modulus E_e is much larger than the real value (Fig. 3.10). However, for values of the aspect ratio a/h close to unity, the assumption that horizontal planes remain plane becomes inappropriate, and both theory and experiment indicate that the last term in Eq. (3.15), $[1 + (a^2/2 h^2)]$, should be replaced by $[1.2 + (a^2/2 h^2)]$ [21, 22]. This change has little effect when the aspect ratio a/h is large and the second term is dominant, and it is clearly incorrect when a/h is small because the leading constant is necessarily unity then. But for blocks with diameters or widths comparable to their thickness, it should be employed in place of Eq. (3.15).

When the ratio a/h is greater than about 5, the effective modulus E_e becomes so large that it is comparable in magnitude to the modulus K of bulk compression. A significant contribution to the observed displacement then comes from volume compression or dilation. The general solution, taking bulk compression into account, yields the pressure distribution [18]:

$$\frac{P}{K \varepsilon} = 1 - \left[\frac{I_0(\alpha r)}{I_0(\alpha a)} \right] \quad (3.16)$$

in place of Eq. (3.14), where $\alpha = (12 G/K h^2)^{1/2}$ and $I_0(x)$ denotes the zeroth order Bessel function of x . The corresponding contribution F_2 to the compressive force F is obtained by integrating this function over the block cross-section, yielding

$$\frac{F_2}{\pi a^2 K \epsilon} = \frac{I_2(\alpha a)}{I_0(\alpha a)} \quad (3.17)$$

where $I_2(x)$ denotes the second-order Bessel function of x . When the term αa is small, this equation reduces to:

$$F_2 = 3 \pi a^2 G \epsilon \left(\frac{a^2}{2 h^2} \right) \quad (3.18)$$

in agreement with Eq. (3.15). But for thin disks, even quite small departures of Poisson's ratio ν from a value of 1/2, corresponding to finite instead of infinitely large values of ratio of the modulus K of bulk compression relative to the shear modulus G (Eq. (3.4)), lead to markedly lower values of the effective modulus, as shown in Fig. 3.10.

When the disk has a central hole in it, so that the pressure there is zero, the effective modulus is much reduced in comparison with that for a solid disk [18, 20]. The result for a completely incompressible material is:

$$\frac{E_e}{E} = \frac{1 + \left[(a_2^2 + a_1^2) - (a_2^2 - a_1^2) / \ln(a_2/a_1) \right]}{2 h^2} \quad (3.19)$$

where a_1, a_2 are the inner and outer radii of the disk. Note that when the inner radius is one-tenth of the outer radius, the effective modulus is reduced to only 58% of that for a solid disk of the same external radius. Even when the inner radius is extremely small, only 1% of the external radius, the effective modulus is reduced to about 78% of that for an equivalent solid disk.

3.2.3.4 Compression of Blocks Between Frictional Surfaces

When a rubber block is compressed between two rigid surfaces having a finite coefficient of friction, the block will slip outwards towards the edges. However, a central region does not slip because the pressure there is large enough to prevent it [23, 24]. Values of the radius r_1 of the central non-slip zone are shown in Fig. 3.11 for a block of circular cross-section. They are plotted as a function of the coefficient of friction μ and the block aspect ratio a/h (the ratio of block radius a to thickness h). It is interesting to note that the size of the non-slip zone is independent of the applied load, and also that some slipping occurs even when the coefficient of friction is quite high. One consequence of slipping at the interfaces is that the compression stiffness of the block is reduced markedly in comparison with that for a similar bonded block. The apparent compression modulus E_a is compared to that for a corresponding bonded block in Fig. 3.12 for various values of the block aspect ratio and friction coefficient μ .

Another consequence of interfacial slipping is that mechanical work is expended against friction, both as the compressive load is applied and again as it is removed. For blocks of high aspect ratio compressed between surfaces with a low friction coefficient, the dissipated energy can amount to a large fraction of the input energy, as high as 50% [24].

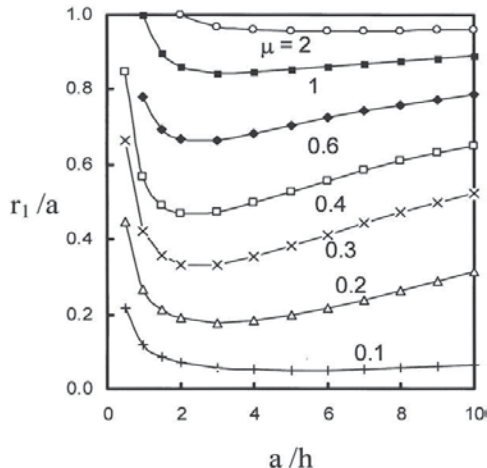


FIGURE 3.11 Radius r_1 of the central non-slip zone for cylindrical blocks as a function of the aspect ratio a/h of block radius to thickness and for various values of the coefficient of friction μ .

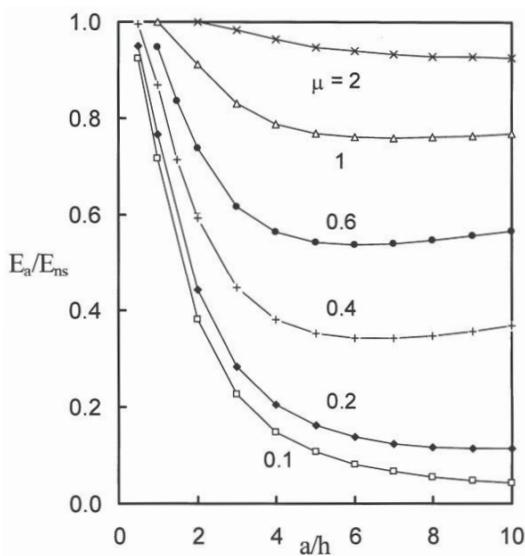


FIGURE 3.12 Apparent compression modulus E_a relative to that for a bonded block as a function of the aspect ratio a/h of block radius to thickness and for various values of the coefficient of friction μ .

3.2.3.5 Maximum Allowable Loads in Tension and Compression

Estimates can be made of the maximum permitted loads in tension and compression, even though the average strain is assumed to be small. In tension, for example, a specific mode of fracture occurs when the local hydrostatic tension (negative pressure) reaches a relatively small critical value, of only about $2.5 G$. At this point, any small cavity that might exist in the central region of the block is predicted to expand greatly in size. In fact, the amount of expansion is predicted by the theory of *large* elastic deformations (see Section 3.3.4, Eq. (3.73)) to become indefinitely large at this value of negative pressure [25], which corresponds to a critical value of the applied tensile stress, obtained by substituting $P = 2.5 G$ in Eq. (3.14), of about $1.25 G$. Large internal cracks and tears are found to develop suddenly in the interior of bonded rubber blocks at well-defined tensile loads that agree with this prediction [25] and also when gases are dissolved in rubber at this pressure and the external pressure is suddenly released [26]. In particular the critical loads and pressures are found to increase in proportion to the elastic modulus for rubber compounds of different hardness, in support of the proposed mechanism of fracture as a consequence of an elastic instability. Rubber apparently contains microscopic cavities that expand in reasonable accordance with Eq. (3.73) and tear open to form large internal cracks. Thus, to avoid internal fractures of this kind, the mean tensile stress in thin bonded blocks or the pressure differential in blocks of any size, must not exceed about $1 G$. In compression, on the other hand, quite large stresses can be applied. A conservative estimate of the maximum permitted stress can be obtained by assuming that the maximum shear stress, developed in the neighborhood of the bonded edges, should not exceed G (i.e., that the maximum shear deformation should not exceed about 100%). This yields a value for the allowable overall compressive strain of $h/3 a$, corresponding to a mean compressive stress of the order of $3 G$ for disks with values of the ratio a/h between about 3 and 10. However, this calculation assumes that the approximate stress analysis outlined earlier is valid right at the edges of the block, and this is certainly incorrect. Indeed, local stresses in these regions will depend strongly on the detailed shape of the free surface in the neighborhood of an edge. They can be minimized by shaping the rubber surface near the edges as sketched in Fig. 3.13a. Moreover, failure is governed by a “critical strain energy release rate” (see Chapters 5 and 6), not by a simple maximum-strain criterion, so that a rather detailed calculation is necessary to find out what mean compressive stress can be tolerated.

As a first approximation, we could assume that a bonded block can support a strain energy density in critical regions of the same general magnitude that could be imposed many times on a homogeneously deformed specimen in simple tension. For a typical soft rubber vulcanizate, this value is about 10 MJ/m^3 (see Chapters 5 and 6). The corresponding value of maximum shear strain is about 170%, equiva-

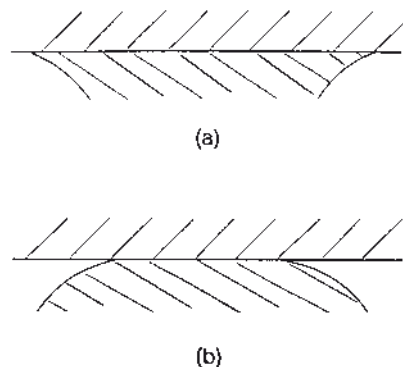


FIGURE 3.13 Good (a) and bad (b) designs of the free surface near a bonded interface.

lent to an allowable mean compressive stress of the order of $5 G$, for the same wide range of ratio a/h as before. And this is still a rather conservative estimate, because growth of a crack that starts near a bonded edge will quickly take it into a less severely strained region [27].

3.2.3.6 Indentation of Rubber Blocks by Rigid Indentors

Classical results for indentation of an elastic block assume that the block is much thicker than a characteristic dimension of the indentor (e.g., the radius of a spherical indentor) and much thicker than the amount of indentation. With these limitations in mind, the following relations hold between indenting force F and amount of displacement d of the rubber surface under the indentor:

(a) For a flat-ended cylindrical punch, of radius a (Figure 3.14) [24],

$$F = 8 G a d \quad (3.20)$$

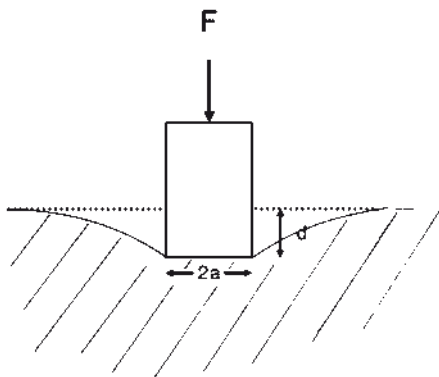


FIGURE 3.14 Cross-sectional view of indentation by a flat ended punch or a long narrow indentor

(b) For a spherical indentor, of radius a [24],

$$F = \left(\frac{16}{3} \right) G a^{1/2} d^{3/2} \quad (3.21)$$

(c) For a conical indentor with a semi-angle of θ [25]:

$$F = \left(\frac{8}{\pi} \right) G d^2 \tan \theta \quad (3.22)$$

In each of these relations the rubber is assumed to be completely incompressible. [For compressible materials the right-hand sides are divided by the factor: $2 (1 - \nu)$.]

Relations for the amount of indentation produced by long, narrow, rigid indentors are more complex. For a given applied load F' per unit length of indentor the amount d of indentation is found to increase logarithmically with the width or thickness of the rubber block, because the block is no longer much larger than the dimensions of the indentor. For example, the indentation d caused by a long, flat-ended indentor of width w pressed into a thick block with a width W smaller than the block thickness but larger than the width w of the indentor ($W = n w$, say) is given by [28]:

$$\frac{F'}{d} = \frac{2 \pi G}{\ln(2n)} \quad (3.23)$$

for $n \gg 1$, where d is measured with respect to the edge of the block. Thus, if the block width W is $100 w$, where w is the width of the indentor, then the indentation referred to the block edges is about 77% greater than for a block with a width of only $10 w$. A similar relation holds between the amount of indentation d and block thickness $T (= n w)$ for blocks with a thickness T smaller than their width W . In this case d is measured with respect to the base of the block. Note that d continues to increase with block thickness, even when the ratio n of thickness to indentor width w is already quite large.

Another approximate relation for the applied force F' per unit length of the indentor that produces an indentation d in a block of thickness T is [29]

$$\frac{F'}{G d} = \frac{1.79}{1 - \exp\left(-0.24 \frac{T}{w}\right)} \quad (3.24)$$

This relation holds reasonably well for a wide range of values of w/T , from about 0.02 to 2.

If the rubber block is compressed laterally while being indented, the amount of indentation is increased markedly, in fact it becomes infinitely large at a critical amount of compression [29, 30]. For equi-biaxial compression, the critical value is 33% and for simple compression it is 55%. Although these compression strains are relatively large and unlikely to arise in practice, smaller compressions can greatly reduce the resistance to indentation.

3.2.3.7 Compression of O-rings

The compression of o-rings is quite complicated to analyze even assuming linear elastic behavior for rubber. Approximate relations have been obtained by considering the o-ring as an elastic cylinder, compressed between rigid plates [31]. The amount d of compression relative to the radius a of the cross-section is obtained as:

$$\frac{d}{a} = \frac{1}{2} \left(\frac{b}{a} \right)^2 \left[\ln \left(\frac{b}{a} \right) - 0.874 \right] \quad (3.25)$$

where b denotes the half-width of the contact patch (Eq. (3.25) is Equation (13) of [31], with Poisson's ratio given the value 0.5 for an incompressible solid). The half-width b is obtained in terms of the applied load P' per unit length of the o-ring (Equation (10) of [31]) as:

$$b^2 = \frac{P' a}{\pi G} \quad (3.26)$$

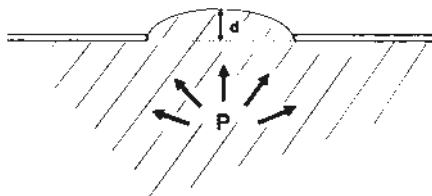
A relation is also given (Eq. (18)) for the outwards bulging d_2 of the O-ring on compression, increasing the original diameter $2a$ to a width of $2(a + d_2)$, where d_2 is given by:

$$d_2 = \frac{a b^2}{2} \quad (3.27)$$

Experiments were in satisfactory agreement with these relations for small compressions up to about 15% [31].

3.2.3.8 Protrusion of Rubber Through a Hole or Slit

When a rubber block is pressurized inside a rigid container with a small hole in one wall (Fig. 3.15), the rubber will bulge out through the hole. For small protrusions the height d of the bulge is proportional to the internal pressure P , in accord with the following equations:

**FIGURE 3.15** Protrusion through an aperture

(a) For a circular hole of radius a [32]:

$$P = \frac{\pi G d}{a} \quad (3.28)$$

(b) For a long narrow slit of width w [33]:

$$P = \frac{4 G d}{w} \quad (3.29)$$

It is interesting to note that in the latter case an explicit relation is obtained for d , even though the slit is assumed to be long.

■ 3.3 Large Deformations

3.3.1 General Theory of Large Elastic Deformations

A general treatment of the stress-strain relations of rubberlike solids was developed by Rivlin [34], assuming only that the material is isotropic in elastic behavior in the unstrained state and incompressible in bulk. It is quite surprising to note what far-reaching conclusions follow from these elementary propositions, which make no reference to molecular structure. Symmetry considerations suggest that appropriate measures of strain, independent of the choice of axes, are given by three strain invariants, defined as follows:

$$\begin{aligned} J_1 &= \lambda_1^2 + \lambda_2^2 + \lambda_3^2 - 3 \\ J_2 &= \lambda_1^2 \lambda_2^2 + \lambda_2^2 \lambda_3^2 + \lambda_3^2 \lambda_1^2 - 3 \\ J_3 &= \lambda_1^2 \lambda_2^2 \lambda_3^2 - 1 \end{aligned} \quad (3.30)$$

chosen so that they become zero in the unstrained state when $\lambda_1 = \lambda_2 = \lambda_3 = 1$. Moreover, for an incompressible material J_3 is identically zero; hence only two independent measures of strain, namely J_1 and J_2 remain. It follows that the strain

energy density W (i.e., the amount of energy stored elastically in unit volume of material under the state of strain specified by $\lambda_1, \lambda_2, \lambda_3$) is a function of J_1 and J_2 only:

$$W = W(J_1, J_2) \quad (3.31)$$

Because stresses are given directly by the derivatives of W with respect to strain, W is a kernel function that contains the stress-strain relations for any type of deformation. Several of these relations are described in later sections. In this section we consider what possible forms the strain energy function W can take.

For example, when the function for W is expanded as a power series in terms of J_1 and J_2 (which are of second order in the strains e_1, e_2, e_3), the strain energy function at sufficiently small strains must take the form

$$W = C_1 J_1 + C_2 J_2 \quad (3.32)$$

where C_1 and C_2 are constants. This particular strain energy function was originally proposed by Mooney [35] and is often called the Mooney-Rivlin equation. It is noteworthy that the C_1 term corresponds to the relation obtained from a molecular theory of rubber elasticity; see Section 3.4 below.

Because J_1 and J_2 contain all terms in e^2 and e^3 , Eq. (3.32) is valid for a greater range of strains than classical small-strain elasticity theory, which neglects terms of higher order than e^2 . However, strains of more than about 25% give rise to fourth-order terms that are not much smaller than third-order terms and therefore cannot be neglected. Thus, although Eq. (3.32) must hold good for small strains, it does not necessarily apply to strains of a size that are commonly encountered. In fact, it is found to hold only for a limited range of strains, much less than unity [36–38], and additional terms in the power-series expansion are needed at larger strains, with a corresponding increase in the number of coefficients, in order to describe stress-strain relations adequately. For example, to include all terms of order J^2 (i.e., all terms of order e^4) it would be necessary to include nine terms in the relation for W for a compressible elastic solid, reducing to five terms for an incompressible elastic solid [39]. Thus, merely to include all terms of order e^4 in the strain energy function for rubber would require five elastic coefficients. Because it is difficult in practice to determine the values of more than two or three elastic coefficients with any accuracy, a power-series expansion for W using more than two or three terms has not been widely employed.

Instead, as described later, it is found that good agreement with experiment is obtained using a simple two-coefficient form for W [40];

$$W = C_1 J_1 + K_2 \ln\left(\frac{J_2 + 3}{3}\right) \quad (3.33)$$

This reduces to the Mooney-Rivlin form at low strains but the second term is now a decreasing function of strain.

3.3.2 Forms for W Valid at Large Strains

Rubber shows strain-hardening at large strains because the long flexible molecules have a finite length and cannot be stretched indefinitely. The strain energy functions considered up to now do not possess this feature and thus fail to describe stress-strain behavior at large strains. Strain-hardening can be introduced by a simple modification to the first term in Eq. (3.33), incorporating a maximum possible value for the strain measure J_1 , denoted J_m

$$J_m = \left(\lambda_1^2 + \lambda_2^2 + \lambda_3^2 - 3 \right)_{\max} \quad (3.34)$$

Equation (3.33) then becomes:

$$W = -C_1 J_m \ln \left(1 - \frac{J_1}{J_m} \right) + K_2 \ln \left(\frac{J_2 + 3}{3} \right) \quad (3.35)$$

Equation (3.35) reduces to Eq. (3.33) when the strains are small and the ratio J_1/J_m is small. It is thus probably the simplest strain energy function that accounts for the elastic behavior to good approximation over the whole range of strains, because it requires only three fitting parameters, C_1 , J_m and K_2 . The first is given by one-half of the small-strain shear modulus G . The second parameter, J_m , is also expected to be a function of G , because for a network of long flexible strands J_m is approximately proportional to λ_m^2 , where λ_m is the maximum stretch ratio of an average strand, and λ_m^2 is inversely proportional to the number N of strands in unit volume and hence to G [36]. Thus, J_m is expected to be inversely proportional to G and to the elastic coefficient C_1 .

Although there is some uncertainty about the physical origin of the third term, the magnitude of the coefficient K_2 is found to be rather independent of the length and number of molecular strands comprising the network, whereas it decreases as the rubber is swollen by a compatible liquid, becoming negligibly small at a volume ratio of rubber of about 25%. These and other features suggest that it is associated with the presence of molecular entanglements within the crosslinked network, as discussed in Section 3.5.3.

Because rubber is highly extensible, the maximum strain ratio λ_m is large, of order 10, and thus J_m is generally a large number, between 50 and 100. The actual value can be employed to relate the maximum extension in one type of strain, for example,

simple extension, to that in another, say equibiaxial extension. In the first case, $J_m = \lambda_1^2 + (2/\lambda_1^2)$ and in the second case $J_m = 2\lambda_2^2 + (1/\lambda_2^4)$, where λ_1 and λ_2 are the major extension ratios in each case. For the value of J_m to be the same in both cases, the corresponding strain ratios at large strains must differ by a factor of about $\sqrt{2}$. The measured breaking strain in biaxial stretching is found to be about 70% of that in uniaxial stretching, in accord with this prediction [41]. Thus, the strain measure J_m appears to be a universal limiting condition for different states of strain.

3.3.3 Stress-Strain Relations in Selected Cases

Stress-strain relations are obtained from the strain-energy function by virtual work considerations: $\partial W = (t_1 / \lambda_1) (\partial W / \partial \lambda_1) \partial \lambda_1 + (\text{corresponding terms in } \lambda_2, \lambda_3)$. They take the form:

$$t_1 = 2 \left[\lambda_1^2 \left(\frac{\partial W}{\partial J_1} \right) - \left(\frac{1}{\lambda_1^2} \right) \left(\frac{\partial W}{\partial J_2} \right) \right] + p \quad (3.36)$$

with similar relations for t_2 and t_3 . The quantity p denotes an unspecified pressure, reflecting the fact that rubber is incompressible and is therefore insensitive to pressure. In any particular case the value of p must be decided by choosing the reference state of stress, as described below. We now examine some simple types of deformation using Eq. (3.36).

3.3.3.1 Simple Extension

A simple extension is defined by strain ratios: $\lambda_1 = \lambda$; $\lambda_2 = \lambda_3 = \lambda^{-1/2}$ (Fig. 3.16). This deformation satisfies the incompressibility condition that the volume remains unchanged on deformation and hence $\lambda_1 \lambda_2 \lambda_3 = 1$. A possible choice of a reference state of stress is to make the sides of the block stress-free, i.e., no stresses are applied in the 2- and 3- directions. Then $t_2 = t_3 = 0$ and Eq. (3.36) for stresses t_2 and t_3 becomes an equation for the unknown pressure p :

$$p = \left\{ -2 \left[\lambda^{-1} \left(\frac{\partial W}{\partial J_1} \right) - \lambda \left(\frac{\partial W}{\partial J_2} \right) \right] \right\} \quad (3.37)$$

Note that p does not represent the actual pressure acting on the chosen surfaces. For a homogeneous deformation, those are the stresses t_1 , t_2 and t_3 . Instead, p is a function that establishes the desired boundary condition; in this case, that $t_2 = t_3 = 0$. When the resulting value for p is inserted in Eq. (3.36) the relation obtained for t_1 ($= t$), is

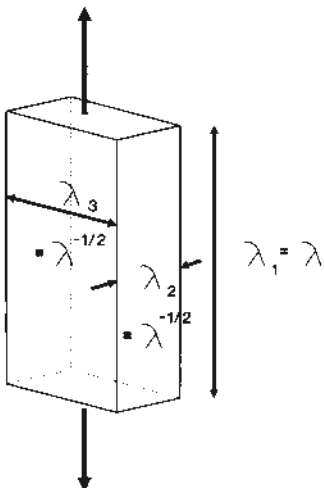


FIGURE 3.16 Principal extension ratios in simple extension

$$t = 2 \left[\left(\frac{\partial W}{\partial J_1} \right) + \lambda^{-1} \left(\frac{\partial W}{\partial J_2} \right) \right] (\lambda^2 - \lambda^{-1}) \quad (3.38)$$

In Eq. (3.38) and elsewhere, the stress t denotes the force acting on a unit of area, where the area is measured in the deformed state. Unfortunately, it has become common practice in the rubber industry to use the word *stress* to denote the force f acting on a unit of *undeformed* cross-sectional area, because this is a more easily measured quantity. To distinguish between these two usages, f is sometimes termed *engineering stress*. For an incompressible material, like most rubbery solids, the imposition of a stretch ratio λ leads to a contraction in cross-sectional area by a factor $1/\lambda$ and thus there is a simple relation between the two measures of stress:

$$f = \frac{t}{\lambda} \quad (3.39)$$

Equation (3.38) is the large-deformation equivalent of the simple result: $t = E e$, applicable at small strains. It gives the stress-strain relation in tension in terms of two properties of the material, $(\partial W/\partial J_1)$ and $(\partial W/\partial J_2)$, denoted hereafter as W_1 and W_2 , that are equivalent, in a way, to elastic moduli. But they are not *constants*, in general; they are derivatives of the strain energy function W evaluated for the particular deformation state under consideration. For example, from Eq. (3.35)

$$W_1 = \frac{C_1}{1 - \frac{J_1}{J_m}}; \quad W_2 = \frac{K_1}{J_2 - 3} \quad (3.40)$$

where an extension strain of λ corresponds to values of $J_1 = \lambda^2 + (2/\lambda) - 3$ and $J_2 = 2\lambda + (1/\lambda^2) - 3$.

3.3.3.2 Equibiaxial Stretching

A relation for equibiaxial tension can be obtained directly from the relations for simple extension. The extension ratios are now denoted $\lambda_2 = \lambda_3 = \lambda$; $\lambda_1 = 1/\lambda^2$ (Fig. 3.17). Also, the stress t_1 is equated to zero because no stresses are usually applied to the major surfaces of the sheet. They are therefore stress-free. Hence the reference pressure p in Eq. (3.36) becomes

$$p = -2(\lambda^{-4} W_1 - \lambda^4 W_2) \quad (3.41)$$

The stresses t_2 and t_3 are then obtained as:

$$t_2 = t_3 = 2(W_1 + \lambda^2 W_2)(\lambda^2 - \lambda^{-4}) \quad (3.42)$$

Note that, again, a highly nonlinear relation is obtained between stress and strain.

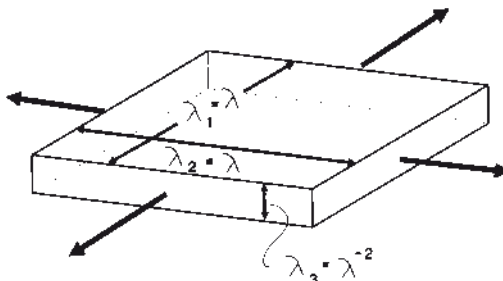


FIGURE 3.17 Principal extension ratios in equibiaxial extension

3.3.3.3 Constrained Tension (Pure Shear)

Another simple deformation state is described as “constrained tension” or “pure shear”, illustrated in Fig. 3.18. It is defined as a tension applied in the 1-direction with the condition that the width in the 2-direction is prevented from altering; i.e., $\lambda_2 = 1$. This is the reason for the term “shear”: a shear deformation is defined as one in which a line parallel to one of the principal axes undergoes no change in length. The term “pure” means that principal axes do not rotate during the deformation. A convenient experimental arrangement is shown in Fig. 3.18. The height h of the specimen in a vertical direction, denoted 1, is chosen to be much smaller than the horizontal width w in the 2-direction, less than one-tenth of w . Then the long horizontal clamps prevent the sample from contracting laterally as it is stretched vertically, except for small, insignificant portions right at the edges, so that $\lambda_2 = 1$.

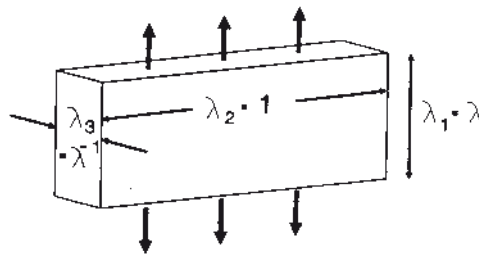


FIGURE 3.18 Constrained tension (pure shear)

Thus, under this deformation, $\lambda_1 = \lambda$, $\lambda_2 = 1$, and $\lambda_3 = 1/\lambda$, while the tension $t_3 = 0$. (Note that the tension t_2 is not zero, it is supplied by the rigid clamps.) From Eq. (3.36), the reference pressure p is obtained as:

$$p = -2(\lambda^{-2} W_1 - \lambda^2 W_2) \quad (3.43)$$

Hence, the tension $t_1 (= t)$ in the stretching direction is

$$t = 2(W_1 + W_2)(\lambda^2 - \lambda^{-2}) \quad (3.44)$$

and the lateral stress t_2 is

$$t_2 = 2(W_1 + \lambda^2 W_2)(1 - \lambda^{-2}) \quad (3.45)$$

In terms of the applied tensile force per unit of unstrained cross-sectional area, Eq. (3.44) becomes

$$f = 2(W_1 + W_2)(\lambda - \lambda^{-3}) \quad (3.46)$$

We note that the stress-strain relation in constrained tension is again a highly nonlinear function of strain and that it involves a combination of the derivatives W_1 and W_2 , somewhat different from that in simple extension, Eq. (3.38). Indeed, by comparing measurements under different types of strain the functions W_1 and W_2 can be evaluated as functions of the strain invariants J_1 and J_2 , and the complete strain energy function can be determined. It is then possible to predict the elastic behavior under any strain, however complex.

3.3.4 Determining the Strain Energy Function W

In order to determine the derivatives of the strain energy function W we need to make measurements of stress-strain relations under different types of strain. Some have already been analyzed; others are analyzed in following sections. Some are particularly suitable for elucidating W because the stress-strain relations depend on only one of the derivatives, which can therefore be determined with greater accuracy [36, 37].

A wide variety of experiments have been carried out using simple natural rubber vulcanizates. They show that W_1 is approximately constant and that W_2 decreases with the amount of strain, primarily as a function of the strain measure J_2 [37]. This variation may be described to a good approximation by the simple empirical relation given previously, Eq. (3.33) [40].

Considerable success has also been achieved in fitting the observed elastic behavior of rubber by strain energy functions that are formulated directly in terms of the extension ratios $\lambda_1, \lambda_2, \lambda_3$ instead of in terms of the strain invariants J_1, J_2, J_3 [42, 43]. Although experimental results can be described economically and accurately in this way, the functions employed are empirical and the numerical parameters used as fitting constants do not appear to have any direct physical significance in terms of the molecular structure of the material. On the other hand, as discussed later, a molecular elasticity theory predicts the first term (W_1) successfully, and the W_2 term has also been correlated with features of the molecular network. In addition, representation in terms of J_1 and J_2 is somewhat simpler mathematically when the deformation involves rotation of the principal axes, for example, in shear and torsion.

If we consider only rather small strains, where rubber must obey the Mooney-Rivlin relation (Eq. (3.32)), then both W_1 and W_2 are constants ($C_1 = K_1$ and $C_2 = K_2/3$) and the relation between “engineering” stress f and strain in simple extension becomes:

$$f = 2 \left(C_1 + C_2 \lambda^{-1} \right) \left(\lambda - \lambda^{-2} \right) \quad (3.47)$$

By expanding in terms of the strain $e (= \lambda - 1)$ and taking e to be small, the ratio f/e at infinitesimally small strains (i.e., the value of the tensile modulus E) is found to be 6 ($C_1 + C_2$) or equivalently $6 C_1 + 2 K_2$. Correspondingly, the shear modulus G is given by

$$G = 2 \left(C_1 + C_2 \right) = 2 \left(K_1 + \frac{K_2}{3} \right) \quad (3.48)$$

Although the Mooney-Rivlin relation, Eq. (3.32), is necessarily valid at small strains, considerable confusion has arisen from its application at somewhat larger strains.

Experimental results in simple extension are in reasonable agreement with this relation because the derivative W_2 happens to decrease with strain in a particular way. This has led to identifying the constants C_1 and C_2 , erroneously, as the derivatives W_1 and W_2 of the strain energy function. Measurements using other types of strain quickly reveal that W_2 is not constant and that Eq. (3.32) does not apply at large strains [36–38]. The real derivatives of the strain energy function for rubber depend on strain as described previously.

In setting up useful approximate representations of the elastic behavior of rubber, one simplification is to ignore terms in J_2 and retain only terms in J_1 , on the grounds that, experimentally, the W_2 term is found to be generally smaller than the W_1 term, ranging from 1/4 to 1/10 of W_1 . (It should be noted, however, that for some types of strain (for example, in equibiaxial stretching) the value of J_2 is much larger than the value of J_1 . Neglecting terms in J_2 might then lead to significant errors.)

If the W_2 term in the strain energy function is ignored, then a simple series expansion for W can be formulated in terms of the strains, based on molecular theory, and employing only two physical constants: the number N of network strands per unit volume, and their contour length L [36, 44, 45]. When enough terms are taken the result is valid over the entire strain range up to the maximum extensibility of the rubber molecules. An approximately-equivalent representation in closed form is obtained from Eq. (3.35):

$$W = -\left(\frac{E J_m}{6}\right) \ln \left[1 - \left(\frac{J_1}{J_m} \right) \right] \quad (3.49)$$

where E is the small-strain tensile modulus, and J_m is the maximum value of J_1 that the molecular network can attain [46].

Equation (3.49) has several desirable features. It involves only two numerical coefficients, both of which have a clear physical significance. At small strains it reduces to the Neo-Hookean form for W predicted by simple molecular theory (see Section 3.5):

$$W = \left(\frac{E}{6}\right) J_1 \quad (3.50)$$

At the other extreme, the stress rises sharply at high strains as the strain invariant J_1 approaches the maximum value J_m , reflecting the fact that rubber molecules have a finite extensibility. Also, it yields simple relations between stress and strain.

Other forms for the strain energy function that use only J_1 have been proposed specifically for use with filled rubber vulcanizates. They are discussed in the following section.

To what degree do the various strain energy functions describe the observed elastic behavior of simple unfilled rubber vulcanizates? Considering that even the most

elastic rubbery material is not perfectly elastic but shows a difference between the extension and retraction stress-strain curves of at least 3%, it is remarkable that a strain energy function of the form of Eq. (3.33) accounts for observed stresses within about 5% for a variety of strains and over a rather large range, up to an extension of about 300%, for example. The coefficients C_1 and K_2 are found to be similar in magnitude, about 1 MPa. Moreover, C_1 is directly related to the structure of the molecular network, increasing with the number of crosslinks introduced by vulcanization, whereas K_2 appears to be rather independent of the degree of crosslinking. Instead, there are indications that it is related to the degree of molecular entanglement.

3.3.4.1 Elastic Behavior of Filled Rubber Vulcanizates

Rubber vulcanizates containing large amounts of a reinforcing filler (usually carbon black or silica) are considerably stiffer than the corresponding unfilled material but they show pronounced softening after prior straining, and soften to a greater degree the larger the previously imposed strain, Fig. 3.4. This feature is termed stress-softening or Mullins softening. It was studied in some detail by Mullins [6] and Mullins and Tobin [47]. They noticed that the softened material followed a stress-strain relation in tension like that for the corresponding unfilled material but with the strain axis condensed. They pointed out that a mechanical model of two phases in series, one hard and relatively inextensible, and one resembling a soft unfilled vulcanize, would behave in the same way. They therefore suggested that a soft phase is created by a stress-induced transformation of the original hard filled rubber vulcanize, possibly by detaching rubber molecules from carbon particles. As the imposed stress increases, the fraction α of soft material is increased and the fraction $(1 - \alpha)$ of hard material simultaneously decreases. Thus, after any given pre-stress, and corresponding degree of softening α , the material follows a stress-strain relation like that for an unfilled vulcanize with the strain axis magnified by a factor $1/\alpha$. (The strain of the soft phase is, of course, greater than the applied strain because it occupies only a fraction α of the sample length.) After the stress reaches the pre-stress value, then more softening occurs and the value of α increases. It was found that α increases more or less in proportion to the applied strain, reaching values of 50% or more after stretching to high strains.

Little experimental work has been done on elastic behavior in other modes of deformation. Charrier and Gent showed that prior extension in one direction did not cause appreciable softening for stretching at right angles [48]. Thus, filled rubber appears to develop anisotropic elastic properties after stretching in one direction. Use of a strain energy function is probably not helpful for anisotropic solids because there are no longer measures of strain corresponding to J_1 and J_2 that are independent of the choice of axes. Nevertheless, a number of empirical relations have been proposed to describe the stress-strain relations of filled rubber vulcanizates. Some

of those that employ a strain energy formalism are discussed here. It is believed that they were applied to experimental stress-strain relations after the material had been softened by a previous stretch. Because the stresses corresponding to J_2 are even less important for filled materials, they are expressed as functions of J_1 only. Othman and Gregory [49] showed that stress-strain relations in tension, compression and shear could be described by a simple relation in terms of J_1 . They proposed stress-strain relations of the form:

$$H \text{ or } G = A + (B J_1^{1/2} + C)^{-1} \quad (3.51)$$

where H and G denote effective “moduli” in simple extension and simple shear, defined by

$$H = \frac{t}{\lambda^2 - \lambda^{-1}} \quad (3.52)$$

where t is the tensile stress and λ is the extension ratio, and

$$G = \frac{t}{\gamma} \quad (3.53)$$

where t is now the shear stress and γ is the shear strain. This formulation requires three elastic coefficients: A , B , and C . The term $[A + (1/C)]$ is the shear modulus (or one-third of the tensile modulus) at small strains. The term in B denotes a strain-dependent softening of the effective modulus, decreasing ultimately to a value of A . Thus, the term C denotes the stiffening effect of filler at small strains and the term A represents the effective modulus of the completely-softened material. Davies, De and Thomas [50] suggested a four-constant strain energy function:

$$W = \left(\frac{A}{2-n} \right) (J_1 + C^2)^{1-(n/2)} + K J_1^2 \quad (3.54)$$

leading to effective moduli of

$$H \text{ or } G = A (J_1 + C^2)^{-n/2} + 4 K J_1 \quad (3.55)$$

where A/C^n denotes the modulus at small strains, C represents a yield strain at which strain-softening begins, n denotes nonlinear behavior due to the presence of filler and H represents strain hardening at large strains. This form for W gave good agreement with experimental stress-strain relations for various filled compounds over a wide range of strains in tension, compression and shear.

A simple expansion of the strain energy function in terms of J_1 alone was proposed by Yeoh [51, 52]:

$$W = C_{11} J_1 + C_{12} J_1^2 + C_{13} J_1^3 \quad (3.56)$$

retaining only the first three terms. This formulation was found to describe elastic behavior with reasonable success over quite large ranges of strain. Moreover, Eq. (3.56) is a natural extension of the concept of a strain energy function, and thus seems somewhat less arbitrary than Eqs. (3.51) and (3.54). However, values of the coefficients C_{11} , C_{12} and C_{13} were chosen to give the best fit: they do not have any obvious physical significance.

3.3.4.2 Does Any Strain Energy Function Apply?

As discussed later (see Section 3.3.5.2), Rivlin showed that the relation between the torsional stiffness M/ϕ for small torsions of a stretched rod and the tensile stress N is independent of the form of the strain energy function [34]. Thus it holds for all elastic materials whatever the form of the strain energy function. Indeed, if the relation is not obeyed, then the stress-strain behavior cannot be described by a strain energy function. This criterion has been used to show that the stress-strain relations for carbon-black-filled rubber compounds [53] and those for unfilled natural rubber under high strains [54] cannot be described by any function expressed solely in terms of the strains because, in both cases, Rivlin's "universal" relation between torsional stiffness and tensile stress did not hold. Instead, theories have been proposed that express the stresses in filled rubber compounds in terms both of the current strains and the history of previous strains [9, 10]. For example, a criterion can be adopted for the amount of irrecoverable internal "damage" (and hence softening) that is caused by previous stretching [9].

3.3.5 Other Stress-Strain Relations Valid at Large Strains

We now consider the stress-strain relations for a number of other simple deformations, if the relevant strain energy function is known.

3.3.5.1 Simple Shear

Rubber shear springs are widely used as springs and flexible mountings. We consider here the stresses set up by a relatively large shear deformation. For a highly-elastic solid, with a strain energy that depends only on the strain measure J_1 (i.e., with $W_2 = 0$), they are [34]:

$$t_{11} = 2 W_1 \gamma^2 + p \quad (3.57)$$

$$t_{22} = t_{33} = p \quad (3.58)$$

$$t_{12} = 2 W_1 \gamma \quad (3.59)$$

where p denotes the reference pressure. These stresses are shown schematically in Fig. 3.19.

First, it should be noted that the shear stress t_{12} is predicted to be proportional to the amount of shear γ , even for large deformations. In practice, the stress-strain relations for many rubber compounds are, indeed, found to be approximately linear in shear up to quite large shears, greater than 100%, with a slope giving their effective shear modulus G . This linearity in shear is a valuable design feature of rubber springs. But we must now consider the various other stresses that are required to maintain a simple shear deformation.

The second-order stresses t_{11} , t_{22} , t_{33} would not have been expected from the classical theory of elasticity because that deals only with small deformations and these stresses depend on the *squares* of the strains. Their magnitudes depend on the boundary conditions. For example, if we assume that the horizontal stress t_{11} , and hence the reference pressure p , is zero, then the vertical stress t_{22} is negative (compressive) and thus a compressive stress must be imposed in order to maintain the block in a state of simple shear. Otherwise the block will increase in height on shearing. Moreover, the required stress t_{22} becomes quite large, comparable to the shear stress t_{12} when the amount of shear is of the order of 100%, and much larger thereafter because it increases in proportion to the square of the amount of shear. It is thus clear that normal stresses cannot be neglected when large deformations are imposed.

Up to this point we have ignored end effects. However, Rivlin [34] showed that, in order to maintain a simple shear deformation, stresses must also be applied to the block edge surfaces. These stresses consist of a normal stress t_n and a shear stress t_s (Fig. 3.19), given by:

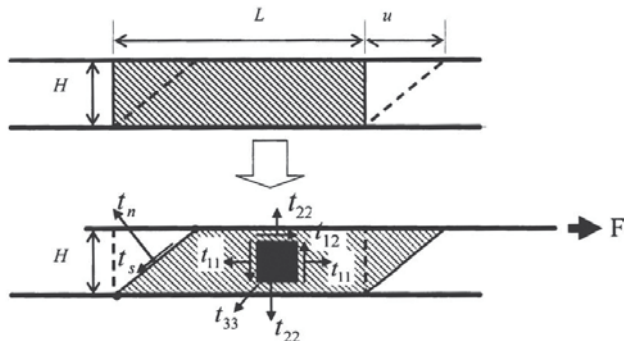


FIGURE 3.19 Stresses necessary to maintain a block in a state of simple shear

$$t_n = \frac{p - (2W_1\gamma)}{1 + \gamma^2} \quad (3.60)$$

$$t_s = \frac{2W_1\gamma}{1 + \gamma^2} \quad (3.61)$$

If they are not applied (as is usually the case in practice) then the previous results do not apply.

An approximation to the stresses in the bulk of the block can be obtained by substituting into Eqs. (3.57) and (3.58) the value of p obtained from Eq. (3.60), putting $t_n = 0$, yielding

$$t_{11} = \frac{2W_1\gamma^2(2 + \gamma^2)}{1 + \gamma^2} \quad (3.62)$$

with corresponding normal stresses t_{22} and t_{33} :

$$t_{22} = t_{33} = \frac{2W_1\gamma^2}{1 + \gamma^2} \quad (3.63)$$

Note that t_{11} , t_{22} and t_{33} have now become *positive* (i.e., tensile) stresses, because the reference pressure p is now a positive quantity.

The most important conclusion from this analysis is that the stresses needed to maintain a block in a state of simple shear depend strongly upon the conditions that hold at the ends of the block. A striking example of this is provided by comparing the stresses set up by shearing two long blocks, one with vertical end surfaces in the unstrained state and the other with inclined end surfaces that become more-or-less vertical in the sheared state, Figs. 3.20 and 3.21 [55].

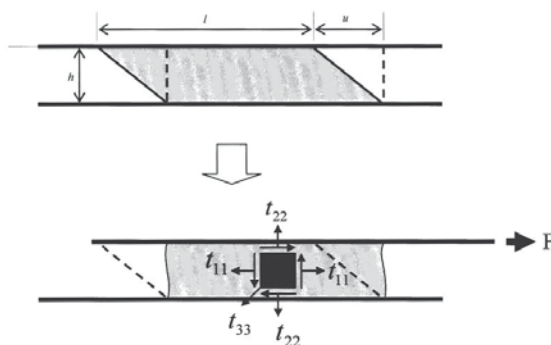


FIGURE 3.20 Sheared blocks with different end shapes

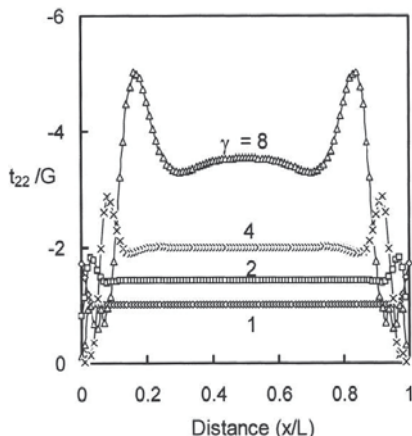


FIGURE 3.21 Normal stresses t_{22} at 100% shear for blocks in Fig. 3.20

In the first case, the normal stress t_{11} is tensile and large, whereas in the second case, it is compressive and small. Note that this striking difference holds however long the block is, relative to its thickness. In other words, the difference in stresses set up by what appears to be the same shear deformation does not arise from an *end effect* that would become unimportant far away from the ends, but is a consequence of a change in *boundary conditions*, and that affects the stresses everywhere.

3.3.5.2 Torsion

Poynting observed that twisted metal wires and rubber rods increased in length by an amount proportional to the square of the torsion [56]. This unexpected effect was shown by Rivlin to follow from the theory of large elastic deformations [34]. He calculated the stress S necessary to hold a stretched cylindrical rod at fixed length and showed that it would decrease in proportion to the square of the amount of torsion (Fig. 3.22).

The required torque M is given by

$$M = (W_1 + W_2) \pi a^4 \psi \quad (3.64)$$

where a is the cylinder radius and ψ is the angular rotation imposed per unit length of the cylinder. The corresponding normal stresses (equivalent to stress t_{22} in Fig. 3.19) vary from point to point over the cross section, depending on the particular form of strain energy function obeyed by the rubber – that is, on the values of W_1 and W_2 that obtain under the imposed deformation:

$$t_{zz} = - \left[2 W_2 r^2 + W_1 (a^2 - r^2) \right] \psi^2 \quad (3.65)$$

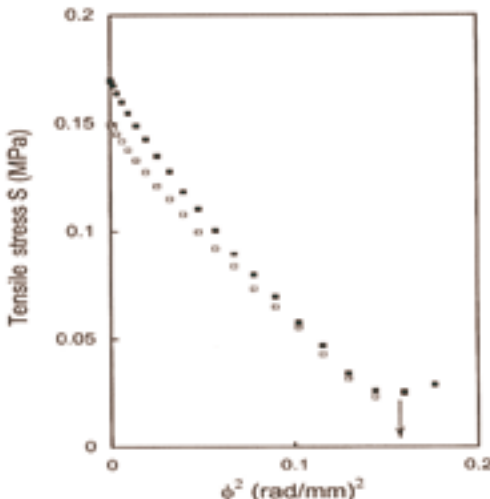


FIGURE 3.22 Decrease in normal force on twisting a stretched rod

where r is radial distance from the cylinder axis [36]. This result is obtained by assuming that the curved surface of the cylinder is stress-free and that the cylinder length is maintained constant. (Note that the normal force is compressive in this case because continuity around the circumference supplies the required stresses t_{rr}) There are several noteworthy features of the solution. First, a twisted rod will elongate if the negative (compressive) stresses t_{zz} are not applied – that is, a pressure is needed to hold the twisted cylinder at its original length. Moreover, the elongation caused by torsion is expected to be proportional to the square of the amount of twist, from the dependence of t_{zz} on ψ^2 . Moreover, measurements of the distribution of normal stresses across a section of a twisted rod enable one to evaluate the strain energy function derivatives rather accurately, because t_{zz} takes values of $-W_1 a^2 \psi^2$ at the center and $-2 W_2 a^2 \psi^2$ at the edge of the cross section, involving only one of the strain energy function derivatives in each case.

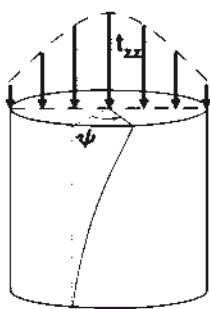


FIGURE 3.23 Distribution of normal stresses set up by twisting a stretched rod

Rivlin derived a “universal relation” between the normal force N required to hold a rod stretched and the torsional stiffness $T (= M/\phi)$ for small torsions of the stretched rod per unit of unstrained length [34]; a relation that holds for *any* strain energy function. It takes the form:

$$T L \lambda = \frac{N a^2}{2(\lambda - \lambda^{-2})} \quad (3.66)$$

where L is the length of the rod and a is its radius in the unstrained state, and λ is the stretch ratio.

If the elastic behavior of a material fails to conform with this relation, we can conclude that no strain energy function will apply. Filled rubber has been shown not to obey this relation, probably because of strain-softening effects and the irreversible nature of the stress-strain relations [53]. Even unfilled natural rubber fails to follow this relation at high strains [54]. The problem probably arises in this case from a strain-induced phase transition (crystallization), causing a pronounced departure from reversibility in the stress-strain relations.

3.3.5.3 Instability in Torsion

As discussed above, the tensile stress necessary to maintain the extension of a cylindrical rod falls as the rod is twisted, approximately in proportion to the square of the amount of torsion, Eq. (3.65). An example was shown in Fig. 3.22. However, at a critical point, marked with an arrow in that figure, the deformation of the rod suddenly changed in character. A small portion of the rod became bent into an S-shaped curve and then collapsed into a tight horizontal ring or kink. This sequence of deformations is shown schematically in Fig. 3.24. The point at which a uniform torsional deformation becomes unstable can be calculated by equating the loss in elastic energy as one twist is released to the increase in energy as the remainder of the rod is stretched further [57]. Thus, the instability can be predicted by considering the elastic behavior of rubber under high strains. Other examples of elastic instability are discussed later.

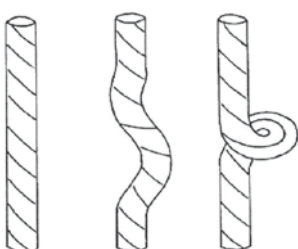


FIGURE 3.24 Instability in torsion (schematic)

3.3.5.4 Inflation of a Thin-Walled Tube [58]

For simplicity in the analysis, the rubber is assumed to have the strain energy function given in Eq. (3.35), with K_2 put equal to zero, i.e., with only two material parameters: C_1 and J_m . The deformation is described by extension ratios λ_1 in the circumferential direction and λ_2 in the axial direction, with the wall thickness w becoming $w/\lambda_1 \lambda_2$ because the rubber volume remains constant. For closed-end tubes, unconstrained in length, the inflation pressure P gives rise to stresses in the circumferential and axial directions:

$$t_1 = 2 t_2 = \frac{(\lambda_1^2 \lambda_2) r P}{w} \quad (3.67)$$

where r is the tube radius in the unstrained state. Putting $t_3 = 0$ defines the reference pressure p :

$$p = \frac{-2 W_1}{\lambda_1^2 \lambda_2^2} \quad (3.68)$$

(Note that in a thin-walled tube of large radius the inflating pressure P is much smaller than the stresses t_1 and t_2 that it generates. Thus P can be neglected in comparison with the stress t_3 in determining the reference pressure p .)

The ratio of the volume contained by the tube in the inflated and uninflated states is denoted V , and is related to the expansion ratio in the axial direction:

$$\lambda_2^3 = \frac{V^2 + 1}{2 V} \quad (3.69)$$

The relation between inflating pressure P and internal volume is then obtained as

$$\frac{P r}{w C_1} = \frac{2(V^2 - 1) \left[2V(V^2 + 1) \right]^{1/3}}{V^2 \left[1 - \left(\frac{J_1}{J_m} \right) \right]} \quad (3.70)$$

where J_i is a function of the extension ratios, given by Eq. (3.30). Relations between P and V are plotted in Fig. 3.25 for various values of the limiting strain measure J_m .

The inflating pressure is seen to pass through a maximum at a volume expansion ratio of about 60%, depending somewhat on the value assumed for J_m . This feature indicates that larger expansions will be unstable. Indeed, thin-walled tubes undergo

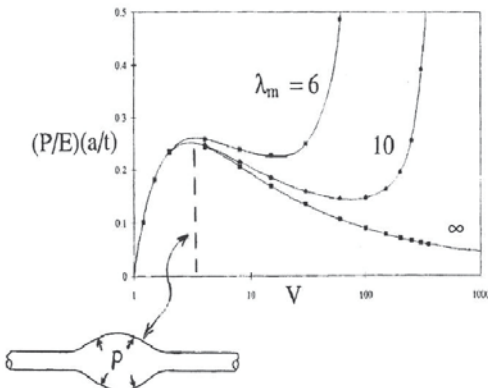


FIGURE 3.25 Inflation pressure p vs tube volume ratio V from Equation 3.70

a strikingly non-uniform deformation at a critical inflation pressure, shown schematically in Fig. 3.25. One portion of the tube becomes highly distended as a bubble or aneurysm while the rest remains less inflated. This phenomenon is attributed to the elastic response of rubber under large deformations, and not to a “weakness” of the material or in the construction of the tube. In the same way, Eulerian buckling of a compressed strut is predicted correctly by the classical theory of elasticity – it is not attributed to a deficiency in the strut. Rubber under inflation shows new elastic instabilities that resemble Eulerian buckling but they arise from the special ability of rubber to undergo large elastic deformations.

In general, two stable deformations can co-exist at the same inflation pressure after the critical state is reached, as shown schematically by the horizontal broken line in Fig. 3.25. However, when J_m is infinitely large the aneurysm can grow indefinitely, and failure would then occur immediately on reaching the critical pressure.

3.3.5.5 Inflation of a Spherical Shell (Balloon)

The pressure P_1 required to inflate a spherical shell of initial radius r_o and thickness d_o to an inflated radius λr_o and thickness d_o/λ^2 can be obtained from Eq. (3.45), using Laplace’s relation between the stresses t in the plane of the shell and inflating pressure (Fig. 3.26):

$$P_1 = \frac{2t d_o}{\lambda^3 r_o} \quad (3.71)$$

Note that this pressure is not the same as the reference pressure p in Eq. (3.36). The inflating pressure P_1 generates a tension stress t in the curved shell. For a typical

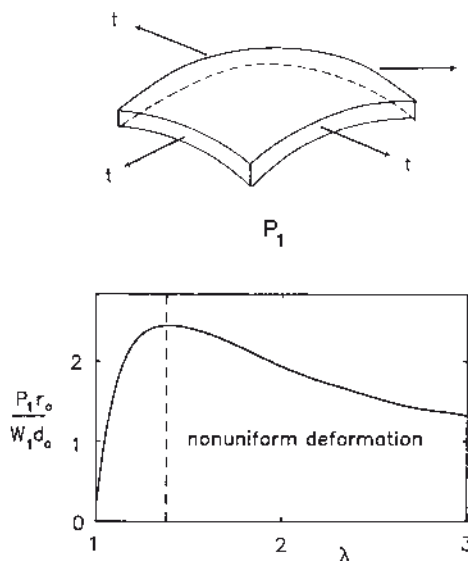


FIGURE 3.26 Inflation of a spherical shell (balloon)

shell, with a radius r_0 much larger than its thickness d_0 , P_1 is negligibly small in comparison with t and thus the stress t_1 normal to the plane of the shell is still effectively zero in Eqs. (3.41) and (3.42). Calculation of the reference pressure p is therefore unaffected by this particular way of stretching the shell biaxially, using an inflation pressure.

On substituting for t in Eq. (3.71), the relation between inflation pressure P_1 and inflation ratio λ is obtained as:

$$P_1 = 4 \left(\frac{d_0}{r_0} \right) (W_1 + \lambda^2 W_2) (\lambda^{-1} - \lambda^{-7}) \quad (3.72)$$

This is a highly nonlinear relation. For illustrative purposes we give W_2 the value zero and plot the behavior predicted by Eq. (3.72) in Fig. 3.26. The inflation pressure is seen to pass through a sharp maximum at an expansion ratio of 38% and then decrease upon further inflation. This is a well-known feature of balloons: after a relatively small inflation it is much easier to continue inflating them.

Another consequence of the maximum in the relation for pressure (Fig. 3.26) is that inflation strains become non-uniform thereafter. Part of the shell stretches to a high degree (until strain hardening sets in) while the rest becomes less inflated, the pressure in the two parts being of course equal.

3.3.5.6 Inflation of a Spherical Cavity; Explosive Decompression

By integrating the result for inflation of a thin-walled spherical shell (Eq. (3.72)), we can obtain a solution for inflation of a thick-walled shell. In the limit, for a shell with an infinitely thick wall (e.g., for a rubber block containing a small spherical cavity in its interior), the relation between inflation pressure P_1 and expansion ratio λ of the cavity radius takes the form:

$$P_1 = W_1 \left(5 - 4 \lambda^{-1} - \lambda^{-4} \right) \quad (3.73)$$

for the especially simple case where W_1 is constant and W_2 is zero [59].

Two features of this result are noteworthy. When the inflation ratio λ is increased indefinitely, the inflation pressure approaches an asymptotic value of $5 W_1$, i.e., $5 G/2$, as shown in Fig. 3.27. Thus, a small cavity is predicted to grow to an infinitely large size at an inflation pressure of this amount. For typical soft vulcanizates this pressure is quite small, only about 1 to 5 MPa. Moreover, the result does not contain the original radius of the cavity, so that a cavity of any size would be expected to expand indefinitely at this pressure.

Experiments with rubber blocks in which high pressure gas is dissolved showed that the interior becomes full of bubbles when the external gas pressure is suddenly released [26]. Thus, dissolved gas must fill microscopic cavities within the rubber and when the external pressure is released the cavities are forced to expand elastically until the limiting extensibility of rubber is reached. At this point the wall of a cavity will tear open and the resulting crack grows further, to form a large gas-filled cavity.

This mechanism needs to be reconsidered, to take into account other energy terms necessary for rubber to tear (see Chapter 5). For example, the initial size of the precursor cavities is found to be an important factor – small cavities are much more

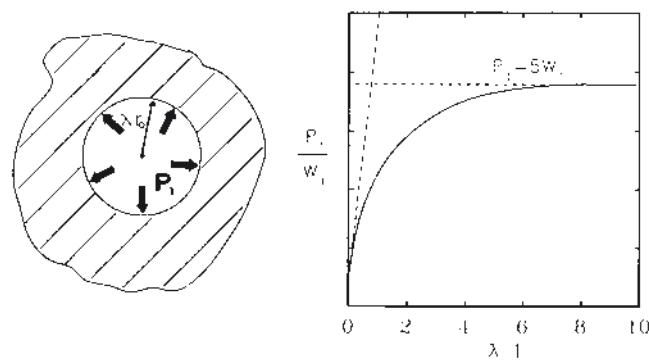


FIGURE 3.27 Inflation of a small cavity

resistant to expansion by tearing than large ones [61, 62]. Nevertheless, rubber appears to contain cavities of a sufficiently large size that Eq. (3.73) gives a good approximation to the critical pressure for formation of the first few large internal cracks.

Note that the solution is unchanged if the internal pressure is replaced by an external tension of the same magnitude. We therefore expect rubber to crack open internally when an external triaxial tension or negative hydrostatic pressure is imposed of the same amount. This phenomenon has also been observed [25]. To avoid internal failures, therefore, rubber should never be subjected to triaxial stresses approaching the magnitude $5 G/2$.

Cavitation can occur under more complex stress states. Solutions have been obtained for the critical hydrostatic tension when shear stresses are also present [63, 64].

These examples of unstable deformations and unexpected fractures illustrate the close connection between rubberlike elasticity and other mechanical properties of rubbery materials.

3.3.5.7 Surface Creasing in Compression

Biot has studied the response of an elastic block to compressions parallel to the surface plane and shown that the surface is expected to become unstable under various types of two-dimensional compression, at rather moderate strains [65]. Three special cases are: simple compression in one direction, compression in one direction with the perpendicular direction constrained (pure shear), and equibiaxial compression. For a simple neo-Hookean material, with the strain energy function given in Eq. (3.50), the corresponding critical compressive strains are predicted to be 55%, 45% and 33%, respectively. Now, when a thick rubber block is bent, the inner surface is subjected to constrained compression and thus the expected critical degree of compression is 45%, corresponding to a tensile strain on the outer surface of about 83%. However, sharp creases are found to appear suddenly on the inner surface at a significantly lower bending strain, when the surface compression at the inner surface is only about 35% and the tensile strain on the outer surface is only about 45% [66]. An example is shown in Fig. 3.28.

This critical compressive strain is substantially smaller than expected, and indicates that another mode of unstable deformation occurs. Whereas Biot considered the stability of surface deformational waves, the observed instability occurs by sharp inwardly-directed surface creasing. Careful analysis of this mode of unstable deformation leads to good agreement with the experimental observations [67].

Rubber articles are often subjected to rather severe bending strains, and the occurrence of sharp creases could lead to high local stress concentrations and premature failure. Surface folds ("Schallamach waves") also appear in rubber surfaces under the

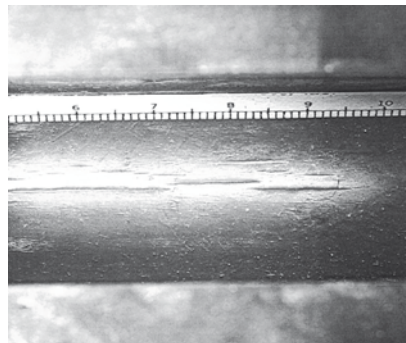


FIGURE 3.28 Creases on the inner surface of a bent block

action of frictional forces [68]. Their formation has been attributed to local buckling of the surface under compressive stresses in the surface plane [69].

■ 3.4 Molecular Theory of Rubber Elasticity

3.4.1 Elastic Behavior of a Molecular Network

A long, flexible molecule can be represented to good approximation by a randomly arranged chain of n freely-jointed links, each of length l . The distribution of end-to-end lengths r obeys a Gaussian probability function, at least for small end-to-end distances:

$$P(r) = C \exp(-\beta^2 r^2) \quad (3.74)$$

where the parameter β^2 is given by $3/2 n l^2$. The mean square distance between the ends, denoted r^2 , is then given by $n l^2$ or $3/2 \beta^2$.

Now a strand having an end-to-end length r has entropic energy w associated with it, given by Boltzmann's relation:

$$w = -k T \ln P = k T \beta^2 r^2 = \frac{3 k T r^2}{2 n l^2} \quad (3.75)$$

and the force-length relation for a single strand is therefore obtained as follows:

$$f = \left(\frac{\partial w}{\partial r} \right) = \frac{3 k T r}{n l^2} \quad (3.76)$$

Thus, a molecule with a size and shape governed by probability considerations is a linearly-elastic spring, with a stiffness that is proportional to absolute temperature and inversely proportional to the number n of links in the molecular strand. However, at large strains, approaching the fully taut configuration, Eqs. (3.74–3.76) cease to be valid, even approximately, because the Gaussian equation, Eq. (3.74), does not apply under these circumstances. A more accurate representation over the entire range of end-to-end distances is given by [70]:

$$\frac{f l}{k T} = L^{-1} \left(\frac{r}{n l} \right) \quad (3.77)$$

where L^{-1} denotes the inverse of the Langevin function,

$$L \left(\frac{f l}{k T} \right) = \coth \left(\frac{f l}{k T} \right) - \left(\frac{k T}{f l} \right) \quad (3.78)$$

A network of Gaussian chains can be treated as if chain end-to-end displacements in the three principal directions were independent. Unfortunately, Eq. (3.77) does not conform to this simple rule: a displacement in one direction alters the probabilities of given displacements in the other directions. As a result, it is not possible to sum up the contributions of a random assembly of network strands to the total strain energy in any simple way. On the other hand, it is easy to do so for a network of Gaussian chains. We are thus able to develop a theory of elasticity for a Gaussian molecular network but it is valid only for moderately small deformations, when r is less than about one-third of the fully-stretched length $n l$ of a representative molecular strand (Fig. 3.29).

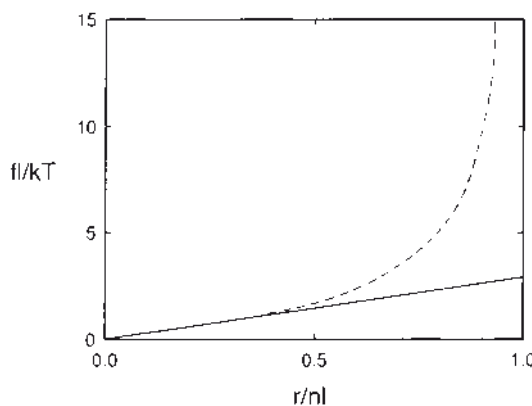


FIGURE 3.29 Elasticity of a single molecule:
solid curve, Gaussian elasticity; dashed curve, inverse Langevin function.

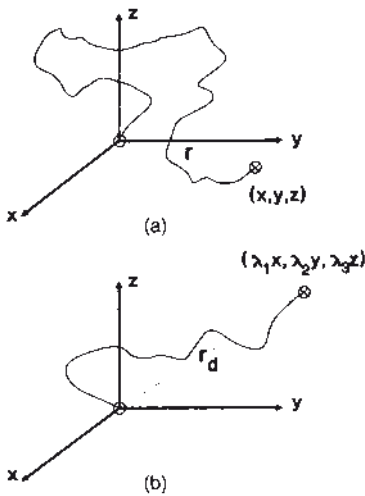


FIGURE 3.30 Sketch of a molecular strand in a network
 (a) in the undeformed state,
 (b) in the deformed state

Figure 3.30 shows a representative molecular strand in the network before and after deformation. We assume that the ends move apart in exactly the same way as macroscopic points in the bulk material, so that (x, y, z) becomes $(\lambda_1 x, \lambda_2 y, \lambda_3 z)$ under a general deformation defined by extension ratios $\lambda_1, \lambda_2, \lambda_3$. The end-to-end length therefore changes from r to r_d , where

$$r_d^2 = \lambda_1^2 x^2 + \lambda_2^2 y^2 + \lambda_3^2 z^2 \quad (3.79)$$

and the energy stored in the strand becomes

$$w = k T \beta^2 r_d^2 \quad (3.80)$$

in place of Eq. (3.75). Thus, the change in strand energy due to the deformation is

$$\Delta w = k T \beta^2 \left[(\lambda_1^2 - 1)x^2 + (\lambda_2^2 - 1)y^2 + (\lambda_3^2 - 1)z^2 \right] \quad (3.81)$$

If we now add up the contributions to Δw from each of N strands in unit volume, and take into account that their x, y , and z coordinates are randomly distributed in the unstrained state, so that their mean values are equal:

$$\bar{x}^2 = \bar{y}^2 = \bar{z}^2 = \frac{\bar{r}^2}{3} \quad (3.82)$$

then the total change W in strain energy becomes

$$W = N k T \beta^2 \bar{r}^2 (\lambda_1^2 + \lambda_2^2 + \lambda_3^2 - 3) \quad (3.83)$$

This result is of the same general form as the first term in the Mooney-Rivlin relation (Eq. (3.32)). Thus, molecular calculations agree with, and clarify, the result obtained from general phenomenological considerations. (The second term in the Mooney-Rivlin relation is discussed below.) We note that the mean square end-to-end distance r^2 in the undeformed state is likely to be similar to that for free chains (i.e., $3/2 \beta^2$, because when crosslinking is carried out in an unoriented polymer melt the crosslinks are likely to form at points where the molecular strands are randomly arranged and in their most probable configurations. The only serious departure from this condition would be for a network that is strained internally before any mechanical stresses are applied, for example, by swelling it with a compatible liquid after crosslinking, or by crosslinking it in an oriented state and then releasing the applied stresses. For such materials, r^2 would be significantly different from $3/2 \beta^2$. Thus, for a network of randomly arranged molecular strands, Eq. (3.83) takes the particularly simple form:

$$W = \left(\frac{N k T}{2} \right) J_1 \quad (3.84)$$

where the only term describing the molecular structure is the number N of network strands per unit volume. Thus the elastic properties at moderately small strains are predicted to be independent of the length or flexibility of the constituent molecular strands, depending only on their number. It is also interesting to note that general nonlinear elastic behavior follows for a network composed entirely of linearly-elastic strands. This feature arises from the geometry of deformation of randomly oriented chains. Indeed, as we have seen, the degree of non-linearity depends on the type of deformation imposed. In simple shear, the predicted relationship is a linear one with a slope (shear modulus G) given by $N k T$.

3.4.3 Effective Density of Network Strands

Let us suppose that the strands formed by crosslinking have an average molecular weight M_c . Then the number N_c of strands per unit volume generated by crosslinking is:

$$N_c = \frac{\rho A}{M_c} \quad (3.85)$$

where ρ is density and A is Avogadro's number. Other network strands are formed by trapped molecular entanglements, at an average spacing of M_e molecular weight units along the molecule. Then,

$$N_e = \frac{\rho A}{M_e} \quad (3.86)$$

and a correction must be made for dangling chain ends that carry no force whatsoever. In sum, a rough guide to the number N of effective molecular strands for use in Eq. (3.83) is [71]:

$$N = \rho A \left[\left(\frac{1}{M_e} \right) + \left(\frac{1}{M_c} \right) \right] \left[1 - 2 \left(\frac{M_c}{M} \right) \right] \quad (3.87)$$

where M denotes the molecular weight of the original molecules before they were linked into a network. Equations (3.83) and (3.87) provide a rough guide to the elastic behavior of a pure rubbery solid in terms of its molecular structure. A more complete analysis has been given by Langley [72, 73].

3.4.4 The Second Term in the Strain Energy Function

The term involving J_2 in the strain energy function leads to additional stresses that are relatively large at small strains (although they are always the smaller part of the observed stress) and they decrease in importance as the strain increases. They also decrease as the network is diluted by swelling with an inert liquid. These features suggest that the J_2 term is associated with constraints on chains in networks (Fig. 3.31) and specifically that it arises from restrictions on the conformations available to entangled chains that are different from those operating at crosslink sites. The constraints appear to become more severe as the strain is increased, so that entanglements become more like real crosslinks. In other words, we reach the surprising conclusion that molecular entanglements lead to additional stress when they are less effective than real crosslinks (i.e., at small strains) and they give smaller contributions to observed stresses when they are fully effective and substantially equivalent to crosslinks. How can this be? A possible explanation is due to Prager and Frisch [74]. They pointed out that a chain that is fixed at one end and compelled to loop around a fixed line will be prevented from having small end-to-end distances but it will not be prevented from having large ones. As a result, the distribution of end-to-end distances is no longer in accord with Gaussian statistics (Eq. (3.74)) but is biased in favor of large values. Moreover, the average tension in the chain is higher than that for a chain that is simply tethered to the fixed line and obeys Gaussian statistics. And these differences diminish as the distance to the fixed line or hole is increased, because the probability of end-to-end distances larger than this becomes small.

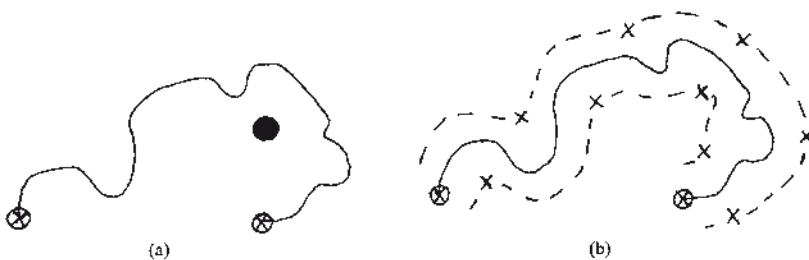


FIGURE 3.31 Constraint on conformations accessible to a molecular strand
 (a) due to passage around a fixed line (represented by the solid circle);
 (b) due to a “tube” of neighboring molecules, represented by crosses

The known features of the second term in the strain energy function are in accord with this hypothetical constraint mechanism. For example, the effect will become smaller in swollen networks, disappearing at moderately high degrees of swelling as the chains become more stretched and entanglements become fully effective. In highly crosslinked networks the contribution is unchanged but it is, of course, now small in comparison with that from “real” network strands. And, whereas molecules in solution appear to obey Gaussian statistics, the second term is highly non-Gaussian, by definition. (Note that it is a property specifically of networks, not of the molecules themselves.) Finally, attempts to prepare networks relatively free from entanglements invariably result in a decrease in the magnitude of the J_2 term.

Other studies of the statistics of chains in networks have been carried out by Flory and his colleagues, as discussed in [75, 76], applying the concept of a variable level of constraint to the crosslink sites, rather than to the chains between them. For simple systems, this leads to a change in the numerical factor in Eq. (3.84) from $\frac{1}{2}$ to $\frac{1}{4}$ as the degree of constraint is lessened. The concept of molecular entanglements has also been replaced by the model of a chain confined by its neighbors to configurations within a tube-like space around it [77, 78], Fig. 3.32 (b), rather than having access to the whole volume that it could sample, in principle, if the neighboring chains were absent. Both of these constraints become relatively less severe for highly-stretched chains and for less concentrated systems, in accordance with the known features of the J_2 term. Fuller discussion and comparison with experiments are given elsewhere [79–81].

3.4.5 Concluding Remarks on Molecular Theories

The simple molecular treatment of rubber elasticity has proved to be remarkably successful in accounting for the elastic properties of rubber under moderate strains,

up to about 300% of the unstrained length (depending on the length and flexibility, hence extensibility, of the constituent chains). It predicts the general form of the stress-strain relationships correctly under a variety of strains, and the approximate numerical magnitudes of stresses for various chemical structures. Moreover, it predicts the effect on the elastic behavior of temperature and of swelling rubber with an inert mobile liquid. It is also consistent with the general phenomenological theory of elasticity, applicable to any elastic solid (Section 3.3). In summary, it constitutes a major advance in our understanding of the properties of materials.

■ Acknowledgments

This chapter was originally prepared during a program of research on the mechanics of elastomers, supported by a grant from the Office of Naval Research (contract N00014-85-K-0222; project officer, Dr. R. S. Miller). It is based in part on an earlier review (“Rubber Elasticity: Basic Concepts and Behavior”, Chapter I in *Science and Technology of Rubber*, 2nd ed., F. R. Eirich, J. E. Mark and B. Erman (Eds.), Academic Press, New York, 1997) and depends heavily on the classic account of rubber elasticity by L. R. G. Treloar (34). It was presented as part of a series of lectures at the University of Minnesota in 1985 and reduced to writing at the suggestion of Professor J. L. Eriksen. Later discussions with Dr. O. H. Yeoh on various aspects of rubber mechanics are gratefully acknowledged. This revision was prepared during a visit to Chonbuk National University, South Korea, supported by the World-Class University Program of the Korean Government. The kind hospitality of Professor C. Nah, Head of the Department of Polymer Science and Engineering, is also gratefully acknowledged.

■ References

- [1] T. Fleischman and M. R. Gurvich, *Rubber Chem. Technol.*, **76**, 912 (2003).
- [2] A. N. Gent, *Trans. Inst. Rubber Ind.*, **34**, 46 (1958).
- [3] B. J. Briscoe and K. S. Sebastian, *Rubber Chem. Technol.*, **66**, 827 (1993).
- [4] L. J. Fetters, D. J. Lohse and W. W. Graessley, *J. Polymer Sci.: Part B: Polymer Phys.*, **37**, 1023 (1999).
- [5] N. R. Legge, G. Holden and H. E. Schroeder (Eds.), *Thermoplastic Elastomers*, Hanser, New York, 1987.
- [6] L. Mullins, *Rubber Chem. Technol.*, **42**, 339 (1969).

- [7] L. Mullins, *Trans. Inst. Rubber Ind.*, **28**, 280 (1948).
- [8] F. Bueche, *J. Appl. Polym. Sci.*, **4**, 107 (1960); **5**, 271 (1961).
[See also F. Clement, L. Bokobza and L. Monnerie, *Rubber Chem Technol.*, **74**, 847 (2001).]
- [9] R. W. Ogden and D. G. Roxburgh, *Proc. Roy. Soc Lond.*, **A455** 2861 (1999).
- [10] C. O. Horgan, R. W. Ogden and G. Saccomandi, *Proc. Roy. Soc Lond.*, **A460** 1737 (2004).
- [11] S. S. Sternstein and A.-J. Zhu, *Macromol.*, **35**, 7262 (2002).
- [12] R. S. Rivlin and D. W. Saunders, *Trans. Inst. Rubber Ind.*, **24**, 296 (1949).
- [13] J. E. Adkins and A. N. Gent, *Br. J. Appl. Phys.*, **5**, 354 (1954).
- [14] J.M. Horton, M.J.C. Gover and G.E. Tupholme, *Rubber Chem. Technol.*, **73**, 69 (2000); **73**, 253 (2000); **79**, 233 (2006).
- [15] S. P. Timoshenko and J. N. Goodier, Mathematical Theory of Elasticity, 3rd ed., McGraw-Hill. New York, 1970. Chapter 9, Section 108.
- [16] A. N. Gent and P. B. Lindley, *Proc. Inst. Mech. Eng. (London)*, **173**, 111 (1959).
- [17] A. N. Gent and E. A. Meinecke, *Polym. Eng. Sci.*, **10**, 48 (1970).
- [18] A. N. Gent, *Rubber Chem. Technol.*, **67**, 549 (1994).
- [19] A. N. Gent, R. L. Henry, and M. L. Roxbury, *J. Appl. Mech.*, **41**, 855 (1974).
- [20] Y. Ling, P. A. Engel and W. L. Brodsky, *J. Engng. Mech.*, **121**, 661 (1995).
- [21] J. M. Horton, G. E. Tupholme and M. J. C. Gover, *ASME J. Appl. Mech.*, **69**, 836 (2002).
- [22] P. Mott and C. M. Roland, *Rubber Chem. Technol.*, **73**, 68 (1995).
- [23] J. S. Thornton, R. E. Montgomery, C. M. Thompson and D. A. Dillard, *Polymer Eng. Sci.*, **28**, 655 (1988); **29**, 432 (1989).
- [24] A. N. Gent, F. M. Discenzo and J. B. Suh, *Rubber Chem. Technol.*, **82**, 1–17 (2009).
- [25] A. N. Gent and P. B. Lindley, *Proc. R. Soc. London, Ser. A*, **249**, 195 (1958).
- [26] A. N. Gent and D. A. Tompkins, *J. Appl. Phys.*, **40**, 2520 (1969).
- [27] P. B. Lindley and A. Stevenson, *Rubber Chem. Technol.*, **55**, 337 (1982).
- [28] I. N. Sneddon, Chapter A, Section 111, in Applications of Integral Transforms in the Theory of Elasticity, ed. by I. N. Sneddon, Springer-Verlag, New York. 1975.
- [29] A. N. Gent and O. H. Yeoh, *Rubber Chem. Technol.*, **79**, 674 (2006).
- [30] M. A. Biot, Mechanics of incremental deformations, Wiley, New York, 1965.
- [31] J. G. Curro and E. A. Salazar, *Rubber Chem. Technol.*, **46**, 530 (1973).
- [32] A. N. Gent and W. Kim, *Rubber Chem. Technol.*, **64**, 814 (1991).
- [33] R. Roscoe, *Phil. Mag. (Ser. 7)*, **40**, 338 (1949).
- [34] R. S. Rivlin, in F. R. Eirich (Ed.), Rheology, Theory and Applications, Vol. 1, Academic Press, New York, 1956, Chapter 10.
- [35] M. Mooney, *J. Appl. Phys.*, **11**, 582 (1940).
- [36] L. R. G. Treloar, The Physics of Rubber Elasticity, 3rd ed., Clarendon Press, Oxford, 1975.
- [37] R. S. Rivlin and D. W. Saunders, *Phil. Trans. R. Soc. London, Ser. A*, **243**, 251 (1951).
- [38] Y. Obata, S. Kawabata and H. Kawai, *J. Polymer Sci.: Polymer Phys. Ed.*, **8**, 903 (1970).
- [39] F. D. Murnaghan, Finite Deformations of an Elastic Solid, Wiley, New York, 1951.
- [40] A. N. Gent and A. G. Thomas, *J. Polym. Sci.*, **28**, 625 (1958).
- [41] R. A. Dickie and T. L. Smith, *Trans. Soc. Rheol.*, **15**, 91 (1971).
- [42] K. C. Valanis and R. F. Landel, *J. Appl. Phys.*, **38**, 2997 (1967).
- [43] R. W. Ogden, *Rubber Chem. Technol.*, **59**, 361 (1986).
- [44] E. M. Arruda and M. C. Boyce, *J. Mech. Phys. Solids*, **41**, 389 (1993).
- [45] P. D. Wu and E. van der Giessen, *J. Mech. Phys. Solids*, **41**, 427 (1993).

- [46] A. N. Gent, *Rubber Chem. Technol.*, **69**, 59 (1996).
- [47] L. Mullins and N. R. Tobin, *Rubber Chem. Technol.*, **30**, 555 (1957).
- [48] J. M. Charrier and A. N. Gent, in "Proc. Internat. Symp. on Elastomer Reinforcement", Obernai, France, 1973, *Colloques Internationale No. 231*, C.N.R.S., Paris, 1974.
- [49] A. B. Othman and M. J. Gregory, *J. Nat. Rubber Res.*, **5**(2), 144 (1990).
- [50] C. K. L. Davies, D. K. De and A. G. Thomas, *Rubber Chem. Technol.*, **67**, 716 (1994).
- [51] O. H. Yeoh, *Rubber Chem. Technol.*, **63**, 792 (1990).
- [52] O. H. Yeoh, *Rubber Chem. Technol.*, **66**, 754 (1993).
- [53] H. R. Ahmadi, J. Gough, A. H. Muhr and A. G. Thomas, in "Constitutive Models for Rubber", ed. by A. Dorfmamm and A. H. Muhr, Balkema, Rotterdam, 1999, pp. 65–71.
- [54] C. Nah et al., *Internat. J. Non-Linear Mech.*, **45**, 232 (2010).
- [55] A. N. Gent, J. B. Suh and S. G. Kelly III, *Internat. J. Non-Linear Mech.*, **42**, 241 (2007).
- [56] J. H. Poynting, *Proc. R. Soc. London, Ser. A*, **82**, 546 (1909); *ibid, Ser. A*, **86**, 534 (1912).
- [57] A. N. Gent and K.-C. Hua, *Internat. J. Non-Linear Mech.*, **39**, 483 (2004).
- [58] A. N. Gent, *Rubber Chem. Technol.*, **72**, 263 (1999).
- [59] A. E. Green and W. Zerna, "Theoretical Elasticity", 2nd ed., Clarendon Press, Oxford, 1975, p. 135.
- [60] B. J. Briscoe, T. Savvas and C. T. Kelly, *Rubber Chem. Technol.*, **67**, 384 (1994).
- [61] M. L. Williams and R. A. Schapery, *Int. J. Fract. Mech.*, **1**, 64 (1965).
- [62] A. N. Gent and C. Wang, *J. Mater. Sci.*, **26**, 3392 (1991).
- [63] O. Lopez-Pamies, M. I. Idiart and T. Nakamura, *J. Mech. Phys. Solids*, **59** (2011) 1463–1487.
- [64] O. Lopez-Pamies, T. Nakamura and M. I. Idiart, *J. Mech. Phys. Solids*, **59** (2011) 1488–1505.
- [65] M. A. Biot, *Appl. Sci. Research*, **A12**, 168 (1963).
- [66] A. N. Gent and I. S. Cho, *Rubber Chem. Technol.*, **72**, 253 (1999).
- [67] W. Hong, Z. Zhao and Z. Suo, *Appl. Phys. Lett.*, **95**, 111901 (2009).
- [68] A. Schallamach, *Wear*, **17**, 301 (1971).
- [69] B. Best, P. Meijers and A. R. Savkoor, *Wear*, **65**, 385 (1981).
- [70] P. J. Flory, Principles of Polymer Chemistry, Cornell University, Ithaca, NY, 1953.
- [71] L. Mullins, *J. Appl. Poly. Sci.* **2**, 1 (1959).
- [72] N. R. Langley, *Macromolecules*, **1**, 348 (1968).
- [73] N. R. Langley and K. E. Polmanteer, *J. Polym. Sci.: Polym. Phys. Ed.*, **12**, 1023 (1974).
- [74] S. Prager and H. L. Frisch, *J. Chem. Phys.*, **46**, 1475 (1967).
- [75] J. E. Mark and B. Erman, Rubber Elasticity – A Molecular Primer, Wiley-Interscience, New York, 1989.
- [76] J. E. Mark and B. Erman, Structures and Properties of Rubberlike Networks, Oxford University Press, New York, 1997.
- [77] S. F. Edwards, *Proc. Phys. Soc. Lond.*, **92**, 9, (1967).
- [78] M. H. Wagner, *J. Rheol.*, **38**, 655 (1994).
- [79] M. Gottlieb, C. W. Macosko and T. C. Lepsch, *J. Polym. Sci.: Polym. Phys. Ed.*, **19**, 1603 (1981).
- [80] J. E. Mark and B. Erman (Eds.), Elastomeric Polymer Networks, Prentice Hall, Englewood Cliffs, New Jersey, 1992.
- [81] W. W. Graessley, Polymeric Liquids and Networks: Structure and Properties, Garland Science, New York, 2004.

■ Problems for Chapter 3

1. A rubbery material has a “Shore A Hardness” of 45 degrees. What is the approximate value of the tensile (Young) elastic modulus E ? What is the approximate value of shear modulus G ? According to the molecular theory of rubber elasticity, what is the approximate number N of molecular strands per cubic meter?
2. Estimate values of E and G for a rubbery material with a Shore A hardness of 75 degrees. [Note that materials of this hardness are almost certainly filled with large amounts of particulate solids, e.g., carbon black and the molecular theory no longer holds.]
3. A rubbery material has a modulus K of bulk compression of 2 GPa and a shear modulus G of 1 MPa. What is the value of Poisson’s ratio? What would the lateral shrinkage strain be if a sample were subjected to a tensile strain of 5%? What would the lateral shrinkage strain be if the tensile strain were 100%? [Is the concept of a constant ratio (Poisson’s ratio) of lateral to longitudinal strain valid when the strains are large?]
4. A rubber tube spring is prepared with the following dimensions: internal radius a_1 of rubber tube (bonded to a rigid cylindrical core), 10 mm; external radius a_2 (bonded to a rigid surrounding tube), 20 mm, and length L 50 mm. The rubber has a shear modulus G of 0.5 MPa. What values would be expected for axial and torsional stiffness?
5. If the temperature were raised from ambient—say, from 20 °C, to 100 °C, what would the spring rates become?
6. Assuming that the material of Question 1 is neo-Hookean ($W_2 = 0$), what tensile stress is required to maintain a tensile strain of 100%? What “engineering” stress is required?
7. A rubber balloon is 25 mm in radius and 1 mm in wall thickness. The rubber compound has a shear modulus G of 0.5 MPa. What pressure is necessary to inflate the balloon to a radial expansion ratio of 2 (i.e., by 100%)? Assume that the material is neo-Hookean (i.e., that the second term W_2 in the strain energy function is zero).
8. A solid rubber cylinder with a radius of 10 mm and a length of 20 mm is twisted through an angle of 90°. What torque is required if the shear modulus G is 0.5 MPa? What end force must be applied to prevent the cylinder from extending as it is twisted? Assume that the material is neo-Hookean (i.e., that the second term W_2 in the strain energy function is zero).

■ Answers to Selected Problems for Chapter 3

4. Using Eqs. (3.8) and (3.9), we expect an axial stiffness of 0.227 MN/m and a torsional stiffness of 41.9 Nm/rad. [This example points out an important feature of tube springs: by a careful choice of dimensions the stiffnesses in different directions can be varied somewhat independently.]
5. From the basic mechanism of rubber elasticity, we would expect the elastic modulus to *increase* in direct proportion to absolute temperature (see Eqs. (3.5) and (3.83)). All the spring rates would then rise accordingly, by a factor of 373/298, or about 25%. However, there are two reasons for expecting a smaller effect than this in practice: most rubbery polymers show a somewhat smaller dependence on temperature than the ideal result, and most practical compounds contain a reinforcing (and stiffening) filler, usually carbon black, which loses much of its stiffening power as the temperature is increased. For a lightly-filled compound, with a shear modulus of about 0.5 MPa, the stiffness would increase by about 20% as a result of the increased thermal energy of rubber molecules, whereas for a rather highly filled compound, containing, say, 50 parts by weight of carbon black per 100 parts by weight of rubber, and with a shear modulus of about 2 MPa, the stiffness would actually *decrease* slightly, instead of increasing.
7. From Eq. (3.72), the pressure when $\lambda = 2$ is given by $P = 0.0788 W_1$, where the coefficient W_1 is given by $G/2$ ($= 0.25$ MPa) on putting $W_2 = \text{zero}$. Thus, $P = 1.97$ kPa. However, to reach this degree of expansion, the balloon must be inflated through the expansion ratio of 38% at which the pressure reaches a maximum. The maximum pressure is obtained from Eq. (3.72) as 2.10 kPa.
8. From Eq. (3.64), the expected torque is 0.617 N-m. The corresponding normal force is obtained by integrating the normal stress, from Eq. (3.65), over the end surface of the cylinder yielding the result: $2 \pi a^4 (W_1 + 2 W_2) \psi^2$.

Thus, the normal force is 97 N in the present case.

4

Dynamic Mechanical Properties

Alan N. Gent, Kenneth W. Scott

■ 4.1 Introduction

The preceding chapter on rubber elasticity was concerned mainly with the ideal behavior of elastomers that are assumed to follow reversible relations between load and displacement. In practice, deviations from such ideal elastic behavior are to be expected. No material is perfectly elastic – they all exhibit some dissipation of the energy expended in deforming them. When subjected to a stress cycle, the stress-strain curve is a hysteresis loop instead of a reversible curve, with the deformation lagging behind the stress as the stress increases and again as the stress decreases. The difference between the loading and unloading curves reflects mechanical energy lost in internal dissipation processes, such as viscous flow or internal bond-breaking induced by stress. All elastomers show some viscous behavior. While this is desirable for shock damping applications, many industrial problems are a consequence of an excessive viscous response. Such common phenomena as stress relaxation, creep, compression set, and unrecovered deformations in general, mechanical irreversibility and energy losses during a deformation cycle (“hysteresis”), limited rebound, heat generation, and temperature rise during flexing are all manifestations of the viscous properties of elastomers. These processes are usually strong functions of test temperature and frequency of oscillation also, as described later.

Note that in the study of internal energy dissipation (the main topic of this chapter) a sample is assumed to deform homogeneously, with every part undergoing the same cycle of stress and deformation. But this is not the case when the stress is changed abruptly and a stress pulse is transmitted. The deformation is then markedly non-uniform, with one part of the sample being stressed more than a neighboring part. Some features of the propagation of stress waves in rubber are discussed in the following section, before we turn to energy dissipation, and visco-elastic losses in particular, in homogeneously-deformed rubbery solids.

■ 4.2 Stress Waves in Rubbery Solids, Transit Times, and Speeds of Retraction

The general equation for the speed v_s of transmission of a stress pulse in an elastic solid is

$$v_s^2 = \frac{S}{\rho} \quad (4.1)$$

where S denotes the appropriate modulus of elasticity and ρ is the density of the solid. For a dilatational pulse, accompanied by volume changes, S is the modulus K of bulk compression, with a typical value for elastomers of about 2 GPa, and hence the speed of a dilatational stress pulse in a rubbery solid having a density of about 10^3 kg/m^3 is about 1.4 km/s. On the other hand, transmission of a distortional shear pulse is much slower, because the shear modulus is much smaller, typically only about 1 MPa, and therefore a shear stress pulse travels with a velocity of only about 32 m/s. Moreover, shear waves are heavily damped in comparison with dilatational waves. Thus the fast, penetrating acoustic waves used for examining rubber for internal defects are primarily dilatational waves.

What is the effect of the finite velocity of stress waves in vibration experiments? Typically, in tests where the sample is subjected to a oscillatory deformation, the sample is assumed to deform homogeneously. But this requires rapid transmission of stresses across the sample. If the frequency of oscillation is, say, 100 Hz, with a period of oscillation of 10 ms, then for a homogeneous response, a stress wave would have to pass from one side of the sample to the other in a small fraction of this time, say in 1% of the period, or 100 μs . Thus, for a typical wave velocity of about 40 m/s, the sample thickness would need to be smaller than about 4 mm. And even thinner samples are needed to show approximately homogeneous deformations at higher frequencies. In this context, it is interesting to consider the speed of retraction of a stretched strip of rubber, Fig. 4.1.

At the instant the strip is released, an unloading pulse starts at the released end and begins to propagate along the strip. Ahead of this pulse the rubber is still in its original state, at a tensile strain of ϵ and tensile stress τ , while behind it the rubber has become virtually unstrained and is moving at the retraction velocity v_r .

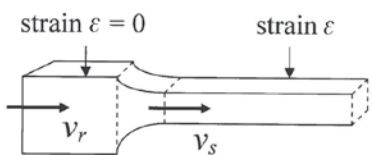


FIGURE 4.1 Retraction of a stretched strip

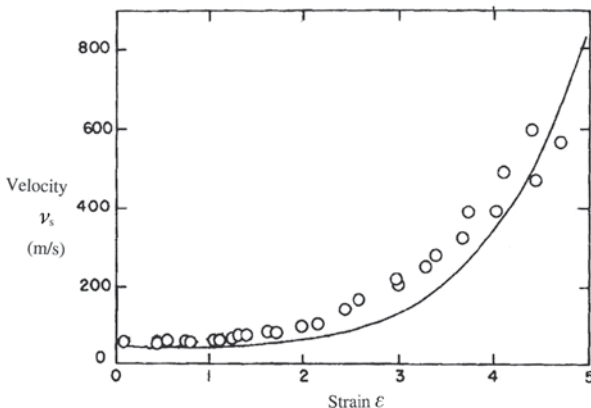


FIGURE 4.2 Velocity v_s of the retraction front vs. extension ϵ for a strip of unfilled natural rubber [2]

The pulse itself may be thought of as a transition region in which the strain is a complicated function of time and position. The leading edge moves through the strip at the velocity v_s of sound, obtained from Eq. (4.1) on taking into account the *incremental* tensile modulus of a stretched strip E_e and the contribution of the tensile stress τ itself.

$$v_s^2 = \frac{E_e + \tau}{\rho} \quad (4.2)$$

This relation is equivalent to that derived by Mason [1] for the velocity of an unloading pulse in a stretched strip, and in the small-strain limit it reduces to Eq. (4.1) with S replaced by the small-strain tensile modulus E . The incremental modulus E_e in Eq. (4.2) is given by the slope of the curve relating true stress τ to tensile strain ϵ . For a sample of unfilled natural rubber, measured values of v_s were found to increase markedly with increasing strain from an initial value of about 55 m/s at zero strain up to about 800 m/s at a strain of 500%, Fig. 4.2. This reflects the increase in incremental modulus. And for a filled rubber sample, v_s was 3 to 10 times higher, depending upon the particular strain used because of its higher modulus.

The velocity v_r of free retraction is related to the velocity of sound in the stretched strip and to the imposed tensile strain ϵ , but corrections are necessary to take into account the rates of motion of the leading and trailing edges of the transition region. At small strains the result is

$$\frac{v_r}{v_s} = \frac{\epsilon}{1 + \epsilon} \quad (4.3)$$

Thus, v_r increases with strain, starting at zero, as shown in Fig. 4.3.

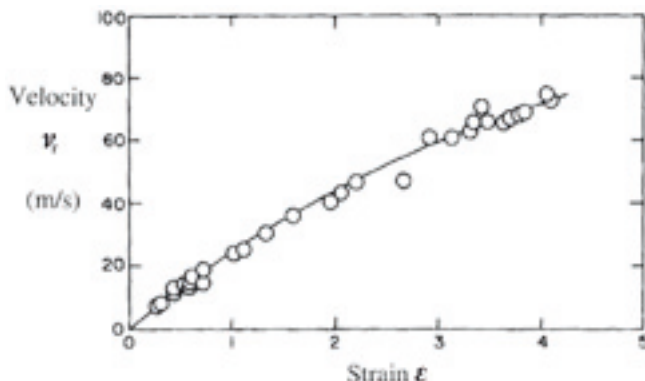


FIGURE 4.3 Velocity v_r of the released end vs. extension ϵ for a strip of unfilled natural rubber [2]

Note that no allowance has been made for dissipative processes in the above discussion. Rate effects have been assumed to arise solely from inertia, and rubber has been treated solely as a non-linear *elastic* solid, with an incremental modulus that depends upon the applied strain. These assumptions account satisfactorily for the speed of stress pulses and rates of retraction without invoking loss processes. We now turn to the effect of loss processes on the behavior of rubber. In this case, the rate of deformation is assumed to be *proportional* to the applied stress; i.e., *linear* visco-elastic behavior is assumed. This implies that the rates of deformation are small compared to any natural frequency of the molecules themselves. Non-linear viscoelasticity is beyond the scope of this chapter.

■ 4.3 Viscoelasticity

An ideal linear elastic solid obeys Hooke's law: stress is proportional to strain. An ideal viscous liquid obeys Newton's law: stress is proportional to rate of change of strain with time. Many materials, and elastomers in particular, have properties intermediate between these two cases. The response of these materials, which act neither as ideal elastic solids nor as ideal liquids, is termed viscoelastic behavior. A Hookean solid may be illustrated by a spring and Hooke's law can be written in the form:

$$F = k x \quad (4.4)$$

where F is force, x is deformation, and k is the spring constant. Newton's law of viscosity may be written in the form:

$$F = c \left(\frac{dx}{dt} \right) \quad (4.5)$$

where c is a viscous damping coefficient. Newtonian viscous behavior is usually illustrated by a viscous element called a dashpot. The laws above may be written alternatively as

$$\sigma = E \varepsilon \quad (4.6)$$

and

$$\sigma = \eta_e \left(\frac{d\varepsilon}{dt} \right) \quad (4.7)$$

where σ is tensile stress, ε is tensile strain, E is the elastic tensile modulus (see the preceding chapter), and η_e is the Newtonian viscosity coefficient in tension. For an incompressible fluid, the tensile viscosity η_e is three times the shear viscosity η . This result is exactly equivalent to the relation between tensile modulus E and shear modulus G for an incompressible elastic solid: $E = 3G$.

Traditionally, viscoelastic behavior has been described by means of phenomenological approaches. Table 4.1 summarizes the simplest of these, employing Maxwell and Voigt elements (Fig. 4.4). Most materials exhibit behavior that is more complex than that of either of these two simple models. For this reason, it is necessary to use generalized models to describe the viscoelastic behavior of a material quantitatively.

TABLE 4.1 Behavior of Viscoelastic Elements

	Maxwell representation (series)	Voigt representation (parallel)
Equation of motion	$\frac{dx}{dt} = \frac{1}{k} \left(\frac{dF}{dt} \right) + \frac{F}{C}$	$F = k x + c \left(\frac{dx}{dt} \right)$
Additive terms	Deformations	Forces
Equal terms	Forces	Deformations
$\tau = c/k$	Relaxation time	Retardation time
Stress relaxation ($dx/dt = 0$ or $x = a$ constant)	$F = F_0 e^{-t/\tau}$	$F = k x$
Creep ($dF/dt = 0$ or $F = a$ constant)	$x = x_0 + \frac{F t}{c}$	$x = \left(\frac{F_0}{k} \right) \left(1 - e^{-t/\tau} \right)$
Constant rate of deformation ($dx/dt = R$)	$F = c R \left(1 - e^{-t/\tau} \right)$	$F = R \left(c + k t \right)$

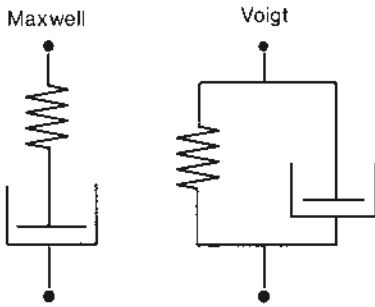


FIGURE 4.4 Models of viscoelastic materials

TABLE 4.2 Generalized Maxwell Model

Stress relaxation modulus	$E(t) = \frac{\sigma(t)}{\varepsilon_0} = \int_0^{\infty} E(\tau) e^{-t/\tau} d\tau = \int_{-\infty}^{\infty} \bar{H}(\ln \tau) e^{-t/\tau} d\ln \tau$
Dynamic modulus	$\begin{aligned} E_1(\omega) &= \int_{-\infty}^{\infty} E(\tau) \left(\frac{\omega^2 \tau^2}{1 + \omega^2 \tau^2} \right) d\tau \\ &= \int_{-\infty}^{\infty} \bar{H}(\ln \tau) \left(\frac{\omega^2 \tau^2}{1 + \omega^2 \tau^2} \right) d\ln \tau \end{aligned}$
Imaginary modulus	$\begin{aligned} E_2(\omega) &= \omega \eta(\omega) = \int_0^{\infty} E(\tau) \left(\frac{\omega \tau}{1 + \omega^2 \tau^2} \right) d\tau \\ &= \int_{-\infty}^{\infty} \bar{H}(\ln \tau) \left(\frac{\omega \tau}{1 + \omega^2 \tau^2} \right) d\ln \tau \end{aligned}$
Creep compliance	$\begin{aligned} D(t) &= \frac{\varepsilon(t)}{\sigma_0} = \int_0^{\infty} D(\tau) \left(1 - e^{-t/\tau} \right) d\tau \\ &= \int_{-\infty}^{\infty} \bar{L}(\ln \tau) \left(1 - e^{-t/\tau} \right) d\ln \tau \end{aligned}$
Stress at constant rate of strain	$\sigma(t) = \dot{\varepsilon} \int_{-\infty}^{\infty} \tau \bar{H}(\ln \tau) \left(1 - e^{-t/\tau} \right) d\ln \tau$
Steady state flow viscosity	$\eta_0 = \int_0^{\infty} \tau E(\tau) d\tau = \int_{-\infty}^{\infty} \tau \bar{H}(\ln \tau) d\ln \tau$
Approximate relations	$\begin{cases} \left[\bar{H}(\ln \tau) \right]_{\tau=1} \approx - \frac{dE(t)}{d(\ln t)} \\ \left[E(\tau) \right]_{\tau=1/\omega} \approx - \frac{dE_1(\omega)}{d(1/\omega)} \\ \left[\bar{H}(\ln \tau) \right]_{\tau=1/\omega} \approx - \frac{dE_1(\omega)}{d(\ln 1/\omega)} \approx \frac{2}{\pi} E_2(\omega) \\ E(t = 0.56/\omega) \approx E_1(\omega) \end{cases}$

A generalized Maxwell model consists of an infinite number of simple Maxwell elements in parallel and is characterized by the so-called distribution of elastic moduli $E(\tau)$ as a function of the relaxation time $\tau = \eta_e/E$ of the simple Maxwell elements. The generalized Voigt model consists of an infinite number of simple Voigt elements in series and is described by the distribution of compliances $D(\tau)$ as a function of the retardation time $\tau (= \eta_e/E)$ of the simple Voigt elements. Both these models (and other generalized systems) are completely equivalent and, in theory, any one may be used to describe all linear viscoelastic behavior. (Linear viscoelastic behavior means that the Boltzmann superposition principle applies; i.e., strain due to the action of a number of stresses $\sigma = \sigma_1 + \sigma_2 + \sigma_3 + \dots$, is equal to the sum of the strains $\varepsilon_1, \varepsilon_2, \varepsilon_3, \dots$ that would be developed as a result of σ_1 acting alone, σ_2 acting alone, σ_3 acting alone, etc.) In practice, it is more convenient to describe stress relaxation experiments by a generalized Maxwell model and creep experiments by a generalized Voigt model. Dynamic mechanical experiments can be described equally well by either generalized model, although the Voigt model is commonly used.

Table 4.2 summarizes relations between the distribution of relaxation times and viscoelastic properties and gives some approximate formulas for determining the distribution of relaxation times from experimental data. Note that the distributions of relaxation times are represented by the functions H and L , defined in terms of a logarithmic time scale, because this is more convenient for viscoelastic solids whose response changes over many decades in time. For a continuous spectrum of Maxwell elements, H is defined by the relation for time-dependent modulus $E(t)$:

$$E(t) = \int_{-\infty}^{\infty} \bar{H} \exp(-t/\tau) d \ln \tau \quad (4.8)$$

Similarly, for a continuous distribution of Voigt elements, the function \bar{L} describing the spectrum of retardation times is defined by the relation for time-dependent tensile compliance $D(t)$:

$$D(t) = \int_{-\infty}^{\infty} \bar{L} [1 - \exp(-t/\tau)] d \ln \tau \quad (4.9)$$

The distribution of relaxation or retardation times may be determined from one linear viscoelastic experiment and then used to calculate the behavior in all other viscoelastic experiments. This phenomenological approach has been quite successful in correlating the results of different types of measurement. It is discussed in detail in [3].

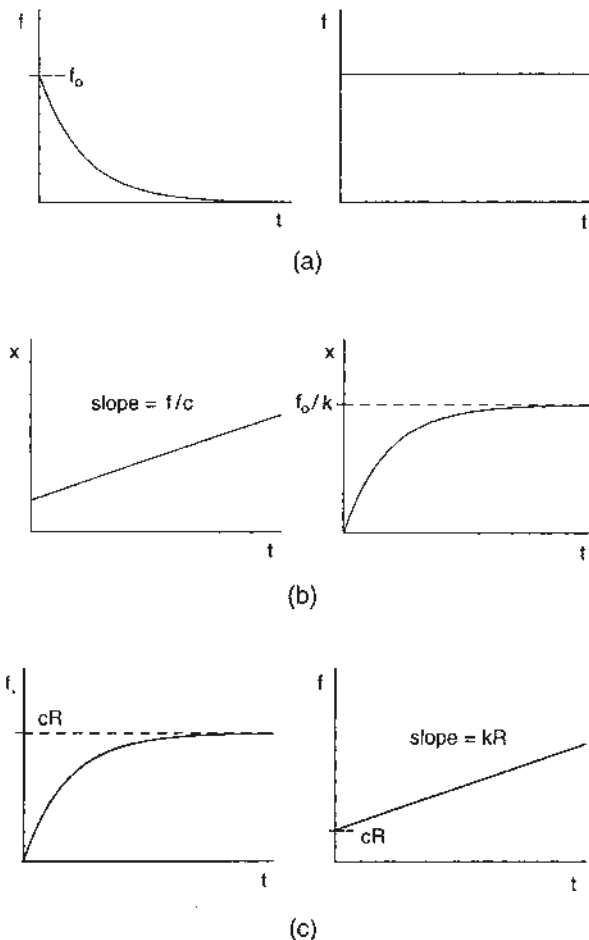


FIGURE 4.5 Behavior of Maxwell and Voigt elements: (a) stress relaxation, (b) creep, and (c) force required to maintain a constant rate R of deformation

4.4 Dynamic Experiments

The term “dynamic mechanical properties of elastomers” refers to the behavior of these materials when subjected to stresses or strains that change with time. For example, in creep experiments one measures the increase in strain with time, the stress being held constant, whereas in stress relaxation experiments one measures the decrease in stress with time under constant strain conditions. Here we shall discuss only the special case of sinusoidally varying stresses and strains. Moreover, we will restrict ourselves to linear viscoelastic systems.

An oscillatory dynamic experiment differs from simple creep and stress relaxation studies in two important respects. First, the time scale is determined inversely by the frequency of the sinusoidal deformation. Second, stress and strain are not in phase in a dynamic experiment; hence, in addition to the ratio of stress to strain, the phase difference or phase angle between them is measured. The phase angle depends on the dynamic viscosity and becomes zero when the viscosity is zero.

Figure 4.6 illustrates the concept of a phase angle. For a perfect spring, the force (stress) and deformation (strain) are in phase (zero phase angle), but for a dashpot the force leads the deformation by $\pi/2$ radians (90°). A viscoelastic material having properties partly of a spring and partly of a dashpot has an intermediate phase angle.

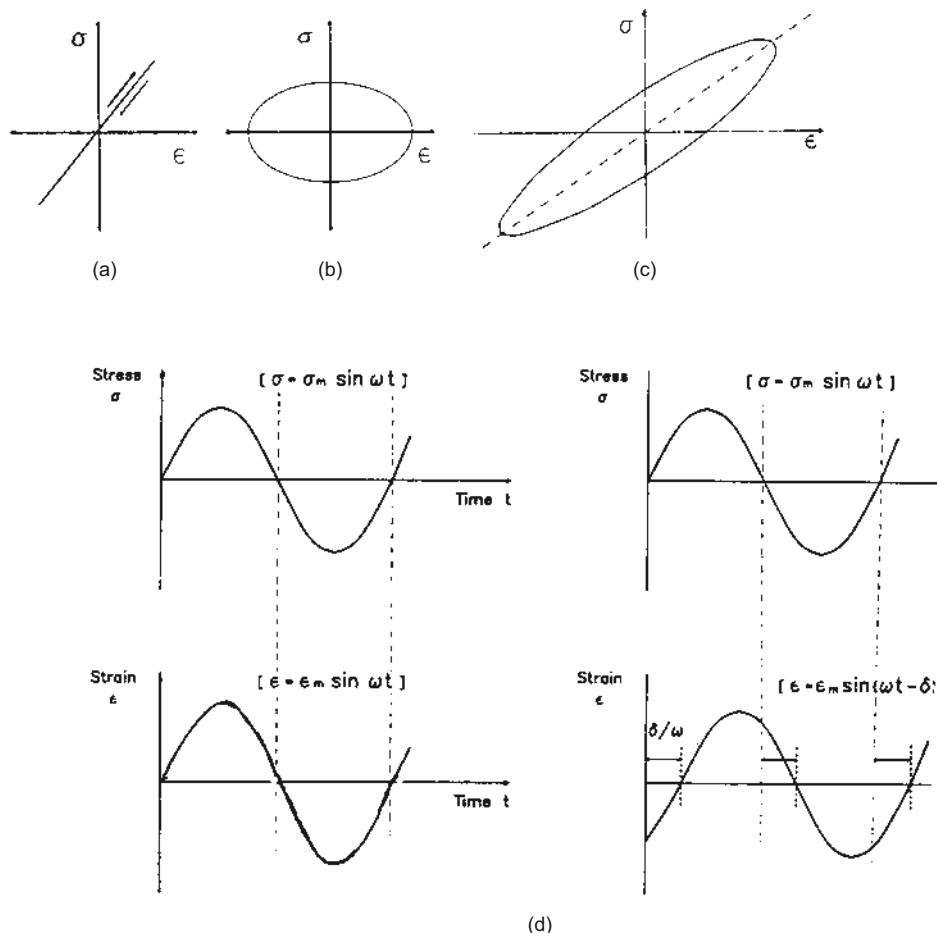


FIGURE 4.6 (a) Relation between instantaneous stress σ and instantaneous strain ϵ for a perfectly elastic solid subjected to an alternating stress. (b) Relation for a simple viscous liquid. (c) Relation for a viscoelastic solid. (d) Relation between stress σ and time, and strain ϵ and time, for a perfectly elastic solid, compared with that for a viscoelastic solid

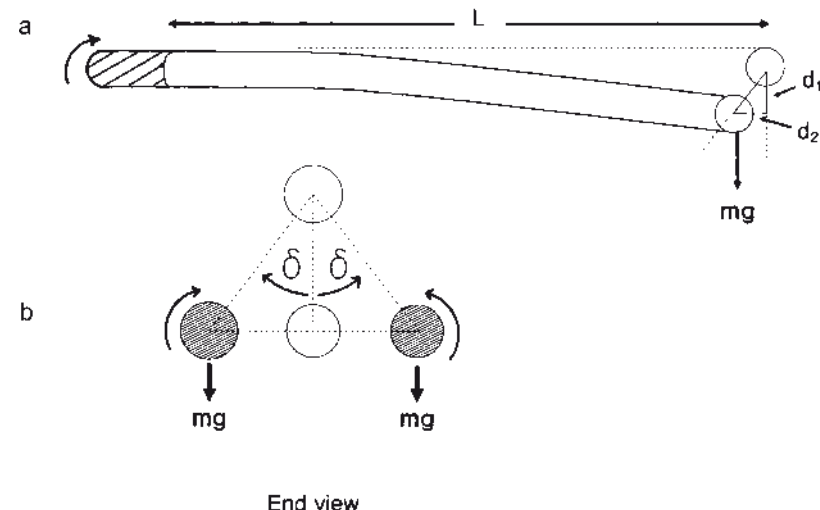


FIGURE 4.7 Vertical (d_1) and horizontal (d_2) displacements of a rotating cantilever

A good example of delayed elastic response is given by the steady rotation of a weighted horizontal cantilever (Fig. 4.7). When the cantilever is stationary, the weighted end hangs vertically below the horizontal axis of rotation, by a distance d that is inversely related to the (static) modulus of elasticity. The exact relation is given by the bending equation for an elastic cantilever:

$$d = \frac{F L^3}{2(1+\nu) E I} \quad (4.10)$$

where F is the applied force (mg), L is the length of the cantilever, ν is Poisson's ratio (see preceding chapter), and I denotes the second moment of area of the cantilever cross section. For a circular cross-section of radius a , $I = \pi a^4/4$, and for a square cross-section, of side length W , $I = W^4/12$. Note that cantilevers of circular and square cross-sections have values of I that are independent of the direction of bending so that cantilevers of this type bend to the same extent as they rotate around their axis. A view from the front of such a cantilever as it is rotated in a clockwise direction is shown in Fig. 4.7b.

It is found that the weighted end moves laterally to a point displaced somewhat to the left of the axis of rotation (i.e., displaced in the same sense as the rotation itself). When the direction of rotation is reversed, the displacement of the weighted end is reversed (Fig. 4.7b). Simultaneously, the vertical deflection d becomes somewhat smaller (d_1), reflecting the fact that the dynamic modulus E_1 is greater than the equilibrium (static) value E .

Sideways displacement of the cantilever end takes place upon rotation because bending stresses are imposed (by gravity) in a vertical direction. All materials are viscoelastic to some degree, and bending strains therefore do not occur exactly in phase with the applied stresses, but are delayed in time. As a result, maximum bending takes place after the maximum stress has passed, when rotation has carried the cantilever end past the axis of rotation. In fact, the angular displacement of the cantilever from a straight-through position is the phase angle δ and the lateral displacement d_2 from the vertical is inversely related to loss modulus E_2 by Eq. (4.10). This simple but elegant example of delayed elasticity has been used for experimental measurements of the dynamic properties of metals [4], plastics [5], and rubber [6]. A close parallel exists between dynamic mechanical theory and alternating current theory. In a reactive circuit, voltage and current are out of phase and the electrical loss factor is given in terms of the electrical loss tangent. Similarly $\tan \delta$ will determine the mechanical energy losses and is termed the mechanical loss tangent or factor. The whole notation system for dynamic mechanical properties is exactly like that used in alternating current theory. As a result, such terms as complex modulus and imaginary modulus are used. These terms are difficult to understand in a mechanical sense and they can cause confusion for the novice. We shall now show how they arise.

Consider the Voigt element in terms of stress σ and strain ε . Then

$$\sigma = E \varepsilon + \eta_e \left(\frac{d\varepsilon}{dt} \right) \quad (4.11)$$

(Hereafter we will use the symbol η for the tensile viscosity η_e .) Let a strain be applied that varies with time in a sinusoidal way so that

$$\varepsilon = \varepsilon_0 \sin \omega t \quad (4.12)$$

where ε_0 is the strain amplitude. We now introduce the complex relation (complex in a mathematical sense only):

$$\varepsilon = \varepsilon_0 \exp(i \omega t) = \varepsilon_0 (\cos \omega t + i \sin \omega t) \quad (4.13)$$

where $i = (-1)^{1/2}$. Since by Eq. (4.12) we are interested only in the dependence of ε on $\sin \omega t$, this means that we are interested only in the imaginary part of Eq. (4.13). (If Eq. (4.12) had been $\varepsilon = \varepsilon_0 \cos \omega t$, we would have been concerned only with the real part of Eq. (4.13).)

The rate of change of strain with time is given by

$$\frac{d\varepsilon}{dt} = i \omega \varepsilon_0 \exp(i \omega t) = i \omega \varepsilon \quad (4.14)$$

Substituting in Eq. (4.11), we obtain

$$\omega = (E + i \omega \eta) \varepsilon \quad (4.15)$$

The term in parentheses in Eq. (4.15) is some type of modulus because it is the ratio of a stress to a strain. It is denoted the complex dynamic modulus E^* . Since E , denoted hereafter E_1 , is the real part of this complex number, it is sometimes referred to as the real dynamic modulus. Likewise $\omega \eta$ is defined as the imaginary dynamic modulus, given the symbol E_2 . Thus, in these terms we may rewrite Eq. (4.15) as follows:

$$\sigma = (E_1 + i E_2) \varepsilon = E^* \varepsilon \quad (4.16)$$

Equation (4.16) defines the real, imaginary, and complex moduli. In practice, E_1 and E_2 alone are sufficient. The following equations are alternative definitions for the real and imaginary components of the complex dynamic modulus:

$$E_1 = \frac{\text{component of stress in phase with strain}}{\text{strain}} \quad (4.17)$$

and

$$E_2 = \frac{\text{component of stress } 90^\circ \text{ out of phase with strain}}{\text{strain}} \quad (4.18)$$

The absolute value of the complex modulus is given by the ratio of stress amplitude σ_0 to strain amplitude ε_0 . Thus

$$E^* = \frac{\sigma_0}{\varepsilon_0} = (E_1^2 + E_2^2)^{1/2} = E_1 \left[1 + (\tan \delta)^2 \right]^{1/2} \quad (4.19)$$

For values of $\tan \delta$ less than 0.2, the error will be less than 2% if we equate the dynamic modulus E_1 with $\sigma_0/E \varepsilon_0$.

■ 4.5 Energy Considerations

The maximum energy U_m stored in a sample per unit volume during a (half) cycle and the energy U_d dissipated in a complete strain cycle per unit volume are given by

$$U_m = \frac{1}{2} E_1 \varepsilon_0^2 \quad (4.20)$$

and

$$U_d = \pi E_2 \varepsilon_0^2 \quad (4.21)$$

Table 4.3 summarizes the relations above.

TABLE 4.3 Relations Between Dynamic Properties: E_1 and E_2 Are Taken as the Primary Parameters

$$\frac{\sigma_0}{\varepsilon_0} = E^* = (E_1^2 + E_2^2)^{1/2} = E_1$$

$$\omega \eta = E_2$$

$$E^* = E_1 + i E_2$$

$$\tan \delta = \frac{E_2}{E_1}$$

Loss in energy per cycle:

$$U_d = \pi E_2 \varepsilon_0^2 = \pi E_1 (\tan \delta) \varepsilon_0^2 \approx \frac{\pi \sigma_0^2 (\tan \delta)}{E_1}$$

$$\frac{\text{Loss in energy per cycle } (U_d)}{\text{Twice the maximum energy stored in each half-cycle } (2 U_m)} = \pi \tan \delta$$

(for a strain cycle about the point (0,0))

Half-power width of resonance curve, $\Delta w / \omega_r := \tan \delta$

Logarithmic decrement of free vibrations $\Delta := \pi \tan \delta$

Rebound resilience (percent of energy returned) $R = 100 e^{-\Delta} \equiv 100 e^{-\pi \tan \delta}$

Real dynamic compliance D_1 (in-phase strain/stress) = $\frac{E_1}{E_1^2 + E_2^2}$

Imaginary dynamic compliance D_2 (90° out of phase strain/stress) = $\frac{E_2}{E_1^2 + E_2^2}$

$$D^* (= D_1 - i D_2) = \frac{1}{E^*}$$

$$\tan \delta = \frac{D_2}{D_1}$$

Dynamic shear modulus $G_1 = \frac{E_1}{3}$

Imaginary dynamic shear modulus $G_2 = \frac{E_2}{3}$

Dynamic shear viscosity $\omega \eta = G_2$

■ 4.6 Motion of a Suspended Mass

The equation of motion used to analyze dynamic experiments is

$$m \left(\frac{d^2x}{dt^2} \right) + c \left(\frac{dx}{dt} \right) + k x = F_0 \sin \omega t \quad (4.22)$$

where m is the mass attached to a Voigt element. It has been shown theoretically that Eq. (4.22) describes the behavior of a linear viscoelastic material at a given frequency, even when the coefficients c and k are themselves functions of frequency. The solution obtained assuming that c and k are constant is still valid. This feature allows actual elastomers, for which c and k vary with frequency, to be described by Eq. (4.22). The steady state solution is

$$x = \frac{F_0 \sin(\omega t - \psi)}{\left[(k - m \omega^2)^2 + (\omega c)^2 \right]^{1/2}} \quad (4.23)$$

where

$$\tan \psi = \frac{\omega c}{k - m \omega^2} \quad (4.24)$$

Note that the tangent of the phase angle of the system (sample + mass) is different from the loss tangent for the sample alone, $\tan \delta = E_2 / E_1 = \omega c / k$. At low frequencies, when k is much larger than $m \omega^2$, they are equivalent, but at high frequencies the mass term becomes dominant and $\tan \psi = \tan \delta = -c / m \omega$.

From Eq. (4.23) the strain amplitude is

$$x_0 = \frac{F_0}{\left[(k - m \omega^2)^2 + (\omega c)^2 \right]^{1/2}} \quad (4.25)$$

illustrated in Fig. 4.8. The amplitude reaches a maximum value at resonance, at an angular frequency ω_r given by

$$m \omega_r^2 = k - \frac{c^2}{2m} \quad (4.26)$$

and then has the value

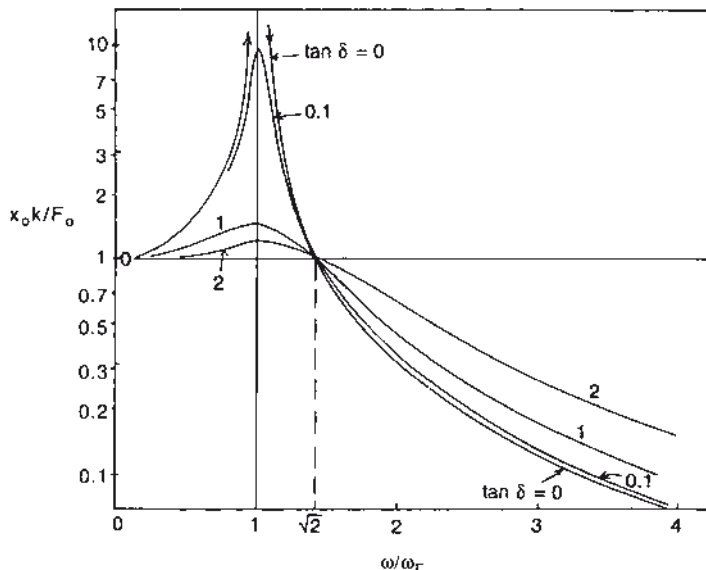


FIGURE 4.8 Amplitude of oscillation for a suspended mass as a function of oscillation frequency ω

$$x_0 (\max) = \frac{F_0}{\left[(\omega_r c)^2 + (c^2 / 2 m)^2 \right]^{1/2}} \quad (4.27)$$

In a forced resonance vibration experiment, the measured terms are x_0 (max), F_0 , ω_r , and m . Equations (4.26) and (4.27) are used to calculate c and k . For values of $\tan \psi$ less than 0.14, the error is less than 1%, if we use

$$k = m \omega_r^2 \quad (4.28)$$

and

$$c \omega_r = \frac{F_0}{x_0 (\max)} \quad (4.29)$$

In a forced nonresonance vibration experiment, the measured terms are x_0 , F_0 , m , ω , and the phase angle ψ , which permit the calculation of spring constant k and damping coefficient c from Eqs. (4.24) and (4.25). For frequencies of less than one-tenth of the resonance frequency, Eqs. (4.24) and (4.25) are less than 1% in error, if simplified to

$$\tan \delta = \tan \psi \quad (4.30)$$

and

$$k = \frac{F_0}{x_0 \left[1 + (\tan \psi)^2 \right]^{1/2}} \quad (4.31)$$

The third type of dynamic experiment is free vibration. No external force acts, $F = 0$, and Eq. (4.22) becomes

$$m \left(\frac{d^2 x}{dt^2} \right) + c \left(\frac{dx}{dt} \right) + k x = 0 \quad (4.32)$$

The solution for values of c less than the critical damping value $2(mk)^{1/2}$ is

$$x = A \exp \left(\frac{-c t}{2m} \right) \cos(\omega t - \alpha) \quad (4.33)$$

where

$$\omega^2 = \frac{k}{m} - \left(\frac{c}{2m} \right)^2 \quad (4.34)$$

and A and α are constants determined by the initial deformation and velocity given to the system. Equation (4.33) represents a damped sinusoidal oscillation (Fig. 4.9). Introducing the logarithmic decrement Δ , defined as the natural logarithm of the ratio of two successive amplitudes of swing,

$$\Delta = \ln \left(\frac{x_{0,n}}{x_{0,n+1}} \right) = \frac{c}{2m f} \quad (4.35)$$

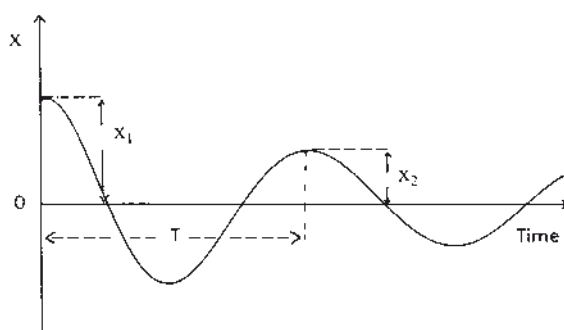


FIGURE 4.9 Amplitude of oscillation versus time for a freely-oscillating suspended mass

where f is the frequency in Hertz, we obtain

$$x_n = A \exp(-n \Delta) \cos(\omega t - \alpha) \quad (4.36)$$

where n is the ordinal number of the oscillation.

Successive amplitudes of the damped sinusoidal oscillation take values

$$x_n = A \exp(-n \Delta) \quad (4.37)$$

Thus, Δ is given by the negative slope of a plot of $\ln(x_n)$ versus n . The loss tangent is given by

$$\tan \delta = \frac{\Delta / \pi}{1 + (\Delta / 2\pi)^2} \approx \frac{\Delta}{\pi} \quad (4.38)$$

while

$$k = (2\pi f)^2 m \left[1 + \left(\frac{\Delta}{2\pi} \right)^2 \right] \approx (2\pi f)^2 m \quad (4.39)$$

and

$$c = 2m f \Delta \quad (4.40)$$

The approximations given in Eqs. (4.38) and (4.39) are good to 1% for values of $\tan \delta$ less than 0.2.

To determine material constants for longitudinal or shear deformation experiments, the following substitutions should be made in the appropriate equations:

$$k = \frac{E_1 A}{L} \text{ or } \frac{G_1 A}{L} \quad (4.41)$$

and

$$\omega c (= 2\pi f c) = \frac{E_2 A}{L} \text{ or } \frac{G_2 A}{L} \quad (4.42)$$

where A is the cross-sectional area of the sample and L is its length or height. For experiments performed in torsion, the moment of inertia I of the torsionally oscillating attached mass is substituted for m in Eqs. (4.22) to (4.40), and k and c are then the torsional stiffness and damping coefficients. Thus, for torsion of a rectangular strip the shear modulus is given [7] by:

$$G_1 = \frac{3 L I \omega^2}{W T^3} \left[1 - 0.63 \left(\frac{T}{W} \right) \right] \quad (4.43)$$

for $W > 2 T$, where W is the width, T the thickness and L the length; $\tan \delta$ is dimensionless and therefore always independent of sample dimensions.

■ 4.7 Experimental Techniques

Several excellent reviews of experimental techniques for determining dynamic mechanical properties are available [8–11].

4.7.1 Forced Nonresonance Vibration

In theory, at least, the forced nonresonance vibration method has the greatest flexibility, particularly with respect to useful frequency range. It is suitable even for extremely high loss materials, for example, in the glass transition region. However, the precision of mechanical loss measurements for values of $\tan \delta$ less than about 0.05 is poor if the phase angle is determined by direct measurement or from the area of a stress-strain ellipse (Fig. 4.6), representing the energy dissipated per strain cycle ($= U_d$, Eq. (4.21)). Research instruments are available based on linear transducers or torsional excitation. They give precise measurements on relatively small samples.

4.7.2 Forced Resonance Vibration

Forced resonance vibration instruments are compact and easy to operate, and they permit the rapid calculation of dynamic properties. Their disadvantages are the need for careful frequency adjustment, limited frequency range (usually between 10 and 500 Hz), and sometimes a lack of adequate power for measurements on stiff materials (e.g., filled rubber compounds at low temperatures). Instruments of this kind have been extensively used for dynamic measurements in compression or shear, and the torsional pendulum has also been adapted for forced vibrations.

4.7.3 Free Vibration Methods

The instruments used for free vibration methods are simple to construct and operate, and they can be adapted to a wide variety of materials. They are highly accurate for measuring low energy loss materials. They have the same frequency limitations as forced resonance vibration methods and are mostly used at frequencies below 10 Hz. They have been used for longitudinal, compression, shear, and torsional deformations.

4.7.4 Rebound Resilience

Measurements of rebound resilience are made by, for example, impacting the upper surface of a rubber block with a free-falling rigid ball and determining the relative amount R of kinetic energy retained after impact, $R = h_2/h_1$, from the height h_2 of rebound relative to the initial height h_1 . Another arrangement employs a rigid rod with a hemispherical end swinging in a vertical plane (Fig. 4.10) and impacting a rubber block at the lowest point of its swing. Again, the relative amount R of retained kinetic energy is determined. Note that energy imparted to the impacting device in the form of mechanical vibrations set up on impact should not be ascribed to energy losses in the rubber.

R is an inverse measure of the loss properties of the material. If an impact is regarded as one half-cycle of a steady oscillation, then Eqs. (4.36) and (4.38) yield

$$\ln R = -\pi \tan \delta \quad (4.44)$$

Because it is based on rather severe assumptions, Eq. (4.44) must be considered to be a rough approximation only. This method is extremely simple to set up and operate, and it is widely used to give an indication of loss properties.

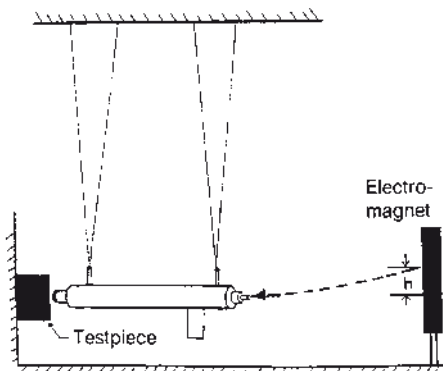


FIGURE 4.10 Method for measuring rebound resilience

4.7.5 Effect of Static and Dynamic Strain Levels

Rubber samples are usually placed under a static compression or extension when measured. These static deformations will have an effect on the observed dynamic properties. Partly, this is because the shape of the sample is changed, so that it becomes effectively a block of different thickness or height. But rubber compounds also show thixotropic effects, especially when filled with carbon black or other stiffening fillers. The elastic modulus is decreased by a previously imposed strain, or by imposing dynamic deformations of increasing amplitude, as described later. Increased energy dissipation accompanies this thixotropic softening, probably associated with the work required to break rubber-filler bonds.

■ 4.8 Application of Dynamic Mechanical Measurements

4.8.1 Heat Generation in Rubber Components

Because the ultimate strength and most other properties of elastomers are diminished at high temperatures, it is desirable to have compounds that generate a minimum of heat in use. The fundamental equation for heat generated per cycle per unit volume of an elastomer undergoing forced sinusoidal vibrations is Eq. (4.21). The amount of heat generated per second is given by $f U_d$, where f is the frequency of oscillation.

We must also consider how heat is lost. For example, if heat is generated uniformly within a rubber block of thickness H , and lost by diffusion to the two surfaces, which are assumed to be connected to effective heat “sinks” and thus to remain at a fixed temperature T , then the maximum temperature reached in the center of the block, at steady state, will be

$$T_m = T + \frac{f U_d H^2}{8 K} \quad (4.45)$$

where K is the coefficient of thermal conduction for rubber.

It is clear that conduction of heat plays an important role in determining the temperature rise. Unfortunately, the value of K is rather insensitive to the choice of elastomer. All elastomers are poor conductors of heat, with values of K of about 0.2–0.3 W/m °C. Even when good conductors – for example, metal powders – are added to rubber compounds, they do not cause a significant increase in K .

The reason is that the particles become surrounded by a layer of rubber and do not form good conducting paths.

It should also be noted that the amount of heat generated per cycle depends strongly on the amplitude ϵ_0 of oscillation (Eq. (4.21)). Thus, when a rubber component is subjected to oscillations of constant load amplitude, a stiffer compound will show less heat generation and a smaller temperature rise owing to the smaller amplitude of oscillation. Because the dependence on strain amplitude is so marked, this effect may well override changes in loss properties. On the other hand, for service conditions that impose a fixed amplitude of oscillation, the material with lower loss modulus will be superior.

Solid tires are an example of an application of rubber in which the load amplitude is fixed. In rubber belting, on the other hand, the amplitude of strain (bending) is fixed by details of the application. Materials would therefore be chosen for these two uses on quite different grounds.

4.8.2 Vibration Isolation

Vibration isolators are basically suspension springs, chosen to give the suspended mass a low resonant frequency, lower by a factor of 3 or more than the exciting or operating frequency. As a result, the amplitude of motion is small (Eq. (4.25), with k chosen to be small).

4.8.3 Shock Absorbers

Shock absorbers are rubber snubbers or cushions, designed to arrest a moving object with minimum load transmission. They act by decelerating the moving mass with a resistive force, and thus they are chosen to have a particular (dynamic) stiffness and to be able to undergo a sufficiently large deflection to bring the mass to rest. It is frequently advantageous for them to have a nonlinear elastic response, softening as the deflection increases, so that the resistive force is large over most of the deflection range. In this way the shock absorbers can function with minimum displacement. Also, some internal damping is useful to minimize rebound. However, this is not the essential attribute of shock absorbers, even though it is commonly believed that suspension springs and shock absorbers are in some way energy dissipation devices and are therefore chosen on the basis of their loss properties. While energy dissipation is a valuable additional feature preventing continued oscillation and unduly large oscillations if a resonance condition is encountered, it must be recognized that these components are basically springs.

For any application, it is necessary that E_1 , E_2 , or $\tan \delta$ be known at the frequency of loading and at the temperature at which the rubber is to be used, because the dynamic properties may, and often do, depend strongly on these variables, as described in the section that follows.

■ 4.9 Effects of Temperature and Frequency

The main cause of delayed elastic response in rubbery solids is internal viscosity between molecular chains. This property is strongly affected by temperature, as one would expect. It depends primarily on the rate φ at which small segments of a molecule move to new positions as a result of random Brownian motion. The value of φ increases strongly with increasing temperature. As a result, internal viscosity and the energy dissipation it gives rise to are much reduced at high temperatures.

The dependence of φ on temperature T follows a characteristic law [12]:

$$\ln \left[\frac{\varphi(T)}{\varphi(T_g)} \right] = \frac{A(T - T_g)}{(B + T - T_g)} \quad (4.46)$$

where A and B are constants, having approximately the same values, 40 and 50 °C, for a wide range of elastomers, and T_g is a reference temperature at which molecular segments move so slowly, about once in 10 seconds, that for practical purposes they do not move at all and the material becomes a rigid glass. The temperature T_g is denoted the glass transition temperature. It is the single most important parameter determining the temperature and dynamic response of an elastomer. Values of T_g for some common elastomers are given in Table I in the Appendix. Equation (4.46) is represented graphically in Fig. 4.11.

In many dynamic applications, molecular motion is required at frequencies higher than $1/10 \text{ s}^{-1}$. For example, for cushioning an impact, we require virtually complete rubberlike response in a time of impact of the order of 1 ms. But molecular segments will move in 1 ms only when φ reaches a rate of about 1000 jumps per second: that is, only at a temperature about 16 °C higher than T_g (Fig. 4.11). Indeed, for coordinated motion of entire molecular strands, consisting of many segments, to take place within 1 ms, the segmental response frequency must be still higher, by a factor of 100 or so. This rapidity of response is achieved only at a temperature about 30 °C above T_g . Thus, we do not expect rapid, fully rubberlike response until a temperature of more than $T_g + 30 \text{ }^{\circ}\text{C}$ is attained.

On the other hand, for sufficiently slow movements, taking place over several hours or days, say, a material would still be able to respond at temperatures significantly

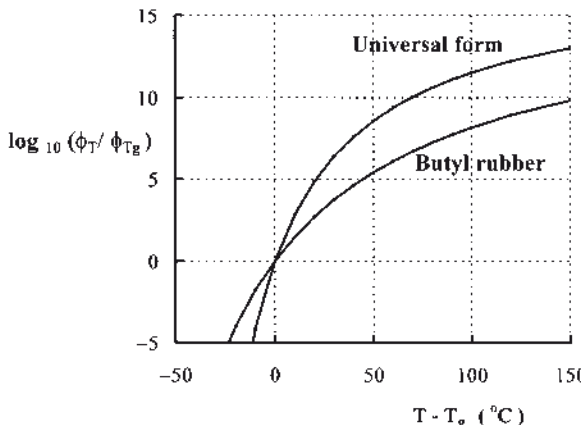


FIGURE 4.11 Dependence of rate φ_T of motion of molecular segments on temperature T (WLF relation); the rate φ_{Tg} at the glass temperature is about 0.1/s

below the conventionally defined glass transition temperature. This region is represented by the portion of the curves below (0,0) in Fig. 4.11. Thus, the conventional glass transition temperature is defined in terms of relatively slow motions, taking place in about one minute, and requiring only small-scale motions of molecular segments rather than motion of entire molecular strands between crosslinks.

The numerical coefficients, 40 and 50 °C, in Eq. (4.46) are about the same for a wide range of elastomers, reflecting the fact that many elastomers have similar values of thermal expansion coefficient and similar sizes for their molecular segments. However, an important exception is polyisobutylene and its common vulcanizable equivalent, butyl rubber. For these materials, the coefficients appear to be about 40 and 100 °C, considerably different from the “universal” values that hold for other common elastomers. This reflects the fact that the rate of segmental motion increases much more slowly above T_g as shown by the second curve in Fig. 4.11. The reason for this peculiarity is probably an unusually large size for the basic moving unit in these polymers.

Equation (4.46) can be used more generally to relate the dynamic behavior at one temperature T_1 to that at another, T_2 . For example, the dynamic modulus E_1 and loss factor $\tan \delta$ are found to depend on the frequency of vibration, as shown schematically in Fig. 4.12. As the imposed frequency is raised, to approach the natural frequency of Brownian motion, the dynamic modulus increases, reaching finally the high value characteristic of glassy solids. At the same time, the dissipation factor rises at first, reflecting increased resistance to molecular motion at high rates, and then falls when the imposed frequency exceeds the natural rate of response and the amplitude of motion becomes less. Eventually, at sufficiently high frequencies, the molecules do not move at all.

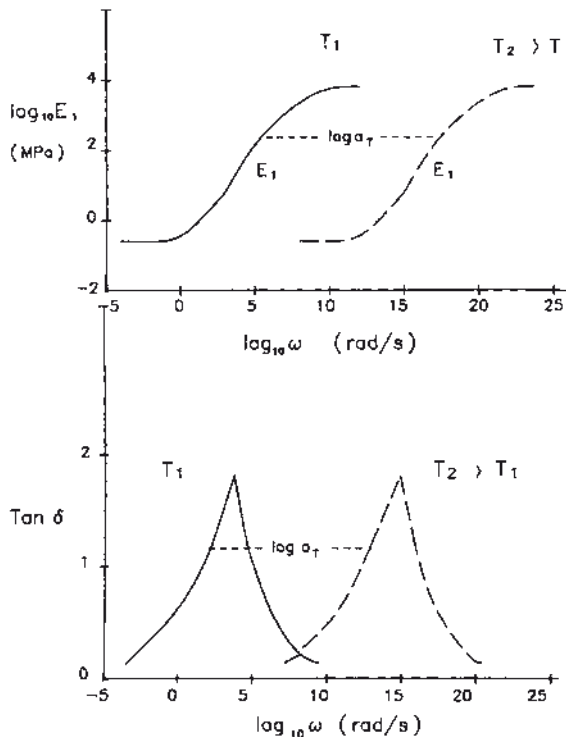


FIGURE 4.12 Dynamic modulus E_1 and $\tan \delta$ versus frequency at two temperatures: T_1 and T_2 , where $T_2 > T_1$

When a logarithmic scale is used for the frequency axis, as in Fig. 4.12, the curves are displaced laterally by a fixed distance when the temperature is raised. The dashed curves in Fig. 4.12 represent the response at a higher temperature T_2 . The amount of the lateral shift, $\ln a_T$, is given by Eq. (4.46), because it reflects the change in characteristic response frequency $\Delta(\ln \varphi)$ of molecular segments when the temperature is changed from T_1 to T_2 . Thus,

$$\ln a_T = \frac{\ln [\varphi(T_2) / \varphi(T_1)] \times 40 \times 52 (T_2 - T_1)}{(52 + T_2 - T_g)(52 + T_1 - T_g)} \quad (4.47)$$

In this way, measurements at one temperature can be applied at another. A temperature change is completely equivalent to a change in inverse frequency, or time. As an approximate guide, valid at temperatures about 50 °C above T_g , a temperature change of about 12 °C is equivalent to a factor of 10 × change in time. Similarly, it is equivalent to a factor of 0.1 × change in frequency, or rate of strain, or speed of loading. Thus, Eq. (4.46) provides a powerful time-temperature, frequency-temperature, and rate-temperature equivalence principle that enables us to correlate

mechanical behavior over wide ranges of time, frequency, and rate with temperature. As an example, measurements can be taken over a limited frequency range at many different temperatures, as shown in Fig. 4.13. They are then superposed by lateral shifts along the logarithmic frequency axis to construct a “master curve”, representing the expected response over an extremely wide frequency range at the chosen temperature (Fig. 4.14).

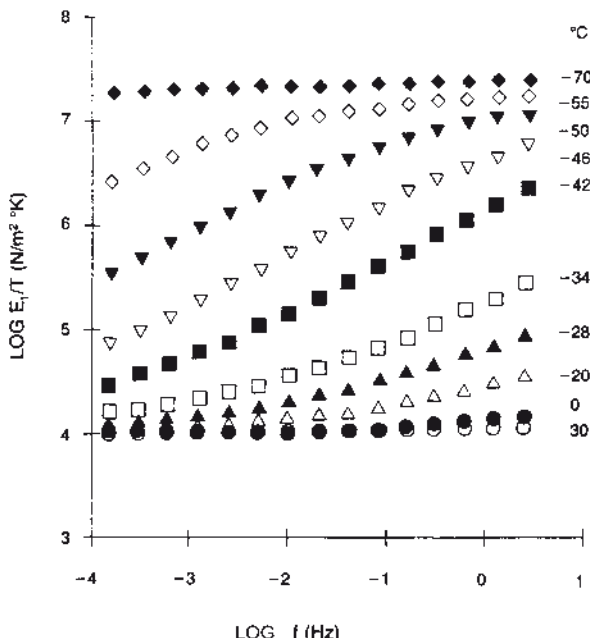


FIGURE 4.13 Dynamic modulus versus frequency for a polyurethane elastomer at various temperatures

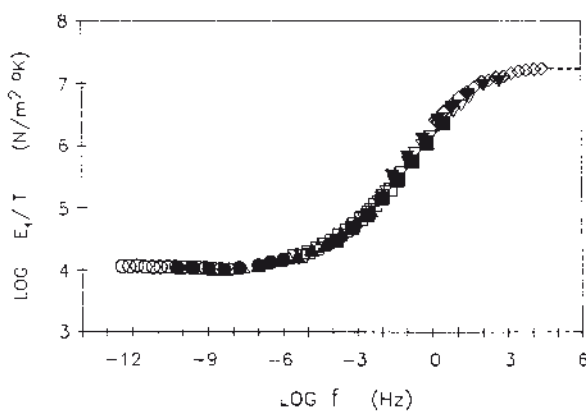


FIGURE 4.14 Results of Fig. 4.13 replotted versus reduced frequency at a reference temperature T_s of -42 °C, using shift factors a_T given by Eq. (4.47)

■ 4.10 Thixotropic Effects in Filled Rubber Compounds

A strong effect is observed of the amplitude of vibration when dynamic properties are measured for practical rubber compounds containing large amounts, of the order of 30% by volume, of carbon black or silica. It takes the form of a striking decrease in the dynamic modulus as the amplitude of imposed vibration is increased from very low levels, 0.1% or less, up to the maximum imposed, as high as 50% shear. Simultaneously, the loss factor $\tan \delta$ rises as the amplitude is first increased and then tends to decrease again after the main softening is over. These changes are shown schematically in Figs. 4.15 and 4.16. They are brought about by increasing the amplitude of vibration, but they are not fully reversible. Much of the softening remains when the amplitude is reduced back to small values and the original modulus is recovered only after a period of heating at temperatures of the order of 100 °C or higher.

The changes are attributed to two main causes: breakdown of weak interparticle bonds at very low amplitudes of oscillation, and rupture of weak associations between rubber molecules and carbon black, starting at somewhat higher amplitudes [13–15]. Because these two processes overlap to a considerable degree, they cannot be readily separated. However, they appear to be a direct consequence of the high stiffening power of certain types of carbon black, notably those with small particle size and highly interactive surfaces. To minimize uncertainty in values of dynamic modulus and $\tan \delta$, it is therefore customary to specify the use of somewhat smaller amounts of less powerfully reinforcing blacks in rubber compounds intended for precise applications. Although the modulus will not be as high as in other compounds – for example, those used for tire treads – it will be much less sensitive to the amplitude of vibration and to the extent of prior deformation.

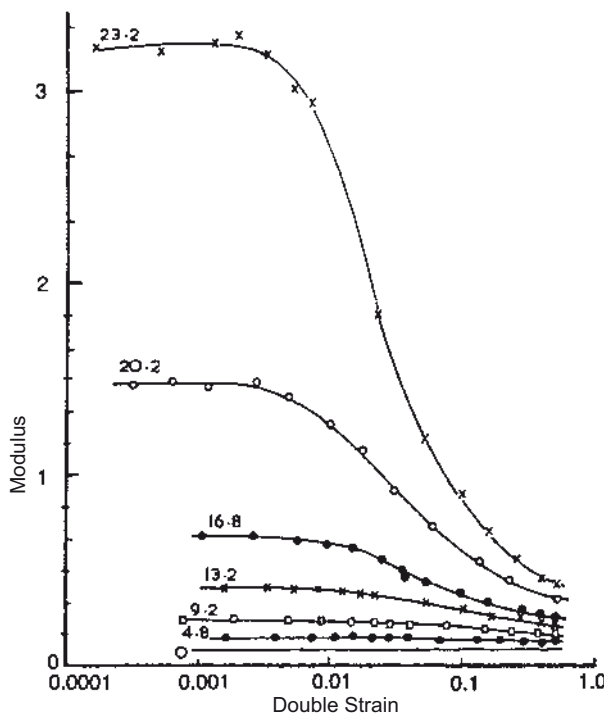


FIGURE 4.15 Changes in dynamic modulus E_1 (MPa) with amplitude of oscillation for a butyl rubber compound containing various volume fractions of N330 carbon black

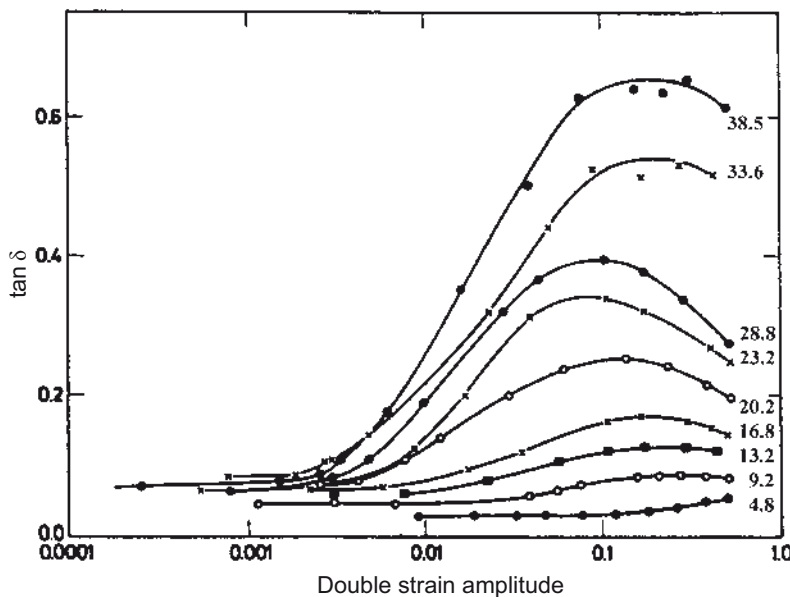


FIGURE 4.16 Changes in $\tan \delta$ corresponding to the changes in E_1 (Fig. 4.15)

Acknowledgments

The authors presented the substance of this chapter in lectures at The University of Akron over many years. Generations of students provided helpful questions and suggestions and encouraged them to prepare a written version.

References

- [1] P. Mason, *Proc. Roy. Soc. London*, **A272**, 315 (1963).
- [2] A. N. Gent and P. Marteney, *J. Appl. Phys.*, **53**, 6069 (1982).
- [3] N. W. Tschoegl, *The Phenomenological Theory of Linear Viscoelastic Behavior*, Springer-Verlag, New York, 1989.
- [4] A. L. Kimball and D. E. Lovell, *Phys. Rev.*, **30**, 948 (1927).
- [5] B. Maxwell, *J. Polym. Sci.*, **20**, 551 (1956).
- [6] A. N. Gent, *Br. J. Appl. Phys.*, **11**, 165 (1960).
- [7] S. P. Timoshenko and J. N. Goodier, *Theory of Elasticity*, 3rd ed., McGraw-Hill, New York, 1970, Section 109.
- [8] J. D. Ferry, *Viscoelastic Properties of Polymers*, 3rd ed., Wiley, New York, 1980.
- [9] J. J. Aklonis and W. J. MacKnight, *Introduction to Polymer Viscoelasticity*, 2nd ed., Wiley, New York, 1983.
- [10] J. M. Ward, *Mechanical Properties of Solid Polymers*, 2nd ed., Wiley, New York, 1983, Chapter 6.
- [11] L. E. Nielsen and R. F. Landel, *Mechanical Properties of Polymers and Composites*, 2nd ed., M. Dekker, New York, 1994, Chapters. 1 and 4.
- [12] M. L. Williams, R. F. Landel, and J. D. Ferry, *J. Am. Chem. Soc.*, **77**, 3701 (1955).
- [13] A. R. Payne and R. E. Whittaker, *Rubber Chem. Technol.*, **44**, 440 (1971).
- [14] L. Mullins, *Rubber Chem. Technol.*, **42**, 339 (1969).
- [15] G. Kraus, *Reinforcement of Elastomers*, Wiley-Interscience, New York, 1965.
- [16] S. Timoshenko, D. H. Young, and W. Weaver, *Vibration problems in engineering*, 4th edition, Wiley, 1974.

Problems for Chapter 4

1. A Voigt element consists of a spring of stiffness $k = 200 \text{ N/m}$ in parallel with a dashpot with a viscous coefficient $c = 1000 \text{ Ns/m}$. What is the retardation time τ ? If a constant force of 2 N is applied suddenly, what deflection would be observed after 0.1 s? After 1 s? After 10 s? After 100 s?

2. A machine with a mass of 400 kg is mounted on a set of light rubber springs with a combined stiffness k of 3.6 MN/m and a damping coefficient c inversely dependent on frequency f and given approximately by 1 kN/m-Hz . (Many rubber compounds show a dependence of damping coefficient on frequency of approximately this form over a common range of mechanical frequencies when the test temperature is far above the polymer glass temperature.)

What is the resonant frequency of this system? And if the machine exerts an out-of-balance oscillating force of amplitude F_0 of 4 kN at the resonant frequency, what would be the amplitude of motion? What would be the amplitude of motion, if the machine exerted the same force, but at a frequency of three times the resonant frequency?

3. Free vibrations of a rubber spring are observed to die away so that every swing is three-fourths of the amplitude of the preceding swing (on the same side of zero). What is $\tan \delta$ for this rubber compound? What rebound would you expect, if a rigid object were dropped onto a block of the same rubber?
4. A rubber layer, 100 mm in length and width, and 10 mm thick, is bonded between two metal plates. One plate moves parallel to the other sinusoidally, through a distance of $\pm 10 \text{ mm}$, at a frequency of 10 Hz, subjecting the rubber layer to an alternating shear strain of $\pm 100\%$. If the rubber has a dynamic shear modulus of 2 MPa and shear loss modulus of 0.2 MPa (i.e., the loss tangent is 0.1), calculate the initial rate of rise of temperature at the center of the block and the final temperature reached there. Assume that the metal plates are large and conduct heat away efficiently, so that they do not heat up significantly.
5. An SBR rubber compound has a reported glass transition temperature of -58°C . In a bending experiment, carried out in a time period of 10 seconds, it is found to stiffen to about twice the value observed at room temperature when the test temperature reaches -30°C . At what temperature would you expect it to reach the same stiffness as at -30°C , if the same experiment were carried rather rapidly, in say, 1 ms?

■ Answers to Problems for Chapter 4

1. Retardation time $\tau = 5 \text{ s}$; deflection after 0.1 s = 0.2 mm; after 1 s = 1.8 mm; after 10 s = 8.65 mm; after 100 s = 10 mm.
2. A first approximation to the resonant frequency can be obtained from Eq. (4.28), assuming that the term $c^2/2 m$ in Eq. (4.26) is small compared to the stiffness k .

The result is $f_r = 15.1$ Hz. At this frequency the term $c^2/2 m$ takes the value 285 kN/m and is, indeed, small compared to k , only about 8% as large. As a result, the second approximation to the resonant frequency, obtained from Eq. (4.26), is 14.5 Hz, rather close to the first. And the third approximation, using the new value for $c^2/2 m$ of 263 kN/m, is 14.55 Hz, probably a sufficiently close approximation to the true value for most purposes.

From Eq. (4.27), the amplitude at resonance takes the value 3.0 mm. When the forcing frequency is raised to 43.65 Hz, three times the resonant frequency, then from Eq. (4.25) the amplitude of the motion is decreased to only 0.15 mm.

3. The logarithmic decrement Δ for this spring is $\ln(4/3)$. From Eq. (4.38), $\tan \delta$ is therefore approximately 0.09. And from Eq. (4.44), we would expect the fractional rebound to be 75%.
4. From Eq. (4.21), the amount of energy dissipated per strain cycle is 0.6 MJ/m^3 . And because strain cycles are imposed at a frequency of 10 Hz, the rate of energy dissipation is 6.2 MW/m^3 . Using a typical value for the thermal capacity of a rubber compound, of $1.8 \times 10^6 \text{ J/m}^3 \text{ }^\circ\text{C}$, the corresponding rate of temperature rise is $3.4 \text{ }^\circ\text{C/s}$.

We note that the thickness of the layer is much smaller than the length or width, so that heat flow will be primarily in the thickness direction. Then Eq. (4.45) gives an estimate of the maximum temperature attained in the center of the layer, relative to the bonded surfaces. Assuming a typical value for thermal conductivity K of the rubber compound, of $0.25 \text{ W/m}^3 \text{ }^\circ\text{C}$, the final temperature rise is obtained as $310 \text{ }^\circ\text{C}$ above ambient.

This is excessively high. Most rubber compounds would decompose rapidly at such temperatures. Steps should be taken to prevent a temperature rise of more than a moderate amount, say $50 \text{ }^\circ\text{C}$, from occurring in practice. For example, a compound could be selected with a much lower loss modulus or a different design could be adopted using thinner rubber layers.

5. A large change is proposed in the effective rate of deformation, by a factor of 10^4 . For a simple viscoelastic solid, the same mechanical response would be obtained if the rate of motion of molecular segments were also increased by the same factor, to become 10^4 times faster than before. From Eq. (4.47), this increase in segmental motion would be found at a temperature T_2 of $+14 \text{ }^\circ\text{C}$ when the prior temperature T_1 was $-30 \text{ }^\circ\text{C}$. Thus, we would expect the stiffness to be doubled at $+14 \text{ }^\circ\text{C}$ instead of $-30 \text{ }^\circ\text{C}$, when the experiment is carried out rapidly.

5

Strength

Graham J. Lake, Alan G. Thomas

■ 5.1 Introduction

Common technological methods of assessing the strength of rubber are by standard tests such as tensile strength or tear measurements. In practice, rubber articles rarely fail in single loadings such as these; rather, failure usually results from crack growth under repeated loading. Thus, these standard tests ought to be regarded as quality control tests rather than as means of obtaining parameters that can be used to predict the failure behavior of an article.

There is considerable evidence that fracture of rubber, like that of all other materials, is initiated from imperfections inadvertently present, or introduced, in the body of the material or on its surface. From these imperfections, cracks may grow under an applied load, often slowly at first, until one or more of them reaches sufficient size for gross fracture to occur. Thus, the crack growth characteristics of a rubber constitute the main factor determining its strength. To study these characteristics and to use them to determine the failure of rubber components, it is necessary to define them in a fundamental manner. The approach adopted for the study of the strength of rubber and other materials is known as fracture mechanics.

■ 5.2 Fracture Mechanics

The physical principle on which the fracture mechanics approach is founded is a consideration of the energy necessary to propagate a crack. Griffith originated the idea (in the 1920 s) when he postulated that a crack in glass would grow, if the elastic energy released by the growth were greater than the surface free energy of the surfaces thus created. He confirmed this by experiment, and thus for glass the basic strength property appears to be simply the surface energy. For rubber and most other materials this is not true.¹ When a crack grows, irreversible processes

¹ Subsequent experiments have shown that even for inorganic glasses, the energy required to cause bulk fracture in many cases considerably exceeds the surface free energy.

occur in the vicinity of the moving tip, leading to energy losses that must be made up from the available elastic energy. The magnitude of these losses is determined by the properties of the rubber, the strain in the crack tip region, and the rate of growth of the crack. In some elastomers, energy losses may occur in the bulk under the applied loading and these must also be taken into account. However, it is the losses in the crack tip region that are of prime importance, and these may be large even for rubbery materials for which the bulk losses (at much lower deformations and rates of strain) are negligible. Thus, the energy necessary to propagate a crack at a particular rate is likely to be a characteristic of the rubber itself, even though it greatly exceeds the thermodynamic surface free energy, and may therefore be independent of the overall shape of the test piece. The elastic energy available to drive a crack may be defined as follows:

$$-\left(\frac{\partial W}{\partial A}\right)_l = G$$

where W is the total elastic energy in the article considered and A the area of one fracture surface of the crack. The partial derivative indicates that the article is considered to be held at constant length l , so that the applied forces do not move, hence do no work. The quantity G is termed “strain energy release rate”, and “tear energy” or “fracture energy”. The term “tear energy” is often used for elastomers. Elastomers that do not crystallize on stretching are often found to tear in a steady, time-dependent manner. The fracture mechanics approach outlined above suggests that the rate of crack growth when expressed in terms of G , rather than simply the load applied to some arbitrarily shaped test piece, should define a relation that is independent of the overall shape of the test piece and should therefore be a characteristic of the rubber itself.

Figure 5.1 illustrates four very differently shaped test pieces. Their common characteristic is that G can be calculated from the easily measurable applied forces or strains, which makes them convenient for experimental purposes. Tear measurements on a non-crystallizing styrene-butadiene rubber (SBR) have been carried out using these test pieces and the results, shown in Fig. 5.2, are expressed in terms of G and the rate of crack growth r . It can be seen that the results are consistent with a single relation, independent of the test piece geometry, as implied by the fracture mechanics approach.

The tear behavior of a strain-crystallizing elastomer, such as natural rubber (NR), differs from that of non-crystallizing elastomers, such as SBR, in that below a critical value of G , denoted G_c , there is normally no time-dependent crack growth. Above G_c , tearing occurs typically in a stick-slip manner. The value of G_c does not depend strongly on the rate of tearing. However, during the process of loading the test

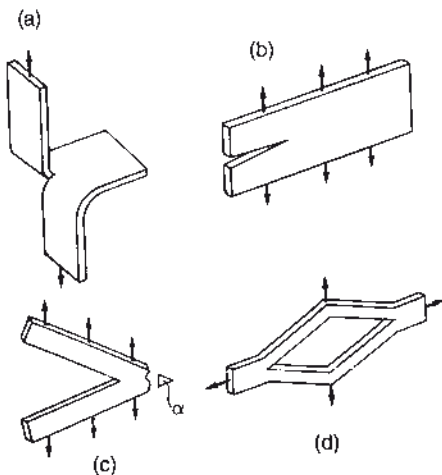


FIGURE 5.1 Crack growth test pieces for which G can readily be calculated:
 (a) “trousers”, (b) pure shear,
 (c) “angled”, and (d) “split”

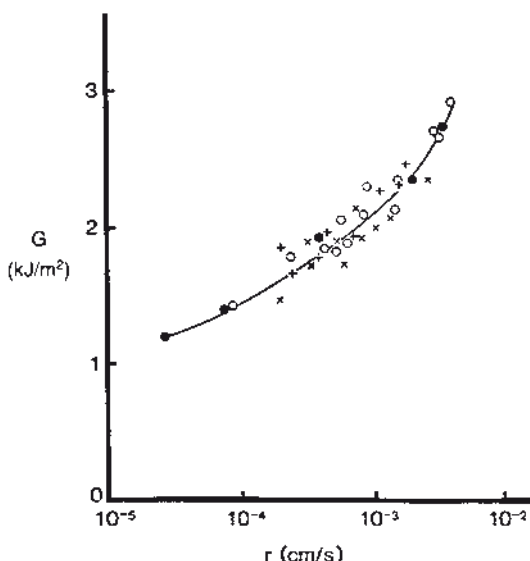


FIGURE 5.2 Strain energy release rate G versus rate of tearing r (logarithmic scale) for an unfilled styrene-butadiene rubber vulcanize using the various test pieces shown in Fig. 5.1:
 \times = trousers; $+$ = pure shear; \circ = split; \bullet = angled

piece, the crack grows by a small amount, although the growth stops if the load is held constant. If the test piece is relaxed and then reloaded, the crack grows again slightly. This crack growth process is the most important failure mechanism for items that are repeatedly cycled, such as rubber springs and tires. It is described more fully in Chapter 6.

5.2.1 Analysis of the Test Pieces

To study the crack growth characteristics of rubber, suitably shaped test pieces are necessary. In principle, any test that can be analyzed to give G in terms of directly measurable quantities can be employed, but some are experimentally more suitable than others. Test pieces that have been widely used are the “trousers” and “pure shear” types shown in Fig. 5.1 and the tensile strip shown in Fig. 5.3.

For the “trousers” test piece (Fig. 5.1a), provided the legs stretch very little under load, the following relation obtains:

$$G \approx \frac{2F}{t} \quad (5.1)$$

where the applied force is F and the thickness is t .

For the pure shear test piece (Fig. 5.1b), we write

$$G = l_0 U \quad (5.2)$$

where l_0 is the unstrained height of the test piece between the grips and U is the strain energy density in the rubber in the pure shear region of the test piece. For there to be such a region, the width-to-height ratio must be sufficiently large. Also, for Eq. (5.2) to apply, the crack has to be long enough to create unstrained regions between the crack and the grips.

For both the foregoing test pieces, G is independent of the crack length. For the pure shear test piece U can be determined from the measured strain in the pure shear region and the (pure shear) stress-strain behavior of the rubber.

For a tensile strip with an edge crack (Fig. 5.3), G is given by

$$G = 2KUc \quad (5.3)$$

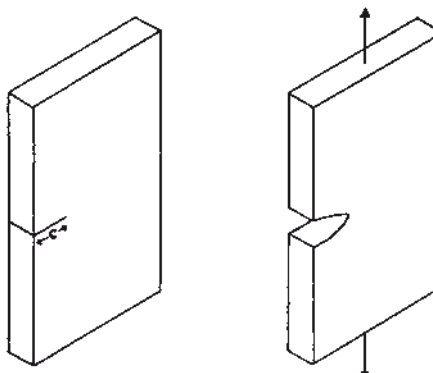


FIGURE 5.3 Tensile strip test piece with an edge crack of length c

where c is the crack length, U the elastic energy density in the simple extension region, and K a slowly varying function of the strain given approximately by

$$K = \frac{3}{\sqrt{\lambda}} \quad (5.4)$$

where λ is the extension ratio in the simple extension region. This dependence of K on extension appears to be directly associated with the lateral contraction of the test piece (and crack) in simple extension (which also goes as $1/\sqrt{l}$). Equation (5.3) also applies for a short crack in the center of a pure shear test piece (Fig. 5.1b) with a value of K (of about 3 or π), which is substantially independent of strain (just as the crack length does not alter with strain in this case) and where c now represents the half-length of the crack. Indeed, a similar relation may be expected to apply more generally for short cracks, provided there are no stress singularities in the immediate crack vicinity and provided also that the bulk stress does not vary rapidly in relation to the crack dimensions (different values of K will be expected to apply for different geometries). In simple shear, a more complex relation for the energy release rate has been obtained (by finite element analysis) for a short crack starting from an edge and propagating along a bonded surface; this probably reflects the effect of the considerable concentration of stress that occurs adjacent to the bonds in nominally simple shear (see Section 5.7).

5.2.2 The Strain Energy Concentration at a Crack Tip

At first sight it is rather surprising that an approach based on the “global” release of strain energy and having, apparently, little or no connection with the region in which fracture is taking place, should be capable of describing crack growth behavior. Insight into why the approach can, and often does, work is provided by an analysis for a model crack having a semicircular tip of diameter d (Fig. 5.4).

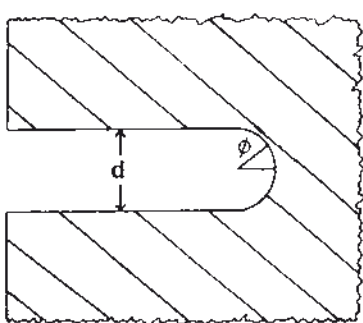


FIGURE 5.4 Model crack having a semicircular tip of unstrained diameter d ; U_ϕ is the strain energy density at the surface at an angle ϕ from the pole

In this case it can be shown that

$$G = d \int_0^{\pi/2} U_\phi \cos \phi \, d\phi \quad (5.5)$$

where U_ϕ is the elastic energy stored per unit volume in the surface layer of the tip at an angle ϕ from the pole (Fig. 5.4). This equation can be derived without making any assumptions about the linearity of the stress-strain behavior for an elastic material or the magnitude of the strains involved. Furthermore, if a suitably averaged strain energy density at the tip is U_t , Eq. (5.5) becomes

$$G = U_t d \quad (5.6)$$

Measurements of the strain, and hence strain energy, distribution around a model crack tip have confirmed the validity of Eq. (5.5), good agreement being found between tearing energies determined in this way and those calculated from the applied forces; also, tear experiments have shown G to increase with d in the predicted way for model incisions with tip diameters of 1–3 mm, with U_t similar to the strain energy density obtained from a tensile test at break.

For a real crack, d is expected to represent an effective unstrained tip diameter. From measured tear strengths and tensile strain energy densities at break, Eq. (5.6) indicates effective tip diameters during tearing to be typically of the order of 0.1 mm. This is much greater than would be expected for the true unstrained tip diameter (the latter may be as little as the distance between crosslinks in the unstrained state – ca. 10^{-5} mm). Two factors are likely to contribute to this discrepancy. First, the effective tip diameter will reflect the roughness of the fracture surface, and the scale of this is often in the region of 0.1 mm for torn surfaces (and can be much greater if “knotty” tearing occurs). Second, the value of U_t is likely to increase as the size of the specimen under test decreases; and this means that values of d from Eq. (5.6) are likely to be overestimates, if they are based on energy densities at break obtained from relatively large tensile test pieces. (The theoretical energy density at break expected from the primary bond strength is at least 2 orders of magnitude greater than that measured in tensile tests.)

There are thus uncertainties about the precise meaning of d for a real crack. Nevertheless, the close interrelation between G and the strain energy density at a crack tip provides insight into why an approach based on the overall strain energy release rate can be successful in treating tear and other fracture phenomena.

■ 5.3 Tear Behavior

Non-crystallizing materials give values of G that depend on the rate of tearing, as the results for SBR in Fig. 5.2 illustrate, but they are independent of the type of test piece used. Similar agreement of tear results for different test pieces is found for other elastomers, although the detailed nature of the tearing and the level of the tear strength may vary.

Thus, the energetics approach provides a means of characterizing tear behavior for various elastomers. The magnitude found for G is of the order of 1 kJ/m^2 and is very much greater than any true surface energy, even when allowance is made for the effect of the long-chain molecular structure of an elastomer.

The fracture energy approach indicates why different conventional tear test pieces rate different materials in different orders. The tearing force, as can be seen from the theory for the test pieces considered above, is governed by a function of G and the modulus of the rubber. This function varies from one test piece to another, giving different sensitivities to modulus and tearing energy changes. As both the modulus and tearing energy vary from one material to another, different ratings are obtained with different test pieces. The analysis also indicates why the variability of results for the trousers test tends to be greater than for other standard tear tests. For the trousers test piece, the tearing force is directly proportional to the tearing energy, if the extension of the legs is negligible, and uninfluenced by the modulus; since the intrinsic variability of fracture processes is generally much greater than that of elastic properties, the variability of the results is correspondingly greater. Thus, the apparently "better" reproducibility of other tear tests simply reflects their lower sensitivity to the property whose measurement is being attempted.

The tear strength of non-crystallizing elastomers depends not only on rate but also on temperature (Fig. 5.5a). These variations parallel closely the variation of viscoelastic properties with rate and temperature, the tear strength increasing with increasing viscoelastic energy dissipation. The same change in viscoelastic behavior can be produced by an appropriate change in either rate or temperature, and an equation developed by Williams, Landel, and Ferry (the WLF equation; see Fig. 5.6a) gives the interrelation between these changes. The glass transition temperature T_g , which characterizes the temperature at which the change from rubber to glass occurs, is of key importance in this relationship. Using this relation, a master curve showing the effect of temperature or rate on viscoelastic behavior, characteristic of a particular polymer, can be constructed as discussed in Chapter 4. It has been found that the tear behavior of "non-crystallizing" elastomers at various rates and temperatures can be similarly treated, except that a modified form of the WLF equation may be required. This modification is believed to be needed because of variations in tip

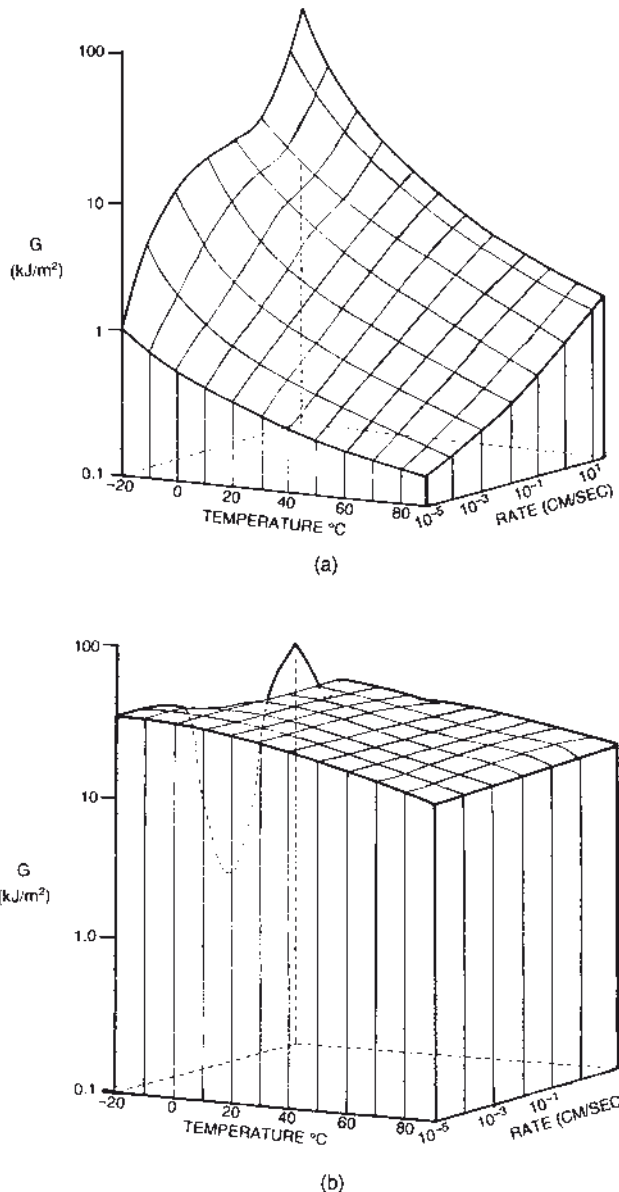


FIGURE 5.5 Tearing energy surfaces for (a) an unfilled, non-crystallizing, SBR vulcanizate, (b) an unfilled, strain-crystallizing, natural rubber vulcanizate

diameter with tear conditions. Indeed, when changes in tip diameter are limited by applying constraints, the shifts required to produce superposition of results obtained at various rates and temperatures are those given by the unmodified WLF equation (Fig. 5.6b).

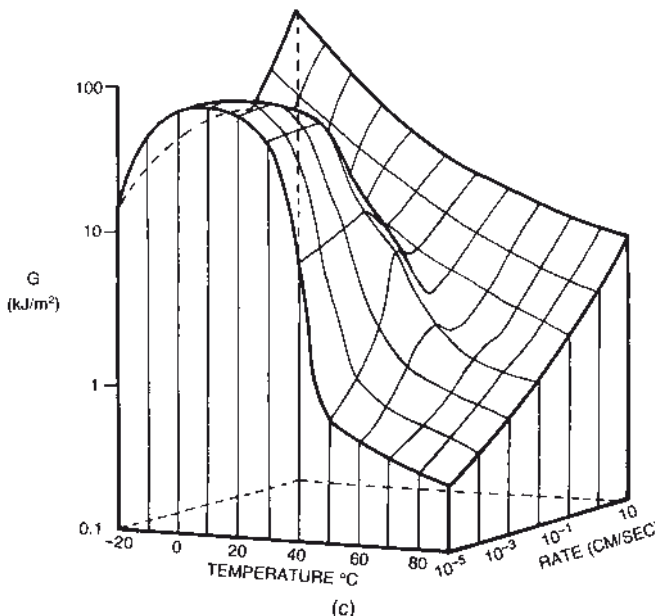


FIGURE 5.5 (c) an SBR vulcanize containing “fine thermal” (FT) black

An alternative demonstration of the importance of viscoelastic properties on tear strength is illustrated in Fig. 5.6c, where the tearing energy at room temperature and a fixed tear rate is plotted against the loss modulus for a family of rubbery copolymers with various glass transition temperatures. Approximate proportionality is found. In this case, it is the importance of variation in T_g rather than in test conditions that is shown.

The T_g of an elastomer is influenced by applying hydrostatic pressure, 1 kbar raising T_g by about 25 °C. The free volume interpretation of the WLF equation predicts this effect, as the free volume will decrease with the hydrostatic compression of the material. Measurements of the tear behaviour under hydrostatic pressure, over a range up to ca. 2 kbar, show an increase in tear strength with pressure, as expected, but there are quantitative discrepancies with the predictions of the free volume theory.

Thus, it appears that irreversible energy dissipation resulting from mechanical hysteresis is one reason why tear strengths often greatly exceed theoretical values. Tearing in non-crystallizing elastomers often proceeds in a “steady”, time-dependent manner in the sense that the force in a trousers test carried out at a constant rate of separation of the legs remains relatively constant. In crystallizing elastomers, by contrast, time-dependent growth is often absent and tearing generally proceeds in a stick-slip manner, with the force increasing during the stick periods until a catastrophic failure point is reached at which the tear jumps forward and, depending on the way in which the force is applied, may completely sever the test piece.

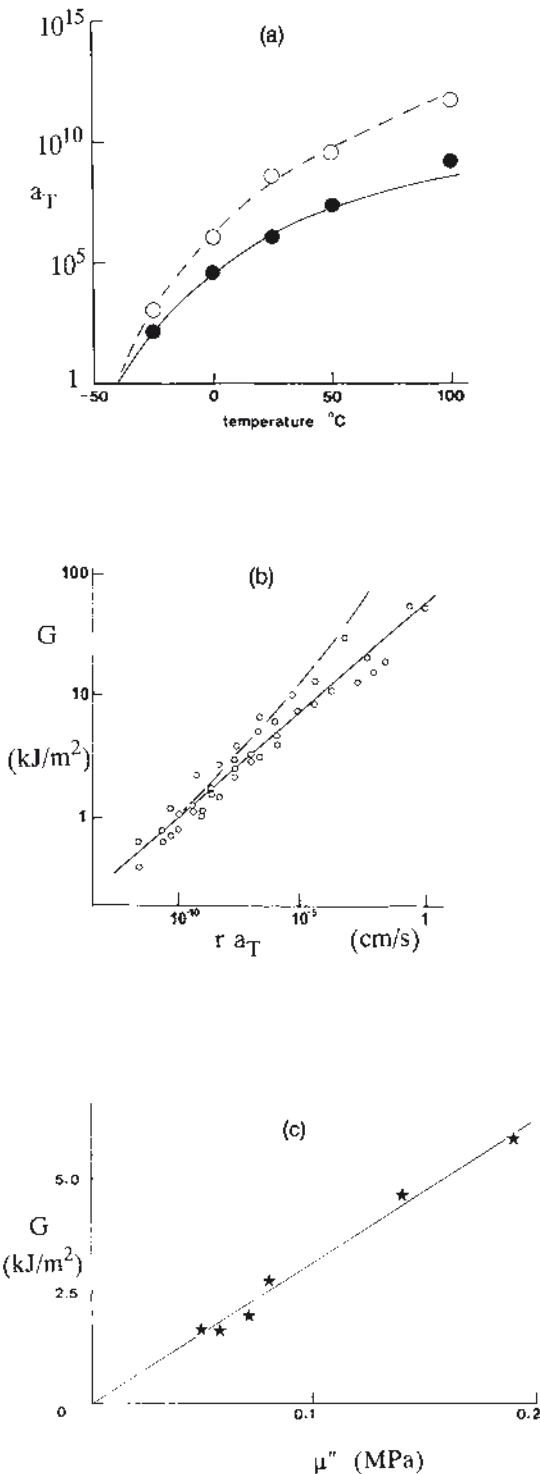
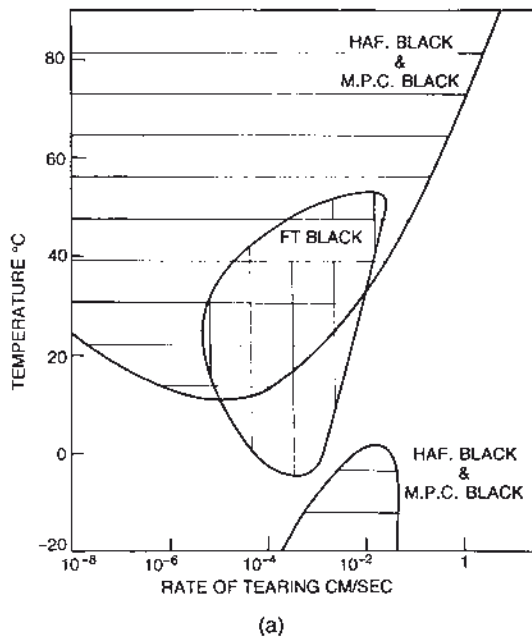


FIGURE 5.6 (a) Dependence of the rate shift factor a_T on temperature according to the Williams-Landel-Ferry relation (see Chapter 4) (●) and the shift factor required to bring tear results at different temperatures into agreement for an unfilled SBR vulcanize with no constraint placed on the tear tip (○).
 (b) Reduced tearing energy versus reduced rate of tearing for the SBR vulcanize at various temperatures from -40 to +100 °C. The rate is multiplied by the shift factor a_T , while G is multiplied by a reference temperature T_s , which is related to the glass transition temperature (-40 °C was used here), divided by the test temperature T (the latter adjustment parallels that made to the modulus in elasticity measurements and is of uncertain validity in relation to strength properties but is relatively small). Results with the tear tip constrained (to prevent deviations > 0.1 mm) indicated by circles (WLF shift factor used). Trend of results with the tip unconstrained [dashed curve: shift factor represented by the dashed curve in (a) is required to bring the results into superposition].
 (c) Dependence of G on loss modulus μ'' for various non-crystallizing elastomers (copolymers of butadiene with styrene or acrylonitrile having T_g 's from -80 °C to -20 °C) at a tear rate of 25 $\mu\text{m/s}$ at 25 °C

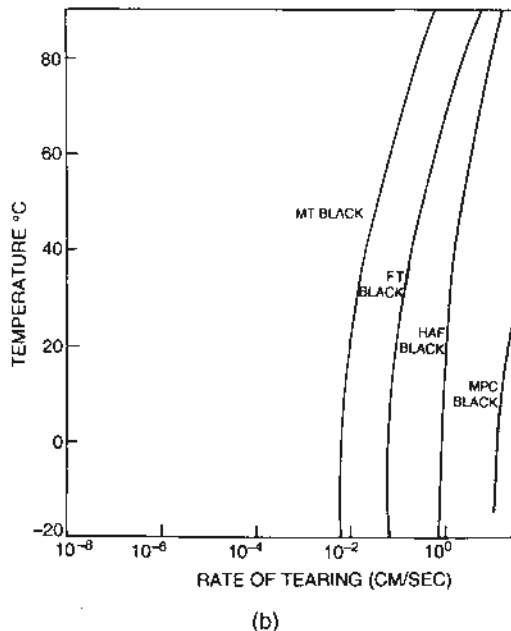
Over wide ranges, the catastrophic tearing energy is insensitive to rate and temperature for a crystallizing rubber, such as natural rubber (Fig. 5.5b); it appears that the effects of crystallization, which can induce very substantial hysteresis at high strains, generally outweigh the viscoelastic effects in such materials. Whatever its detailed causes, a further consequence of hysteresis is that the strain concentration at the tip of a crack that has propagated into hysteretic material may be very much less than if the material were perfectly elastic.

Another factor that can greatly increase tear strength is blunting of the tip of a tear. As Eq. (5.6) indicates, this is in principle an effect distinct from that of hysteresis, although it is clear from the evidence given above that viscoelastic behavior is one factor that can influence the tendency for blunting to occur. Whatever its causes, experiments with very sharp crack tips have shown how large a part blunting can play in increasing tear strength. In extreme cases, blunting can take the form of “knotty” tearing in which a tear tip circles around on itself under increasing force until finally a new tear breaks ahead. Although knotty tearing is not exclusive to filled rubbers, the tendency for it to occur can be greatly increased by fine-particle fillers, with corresponding large increases in tear strength. If lateral tear deviation is restricted by constraints, these large increases can be almost entirely suppressed. It seems probable that a strength anisotropy arising from orientation effects is at least partly responsible for tear deviations. Evidence supporting this view has been obtained by experiments in which the rubber is pre-stretched in the direction of tearing, when marked reductions in strength are found.

The occurrence of knotty tearing resulting from the presence of a filler can greatly alter the shape of the tear “surface” for a non-crystallizing rubber, as Fig. 5.5c illustrates. The tendency for knotty tearing to occur is influenced by viscoelastic effects as well as by the type of filler, and the behavior may be complex in non-crystallizing elastomers (Fig. 5.7a). In strain-crystallizing natural rubber, a more straight-forward picture applies (Fig. 5.7b), with knotty tearing occurring below a certain tear rate, which again depends on the type of filler used but is not much influenced by temperature. The latter feature probably reflects the influence of crystallization, and it appears probable that the critical rate reflects the time required for the formation of an anisotropic structure, involving crystallization and to some extent the filler, at the tear tip.



(a)



(b)

FIGURE 5.7 (a) Regions of "knotty" tearing for SBR vulcanizates containing 50 parts per hundred parts of rubber by weight (phr) of various carbon black fillers.
 (b) Similar results for filled natural rubber vulcanizates: the regions of "knotty" tearing lie to the left of the appropriate curves

■ 5.4 Crack Growth under Repeated Loading

Although under many circumstances time-dependent crack growth is not observed in crystallizing elastomers, small-scale crack growth does occur while the load (and tearing energy) is increasing. This can be observed in a single loading cycle, although often the growth does not become significant until many cycles have occurred. A similar process occurs in non-crystallizing elastomers, and it appears that for these materials there can be a cyclic component in the growth in addition to the component expected as a result of time-dependent tearing. For both types of elastomer, the growth during each cycle is often found to be determined mainly by the maximum tearing energy attained, rather than by the way in which the maximum is reached (i.e., waveform, rate of strain), at least when the unstrained state is visited for part of each cycle (cf. later discussion of “non-relaxing” effects).

Measurements of the crack growth behavior under repeated stressing using various test pieces may be expressed as the crack growth per cycle (dc/dn) as a function of G , where, following the discussion above, this is now understood to represent the maximum value attained during cyclic loading. Results for a natural rubber (NR) compound (Fig. 5.8) indicate that, as for tear behavior, the crack growth under repeated stressing is independent of the test piece geometry; hence it is a true strength property of the material.

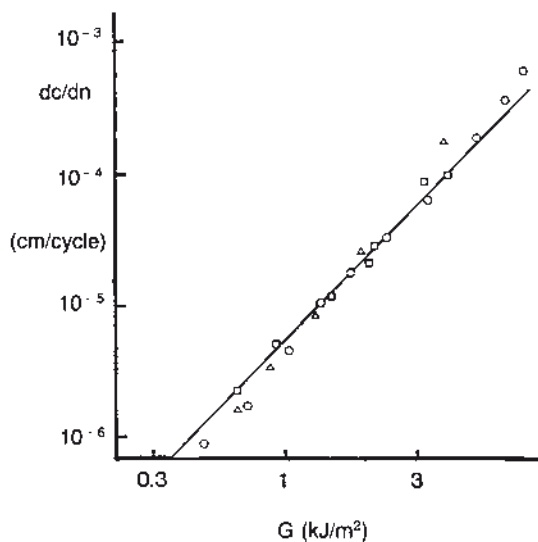


FIGURE 5.8 Cyclic crack growth rate dc/dn versus maximum tearing energy of the cycle (minimum zero) for an unfilled natural rubber vulcanize obtained using various test pieces (cf. Figs. 5.1 and 5.3): \square = trousers; Δ = pure shear; \circ = tensile strip with an edge crack

Figure 5.8 is a logarithmic plot and shows that, over the range covered,

$$\frac{dc}{dn} = B G^\beta \quad (5.7)$$

where B and β are constants. It is found experimentally that this approximately represents the behavior of various vulcanizates over a useful, but limited, range of G values. For natural rubber, β is often about 2, whereas for non-crystallizing elastomers (such as SBR) it may be about 4.

If rubber articles are repeatedly stressed, cracks may grow and eventually cause failure. In many cases the cracks appear to be initiated from flaws at the surface, possibly due to dirt, molding defects, or mechanical damage. Ultimately an article may fail by breaking in two. The fatigue life – the number of cycles to failure – can be quantitatively related to the initial flaw size and the crack growth characteristics of the rubber using the fracture mechanics approach, as described in Chapter 6.

5.4.1 The Fatigue Limit and the Effect of Ozone

As pointed out earlier, the power law dependency of crack growth rate is valid only over a limited G range. Figure 5.9, which presents the crack growth relations for NR and SBR vulcanizates over a wider G range, shows the breakdown of the power law. In particular, below a critical value of G , G_0 , it is found that the crack growth rate is virtually zero, as shown in the insert to Fig. 5.9, where linear scales are used. At G values less than G_0 , mechanical crack growth is absent and ozone attack is the only mechanism that produces growth. This region appears on the log–log plot as the constant rate region below G_0 values of about 50 J/m^2 . The existence of G_0 means that if this value is not exceeded during fatigue cycling of an article, the life of the article will, in the absence of ozone attack, be virtually indefinite. Thus, rubber can, like other materials such as metals, exhibit a fatigue limit. This limit is also discussed in the next chapter.

In the region immediately above G_0 , linear relationships often apply for cyclic crack growth (cf. inset to Fig. 5.9), so that the growth can be represented by an equation of the form:

$$\frac{dc}{dn} = A(G - G_0) + r_z \quad (5.8)$$

where A is a mechanical (strictly, “mechanico-oxidative” – see later) crack growth constant and r_z represents the ozone contribution to the growth (which is all that occurs below G_0).

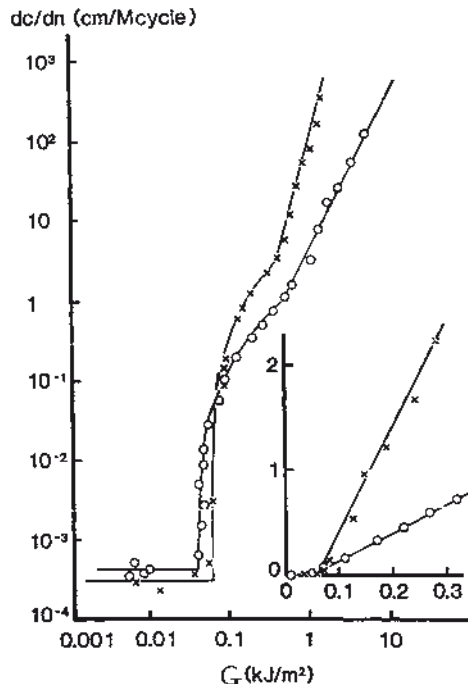


FIGURE 5.9 Cyclic crack growth rate dc/dn plotted against the maximum tearing energy of the cycle (minimum zero) on logarithmic scales for vulcanizates of natural rubber (\circ) and SBR (x). Inset shows the region near the threshold energy for mechanical crack growth G_0 plotted on linear scales

5.4.2 Physical Interpretation of G_0

The magnitude of the energy G_0 required to initiate mechanical crack growth is of similar order ($\approx 50 \text{ J/m}^2$) for a range of elastomers including natural rubber and SBR, as illustrated in Fig. 5.9, and polychloroprene and butyl rubber, which differ widely in tear and tensile strengths. Similar values are observed for SBR for cyclic and time-dependent growth. The similarity of the G_0 values suggests that G_0 may be governed fairly directly by the primary strength of the carbon-carbon bonds for these elastomers. An estimate of the minimum tearing energy required for bond rupture can be made using Eq. (5.6), if it is assumed that the tip diameter has its smallest possible value, which for an elastomer is of the order of the distance between crosslinks in the unstrained state; this gives $d = \xi m^{1/2}$, where ξ is the length of a monomer unit and m the number of monomer units between crosslinks. Assuming forces to be transmitted primarily via the crosslinks, the energy stored by the carbon-carbon double bonds will be small at the breaking force of the single bonds; also, if the chains are substantially straight at rupture, the force on each

bond will be essentially the same, so that the maximum possible energy density will be of the order of $b J$, where b is the number per unit volume of load bearing single carbon-carbon bonds (ignoring those in any side groups) and J is the energy stored by each single bond at its rupture point. Substitution in Eq. (5.6) yields

$$G_0 = b J \xi m^{1/2} \quad (5.9)$$

For a typical natural rubber vulcanize, the following approximate values hold: $\xi = 5 \times 10^{-8}$ cm, $b = 2.4 \times 10^{22}$ cm $^{-3}$, $m = 100$, and $J = 3.3 \times 10^{-12}$ erg (the dissociation energy of the weakest C-C bond in the isoprene unit). Equation (5.9) then gives $G_0 = 40$ J/m 3 . A more precise calculation yields about half this value, which is nevertheless in good agreement with the experimental results in view of various uncertainties. Variations between different elastomers would be expected to be fairly small on this basis, as is observed. Thus, G_0 can be related approximately to the primary bond strength and molecular structure of a vulcanize.

The calculation above is similar to a normal surface energy calculation, but is modified to take account of the long-chain molecular structure of a rubber. Because of this, breaking a bond crossing the fracture plane requires that many other bonds (in the same chain between crosslinks) be taken essentially to the breaking point; thus, the energy required is correspondingly magnified. The question now arises: Why does failure not occur in bulk when G_0 is reached?

Indeed, for certain elastomeric materials, such as very highly crosslinked or very highly swollen ones, bulk failure does occur close to G_0 . However, for most elastomers this is not the case, and the tear strength is much greater than G_0 . One reason for this is believed to be the irreversible energy dissipation arising from viscoelastic or other sources of hysteresis, referred to earlier. When G_0 is exceeded, the occurrence of crack growth means that retraction of material occurs in certain regions in the vicinity of a crack tip. Thus, the mechanical hysteresis of the material will influence the stress concentration at the tip, hence contributing to the complex picture that applies to crack growth at higher severities. Roughening of the crack tip can also strongly influence the tear strength as normally measured, as has already been discussed, whereas the agreement between the G_0 theory and experimental evidence, such as that in Fig. 5.9, suggests that the limiting molecular sharpness often occurs in the vicinity of G_0 .

There is considerable evidence supporting the existence of a threshold energy for crack growth and its physical interpretation both for constant and for cyclic stressing. By contrast, the conventional tear and tensile strengths which, as they represent the upper bounds of the macroscopic failure spectrum, are relatively easy to measure, are much more complex properties and do not appear likely to be amenable to straightforward, if any, fundamental interpretation.

5.4.3 Effects of Type of Elastomer and Filler

The conclusion that the fundamental strength property of a rubber is its crack growth characteristics means that to predict the failure, due to crack growth, of an article under stress, this behavior has to be evaluated for materials of interest. Usually it is repeated stressing that is relevant for such articles as rubber springs or tires, but crack growth can occur under a constant stress, particularly in non-strain-crystallizing rubber. In this case the “static” time-dependent crack growth behavior is relevant.

Crack growth curves under repeated stressing for a range of materials are given in Chapter 6. They show differences in the form of the characteristics (slope and shape of the curves) for different elastomers. Also, improvements due to the introduction of carbon black, which appear mainly to be associated with tip blunting effects, are shown. These effects, which in extreme cases lead to the crack deviation phenomenon of knotty tearing referred to earlier, are believed to be associated with the development of strength anisotropy in the highly strained region ahead of the crack tip. Crack growth measurements on NR black-filled rubbers which are pre-strained in the direction of growth do indeed show much enhanced rates at pre-strains of more than 50%, supporting this view. This also suggests that the crack growth behavior of filled materials in service may be modified, if a crack is growing in a region of biaxial strain. There is evidence that repeated small deformations can induce significant anisotropy under service conditions.

The type and degree of crosslinking may also affect the crack growth characteristics for a particular elastomer, but the effects are generally less than when the elastomer is varied. In tension or compression, and in shear, the available energy G depends on the elastic energy density in the body of the sample. At a particular strain, this increases with the modulus of the elastomeric material. Thus, improvements in crack growth characteristics conferred by carbon black may not be evident if comparison is made on a strain basis.

5.4.4 Effect of Oxygen

The presence of oxygen in the test atmosphere can affect the extent of mechanical crack growth. This is shown in Fig. 5.10 for unfilled natural rubber. In a vacuum, the G value required for a particular crack growth rate is increased by a factor of around 2. It is rather better to consider oxygen as affecting the G value instead of the rate of growth because, at low G values, in the vicinity of G_0 (below which mechanical tearing ceases), the effect on growth rate (at constant G) can be very large. Indeed, there is a region in which mechanical crack growth occurs at atmospheric pressure

where no growth is observed in vacuo. Although the term “mechanical” is often used here, it is thus generally more correct to describe the process as “mechanico-oxidative” crack growth. The influence of oxygen on crack growth is quite distinct from oxidative aging, there being no deterioration in bulk properties, and parallels the effect observed in mastication.

The oxygen effect is dependent on the rate of crack growth, hence on the rate of cycling. At high enough crack growth rates, oxygen has little effect. Presumably there is a stress-activated oxidative scission process leading to the breakage of molecular chains, and this is time dependent (and also, no doubt, temperature dependent). According to the molecular theory discussed above, the reduction of G_0 by oxygen is ascribed to an effective reduction in the energy J stored in the bonds at rupture, of magnitude some two- to three-fold for natural rubber from the data in Fig. 5.10 (note that this reduction is primarily in the energy stored by the single bonds, although it is the double bonds that are expected to interact with oxygen). Suitable anti-flex-cracking agents (certain antioxidants) mitigate the effect of oxygen and give crack growth behavior typically about midway between the two curves shown in Fig. 5.10.

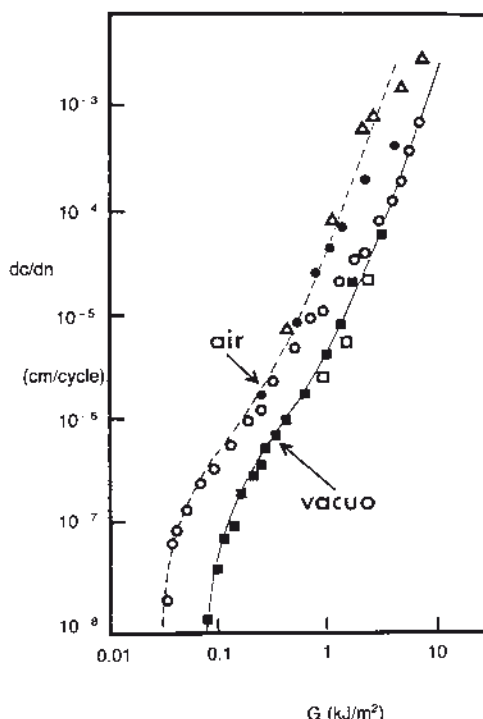


FIGURE 5.10 Effect of atmosphere and frequency on cyclic crack growth in a natural rubber vulcanizate containing no added anti-flex-cracking agent.

Experiments at atmospheric pressure; \circ = approximate frequency 2 Hz; \bullet = 0.02 Hz; Δ = 0.0002 Hz. Experiments in vacuo ($< 10^{-2}$ torr); \blacksquare = 2 Hz; \square = 0.02 Hz

5.4.5 Effects of Frequency and Temperature

The effects of frequency and temperature follow broadly what might be expected from tear behavior. Thus, little effect of frequency (or strain rate) is observed for crystallizing natural rubber over a wide range. The effects are rather greater for non-crystallizing SBR, although even for an unfilled vulcanize, the growth step is substantially constant for frequencies above about 0.1 Hz at 20 °C. Similarly, the effect of temperature is small over a range from about 0 to 100 °C for natural rubber; at higher temperatures, crystallization may be impeded and crack growth strongly affected by temperature, as well as by variations in the vulcanizing system. A much stronger temperature dependence is observed over the whole range for unfilled SBR, but this is moderated by incorporation of filler to an extent that depends on the type and amount of filler.

5.4.6 Nonrelaxing Effects

An important effect is observed when the strain is not relaxed to zero for part of each cycle: for strain-crystallizing elastomers, such as natural rubber – the crack growth rate may be very substantially reduced. Figure 5.11 shows some results for an unfilled NR vulcanize. In this instance, with a minimum tearing energy of about 6% of the maximum, the threshold energy is effectively increased and the crack growth rate at higher energies is reduced. Many rubber springs are subjected to an oscillating load superimposed on a dead load, and thus the nonrelaxing behavior may be of prime importance. It is, by its nature, rather more difficult to measure than the completely relaxing case. Much smaller nonrelaxing effects tend to be observed in non-crystallizing elastomers, in part because of the occurrence of time-dependent mechanical crack growth.

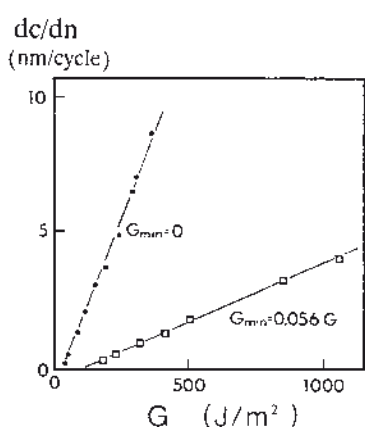


FIGURE 5.11 Effect of nonzero minimum tearing energy (nonrelaxing conditions) on cyclic growth in natural rubber. Cyclic crack growth rate dc/dn versus maximum tearing energy G of the cycle with minimum tearing energy, G_{min} , zero and with G_{min} equal to about 6% of the maximum.

5.4.7 Time-Dependent Failure

In non-crystallizing elastomers, such as SBR, time-dependent failure under constant force discussed earlier in the context of tearing, can occur at much lower rates and energies, right down to the mechanical threshold. Indeed, at low frequencies, the cyclic growth that is observed with SBR is simply the summation of time-dependent growth over the loading cycle, although at higher frequencies there is a distinct cyclic component, as noted earlier. Apart from this, the characteristics of time-dependent growth are very similar to those of cyclic growth, and show similar energy dependencies and threshold energies. Time-dependent crack growth can lead to mechanical failure under constant load, again with a fatigue limit similar to that observed under cyclic conditions. Fillers, particularly fine-particle ones, can considerably reduce rates of time-dependent crack growth in non-crystallizing elastomers, but with most types and loadings such failure still occurs.

■ 5.5 Ozone Attack

As mentioned above, ozone attack can be a significant factor in failure. Ozone reacts very rapidly with carbon-carbon double bonds and causes time-dependent crack growth even under constant loading; this can occur at very small G values in a susceptible, unprotected rubber (i.e., one with carbon-carbon double bonds in the main chain and without added antiozonant). Under cyclic loading, when mechanical crack growth is very slow or absent, ozone attack may be the dominant crack growth process until the cracks are large enough to permit mechanical growth to take over: that is, until G_0 is reached (Fig. 5.12). For continuous cyclic loading at upward of very low frequencies, the ozone contribution normally soon becomes negligible once G_0 has been exceeded, as Fig. 5.12 illustrates.

The cyclic ozone crack growth referred to above closely parallels the behavior observed for the growth of a single crack by ozone under fixed load (or deformation). In the latter case the growth is time dependent and, provided the temperature is well above the glass transition temperature for the elastomer, the rate is commonly found to be proportional to the ozone concentration and independent of the tearing energy, provided this exceeds a threshold value, G_z (Fig. 5.13). Thus, the time-dependent growth can be represented by an equation of the form

$$\frac{dc}{dt} = \alpha [O_z] \quad G > G_z \quad (5.10)$$

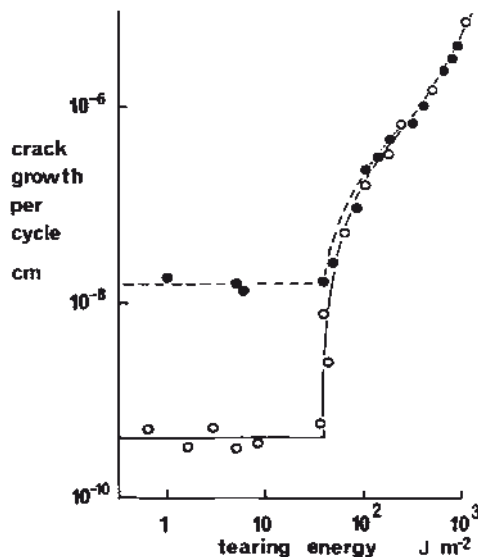


FIGURE 5.12 Effect of ozone on cyclic crack growth in a natural rubber vulcanizate.

Experiments in the laboratory atmosphere (○): ozone concentration about 0.3 parts per hundred million (pphm) of air by volume; experiments in an ozone chamber (●): concentration 20 pphm. The G_0 value for this vulcanizate is about 40 J/m^2

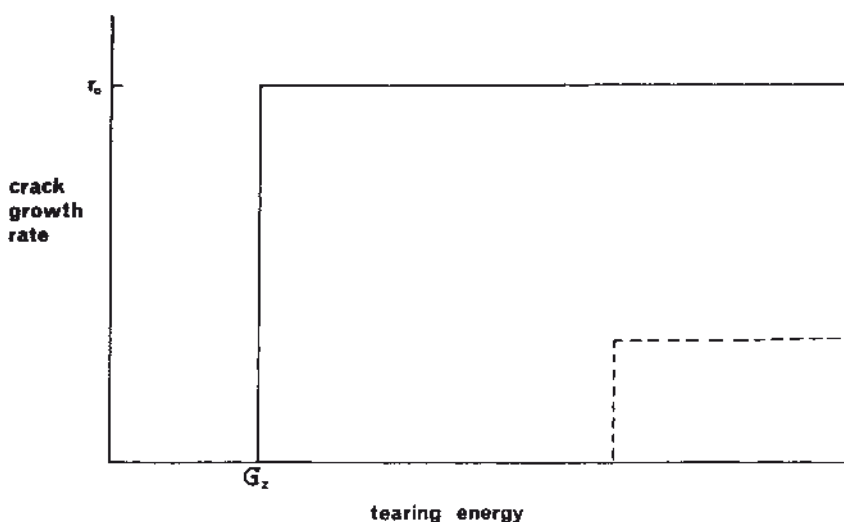


FIGURE 5.13 Characteristics of single crack growth under fixed load due to ozone (schematic):

G_z represents the threshold energy and r_0 the energy-independent rate of growth above G_z (cf. Eq. (5.10)). The dashed line indicates the effects of a good chemical antiozonant

where α is a constant representative of the vulcanizate (α may be influenced by the degree of crosslinking, fillers, and other vulcanizing ingredients, as well as by elastomer type). The behavior represented by Eq. (5.10) is consistent with a simple mechanistic picture, in which the rate of crack growth is controlled mainly by the rate of impact of ozone molecules on the rubber chains at the crack tip. At lower temperatures (in relation to the glass transition), the rate may be greatly reduced and may become controlled by the viscoelastic behavior of the rubber. Mechanistically, it appears that the retraction of severed chain ends, after ozone scission has occurred, is the rate-limiting factor in this region.

For vulcanizates containing no protective agents, G_z is typically only 0.1 J/m^2 . This compares with some 50 J/m^2 for the mechanical threshold G_0 . The very low ozone threshold is comparable with twice (since there are two crack surfaces) the surface energy of simple organic liquids and is believed to represent the energy required to separate chain ends after ozone has caused direct cleavage of carbon-carbon double bonds in the backbone chains. If rubber is unstressed (or if the energy at flaws is less than G_z), ozone attack does occur but is much less apparent, since it is restricted to a very slow, uniform erosion of the surface with no visible cracks.

Ozone cracking in a surface held at constant deformation is a good deal more complex than might be expected from the simple, single crack growth behavior just described. It has some unusual and, at first sight, perplexing features. Thus, the crack density increases with increase in strain (Fig. 5.14), while there is a concomitant decrease in the rate of growth. The increase in crack density can be understood in terms

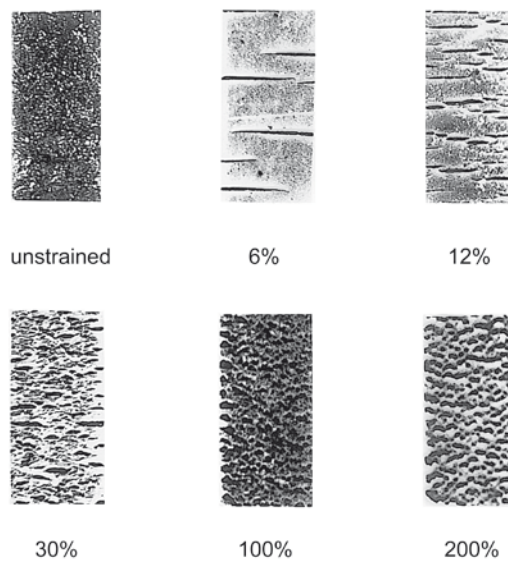


FIGURE 5.14 Variation with strain of the ozone cracking pattern in a surface held at constant strain (unprotected natural rubber vulcanize; same ozone exposure conditions at each strain)

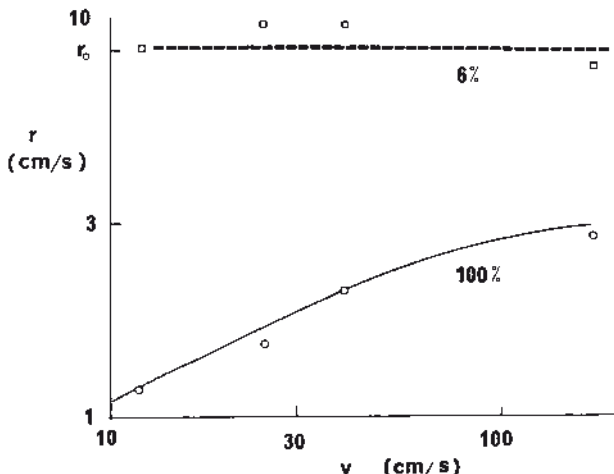


FIGURE 5.15 Variation of the rate r of ozone crack growth in a surface held at constant strain with speed of the gas stream passing over the surface v for strains of 6 and 100% (unprotected natural rubber vulcanizate); r_0 is the single crack rate of growth (cf. Eq. (5.10) and Fig. 5.13)

of a distribution of surface flaws, with the threshold energy G_z being attained at progressively smaller flaws as the strain increases. At any given strain, except at very early stages of exposure, the crack density tends to decrease with time, owing to crack coalescence or obsolescence (cracks being overtaken by larger cracks and ceasing to grow because the necessary energy is no longer available). The variation in rate of growth with strain applies not only to growth in the surface (Fig. 5.14) but also (and more importantly from a strength viewpoint) to growth perpendicular to the surface. The rate is also found to depend on the fluid flow rate over the surface (Fig. 5.15) and the size of the article involved; moreover, it is much slower, if the medium carrying the ozone is a liquid rather than a gas. The rate may also decrease with increase in crack length normal to a surface, for deep enclosed cracks. These features are ascribable to diffusion control mechanisms, which arise because ozone reacts rapidly with, and is destroyed by, stretched rubber; indeed, the greater the number of cracks that are growing, the more rapid the destruction. Thus, the rate of growth may be controlled by the need for ozone to diffuse across the boundary layer of fluid adjacent to a rubber surface, or within a crack itself. For repeated loading, at fairly high frequency, the diffusion effects would be expected to be much smaller, consistent with the simpler picture observed in this case (cf. Fig. 5.12).

Incorporation of a chemical ‘antiozonant’ in the rubber can effectively increase the threshold energy by several orders of magnitude from the value of about 0.1 J/m^2 for an unprotected vulcanize containing main-chain unsaturation. The most effective antiozonants form a protective layer on the rubber surface by reaction with ozone, diffusion of antiozonant from the interior being necessary for a layer to build up.

Thus, high glass transition temperature elastomers, such as nitrile rubber or epoxidized natural rubber, in which antioxidants diffuse more slowly, are more difficult to protect than natural rubber or SBR. Under continuous cyclic loading the layer tends to break down mechanically, so that protection is lost. However, chemical antiozonants also reduce the rate of ozone crack growth and this benefit applies equally under cyclic loading. When cycling is intermittent, significant threshold effects may be retained, especially at the low ozone concentrations that often apply in service.

■ 5.6 Tensile Strength

In engineering applications it is unlikely that failure will take place in only one loading cycle; thus conventionally measured tensile strength behavior is not directly relevant. However, it is the most commonly used laboratory test method for evaluating strength, so it is of interest to consider the relation between tensile strength and crack growth behavior. The close interrelation between fatigue failure – failure after many loading cycles – and crack growth was referred to earlier and is discussed more fully in Chapter 6, where it is shown that the number of cycles to failure can be quantitatively related to the crack growth characteristics and the size of flaw that is present initially. In essence, tensile failure can be regarded as a single-cycle fatigue test, in which crack growth occurs from a pre-existing flaw as the test piece is extended, although there are complications in the analysis owing to scale and other effects.

For non-crystallizing elastomers, the tensile strength (or work to break, which is the quantity obtained explicitly from the fracture mechanics approach) varies with rate of extension in the way expected from the observed time-dependent mechanical crack growth. For crystallizing elastomers, the virtual absence of such growth corresponds to a substantial lack of dependence of the strength, or work to break, on rate (at least in the absence of oxidative effects, which can occur at very slow rates of extension (Fig. 5.16)). This effect parallels that of frequency in cyclic crack growth at lower tearing energies (cf. Fig. 5.10). For crystallizing elastomers, the cyclic growth component will occur as a test piece is extended, but an additional complication is that if the bulk of the test piece becomes crystalline (as is usually the case prior to tensile failure), catastrophic tearing does not occur. Under these circumstances, the cyclic growth component continues at higher tearing energies, and this eventually leads to unstable crack propagation and failure. A corresponding change in failure mechanism is observed when the dependence of the breaking stress on flaw size is investigated (Fig. 5.17) and can also occur in the absence of inserted flaws at elevated temperature (when crystallization in the bulk is suppressed).

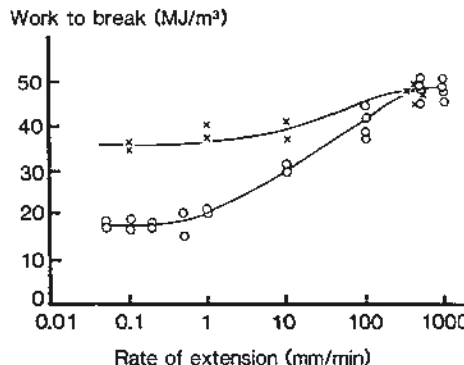


FIGURE 5.16 Dependence of the work to break in a tensile test on rate of extension for NR vulcanizates without antioxidant (O) and with 1 phr of a good flex-cracking antioxidant (×)

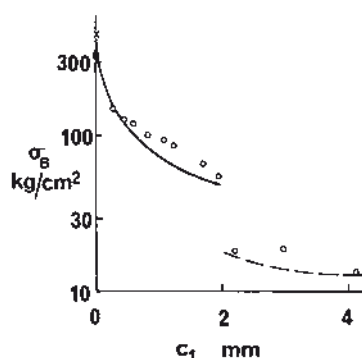


FIGURE 5.17 Tensile breaking stress σ_B versus size of inserted edge cut c_1 for a natural rubber vulcanizate (O). The theoretical curves assume failure to occur when the catastrophic tear strength is reached (dashed curve) and as a result of unstable crack growth (solid curve). The transition from one mechanism to the other occurs when crystallization takes place in the bulk. The tensile strength (in the absence of an inserted cut) is shown by a solid circle (●), and the calculated value (from the fracture mechanics based unstable crack growth theory, assuming the same initiating flaw size as for fatigue failure: cf. Chapter 6) by (X)

The crack growth behavior relevant to tensile failure occurs in a region different (higher severity) from that relevant to most fatigue applications. Because of variations in the form of the crack growth characteristics for different materials (cf. earlier discussion), tensile strength is not likely to be a useful indicator of fatigue performance, except possibly at very high strains. Tensile measurements should therefore be regarded as primarily of interest from a quality control viewpoint and, for this reason, the failure mechanisms are not discussed in more detail here.

■ 5.7 Crack Growth in Shear and Compression

Applications of the fracture mechanics approach that have features in common with some engineering uses of rubber involve treatments of crack growth in a bonded block or cylinder subjected to simple shear. Figure 5.18 illustrates the geometry for the block. If the crack is long enough compared with the height h , then simple considerations of the geometry show that there will be a region (region 4 in Fig. 5.18b) that is essentially unstrained, another region in simple shear (region 2), with an elastic energy density of U , say, and an edge region (region 1). A region of complex strain (region 3) will move with the crack so that the tearing energy will be given by

$$G = U h \quad (5.11)$$

which is the same as for a long crack in pure shear (Eq. (5.2)).

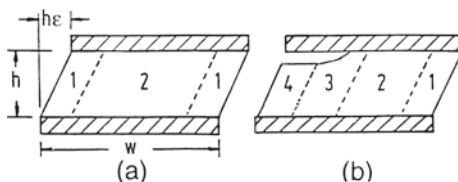


FIGURE 5.18 Bonded unit subjected to simple shear strain ε : (a) with no crack and (b) with a crack adjacent to a bonded surface. The numbered regions relate to the derivation of the strain energy release rate for crack growth as discussed in the text

If a suitable crack is introduced near the bond, and the test piece cycled in shear, the observed rate of crack growth can be compared with that deduced from independent experiments on the rubber using, for example, a tensile strip test piece. The results (Fig. 5.19) compare well with the independent measurements.

For small cracks, Eq. (5.11) does not hold. With this geometry there are stress concentrations near the bonded edges at the corners of the block and large strain gradients in these regions. Energy release rates therefore vary strongly with crack length c . A finite element analysis has been carried out for a range of crack lengths and values of G have been calculated from the change of total elastic energy with c . The stress concentrations near the ‘leading’ and ‘trailing’ corners (with respect to the shear displacement) of the block shown in Fig. 5.18 – the stresses near the edge of the rubber-metal bond are tensile in nature. Results for these corners are shown in Fig. 5.20. The dependence of G on c shows the interesting feature that as the crack grows away from the edge, the effect of the stress concentration diminishes rapidly, and G then falls before increasing to the final value given by Eq. (5.11). Thus a crack initiating at the corner may not grow beyond a short

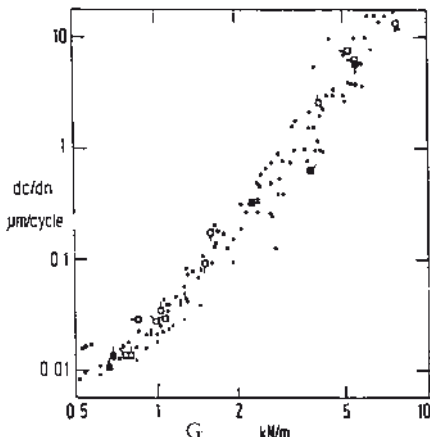


FIGURE 5.19 Comparison of cyclic crack growth characteristics obtained from tensile strip test pieces with edge cracks (Fig. 5.3 and Eq. (5.3)) with crack growth behavior measured in shear units (with G calculated from Eq. (5.11)): □ = single shear units; ■ = double shear units. Different flags indicate different unit heights (h , Fig. 5.18) as follows: □ = 1 mm; □ = 2 mm; □ = 3 mm; □ = 4 mm; □ = 5 mm; □ = 6 mm. The crack length in the shear units was at least 3 h

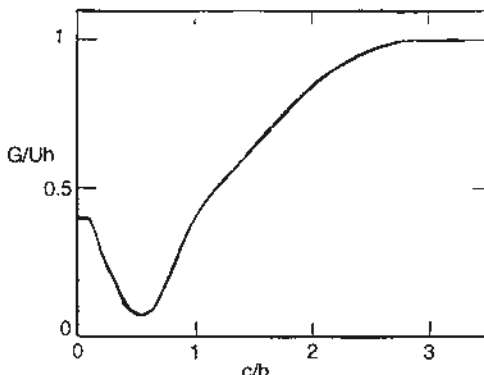


FIGURE 5.20 Variation of strain energy release rate G with crack length c derived from finite element analysis for a crack near a bonded surface in a shear unit. Reduced variables are used, U being the strain energy density in the bulk and h the unit height (cf. Fig. 5.18)

distance, if the minimum G value is below the crack growth limit G_0 . The stress concentrations at the ‘trailing’ corners are compressive and lead to relatively low G values for short cracks.

Similar considerations to those above apply for a crack growing in a long cylindrical elastic tube, bonded between a rigid cylindrical core and a rigid surrounding tube, and subjected to axial shear. In this case, strain energy release rates for a cylindrical crack growing from one end adjacent to the inner bonded interface have been

investigated by finite element analysis for a range of crack lengths and cylinder dimensions. Broadly, the conclusions are similar to those described above but show, additionally, that the energy release rate may depend on the direction of propagation. For a crack propagating from the tensile stress concentration end (i.e. equivalent to the lower left or upper right corners of the block shown in Figure 5.18), the energy will not exceed and, depending on the radial dimensions, may be less than that for a crack growing from the other end once the crack becomes large (relative to the radial thickness). A similar consideration appears likely to apply for the rectangular block. For the co-axial cylinder, it was concluded that failure at or near the interface with the core was more likely than growth of a crack through the elastic material under the influence of the maximum tensile stress.

Another test piece geometry that has been employed is a circular rubber disc bonded between two plates and subjected to repeated twisting. A circumferential crack introduced in the outer surface grows radially inwards, and an approximate fracture mechanics analysis allows the observed crack growth rate to be expressed in terms of G . Comparison with previously published data on similar materials shows satisfactory agreement. This geometry, like that of simple shear described above, involves growth under a shear deformation. As pointed out earlier, this often occurs in practical applications. Also, in these experiments the effective thickness of the rubber at the tip is relatively large and, as crack growth data are usually obtained on sheets only about 1 to 2 mm thick, the agreement found indicates that thickness effects are not large over this range. Thus, there is a good prospect that conventional crack growth data can be used successfully to predict the behavior in practical engineering applications.

Uniaxial compression of bonded units (and of unbonded units when there is no slip at the interfaces) induces tensile stresses in surface regions (again particularly near bonded edges). Crack growth may result, and it appears that the fracture mechanics approach can be applied to relate the rate of growth to independent measurements of the crack growth characteristics of the rubber. For high shape factor bonded units in compression, an equation of the form of Eq. (5.11) has been found to apply for cracks growing essentially parallel to the bonded surfaces. A similar equation has also been found to apply for crack growth between the plies in rubber-cord laminated structures, such as are used in tires and other articles, in which the deformations can be very complex. These aspects are discussed more fully in Chapter 6. Caution may be needed when there are compressive stresses. In cases of adhesion failure, for example, energy release rates have been found to be reduced by frictional effects.

It is interesting to note that in the application of fracture mechanics to other, relatively rigid, materials it has been found necessary to invoke different strength behaviors for different fracture modes. This appears to be unnecessary for rubber.

■ 5.8 Cavitation and Related Failures

The preceding discussion of failure has been concerned with crack growth or tear behavior, using a fracture mechanics approach. If a rubber vulcanize is subjected to a hydrostatic tension – that is, all three principal stresses are equal and tensile – then failure may take place by what appears to be a different mechanism, namely cavitation. This state of stress may be approached in bonded rubber-metal components when a tensile load is applied because of constraints imposed by the rigid rubber-metal interfaces. The phenomenon of cavitation has been studied using rubber-metal bonded cylinders of large diameter-to-height ratios. When loaded in tension, a critical state is reached when cavities suddenly grow in the body of the rubber, producing a drop in the extending force. Subsequent examination of the samples reveals the presence of internal cracks, which can initiate catastrophic failure if the load is increased further.

In a theory that has been remarkably successful in explaining the phenomenon, cavitation is attributed to elastic instability. The theory is based on the large-strain elastic solution of the problem of the dilation of a spherical cavity in an infinite rubber block subjected to uniform hydrostatic tension at infinity. This solution shows that, for a rubber obeying the statistical theory of rubber-like elasticity, the tensile stress asymptotes to a value of $5 E/6$ as the cavity radius increases, where E is the tensile modulus. Hence, if this stress is reached, the cavity is expected to increase in size without limit.

The stress is independent of the initial radius of the cavity, provided this is sufficiently large ($> \sim 10^{-7}$ m) for surface energy effects to be negligible. Thus, if the rubber has internal imperfections (of sufficient size) that can be modelled by spherical holes, the stress of $5 E/6$ can be identified with that required to produce the observed cavitation.

The cracking stress is thus predicted to be proportional to the modulus and independent of the intrinsic strength characteristics of the material. These features are in accord with experiment, although the distribution of flaws in a material influences how many cavities are initiated and the tear strength affects how easily failure then propagates through the sample.

Since critical tensions for cavitation are much lower than typical compression stresses that can be sustained safely by many components, care is necessary to avoid substantial hydrostatic tensions in either the use or proof testing of bonded components. Approximate analytical solutions are available that give the maximum hydrostatic tensions for extension and tilting deformations of bonded rubber blocks. For example, for a bonded cylinder of fairly large diameter-to-thickness ratio, the maximum hydrostatic tension is approximately twice the tensile stress applied to the cylinder.

If gas is dissolved in rubber under pressure and this pressure is suddenly released, bubbles may develop and grow with time, provided the initial pressure was high enough. It is thought that this process is essentially the same as that described above, except that a hydrostatic pressure is applied to the interior of the cavity rather than a tensile stress to the rubber at infinity. These two situations are equivalent because of the incompressibility of rubber. This phenomenon has become of particular importance with the widespread use of deep-sea oil drilling; this has led to the occurrence of what has been termed explosive decompression failure of rubber seals, when the pressure of a gas, which is in external contact with the rubber and is particularly soluble in it, is suddenly decreased from a high value. This can lead to such rapid and extensive bubble growth that the seal may fail catastrophically.

A theory similar to that for cavitation has been proposed to explain the phenomenon described above in terms of an elastic instability. The predictions of the theory are in remarkably good agreement with the experimental results for both cavitation and bubble formation. However, observation of the failure regions shows that cracks have formed, so that a fracture process has taken place. A finite strain fracture mechanics analysis of the inflation of a penny-shaped crack in an infinite block gives G in terms of the inflating pressure, rubber modulus and initial crack diameter. At low pressures, the small strain solution is followed as expected with G increasing as the square of the pressure. At higher pressures, of the order of E , G increases more rapidly and crack growth followed by failure may be anticipated, although the detailed crack growth behavior of the material will have an influence on the detailed way in which this occurs.

■ 5.9 Conclusions

The fracture mechanics approach appears to provide a rational basis for predicting crack growth behavior in rubber articles. It is necessary for the intrinsic crack growth behavior of the rubber itself to be determined, at least approximately, using one or more of the appropriate test pieces. The complementary knowledge of the energy release rate for an article must be obtained from an appropriate elastic analysis of the article, either by an analytical (probably approximate) calculation or by a finite element approach.

■ References

Reviews

- Atkins, A. G., and Mai, Y.-W., "Elastic and Plastic Fracture", Ellis Horwood, U.K., 1985.
- Gent, A. N., "Some Outstanding Problems in the Mechanics of Rubbery Solids", Chapter 1 in A. K. Bhowmick (Ed.), "Current Topics in Elastomers Research", CRC Press, 2008.
- Greensmith, H. W., Mullins, L., and Thomas, A. G., "Strength of Rubbers", in L. Bateman (Ed.), The Chemistry and Physics of Rubber-like Substances, Maclarens, London, 1962, p. 249.
- Lake, G. J., "Mechanical Fatigue of Rubber", *Rubber Chem. Technol.*, **45**, 309 (1972).
- Lake, G. J., "Aspects of Fatigue and Fracture of Rubber", *Prog. Rubber Technol.*, **45**, 89 (1983).
- Lake, G. J., and Thomas, A. G., "Strength Properties of Rubber", in A. D. Roberts (Ed.), Natural Rubber Science and Technology, Oxford University Press, Oxford, Chapter 15, 1988.
- Treloar, L. R. G., The Physics of Rubber Elasticity, 3rd ed., Clarendon Press, Oxford, 1975.

Fundamentals

- Ahagon, A., and Gent, A. N., "Threshold Fracture Energies for Elastomers", *J. Polym. Sci., Polym. Phys. Ed.*, **13**, 1903 (1975).
- Andrews, E. H., "Rupture Propagation in Hysteresial Materials: Stress at a Notch", *J. Mech. Phys. Solids*, **11**, 231 (1963).
- Bell, C. L. M., Stinson, D., and Thomas, A. G., "Measurement of Tensile Strength of Natural Rubber Vulcanizates at Elevated Temperature", *Rubber Chem. Technol.*, **55**, 66 (1982).
- Bhowmick, A. K., Gent, A. N., and Pulford, C. T. R., "Tear Strength of Elastomers Under Threshold Conditions", *Rubber Chem. Technol.*, **56**, 206 (1983).
- Gent, A. N., and Tobias, R. H., "Threshold Tear Strength of Elastomers", *J. Polym. Sci., Polym. Phys. Ed.*, **20**, 2051 (1982).
- Greensmith, H. W., "Rupture of Rubber Part 10: The Change in Stored Energy on Making a Small Cut in a Test Piece Held in Simple Extension", *J. Appl. Polym. Sci.*, **7**, 993 (1963).
- Greensmith, H. W., "Rupture of Rubber Part 11: Tensile Rupture and Crack Growth in Noncrystallizing Rubber", *J. Appl. Polym. Sci.*, **8**, 1113 (1964).
- Griffith, A. A., "The Phenomena of Rupture and Flow in Solids", *Phil. Trans. R. Soc. London, Ser. A*, **221**, 163 (1920).
- Lake, G. J., and Thomas, A. G., "The Strength of Highly Elastic Materials", *Proc. R. Soc. London, Ser. A*, **300**, 108 (1967).
- Lake, G. J., and Yeoh, O. H., "Effect of Crack Tip Sharpness on the Strength of Vulcanized Rubbers", *J. Polym. Sci. Polym. Phys. Ed.*, **25**, 1157 (1987).
- Lake, G. J., Lindley, P. B., and Thomas, A. G., "Fracture Mechanics of Rubber", in Proceedings of the Second International Conference on Fracture, Brighton, Chapman & Hall, London, 1969, p. 493.
- Lindley, P. B., and Thomas, A. G., "Fundamental Study of the Fatigue of Rubbers", in Proceedings of the Fourth Rubber Technology Conference, London, IRI, London, 1962, p. 428.

- Mullins, L., "Rupture of Rubber Part 9: Role of Hysteresis in the Tearing of Rubbers", *Trans. Inst. Rubber Ind.*, **35**, 213 (1959).
- Rivlin, R. S., and Thomas, A. G., "Rupture of Rubber Part 1: Characteristic Energy for Tearing", *J. Polym. Sci.*, **10**, 291 (1953).
- Thomas, A. G., "Rupture of Rubber Part 2: The Strain Concentration at an Incision", *J. Polym. Sci.*, **18**, 177 (1955).
- Thomas, A. G., "Rupture of Rubber Part 6: Further Experiments on the Tear Criterion", *J. Appl. Polym. Sci.*, **3**, 168 (1960).
- Thomas, A. G., "Fracture of Rubber: Physical Basis of Yield and Fracture", in Conference Proceedings Oxford, Institute of Physics and Physical Society, London, p. 134, 1966.
- Thomas, A. G., and Whittle, J. M., *Rubber Chem. Technol.*, **43**, 222 (1970).
- Williams, M. L., Landel, R. F., and Ferry, J. D., "The Temperature Dependence of Relaxation Mechanisms in Amorphous Polymers and Other Glass Forming Liquids", *J. Am. Chem. Soc.*, **77**, 3701 (1955).

Failure Processes

Cavitation

- Busfield, J. J. C., Davies, C. K. L., and Thomas, A. G., "Aspects of Fracture in Rubber Components", *Progress in Rubber and Plastics Technology*, **12**, 191 (1996).
- Gent, A. N., and Lindley, P. B., "Internal Rupture of Bonded Rubber Cylinders in Tension", *Proc. R. Soc. London, Ser. A*, **249**, 195 (1958).
- Gent, A. N., and Meinecke, E. A., "Compression, Bending, and Shear of Bonded Rubber Blocks", *Polym. Eng. Sci.*, **10**, 48 (1970).
- Gent, A. N., and Tompkins, D. A., "Nucleation and Growth of Gas Bubbles in Elastomers", *J. Appl. Phys.*, **40**, 2520 (1969).
- Gent, A. N., and Wang, C. "Fracture Mechanics and Cavitation in Rubber-Like Solids", *J. Mat. Sci.*, **26**, 3392 (1991).

Crack Growth

- Aboutorabi, H., Ebbott, T., Gent, A. N., and Yeoh, O. H., "Crack Growth in Twisted Rubber Disks, Part I. Fracture Energy Calculation", *Rubber Chem. Technol.*, **71**, 76 (1998).
- Busfield, J. J. C., Ratsimba, C. H., and Thomas, A. G., "Crack Growth and Strain Induced Anisotropy in Carbon Black Filled Natural Rubber", *J. nat. Rubb. Res.*, **12**, 131 (1997).
- Cadwell, S. M., Merrill, R. A., Sloman, C. M., and Yost, F. L., "Dynamic Fatigue Life of Rubber", *Ind. Eng. Chem. Anal. Ed.*, **12**, 19 (1940).
- Gent, A. N., and De, D. K., "Part II. Experimental Results", *Rubber Chem. Technol.*, **71**, 84 (1998).
- Gent, A. N., Lindley, P. B., and Thomas, A. G., "Cut Growth and Fatigue of Rubbers Part 1: The Relationship Between Cut Growth and Fatigue", *J. Appl. Polym. Sci.*, **8**, 455 (1964).
- Lake, G. J., and Lindley, P. B., "Cut Growth and Fatigue of Rubbers Part 2: Experiments on a Noncrystallizing Rubber", *J. Polym. Sci.*, **8**, 707 (1964).
- Lake, G. J., and Lindley, P. B., "The Mechanical Fatigue Limit for Rubber, and the Role of Ozone in Dynamic Cut Growth of Rubber", *J. Appl. Polym. Sci.*, **9**, 1233, 2031 (1965).
- Lake, G. J., Samsuri, A., Teo, S. C., and Vaja, J., "Time-Dependent Fracture in Vulcanized Elastomers", *Polymer*, **32**, 2963 (1991).

- Lake, G. J., Thomas, A. G., and Lawrence, C. C., "Effects of Hydrostatic Pressure on Crack Growth in Elastomers", *Polymer*, **33**, 4069 (1992).
- Lindley, P. B., "Relation Between Hysteresis and the Dynamic Crack Growth Resistance of Natural Rubber", *Int. J. Fract.*, **9**, 449 (1973).
- Lindley, P. B., "Nonrelaxing Crack Growth and Fatigue in a Noncrystallizing Rubber", *Rubber Chem. Technol.*, **47**, 1253 (1974).
- Thomas, A. G., "Rupture of Rubber Part 5: Cut Growth in Natural Rubber Vulcanizates", *J. Polym. Sci.*, **31**, 467 (1958).

Ozone Attack

- Braden, M., and Gent, A. N., "The Attack of Ozone on Stretched Rubber Vulcanizates. Part I: The Rate of Cut Growth. Part II: Conditions for Cut Growth", *J. Appl. Polym. Sci.*, **3**, 90 and 100 (1960).
- Lake, G. J., "Ozone Cracking and Protection of Rubber", *Rubber Chem. Technol.*, **43**, 1230 (1970).
- Lake, G. J., "Corrosive Aspects of Fatigue", in *Proceedings of the International Conference on Corrosion Fatigue*, University of Connecticut, 1971, p. 710. *Rubber Age*, **104**(8), 30; **104**(10), 39 (1972).
- Lake, G. J., and Lindley, P. B., "Ozone Cracking, Flex Cracking, and Fatigue of Rubber. Part 1: Cut Growth Mechanisms and How They Result in Fatigue Failure. Part 2: Technological Aspects", *Rubber J.*, **146**(10), 24; **146**(11), 30 (1964).
- Lake, G. J., and Mente, P. G., "Ozone Cracking and Protection of Elastomers at High and Low Temperatures", *J. Nat. Rubb. Res.*, **7**, 1 (1993).
- Lake, G. J., and Mente, P. G., "Mechanisms of Antiozonant Protection of Elastomers", *Polymer Degradation and Stability*, **49**, 193 (1995).

Tear

- Brown, P., Porter, M., and Thomas, A. G., "The Dependence of Strength Properties on Crosslink Structure in Vulcanized Polyisoprene", *Kautsch. Gummi Kunst.*, **40**, 17 (1987).
- Gent, A. N., and Henry, A. W., "On the Tear Strength of Rubbers", in *Proceedings of the International Rubber Conference*, Brighton, Maclarens, London, p. 193, 1967.
- Gent, A. N., and Kim, H. J., "Tear Strength of Stretched Rubber", *Rubber Chem. Technol.*, **51**, 35 (1978).
- Greensmith, H. W., "Rupture of Rubber. Part 4: Tear Properties of Vulcanizates Containing Carbon Black", *J. Polym. Sci.*, **21**, 175 (1956).
- Greensmith, H. W., "Rupture of Rubber. Part 8: Comparisons of Tear and Tensile Rupture Measurements", *J. Appl. Polym. Sci.*, **3**, 183 (1960).
- Greensmith, H. W., and Thomas, A. G., "Rupture of Rubber. Part 3: Determination of Tear Properties", *J. Polym. Sci.*, **18**, 189 (1955).
- Kadir, A., and Thomas, A. G., "Tear Behaviour of Rubbers over a Wide Range of Rates", *Rubber Chem. Technol.*, **54**, 15 (1981).
- Kadir, A., and Thomas, A. G., "Tearing of Unvulcanized Natural Rubber", *J. Polym. Sci., Polym. Phys. Ed.*, **23**, 1623 (1984).

Applications

- Breidenbach, R. F., and Lake, G. J., "Mechanics of Fracture in Two-Ply Laminates", *Rubber Chem. Technol.*, **52**, 96 (1979).

- Breidenbach, R. F., and Lake, G. J., "Application of Fracture Mechanics to Rubber Articles, Including Tyres", *Phil. Trans. R. Soc. Lond.*, **A299**, 189 (1981).
- Gent, A. N., and Wang, C., "Strain Energy Release Rate for Crack Growth in an Elastic Cylinder Subjected to Axial Shear", *Rubber Chem. Technol.*, **66**, 712 (1993).
- Lindley, P. B., "Energy for Crack Growth in Model Rubber Components", *J. Strain Anal.*, **7**, 132 (1972).
- Lindley, P. B., and Teo, S. C., "Energy for Crack Growth at the Bonds of Rubber Springs", *Plast. Rubber Mater. Appl.*, **4**, 29 (1979).
- Lindley, P. B., and Stevenson, A., "Fatigue Resistance of Natural Rubber in Compression", in Fatigue '81: Conference Proceedings, Warwick, Westbury House, Guildford, p. 233; *Rubber Chem. Technol.*, **55**, 337 (1981).
- Stevenson, A., "Fatigue Crack Growth in High Load Capacity Rubber Laminates", *Rubber Chem. Technol.*, **59**, 208 (1986).

■ Problems for Chapter 5

1. The extent of vulcanization of an elastomer can be characterized by the molecular weight between crosslinks. How is the intrinsic strength of a vulcanized elastomer expected to vary according to Eq. (5.9), with: (a) the molecular weight between crosslinks, and (b) the shear modulus of the rubber? What other aspects of molecular structure are expected to affect the strength on this basis? Are there other factors, which do not appear in Eq. (5.9), which may also have effects?
2. An unprotected vulcanize has a threshold energy for ozone crack growth, G_z , of 0.09 J/m² and for mechano-oxidative crack growth, G_0 , of 25 J/m²; the Young's modulus of the vulcanize is 2 MPa, and the largest of the "naturally occurring" flaws present is equivalent to a crack of length 0.025 mm. Calculate the threshold strain in simple extension for each type of cracking. (The tensile stress-strain curve may be assumed linear and K taken as 2.)
3. Would you expect a vulcanized elastomer to fail catastrophically once the mechanical threshold energy is attained? If not, why not? Would you expect the tear strength and tensile strength to be closely interrelated to the threshold strength or to one another for vulcanizates of: (a) a strain-crystallizing elastomer; (b) a non-crystallizing elastomer? Discuss the reasons for your answer.
4. Two strain-crystallizing materials having widely different moduli are to be evaluated by the "trousers" and crescent tear tests. The Young's modulus E is measured to be 2 MPa for material A and 8 MPa for material B, with a variability of $\pm 5\%$ in each case. The tear strengths measured using "crescent" test pieces are found to be the same, within a variability approaching $\pm 30\%$. The tear "strengths" measured using "trousers" test pieces, with the legs reinforced to prevent their extension, are 10 N/mm for material A and 2.5 N/mm for material B, each with

a variability of $\pm 50\%$. Are the two sets of results consistent? (For the purposes of this example, the crescent tear test piece may be taken to be a tensile strip 2 cm wide and 2 mm thick containing an edge crack 1 mm long; the force-deflection curve may be assumed linear and K taken as 2.)

5. Three lightly-filled non-crystallizing elastomers have glass transition temperatures of -80°C , -50°C , and -20°C . Their tearing energies measured at room temperature (20°C) by tests in which the tear tip is constrained to keep deviations to $< 0.1\text{ mm}$, are about 2 kJ/m^2 , 4 kJ/m^2 , and 9 kJ/m^2 , respectively. What would the tear strengths be expected to be at (a) 0°C and (b) 60°C at the same rate of tearing? Suggest possible chemical compositions for these elastomers.

Effects of rate and temperature on the viscoelastic properties of the elastomers are generally given by Eq. (4.46) of Chapter 4 (with $A = 40^\circ\text{C}$ and $B = 50^\circ\text{C}$). The tearing energy may be assumed to vary as the one-sixth power of the reduced rate of tearing (the product of the rate and the shift factor a_T , cf. Fig. 5.6b). The possible correction of the tear energy according to the absolute temperature may be ignored.

6. A bonded shear unit has a height of 1 cm. The rubber has a shear modulus of 1 MPa, a threshold energy for mechanical crack growth (under fully relaxing conditions) of 50 J/m^2 , and a crack growth constant A (cf. Eq. (5.8)) of $2 \times 10^{-8}\text{ (m/cycle)/(kJ/m}^2)$. What is the maximum cyclic strain for which no mechanical crack growth will occur parallel to the bonded surfaces for a long crack? If a maximum cyclic strain of 20% is applied 10^6 times per year, what will the crack growth per year be when a steady rate is attained? (The minimum strain may be taken as zero and the shear stress-strain curve and crack growth characteristics assumed to be linear; ozone crack growth may be assumed to be negligible).

■ Answers to Problems for Chapter 5

1. The molecular weight between crosslinks, M_c , is related to the number of monomer units between crosslinks, m in Eq. (5.9), by

$$M_c = M_1 m$$

where M_1 is the mass of a monomer unit. The number of effective single bonds per unit volume, b , can be written as

$$b = \frac{p \rho}{M_1}$$

where p is the number of single bonds in the backbone molecular chain for each monomer unit and ρ is the density of the polymer. Substitution in Eq. (5.9) yields

$$G_0 = p \rho J \xi \left(\frac{M_c}{M_1^3} \right)^{1/2}$$

Thus, the threshold energy is predicted to increase as the square root of the molecular weight between crosslinks for a given elastomer, a dependence that has been found to hold reasonably well over much of the practical range (see below).

According to the statistical theory of rubber elasticity (Chapter 3), the shear modulus μ is related to the number of elastically effective molecular strands per unit volume N by

$$\mu = N k T$$

where k is Boltzmann's constant and T is the absolute temperature. Putting $N = \rho/M_c$ yields

$$G_0 = p J \xi \left(\frac{\rho^3 k T}{M_1^3 \mu} \right)^{1/2}$$

Thus, for a given elastomer, G_0 varies inversely as the square root of the shear modulus. (Note that the apparent dependence of G_0 on the square root of the absolute temperature arises only through the corresponding dependence of the shear modulus). Other important aspects of the molecular structure are the number of single bonds in the backbone chain relative to the mass of a monomer unit and the energy stored by a single bond at its point of rupture J . From a load-bearing viewpoint, material in side-groups is wasted, and consistent with this, vulcanizates of polybutadiene show the highest threshold energies of any elastomer. Although most elastomers have carbon-carbon backbone chains, some differences in J are expected because of variations in side-groupings. For elastomers with other backbone chains, larger differences [and lower values] of J are expected. Observations are broadly in accord with this.

Note that a number of simplifications and approximations are made in deriving Eq. (5.9). The distance between crosslinks in the unstrained state is calculated for freely-jointed chains. In practice, the chains will be less flexible, to various degrees. On this basis, a somewhat greater chain length (and G_0 value) would be expected for *trans*-polyisoprene than for *cis*-polyisoprene. A higher threshold energy is observed for *cis-trans* isomerized natural rubber than for ordinary

natural rubber, in qualitative agreement with this. For lightly-crosslinked materials, the effect of chain ends, which are wasted, is expected to be large, and threshold energies will be lower than predicted above. The molecular weight of the parent molecules, before any crosslinks are introduced, also affects the amount of wasted material). Although it is possible to take into account a distribution of chain lengths and random crosslinking, these variations are found to have relatively small effects. Whether physical (including entanglements) or chemical crosslink densities should be used is not entirely clearcut. Copolymers can be treated by suitable averaging of the contributions of the individual molecular constituents, bearing in mind that the weakest bond will determine the breaking force of a chain. For elastomers, including natural rubber and SBR, that contain unsaturation in their backbone molecular chains, G_0 may be lowered by atmospheric oxygen. This effect probably results from a reduction in the magnitude of J .

- Putting $K = 2$ and $U = \frac{1}{2} E \varepsilon^2$, where E is the Young's modulus and ε the tensile strain, in Eq. (5.3), gives

$$G = 2 E \varepsilon^2 c$$

which upon rearrangement gives for the threshold strain

$$\varepsilon_i = \left(\frac{G_i}{2 E c_0} \right)^{1/2}$$

where G_i is the corresponding threshold energy and c_0 the equivalent flaw size. Thus for ozone cracking

$$\varepsilon_z = \frac{0.09}{\left(2 \times 2 \times 10^6 \times 0.025 \times 10^{-3} \right)^{1/2}} = 0.03 \text{ or } 3\%$$

while for mechanico-oxidative crack growth

$$\varepsilon_0 = \frac{25}{\left(2 \times 2 \times 10^6 \times 0.025 \times 10^{-3} \right)^{1/2}} = 0.5 \text{ or } 50\%$$

- In general, catastrophic failure does not occur until energy much higher than the threshold energy is attained. This is believed to be because of the imperfect elasticity of most vulcanized elastomers. Their stress-strain curves are not perfectly reversible, displaying hysteresis loops which may be pronounced, particularly at high strains. When a crack grows, there are regions *near* the tip where the stresses are decreasing and are thus influenced by the retraction curve. The stress *at* the

tip will therefore be affected by the imperfect elasticity. Certain vulcanizates, for example, very highly swollen ones, which display little hysteresis, do exhibit catastrophic failure at energies close to the threshold.

Other factors can increase resistance to crack propagation at energies above the threshold. Crystallization induces very substantial hysteresis at the high strains relevant to fracture, and also produces a strong, oriented structure which probably both resists and diverts crack growth. Oriented structures associated with carbon black filler can act in a similar way, producing very blunt crack tips, of which “knotty” tearing is an extreme example, with correspondingly large energy increases. Tip blunting is very widely observed, even in unfilled non-crystallizing elastomers (cf. Fig. 5.6b). This must be due to other mechanisms, perhaps including random diversions as a crack advances due to molecular-scale inhomogeneities. Thus, the tear strength is influenced by various additional factors and is not expected to correlate directly with the threshold energy.

For crystallizing elastomers, failure in a tensile strength test normally occurs after the material has crystallized in the bulk. As a result, the tensile strength generally does not correlate with the tear strength, the two showing different dependencies on the degree of crosslinking, for example. For non-crystallizing elastomers, closer correlation between tear and tensile strengths is shown, for example, in rate and temperature dependencies. Even in this case, however, there are quantitative discrepancies associated with scale effects, because of the very much smaller amount of crack growth required to produce tensile failure. The latter factor is also likely to contribute for crystallizing materials and may be the reason for the relatively large naturally-occurring flaw sizes needed to account quantitatively for tensile failure stresses.

4. According to standard procedures, the tear “strength” for the “trousers” test piece is expressed as the tear force per unit thickness, which, rearranging Eq. (5.1), is

$$\frac{F}{t} = \frac{G_c}{2}$$

where G_c is the catastrophic tear strength. The results of the trousers tear test thus indicate G_c values of 20 kJ/m^2 ($= \text{N/mm}$) for material A and 5 kJ/m^2 for material B.

If Eq. (5.3) for the tensile strip is applied to a crescent test piece, then the tear “strength” again calculated according to standard methods as the force per unit thickness, is given, for linear force-deflection behavior and with $K = 2$, by

$$\frac{F}{t} = w \left(\frac{G_c E}{2 c} \right)^{1/2}$$

where w is the test piece width. For the above values of G_c , E , w , and c the tear strength is calculated to be about 90 N/mm for each material, with a variability of about $\pm 28\%$ from the modulus and G_c variations. Thus, the two sets of results are quite consistent, the difference in the assessments of tear resistance from the two methods being entirely associated with the difference in modulus.

Notes

- For the “crescent” tear test piece, the tear force may be very sensitive to the sharpness of the tip of the inserted cut (cf. Section 5.2.2).
 - Which, if either, of the tear results would correlate best with service performance in an application for which tear resistance was relevant would depend on the mechanics of the application. The advantage of the trousers test from a basic viewpoint is that a measure of tear strength is obtained that does not include any modulus contribution (provided extension of the legs is prevented or is allowed for).
5. Equation (4.46) of Chapter 4 can be used to calculate effective changes in rate of tearing caused by changes in test temperature. These can then be converted into energy changes using the relationship given in the question. The calculations yield for the tear strengths at 0 °C: 2.8, 7 and 29 kJ/m²; and at 60 °C: 1.3, 2.0 and 2.8 kJ/m², respectively. Note the much wider spread at the lower temperature. The elastomers might be a butadiene rubber, a styrene-butadiene copolymer, or a nitrile rubber respectively (cf. Table 1 of the Appendix).
6. For linear shear stress-strain behavior, the strain energy density is given by

$$U = \frac{1}{2} \mu \varepsilon^2$$

where μ is the shear modulus and ε the strain. If ε_0 is the value of ε for which the strain energy release rate for a long crack equals the mechanical threshold G_0 , then from Eq. (5.11),

$$\varepsilon_0 = \left(\frac{2 G_0}{\mu h} \right)^{1/2}$$

With $\mu = 1 \text{ MPa}$, $G_0 = 50 \text{ J/m}^2$, and $h = 0.01 \text{ m}$, substitution gives

$$\varepsilon_0 = \left(\frac{2 \times 50}{10^6 \times 10^{-2}} \right)^{1/2} = 0.1 \text{ or } 10\%$$

Thus for maximum strains of 10% or less, no mechanical crack growth would be expected to occur for a long crack. This will apply even if initiation of a shorter

crack occurs as a result of a high stress concentration. (The latter behavior would not be expected for the dependence of the energy release rate on crack length shown in Fig. 5.20, but it may occur under other circumstances – for example, in rubber–cord laminated structures such as are used in tires, where very high stress concentrations can occur near cord ends.)

From Eq. (5.8), when the ozone contribution is negligible, the cyclic crack growth rate will be given by

$$\frac{dc}{dn} = A (G - G_0)$$

For a long crack, from Eq. (5.11)

$$G = \frac{1}{2} (\mu \varepsilon^2 h)$$

which upon substituting the given values of μ and h , and with $\varepsilon = 20\%$, gives

$$G = \frac{1}{2} \times 10^6 \times 0.2^2 \times 0.01 = 200 \text{ J/m}^2 \text{ or } 0.2 \text{ kJ/m}^2$$

Thus with $A = 2 \times 10^{-8}$ (m/cycle)/(kJ/m²), the cyclic rate becomes

$$\frac{dc}{dn} = 2 \times 10^{-8} (0.2 - 0.05) = 3 \times 10^{-9} \text{ m/cycle}$$

which for 10^6 cycles per year gives a growth rate of 3 mm/year in the steady rate region.

6

Mechanical Fatigue

Maria D. Ellul

■ 6.1 Introduction

Mechanical fatigue is demonstrated in rubbery materials by a progressive weakening of physical properties as a result of slow crack growth during application of dynamic loads or deformations. The most obvious of the changes is a gradual reduction in stiffness. Protracted static loading causes stress relaxation and may also result in time-dependent cracking of most synthetic amorphous elastomers, but usually not natural rubber. Under a steady load natural rubber crystallizes, and the crystallites apparently prevent further growth of cracks.

Various atomic and molecular processes take place during fatigue. Although such processes have been studied extensively in metals, rubber fatigue studies to date have treated rubber as a continuum because of the complexities of its structure. Thus, fatigue characteristics of rubber remain empirical to a great extent. The only exception here is the mechanical fatigue limit, which represents the stressing condition below which mechanical fatigue failure does not occur on any realistic time scale. The limiting strength of rubber can now be understood in molecular terms, as discussed in Chapter 5.

Excellent reviews on rubber fatigue and fracture by G. J. Lake [1] and others [2] contain original references. A review by Hamed [3] covers the molecular aspects of the fatigue and fracture of rubber, including discussions of mechano-chemical fatigue, reinforcing mechanisms, the role of energy dissipation, particulate reinforcement, strain crystallizability, and crack blunting and deviation. Another review [4] deals with the fracture mechanics analysis of rubber fatigue. It emphasizes the fatigue threshold and includes a section on how to calculate fatigue lifetimes from crack growth data and an experimental section describing fatigue tests on two natural rubber compounds. More recent literature [5] surveys fatigue analysis approaches for rubber from both the ‘nucleation’ and ‘fracture mechanics’ viewpoints. The value of the nucleation view is its ability to quantify potential for flaw development across a large number of possible initial flaw locations and orientations.

The value of the fracture mechanics view is its ability to provide an accurate and detailed account of the driving forces acting on any specified crack. In this chapter these reviews are updated and the applications of various basic concepts developed earlier are emphasized. In particular, emphasis is given to failure by the propagation of a flaw, the roles played by testing and material parameters, and the application of fracture mechanics. The use of fractography to infer the micromechanisms of fatigue failure is not discussed.

The predominant type of fatigue fracture in crosslinked rubbers is brittle fracture because there is virtually no plastic deformation. The main causes of fatigue cracking in rubber are mechanical, thermal, environmental (oxygen, ozone, and ultraviolet radiation) and chemical (e.g., oil, sour gasoline). Typical failures are certain tread and ply separations in tires and failures in motor mounts and suspension bushings. Environmental cracking normally shows up as small surface cracks. Rubber components often contain protective agents, such as antioxidants and antiozonants, to slow down environmental cracking, and carbon black to guard against ultraviolet radiation and to improve mechanical properties. Unlike sunlight crazing, which is random, ozone cracks normally grow perpendicular to the stressing direction. Whether ozone cracks become mechanical fatigue cracks depends on the rubber composition, the loads during service, and the geometry (design) of the rubber article. Many rubber components (e.g., natural rubber bridge bearings) develop ozone cracks on the surface but are still serviceable after more than 50 years because of their large size. Also, such units are normally under a combination of compression and shear, and thus harmful tensile stresses necessary for ozone cracking are absent from the interior. Typical rates of growth for ozone cracking in rubber protected by antiozonants are about 0.1 mm per year for an ozone concentration of about 1 part per hundred million. This aspect of fatigue is discussed in detail in Chapter 5. Until the early 1930 s, standard engineering practice for fatigue endurance design was to ensure that no applied stress exceeded the elastic limit of a material. This approach has proved to be inadequate, as evidenced in that decade by failure of several bridges and ships at applied stresses significantly below the materials' yield stress. The overriding importance of local stress concentrations around structural flaws was thus realized. Hence the fracture mechanics approach evolved.

■ 6.2 Application of Fracture Mechanics to Mechanical Fatigue of Rubber

Fracture mechanics seeks to derive parameters that are inherent failure characteristics of the material, independent of geometry and loading [6]. As explained in the preceding chapter, an energy criterion for crack growth was proposed by Griffith [7] in 1920. He contended that every body contains a distribution of flaws and that failure starts at the largest of these. Griffith proposed that an initial crack of length C in a body of thickness t and at a fixed displacement l will grow, if the decrease in the total elastic energy W of the body per unit increase in the crack length C is at least equal to the surface energy G required to form new crack surfaces. Thus:

$$-\left(\frac{1}{t}\right)\left(\frac{\partial W}{\partial C}\right)_l \geq G \quad (6.1)$$

Under conditions where l is not constant, the Griffith criterion is modified to include work done by external forces.

This concept was first applied successfully to the tearing of rubber by Rivlin and Thomas [8]. In this case, G in Eq. (6.1) is no longer equal in magnitude to the surface energy because rubber is not perfectly brittle. In fact, stresses induced at the tip of a flaw cause large local deformations and result in much more energy being dissipated. The strain energy release rate criterion is still valid for rubber, however, provided the energy dissipation is confined to a small zone at the crack tip.

For well-defined geometries, analytical solutions for the tearing energy that have been derived from general considerations [1, 2, 7] are valid for nonlinear elastic stress-strain relations. Figure 6.1 shows three geometries that can be classified as mode I or opening mode of crack growth, namely: tensile, pure shear, and angled test pieces respectively (see Fig. 6.1a–c). In Fig. 6.1d, the trousers test piece illustrates a mode III type fracture, also known as the out-of-plane shear mode of crack propagation. For the tensile geometry [1, 7–9] (Fig. 6.1a):

$$G = 2 k U C \quad (6.2)$$

where [9, 10]

$$k = \frac{2.95 - 0.08 \varepsilon}{(1 + \varepsilon)^{1/2}} \equiv \frac{\pi}{(1 + \varepsilon)^{1/2}} \quad (6.3)$$

and ε is the strain and U the strain energy density.

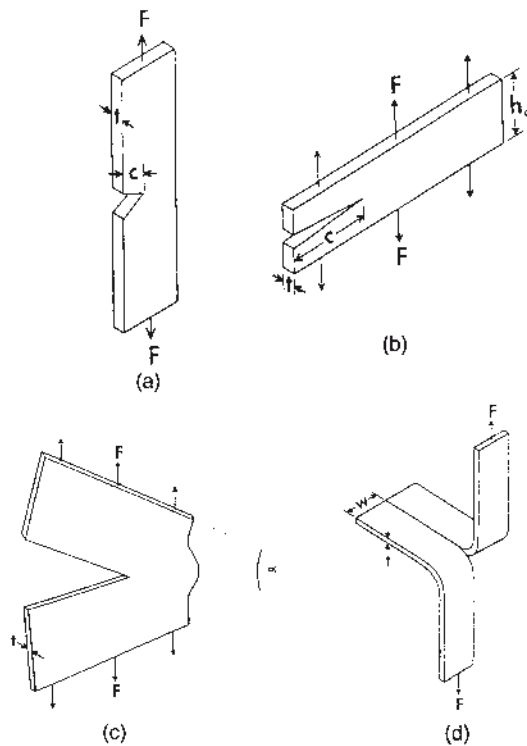


FIGURE 6.1 (a) Tensile geometry with a single edge cut c , (b) pure shear geometry with a single edge cut, (c) angled test piece with edge cut: a rectangular strip clamped on the long axis and inclined at an angle α , and (d) trousers test piece

For the pure shear geometry [1, 8] (Fig. 6.1b):

$$G = U h_0 \quad (6.4)$$

where h_0 is the original height of the test place.

For the angled test piece [2] (Fig. 6.1c):

$$G = 2 \left(\frac{F}{t} \right) \frac{\sin \alpha}{2} \quad (6.5)$$

where α is the angle of the clamps and F is the applied force.

For the trousers test piece [1, 2] (Fig. 6.1d):

$$G = \frac{2 F \lambda}{t} - w U \quad (6.6)$$

If the width w of the test piece is sufficiently great relative to the thickness t , then λ , the extension ratio, approaches unity and $w U$ in Eq. (6.6) is negligible.

These relationships (Eqs. (6.2–6.6)) were originally applied to the catastrophic tearing of rubber. At energies below the catastrophic tear strength G_c , small-scale intermittent crack growth can occur under repeated stressing. In the case of non-strain-crystallizing rubbers under constant stress, slow crack growth also occurs, and this phenomenon is referred to as time-dependent tearing. Small-scale crack growth is the slow incremental tearing of rubber ultimately resulting in fatigue failure. The tearing energy concept is also valid for mechanical fatigue cracking, because as shown in Fig. 5.8, a single plot of crack propagation rate (dC/dN) for various test pieces [1] is a function only of tearing energy G . The tearing energies involved in the mechanical fatigue of rubber cover a broad range from less than 100 J/m^2 up to the catastrophic tearing energy, several kilojoules per square meter.

In Fig. 6.1, all the geometries other than the tensile geometry are referred to as stable because the tearing energy is independent of the crack length. Thus, the rate of crack propagation is controlled only by the input of external work and can be stopped or started at will. Unstable crack growth occurs when the internal energy release rate of the system is in excess of that required to cause crack propagation so that acceleration occurs and growth becomes uncontrollable, as is the case in tension at energies close to the catastrophic tear strength. To apply the Griffith criterion to a rubber component in an engineering application, it is necessary to calculate the tearing energy for the particular geometry.

■ 6.3 Initiation and Propagation of Cracks

6.3.1 Fatigue Crack Initiation

Initiation of mechanical fatigue cracks in rubber has received little attention until recently. Indeed, one of the basic premises of fracture mechanics is the presence of natural defects or flaws in any object. Crack nuclei are therefore assumed to be present in any rubbery material. The exact nature of these nuclei is often obscure. Compounded rubbers contain various additives such as curatives, process aids, and fillers. They therefore exhibit various degrees of inhomogeneity on a microscopic scale, probably of the order of $10 \mu\text{m}$ in size, depending on the particular additives. Rubber without these additives may contain gel particles, microvoids, and roughnesses at cut or molded edges, which can also act as nuclei for crack initiation. All these inhomogeneities have one thing in common: they form highly localized stress concentrations that initiate fatigue failure. For natural rubber, the effective size of initial flaws is estimated to be about $25 \mu\text{m}$ [1]. Another precursor to mechanical fatigue cracks are cracks initiated by ozone attack at areas on the surface where tensile stresses are present.

When a rubber part is subjected to repeated stresses, a certain time passes before visible fatigue cracks appear. Whether this induction time should be considered to be part of a crack initiation process is often a subject of debate. The distinction between crack initiation and propagation is not clear-cut. What matters in practice is how fast a crack of a certain size will propagate under certain loading conditions. With laboratory test pieces, the random process of crack initiation from a natural flaw is obviated by introducing a precrack. This leads to a much more reproducible test, since sensitivity to defects that are not inherent material properties is eliminated. Furthermore, testing a large number of samples is not necessary. The focus in fracture mechanics is thus on fatigue crack propagation. An initial crack size is chosen that reflects the material's known defect size or the minimum crack size detectable by inspection of a product by, for example, holography or ultrasound. Fracture mechanics may also be employed to predict in a given structure the crack size range that will propagate slowly under specified loading until it reaches the critical size from which it will propagate rapidly to catastrophic rupture. In the last decade, fatigue analysis approaches for initiation have seen significant development, including a definition of a new predictor for multiaxial fatigue crack nucleation in rubber [11, 12].

6.3.2 Fatigue Life and Crack Growth

The fatigue life is the number of cycles required to break a specimen into two pieces at a particular stress for a stress-controlled test (or strain for a strain-controlled test). The fatigue life is normally determined from experimental data by assuming either a log normal or a Weibull distribution. Traditionally, the fatigue characteristics of materials including rubbers were determined by a "Wohler" curve, also known as an *S-N* curve (*S* denotes the applied dynamic stress σ for a stress-controlled test or, alternatively, strain ε for a strain-controlled test, and *N* is the number of cycles to failure). Normally the dynamic stress range (or strain range) is plotted against the number of cycles to failure (on a logarithmic scale). Figure 6.2 is a schematic presentation of the *S-N* curve for rubber. The important feature of Figure 6.2 is that upon reducing the dynamic stress or strain of the cycle toward a certain value, the fatigue life approaches infinity. This gave rise to the concept of a limiting stress or strain.

Since cracks initiate from some flaw in the sample, large scatter is found in the fatigue lives of specimens without a defined precrack. Hence such tests require a large number of samples and are very tedious and time-consuming. Moreover, tests of this type are not helpful from a basic standpoint. Information obtained is specific only to the particular specimen used, which may not be representative of a typical

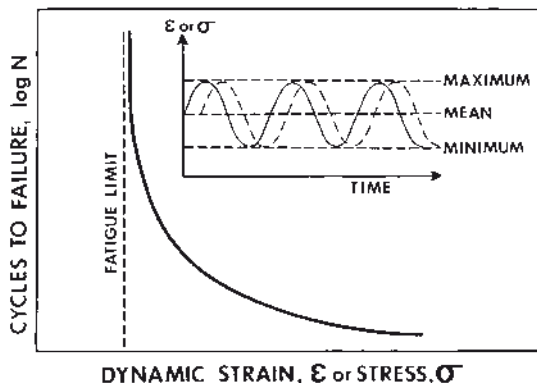


FIGURE 6.2 “Wohler” (S-N) curve for rubber: S is the range of applied dynamic stress σ , or strain ϵ , in the cycle, which equals the maximum minus the minimum values, and N is the number of cycles. Inset shows maximum, minimum, and mean stress or strain

component in service. Also, comparisons of materials with different moduli are not straightforward as discussed later (see Section 6.5). Conventional fatigue tests can be categorized as follows:

1. Periodic loading between fixed stress limits, in tension or compression (load control)
2. Periodic loading between fixed strain limits in tension or compression (displacement control)
3. Reversed shear stresses obtained by torsional deformation
4. Reversed bending stresses in one dimension (flexing of a sheet) or two dimensions (rotary deflection of a cylinder)

A variety of flex-cracking and cut growth testers have been used to generate fatigue life data in bending, many of them intended to simulate service conditions for particular products such as belting, coated fabrics, and footwear. A useful review was given by Buist and Williams [13]. There are several disadvantages associated with many of these testers. The principal problem is difficulty in controlling the bending strain, which may vary with modulus of the rubber. Hence misleading results can be obtained because the fatigue life of rubber is sensitive to both the magnitude and type of applied strain. This partly explains why results obtained in the laboratory using, for example, the de Mattia test machine [14] rarely correlate with service performance. Moreover it is worth remembering that most products are subjected to more complex strain patterns than are seen in a laboratory test. Another problem encountered with many laboratory flex fatigue tests is heat generation. Unless the test sample is thin enough to dissipate the hysteretic heat generated during cycling, failure will be compounded by thermal effects.

The most scientific basis for selection of materials for fatigue life optimization is to determine experimentally the fatigue crack growth rate over a broad range of tearing energies. A relationship between crack growth rate and fatigue can then readily be established (see Section 6.3.4). A practitioner should use fracture mechanics tests to characterize sensitivities to load levels, and should use nucleation tests to characterize initial flaws. Fracture mechanical analysis should be used when enough is known about failure mode and progression to make good assumptions about initial crack geometry and its progression. Nucleation analysis should be used to survey potential failure sites, and is subject to the limitation that initial flaw size must be “small enough”.

6.3.3 Fatigue Crack Propagation: The Fatigue Crack Growth Characteristic

The relationship between the crack growth rate dC/dN and tearing energy G is known as the crack growth characteristic of the material because it is independent of test piece geometry. Typical curves for a natural rubber (NR) and a styrene-butadiene rubber (SBR) compound [1] cycled under relaxing conditions (minimum tearing energy equals zero) are shown in Figs. 5.9 and 6.3. Figure 6.3 can be divided into four regions. In region I the tearing energies G are less than the threshold tear energy G_o ; hence no *mechanical* crack growth occurs. G_o is the mechanical fatigue limit (see Section 6.3.2). Below G_o , crack growth is caused solely by ozone [1] and takes the form:

$$\frac{dC}{dN} = k_z [O_z] = R_z \quad G < G_o \quad (6.7)$$

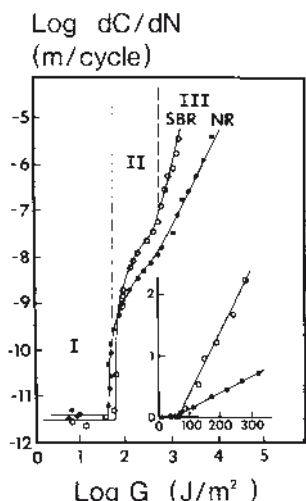


FIGURE 6.3 Cyclic crack growth rate dC/dN , for unfilled NR (●) and SBR (○) compounds as a function of the maximum tearing energy of the cycle, the minimum being zero. Inset shows the region near the threshold tearing energy for mechanical fatigue G_o ($\times 10^{-8}$) plotted on linear scales (data from [1], p. 102)

where k_z is the rate constant due to ozone, O_z is the ozone concentration, and R_z is the crack growth rate. The chemical reaction between ozone and carbon-carbon double bonds, which are present in the backbone of natural and various olefin rubbers, is very rapid, resulting in molecular scission. Ozone will attack rubbers above a critical tensile stress that provides an energy requirement of about 0.1 J/m^2 for unprotected NR and SBR compounds. Above this critical energy level, the rate of crack growth is proportional to ozone concentration O_z and independent of tearing energy, as represented by Eq. (6.7).

In region II, crack growth is dependent on both ozone and mechanical factors in an approximately additive and linear fashion. Hence:

$$\frac{dC}{dN} = R_z + A(G - G_0) \quad G_0 < G < G_A \quad (6.8)$$

where A is a crack growth constant for region II.

In region III, a power law dependency between crack growth rate and G has been found for many rubbers as well as for non rubbery materials [15]. Thus:

$$\frac{dC}{dN} = B G^\beta \quad G_A < G < G_C \quad (6.9)$$

where B and β are constants characteristic of region III (see Fig. 6.3). For natural rubber β is about 2, whereas for *cis*-polybutadiene and SBR, β is about 3 and 4, respectively. In general, β ranges between 2 and 6 for most rubber vulcanizates, depending mainly on the elastomer used and to a lesser extent on secondary factors such as compounding ingredients.

A change in morphology of the fatigue surfaces normally accompanies the transition regions I to IV. In region IV (not shown in Fig. 6.3), dC/dN approaches the velocity of elastic waves in rubber, about 50 m/s. Thus

$$G = G_c \quad (6.10)$$

Division of the crack growth characteristic into distinct parts, I to IV, governed by the empirical Eqs. (6.7) to (6.10) is however oversimplified. In practice, many materials follow more complex empirical relationships. In other cases, however, the power law may hold over a broad range from G_0 to G_c .

Recently a “crack layer” theory [16] has been proposed to model the main crack tip and its surrounding damage zone, called a “crack layer”. A “constitutive” model is proposed to describe the fatigue crack propagation characteristics of an NR vulcanizate. Thus:

$$\frac{dC}{dN} = \frac{\delta G^2}{\gamma G_c - G} \quad (6.11)$$

where δ and γ are coefficients of energy dissipation and damage evolution, respectively. Although damage cannot be easily detected in rubber samples, nevertheless, γ is predicted to increase during stable crack propagation. The value of γ evolves differently for each compound, approaching unity at catastrophic failure. This model derives from both energy balance and irreversible considerations. The basic factors, namely hysteresis and crack tip variations, which determine the crack growth characteristics are however still ill understood.

Progress has been made in relating G_o , the energy required for the onset of mechanical crack growth, to the energy required to fracture primary chemical bonds across a plane (see Chapter 5). Above G_o Andrews and Billington [17] have given a general theoretical treatment for steady tearing in terms of a product of G_o and a viscoelastic loss function, $\Phi(V a_T)$, which itself is dependent on the velocity of crack propagation V and temperature, as represented by the shift factor a_T . Thus:

$$G = G_o \Phi(V a_T) \quad (6.12)$$

A similar approach could in principle be used for fatigue crack growth data. The ultimate goal is to develop a theory for the prediction of crack growth characteristics from crack tip dimensions and elastic and viscoelastic material constants. Much more fundamental understanding of the fracture process zone is needed. Lake and Thomas [2] have shown that the diameter of the tip of a tear or crack is an important factor. In addition, Lake and Yeoh [18] have demonstrated that variations in crack tip sharpness occur during cyclic crack growth and influence the crack growth characteristics.

6.3.4 Fatigue Life Determinations from the Crack Growth Characteristics

“Theoretical” S-N curves can be predicted from the fatigue crack growth characteristics. This methodology is illustrated in detail in [1]. Fukahori [19] has also used a similar methodology to estimate the fatigue life of elastomers. Application to tire breakers has recently been proposed by Grosch [20]. A simpler example is the tensile test piece (shown in Fig. 6.1a) under relaxing cyclic conditions. From the fatigue crack growth characteristic (e.g., Fig. 6.3), we can write:

$$\frac{dC}{dN} = f(G) \quad (6.13)$$

The function $f(G)$ depends on the tearing energy range relevant to the particular application. For moderate and high strains, it can be approximated by the power law relationship (i.e., Eq. (6.9)). Substituting Eqs. (6.2) and (6.9) into Eq. (6.13) and integrating between the limits of C_0 the initial flaw size, to a final failure size C_f , we obtain:

$$N = \frac{1}{(\beta-1) B (2 k U)^\beta (C_0^{\beta-1} C_c^{\beta-1})} \quad (6.14)$$

When $C_c \gg C_0$,

$$N = \frac{1}{(\beta-1) B (2 k U)^\beta C_0^{\beta-1}} \quad (6.15)$$

Equation (6.15) has been found to work well at moderate to high strains. The flaw size C_0 required for quantitative agreement is typically a few thousandths of a centimeter and is consistent with observable imperfections in rubber.

If service strains are low, this approach can be applied to lower severities, but instead of only the power law (Eq. (6.9)), we use Eq. (6.8) first and then Eq. (6.14). The integration limits for the latter are now C_A and C_C . Therefore, for natural rubber:

$$N = \frac{1}{2 K U} \left\{ \frac{1}{A} \ln \left[\frac{G_A - G_0 + (R_z / A)}{2 k U C_0 - G_0 + (R_z / A)} \right] + \frac{1}{B} \left(\frac{1}{G_A} - \frac{1}{G_C} \right) \right\} \quad (6.16)$$

where G_A is the tearing energy at which the transition from a linear relationship (Eq. (6.8)) to a power law (Eq. (6.9)) occurs. Other symbols are as before. In deriving Eq. (6.16), β for NR was taken as 2.

Figure 6.4 shows experimental fatigue life results for an unfilled natural rubber vulcanizate over a broad range of strains. The fatigue life was measured on dumbbell test pieces without any edge cuts, which were cycled until failure. The “theoretical” $S-N$ curve in Fig. 6.4 was drawn using the following values of the constants derived from the experimental crack growth characteristic:

$$G_0 = 40 \text{ J/m}^2; \quad G_A = 450 \text{ J/m}^2; \quad G_c = 10 \text{ kJ/m}^2$$

$$R_z = 1.2 \times 10^{-11} \text{ m/s (laboratory atmosphere)}$$

$$A = 2.5 \times 10^{-8} \text{ m/cycle/kJ/m}^2; \quad \beta = 2$$

$$B = 5 \times 10^{-8} \text{ m/cycle/kJ}^2/\text{m}^4; \quad C_0 = 25 \mu\text{m}$$

The strain energy density U at various strains was obtained by numerical integration of the tensile stress-strain curve. All the constants above are measured quantities except C_0 , whose assigned value is chosen to give the best fit. The value adopted is in line with the sizes of imperfections in rubber. In general the fatigue life N of any rubber component can be predicted by integrating Eq. (6.13):

$$N = \int_{G_i}^{G_c} \left(\frac{1}{dG/dC} \right) \left[\frac{dG}{f(G)} \right] \quad (6.17)$$

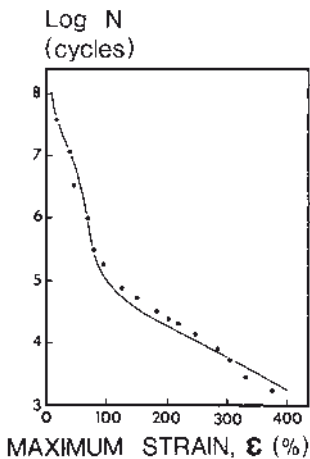


FIGURE 6.4 Tensile fatigue life N as a function of maximum strain ϵ (minimum strain for each cycle is zero) for an NR vulcanizate tested in air; each point is the average of 4–8 experimental results. The theoretical curve was derived from the crack growth characteristics, assuming a natural flaw size of 25 μm (data from [1], p. 104)

To evaluate Eq. (6.17), the initial tearing energy G_i , which depends on the size of the starting crack, and the dependence of G on crack length C must be known.

■ 6.4 Fatigue Crack Growth Test Methodology

6.4.1 Experimental Determination of Dynamic Tearing Energies for Fatigue Crack Propagation

In principle, any of the fracture mechanics geometries depicted in Fig. 6.1 can be used. The tensile test piece (Fig. 6.1a) is most suitable for tearing energies close to G_0 ; otherwise the pure shear test piece is preferred because the tearing energy is independent of crack length in this geometry. A minimum width-to-height ratio (w/h_0) of about 10, preferably more, is recommended to minimize edge effects. A study of sample preparation effects has been reported [21]. There is a need to keep track of the strain energy density U during the test, especially for filled compounds, which are dependent on strain history [22, 23]. The most accurate way to accomplish this is to have a pure shear sample without a crack, cycling under exactly the same conditions as the sample with the crack. The strain energy density is determined on the former, and the incremental crack length as a function of number of cycles is measured on the latter. The sample is normally preconditioned at the highest strain amplitude to be employed in later crack growth measurements. This reduces the strain softening. An alternative way is to take the uncracked width ($w-C$) when measuring the force-deflection characteristic as the effective width of the sample.

Since filled rubbers are hysteretic, U should be obtained from the area under the retractive force-extension curve because it is this elastic energy which is released during crack growth [24–26]. It is also advisable to use thin samples to minimize heat buildup. There is now an ISO standard for pure shear fatigue crack growth testing: ISO 27727:2008(E).

Recently Muhr and Thomas [27] have used an angled test piece under force control for crack growth measurements. This sample is attractive because there is no need to monitor U during the test but simply the force. However, relatively large buckling corrections are necessary at low tearing energies.

6.4.2 Kinetics of Crack Growth

A sharp razor blade crack is normally inserted at the beginning of each test. Initially, the rate of crack growth is fast and the crack surfaces are smooth. When the pure shear test piece is used, tearing gradually slows down as the crack surfaces become rougher, until eventually a constant rate is reached as shown in Fig. 6.5. This rate is assumed to resemble growth from a natural fatigue crack at that particular tearing condition. Crack growth is conventionally measured to a precision of at least a few hundredths of a millimeter. Measurements are taken until the crack C is above one-tenth of the sample thickness. An automated video measuring system was reported in 1985 [28]. Another method for automating crack growth measurements on rubber entails the deposition of a thin film of conductive material. The attenuation in resistance is calibrated to yield the equivalent change in crack length. This method has been recently applied to monitor crack propagation in ceramics [29].

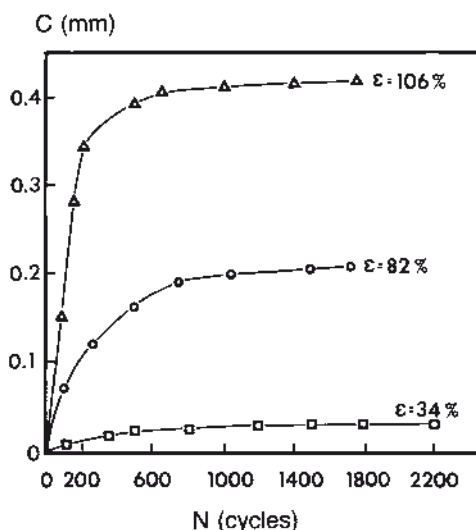


FIGURE 6.5 Crack growth C from a sharp razor blade cut, as a function of number of cycles N for a carbon black filled polybutadiene rubber at various maximum strains ϵ (minimum strains = 0) (unpublished data, M. D. Ellul)

6.4.3 Effects of Test Variables on Fatigue Crack Growth Characteristics and Dynamic Fatigue Life

6.4.3.1 Waveform

Most studies of fatigue crack propagation have utilized simple sinusoidal excitations. To simulate particular products, it may be useful to consider nonsinusoidal inputs that relate to the service conditions of the particular component. For instance, haversine and other waveforms are representative of some tire deformations, whereas dual-sine waveforms occur in engine mounts. Systematic studies of the effect of different waveforms on fatigue crack growth are not available in the literature. Since changing waveforms translate to variations in strain rate, we would expect synthetic rubbers to show bigger effects than NR because their strength is highly dependent on viscoelasticity.

6.4.3.2 Frequency

A change in test frequency alters the strain rate, the number of cycles per unit time, and the time under deformation for each cycle. If the maximum strain of the cycle is changed to generate the crack growth characteristic, a constant strain rate can be maintained by appropriate change in the test frequency [30]. Significant effects of frequency have been found for non-crystallizing rubbers because of time-dependent continuous crack growth, which is superimposed on the dynamic crack growth [1]. This steady component of crack growth is especially important at frequencies below about 0.2 Hz. It owes its origin to viscoelastic effects. For natural rubber, very little effect of frequency on fatigue cracking has been observed over the range of 10^{-3} to 50 Hz [1, 2].

If the frequency of stressing is too high, especially for a thick sample, excessive heat generation results. The predominant cause of failure is now no longer mechanical fatigue but rather high temperature degradation. This type of failure, often referred to as thermal runaway [31], leads to blowout of solid tires. Pneumatic tires which run under very severe conditions, such as very high speeds or overloads, are also likely to fail in this way. These failures should not be confused with mechanical fatigue. Failures related to heat generation have been reported for the shoulder area of heavy-duty tires and for tank track pads in an earlier review of fatigue by J. R. Beatty [32].

6.4.3.3 Temperature

The effects of temperature are also greatest in non-strain-crystallizing rubbers, whose strength derives from viscoelasticity. Thus a 10^4 -fold decrease in fatigue life is observed for unfilled SBR on going from 0 to 100 °C, in contrast to unfilled

NR, which exhibits only a fourfold decrease [33] (see Fig. 6.6a). Measurements by Young [30] on carbon black reinforced materials at a fixed strain rate showed that the rate of crack propagation of NR and most synthetic rubbers was generally higher at higher temperatures, but for NR and chlorobutyl, crack growth rates at 25 °C were lower than at 0 °C (see Figs. 6.6b and 6.6c).

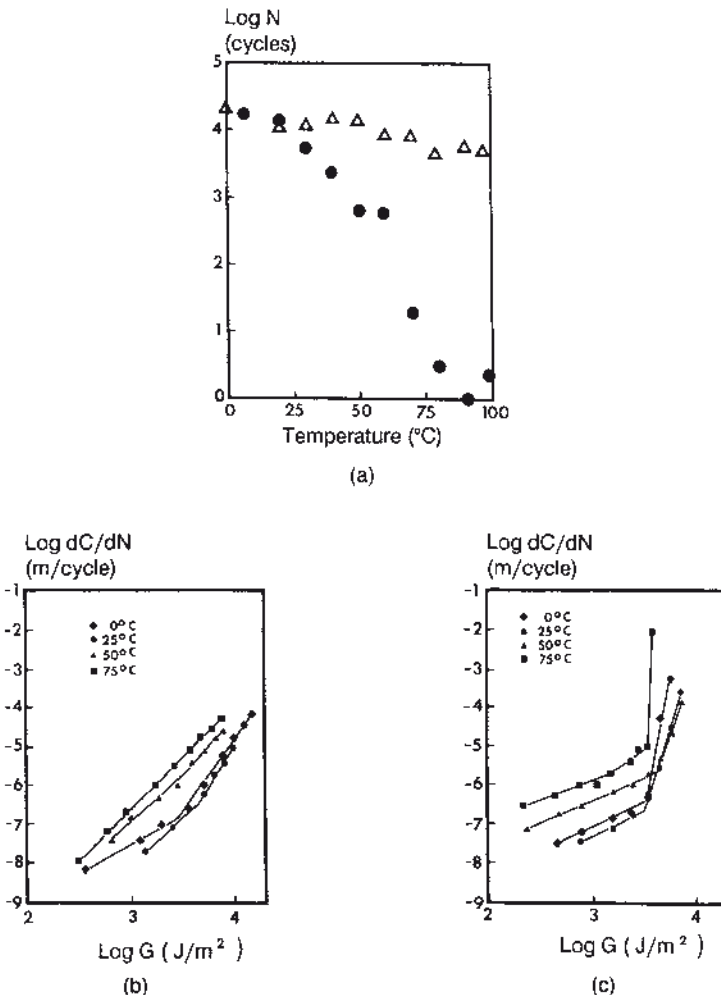


FIGURE 6.6 (a) Effect of temperature on the dynamic fatigue life of dumbbell test pieces at 1000 cycles/minute: ● = SBR at 175% maximum strain, Δ = NR at 250% maximum strain (minimum strain equals zero for both SBR and NR) (data replotted from [33]); (b) fatigue crack growth rate of chlorobutyl rubber at various temperatures: ■ = 75 °C; ▲ = 50 °C; ▽ = 25 °C; ♦ = 0 °C. Strain rate, 20 s⁻¹, air atmosphere; (c) fatigue crack growth rate of natural rubber at various temperatures: ■ = 75 °C; ▲ = 50 °C; ▽ = 25 °C; ♦ = 0 °C. Strain rate, 20 s⁻¹, air atmosphere (data from [30])

6.4.3.4 Static Strain/Stress

When the minimum strain in a cyclic deformation is not zero, the deformation is referred to as nonrelaxing. Nonrelaxing conditions are normally expressed in terms of a parameter R , the ratio of minimum to maximum deflection (or minimum to maximum load in the case of a load-controlled test). For a periodic waveform of fixed amplitude, the mean stress increases with increase in the minimum load. In general, the fatigue life of metals decreases with increase in the mean stress. However, with rubber the behavior is quite different.

The relationships given earlier were based on a return to zero strain during each cycle. Practical rubber units in service are usually subjected to nonrelaxing fatigue, whereby small oscillations are superimposed on comparatively large static deformations as a result of the loads they support. In contrast to metals, the fatigue life of rubbers that strain-crystallize (e.g., NR) is prolonged significantly under nonrelaxing conditions, probably because the strain-crystallized rubber at the crack tip is extremely resistant to further crack growth. This effect is taken advantage of in most rubber spring applications. The extensive fatigue life data obtained by Cadwell and coworkers [34] on NR cylinders are reproduced in Fig. 6.7 to illustrate this point for a variety of strains and strain cycles. It is observed that the fatigue life of NR is enhanced with increasing minimum tensile strains up to some maximum value, even if the dynamic strain range ($\varepsilon_{\max} - \varepsilon_{\min}$) is kept constant.

There is a considerable increase in crack growth resistance of strain-crystallizing rubbers. As shown in Fig. 5.11, when the minimum tearing energy is not zero, but $0.056 G_{\max}$, there is an increase in the threshold tearing energy G_0 and a reduction in the rate of crack growth once the new G_0 has been exceeded. Similarly, the fatigue life of NR is improved by a hundredfold at a minimum strain of about 45% (see Fig. 6.8).

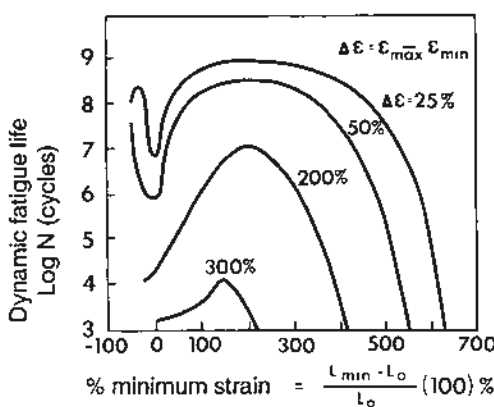


FIGURE 6.7 Nonrelaxing (minimum strain > 0) fatigue life data from [34]; fatigue life of NR cylinders as a function of the minimum dynamic strain at various fixed dynamic strain ranges $\Delta\varepsilon$ of 25, 50, 200, and 300%, respectively.

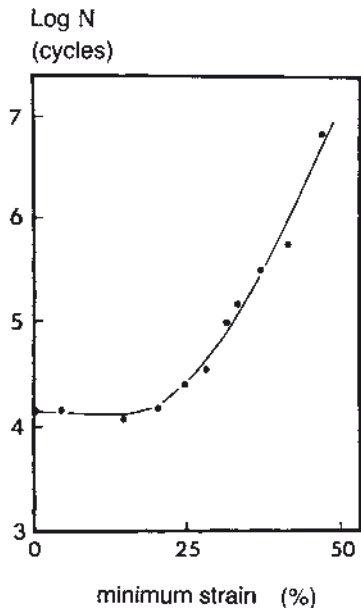


FIGURE 6.8 Effect of static strain (minimum dynamic strain) on fatigue life for an unfilled NR vulcanize at 250% total maximum strain (data from [1], p. 109)

Enhancements in crack growth resistance have also been observed in non-strain-crystallizing rubbers (e.g., SBR) under nonrelaxing conditions. In this case, the total crack growth per cycle is the sum of steady and cyclic contributions [35]:

$$\left(\frac{dC}{dN} \right)_{\text{total}} = \frac{2\pi}{\omega} \left(\frac{dC}{dt} \right)_{\text{steady}} + \left(\frac{dC}{dN} \right)_{\text{cyclic}} \quad (6.18)$$

where ω is the angular velocity, t is the time, and other symbols are as defined before. The improvement in crack growth and fatigue resistance for non-strain-crystallizing rubbers under nonrelaxing conditions is mainly attributable to a reduction in the strain energy of the cycle.

Experimentally, nonrelaxing tests under displacement control are much more difficult than relaxing tests because of creep. Load-controlled tests are more convenient experimentally. Moreover, oxygen and ozone sensitivity can become an important factor because of the longer test duration under nonrelaxing conditions. Nevertheless, energy methods have been applied successfully to quantify nonrelaxing crack growth. Lindley [35] used two parameters, namely G_{\max} and x , the ratio of G_{\min} to G_{\max} . The original references should be consulted for more details [1, 2]. See also reference [36].

■ 6.5 Material Variables and Their Effect on Fatigue Crack Growth

6.5.1 Reinforcing Fillers and Compound Modulus

Black reinforcing fillers protect against ultraviolet degradation. In addition, they affect significantly mechanical fatigue cracking. The effects of both high (HAF carbon black) and low (MT carbon black) reinforcing fillers on the fatigue crack growth of several rubber types are shown in Fig. 6.9 [37] and compared to the corresponding unfilled elastomer. The compounding ingredients are otherwise the same. HAF black markedly improves the cut growth resistance of all the vulcanizates, except

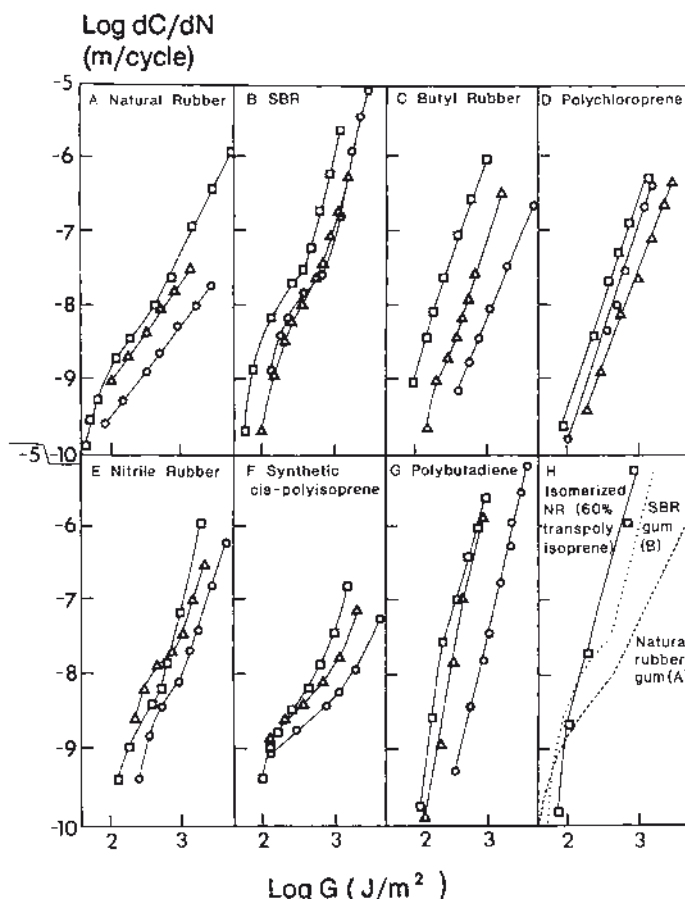


FIGURE 6.9 Mechano-oxidative crack growth characteristics of vulcanizates from different polymers:
 □ = gum; Δ = with 50 phr MT carbon black; \circ = with 50 phr HAF carbon black at room temperature (data from [35], p. 33)

polychloroprene. A low reinforcing MT black has a beneficial effect on SBR, butyl, and polychloroprene. Carbon black provides for

- an additional source of hysteresis and
- an increased propensity to crack tip blunting and branching.

These two mechanisms are mainly responsible for the increased resistance to cut growth.

At low tearing energies, close to the fatigue limit, reinforcing fillers increase the value of G_0 by about 50% [37]. Above G_0 , hysteresis enhances the crack growth resistance of materials by dissipating energy that would otherwise be expended in crack growth. Hysteresis, however, also causes heat build-up; unless this heat is dissipated, it may promote further fatigue cracking.

The inclusion of a filler also increases the modulus, thus resulting in a reduction of the conventional mechanical fatigue limit, if this is deduced from plots of the number of cycles N as a function of strain ε (e.g., Fig. 6.4). This is because at fixed strain (or deflection) testing conditions, a stiffer compound has a higher level of strain energy density at a given strain. The converse is true for a load-controlled test. To understand this point further, consider two hypothetical compounds 1 and 2, whose stress-strain curves are shown in Fig. 6.10. The compound that will be better in service can be determined on the basis of whether the rubber is in a load- or displacement-controlled application.

For displacement control, that is, fixed strain ε_1 (see Fig. 6.10a), the low modulus compound 2 should be better for fatigue durability, since the area OAB under its stress-strain curve, the strain energy density U_2 , is smaller than the area OAC (U_1) for compound 1. Of course this is true, if the crack growth rate corresponding to the tearing energy for the U_2 condition is also smaller than that which corresponds to the tearing energy for U_1 . Conversely, for a load-controlled application (Fig. 6.10b),

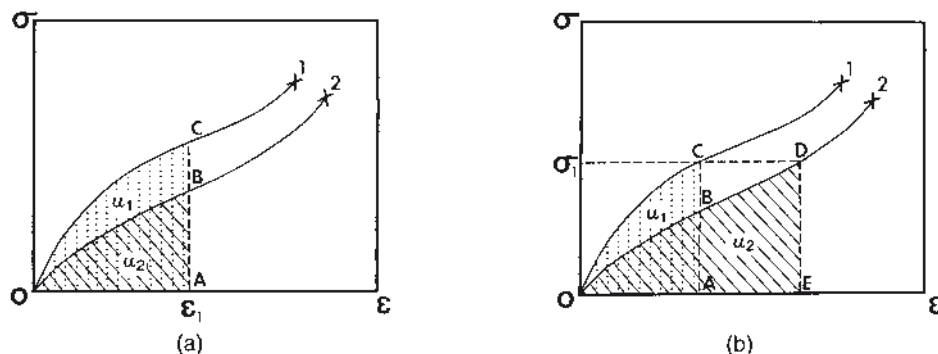


FIGURE 6.10 Hypothetical stress-strain curves for materials 1 and 2, showing the energies U_1 and U_2 involved in fatigue crack growth for (a) a displacement-controlled application and (b) a load-controlled application

the higher modulus compound 1 will have a lower strain energy density U_1 (area OAC) and therefore a longer fatigue life. Again, this is assuming that the crack growth rate corresponding to the tearing energy for the U_1 condition is lower than that corresponding to the tearing energy for U_2 .

6.5.2 Elastomer Type

Crack growth resistance for different elastomers is shown in Fig. 6.9. The power law exponent β , from Eq. (6.9), can be used to differentiate between different elastomers. Table 6.1 shows values of β taken from [38]. The differences are mainly attributed to various degrees of mechanical hysteresis in these materials. The minimum value of β for perfectly dissipative materials is about 2. This is because the stress distribution for a sharp crack leads to growth steps that depend on the square of the tearing energy [39]. The mechanical hysteresis is large for NR at high strains because of strain-induced crystallization. For relatively elastic materials, β should be significantly greater than 2, approaching infinity for a perfectly elastic solid.

Values of β can be affected by both strain level and strain rate. Thus values for NR have been found to range from 1.08 to 2.38 at low strain levels and from 3.2 to 46 in the high strain region [30]. For design purposes, comparisons of different elastomers are best made directly in terms of tearing energy. Assuming that an estimate of the operating tearing energies encountered during service can be made, the materials can be ranked in terms of respective crack growth rates. Engineering design of a rubber component must ensure that operating tearing energies are well below the catastrophic tear strength.

Figure 6.11 shows some comparisons of fatigue crack growth characteristics for different elastomers, plotted on the same scale [40]. No single material will have the best fatigue life over the whole tearing energy range (i.e., G_0 to G_c).

TABLE 6.1 Exponent β Values

Rubber	Unfilled	Filled
NR	2.0	2.0
IR	3.8	2.0
SBR	2.3	2.4
BR	3.6	3.0
NBR	2.7	2.8
CR	1.7	3.4
EPDM	3.4	3.2

Source: [38]

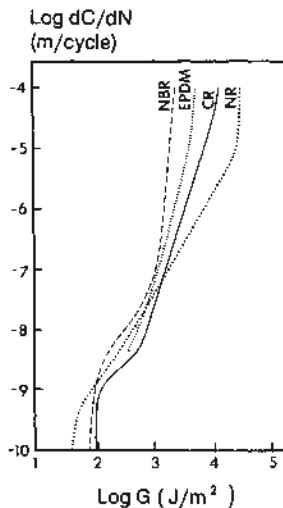


FIGURE 6.11 Fatigue crack growth rate as a function of tearing energy at 22 °C for various elastomers (minimum tearing energies per cycle equal zero) (data from [40])

Inspection of Fig. 6.11 suggests that at high tearing energies, NR is the best material and NBR (acrylonitrile-butadiene rubber) is the worst. In contrast, at lower tearing energies, CR (polychloroprene) is significantly better than NR. There is much scope for development of blends of elastomers to optimize the fatigue life over a broad tearing energy range.

Fatigue crack propagation in carbon black filled fluoroelastomers and post failure analysis by SEM has been described [41]. As the crack speed increased, the roughness of the surface decreased. On a microscopic level, the fracture surface exhibited microcracks and microvoids with evidence of void coalescence.

6.5.3 Vulcanizing System

The crack growth characteristics of unfilled natural rubber vulcanized by different curing systems are quite different [2, 37]. Table 6.2 shows formulations and G_0 results for several NR compounds. The polysulfide curing system was better overall than the monosulfide or direct carbon-carbon crosslinkages by a factor of up to 2. A similar twofold variation was observed in the rates of crack growth. Comparable results were obtained for the effect of vulcanizing system on strength of filled NR compounds [42].

Thus it appears that the most labile polysulfidic crosslinks are better than the stronger monosulfide or carbon-carbon bonds for fatigue resistance. Thomas et al. [2, 43] postulated that the polysulfide crosslinks break before the main backbone chain

TABLE 6.2 Effect of Vulcanization System on G_0

Material ^a	Vulcanizing system		
	Conventional	TMTD-sulfurless	Peroxide
Natural rubber	100	100	100
Zinc oxide	5	4	5
Stearic acid	1	-	-
Sulfur	4	-	-
CBS	1.5	-	-
TMTD	-	10	-
Dicumyl peroxide	-	-	4
Young's modulus, MPa	2.7	2.6	2.7
G_0 , J/m ²	50	22	< 30

^a Abbreviations: CBS, *N*-cyclohexyl-2-benzothiazole sulfenamide; TMTD, tetramethyl thiuram disulfide

Source: [37]

under the high stresses around the crack tip. The stress is therefore redistributed over a larger volume of material. This effect is presumably absent in the case of carbon-carbon crosslinks, which are relatively strong. On the other hand, Brydson [44] suggested that the different strengths in natural rubber are due to the effect of different crosslink structures on strain-induced crystallization. Results obtained (Fig. 6.12) on isomerized NR, which does not strain-crystallize, are however similar to those for regular NR [43].

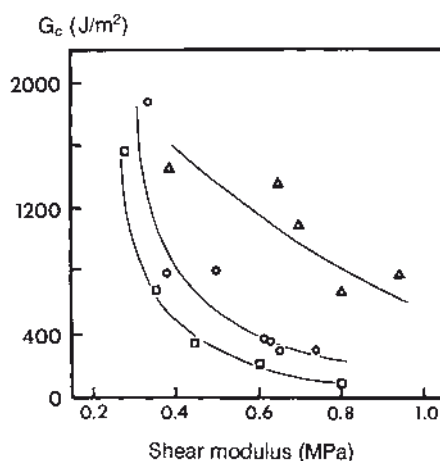


FIGURE 6.12 Effect of vulcanization system on catastrophic tearing energy G_c , measured at a velocity of 10 µm/s for isomerized NR: □ = peroxide (carbon-carbon crosslinks); ○ = mainly monosulfide crosslinks; Δ = mainly polysulfide crosslinks (data from [43])

6.5.3 Fatigue of Double Network Elastomers and Blends

Double networks were prepared from guayule rubber (GR), deproteinized natural rubber (DPNR), and styrene butadiene rubber (SBR), and their properties compared to conventional “single networks” having the same crosslink density. Substantial residual strains were obtained in all double networks, whereby the modulus parallel to the residual strain was enhanced. For the two strain-crystallizing elastomers, GR and DPNR the fatigue resistance of the double networks (for extensions parallel to the residual strain) was higher than for their single network counterparts [45]. Moreover, the guayule rubber, which is more strain-crystallizable than DPNR, exhibited the greater enhancement. For the amorphous SBR, on the other hand, the network structure had an insignificant effect on the fatigue life. These results demonstrate that longer mechanical fatigue lifetimes in double network rubbers are a consequence of their intrinsic orientation. This provides the capacity to retain crystallinity at the front of growing cracks, even in the absence of stress. The origin of the improved fatigue resistance is similar to the mechanism responsible for the better performance of strain-crystallizing rubbers subjected to non-relaxing cyclic deformations.

Fatigue behavior in a blend of natural rubber (NR) and polybutadiene rubber (BR) has recently been investigated. The energy release rates measured from load-displacement curves recorded during the fatigue test could be used to characterize the fatigue crack propagation (FCP) history of a NR/BR blend. Crack propagation kinetics showed an initial low slope “ozone crack regime” with an S-shaped “mechanico-oxidative cut growth regime”. The blend has a mechanical fatigue limit of 2.4 kJ/m^2 . The crack initiation constituted 25% of the total fatigue life and the low slope stage comprised 40% of the crack propagation life. Examination of the fracture profile and the fracture surface revealed that microcracks and crack tip roughening were two damage mechanisms controlling the resistance to crack propagation in the “mechanico-oxidative cut growth regime”, while the reverse herringbone pattern near the notch corresponded to the “ozone crack regime” [46].

■ 6.6 Fatigue and Crack Growth of Rubber under Biaxial Stresses and Multiaxial Loading

Most rubber components in service are normally under a combination of compression, shear, and bending. Consequently, an understanding of the fatigue of rubber under such multiple stress states is very important to verify whether results from simpler tests such as uniaxial tension can be used to predict fatigue crack growth in more complex states. We shall discuss first fatigue under equibiaxial extension [47]. The fatigue life was found to be greater than that in uniaxial tension at the same value of strain energy. However, if comparisons are made on the basis of strain, the uniaxial fatigue life is greater than that in equibiaxial extension. Roach [48] described the fatigue life in both uniaxial and equibiaxial extension by:

$$N \propto (2k\Delta U)^{-\beta} \quad (6.19)$$

where ΔU is the available energy and other symbols are as defined earlier. In the equibiaxial case, ΔU is the difference between the energy for equibiaxial stretching and the energy for uniaxial stretching at the same strain. The energies were determined experimentally from the respective areas under the uniaxial and biaxial stress-strain curves.

Experimental results are shown in Fig. 6.13. For NR (Fig. 6.13a), no significant differences were observed in the fatigue life in equibiaxial extension and uniaxial tension. Small differences were observed for SBR (Fig. 6.13b). A rather unexpected

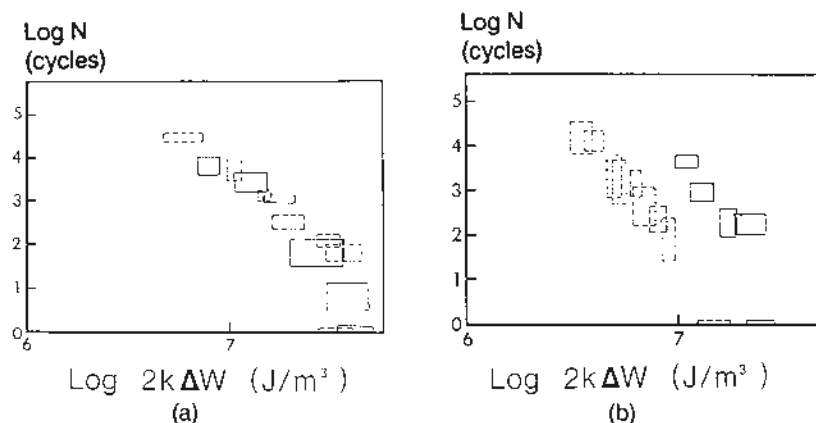


FIGURE 6.13 Fatigue life of unfilled vulcanizates as a function of the available energy for both uniaxial (dashed boxes) and equibiaxial (solid boxes) tests; (a) NR vulcanize and (b) SBR vulcanize

observation is that the fatigue lives of NR and SBR under equibiaxial extension are surprisingly similar; at least in the region covered by these experiments. There is no apparent advantage in having a strain-crystallizing rubber in equibiaxial extension.

Crack growth of carbon black filled and unfilled NR has been studied in pure shear with various static strains ε_1 imposed perpendicular to the shear direction [48]. In this case, the tearing energy G for the deformed test piece is

$$G = U h_0 (\varepsilon_1 + 1)^{-1/2}_{\text{static}} \quad (6.20)$$

where U is the stored strain energy per unit volume and h_0 is the original sample height. Results are shown in Fig. 6.14. Again, no significant change in the rate of crack growth was observed between biaxial and uniaxial experiments.

A novel specimen for investigating mechanical behavior of elastomers under multiaxial loading conditions was recently proposed by Mars and Fatemi [49] and used to study multiaxial stress effects on fatigue behavior of filled natural rubber [50]. Under multiaxial loading, it becomes essential to account for the experiences of individual material planes [51, 52].

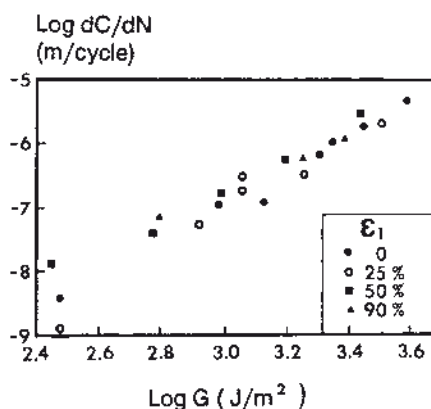


FIGURE 6.14 Fatigue crack growth rate of an unfilled NR as a function of the available tearing energy for the pure shear test piece, with various static strains ε_1 imposed perpendicular to the cyclic deformations. Inset shows values of ε_1 .

6.7 Fatigue in Rubber Composites

Cords are relatively inextensible when compared with rubber, and therefore cord-rubber composites are heterogeneous and anisotropic. Tensile and in-plane shear geometries have been investigated [53]. The tearing energies of the mode I composites shown in Fig. 6.15a and 6.15b were calculated using Eqs. (6.2) and (6.4),

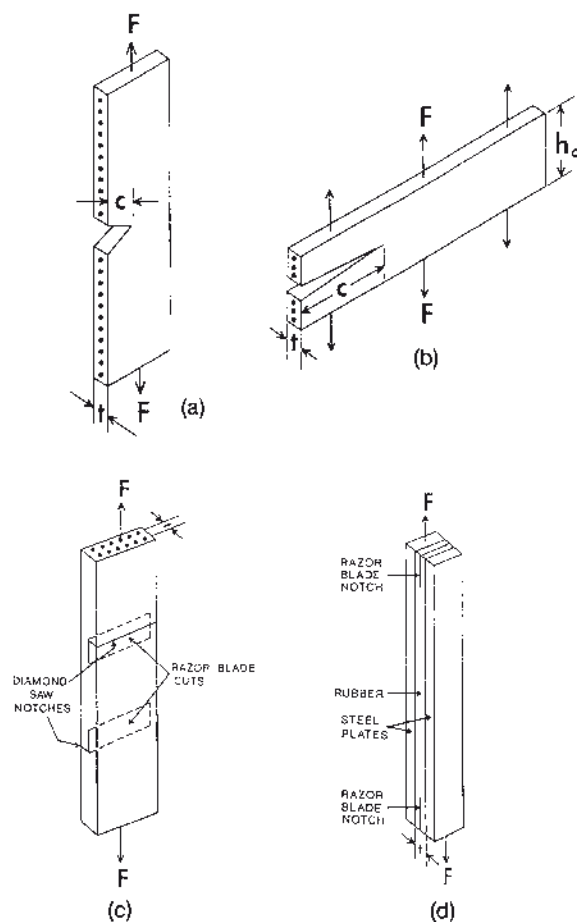


FIGURE 6.15 Mode I test geometries: (a) simple extension test piece with an edge crack and brass-plated steel wires of diameter 0.175 mm, aligned perpendicular to the applied force and (b) pure shear test piece also with an edge crack and wires aligned in the width direction. Mode II test geometries: (c) notched shear specimen consisting of double layers of unidirectional cord-reinforced material (notches of half-thickness deep were made by a diamond saw on both sides of the specimen and artificial delaminations inserted in the midplane from these notches by a razor blade) and (d) single-lap shear specimen with artificial razor blade delaminations inserted in the midplane at both ends of the specimen

respectively. In each case U was computed empirically from the unloading portion of the dynamic stress-strain curve.

In the case of the mode II geometries (Figs. 6.15c, 6.15d), the tearing energy for type 1 (Fig. 6.15c) was

$$G = U_c t \quad (6.21)$$

where U_c is the strain energy density in the central region and t is half the average thickness of the rubber. For type 2, (Fig. 6.15d), the same equation was applied, but t is now the thickness of the rubber between steel plates.

6.7.1 Effect of Wires, Cords, and Their Spacing on Fatigue Crack Propagation

Fatigue crack propagation (FCP) results [53] for tensile test pieces (Fig. 6.15a) over a tearing energy range of 600–3000 J/m² showed crack growth rates of the rubber alone approximately equal to the rates for the wire-rubber and cord-rubber composites irrespective of the wire or cord spacing. Comparisons are made on the basis of available tearing energies. Essentially similar conclusions are reached in pure shear and simple shear [53] using the test pieces shown in Figs. 6.15b and 6.15c. The results are somewhat scattered but are in reasonable agreement.

6.7.2 Effect of Minimum Strain or Stress

As discussed earlier, the effect of a static strain superimposed on a dynamic strain is large in NR because of stress-induced crystallization. Thus under nonrelaxing conditions ($R > 0$), a crack in NR tends to propagate parallel to the load and sometimes even arrests. For composites with wires aligned in the width direction (Figs. 6.15a and 6.15b), when R exceeds 0, this deflection of the crack is suppressed. The results are shown in Fig. 6.16a. The abscissa is the maximum tearing energy of the cycle and R is the ratio of minimum to maximum load. The lines are drawn through the points for $R = 0$ and $R = 0.15$, respectively.

An effect of stress ratio R was also observed in a non-strain-crystallizable SBR tensile specimen (Fig. 6.16b). The higher the R value, the greater was the slope of the FCP characteristic. Compare a slope of 4.3 for $R = 0$, with 5.1 for $R = 0.3$.

The effect of negative R values can be studied by means of the geometry shown in Fig. 6.15 d. Reversing the direction of the applied load ($R = -1$) was found to increase crack propagation by at least an order of magnitude, as shown in Fig. 6.16c.

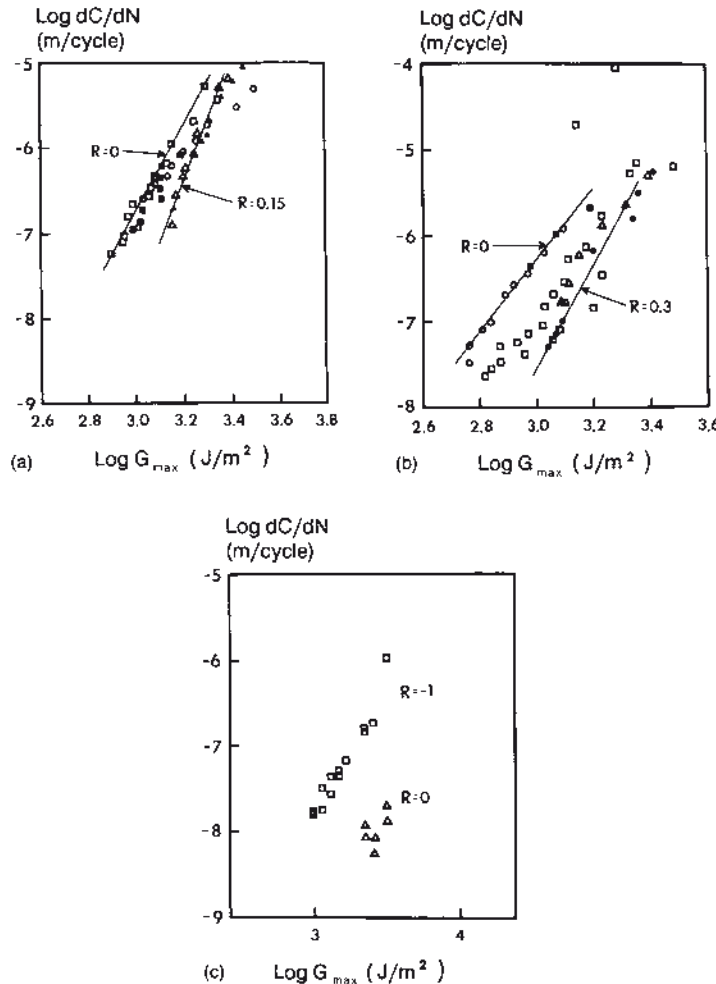


FIGURE 6.16 Effect of stress ratio or R value. (a) Fatigue crack growth rate as a function of maximum tearing energy (minimum $G > 0$) for unfilled NR and its respective wire composites in a single edge-notched tensile specimen: wire spacing, 26.6 wires/cm; test frequency, 2.5 Hz; \square : $R = 0$; \blacksquare : $R = 0.1$; Δ : $R = 0.15$; \blacktriangle : $R = 0.2$; \circ : $R = 0$ (wireless). (b) Fatigue crack growth rate as a function of maximum tearing energy for a carbon black filled SBR in a single edge-notched specimen: wire spacing, 26.6 wires/cm; test frequency, 2.5 Hz; \blacksquare : $R = 0$; \square : $R = 0.1$; Δ : $R = 0.2$; \bullet : $R = 0.3$; \circ : $R = 0$ (wireless). The lines are drawn only for the points at $R = 0$ and $R = 0.3$, respectively. (c) Fatigue crack growth rate of a carbon black filled NR in a single-lap shear geometry (mode II, type 2, see Fig. 6.15d: \square : $R = -1$; Δ : $R = 0$ (data from [53]))

6.7.3 Comparison of S-N Curve and Fatigue Crack Propagation Constants for Rubber-Wire Composites [53]

A study was carried out on notched tension specimens with wires (Fig. 6.15a) to compare fatigue life data (*S-N* curves: Fig. 6.17a) and fatigue crack propagation results (Fig. 6.17b). The specimen lifetime is the integrated effect of the crack velocity and should follow the same stress exponent as for a fatigue crack propagation experiment. Assuming linear elasticity theory, we can rewrite Eq. (6.15) in terms of stress σ to derive:

$$N^{-1} = \left[B \left(\frac{k}{E} \right)^\beta C_0^{\beta-1} \right] \sigma^{2\beta} \quad (6.22)$$

or

$$N^{-1} = K' \sigma^{2\beta} = K' \sigma^{1/m} \quad (6.23)$$

where k is as defined earlier by Eq. (6.3), E is Young's modulus, and all other constants are as described previously. The constants in the square brackets in Eq. (6.22) are represented by K' . Therefore from Eq. (6.23), the slope m of the *S-N* curve (Fig. 6.17a) should equal $-1/2\beta$, which in this case is -0.15 . Hence, $\beta = 3.3$.

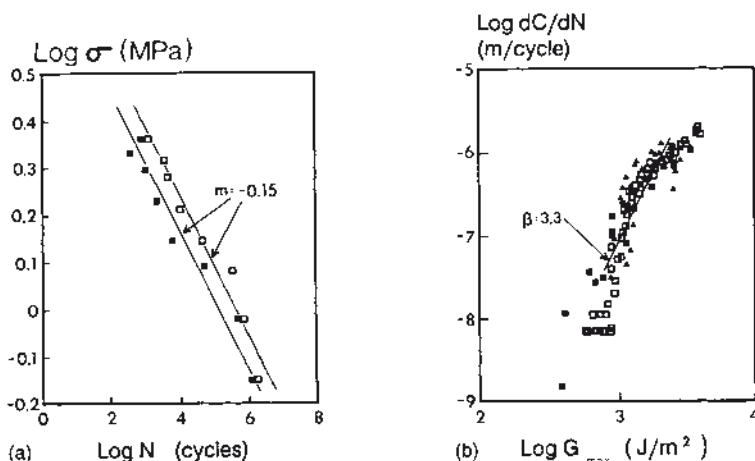


FIGURE 6.17 (a) *S-N* curves of carbon black filled NR-wire composites (S is the maximum stress σ_{\max} and N is the number of cycles). Tension specimens had a single edge crack and wires aligned in the width direction. Test conditions: $R = 0.1$; frequency, 3 Hz; wire spacing, 26.6 wires/cm; \square = 2 mm notch; \blacksquare = 3 mm notch. (b) Comparison of the linear relation based on the slope m value obtained from the *S-N* results (Fig. 6.17a) with the fatigue crack propagation rate data for carbon black filled NR-wire composites. Test conditions: $R = 0.1$; frequency, 2.5 Hz; wire spacing, 26.6 wires/cm; tensile geometry with edge cut; \square = smooth surface; \blacktriangle = rough surface; \blacksquare = pure shear with an edge cut (data from [53])

In Fig. 6.17b, a line of slope 3.3 is drawn through the FCP data in the region of tearing energies described by Eqs. (6.9) and (6.22). Thus, values of the exponent m , obtained from the S - N curves (Fig. 6.17a), agree reasonably well with the exponent β fitted to the fatigue crack propagation results (Fig. 6.17b). Note that S - N curves are dependent on notch size, but the curves are parallel. In principle, “theoretical” S - N curves for rubber-wire composites can be derived from FCP data. As noted in Section 6.3.4, work on rubber alone successfully predicted S - N curves from FCP data, mostly under relaxing conditions, although work under nonrelaxing conditions was pointing in the same direction.

6.7.4 Fatigue of Two-Ply Rubber-Cord Laminates

Lake and Breidenbach [1, 54] examined crack propagation in rubber-cord laminates containing two sets of symmetrically arranged cords with cord angles $\pm\theta$, under repeated tensile loading. Such laminated structures are prevalent in tires, conveyor belts, and hose. Under these conditions the investigators found that very large local shear strains (up to 1000%) develop near the cords’ ends even when the overall tensile loads are only a few percent. Cracks initiate at the cord ends and propagate toward the center of the specimen between the two layers. It was concluded that the crack propagation in the interior was driven by the average tearing energy in the central region, not by the edge shear strains. This failure mode was referred to as “interply shear cracking”. The strain energy release rate was calculated in terms of the thickness t of the rubber layers and the average strain energy density in the central region U_c giving:

$$G = U_c t \quad (6.24)$$

This expression is analogous to that for the pure shear test piece. Average rates of crack growth for interply cracking of these laminates were comparable to those obtained on tensile strips of the ply rubber alone. Alternatively, if failure occurs by the growth of roughly cylindrical cracks around individual cords, termed “socketing”, the strain energy release rate is given by

$$G = \frac{U_c t}{\pi n D} \quad (6.25)$$

where n is the number of cords per unit length perpendicular to the cord direction and D is the diameter of a crack around a cord. The theory predicts that there will be a transition from interply cracking (Eq. (6.24)) to socketing (Eq. (6.25)) when the number of cords per unit length is reduced to a value of $1/(\pi \times \text{cord diameter})$. Satisfactory agreement was found between experiment and predictions for these failure mode transitions, and for the rates of crack growth in each case.

Fatigue lives of model single and two-ply cord-rubber composites were recently predicted with fairly good accuracy from the cord dimensions and the crack growth characteristics of the rubber alone [55]. The practical advice implications of this work are: (1) use rubber resistant to crack propagation and (2) design the laminate to reduce the strain energy release rate. For example, an edge filler in the laminate increases the interply distance at the edges and may reduce the local strain energy density, thus retarding the formation of starter cracks. Other design variables include optimization of cord angles and rubber thickness between cord layers to minimize the strain energy release rate in the central region.

■ 6.8 Fatigue Cracking of Rubber in Compression and Shear Applications

6.8.1 Crack Growth in Compression

Compression and simple shear are deformations of great practical importance in engineering components. As a first approximation it would be logical to assume that compressive stresses will close a crack, but early work by Cadwell et al. [34] pointed to failures of rubber cylinders under repeated compression cycles (Fig. 6.7). More recently, fractures were observed in railway buffers under compression. Chunks of rubber separated from exposed areas. However, since crack growth is limited to the outer surface, rubber blocks in compression may be considered to be fail-safe. A fracture mechanics approach has been applied to fatigue crack growth in bonded rubber cylinders subjected to uniaxial compression. Figure 6.18 shows typical stages of crack growth in uniaxial compression [56]. These experimental observations suggested that the locus of crack growth in bonded rubber units under cyclic compression defines a surface that is approximately parabolic [56]. A linear analysis based on this model gives the tearing energy relation

$$G = 0.5 U h \quad (6.26)$$

where h is the original height of the cylinder.

If the force-deflection relation is linear, the strain energy density U can be calculated from the effective compression modulus; otherwise empirical methods must be used. The compression modulus is given in terms of the shape factor s , where

$$s = \frac{\text{one loaded area}}{\text{force-free area}} \quad (6.27)$$

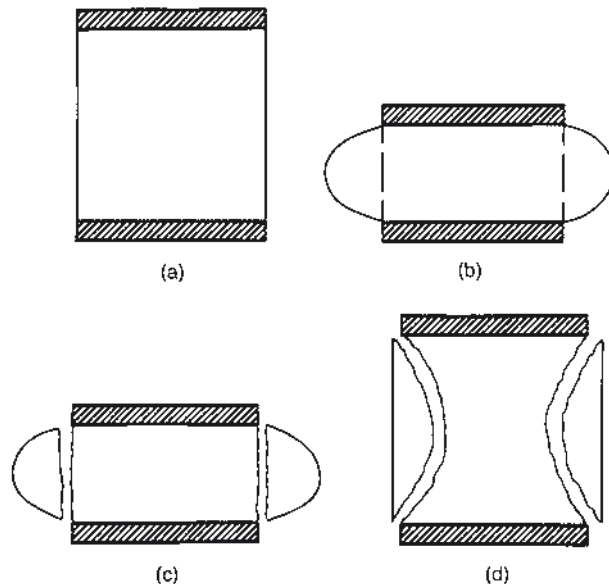


FIGURE 6.18 Schematic representation of the sequence of crack growth for bonded rubber units in compression: (a) unstrained, (b) compressed-crack initiation at bond edges, (c) compressed-bulge separates from core, and (d) unstrained-showing parabolic crack locus (from [56])

For shape factors below approximately 10, the effective compression modulus is given to a good approximation by (see Chapter 3):

$$E_c = E \left(1 + K s^2\right) \quad (6.28)$$

where E is the small-strain tensile modulus of the rubber and K is a numerical factor. As the shape factor increases, the compression modulus E_c increases toward the bulk modulus. The effect of bulk compression must then be included. An average value of the stored energy density U can be computed in terms of the modulus if a linear force deflection characteristic is assumed. Thus:

$$U = 0.5 E_c \varepsilon_c^2 \quad (6.29)$$

where ε_c is the compression strain. A more accurate formulation for the tearing energy in compression can be found in [56].

Thus for rubber cylinders in compression, cracks grow to remove the rubber which, at the maximum compression, bulged outside the original profile of the cylinder. Since Eq. (6.26) does not contain the crack length, propagation is stable in this geometry and the crack will not accelerate. Results of crack growth rates in compression were found to correlate well with values obtained in tension, as shown in Fig. 6.19.

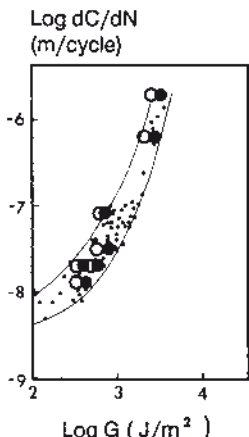


FIGURE 6.19 Crack growth rate as a function of tearing energy: ● = compression-experimental results; ○ = compression-theoretical results; · = simple extension-experimental results (data from [56])

This suggests that the fatigue crack growth rates of compression samples can easily be determined from tension experiments on thin specimens.

This approach has been extended to predict fatigue in multiple rubber-metal bonded layers of shape factors up to 50 [57]. These laminated NR bearings often experienced compressive loads of up to 500 tons. The tearing energy was given by

$$G = 0.5 U t \quad (6.30)$$

where t is the thickness of the rubber layer. Results are shown in Fig. 6.20. A numerical example to illustrate the use of the crack growth characteristic (Fig. 6.20) to predict lifetime of the bonded rubber layers in compression follows:

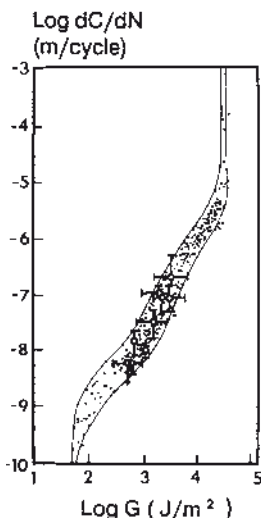


FIGURE 6.20 Fatigue crack growth rate as a function of tearing energy G , for simple extension test pieces (●), and laminates of high shape factor under uniaxial compression (○) (from [57])

A rubber bearing of shape factor less than 10 consists of multiple rubber layers of thickness 4 mm, each bonded to a steel plate. In service it is subjected to a maximum compression strain ε_c of 10%. The effective compression modulus E_c of the rubber is estimated as 100 MPa. What is the minimum lifetime, if failure occurs when a crack reaches a size of around 0.1 m? Assume crack growth data from Fig. 6.20.

From Eq. (6.30) the maximum tearing energy operating in service, written in terms of strain, is

$$G = \frac{1}{4} (E_c \varepsilon_c^2 t) = \frac{1}{4} (100 \times 10^6) (0.1^2) (0.004) = 1 \text{ kJ/m}^2$$

But from Fig. 6.20, $dC/dN = 10 \text{ nm/cycle}$ at $G = 1 \text{ kJ/m}^2$. Therefore, the expected minimum lifetime of the bearing is about 10 million cycles.

6.8.2 Crack Growth in Shear

A relationship for G was derived for bonded simple shear test pieces of thickness t . For short cracks ($C < t$) [58], we write:

$$G = 0.4 U t \quad (6.31)$$

Actually the numerical coefficient can vary between 0.2 and 1, depending on the relative size and configuration of the crack (see Fig. 5.20). A “simple” shear deformation is difficult to achieve in practice, and the situation for very short cracks is complicated by stress concentrations. Furthermore, the tensile component of the stress tends to drive cracks toward either boundary, so that failure occurs at or close to the interface. Simple shear deformation is of importance for several engineered rubber goods (e.g., engine mounts and suspension bushings). Fracture in twisted rubber discs was analyzed by De and Gent [59].

Pure shear deformation was discussed earlier. It is analogous to simple shear, except that there is no rotation of the principal strain axes in the pure shear case. This type of deformation is not only of academic significance. Deformations of this type are encountered in actual service of certain components (e.g., in tire grooves). Clapson and Lake [60] used this model to calculate the tearing energy in a truck tire groove. Thus, knowing the groove dimensions, modulus, and crack growth rates of the rubber, a quantitative prediction of groove cracking in tire treads was achieved.

More recently, Gent and Razzaghi studied the energy release rate for a crack in a tilted rubber block bonded between two rigid plates. Application of repeated tilting deformations to a bonded rubber block appears to be a simple way of measuring crack growth rates under mechanical fatigue. Moreover, a wide range of energy release rates can be employed using a single specimen [61].

■ 6.9 Environmental Effects

The ubiquitous presence of natural flaws in rubber was discussed earlier. Such flaws grow by cumulative tearing steps when the rubber is repeatedly strained, causing *mechanical fatigue*. However, mechanical rupture of chains can be considerably enhanced by oxygen, particularly if the rubber has no antioxidant. Figure 5.10 shows fatigue crack growth data in air and in vacuo for an unprotected natural rubber vulcanizate [1]. Oxygen decreased G_0 of this NR compound by about a factor of 4. Also, the crack growth rate increased immediately above G_0 . Effects of oxygen extend to progressively higher energies, if the frequency of testing is reduced, as shown in Fig. 5.10. Gent and Hindi have investigated the effect of oxygen on tear strength of various elastomers [62]. Oxygen had a much bigger effect on SBR and BR than on NR. At low tearing energies ($G < 1 \text{ kJ/m}^2$), the rate of crack growth for these elastomers was reduced by a factor of up to 10 in the absence of oxygen. Thus, mechano-oxidative fatigue is a more precise term for slow crack growth. At high tearing energies ($> 1 \text{ kJ/m}^2$), the effects of oxygen are negligible. In any case the effects of oxygen can be partially mitigated if suitable antioxidants are incorporated in the rubber. Another environmental agent causing crack growth is ozone. Ozone reacts very rapidly with carbon-carbon double bonds and causes scission. This results in multiple cracks of an unprotected rubber article, held under a small static stress. A small stress, corresponding to a tearing energy G_z , of about 0.1 J/m^2 , is necessary for cracks to grow by ozone; above this condition, the rate of crack growth is independent of tearing energy and proportional to the ozone concentration. The rate is similar for a number of polymers including NR and SBR [63]:

$$\frac{dC}{dt} = \alpha [O_z] \quad G < G_0 \quad (6.32)$$

where α is an ozone crack growth constant.

In rubber-metal bonded components, cracking by ozone occurs close to the interface where the stress concentrations are highest [64], but growth appears to be more complex than would be expected from Eq. (6.32).

Under cyclic conditions, Eq. (6.32) becomes

$$\frac{dC}{dN} = \left(\frac{\tau}{\nu} \right) \alpha [O_z] = R_z \quad G < G_0 \quad (6.33)$$

where τ is the time fraction of each cycle for which the sample is under stress and ν is the frequency. The effect of ozone under cyclic conditions can therefore be predicted from static tests. The ultimate in resistance to ozone is found in fully saturated elastomers, such as ethylene-propylene copolymers. Unsaturated elasto-

mers are normally protected by incorporation of waxes and antiozonants. Waxes are mostly effective in static applications. A review by Lewis [65] should be consulted for more details.

■ 6.10 Modeling and Life Predictions of Elastomeric Components

A technique to predict failure of rubber compounds under repeated complex straining was proposed by Busfield et al. [66]. A software package developed specifically for analyzing fatigue in elastomers was marketed by Materials Engineering Research Laboratory Limited (MERL) under the tradename FLEXPAC [67]. This was a non-linear large deformation finite element code with special features for modeling internal crack growth and for predicting crack direction. However, the code is no longer commercially available as in more recent times the ability to analyze crack growth in rubber components has become widely available in general purpose finite element codes. The modeling of crack growth using finite element analysis can be challenging, especially in 3D. In general, modeling open cracks in tension is possible, but modeling closed cracks in compression may present solution difficulties due to the complexities of modeling the contact between the crack faces. However as the capabilities of codes continue to evolve and the speed and size of computers increases, these types of analysis will become more practical (see Chapter 9).

■ 6.11 Fatigue Crack Propagation of Thermoplastic Elastomers

In one class of thermoplastic elastomers (SBS) the phase-separated polystyrene domains act as physical crosslinks and also as reinforcing particles. The cut growth properties of these SBS materials have been reported [68]. Another large group of thermoplastic elastomers (TPEs) consists of dynamically vulcanized blends of an elastomer with a thermoplastic [69]. Typical are heterophase TPEs comprising a polypropylene matrix and dispersed micron-sized domains of crosslinked EPDM [70]. These materials have proven to be quite tough and fracture resistant and have been steadily replacing many thermoset elastomers in a variety of applications [71, 72]. Figure 6.21 illustrates fatigue crack propagation of two dynamically vulcanized TPEs containing 33% of EPDM and 67% of polypropylene at -40 °C and 125 °C

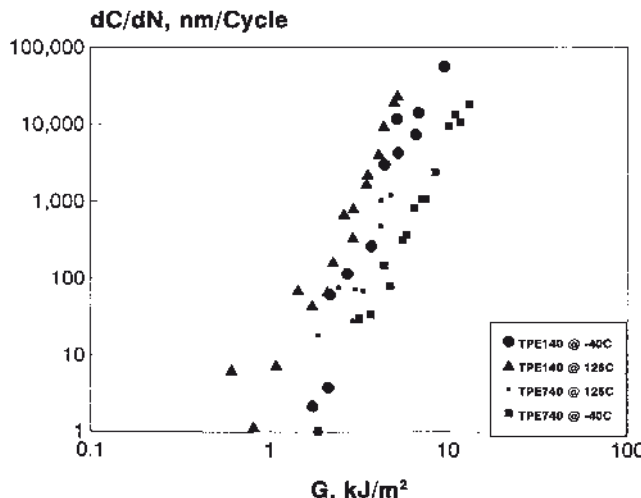


FIGURE 6.21 Fatigue crack growth rate as a function of tearing energy for two dynamically vulcanized EPDM-polypropylene thermoplastic elastomers at 3 Hz and temperatures of 125 °C and –40 °C. Strain energy density calculated from the loading curve

and at 3 Hz. Other fatigue studies on thermoplastic elastomers include fatigue crack propagation of medically implantable polyurethane [73], the effect of soft segment on the fatigue behavior of segmented polyurethanes [74], and the morphology of fatigue fracture surfaces of various thermoplastic elastomers [75]. A relationship between wear rate and mechanical fatigue in sliding of urethane thermoplastic elastomer (TPU) was developed and the wear process in TPU confirmed to be the result of crack propagation in the subsurface layer of the material at small scale [76]. For other recent work, see references [77] and [78].

■ 6.12 Durability of Thermoplastic Elastomers

Although the fracture mechanics methods for evaluating strength and fatigue resistance of elastomers have been well established, they are not as widely used as other, more empirical methods. It is more common in industry to measure ultimate tensile and elongation properties over a broad spectrum of aging times and temperatures and then plot the data in 3D graphs (Figs. 6.22 and 6.23). From this data is determined the continuous upper service temperature, defined according to SAE J2236 as the highest temperature at which a material retains a minimum of 50% of both the tensile strength and elongation at break after 1008 hours in an air circulating oven. This is one measure of durability commonly used in elastomers and plastics specifications.

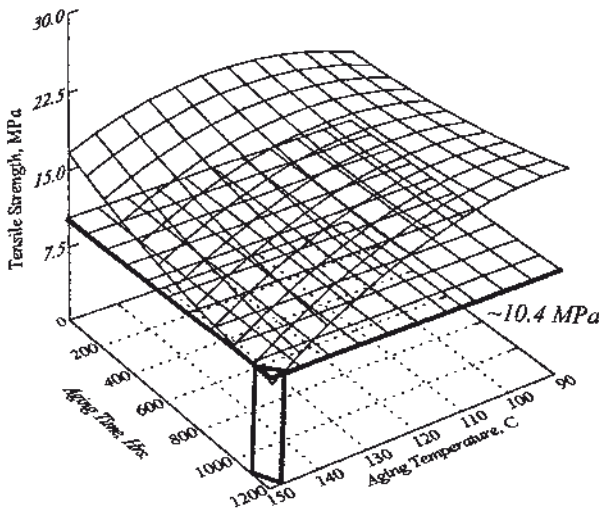


FIGURE 6.22 Tensile strength of a 30% EPDM/70% PP dynamically-vulcanized thermoplastic elastomer, TPE140, as a function of aging time and temperature in air. The continuous service temperature range from SAE J2236 is indicated

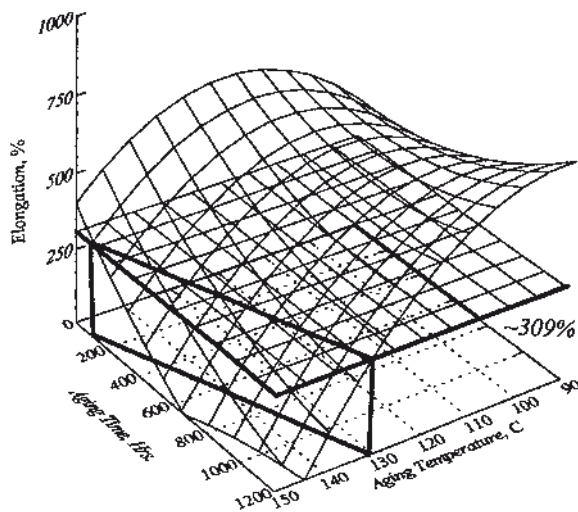


FIGURE 6.23 Breaking elongation of a 30% EPDM/70% PP dynamically-vulcanized thermoplastic elastomer, TPE140, as a function of aging time and temperature in air. The continuous service temperature range from SAE J2236 is indicated

■ 6.13 Summary

The lifetime of a structure is a feature that the engineer needs to be able to quantify. This chapter has reviewed the fatigue failure of rubber under repeated loading. A fracture mechanics approach based on a tearing energy fracture criterion has been found to be reasonably successful in predicting rubber fatigue life in simple geometries either under continuous loads or under repeated excitations. This approach has been extended to rubber composites in uniaxial compression and shear deformations.

The basis of fatigue mechanics of rubber is a crack growth rate dC/dN , which is a function of the available tearing energy G . The complete characterization of a material for mechanical fatigue requires measurement of crack growth rates over a broad range of tearing energies, from the threshold value G_0 to the catastrophic tearing energy G_c . Crack growth tests require fairly elaborate experimental techniques but yield fundamental information on the fatigue behavior of rubber for predictions of service life.

The onset of mechanical fatigue depends on both service conditions, namely loads and temperature, and inherent material characteristics. The molecular structure of the rubber is an important material variable. Because of its stereoregular structure, natural rubber crystallizes under strain, and crack growth is inhibited under steady loading conditions. On the other hand, elastomers that do not strain-crystallize show time-dependent mechanical fatigue. Strain crystallization does not, however, preclude attack by ozone. Above a small critical stress, ozone cracking is independent of tearing energy and is limited primarily by the ozone concentration and presence of an anti-ozonant (see Chapter 5).

In practice, to predict the lifetime of a rubber part, it is necessary to first generate a spectrum of loads and displacements. This permits derivation of the tearing energies during service. If the geometry of the part is complex, analytical solutions for the elastic behavior and the operating tearing energy may not be feasible. Numerical or experimental methods must be developed. When the operating tearing energies are known, the crack growth rate can be estimated from the fatigue crack growth characteristics of the rubber alone, measured in a much simpler geometry. Thus, experiments under a uniaxial loading condition, such as simple tension or pure shear, can be employed to predict the fatigue crack growth rate of rubber under complex stress states.

Acknowledgments

The author expresses her gratitude to the late Mr. Charles E. Barnes for creating the figures.

References

- [1] G. J. Lake, *Prog. Rubber Technol.*, **45**, 89 (1983).
- [2] G. J. Lake and A. G. Thomas, in A. D. Roberts (Ed.), *Natural Rubber Science and Technology*, Oxford University Press, Oxford, 1988, pp. 731–772.
- [3] G. R. Hamed, *Rubber Chem. Technol.*, **67**(3), 529–536 (1994).
- [4] R. Selden, *Prog. Rubber Plast. Technol.*, **11**(1), 56–83 (1995).
- [5] W. V. Mars and A. Fatemi, *International Journal of Fatigue*, **24**, 949 (2002).
- [6] J. G. Williams, *Fracture Mechanics of Polymers*, Ellis Horwood, Chichester, 1984.
- [7] A. A. Griffith, *Phil. Trans. R. Soc. London, Ser. A*, **221**, 163 (1920).
- [8] R. S. Rivlin and A. G. Thomas, *J. Polym. Sci.*, **10**, 291 (1953).
- [9] H. W. Greensmith, *J. Appl. Polym. Sci.*, **7**, 993 (1963).
- [10] P. B. Lindley, *J. Strain Anal.*, **7**, 132 (1972).
- [11] W. V. Mars and A. Fatemi, *Journal of Materials Science*, **41**, 7324 (2006).
- [12] E. Verron and A. Andriyana, *Journal of the Mechanics and Physics of Solids*, **56**, 417, (2008).
- [13] J. M. Buist and G. E. Williams, *India Rubber World*, (New York), **124**, 320, 447, 567 (1951).
- [14] R. P. Brown, *Physical Testing of Rubber*, Applied Science Publishers, London, 1979, pp. 214–223.
- [15] R. W. Hertzberg and J. A. Manson, *Fatigue of Engineering Plastics*, Academic Press, New York, 1979.
- [16] A. Moet, *Int. J. Fract.*, **40**, 285 (1989).
- [17] E. H. Andrews and R. A. Billington, *J. Mater. Sci.*, **11**, 1354 (1976).
- [18] G. J. Lake and O. H. Yeoh, *J. Polym. Sci.*, **25**, 1157 (1987).
- [19] Y. Fukahori, *International Polymer Science and Technology*, **13**, No. 3, T/37 (1986); Nippon Kyokaishi, **58**, No. 10, 625 (1985).
- [20] K. Grosch, *Rubber Chem. Technol.*, **61**, 42 (1988).
- [21] D. G. Young, *Rubber Chem. Technol.*, **58**, 785 (1985).
- [22] L. Mullins, *J. Rubber Res.*, **16**, 275 (1947).
- [23] A. R. Payne, *J. Appl. Polym. Sci.*, **11**, 57 (1962); ibid., **7**, 873 (1963).
- [24] A. N. Gent and H. J. Kim, *Rubber Chem. Technol.*, **51**, 35 (1978).
- [25] E. H. Andrews, *J. Mater. Sci.*, **9**, 887 (1974).
- [26] A. Kadir and A. G. Thomas, *J. Polym. Sci.*, **23**, 1623 (1984).
- [27] A. Muhr and A. G. Thomas, *Rubber Chem. Technol.*, **62**, 219 (1989).
- [28] T. S. Fleischman and D. O. Stalnaker, in “Proceedings of the 1985 SEM Spring Conference of Experimental Mechanics”, Las Vegas, June 9–14, 1985, pp. 688–694.
- [29] R. H. Dauskardt and R. O. Ritchie, *Closed Loop*, Springer 1989, pp. 7–17.

- [30] D. G. Young, *Rubber Chem. Technol.*, **59**, 809 (1986).
- [31] G. J. Lake, R. M. Rollason, R. D. V. Bennett, and H. Ceato, in *Proceedings of the International Rubber Conference*, Kuala Lumpur, 1975.
- [32] J. R. Beatty, *Rubber Chem. Technol.*, **37**, 1341 (1964).
- [33] G. J. Lake and P. B. Lindley, *J. Appl. Polym. Sci.*, **8**, 707 (1964).
- [34] S. M. Cadwell, R. A. Merrill, C. M. Sloman, and F. L. Yost, *Ind. Eng. Chem., Anal. Ed.*, **12**, 19 (1940).
- [35] P. B. Lindley, *Rubber Chem. Technol.*, **47**, 1253 (1974).
- [36] W. V. Mars, and A. Fatemi, *Rubber Chem. Technol.*, **76**, 1241 (2003).
- [37] G. J. Lake and P. B. Lindley, *Rubber J.*, October 1964, p. 24; *ibid.*, November 1964, p. 30.
- [38] R. Clamroth and V. Eisele, *Kautsch. Gummi Kunst.*, **28**, 433 (1975).
- [39] E. H. Andrews, *J. Appl. Phys.*, **32**, 542 (1961).
- [40] A. Stevenson, *Rubber Plast. News*, Feb. 22, 1988, p. 42.
- [41] R. Elleithy, H. Aglan, and A. Letton, *J. Elastomers Plast.*, **28**(3), 199 (1996).
- [42] L. C. Yanyo, *Int. J. Fract.*, **39**, 103 (1989).
- [43] P. Brown, M. Porter and A. G. Thomas, *Kautsch. Gummi Kunst.*, **40**, 17 (1987).
- [44] J. A. Brydson, *Rubber Chemistry*, Applied Science Publishers, London, 1978.
- [45] P.G.Santangelo and C.M, Roland, *Rubber Chem. Technol.*, **76**, 892 (2003).
- [46] M.-P. Lee and A. Moet, *Rubber Chem. Technol.*, **66**, 304 (1993)
- [47] B. J. Roberts and J.B. Benzie, in *Proceedings of the International Rubber Conference, Brighton*, Chameleon Press, London, 1977, p. 21.
- [48] James F. Roach, "Crack Growth in Elastomers Under Biaxial Stress", Ph. D. Dissertation, University of Akron, 1982.
- [49] W. V. Mars and, A. Fatemi, *Experimental Mechanics*, **44**, 136 (2004).
- [50] W. V. Mars and A. Fatemi, *International Journal of Fatigue*, **28**, 515 (2005).
- [51] W. V. Mars, book chapter, "Elastomers and Components – Service Life Prediction; Progress and Challenges" in Heuristic Approach for Approximating Energy Release Rates of Small Cracks under Finite Strain, Multiaxial Loading, V. Coveney (Ed.), OCT Science, Philadelphia, pp. 89–109, Oct 2006.
- [52] Yost, W. V. Mars, A. Fatemi, *Rubber Chem. Technol.*, **79**, 589 (2006).
- [53] Jiro Kawamoto, "Fatigue of Rubber Composites", Ph. D. thesis, M.I.T., 1988.
- [54] R. F. Breidenbach and G. J. Lake, *Phil. Trans. R. Soc. London, Ser. A*, **299**, 189 (1981).
- [55] Y. S. Huang and O. H. Yeoh, *Rubber Chem. Technol.*, **52**, 709 (1989).
- [56] A. Stevenson, *Int. J. Fract.*, **23**, 47 (1983).
- [57] A. Stevenson, *Rubber Chem. Technol.*, **59**, 208 (1986).
- [58] P. B. Lindley and S. C. Teo, *Plast. Rubber Process. Appl.*, **4**, 29 (1979).
- [59] D. K. De and A. N. Gent, *Rubber Chem. Technol.*, **71**, 84 (1998).
- [60] B. E. Clapson and G. J. Lake, *Rubber J.*, **152**(12), 47 (1970).
- [61] M. Razzaghi-Kashani and A.N. Gent, *Rubber Chem. Technol.*, **73**, 818 (1998).
- [62] A. N. Gent and M. Hindi, *Rubber Chem. Technol.*, **63**, 123 (1990).
- [63] M. Braden and A. N. Gent, *J. Appl. Polym. Sci.*, **3**, 100 (1960).
- [64] P. B. Lindley, *J. IRI*, **5**, 213 (1971).
- [65] P. M. Lewis, *Polym. Degradation Stab.*, **15**, 33 (1986).
- [66] J. J. C. Busfield, C. H. Ratsimba, and A. G. Thomas, 1997, *J. Nat. Rubber Res.*, **12**(3), 131 (1997).
- [67] Flexpac, Materials Engineering Research Laboratory, Hitchin U.K.
- [68] D. G. Hirst and A. S. Farid, "Cut Growth of SBS Thermoplastic Elastomers", presented at the ACS Rubber Division Meeting, Chicago, April, 1999.

- [69] A. Y. Coran and R. P. Patel, "Thermoplastic Elastomers Based on Dynamically Vulcanized Elastomer-Thermoplastic Blends", in "Thermoplastic Elastomers", 2nd ed., G. Holden, N. R. Legge, H. E. Schroeder, and R. P. Quirk (Eds.), Hanser Publications, 1996, pp. 133–161.
- [70] M. D. Ellul, J. Patel, and A. J. Tinker, *Rubber Chem. Technol.*, **68**, 573 (1995).
- [71] M. D. Ellul, *Plastics and Rubber Composites Processing Applications*, **26**(3), 137 (1997).
- [72] M. D. Ellul, G. J. Lake, and A. G. Thomas, *Proc. ACS Division of Polymeric Materials: Science and Engineering*, **79**, 109 (1998).
- [73] H. Aglan, *J. Elastomers Plast.*, **22**(3), 199 (1990).
- [74] E. L. Rodriguez, *J. Mater. Sci. Lett.*, **16**(24), 1994 (1997).
- [75] G. Jimenez, A. Shishido and M. Sumita, *European Polymer Journal*, **36**(9), 2039 (2000).
- [76] F.J. Martinez, M. Canales, J.M. Bielsa, M.A. Jimenez, *Wear*, **268**(3–4), 388 (2010).
- [77] W. Michaeli and A. Schobel, "Determination of Load Limits of thermoplastic elastomers under multiaxial load cases", *TPE Magazine*, **2**, 94–98, (2010).
- [78] El Fray, M. and Alstaedt, V., "Fatigue behavior of multiblock thermoplastic elastomers; Stepwise increasing load testing of poly(aliphatic/aromatic-ester) copolymers", *Polymer*, **44**, 4635–4642 (2003).

■ Problems for Chapter 6

1. In developing the fracture mechanics expressions for through-cracks in a sheet of uniform thickness, what is the implicit assumption concerning the area of the growing crack?
2. Derive an expression for the tearing energy in the tensile geometry in terms of stress or strain and modulus, assuming for simplicity linear elastic behavior of the rubber.
3. Fracture mechanics defines a critical crack size for a given level of operating stress as the size below which an initial crack can withstand the first application of stress, but beyond which the crack propagates rapidly to fracture. For a given material subject to repeated loading, what parameter governs the critical crack size?
4. (a) Define the mechanical fatigue limit in terms of the threshold tearing energy G_0 for the simple extension test piece without an edge crack.
 (b) What is the order of magnitude of G_0 and the natural flaw size for rubber?
 (c) What are the main factors that determine G_0 ?
5. A rubber bushing is subject to a steady radial load on which is superimposed a cyclic torsion deformation. It develops an initial crack C_i of length 0.1 mm in the rubber toward the inner wall.

- (a) Derive an expression for the fatigue life N , assuming that the tearing energy is directly proportional to the crack length times the available strain energy density ΔU , and that the crack growth rate versus tearing energy relationship approximates a power law.
- (b) Calculate the fatigue life N assuming the following values of the constants: $\beta = 2$, $B = 7 \times 10^{-8}$ m/cycle/kJ²/m⁴, $k = 6$, $\Delta U = 20$ kJ/m³.
6. Two rubber bands, one made of NR and the other one of SBR, are stretched around a mandrel at strains that correspond to tearing energies of about 2000 J/m². Both rubbers are very well protected by antiozonants/antioxidants. Which rubber band is expected to last the longest and why?

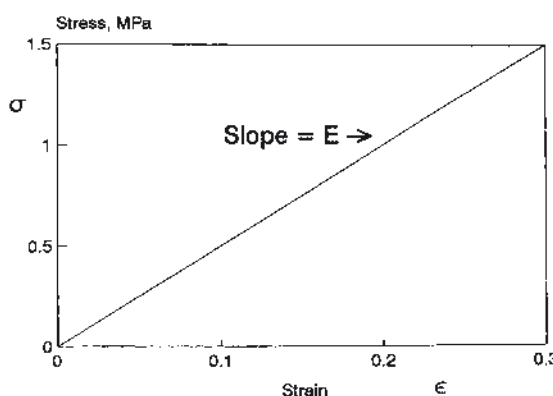
■ Answers to Problems for Chapter 6

1. The change of area is assumed to occur in a self-similar manner from its previous shape. Thus only one parameter, the crack length C , is necessary to define crack propagation because the thickness is constant.
2. Recall Eq. (6.2)

$$G = 2 k U C$$

For a linear elastic material in tension, the Young's modulus E describes the stress-strain behavior. Thus,

$$E = \frac{\sigma}{\epsilon}$$



Therefore

$$U = 0.5 \varepsilon \sigma = 0.5 \varepsilon^2 E = \frac{0.5 \sigma^2}{E}$$

Thus we can write:

$$G = k C \varepsilon^2 E = \frac{k C \sigma^2}{E}$$

3. The critical crack size is determined by the tearing energy. From Fig. 6.3 and Eqs. (6.2) and (6.10) it is seen that a subcritical crack grows to the critical crack size as the catastrophic tearing energy G_c is approached.
4. (a) $G_0 = 2 k U_0 C_0$, where k is a constant defined by Eq. (6.3), U_0 is the minimum strain energy density required for mechanical crack growth, and C_0 is the natural flaw size.
- (b) The order of magnitude of G_0 for rubber is about $10\text{--}50 \text{ J/m}^2$; C_0 is about 0.02 mm .
- (c) G_0 is mainly determined by the molecular structure of the rubber and the molecular weight between crosslinks. (See Chapter 5 and Lake and Thomas [2] for more details.)
5. (a) For small crack lengths (relative to the specimen size), a good approximation for the tearing energy of this bushing is [1]:

$$G = k C \Delta U \quad (6.2)$$

where ΔU is the peak-to-peak change of the strain energy density and other symbols are as defined earlier in Eq. (6.2) (see H. L. Oh, *Rubber Chem. Technol.*, **53**, 1226 (1980)).

If a power law relation between the crack growth rate dC/dN as a function of tearing energy G is assumed, then:

$$\frac{dC}{dN} = B (\Delta G)^\beta \quad (6.9)$$

where ΔG denotes the peak-to-peak change of the tearing energy or the available energy for the cyclic crack growth. Substituting Eq. (6.2) into Eq. (6.9) and integrating between the limits of initial crack length C_i to the final crack length C_f yields:

$$N = \int_{C_i}^{C_f} \left[\frac{1}{B(k C \Delta U)^\beta} \right] dC = \frac{(C_i)^{1-\beta} \left[1 - (C_i / C_f)^{\beta-1} \right]}{(\beta-1) B(k \Delta U)^\beta}$$

but at failure $C_f \gg C_i$, so $(C_i / C_f)^{\beta-1} \rightarrow 0$.

Thus

$$N = \frac{1}{(\beta-1) B(k)^\beta (C_i)^{\beta-1} (\Delta U)^\beta}$$

$$(b) N = 1/7 \times 10^{-8} (6)^2 (0.1 \times 10^{-3}) (20)^2 = 9.9 \times 10^6 \text{ cycles}$$

6. The lifetime of the rubber band made from NR is expected to be the longer, because the strain crystallization that develops in NR will delay substantially and even stop crack growth.

7

Durability

Andrew Stevenson, Robert Campion

■ 7.1 Introduction

Durability assessment should be an integral part of the engineering design process with rubber. All polymers, and elastomers in particular, are potentially sensitive to the temperatures, fluids, and mechanical conditions they are likely to encounter in service, and they can undergo changes in property magnitudes large enough to cause failure. This sometimes surprises engineers whose professional training in materials science has been restricted to metals, and in the extreme may lead to the false conclusion that polymer engineering components are always unreliable. Most of these changes are understood scientifically and can be anticipated if the material has been adequately characterized. It is important for engineers to appreciate the factors that may affect durability of the main categories of elastomers in different service environments.

Durability then is defined here as resistance to any change in property levels due to the service environment. Elastomers vary widely in their resistance to specific environments, depending on material type and composition. The detailed composition and microstructure of elastomeric materials, which are essentially created during the polymerization of the elastomer and the manufacture of the component, depend both on the ingredients selected for the compound and the forming process used. This again is different from the situation for metals, where components are generally formed from materials whose composition is not substantially changed by the production process. Different elastomers can vary in their property behavior as widely as different metals (e.g., gold, copper, steel). There is at present no accepted standardization of elastomer compounds, and their formulations are usually proprietary secrets of component manufacturers.

In practice, assessment of durability is often qualitative and derived from simply cataloguing changes in standard test property values and comparing with earlier data. Although this approach does give some guidance, with some such information included in this chapter, it is nevertheless usually inadequate for critical engineering components with demands for quantitative life assessment. Hence life assessment

requires first identifying whether there are properties that reflect the function of the component and, if so, then defining acceptable limits within which they may change in magnitude before being deemed to have failed; ensuing tests will focus only on these properties. Otherwise, if the component's mode of function does not relate easily to the mode of any standard test property, special tests may then be devised to measure more appropriate rates of change, and these rates may be used for a more direct quantitative life prediction.

One of the most important changes that can limit component durability is the growth of cracks in the material. These normally arise due to oscillating or static stressed mechanical conditions of service. Cracks may grow in any mode of deformation, and growth rates may range from slow and stable to catastrophic. Use of fracture mechanics is the most scientific approach to the characterization of fatigue life, defined by the growth of cracks. This approach has been used with success for elastomeric components, and there is a growing body of literature documenting a wide range of case studies [1–5]. This topic is covered in Chapters 5 and 6 and so is not considered here, but [1] describes a case history in which fracture mechanics was used successfully to predict the life of critical components in the offshore oil industry.

As recognized in Chapter 6, one area of fatigue not covered well by fracture mechanics is crack initiation. In an alternative approach, fatigue assessment in this area is sometimes made empirically by testing (usually in tension) numerous replicate testpieces possessing no deliberately-added cuts or cracks, applying different maximum stress values to each testpiece. The results are plotted as an S - N plot – that is, with maximum cyclic stress plotted against number of cycles to failure. Tensile dumbbells are frequently employed but, where appropriate, testpieces relating better to a service application might be used instead. S - N plots usually resemble simple hyperbolic curves, which means that the onset of significant fatigue failure normally occurs across a relatively small stress region.

Other physical and chemical processes may cause elastomer property levels to change with time in service environments. Some of these processes, such as physical creep and stress relaxation and crystallization, are in principle reversible and should not cause permanent damage. However, they may cause changes to property levels that diminish the ability of a component to function and, in that sense, limit component durability: moreover, in practice, it may be impossible to reverse the process. An example is a rubber bearing in service. The consequence of either crystallization due to cold environments or age hardening due to aerobic effects in hot sunny climates may double the elastomer modulus (stiffness): the reduction in service performance would then be the same in both cases, even though the stiffening was due to a theoretically reversible process in the first case and an irreversible process in the second.

Service environment is also a major effect in durability. Aerobic attack is one common example of chemical degradation that causes permanent changes in property levels, especially at elevated temperatures. Oxygen is the most common factor in age hardening of elastomers. However, other permanent chemical changes can occur in anaerobic conditions at high enough temperatures by the continuation of cure. Exposure in service to chemically hostile fluids can again cause deterioration in elastomers, for instance, hydrogen sulphide in oilfield operations, especially if the oil-resistant seals or hose linings involved are nitrile rubbers. The consequences of certain purely physical effects can also cause permanent changes. Large amounts of swelling can occur in hydrocarbon liquids which will cause weakening. Gases can permeate elastomers to a considerable extent at high pressures; if this permeation occurs across a seal or hose lining, environmental contamination might result. In addition, a rapid removal of the high pressures can quickly change a hitherto stable situation for the dissolved gas into an unstable one, resulting in fracture and breakup of the elastomer in extreme cases – in popular jargon, this phenomenon is termed ‘explosive decompression’ or is otherwise known as rapid gas decompression.

Assessment of the overall durability of an elastomeric component should take account of the mechanical effects of fatigue crack growth and strength and environmental durability associated with service fluids, temperatures, and pressures. Interactions between all mechanisms of deterioration need also to be considered in detail for some applications. An improved appreciation of mechanisms of deterioration and factors limiting durability will allow engineers to design elastomeric components for more critical applications and with increased reliability. This approach to reliability analysis is required in some documents of the International Standards Organization (ISO).

This chapter focuses on describing mechanisms affecting durability that are not directly concerned with crack growth fatigue. Discussions on interactions between fluid aging and fracture mechanisms are also beyond the scope of this book.

■ 7.2 Creep, Stress Relaxation, and Set

Creep is a time-dependent increase in deformation under constant load, while stress relaxation is a time-dependent reduction in stress under constant deformation. Both are referred to as “relaxation” phenomena. Theoretical relationships between creep and stress relaxation rates are mathematically complex, but in practice either rate can be deduced from the other, if the shape of the force-deflection curve is known – see Section 7.2.2. Set is “permanent” deformation which remains when a material is released from the strain imposed. These phenomena occur in all materials,

but are often more evident in elastomers because of the high initial deformations to which they may be subjected.

7.2.1 Creep

If an elastomeric component is subjected to a static preload, then this load will cause a progressive increase in deformation as a function of time. This can be important in a wide variety of applications, from building mounts to automotive suspensions and engine mounts to elastomeric tensioners for oil platforms [2]. Creep is usually expressed as a percentage of the initial deflection. Thus:

$$\text{creep at time } t = \frac{x_t - x_0}{x_0} \times 100\% \quad (7.1)$$

where x_0 is the initial deflection, and x_t is the deflection at time t .

The initial deflection must be measured at a defined initial time t_0 , which should be about 10 times longer than the time taken to apply the deformation. Creep rate is expressed as creep divided by a function of time. This function may be the logarithm of time if the relaxation mechanism is physical or time if it is chemical.

Creep in rubber consists of both physical creep (due to molecular chain slippage) and chemical creep (due to molecular chain breaking). Physical creep rates (A) decrease in time and are usually expressed as a percentage of the original deflection per decade (factor of 10 increase) of time. Chemical creep rates (B) at a constant temperature are approximately linear with time, and thus the total creep is given by:

$$\text{creep (\%)} = A \log_{10} \left(\frac{t}{t_0} \right) + B(t - t_0) \quad (7.2)$$

This approach has proven successful in characterizing large-scale components, and good correlations between laboratory expectations and site measurements exist for up to 15 years' service of building mounts [6].

7.2.2 Stress Relaxation

When an elastomer is held at a constant deformation, there is a decrease in stress as a function of time. This phenomenon can be of great importance in low pressure sealing applications, where the sealing force is mainly brought about by prior mechanical compression of the seal. During service, the material of the seal is required to remain at above a specific sealing force to prevent leakage. Stress relaxation dominates the effective life of the seal at low pressures. In contrast, at high pressures, transference of the pressurized fluid "energizes" the seal to bring about sealing.

Stress relaxation is usually defined as the loss in stress expressed as a percentage of the initial stress. Thus:

$$\text{stress relaxation} = \frac{\sigma_0 - \sigma_t}{\sigma_0} \times 100\% \quad (7.3)$$

The rate of stress relaxation is then the stress relaxation divided by some function of time.

Stress relaxation and creep rates are related to one another, if the shape of the force-deflection curve is known, using a method proposed by Gent in 1962 [7]. According to this, the relationship between the two parameters is determined by the incremental stiffness at the point on the force-deflection curve relevant to the stress relaxation or creep measurement. Thus

$$C = \frac{\sigma}{\varepsilon} \left(\frac{d\varepsilon}{d\sigma} \right) S \quad (7.4)$$

where C is the creep rate, S is the stress relaxation rate, ε is the strain, and σ is the stress.

Since it has been established that creep and stress relaxation can be related in this way, in the following discussion both are referred to as relaxation processes.

7.2.3 Physical Relaxation

Relaxation mechanisms are usually divided into two categories, namely physical and chemical. Physical relaxation is not very sensitive to temperature at normal operating temperatures, whereas chemical relaxation is. Physical relaxation is associated with reorientation of the molecular network under strain, with disengagement and rearrangement of chain entanglements, with the breaking of bonds due to secondary valence forces between chains, between filler particles, or between chains and filler particles. The strain history of the material can also be influential. These processes are relatively rapid initially and slow down with time. Physical relaxation usually decreases linearly with the logarithm of time. Figure 7.1 shows the stress relaxation of two elastomers at elevated temperature. In each case the behavior is *initially* log-linear, and can be described in this region by the relation

$$\frac{\sigma_0 - \sigma_t}{\sigma_0} = A \log_{10} \left(\frac{t}{t_0} \right) \quad (7.5)$$

where A is the stress relaxation rate in percent per decade of time (ppd).

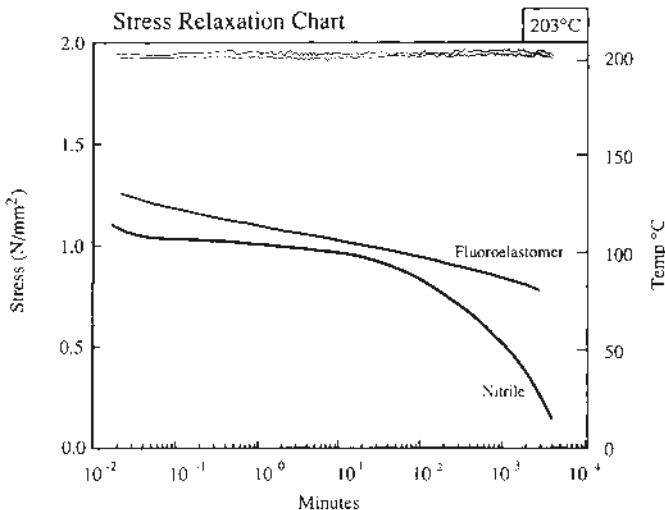


FIGURE 7.1 Stress relaxation of acrylonitrile-butadiene rubber (NBR) and a fluoroelastomer (FKM) at 203 °C (upper thin traces, in situ thermocouple outputs); lower bold traces, typical stress relaxation data for NBR and FKM elastomers

The proximity of the service temperature to the glass transition temperature T_g is normally the dominant factor in determining physical relaxation rate. Thus physical rates are high near to T_g and decrease as the temperature rises and molecules become more mobile.

The degree and type of crosslinking of the elastomer also affect the relaxation rate, with increasing crosslink density decreasing relaxation rate. Since fillers cause additional relaxation mechanisms, filled elastomers have higher physical relaxation rates. Relaxation rates are not generally strongly dependent on strain or the mode of deformation: compression, tension, or shear.

Physical relaxation rates may be affected by the absorption of small amounts of fluids, such as water vapor. Thus a natural rubber vulcanizate in 88% relative humidity has been shown [8] to absorb less than 1% of water, but this caused an increase in stress relaxation by 60% compared to dry conditions. However, excessive swelling due to absorption of organic solvent has been seen to overcome initial relaxation, increasing stresses significantly [9].

Temperature cycling while an elastomer is under stress or strain does indeed affect physical relaxation significantly, and so careful temperature control is essential when making measurements [9].

7.2.4 Chemical Relaxation

At high temperatures and long times, chemical relaxation usually predominates over physical relaxation. The rate of chemical relaxation is approximately linear with time, at least in the early stages. Chemical relaxation has the usual sensitivity to temperature associated with chemical reactions: the rate can almost double with a 10 °C change in temperature (but see Section 7.6.4 and Chapter 7 Problem no. 3). Chemical relaxation is associated with a scission of chemical bonds, either in the polymer chains or in the crosslinks. Scission is mostly oxidative, but can still occur under anaerobic conditions (e.g., overcure within a mold sealed by the flash rubber). Except for anaerobic relaxation, chemical relaxation is strongly influenced by specimen thickness because the chemical degradation process needs to be induced by the fluid (e.g., oxygen) which causes it, and only the thinnest sections have sufficient supply to exhibit a “true” chemical relaxation rate. When testing in air, for specimen thicknesses above about 0.25 mm, oxygen cannot diffuse in fast enough to sustain the highest possible chemical relaxation rates, and so the reaction is “diffusion controlled”. This effect becomes most important at higher temperatures. For example, the chemical rate for natural rubber in air at 110 °C has been found [8] to be about 50% less for a 7 mm thick section than for a 0.25 mm thick section. A total relaxation rate can be determined by combining physical and chemical rates. Thus

$$\text{total relaxation} = A \log_{10} \left(\frac{t}{t_0} \right) + B(t - t_0) \quad (7.6)$$

(where A is the physical relaxation rate and B is the chemical relaxation rate) is the general form of Eq. (7.2).

Figure 7.1 illustrates the type of relaxation behavior that may occur in nitrile rubber when chemical mechanisms become important, here at 203 °C. The influence of the second coefficient B may be seen in the departure from logarithmic/linear behavior beyond a certain time. The greater chemical resistance of FKM is shown by the minimal nature of such a change. In-situ test techniques are required to provide relaxation charts of the type illustrated in Fig. 7.1.

7.2.5 Compression Set and Recovery

Theoretically, set is the deformation that remains after an imposed strain has been removed. Thus set measures the ability of the elastomer to recover its original dimensions. When the deformation is compressive, it is referred to as compression set. Hence, compression set is defined as

$$\text{set} = \frac{h_0 - h_r}{h_0 - h_s} \times 100\% \quad (7.7)$$

where h_0 is the initial thickness, h_r is the recovered thickness, and h_s is the compressed thickness – in practice, the thickness of an associated steel spacer which prevents further compression by the clamping plates.

Practically, the recovered thickness will increase as a function of time from release of compression. Hence appropriate recovery times need to be specified. In “standard” testing (e.g., ASTM), rubber disks are compressed by 25% at room temperature, then exposed to the test temperature for a specified time (e.g., 24 hours), and released to allow recovery. Then h_r is measured after a 30 minute recovery at room temperature.

The main use of the standard test is to provide a quality control check on the state of cure. An undercured specimen will show excessive set because of the formation in the compressed state of extra crosslinks, which prevent recovery. Attempts to interpret the standard test beyond this can be meaningless. The large specimen size means that oxidative effects will not occur evenly, because the time scale of the test is usually too short for oxygen to be present at equilibrium other than at the surface.

Compression set does not measure the same changes as stress relaxation and there is no reason any correlation should exist between the two properties. After compression of an elastomer to a fixed deformation, breakdown of the network of long-chain polymer molecules occurs, and this is to some extent measured by stress relaxation. However, crosslinks may form in the strained state and form a “second network”. These crosslinks will have no effect at all on stress relaxation but can dominate the value of compression set, because the bonds so formed oppose recovery after release of compression.

In sealing applications, the ability of the seal to recover can be important if there is movement in the surrounding metalwork. Whether instant recovery or just the ability to recover at all is more important depends on the design and the application. In either case, recovery at 30 minutes is not a useful measure, as it represents a mixed case between instant and permanent recovery. Where ability to recover is more important than speed of recovery, it is recommended that the set 24 hours after release be used as a measure of “permanent” set. Alternatively, although a non-standard approach, for testing at elevated temperatures, the optimal recovery will be obtained if carried out *still at the test temperature* until equilibrium. Where speed of recovery is important, then the set 10 seconds after release may be used, which requires *in situ* measuring equipment.

If temperatures fall below T_g (see Section 7.4.1) and then increase again, a form of compression set can occur from physical reasons only. Again, this may be important in some sealing applications.

7.2.6 Case History Study

A detailed case history study has been made of a set of building mounts over a period of 15 years [6, 10]. The building, Albany Court in London, was supported by 13 bearings, of a capacity between 60 and 200 tons, which isolated the building from vibrations from an underground railway (“tube”) line, as shown schematically in Fig. 7.2. Provision was made for easy access to the bearings with jacking points to facilitate replacement, should this prove necessary. One of the main concerns was that creep in the rubber should be neither excessive nor uneven, because this could cause uneven settlement and structural damage to the building. Extensive laboratory tests were performed to establish the creep rates for the rubber compound used. The physical creep rate A was measured as $6.6 \pm 1.2\%$ per decade and the chemical creep rate B was $0.47 \pm 0.2\%$ per year. Using these laboratory values, calculations were performed for the full-scale building mount, which estimated that creep in the rubber bearings would be not more than 6 mm after 100 years of service.

Following construction, detailed measurements of creep were made at regular intervals on site for up to 15 years. The results of these measurements were in good agreement with the predictions from laboratory tests. There was no evidence of a diffusion control mechanism at this ambient temperature. The results are shown in Fig. 7.3.

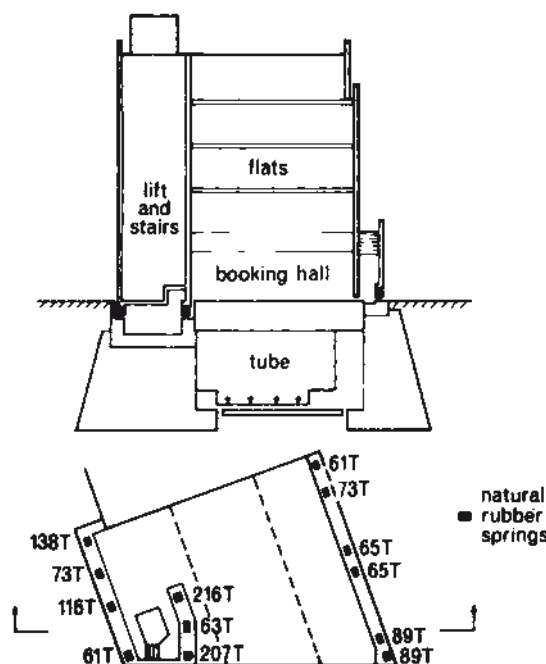


FIGURE 7.2 Albany Court building mounts: schematic view showing the locations (◆) of the rubber bearings in the building

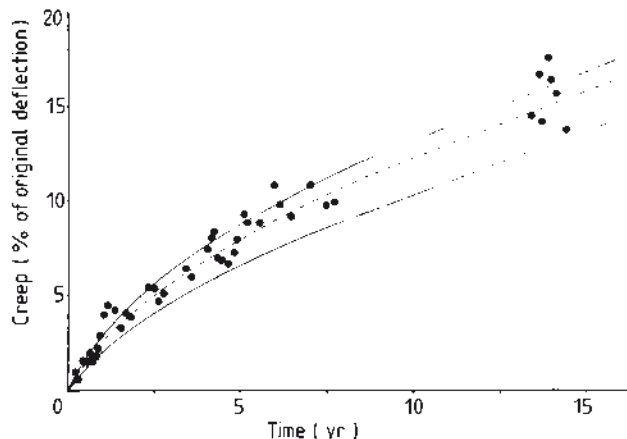


FIGURE 7.3 Creep of building mounts after 15 years service in Albany Court: circles show site measurements on building; curves indicate envelope and median of laboratory predictions made before building construction

The upper and lower bounds of the laboratory predictions are shown by the solid curves, while the site measurements are represented by circles. After 15 years, the amount of creep is close to the predicted value and the trend is still consistent with the ultimate prediction “less than 6 mm after 100 years”. All the measurements shown are averages from readings on seven different bearings and all have been corrected for seasonal fluctuations in temperature. The general condition of the rubber in all these bearings still appears to be excellent, and no replacement has proved necessary. There is thus good evidence that creep in elastomers over long periods of time can be correctly predicted from short-term laboratory tests.

■ 7.3 Longevity of Elastomers in Air

7.3.1 Durability at Ambient Temperatures

There is also evidence that rubber can survive very long periods in service at ambient temperatures up to at least 30 °C without any measurable deterioration. By 1983, a range of polychloroprenes and fluoroelastomers had been characterized in 14-year trials of longevity at an outdoor weathering site in Panama [11]. Elsewhere, natural rubber and polychloroprene bridge bearings have been in continual service for more than 30 years with no need for maintenance or replacement.

However, durability at ambient temperatures can be affected adversely by poor processing (e.g., incomplete cure). Slow continued crosslinking may then occur,

causing hardening. Some elastomer compounds are more vulnerable to this than others. Results from thin standard test pieces can be misleading when attempting to judge the durability of real engineering components. Some case studies follow.

7.3.2 Sunlight and Weathering

Effective protection against direct sunlight is given by the carbon black filler incorporated in most rubber compounds. Carbon black filters ultraviolet radiation. Additionally, rubber units are often placed so that they are shielded from direct sunlight. Surface degradation of rubber, variously described as perished, cracked, crazed, or weathered, can normally be attributed to attack by atmospheric ozone, oxygen, and sunlight. This can occur particularly in compounds not protected by antioxidants and antiozonants – a situation which has not generally applied for many years. However, this phenomenon affects only the relatively thin outer layer of rubber, and so may remain only a surface effect for structural bearings. Bearing pads of natural rubber installed in 1890 were examined in 1986, and although the outer 1 to 2 mm of rubber had degraded after 96 years of exposure to the atmosphere, the inner core of rubber was still in good condition. Most likely, oxidation was so limited because diffusion of further oxygen through oxidized rubber is much slower than through new rubber; the oxidized material had formed a thin protective skin on the surface of the bearing.

Some standard laboratory aging tests on thin strips of rubber can be very misleading because of these skin effects, the skin here being a significant proportion of the rubber test piece. They do, however, provide a guide to the relative weathering resistance of thin sections of different types of rubber, for instance, for roofing membranes.

7.3.3 Ozone Cracking

Minute concentrations of ozone in the atmosphere can cause cracking within a few weeks in unprotected rubber components (i.e., with no antiozonants present in the formulation). For this to occur requires the presence of a minimum surface tensile strain, the cracks then growing in a direction perpendicular to the strain (see Fig. 5.14). The latter characteristic distinguishes ozone cracks from crazing induced by sunlight. The rate of crack growth depends on the type of rubber and on the ozone concentration. Nitrile rubber and natural rubber are intrinsically less resistant to this effect than polychloroprene or ethylene-propylene diene monomer (EPDM). Protection is usually provided by the incorporation of waxes or chemical antiozonants.

The subject of ozone cracking is not considered here in detail because it is treated as a crack growth mechanism in Chapters 5 and 6. Most national standards for bridge bearings require a certain level of ozone resistance, as judged by an accelerated test in a high ozone concentration. The best level of protection is required by the German standard DIN 1400, which requires resistance to 200 parts per hundred million (pphm) concentration of ozone for elastomeric bridge bearings.

7.3.4 Structural Bearings: Case Histories

7.3.4.1 Natural Rubber Pads for a Rail Viaduct after 100 Years of Service

Pads of natural rubber were installed in 1889 between the steel superstructure and the supporting piers in a rail viaduct between Flinders Street and Spencer Street, Melbourne, Victoria, Australia (see Fig. 7.4). The viaduct was opened to traffic in 1891 and was still one of the most heavily traveled structures of the Victoria Railway system in the 1990's, with up to 30 trains per hour. It is believed that the rubber pads were installed to absorb impact and noise rather than to accommodate any temperature-induced horizontal movement of the cross-girder relative to the piers. In those days, there was no satisfactory method of bonding rubber to metal plates, and so unbonded pads were used, which have since in places squeezed out partially from beneath the steel plate of the superstructure. This enabled a sample of rubber to be cut away from one edge and tested in the laboratory.

The rubber pads were about 0.5 in thick and made from "best red rubber", composed of natural rubber, clay, sulfur, and iron oxide. The sulfur level was found to

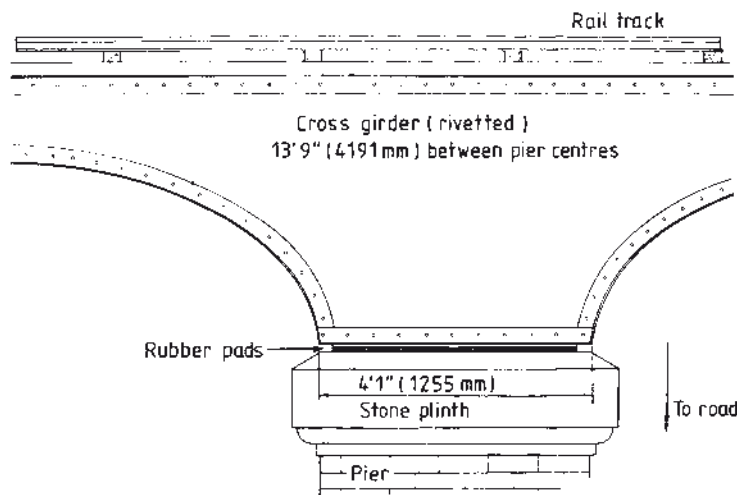


FIGURE 7.4 Location of 100-year-old rubber rail pads in bridge in Melbourne, Australia

be several times higher than in modern NR compounds, and there were no added antioxidants. Although the surface of the rubber is now hard and shows evidence of oxidation, below a depth of about 1.5 mm the rubber is free from such degradation and has a hardness of only 63 IRHD (International Rubber Hardness degrees). There is no evidence of significant deterioration of the rubber below this depth or in the center of the pad. This convincingly illustrates that weathering of rubber in normal conditions is limited to the surface regions. It suggests also that so-called accelerated tests exposing thin rubber sheets to elevated temperatures can give a misleadingly pessimistic view of the longevity of rubber pads for civil engineering applications. As already noted, the skin of oxidized rubber forming as a result of aging can act as a protective layer to inhibit further ingress of oxygen to rubber deep inside a thick block. It is, of course, the bulk stiffness of the pads that determines whether they will continue to function satisfactorily in this type of application, not the appearance of a surface skin.

The rubber pads discussed here were made from what would today be considered to be an inferior and unprotected compound. Yet they were still functioning satisfactorily 100 to 110 years after installation. Modern elastomer compounds with chemical antioxidants are expected to show even greater durability. Compounds of synthetic elastomers, such as polychloroprene, can also be used as coatings to reduce degradation in the outer skin of a large bearing based on natural rubber.

7.3.4.2 Laminated Bridge Bearings after 20 Years of Service

Laminated polychloroprene and natural rubber bearings have been in documented service for more than 30 years in the U.S. and in the United Kingdom with no reports of serious deterioration. In the UK, a detailed case study [6] was made of natural rubber bridge bearings taken from a bridge carrying the main London-to-Kent M2 Motorway. The specimens were removed for laboratory study in December 1982 after 20 years of service. The study was commissioned by the British Department of Transport to help assess any future needs for replacement of elastomeric bearings in bridges. The bridge is 52 m long and has twin two-lane carriageways with hard shoulders. There are 32 bearings located in two rows, one row at each end of the bridge deck. Figure 7.5 shows a close-up view of a bearing *in situ* supporting the bridge deck. For a period of one year, detailed measurements were made of the functioning of the bearing using displacement transducers, positioned to monitor shear movements in the bearing.

Two bearings were removed by raising the bridge deck using hydraulic jacks. The compression and shear stiffnesses of the removed bearings were measured, and one bearing was sectioned to study the condition of the rubber. Figure 7.6 shows the results for that bearing. The compression stiffness was within the range of original test results quoted by the manufacturers for this set of bearings prior to installation

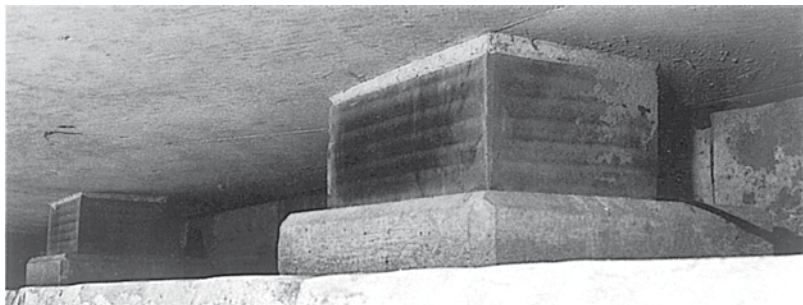


FIGURE 7.5 Close-up of 20-year-old rubber bearing under bridge deck in England

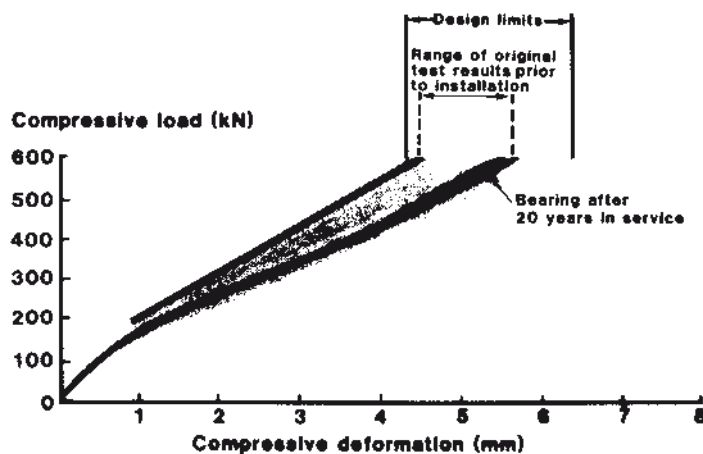


FIGURE 7.6 Compressive load-deflection characteristics of 20-year-old bridge bearing after removal from bridge deck in Fig. 7.5

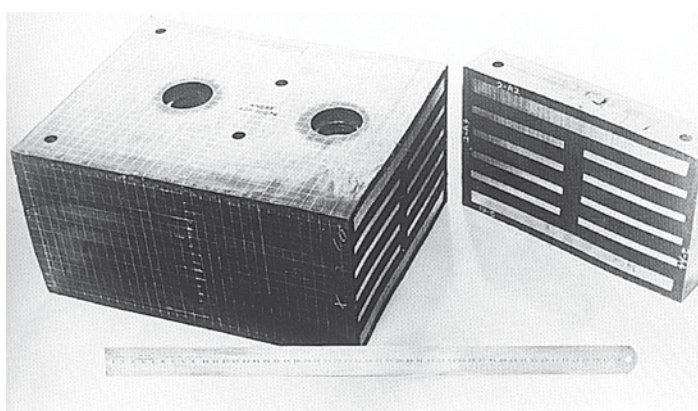


FIGURE 7.7 Photograph of sectioned 20-year-old bearing after tests shown in Fig. 7.6

and also within the design limits for the bridge. Tests on whole bearings gave no evidence of any significant change in either shear or compression stiffness. The stiffnesses of the 20-year-old bearing were also very close to that of new replacement bearings supplied by the manufacturers (Andre Rubber Ltd).

Figure 7.7 shows the structure of the bearing. It had an outer rubber cover about 12 mm thick, for environmental protection. This illustrates the main principle of providing durability for elastomeric structural beatings. All edges of reinforcing metal plates need to be encapsulated and protected from the environment by an outer rubber cover.

The general appearance of the bearings was excellent, with no evidence of any ozone cracks or oxidation. All the bonds to the steel plates still appeared to be in perfect condition, with no evidence of delamination anywhere [6]. In the laboratory, the entire outer surface of one bearing was marked with a grid, and hardness and puncture measurements were taken for each grid square. These results enabled contour maps of hardness and puncture strength to be constructed for each surface of the bearing.

Figure 7.8 shows a contour map obtained from the puncture test. Puncture strength is quoted simply as puncture force, but this can be related to tear strength. There was no significant difference in hardness or puncture strength between the outer exposed surface of the rubber and the cut surface from inside the bearing. Apart from a few high and low values, most puncture forces were in the range 15 to 20 N. In addition to the contour maps, standard tests were carried out on specimens extracted from the bearing, as required under both past British Standards and those later ones applying at the time of the examination. The results are shown in Table 7.1. It was found that the elastomer would still pass standard test requirements for a new bearing of this type.

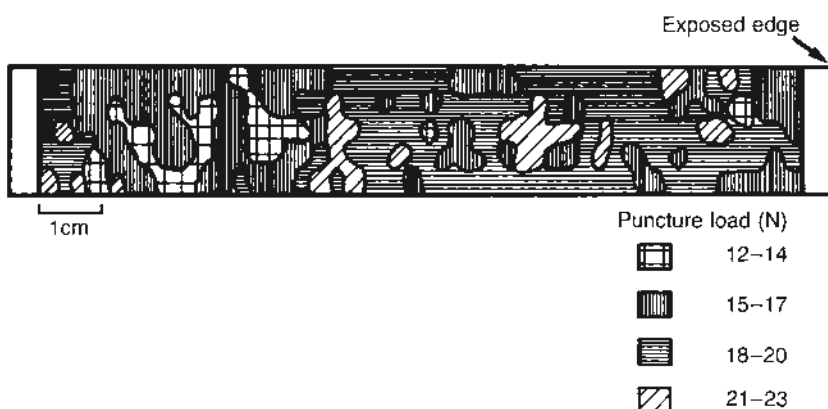


FIGURE 7.8 Contour maps of puncture strength in 20-year-old bridge bearing of Fig. 7.7

TABLE 7.1 Comparison of Test Data from a 20-Year-Old Bearing with Requirements of British Standards

Property	Original 1952 standard: BS 1154		1983 standard:	Results on rubber cut from bearing and ground flat	
	Z14	Z15	BS 5400	From load-bearing layers between reinforcement inside bearing	From outer rubber cover
Hardness, IRHD	62–70	72–80	66–75	71	68
Tensile strength (TS) MPa	13.8 (min)	10.4 (min)	15.5 (min)	17.1	14.7
Elongation at break (EB) %	350 (min)	250 (min)	300 (min)	439	403
Compression set, %	30 (max)	35 (max)	30 (max)	15	20
Change after 7 days at 70 °C					
Hardness, IRHD	-0, +4	-0, +4	±10 (max)	+2	+3
TS, %	10, +10	-10, +10	±15 (max)	-8	+1
EB, %	15, +0	-15, +10	±20 (max)	-5	+8

After this study, it was concluded that there was no evidence of any significant deterioration of the bearings or of the rubber material over the 20-year period that the bearings had been in service.

■ 7.4 Effect of Low Temperatures

7.4.1 Glass Transition

On cooling to very low temperatures, all elastomers undergo a transition, occurring across a few degrees only, to the glassy state, becoming brittle and stiffening by factors of up to 1000. In this state they clearly cannot display elastomeric properties. The temperature range over which this occurs differs widely for different elastomers, depending mainly on the molecular structure of the polymer. Some elastomer glass transition temperatures T_g , representing the mid-point or thereabouts of this range, are given in the Appendix, Table 1.

There can be significant changes in mechanical properties compared with ambient temperature values at temperatures even 20 °C or more above the actual transitional temperature range. Stiffness and modulus may increase along with hysteresis, creep, stress relaxation, and set. In dynamic applications, T_g will increase, perhaps by many tens of degrees, if frequency is increased, with amplitude effects occurring as well. The maximum in hysteresis occurs at a “dynamic T_g ”. Viscoelastic properties are

discussed in Chapter 4. Engineering design with elastomers for dynamic purposes must allow for the associated stiffening at temperatures well above the “static” T_g .

7.4.2 Crystallization

Some elastomers can also crystallize. This occurs at temperatures well above T_g , but can be still below ambient. Polychloroprene (CR) and natural rubber (NR) are the principal types of crystallizing rubber, having maximum crystallization rates at -10 and -25 °C respectively. In fact, the extremely good strength and fatigue resistance of CR and NR derive largely from their ability to strain-crystallize locally at a crack tip, even at working temperatures. EPDM can also crystallize, depending on the ethylene content (high for crystallization).

While the glass transition happens rapidly on cooling sufficiently, crystallization occurs slowly and may take months to reach equilibrium. The most important consequence for engineering applications is an increase of modulus by factors of 1 to 100 [2]. In addition to the choice of elastomer, the choice of vulcanization system is important; as an example, for natural rubber, a “conventional” sulfur-curing formulation with a high-sulfur/low-accelerator ratio is preferable for resisting crystallization. The resulting polysulfidic crosslinks are thought to cause local disruption of the molecular chain regularity needed for crystallization.

Natural rubber possesses intrinsically greater resistance to low temperature crystallization than polychloroprene, so that the most resistant NR formulations are more resistant than the most resistant CR formulations – which are also those generally with poorer aging resistance at elevated temperatures. However, at some temperatures, some other formulations of NR will exhibit greater crystallization at the same temperature (e.g., at -10 °C) than some formulations of CR. Under zero-strain conditions, crystallization can occur over a temperature range of 70 °C or so, but times to equilibrium will be long at the extremes of the range. There can be substantial stiffness increases in some types of CR and NR after prolonged exposure to a temperature of +3 °C. This stiffening effect should be considered carefully when designing structural bearings for cold climates.

The strong dependence of low temperature resistance on compound formulation means that it is essential to have a performance-related low temperature test for engineering components likely to experience cold environments in service. The most accurate and reliable way to characterize resistance to low temperature crystallization is to measure elastic modulus directly. Other tests have been used (e.g., low temperature hardness, volume change, low temperature compression set) but, as Fig. 7.9 illustrates, these tests can underestimate the extent of low temperature stiffening.

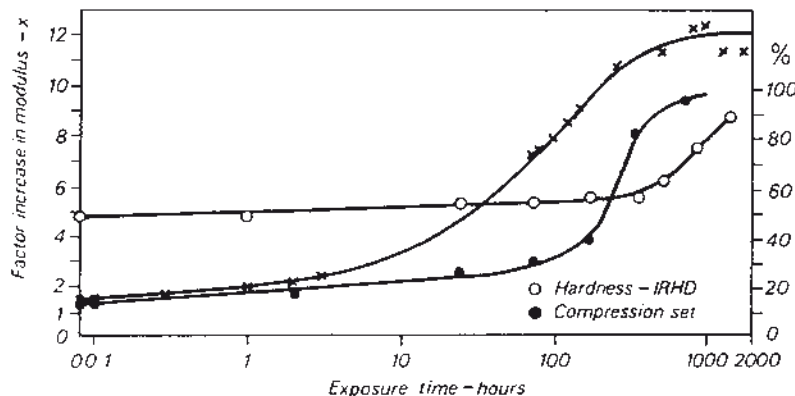


FIGURE 7.9 Correlation between low temperature modulus increase (x), compression set, and hardness for a natural rubber vulcanizate

Crystalline rubber still possesses high strength, but it is no longer a highly-elastic rubbery material. It yields like a thermoplastic above about 7% extension. The degree of crystallinity is, in fact, rather low, below 40% at equilibrium. Melting of the crystallites will begin at temperatures approx. 10 °C above the temperature of crystallization. Melting is a much more rapid process than crystallization, but can still be a lengthy process for a large bulk of rubber. During crystallization, rubber shows very high rates of stress relaxation (50% per decade), which can be extremely damaging in sealing functions and some other applications.

Low temperature stiffening does not in itself damage the rubber, and the effects usually are fully reversible by warming for long enough above either T_g or the equilibrium melting temperature of the rubber crystallites. Durability of a component may however be adversely affected in an engineering application that would force the glassy or semicrystalline bearing to deform to a given initial strain, creating abnormally high stresses.

■ 7.5 Effect of Elevated Temperatures

At sufficiently elevated temperatures, all types of rubber will undergo degradation reactions, leading to a loss of mechanical properties. Moderately elevated temperatures may cause the exchange of crosslinks and formation of additional crosslinks, leading to some hardening of the rubber. At higher temperatures, scission of crosslinks may outweigh crosslink formation, with breakdown in structure and a net softening of the rubber. At very high temperatures, the molecular chains break down and charring and embrittlement of the rubber occur. Under deformation, all three changes are the basis for compression set testing.

TABLE 7.2 Resistance to Thermal Degradation

Highest service temperature (°C)	Rubber type
75	Polyurethane Styrene-butadiene rubber
85	Butadiene rubber Natural rubber
100	Polychloroprene
125	Epichlorohydrin Nitrile rubber Butyl rubber Ethylene-propylene diene monomer
150	Chlorosulfonated polyethylene Hydrogenated nitrile rubber Polyacrylic rubber
200	Fluoroelastomer ^a Fluorosilicone rubber Terfluoroelastomer copolymer Tetrafluoroethylene-propylene copolymer
250	Silicone rubber
300	Perfluoroelastomer

^a Greater resistance with increasing fluorine content.

The presence of oxygen is a very important factor in influencing the resistance of rubber to elevated temperatures. In the absence of oxygen, most types of rubber (even natural rubber) could survive temperatures of 175 °C, although at this temperature degradation would occur very rapidly in the presence of oxygen. Table 7.2 summarizes in general terms the realistic upper service limits of most types of rubber in the context of engineering applications that normally use rubber in reasonable thicknesses. Any such guide has to be approximate, because the actual suitability will depend on the properties measured, the exact compounds used (some NR compounds provide prolonged service only below 70 °C), and also the length of service required at that temperature.

For most engineering applications outside the oil and gas production sector, oxidative degradation is the most important factor determining durability. For a thick enough section of rubber, the availability of oxygen is limited by diffusion, and components with bulky rubber layers (e.g., engine mounts or bridge bearings) can be considerably more resistant to elevated temperatures than the behavior of the thin strip specimens used in standard tests would suggest. As already noted, an outer skin of rubber may form, which can further limit oxygen ingress. Such a skin was found to play an important part in the durability of the 100-year-old bridge pad discussed in Section 7.3.4.1. At elevated temperatures (e.g., 100 °C) rubber in large components

can show surprisingly good resistance because of its low thermal conductivity and tendency to form a charred outer skin, which can act as an intumescent material. Above its highest service temperature it will eventually degrade, becoming sticky.

Silicone and highly fluorinated elastomers show by far the greatest resistance to high temperatures (≥ 200 °C). Figure 7.1 illustrates the difference in chemical degradation at 203 °C between typical NBR and FKM compounds. However, at less elevated temperatures other factors (e.g., mechanical strength) may cause other elastomers to be preferred. Under thermal aging all chlorine-containing elastomers (e.g., epichlorhydrin) may evolve hydrogen chloride gas, if insufficient acid acceptor is present or if temperatures are high enough. Fluorine-containing elastomers may evolve hydrogen fluoride gas, and so in extreme circumstances appropriate care should be exercised.

Thermal degradation is an extreme case of the aerobic chemical relaxation mechanisms outlined in Section 7.2.4. Kinetics of chemical reactions in fluids are discussed in Section 7.6.4.

■ 7.6 Effect of Fluid Environments

The flexibility associated with an elastomer – essential for performing its many functions (sealing, isolating vibrations, etc) – stems from the 10% or so of space between its molecular chains – the “free volume”, which takes an everchanging shape-pattern reflecting the kinetic motion of the chains. However, this internal space leads to other, less welcome characteristics: it provides the physical means for fluid (gas and liquid) molecules to enter the elastomer. No elastomer is completely resistant to chemical and/or physical effects arising from contact with fluids. Different elastomers can withstand such attacks to different extents. If a rubber absorbs a large volume of liquid, it generally swells and becomes weak and useless for most engineering applications. Moreover, chemical attack can cause further deterioration. In either case, initial weakening is progressive: in the chemical case, weakening or embrittlement will continue throughout the service life. It is clear from these observations that durability of an elastomeric component is influenced by its environment. Elastomer selection therefore needs to take account of the service fluid composition. Organic liquids tend to weaken elastomers by physical means only, whereas corrosive liquids, such as acids and alkalis, tend to attack chemically.

Rubber and ebonite are used as coatings and linings to protect chemical plant, pipes, and other equipment against corrosion and abrasion. In that context, they may come into contact with various chemical solutions. Table 7.3 summarizes the resistance at room temperature of several elastomer types to a range of aqueous

and other liquids; the behavior may, however, be different at elevated temperatures. Such tables are inevitably very approximate and should be used for preliminary guidance only, since different results may be obtained with different compounds of the same base elastomer. Also, different applications may render the same elastomer compound satisfactory or unacceptable, even with the same liquid. Many such tables are given by material producers and manufacturers, and before concluding that the classification is relevant for the application at hand, the engineer should always inquire exactly which tests were performed to confirm the classification and whether the formulation of the elastomer compound is suitable.

TABLE 7.3 Chemical Resistance of Several Types of Rubber and Ebonite:
S = Satisfactory; L = Limited Applications; X = Not Recommended

Chemical environment	NR and SBR		NBR		Butyl	Poly-chloroprene	Chlorosulfonated polyethylene
	Soft	Ebonite	Soft	Ebonite			
Acids							
Acetic (glacial)	X	S	L	S	L	X	S
Aqua regia	X	X	X	X	X	X	X
Chlorine water	L	S	L	S	X	X	S
Chromic, 50%	X	X	X	X	X	X	L
Hydrochloric	S	S	L	S	S	L	S
Hydrofluoric, 50%	S	S	L	L	S	L	S
Nitric, 20%	X	X	X	X	S	X	S
Nitric, 40%	X	X	X	X	X	X	S
Nitric, fuming	X	X	X	X	X	X	X
Phosphoric, 80%	L	S	L	S	S	L	S
Sulfuric, 25%	S	S	L	S	S	S	S
Sulfuric, 50%	S	S	L	S	S	L	S
Inorganic Salts and Alkalies							
Alums	S	S	S	S	S	S	S
Ammonia, 25%	S	S	S	S	S	S	S
Ammonium hydroxide	S	S	S	S	S	L	S
Copper chloride	L	S	S	S	S	S	S
Ferric chloride	L	S	S	S	S	L	S
Ferrous sulfate	S	S	S	S	S	S	S
Potassium hydroxide	S	S	L	S	S	S	S
Silver nitrate	L	S	L	S	S	S	
Sodium thiosulfate	S	S	S	S	S	S	S
Zinc chloride	S	S	S	S	S	S	S

TABLE 7.3 (continued)

Chemical environment	NR and SBR		NBR		Butyl	Poly-chloroprene	Chlorosulfonated polyethylene
	Soft	Ebonite	Soft	Ebonite			
Organic Materials							
Acetone	S	S	X	S	S	X	S
Alcohols	S	S	S	S	S	L	S
Cresol	X	X	X	X	X	L	X
Ethers	X	X	S	X	L	L	S
Ethyl glycol	S	S	S	S	S	S	S
Fatty acids	X	L	L	L	L	L	L
Glues	S	S	S		S	S	S
Glycerine	S	S	S	S	S	S	S
Hexane	X	X	S	S	X	S	S
Methyl chloride	X	X	X	X	L	X	X
Mineral oils	X	L	S	S	X	L	S
Petroleum oils	X	L	S ^a	S	X	L	L
Phenol	L	S	X	S	L	X	X
Soap solutions	S	S	S	S	S	S	S
Turpentine	X	X	S	S	X	X	X
Vegetable oils	X	L	S	S	S	L	
Plating solutions							
Brass, copper, lead	S	S	S	S	S	S	S
Chromium	X	X	X	X	L	X	S
Gold, silver	S	S	X	S	S	S	S
Nickel (dull)	S	S	L	S	S	S	S
Nickel (bright)	S	S	L	L	S	S	S
Tin, zinc	S	S	X	S	S	S	S

^a A high-aromatic oil might swell a low-ACN nitrile rubber excessively.

Oil and gas can come into direct contact with rubber in downhole applications in exploration for, and production of, hydrocarbons. The rubber may be exposed in the form of seals, flex joints, flexible pipes, or hoses to crude oil containing methane and other hydrocarbon gases, carbon dioxide, and sometimes hydrogen sulfide gases, often at elevated temperatures. In general, the types of elastomer that have best resistance to oil and gas are also among the better rubbers for resisting temperatures of 100 °C and above, and so Table 7.2 provides a rough guide to fitness for this purpose (although solely-hydrocarbon elastomers should be avoided).

Two physical processes are involved in fluid uptake (absorption) by an elastomer. Liquids and gases dissolve in the surfaces of elastomers (adsorb) and penetrate further by diffusion. Since the rate of absorption is diffusion-controlled, the resistance to swelling of an elastomeric component increases as the square of its thickness and with increasing viscosity of liquid diffusants.

For gas or liquid as the penetrant, the initial surface concentration c_0 is determined by the process of adsorption. With liquids, c_0 is usually obtained by dividing original sample volume into the equilibrium (maximum) mass uptake m_∞ ultimately attained throughout the elastomer – the solubility – and is essentially independent of actual pressure, being dependent on vapor pressure. For gases, the adsorption process is dependent on actual gas pressure.

The rate of diffusion into the elastomer bulk is independent of pressure at normal pressures. However, a considerable effect shows up at high pressures, and this is illustrated to a marked degree in gas permeation. This phenomenon refers to the passage of gas right through an elastomeric sample; that is, it involves both surface solution (adsorption) and diffusion, and evaporation is treated mathematically as the (anti)solution process on “the far side” of the sample.

Whether a particular elastomer will absorb large quantities of a fluid depends on thermodynamic considerations. A drive exists for a fluid and a polymer to mix if a negative free energy change ΔG takes place during the mixing. The free energy change is

$$\Delta G = \Delta H - T \Delta S \quad (7.8)$$

where ΔH is the change in heat content (enthalpy), ΔS is the change in entropy, and T is absolute temperature. Thus, the requirement for mixing is that $T \Delta S$ be greater than ΔH – in practice, the reverse is normally sought, to eliminate or minimize swelling and associated effects. For liquid and polymer, the enthalpy change is largely influenced by the difference in their solubility parameter δ values [12], where δ^2 is the cohesive energy density – a measure of the energy of attraction between like molecules. Liquid δ values vary from approximately $6 \text{ (cal/cm}^3\text{)}^{1/2}$ – that is, $12.3 \text{ MPa}^{1/2}$ – to about $23 \text{ (cal/cm}^3\text{)}^{1/2}$ ($47.2 \text{ MPa}^{1/2}$ – the value for water), with the range of rubber types roughly covering the lower half of that range. ΔH will be less than $T \Delta S$ only when certain conditions for δ are met: for instance, if δ values for an elastomer and a solvent are within about 1 to $2 \text{ (cal/cm}^3\text{)}^{1/2}$ (2.05 – $4.1 \text{ MPa}^{1/2}$) of each other. Then considerable swelling can occur. If the liquid is a moderately viscous oil, this maximum acceptable difference in δ reduces to about $0.8 \text{ (cal/cm}^3\text{)}^{1/2}$. Practically, to avoid swelling, elastomer and liquid combinations with significantly different δ values are used. If this is not possible for other reasons, then structural aspects, such as high crosslink density, high T_g (equivalent to low free volume), high filler content, among others, can reduce $T \Delta S$, to oppose the effects of the similar δ values, and thus lessen swelling.

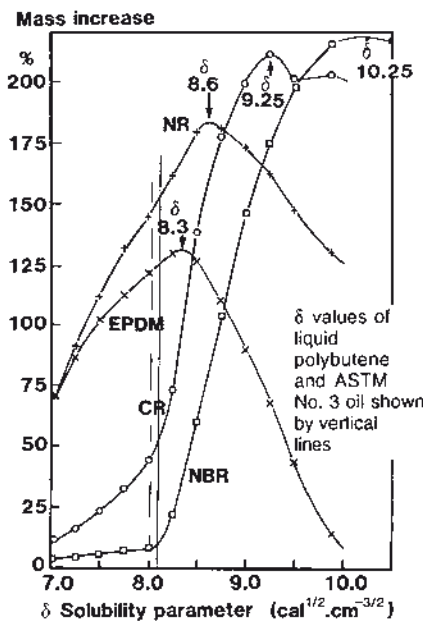


FIGURE 7.10 Solubility parameter spectra for four elastomers: NR, EPDM, CR, and NBR

Figure 7.10 shows the degree of equilibrium swelling for a series of well-prepared samples of four common elastomers when immersed in solvents with a relatively small range of known δ values. Diffusion is sufficiently fast at room temperature for equilibrium to be reached in a few days. The figure illustrates δ values of about $8\text{--}10 \text{ (cal/cm}^3\text{)}^{1/2}$ for the elastomers, obtained from the maxima given by so-called solubility parameter spectroscopy (SPS) plots. SPS arises from early work by Gee [13] and is a weighing technique employing solvent mixtures as the swelling media: the solvents are carefully chosen to avoid interactions and are completely miscible [14], and are mixed according to appropriate volume fractions to give many liquids of different, but known, δ values. NBR has a high δ value and is an oil-resistant elastomer. FKM's with even greater oil resistance have even higher δ values than NBR. The application of solubility parameters becomes more complex at values of about $15\text{--}23 \text{ (cal/cm}^3\text{)}^{1/2}$ because of hydrogen bonding effects, and others. This applies especially to water absorption. Many values of δ (obtained in various ways) are listed in the literature [15, 16] for all common elastomers and liquids; a selection for liquids is shown in Table 7.4.

As already mentioned, the final concentration m_∞ is lower for a highly cross-linked or highly filled elastomer, even for a liquid of similar δ . Another feature determining whether a liquid will dissolve quickly in an elastomer is the liquid's viscosity; this can diminish the extent of swelling indicated by SPS plots which use appropriate low-viscosity solvents. High molecular weight liquids cause both m_∞ and the rate of

TABLE 7.4 Solubility Parameter δ Values [16] for a Selection of Solvents at 20 °C

Solvent	δ (cal/cm ³) ^{1/2}
Hexane	7.33
Octane	7.60
Decane	7.77
Benzene	9.22
Toluene	8.97
<i>o</i> -Xylene	9.03
<i>m</i> -Xylene	8.87
<i>p</i> -Xylene	8.83
1,2-Dichloroethane	9.96
Acetone	9.74
Methyl ethyl ketone	9.56
Diethyl ether	7.74
Ethyl acetate	9.10
Methanol	14.52
Ethanol	12.97
Propanol	12.02
Ethylene glycol	14.52

Source: G. Allen, G. Gee, and J. P. Nicholson; *Polymer*, 1, 56 (1960)

diffusion to be reduced considerably compared with typical solvents. The diffusion of liquids in elastomers is discussed in Section 7.6.2. The relationship of permeation, diffusion, and solubility for gases in elastomers is presented in Section 7.6.3. Solubility parameters also apply to gases at high pressures when they are supercritical and possess liquid-like densities. δ values are complex here; significant changes are possible, increasing with further pressure and decreasing at higher temperatures.

7.6.1 Aqueous Liquids

All elastomers absorb at least one or two per cent of water over long periods of time. Only small amounts would be expected from δ considerations. However, other factors can cause increases. Water absorption leads to an increase in mass and volume, but does not usually have much effect on the modulus or strength. However, stress relaxation can be significantly affected (see Section 7.2.3). Some compounding ingredients can leach out. For example, some types of antioxidant can

TABLE 7.5 Water Uptake of Some Engineering Elastomers after 2 Years in Seawater at 23 °C

Elastomer	Equilibrium (% mass uptake of water)
Natural rubber	4
Acrylonitrile-butadiene rubber	5
Polychloroprene cured with litharge	> 5.5
Polychloroprene cured with magnesium oxide	> 32

be lost in this way, with a consequent loss of fatigue resistance under oxygenated conditions. Plots against time of mass uptake measurements can be misleading, if not corrected for mass loss effects by means of separate drying tests conducted on replicate samples. Table 7.5 shows some typical (corrected) values for water absorption by some common elastomers after 2 years of immersion in seawater. Use of hydrophilic fillers or metal oxides in the cure system generally has a larger effect than polymer type. Thus, polychloroprene cured with litharge does not absorb much water, whereas polychloroprene cured with magnesium oxide absorbs large amounts. Conversely, if hydrophilic impurities are removed from a rubber, as in deproteinized natural rubber, the water uptake can be reduced (e.g., from 4% to 1% for NR and DPNR).

Salt water is not generally a deleterious environment for rubber. If care is taken over certain points, a long and maintenance-free life can be expected for rubber engineering components, unlike the situation for metals, where corrosion processes of various types need to be constantly checked.

Polychloroprene has been used successfully for coating subsea pipes in offshore engineering applications to protect the pipes from salt water corrosion. There are few reports of any problems, even after 10 years of service. This has been a leading use of elastomers in offshore corrosion protection. Special polychloroprene compounds developed by the pipe coating manufacturers include ingredients to inhibit marine fouling.

In a case study made of a rubber tire after 42 years of exposure to seawater, the condition of the rubber was found to be still excellent. The tire was recovered from a shipwreck and sealed subsea to preserve all water uptake. Chemical analysis showed the tire material to be natural rubber. Apart from some poor rubber-metal bonding to the carbon steel wires, there was no corrosion of the wires and no obvious deterioration of the rubber after 42 years in seawater [17]. Laboratory drying experiments showed that no more than 5% of water had been absorbed in this time. This value is in line with predictions from shorter term laboratory tests for this type of vulcanizate. This gives reasonable confidence in the ability of laboratory tests, accelerated by using thin-walled sections, to predict correctly the effects of seawater.

Natural rubber, sometimes blended with styrene-butadiene rubber, has been used to line water purification vessels used in power generation applications for more than 20 years, and although there may have been some long-term deterioration of the lining in purified water, nevertheless, protection of these vessels from large-scale corrosion has been very successful. Chlorobutyl rubber is frequently a better choice for such applications, because it combines relatively good adhesion when cured *in situ* at low temperatures with low water permeation.

Another case history that illustrates the excellent durability of elastomers in seawater is provided by the Hutton tension leg oil production platform (TLP) in the North Sea. This is a compliant structure with the compliance provided by a set of flex elements, each of overall diameter of 1 to 2 m. Each flex element consists of alternating layers of nitrile rubber and spherical section stainless steel reinforcements. Figure 7.11 shows a schematic view of a similar component, a flex joint, illustrating its ability to sustain a conical angle displacement of 16°. The entire platform, with accommodation for 200 people, rests on the flex elements, which are structurally critical units. Such components should not be regarded as “off the shelf”, but the success of this project in a hostile region of the North Sea illustrates the reliability and durability of elastomeric components, provided there is adequate analysis and testing for the service environment. A case study [1] of the elements was performed after 5 years of service. The nitrile rubber has shown excellent resistance to seawater with no measurable deterioration. The study included a fracture mechanics analysis, combined with extensive environmental and full-scale testing. At the time of the study, performance in service had been as predicted from this program of laboratory testing and fracture mechanics analysis.

Ingress of water into the bulk of an elastomer is a diffusion-controlled process. This has been well studied, and at least the short-term aspects are understood [18]. Considering migration in natural rubber, water is only slightly soluble in the pure rubber hydrocarbon (since the two solubility parameters are very different).

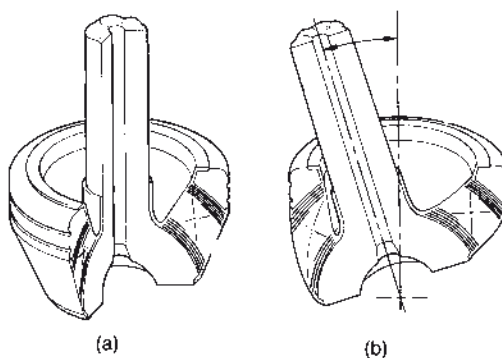


FIGURE 7.11 Schematics for the Hutton TLP flex joint: (a) no deflection and (b) 16° conical deflection

However, diffusing water collects around the hydrophilic impurities arising naturally in this elastomer, so that the overall water content reaches a level higher than would be expected. Droplets of water form, and increase in size until their osmotic pressure is balanced by opposing elastic forces; Muniandy and Thomas performed calculations based on chemical potentials to illustrate this [19]. After long periods of time, this effect progresses into the inner regions of the elastomer.

7.6.2 Hydrocarbon Liquids

As already noted, when a liquid contacts an elastomer, it adsorbs rapidly up to a concentration c_0 at the surface, followed by diffusion of the liquid further into the elastomer. The thermodynamic drive for adsorption is to equilibrate chemical potential of adsorbed and external liquid, the latter effectively given by the liquid's vapor pressure. For hydrocarbons and other nonaqueous liquids, diffusion dominates the movement of liquid into the elastomer bulk. In diffusive motion, individual molecules of the liquid move by "jumping" into adjacent free volume holes formed momentarily in the elastomer matrix during random thermal motions arising from kinetic energy. The thermodynamic drive is due to a tendency to equalize chemical potential (i.e., concentration) of the diffusing liquid throughout the elastomer.

The rate of this diffusive migration is governed by Fick's laws of diffusion. These laws also apply if the diffusant is gaseous: the difference in mathematical treatment between gas-elastomer and liquid-elastomer systems lies in the different boundary conditions that are applied when Fick's second law is integrated. If amount dm of substance diffuses across area A in time dt to give a concentration gradient dc/dx , Fick's first law states:

$$\left(\frac{1}{A}\right)\left(\frac{dm}{dt}\right) = -D\left(\frac{dc}{dx}\right) \quad (7.9)$$

where D is the diffusion coefficient (or constant), in square meters per second. By considering incremental increases in concentration along the path of the migrating species, Fick's second law is obtained:

$$\left(\frac{dc}{dt}\right) = D\left(\frac{d^2c}{dx^2}\right) \quad (7.10)$$

These equations assume D to be independent of concentration; however, for a small molecule diffusing in a polymer, D depends in reality on the local concentration and other conditions. D is affected inversely by the molecular size of the diffusant.

As diffusion progresses, concentration-distance curves with shapes analogous to error function curves “erf z ” develop. During this period, the average distance traveled by a particle in time t from $x = 0$ is $(2 D t)^{1/2}$. The form of this expression indicates why, in practice, times of diffusion-related phenomena (e.g., swelling) increase with the square of elastomer thickness.

Mathematical solutions of Fick's second law are complex, but have been obtained for many situations [20]. A current approach uses finite elements, with simple solutions applying to elements being summed for whole, complex, geometries. It is useful therefore to have one relatively easy means of determining D , so that the result can be employed in finite element procedures for extrapolation to actual service conditions. This easy means of measurement is by mass uptake-immersion of sheet samples into the liquid of interest, and removal of these samples at appropriate time intervals for careful but rapid weighing before returning to the liquid, continuing until equilibrium mass uptake is attained.

To determine D for a sheet sample immersed in liquid, the solution of Fick's second law with appropriate boundary conditions gives:

$$\frac{m_t}{m_\infty} = \left(\frac{2}{h} \right) \left(\frac{D t}{\pi} \right)^{1/2} \quad (7.11)$$

where m represents mass uptake at time t and at equilibrium swelling, respectively, and $2 h$ is thickness. Eventually D can become concentration-dependent for elastomer/liquid combinations where, after a while, liquid that has already entered the elastomer contributes to the rate at which fresh liquid diffuses.

One simple and convenient method of obtaining a representative value of diffusion coefficient is to measure D_{av} an “average” D at the point of 50% mass uptake, so that:

$$0.5 = \left(\frac{2}{h} \right) \left(\frac{D_{av} t_{av}}{\pi} \right)^{1/2} \quad (7.12)$$

As for water uptake (Section 7.6.1), corrections for the leaching of soluble constituents out of the elastomer are made by reading values off desorption curves from drying tests performed on samples swollen to different degrees, and adding these values to the mass uptake curves at the appropriate times.

From the form of the equations above, plots of mass uptake versus square root of time should be informative. Figure 7.12 shows plots obtained when natural rubber sheet samples were immersed at 43 °C in liquid hydrocarbons of various viscosities. Overall, Fig. 7.12 illustrates the expected effect, namely that increases in viscosity clearly reduce diffusion rate and the magnitude of t_{av} . The portion of the plots in the region around 50% mass uptake is essentially linear, permitting calculated D_{av}

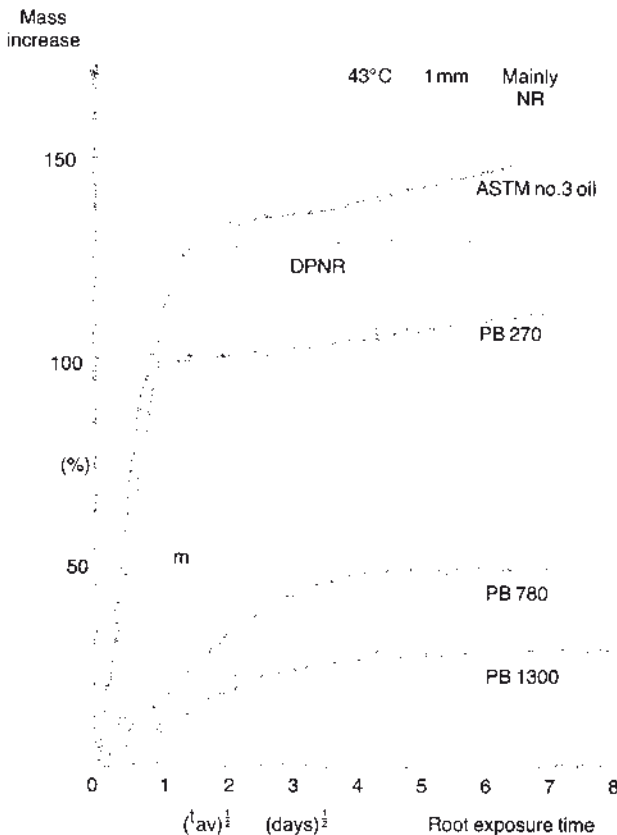


FIGURE 7.12 Example of hydrocarbon liquid diffusion in elastomers – polybutenes (Mn shown) in NR

values to be obtained, representative of the diffusion rates. When a sample nears saturation, the rate of uptake diminishes until the equilibrium mass uptake values m_∞ are reached, ideally signified by a plateau. As a point of interest, the m_∞ “plateau” for each of the two lowest viscosity hydrocarbons showed a low, but positive slope. This observation is attributed to a secondary effect: the slow absorption of these hydrocarbon liquids by the proteinous nonrubber content of natural rubber (the species that dominates water uptake in NR). This hypothesis was supported by repeating the experiment for one hydrocarbon liquid (ASTM No. 3 oil), but replacing NR by deproteinized natural rubber, to give a plot (shown in Fig. 7.12 by the dashed curve) displaying a near-equilibrium plateau for m_∞ . Table 7.6 shows the diffusion coefficients D_{av} , the equilibrium mass uptakes m_∞ , and associated equilibrium concentrations c for the four hydrocarbons in NR.

The phenomenon of permeation (involving passage of fluid right through an elastomeric article) is more common for gases rather than for liquids. Permeation issues are discussed in Section 7.6.3. However, liquid permeation is important, for instance

TABLE 7.6 The Diffusion of Oil and Polybutenes into NR Elastomer at 43 °C:
Sheet Samples, Nominal Thickness 1 mm

Diffusant	Diffusion coefficient D_{av} ($\text{m}^2/\text{s} \times 10^{-13}$)	Equilibrium mass uptake m_∞ (%) ^a	Equilibrium concentration c (g/cm^3)
ASTM No. 3 oil	12.5	136	1.44
Polybutene			
▪ M_n 270	30.8	101	1.07
▪ M_n 780	2.1	48	0.51
▪ M_n 1300	1.9	28	0.30

^a Referred to initial sample weight.

in the automotive sector, where stringent laws on emission now apply in certain countries and states. The simplest permeation test for a liquid is a ‘cup’ test [21], in which test liquid is placed in a steel (or other material, as appropriate) flanged beaker and an elastomeric sheet sample is clamped and sealed over the top of the beaker, using the flanges. The assembly is weighed, heated to test temperature (band heaters, oven, water-bath), and weighed again at intervals, noting the mass loss of test liquid due to permeation through the sample. Testing can be stopped when a steady-state condition is reached. The coefficients described in Section 7.6.3 can be obtained similarly, but the liquid’s vapor pressure is used instead of pressure for P_1 and P_2 in Eq. (7.17).

For any polymer/liquid system, permeation rates can be estimated from absorption tests, the latter being easier to carry out. A relationship between the two phenomena has been proposed [22] and, after appropriate testing, validated [23].

7.6.3 Hydrocarbon and Other Gases

While absorption measurements (involving weighing until the sample is saturated) are more convenient when assessing diffusion-related properties of elastomer/liquid systems, permeation measurements are more suitable when the fluid is gaseous. When an elastomeric polymer is exposed to gas at high pressure and the gas enters the bulk of the elastomer by the two-stage process of adsorption and diffusion, unlike the liquid case, the amount adsorbed is dependent on applied (partial) gas pressure. The diffusion stage is once again largely independent of pressure. In the oil and gas sector, engineering, pressures above 1,000 atm can be met. Under these conditions the amount of gas that has entered the elastomer after a few days can be considerable, and if an elastomer is constrained, e.g., in a seal housing and becomes essentially saturated at equilibrium, this amount of absorbed gas again

relates directly to applied pressure, as the concentration originally adsorbed is eventually achieved throughout the bulk.¹

The theory for absorption and permeation of fluids is well established [20, 22, 24, 25] and concerns the interrelated processes of adsorption and diffusion. Adsorption of a single gas into the elastomer surface is governed by Henry's law, which applies to dilute solutions:

$$c = s P \quad (7.13)$$

where c is concentration, P is the applied pressure, and s is the solubility coefficient. To determine the concentration of one of the gases in the surface when a gas mixture contacts the elastomer, the partial pressure of that gas is employed in the expression above. This expression also applies to a liquid, but to its *vapor* pressure, not actual (hydrostatic) pressure: the former is only marginally affected by large changes in the latter – hence the comment early in Section 7.6 that liquid solubility is essentially independent of pressure.

For gases, with vapor pressure now equaling the applied pressure, this expression suggests a linear relationship between concentration of dissolved gas and pressure *for all pressures*. Clearly this cannot be the case. At high pressures, the solubility coefficient s of the gas is much lower. Eventually, at very high pressures, an equilibrium situation should be reached, where further increases in pressure essentially cause no further increase in absorbed gas concentration or rate of permeation. From experience, Eq. (7.13) can be used at pressures of up to about one thousand atmospheres, but then s becomes a significant function of pressure..

Once molecules have been adsorbed (dissolved) in the elastomer surface, their diffusion into the bulk is generally independent of external gas pressure (except at high pressures, which cause compression of the elastomer and thus, in turn, change the rate of gas movement). As with liquids, the rate of diffusive migration is governed by Fick's law. For a plane sheet of elastomer of area A , steady state diffusion of dissolved gas from one surface through to the other is given by an integrated version of Fick's first law:

$$\left(\frac{1}{A}\right)\left(\frac{q}{t}\right) = \frac{D(c_1 - c_2)}{h} \quad (7.14)$$

where a gas volume q diffuses through thickness h in time t ; c_1 and c_2 are the surface concentrations.

¹ Of course, the local region of seal adjacent to the extrusion gap will be at a lower concentration.

The process of permeation – the passage of gas from a high pressure region into, through, and out into the opposite low pressure side of an elastomer membrane – involves adsorption, diffusion, and evaporation. The last-named is treated mathematically in terms of negative adsorption on the low pressure side. By combining Eqs. (7.13) and (7.14), we get for steady state permeation:

$$\frac{q}{t} = \frac{D s A (P_1 - P_2)}{h} \quad (7.15)$$

where condition 1 is the high pressure side and 2 is the low pressure side. The product of the coefficients D and s is termed the permeation coefficient (or permeability) Q :

$$Q = D s \quad (7.16)$$

and

$$\frac{q}{t} = \frac{Q A (P_1 - P_2)}{h} \quad (7.17)$$

This is the general gas permeation equation for a sheet at equilibrium (steady state) conditions. Hence, if an elastomer is employed in service as a sheet-like diaphragm, in a situation that permits gas to migrate through it, and if Q for the system is known from laboratory testing, Eq. (7.17) can be employed to assess the permeation rate through the sheet. For other articles, e.g., hose linings or O-rings, analogous versions of Eq. (7.17) allowing for the different geometrical aspects would apply – see Chapter 7, Problem 6, for this equation for a hollow cylinder. Methods are known for measuring permeation rates at pressures up to 100 atmospheres or so [25], or even up to 1,000 atms [26]. When steady state permeation is attained, plots of q versus t give lines of gradient $Q A (P_1 - P_2)/h$, so that Q can be calculated. At the onset, a certain time elapses before steady state permeation occurs. This transient stage has been used by Daynes to provide a separate determination of D (analyzed in [24]):

$$D = \frac{h^2}{6 \tau} \quad (7.18)$$

where τ is the time that the steady state line lags behind a line of the same gradient starting from the origin. After Q and D have been determined, s is easily obtained as Q/D . Knowledge of values of Q enables us to minimize the amount of gas that will pass through a membrane or a thick-walled hose, for example. Knowing the value of D is helpful in estimating the average distance traveled in time t from $x = 0$ using $(2 D t)^{1/2}$; s affects explosive decompression, which is discussed later, because the product sP gives the concentration c_1 of gas present at the high pressure surface, from Henry's law, Eq. (7.13).

If the elastomer is used in an application with no outlet for the gas (e.g., as an inner lining inside a steel pipe), Eq. (7.13) governing gas adsorption applies, but subsequent migration of gas would be governed by a solution of Fick's law using appropriate boundary conditions until the gas concentration reached equilibrium throughout the elastomer: here the gas would be absorbed. Clearly, a permeation test for an unrestricted system can also lead to a calculation of the amount of gas absorbed in a confined situation, as the c_1 value for permeation equates with the eventual c_∞ value for absorption.

Elastomers for engineering use are obviously fully compounded, and some additives can influence permeation. The influence of ingredients that affect the degree of crosslinking is merely to alter the magnitude of coefficients such as Q , while retaining the form of the equations given in earlier sections. Increasing the number of crosslinks decreases Q ; but it is not known whether this results from changes in both D and s or just one of these coefficients.

The effect of carbon black and other fillers is more pronounced, causing a diluting effect, as well as increased "tortuosity" (i.e., the path length between and around filler particles). Both these effects decrease permeation rate. In addition, filler particles can adsorb diffusant molecules, to upset the normal behavior reflected in Fick's and Henry's laws.

Many data exist for the coefficients mentioned here. A selection is given in the Appendix, Table 5. As a result, permeation rates can be estimated for many service applications involving elastomers and gases at moderate pressures. However, it is often not valid to extrapolate these data to high pressures. High pressures can reduce the permeation coefficient dramatically [26], as indicated in Fig. 7.13. A probable reason is that above certain pressures the elastomer becomes compressed significantly and the free volume between polymer molecular chains decreases; hence, the diffusion rate decreases. This effect is displaced to higher pressures as the temperature is raised.

Added factors involved at high pressures are local strain effects and swelling effects. The latter are more often associated with liquid diffusion, but at high pressures, gas densities can approach liquid values (see comment immediately before Section 7.6.1).

Two phenomena frequently found in oil field applications, which occur as a result of gas permeation, are "explosive" or "rapid gas decompression" (ED or RGD) and "doming". When an elastomer is saturated as a result of exposure to high pressure gas, or approaches this condition, rapid removal of the high pressure means that the situation quickly becomes one of supersaturation. The amount of gas present now exceeds the concentration associated with the new low external pressure. The excess gas possesses a thermodynamic drive to come out of solution, and it can do so by collecting at existing or incipient flaws, or initiating nucleation processes that

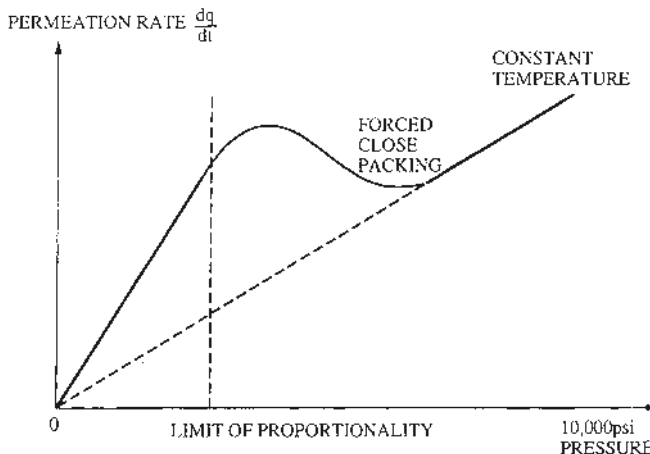


FIGURE 7.13 High pressure gas permeation in elastomers

lead to flaws. The continued arrival at the flaws of more gas by diffusion can lead to bubble growth. At some threshold amount of dilation, this growth causes fracture, and subsequent expansion of the flaw includes tearing as a major component. This is the phenomenon of explosive decompression failure. It causes an elastomer to become unable to seal, for example. Carbon dioxide, which is highly soluble in many elastomers, is particularly likely to cause this effect.

When gas is driven out of solution near a bonded interface in a composite structure, the bonding can be fractured in an analogous way; this is the phenomenon of doming, which can force the linings of flexible pipes to collapse into the flow passage. Both doming and ED have been the subject of research [e.g., 27–30]. International and other standards applying to the oil and gas sector [31] include appropriate ED test methods for qualifying materials. However, questions remain about ED, because failure can occur in one area of a sample and not another and some samples fail when other samples do not under the same conditions.

Some techniques to minimize the ED problem include reducing the amount of gas present by

- (i) choosing low-solubility elastomers
- (ii) allowing the gas to escape as quickly as possible during decompression by using high-diffusion elastomers
- (iii) increasing the resistance to bubble growth and fracture by optimizing
 - (a) modulus and (b) tear strength of the elastomer
- (iv) introducing mechanical constraints which minimize material expansion. Reducing the decompression rate will also diminish ED damage, if service operational circumstances allow. More details are given in [30].

However, regarding point (iii), increasing either modulus or tear strength normally causes the other property to deteriorate. Biphasic single component elastomers have been developed to optimize both properties simultaneously [32], using an interwoven two-phase structure of the same elastomer at different states of cure. Explosive decompression resistance has increased significantly in these elastomers.

7.6.3.1 Pressurized CO₂ for Assessing Interface Quality in Bonded Rubber/Rubber Systems

ED has been employed by Lewan and Campion [30], using CO₂ at low pressures, and a moderate rate of decompression as a gas diagnostic (GD) tool to assess the quality of adhesion between two cured layers of the same rubber. If two identical elastomer sheets are pressed together and cured, they will adhere if the uncured compound is tacky (possesses a high degree of autohesion), as the surfaces then remain in intimate contact and allow interdiffusion of curatives during the early stages of cure. Interfacial crosslinks then form to provide good adhesion. The high tack of an uncured NR compound led to high adhesion test values of cured samples, with test pieces tearing across tabs (“cohesive failure”) rather than along the original interface. A similar result was obtained for test pieces exposed to the GD procedure before testing – there was no “memory interface” remaining from the assembly stage.

When a non-tacky EPDM elastomer was examined, its tack was so low that no rubber-to-rubber bond formed in the cured state, and the peel sample separated cleanly, at very low separation forces. No GD stage was necessary. With an SBR elastomer of moderate tack, on the other hand, cured adhesion was high, with cohesive failure. However, when samples were exposed to the GD procedure before peel testing, peel forces were reduced by 80%, and separation occurred at the original interface. Regions of weak interface – which, if present in engineering products, could give rise to fatigue problems in service – had been present, although adhesion tests alone had not revealed this.

7.6.4 Effects of Temperature and Chemical Fluid Attack

Two basic forms of chemical aging exist: continuation of cure at elevated temperatures due to unstable cure systems, and exposure to hostile fluids (the latter occurring initially at the elastomer surface, depending on diffusion to access the bulk unless surface cracking provides a more rapid route). The ubiquitous roles of oxygen and ozone have already been discussed. In the oil and gas sectors, hostile fluids can include hydrogen sulfide (produced in some wells) and various amines and amides used as corrosion inhibitors. The former can attack unsaturated sealing elastomers such as nitriles, so that use of hydrogenated nitrile rubbers (and FKM)s

can be beneficial here. Even some of the FKM s are prone to attack by amines at high temperatures, a process accelerated [33] by application of stress (presumably the increase in stored energy also increases chemical potential). This is an instance of environmental stress cracking (ESC), which can involve chemical or physico-chemical attacks; the correct FKM should be selected for the application. Similarly, some FKM s are attacked by methanol by a process which can be shown to be reversible – and the application of stress again exacerbates it.

When a diffusant can also chemically react with the elastomer matrix, two main questions arise.

- Are some diffusant molecules deactivated by the chemical interaction, so that the overall diffusion rate decreases?
- Is the chemical reaction aggressive enough to embrittle and/or break up the elastomer?

Such questions can be resolved only by experiments. Both the physicochemical and hostile chemical processes can be governed by Arrhenius-type equations. Hence, for diffusion coefficient D , we write

$$D = D_0 \exp\left(\frac{-E_d}{R T}\right) \quad (7.19)$$

where D_0 is a frequency factor correlating with the initial concentration dependence of D , T is absolute temperature, R the gas constant, and E_d is the activation energy for diffusion. Similar equations apply for s and Q . Tests show that the expected linearity from this equation in plots of $\log D$ etc. versus I/T does frequently occur in practice.

In addition, an Arrhenius equation applies to the kinetics of chemical reactions:

$$k = A \exp\left(\frac{-E_a}{R T}\right) \quad (7.20)$$

where k is the rate of chemical reaction, the frequency factor A is now concerned with molecular collisions, and the activation energy E_a is the critical energy needed for reactions to occur. Regarding the attack of hostile fluids on high molecular weight elastomers, it can be tentatively assumed from statistical network theory that applied stress (and associated modulus or stiffness magnitudes) vary directly with elastomer crosslink density to a first approximation. Hence, the kinetics of reactions (classically based on concentrations of reactants and/or products) can be followed by changes in stiffness or modulus. In accelerated aging tests, one means of representing k is by measuring time ($1/k$) to a point at which a chosen property has changed by a specified amount, say 20%. (This value might, for instance, represent a stiffness increase above which a bearing would no longer accommodate design frequencies – hence the bearing has ‘failed’ in this case). The commonly cited rule-

of-thumb that chemical reaction rates more-or-less double with every 10 °C increase in temperature should be attributable to an appropriate E_a value applying to these reactions: the reader is invited to determine this E_a value in one of the problems listed at the end of the chapter, where the true picture is seen to be more complex.

One complication is that interaction of diffusion and chemical reactions, with their different activation energies, could mean that the 20% change in stiffness used above occurs because the deterioration is shared quite evenly throughout the elastomer (i.e., rapid diffusion, slow chemistry) or that it occurs because the outer regions only have embrittled extensively (i.e., slow diffusion, rapid chemistry). Empirical solutions are necessary in this area.

7.6.5 Effect of Radiation

Most elastomers increase in hardness when irradiated, but butyl and polysulfides soften and become liquid. Free radical mechanisms are involved; an analogous phenomenon prevents peroxide curing of these two elastomers. Carbon black filled vulcanizates are more resistant to radiation than unfilled vulcanizates. Table 7.7 indicates the radiation resistance of some elastomers.

TABLE 7.7 Radiation Stability of Elastomers

Damage:	Incipient to mild	Mild to moderate	Moderate to severe
Utility of rubber:	Nearly always usable	Often satisfactory	Limited use
Rubber	Gamma exposure dose (kJ/kg)		
Polyurethane rubber (AU, EU)	70	280	1670
Natural rubber (NR)	15	310	1670
Adduct rubbers ^a	24	200	820
Styrene-butadiene rubber (SBR)	15	108	420
Fluororubber (Viton) (FKM)	30	200	650
Cyanosilicone rubber ^a	30	100	320
Vinyl pyridine rubber ^a	25	80	250
Nitrile rubber (NBR)	15	50	170
Chloroprene rubber (CR)	15	34	100
Chlorosulfonyl polyethylene (CSM)	8	25	80
Fluororubber (Kel-F) (FKM)	20	44	83
Silicone rubber (Q)	11	27	63
Polyacrylate (ACM)	10	22	54
Butyl rubber (IIR)	16	25	42
Polysulfide rubber (TR)	3	12	26

^a Specialty materials

The incorporation of protective agents, known as antirads, can improve resistance by an order of magnitude. When rubbers are irradiated and then compressed at high temperatures, they generally acquire high compression set.

■ 7.7 Durability of Rubber-Metal Bonds

Many elastomeric-based components involve composite structures with the elastomer (rubber) strongly bonded to steel or another rigid material. Using suitable adhesives, rubber-metal bonds are usually formed during vulcanization of the rubber and are generally as strong or stronger in dry conditions than the rubber itself; thus, when failure does occur (e.g., on a pull-to-failure test), it occurs through the rubber (often denoted as 100%R) for a good bond. In that case a precise quantitative measure of bond strength is not possible, but it is probably not necessary for practical purposes. With most rubbers, the occurrence of interfacial rubber-metal bond failure usually indicates a manufacturing process error, but in some cases (e.g., some FKM elastomers) the bond strength may be moderate only. Prolonged exposure to liquids (especially aqueous liquids) can however cause failure of an initially strong bond. Only “hot formed bonds” produced during the vulcanization of the rubber will be durable in water; cold bonded systems (e.g., with epoxy resins or cyanoacrylates, even when applied to oxidized surfaces to enhance wetting) usually give weaker initial bonds and more rapid deterioration in service environments.

7.7.1 Adhesion Tests

There are a number of tests for rubber-metal bond strength, but the simplest and most effective are probably the double-shear test and the peel test, as depicted in Fig. 7.14. Since fracture mechanics solutions exist for both test piece geometries, interfacial bond strength can be measured in fundamental terms, and the fatigue life of the adhesive bond can be analyzed for cohesive failure of the rubber itself. The double-shear test piece has advantages when it is desired to maintain a constant shear strain on the adhesive joint during an environmental exposure test, for example, to simulate specific mechanical aspects of service conditions. For general characterization of bond strength and durability, however, the peel test is usually more convenient. It can also be adapted for testing of samples applied “on site” (e.g., of pipe linings or coatings) as a quality control (QC) check.

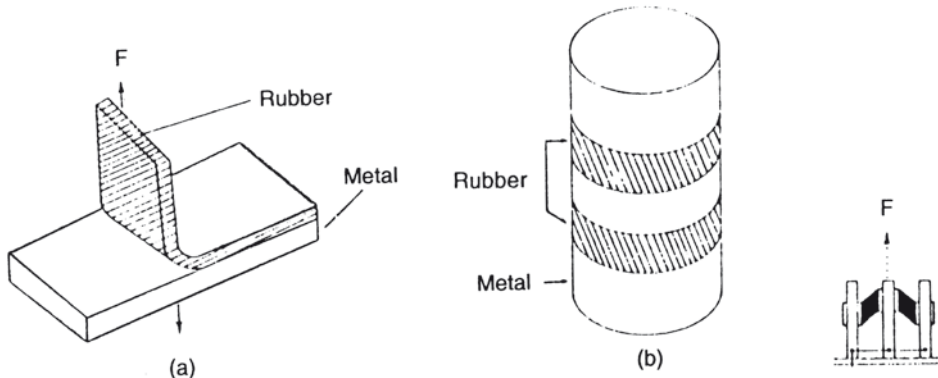


FIGURE 7.14 Test piece geometries for rubber-metal bond tests:
(a) peel test at 90° and (b) double-shear test

For the peel test piece, peel energy P is expressed [34] as follows:

$$P = \frac{F}{w} (\lambda - \cos \Phi) - U h \quad (7.21)$$

where U is strain energy density in the peeled leg, Φ the peel angle, λ the extension ratio, h the unstrained strip thickness, w the width of the peel strip, and F the peel force.

For linear stress-strain behavior, Eq. (7.21) can be rewritten [35]:

$$P = \frac{F}{w} (1 - \cos \Phi + e / 2 l) \quad (7.22)$$

where e is the elongation (displacement) at force F , and l the original elastomer tab length. Thus all factors are obtainable from original dimensions or readings from the test force versus elongation plot. At 90° , Eq. (7.22) reduces to:

$$P = \frac{F}{w} (1 + e / 2 l) \quad (7.23)$$

In the case of linear stress-strain behavior, and if the peel leg is constrained to be approximately inextensible so that $\lambda = 1$ or $e = 0$ (e.g., by incorporating fabric backing) then generally:

$$P = \frac{F}{w} (1 - \cos \Phi) \quad (7.24)$$

and, for $\Phi = 90^\circ$, $P = F/w$, and at $\Phi = 180^\circ$, $P = 2 F/w$.

Tests performed at 180° avoid inaccuracies due to changes in the peel angle during the test. For thick peel strips, however, lower peel angles avoid inaccuracies due to bending of the peel strip during testing. At low angles, forces can be high, and breaking of the tab is common. A useful compromise angle is 90°.

A subsequently developed double peel test uses two single peel test pieces (Fig. 7.14a) clamped together back-to-back and head-to-tail, so that the rubber tabs are both held in the test machine grips. This arrangement allows a rotation through a wide range of angles during testing. It has been shown to give, during the early stages of rotation, rubber-metal bondline failure even for well-bonded systems – those giving rubber tearing failure with normal peel tests [36]. This is a useful feature for mechanistic studies but, clearly, a geometry to be avoided when designing bonded rubber/metal composite components.

7.7.2 Rubber-Metal Adhesive Systems

There are a number of proprietary rubber-metal primers and adhesives available. The most widely used and researched system is the Chemlok 205 primer and Chemlok 220 adhesive (or equivalent) supplied by Lord Corporation (USA) and Henkel (Germany). For some synthetic elastomers (e.g., for fluoroelastomers), specialty adhesives are available. For fluorocarbon elastomers, Chemlok 607 is recommended, and for hydrogenated nitrile elastomers, Chemlok 233, with Chemlok 205 as the metal primer in each case. Nitrile rubber will bond well to this primer alone. The methods of applying primers and adhesives are important, and it is recommended that appropriate adhesive tests be performed during component development. For critical engineering components, peel tests should be performed on a QC basis during production. An acceptable level of adhesion strength from QC tests then “signs off” a production batch

Three factors are of key importance in ensuring bond durability:

- Good initial procedure for degreasing, grit blasting, and metal surface preparation
- Strict quality control for application of primer and bonding agent
- Use of an appropriate cure schedule for the rubber component (time, temperature, and pressure during cure) with regard to the adhesive system selected.

Good initial bonds, formed in the circumstances above, can remain intact even after several years of immersion in salt water. Some factors affecting durability, such as electrochemical potentials, are discussed in the next section.

7.7.3 Durability in Salt Water: Role of Electrochemical Potentials

It is almost certainly beneficial to cover all metal parts of a structural bearing scheduled for salt water service with several millimeters of rubber. This will substantially retard both metal corrosion processes and bond failure mechanisms to achieve a reasonable life span. If sacrificial anodes are used to protect adjacent steelwork, the bond edge should be encapsulated in rubber and electrically isolated where possible.

Although well-made rubber-metal bonds can be extremely durable, it has been shown [37] that if the metal adherends are not inert then rapid bond failure can occur. The highest potential (commonly used in engineering applications of cathodic protection) is provided by a zinc sacrificial anode in combination with carbon steel adherends. This produces a measured cathodic potential of 1040–1070 mV at the rubber-metal interface (with reference to a silver-silver chloride reference electrode). Bond failure is then rapid at all temperatures tested, but there is no corrosion of the carbon steel.

A failure surface consists in general of three regions. There is a first region, where failure occurred through cohesive fracture of the rubber. Adjacent to this region of polymer fracture is a gray region, where failure is predominantly at the interface between the metal and its primer coating when a pull-to-failure test is performed. The third region is of bond failure, occurring *in situ* during exposure, before the pull-to-failure test has been performed.

When determining any change in adhesive bond strength (interfacial failure energy), it is important to know whether there is any change in the cohesive strength of the polymer. Clearly if the rubber tear strength decreased during water exposure, the area of bond failure could be anomalously lower than if it had remained constant. To investigate this, the energy required to cause fracture may be measured by integrating the force-deflection curve from a shear pull-to-failure test. This energy can then be used to derive a characteristic stored energy density U at fracture. In the absence of bond failure, U characterizes the critical fracture energy of the polymer, and indeed yields a value comparable to results from standard fracture or tear tests. With an area of partial bond failure, however, the fracture geometry is more complicated, although the same approach can be used.

The characteristic stages of the bond failure process are illustrated in Fig. 7.15, where bond failure penetration depth is plotted against the square root of seawater exposure time (days). If diffusion processes are involved, a linear relation between penetration depth and the square root of time is expected from diffusion theory.

The first stage is a time lag observed before any bond failure is measured (i.e., 0.5 mm failure penetration depth). This “induction period” increases with decreasing potential and decreasing temperature. The second stage is a period of increasing area of bond failure as an approximately linear function of the square root of

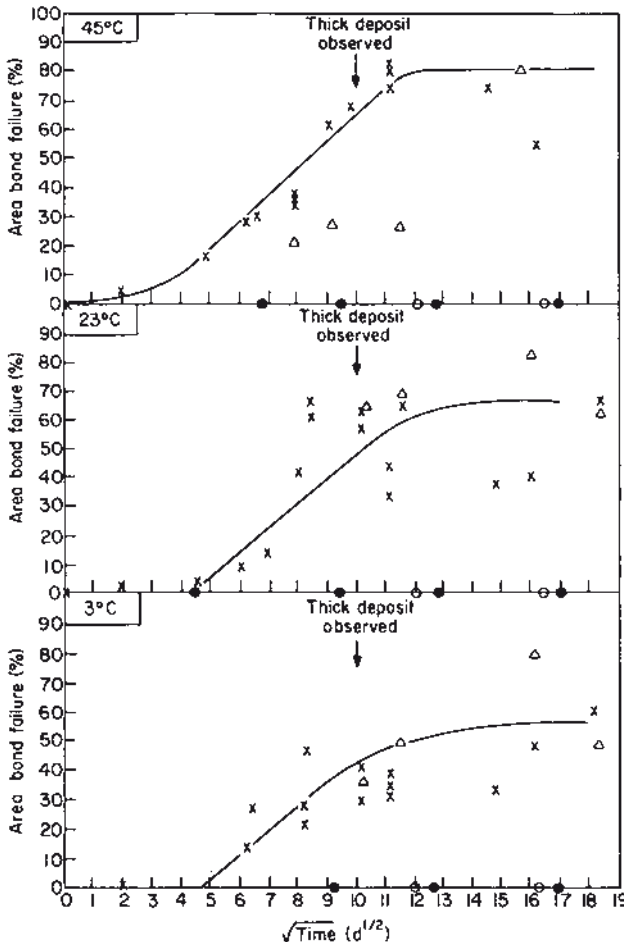


FIGURE 7.15 Bond failure rates in seawater with cathodic potentials of 1.05 V; test pieces were NR-carbon steel with C205/C220 adhesive system

exposure time. This suggests that liquid diffusion is a controlling factor, although only diffusion along the interface is considered important, not (unlike the case for organic coatings) diffusion through the bulk polymer. A failure penetration rate can be defined for each test condition. Finally, there is an approach to an “equilibrium” depth of bond failure.

The effect on carbon steel test pieces of potential differences lower than 1.05 V may be characterized by a potentiostatic arrangement to supply a constant impressed current at a chosen potential difference (e.g., 0.95, 0.85, 0.75, and 0.61 V) at the bond edge.

Induction period increases as the level of imposed cathodic potential is reduced, for example, from one day at 1050 mV to 30 days at 610 mV for NR-steel test pieces

[37]. After the induction period, bond failure begins, and the failure penetration rates are approximately the same for all potentials. After very long exposure periods (up to 3 years), the penetration depth for NR-steel with C205/C220 bonding agents approached an equilibrium value, which increased from 4 mm at 610 mV to the maximum possible (≥ 12.5 mm) at 1050 mV. Identical test pieces exposed to sea water in the same restraining jigs but without electrical connection to a potentiostat or to a dissimilar metal (i.e., 0 mV) showed no bond failure whatsoever, even after more than 3 years of seawater exposure.

The effect of dissimilar metals in contact can be similar, as a result of local potential differences set up by differences in the galvanic series. Adherends of Inconel, two types of titanium, and stainless steel were exposed to seawater at 3, 23, and 45 °C in holding jigs of carbon steel. The system was not electrochemically inert for the Inconel, stainless steel, or titanium test pieces, and the possibility existed of electrochemical interactions throughout the seawater exposure period. Different metals contacting steel showed different rates of bond failure [37].

The rate of bond failure is not necessarily accelerated by higher exposure temperatures. In some cases higher rates of bond failure have been found at lower temperatures. This is due to a variety of interacting environmental factors [38].

■ 7.8 Life Prediction Methodology

Quantitative prediction of the durability of an engineering component becomes an increasingly important requirement as elastomers are used for more critical engineering applications. Life prediction methodology embraces all aspects of processes that may affect the function of the component. The first step is to define the function of the component clearly enough for a failure criterion to be derived. This criterion may be an unacceptable change in stiffness for a bearing or antivibration device, unacceptable leakage for a sealing component, or unacceptable crack depth. Definition of the failure criterion requires an understanding of the engineering end use. Examples follow for possible failure criteria for oilfield production applications [39, 40]:

- Increase or decrease in stiffness to values outside design limits (e.g., for hoses, seals, flex elements)
- Occurrence of surface cracks
- Dynamic growth of service cracks to unacceptable limits (e.g., for flex elements, flex joints)
- Formation of cracks/blisters in bulk (e.g., in high pressure gas applications, from explosive decompression, for seals, flex joints)

- Loss of sealing stress by stress relaxation (seals in low pressure applications, end-fittings for hoses)
- Extrusion of seal/hose lining into surrounding gap
- Weakening by excessive liquid absorption and swelling (and effects on factors above)
- Excessive build-up of gas due to seal leakage (from factors above or thermal changes) and permeation
- General degradation (hoses, seals, in extremely hostile fluids)

After the failure criterion has been defined, the changes in the elastomer material that could cause this failure may be analyzed. Durability of rubber components can be defined quantitatively on this basis. Crack growth is clearly one such change, age hardening is another, and swelling in or permeation of fluids is another. Fracture mechanics analysis of the rubber layer(s) in the component is the only known way of predicting crack growth rates in elastomeric components. This approach has a documented track record of successful application to actual components [1, 3–5].

Further work is needed to extend the range of geometrical solutions to which fracture mechanics can be applied, and there is some discussion of this in other chapters in this book. Other changes in the material (e.g., oxidative age hardening) may affect rates of crack growth. Alternatively, there may be no crack growth but only hardening of the material. Liquid ingress could cause weakening; gas ingress could cause explosive decompression fracturing. Whatever the mechanism, each process needs to be identified and its rate characterized separately. Only then can interactions between different mechanisms be considered for life predictions on a sound basis.

Tests on materials should be performed at different levels of severity and at different time intervals to ensure that the rate of change is measured. Change in physical property levels over many years are described in [41], mainly for air aging. Care must be taken to match the test condition to the service conditions in as realistic a way as possible. For example, if measurements of rate cannot be made at the service temperature in the time available, accelerated tests may be used at elevated temperatures or increased frequency, provided a clear proof exists that the acceleration is an actual increase in rate of the same process. This point needs to be validated for each material. After the rate of each process has been determined under the accelerated condition(s), the rate at the service condition may be determined by extrapolation. It is conventional to use an Arrhenius plot of log (failure rate) against reciprocal temperature (see Section 7.6.4) to enable extrapolations to be made to long times (low rates) at lower temperatures. A case study for this is included in [39].

After each process is separately understood in this way, interactions can be put together to provide a life prediction of the durability of the component under service conditions. This should then be validated by selected prototype testing.

Figure 7.16 is a flow diagram for a complete life prediction methodology used at Materials Engineering Research Laboratory to estimate the durability of a polymer engineering component. This approach has provided a useful basis for development work on several types of component. Once all relevant parts of the life prediction chart have been characterized, the database also provides a sound basis for computer-aided design, which can eventually model durability processes to reduce the need for complex and costly prototype testing.

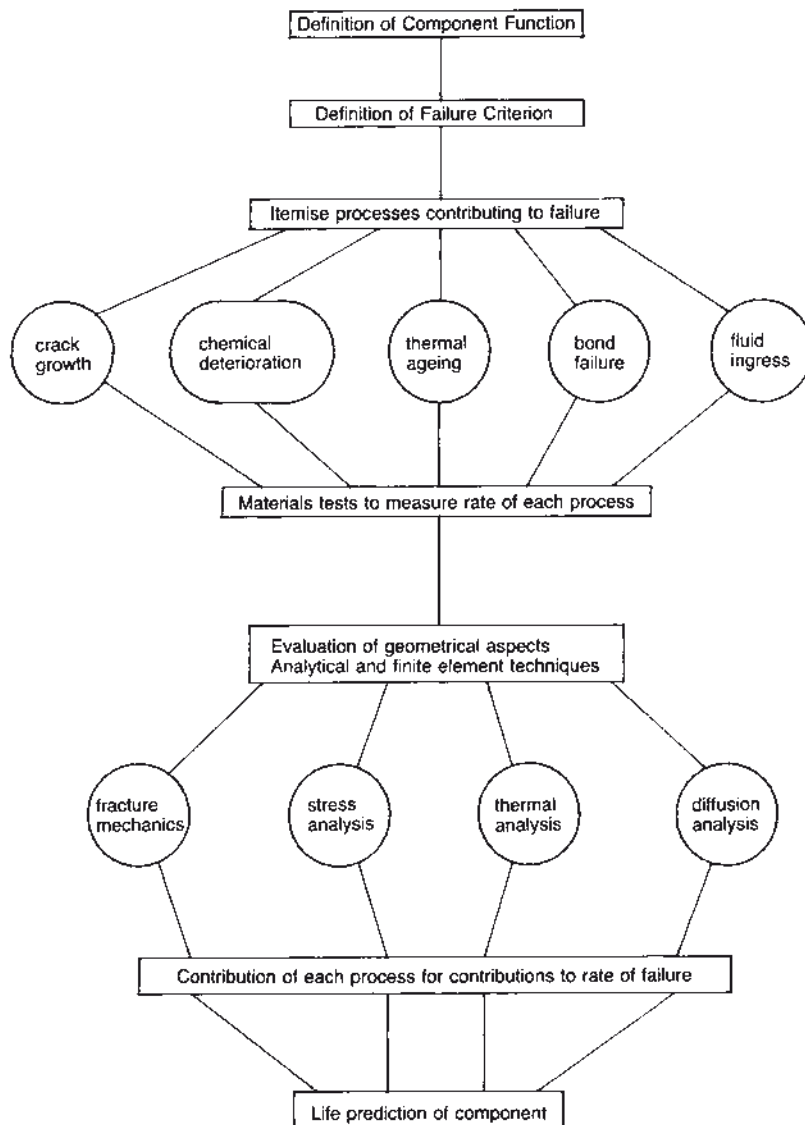


FIGURE 7.16 Flow diagram for life prediction methodology to establish rubber engineering component durability

Acknowledgment

The authors thank Mr. C. J. Derham of Materials Engineering Research Laboratory (MERL Ltd.) for his contributions to the understanding of creep and stress relaxation, without which the first section of this chapter would not have been possible.

References

- [1] A. Stevenson and W. McIntosh, "Operating Experience with Elastomer Composites on the Hutton Tension Leg Platform", in *Proceedings of the Ninth International Conference on Offshore Mechanics and Arctic Engineering*, Houston, February 1990. Published by American Society of Mechanical Engineers, New York (1990).
- [2] A. Stevenson, "Rubber in Engineering", in *Kempes Engineering Yearbook (1986-90)*, Morgan Grampian Publishers, London, Chapter C3.
- [3] H. L. Oh, *Rubber Chem. Technol.*, **53**, 1226 (1980).
- [4] R. F. Breidenbach and G. J. Lake, *Phil. Trans. R. Soc. London, Ser. A*, **299**, 189–202 (1981).
- [5] D. G. Young, presentation at American Chemical Society, Rubber Division Conference (1989).
- [6] A. Stevenson, "Longevity of Natural Rubber in Structural Bearings", *Plast. Rubber Process. & Appl.*, **5**, 253 (1985).
- [7] A. N. Gent, *J. Appl. Polym. Sci.*, **6**(22), 442 (1962).
- [8] C. J. Derham, *Rubb. India*, **16** (Oct. 1974).
- [9] C. J. Derham, *Plast., Rubber Compos. Process. Appl.*, **26**(3), 129 (1997); (different article illustrating temperature effects only) *J. Mater. Sci.*, **8**, 1023 (1973).
- [10] C. J. Derham and R. A. Waller, *The Consulting Engineer*, **39**, 49 (1975).
- [11] D. Cumberland, Panama Weathering Study, DuPont Technical Report 515 (1983).
- [12] J. H. Hildebrand, J. M. Prausnitz, and R. L. Scott, *Regular and Related Solutions*, Van Nostrand Reinhold, New York (1970).
- [13] G. Gee, *Trans. Inst. Rubb. Ind.*, **18**(6), 266 (1943).
- [14] D. Lawson et al., *Proc. Conf. 18th Canadian High Polymer Forum*, McMaster Univ, Hamilton, Ontario, Canada, paper 35 (1975).
- [15] C. J. Sheehan and A. L. Bisio, *Rubb. Chem. Technol.*, **39**(1), 149 (1966).
- [16] G. Allen, G. Gee, and J. P. Nicholson, *Polymer*, **1**, 56 (1960).
- [17] K. Ab-Malek and A. Stevenson, *J. Mater. Sci.*, **19**, 585 (1984).
- [18] E. Southern, in A. Stevenson (Ed.), *Rubber in Offshore Engineering*, Adam Holger, Bristol, UK, Chapter 19 (1984).
- [19] K. Muniandy and A. G. Thomas, *Proc. Conf. Polymers in a Marine Environment*, London, *Trans. I Mar. E. (C)* (**97**), 87 (1984).
- [20] J. Crank, *The Mathematics of Diffusion*, 2nd ed., Oxford University Press, Oxford (1956).
- [21] International Standard ISO 6179.

- [22] R. P. Campion, *Permeation through Polymers for Process Industry Applications*, MTI publication No. 53, Materials Technology Institute of the Chemical Processing Industry, St Louis MO, USA, distributed by Elsevier Science, Amsterdam, The Netherlands, 55–56 (2000).
- [23] N. L. Smith and R. P. Campion, *Proc. 2nd Conf. Polymers in Automotive Fuel Containment*, Hanover, Germany, publ. Rapra Technology Ltd., Shawbury, UK, paper 16 (2005).
- [24] G. J. van Amerongen, “Diffusion in Elastomers”, *Rubber Chem. Technol. (Rubber Rev.)*, **37**, 1065 (1964).
- [25] J. Crank and G. S. Park, *Diffusion in Polymers*, Academic Press, London (1968).
- [26] R. P. Campion, *Proceedings of Corrosion 91*, NACE, Cincinnati, paper 456 (1991); also (with G. J. Morgan) *Plastics, Rubber & Composites Processing & Applications*, **17**(1), 51–58 (1992).
- [27] R. P. Campion, *Cellular Polymers*, **9**(3), 206 (1990).
- [28] A. Stevenson and G. J. Morgan, *Rubb. Chem. And Technol.*, **68**(2), 197 (1995).
- [29] B. J. Briscoe, T. Savvas and C. T. Kelly, *Rubb. Chem. And Technol. (Rubb. Reviews)*, **67**(3), 384 (1994).
- [30] R. P. Campion, C. J. Derham, G. J. Morgan and M. V. Lewan, in A. N. Bhowmick (Ed.), *Current Topics in Elastomer Research*, CRC Press, Boca Raton FL, USA, chapter 23 (2008).
- [31] International Standard ISO 23936-1 (for thermoplastics) and ISO 23936-2 (for elastomers, nearing completion); Norwegian National Standard NORSO M-710 Rev 2 (mainly for elastomers).
- [32] R. P. Campion and B. Thomson, *Offshore Research Focus*, **114** (publ. OSO, Glasgow, UK), 5 (Oct. 1996).
- [33] G. J. Morgan, R. P. Campion and C. J. Derham, *Proc. Conf. American Chemical Society, Rubber Division*, Chicago IL, USA, 56 (1999).
- [34] P. B. Lindley, *J. IRI*, **5**, 243 (Dec. 1971).
- [35] R. P. Campion and P. J. Corish, “Elastomer – Metal Adhesion Processes” in P. J. Corish (Ed.), *Concise Encyclopedia of Polymer Processing & Applications*, Pergamon Press, Oxford, UK, 211–216 (1992).
- [36] R. P. Campion, *Proc. Conf. American Chemical Society, Rubber Division, Fall Meeting*, Cleveland, Ohio, paper 24 (Oct. 1997).
- [37] A. Stevenson, *J. Adhes.*, **21**, 313–327 (1987).
- [38] A. Stevenson and B. Thomson, *Proceedings of Rubber/Metal Bonding Conference*, Frankfurt, Germany (Dec. 1998), publ. RAPRA, Shawbury, UK (1998).
- [39] R. P. Campion, *Rubb. Chem. Technol. (Rubb. Rev.)*, **76**(3), 719 (2003).
- [40] R. P. Campion, *Proceedings of Elastomer – Service Life Prediction Symposium '98*, publ. ARDL, Akron, Ohio, paper C (Sept. 1998).
- [41] R. P. Brown and T. Butler, “Natural Ageing of Rubber”, Rapra Technology Ltd., Shawbury, UK, 2000.

■ Problems for Chapter 7

1. A building mount consists of three rubber layers bonded between horizontal steel plates. Each rubber layer is 15 mm thick, and rectangular in cross-section: 200 mm \times 600 mm. The shear modulus G of the rubber is 0.99 MPa. When the mount is loaded to 2070 kN (taking 1 minute), the initial compressive deflection is 6.9 mm. Calculate the compression stiffness of the mount. (Obtain a check to this answer to within about 5 MN/m using the bearing dimensions and rubber properties provided in Chapter 8, Section 8.2. Use interpolated shear modulus and associated values from Table 8.1, and allow for the contribution from bulk compression for a flat sandwich block.) If the physical creep rate A is 6.6% per decade and the chemical creep rate B is 0.47% per year at the average service temperature of 20 °C, what is the expected creep after 1 year, 5 years, 10 years, 20 years, and 50 years? When does the amount of chemical creep equal the amount of physical creep? How long does it take for the total deflection to reach 12 mm?
2. Briefly discuss factors to be considered in selecting rubbery materials for sealing against:
 - (a) hydrocarbon liquids such as ASTM No. 3 oil at (i) 80 °C; (ii) 180 °C (iii) -30 °C.
 - (b) sea water at 80 °C
 - (c) methanol at 80 °C.

From information given in this chapter, if 25 mm thick NR sheets are immersed in ASTM No. 3 oil for one year at 43 °C, how far will the oil penetrate into the rubber through each face on a root-mean-square basis?
3. (a) Two reactions each possess the same activation energy E_a but their rates differ at the same temperature. Explain this in terms of the Arrhenius equation.
(b) If a chemical reaction has a value for E_a of 21 kcal/mol, how much faster does the reaction proceed at 160 °C compared with 140 °C, taking the gas constant R to be 1.987 cal/deg/mol?
(c) As a rough rule of thumb, it is often stated that increasing the temperature of a chemical reaction by 10 °C doubles its rate. By constructing Arrhenius-type plots for the temperature range 20 °C to 180 °C, compare the “doubling” method with a true Arrhenius approach and see if you can calculate an equivalent E_a value (in kcal/mol and kJ/mol) for this range. Also determine equivalent E_a values for the smaller temperature ranges: (i) 20 °C to 40 °C, and (ii) 160 °C to 180 °C. Comment on your findings.

4. Thin strips of a rubber sample were exposed at an elevated temperature to a chemically-hostile liquid which saturated the strips in a few days, causing some swelling. Strips were removed at intervals of time and low-strain tensile moduli were obtained immediately at 23 °C. The whole procedure was repeated for exposures at two other temperatures. The values obtained for tensile moduli are given below.

Modulus Values (MPa)

Temper- ture (°C)	Time (days)											
	0	1	3	5	7	14	28	56	84	112	140	168
160	10	8.5	8	10	12.5	12.5	10	9	8.5	8	7.5	7.5
140	10	9	8.5	8	8.5	10	14	12	10	9	8.5	8
120	10	9.5	9	8.5	8	8	9	12	15	14.5	13.5	12.5

It can be seen that the modulus changes in three stages: first decreasing, then increasing, and finally decreasing again. Explain how this might be. Determine activation energies for three cases: (a) the early minimum modulus, (b) the maximum modulus, and (c) the original modulus level when it is achieved again following the maximum. N.B. One of these cases will require a time-based extrapolation.

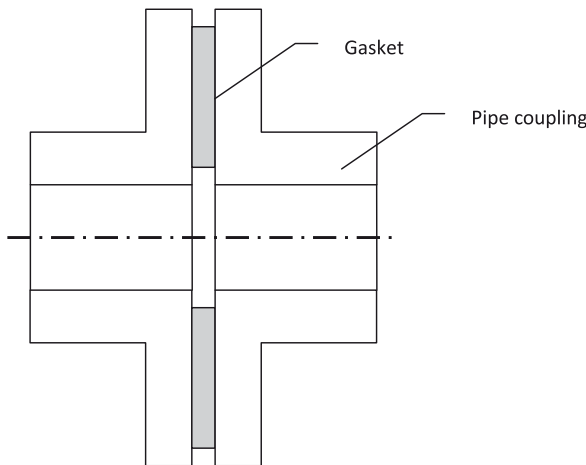
According to an Arrhenius prediction, how long would it take to attain these three levels of modulus at 60 °C in the same fluid? Comment on your degree of confidence in the findings.

5. A series of gas permeation tests gave the following results for CO₂ passing through a rubber sheet (cf. Eqs. (7.16–7.18)):

Temperature (°C)	Q (m ² /s/atm) × 10 ⁻¹⁰	D (m ² /s) × 10 ⁻¹⁰	S (atm ⁻¹)
195	4.1	23.0	0.18
155	2.6	10.0	0.26
130	1.8	5.2	0.35
100	1.1	2.0	0.55

Determine the activation energies of permeation, diffusion and solubility for this system. In an application, the rubber is to be exposed to CO₂ gas at 345 atm and 70 °C until saturated and then the external pressure will be rapidly removed. Assuming that there is a critical gas concentration c_c of 200 cm³ (S.T.P) per cm³ of rubber at 70 °C, above which explosive decompression (ED) failure is probable, determine whether this critical value will be exceeded. What other factors influence failure by explosive decompression?

6. (a) With reference to molecular- and micro-structures of polymers, explain the relatively high permeability and absorption characteristics of elastomers.
- (b) Consider an assembly comprising a gasket separating two clamped-together horizontal pipe sections as indicated below:



A pressurized gas is being transported through the sealed pipe system shown. To calculate the rate of leakage by permeation radially outwards through the gasket, Fick's 2nd law of diffusion is integrated to the correct boundary conditions to give the permeation equation for permeation outwards through a hollow cylinder of length L . A gasket is then considered as a squat cylinder so that the flow rate can be given by

$$\dot{Q} = \frac{2 \pi Q L (P_1 - P_2)}{\ln(r_2 / r_1)}$$

where Q is the permeation coefficient, L here is the *thickness* of the gasket as viewed, P_1, P_2 are the pressures of the gas on the inside and outside of the gasket, respectively, and r_1 and r_2 are the inner and outer radii of the gasket, respectively. Calculate the gas flow rate in cm^3/hour escaping into the atmosphere radially outwards across a nitrile elastomer gasket of thickness 5 mm, outer diameter 150 mm and bore 50 mm for methane at 17.2 MPa and 100 °C if its permeation coefficient at these conditions is $0.3 \times 10^{-6} \text{ cm}^2/\text{s/atm}$. (Assume 10 atm = 1 MPa)

■ Answers to Problems for Chapter 7

1. Compression stiffness = 300 MN/m.

Taking t_0 as 10 min, the amount of creep (increase in deflection) is 2.20 mm, 2.65 mm, 2.95 mm, 3.40 mm, 4.55 mm, respectively, after the given periods under load.

Time for creep contributions to be equal = 94 years.

Time for total deflection to reach 12 mm = 65.5 years.

2. (a) On a solubility parameter basis, NBR, HNBR, FKM, or perfluoroelastomer FFKM can be chosen: NBR is the cheapest, but HNBR has the best mechanical properties. (FFKM is expensive, but becomes necessary at temperatures above 200 °C. TFE/P copolymer can also be used above 200 °C because, even though the value of δ is only 9 (cal/cm³)^{1/2}, this polymer is resistant to swelling by oil for structural reasons.) Hence:

- (i) NBR (or HNBR, if high strength is required).
 - (ii) FKM or FFKM.
 - (iii) Low-acrylonitrile NBR, so that T_g is below -30 °C.
- b) Most elastomers not containing hydrophilic groups are suitable (ECO or high acrylonitrile NBR are examples that would not be recommended). Also, some curing systems (e.g., litharge-cured CR) and hydrophilic fillers should be avoided.
- c) NBR, HNBR. Some FKMs; others will swell excessively; contact the manufacturer for advice.

Penetration distance = 8.9 mm, by applying the expression $(2 D t)^{1/2}$ and using the appropriate value for D from Table 7.6.

3. (a) The two reactions have a different frequency factor A_0 . E_a does not predict actual rates – only how the rate of a particular reaction will change from one temperature to another.

- (b) A factor of 3.26 faster.

(Apply Eq. (7.20) in logarithmic form to the two temperatures, and subtract.)

- (c) Taking the rate k at 20 °C to be unity and doubling 16 times to 180 °C gives values for plotting as the natural logarithm $\ln k$ against reciprocal temperature $1/T$. The result is clearly not linear, but it might be considered near enough for a reasonable linear fit to be obtained (statistical $r^2 = 0.986$). From the slope $(-E_a/R)$ of the best-fit straight line, a value of E_a is obtained of 18.3 kcal/mol (= 76.6 kJ/mol). However, from the slopes at the temperature extremes, we have

- (i) $E_a = 12.6 \text{ kcal/mol} (= 52.9 \text{ kJ/mol})$ for the temperature range 20 °C to 40 °C
- (ii) $E_a = 27.3 \text{ kcal/mol} (= 114.1 \text{ kJ/mol})$ for the temperature range 160 °C to 180 °C. Obviously the “doubling” rule of thumb only applies over a very limited temperature range.
4. An initial softening occurs due to swelling. A secondary crosslinking reaction, brought about by the chemically hostile species, then dominates the second stage. A degradation reaction, causing softening again, takes over during the third stage, perhaps due to absorbed oxygen or involving a product of the second-stage crosslinking.
- (a) 10.5 kcal/mol; (b) 17.5 kcal/mol; (c) 18.0 kcal/mol, after extrapolating the property versus time plot to give a time of 238 days to a third-stage modulus of 10 MPa.
- (a) 118 days; (b) 13 years; (c) 42 years. Ideally, many more repetitions of this aging test, preferably involving more temperatures and times, are required to give adequate confidence in the longer predictions because a small error in E_a can make a large difference in a predicted value over a long time. It can be the case (e.g., in oil field engineering) that major construction goes ahead irrespective of the status of prediction tests for rubber components, so that only a few data points are available for prediction purposes. It is imperative under these circumstances to use error bars to indicate the worst-case prediction.
5. From best-fit lines, $E_a(Q) = 4.82 \text{ kcal/mol}$; $E_a(D) = 8.92 \text{ kcal/mol}$; and $(E_a)s = -4.07 \text{ kcal/mol}$. Reasonable agreement with Eq. (7.16) is thus demonstrated. From an Arrhenius extrapolation $s = 0.865 \text{ atm}^{-1}$ at 70 °C, so that at 345 atm, $c = 298 \text{ cm}^3/\text{cm}^3$. Hence the limit c_c is exceeded and ED would be expected to occur. (Note that the existence of such a limit is not yet established.)
- See last paragraph in Section 7.6.3 for other factors affecting ED.
6. (a) An elastomer, like all polymers, consists of interwoven long chain molecules moving according to the kinetic theory, especially when amorphous. Thermoplastics possess crystalline regions distributed amongst their amorphous regions which resist permeation and absorption. Elastomers are usually fully amorphous; what distinguishes them from the other polymer class that cross-links (thermosets) is that elastomers have relatively few crosslinks. Therefore, an elastomer possesses a relatively large amount of free volume, which gives rise to the material's relatively high permeability and absorption of fluids.
- (b) Leakage flow rate = $2\pi(0.3 \times 10^{-6})(0.5)(172 - 0)/\ln[(15/2)/(5/2)] \text{ cm}^3/\text{s}$
 $= 0.0001475 \text{ cm}^3/\text{s} \equiv 0.53 \text{ cm}^3/\text{hour}$

NB: P_2 is zero, because permeated (escaped) gas is swept away as it reaches the atmosphere.

8

Design of Components

*Patrick M. Sheridan, Frank O. James,
Thomas S. Miller*

■ 8.1 Introduction

Elastomers have found use in a wide range of applications, including hoses, tires, gaskets, seals, vibration isolators, bearings, and dock fenders. In most applications, the performance of the product is determined by the elastomer modulus and by details of the product's geometry. Chapter 3 discusses the elastomer modulus and many factors that may cause it to change. This chapter addresses some simple geometries common to applications for elastomeric products. In particular, sample calculations are given for products in which the elastomers are bonded to rigid components and are used to accommodate motion, isolate from vibration, or protect from shocks. Section 8.4 identifies potential design resources for elastomeric products in general. Depending on the application, many different characteristics of an elastomer may be of interest to the designer. Some of these characteristics are:

- Ultimate strength, both stress and strain at break
- Sensitivity to changes in temperature
- Sensitivity to changes in strain
- Resistance to fluids and other contaminants
- Compatibility with mating material (adhesives, metals, etc.)
- Resistance to "set" and "creep" (dimensional stability under load)
- Internal damping

In some cases, these properties are related. Examples include:

- Minimizing "creep" usually requires a material with very low damping. As damping increases, the rate and amount of creep typically increases.
- Selecting a properly compounded silicone material will minimize sensitivity to temperature, for example, but because of the lower strength of silicone rubber, it results in lower allowable values of stress and strain in the design.
- Fatigue performance depends on both the material properties and the detailed product design. The fatigue performance of any given design can be seriously compromised by environmental factors such as deleterious fluids and heat.

The first step in most product designs is selecting the material to be used, based on the above characteristics. The material selected in turn defines the design allowables. This chapter uses conservative, generic design allowables. Although most manufacturers consider their design criteria proprietary, the information sources noted in Section 8.5 provide some general guidelines.

For most designs, the spring rate (sometimes called stiffness) is a key design parameter. The units for stiffness or spring rate are Newtons per millimeter (N/mm). In terms of function, the spring rate of a part is defined by Eq. (8.1) as the amount of force required to cause a unit of deflection:

$$K = \frac{F}{d} \quad (8.1)$$

where F is the applied force (N) and d is the deflection (mm). The spring rate K can be for shear, compression, tension, or some combination of these, depending on the direction of the applied force with respect to the principal axes of the part.

The spring rate K of a part is defined by Eq. (8.2) in terms of geometry and modulus:

$$\text{Shear: } K_s = \frac{A G}{t} \quad (8.2a)$$

$$\text{Compression: } K_c = \frac{A E_c}{t} \quad (8.2b)$$

$$\text{Tension: } K_t = \frac{A E_t}{t} \quad (8.2c)$$

where A is effective load area (m^2), t is thickness (m) of the undeformed elastomer, and G , E_c , and E_t represent the shear, compression, and tension moduli (KPa or KN/m²) of the elastomer. Figure 8.1 (Section 8.2.1) defines area and thickness.

Using Eqs. (8.1) and (8.2), the product designer can relate forces and deflections to the design parameters of area, thickness, and material modulus. It is important to use the correct modulus to calculate the appropriate spring rate.

Usually design allowables such as maximum material strength are given in terms of stress σ and strain ε . Stress is applied force divided by the effective elastomer load area, and strain is deflection divided by the undeflected elastomer thickness.

$$\sigma = \frac{F}{A} \quad (8.3)$$

$$\varepsilon = \frac{d}{t} \quad (8.4)$$

For the applications considered in this chapter, the usual design aims include the abilities to maximize fatigue life, provide specific spring rates, minimize set and drift, and minimize size and weight. Maximizing fatigue life means minimizing stress and strain, which translates to large load areas and thicknesses. The load area and thickness are also limited by the available range of elastomer modulus. Therefore, the final design represents a trade-off among size, fatigue life, and spring rate.

The design examples in this chapter assume that operation remains in the linear range of the elastomer modulus. Typically, this is less than 75–100% strain for shear and less than 30% strain for tension and compression.

Also, the design examples are limited to fairly simple geometries. Typically, the shear modulus G is not a function of geometry. However, compression modulus (E_c) is strongly affected by the geometry of a design. If the two designs in Fig. 8.1 have the same modulus elastomer, load area, and thickness, the shear spring rate K_s will be equivalent for both designs, while the different shapes will have different compression spring rates. The equations used here are good for close approximations of performance and are generally adequate for design purposes. The basic equations must be modified to account for more complex geometry effects and/or for nonlinear elastomer properties.

For all the sample problems in the sections that follow, the international system (SI) of units is used. The equations presented are independent of the unit system. Section 8.5 includes some common conversion factors from SI to English units.

■ 8.2 Shear and Compression Bearings

The ability to mold rubber into a wide variety of shapes gives the design engineer great flexibility in the selection of stress and strain conditions in a finished part. This section outlines some fundamental equations for static stress-strain relationships in bonded rubber components of various geometrical configurations. The sample problems are intended to show how these basic equations can be applied to component design.

8.2.1 Planar Sandwich Forms

Simple flat rubber and metal sandwich forms are the basic geometric shapes for a large number of rubber mounts and bearings. Typical shapes are shown in Fig. 8.1. Equations will be presented for the two principal modes of loading, simple shear and compression.



FIGURE 8.1 Rectangular and circular shear pads

Combining Eqs. (8.1) and (8.2a) yields a basic equation relating shear spring rate and product design variables.

$$K_s = \frac{F_s}{d_s} = \left(\frac{A G}{t} \right) \quad (8.5)$$

Where

K_s = shear spring rate

F_s = applied force in the shear direction

d_s = shear displacement

A = load area

G = shear modulus

t = rubber thickness

Equation (8.5) can be applied to the majority of simple shear calculations for flat “sandwich” parts. The equations are valid only when shear deformation due to bending is negligible. When the ratio of thickness to length exceeds approximately 0.25, the shear deformation due to bending should be considered. The effect of bending is shown in Fig. 8.2 and can be quantified by the following equation:

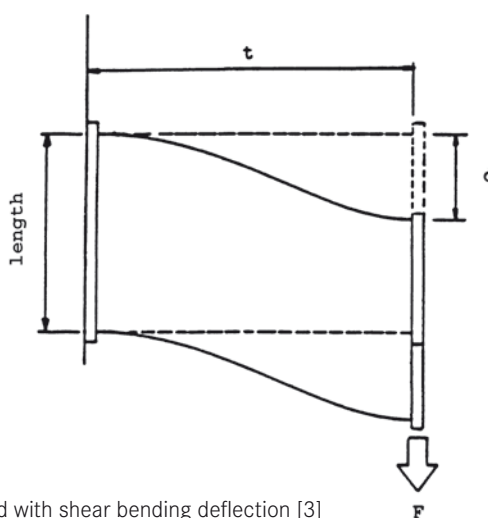


FIGURE 8.2 Shear pad with shear bending deflection [3]

$$K_s = \frac{F_s}{d_s} = \left(\frac{A G}{t} \right) \left(\frac{1}{1 + t^2 / 36 r_g^2} \right) \quad [3] \quad (8.5a)$$

where $r_g = (I_b/A)^{1/2}$ is the radius of gyration of the cross-sectional area about the neutral axis of bending and I_b is the moment of inertia of the cross-sectional area A about the neutral axis of bending. Chapter 3 includes other methods for estimating bending.

Two other factors that can affect shear spring rate are mentioned here but, because of the limited scope of this chapter, no detailed derivation is given. When the shear strain d_s/t exceeds approximately 75%, or when the part has an effective shape factor of less than 0.1, the effect of rubber acting in tension may also need to be considered. At this point the rubber is no longer acting in simple shear only; there is now a component of tensile force in the rubber between the two end plates. Another important consideration for some components may be a change in shear spring rate due to an applied compressive stress [1]. With components of high shape factor, the shear spring rate increases as a compressive load is applied. This effect increases with increasing shape factor and increased compressive strain, as shown graphically in Fig. 8.3. The shape factor is defined in Eq. (8.9).

Combining Eqs. (8.1) and (8.2b) yields a basic equation relating compression spring rate and product design variables.

$$K_c = \frac{F_c}{d_c} = \frac{A E_c}{t} \quad (8.6)$$

where

K_c = compression spring rate

F_c = applied force in compression direction

d_c = compression displacement

A = load area

E_c = effective compression modulus

t = thickness

Successful use of this equation depends on knowing the effective compression modulus E_c . The value of E_c is a function of both material properties and component geometry, as discussed in Chapter 3. Many different analytical techniques can be used to calculate E_c , and the method described here yields reasonable approximations for compression spring rates of many simple components. More advanced analytical solutions as well as finite element analyses are available for more accurate spring rate calculations. For a more rigorous analytical solution of compression, bending, and shear in bonded rubber blocks, see Gent and Meinecke [2].

Approximation of Change in Shear Modulus as a Function of Shape Factor and Percent Compressive Strain.

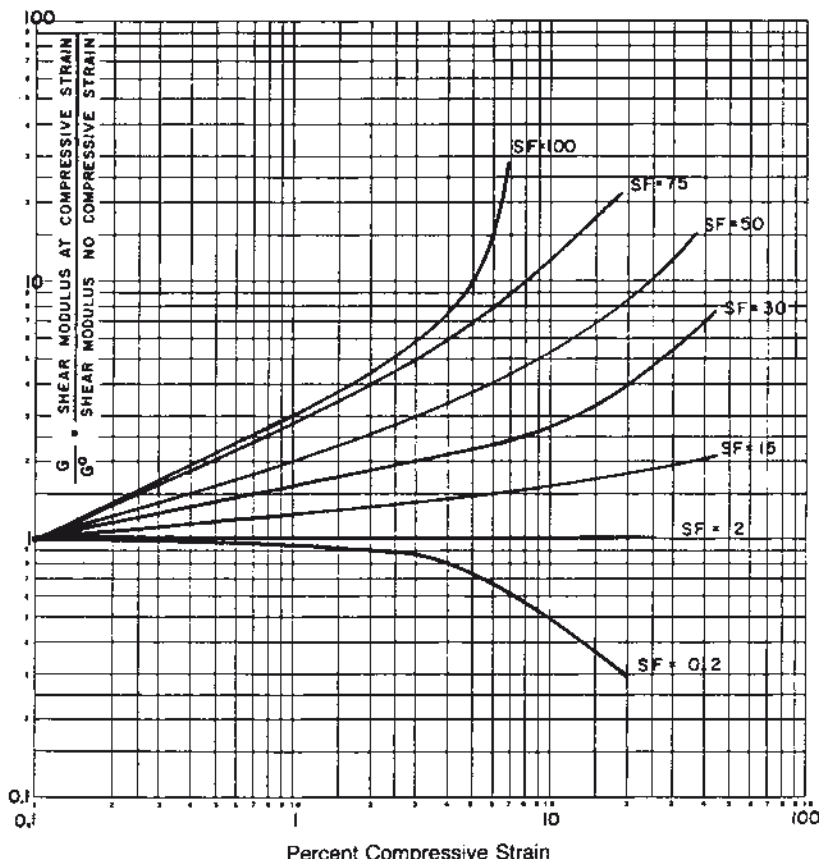


FIGURE 8.3 Influence of compressive strain and shape factor (SF) on shear modulus [3]

The effective compression modulus for a flat sandwich block is given by the equation:

$$E_c = E_0 (1 + \phi S^2) \quad \text{for bidirectional strain (blocks)} \quad (8.7)$$

or

$$E_c = 1.33 E_0 (1 + \phi S^2) \quad \text{for one-dimensional strain [4]} \quad (8.8)$$

(long, thin compression strips)

where

E_0 = Young's modulus (see Table 8.1)

ϕ = elastomer compression coefficient (see Table 8.1)

S = shape factor (defined below)

TABLE 8.1 Material Properties [3]

Shear modulus, <i>G</i> (kPa)	Young's modulus, <i>E</i> ₀ (kPa)	Bulk modulus, <i>E</i> _b (MPa)	Material compress- ibility coefficient, ϕ
296	896	979	0.93
365	1158	979	0.89
441	1469	979	0.85
524	1765	979	0.80
621	2137	1,007	0.73
793	3172	1,062	0.64
1034	4344	1,124	0.57
1344	5723	1,179	0.54
1689	7170	1,241	0.53
2186	9239	1,303	0.52

The coefficient ϕ is an empirically determined material property, which is included here to correct for experimental deviation from theoretical equations. Table 8.1 gives values of ϕ for varying elastomer moduli. The modulus and material compressibility values in Table 8.1 are used to solve Problem 8.2.1.1 (below), as well as the other numbered problems in this chapter.

The shape factor S is a component geometry function that describes geometric effects on the compression modulus. It is defined as the ratio of the area of one loaded surface to the total surface area that is free to bulge:

$$\text{shape factor } S = \frac{\text{load area}}{\text{bulge area}} = \frac{A_L}{A_B} \quad (8.9)$$

For example, the shape factor for the rectangular block of Fig. 8.1 would be:

$$\begin{aligned} S &= \frac{A_L}{A_B} = \frac{(\text{length})(\text{width})}{2t(\text{length}) + 2t(\text{width})} \\ &= \frac{(\text{length})(\text{width})}{2t(\text{length} + \text{width})} \end{aligned}$$

Results from this method of calculating compression modulus are summarized graphically in Fig. 8.4. Given shape factor and shear modulus, this graph can be used to find effective compression modulus for a component.

Generally, rubber can be regarded as incompressible. In some cases bulk compressibility makes an appreciable contribution to the deformation of a thin rubber pad in compression [3, 4]. The reason is that a thin pad offers great resistance to compression, and the apparent compression modulus approaches the bulk modulus in

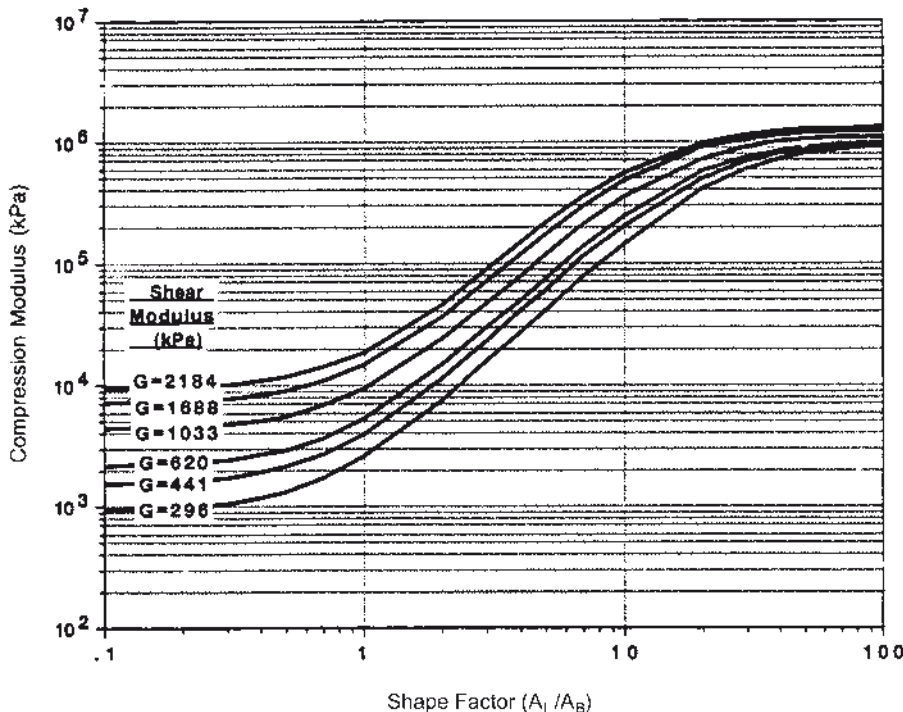


FIGURE 8.4 Compression modulus E_c versus shape factor S for various shear moduli [3]

magnitude. To account for this decrease in spring rate, the calculated compression modulus should be multiplied by the following factor:

$$\frac{1}{1 + E_0 / E_b} \quad (8.10)$$

where E_b is the modulus of bulk compression, about 1.1 GPa (approximation from Table 8.1).

Problem 8.2.1.1

Calculate compression and shear spring rates and their ratio K_c/K_s for a rectangular block measuring 50 mm \times 75 mm \times 10 mm thick, made with rubber of shear modulus $G = 793$ kPa. Assume bulk compressibility effects to be negligible. The solution is arrived at as follows:

$$K_s = \frac{(0.050 \text{ m} \times 0.075 \text{ m}) \times (793 \text{ kN/m}^2)}{0.01 \text{ m}} \quad (\text{per Eq. (8.2a)})$$

$$= 297 \times 10^3 \text{ N/m}$$

$$S = \frac{50 \text{ mm} \times 75 \text{ mm}}{(2 \times 10 \text{ mm}) \times (50 \text{ mm} + 75 \text{ mm})} \\ = 1.5$$

$$E_c = 3172 \text{ kPa} \left[1 + 2(0.64)(1.5)^2 \right] \quad (\text{per Eq. (8.7)) and Table 8.1}) \\ = 12,300 \text{ kPa}$$

$$K_c = \frac{(0.050 \text{ m} \times 0.075 \text{ m})(12.3 \text{ MPa})}{0.01 \text{ m}} \quad (\text{per Eq. (8.2b)}) \\ = 4.61 \times 10^6 \text{ N/m}$$

$$K_c / K_s = \frac{4.61 \times 10^6}{297 \times 10^3} = 15.5$$

8.2.2 Laminate Bearings

The introduction of rigid shims into the elastomeric section of a bearing is often used as a technique to increase compression spring rate while maintaining the same shear spring rate. In the case of a laminate bearing, the compression spring rate equation becomes:

$$K_c = \frac{F_c}{d_c} = \frac{A E_c}{t N} \quad (8.11)$$

where

N = number of identical elastomer layers

t = individual layer thickness

E_c = individual layer compression modulus

The shear spring rate remains unchanged, assuming that the total elastomer thickness is unchanged.

Problem 8.2.2.1

Calculate the shear and compression spring rates and their ratio K_c/K_s for the bearing in Problem 8.2.1.1 if the elastomer is divided into five equal thickness sections by rigid shims (Fig. 8.5). The load area and total elastomer thickness are the same, so the shear spring rate remains unchanged.

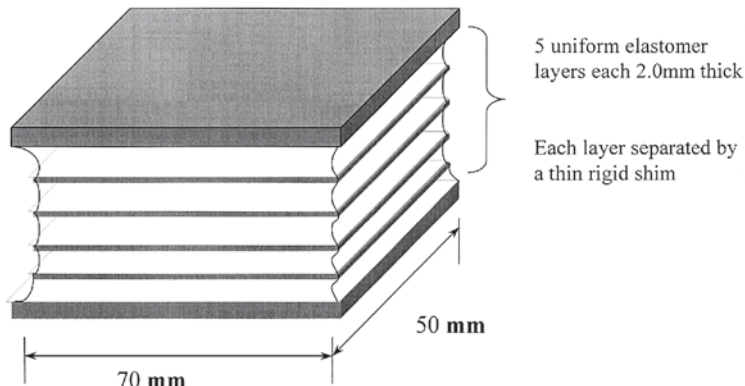


FIGURE 8.5 Laminate bearing (5 layers)

$$K_s = 297 \times 10^3 \text{ N/m}$$

The compression spring rate becomes:

$$K_c = \frac{A E_c}{t N}$$

where

$$S = \frac{50 \text{ mm} \times 75 \text{ mm}}{2 \times 2 \text{ mm} \times (50 \text{ mm} + 75 \text{ mm})} \quad (\text{per Eq. ((8.7))})$$

$$= 7.5$$

$$E_c = 3172 \text{ kPa} \left[1 + 2(0.64)(7.5)^2 \right]$$

$$= 232 \text{ MPa}$$

Including the bulk correction factor, we write

$$E_c = \frac{232 \text{ MPa}}{1 + (3172 \text{ MPa}/1062 \text{ MPa})}$$

$$= 231 \text{ MPa}$$

$$K_c = \frac{(0.050 \text{ m} \times 0.075 \text{ m})(231 \text{ MPa})}{5 \times 0.002 \text{ m}} \quad (\text{per Eq. (8.11)})$$

$$= 87 \times 10^6 \text{ N/m}$$

$$K_c / K_s = \frac{87 \times 10^6}{297 \times 10^3} = 293$$

Problem 8.2.2.1 illustrates the ability to increase the ratio of compressive to shear spring rate significantly, while keeping the overall volume of the part essentially unchanged (ignoring the thickness of the rigid shims).

If the part is simultaneously subjected to both compression and shear loading, the shear spring rate may increase with increasing compression load, as shown in Fig. 8.3.

8.2.3 Tube Form Bearings and Mountings

Tube form mountings and rubber bushings are widely used products as they offer flexibility in torsion, tilt (cocking), axial and radial directions. They provide high load-carrying capacity in a compact shear isolator. In the torsion and axial directions the rubber is used in shear and provides relatively soft spring rates. In the radial direction the rubber is used in compression and tension which provides much stiffer spring rates and hence greater stability. When used as spring elements, the torsion and/or axial shear spring rates are generally the key design parameters. However, the radial and cocking spring rates also affect the behavior of the design. Determination of these spring rates is often necessary in order to ensure that excessive forces or deflections will not occur, or that resonant frequencies will not fall within the operating range of a machine. The relevant stiffnesses for small radial, axial, and tilting deformations have been determined by Horton, Glover and Tupholme [5-7]. In this section, simpler and more approximate relations are employed.

A general equation for torsional stiffness of a tube form elastomeric bearing with plane ends (given in slightly different form in Chapter 3, Eq. (3.9)) is:

$$K_{\text{tor}} = \frac{T}{\theta} = \frac{\pi G L}{1/(d_i)^2 - 1/(d_o)^2} \quad (8.12)$$

where

K_{tor} = torsional spring rate

G = shear modulus

L = bearing length

d_i = bearing inner diameter

d_o = bearing outer diameter

T = applied torque

θ = angular deflection (radians)

Problem 8.2.3.1

A spring-loaded arm is used to maintain wire tension on a wire winding machine. The wire passes over several pulleys, two of which are on the hinged arm, which allows for wire slack take-up by arm rotation (see Fig. 8.6). The arm should move $\pm 5^\circ$ with $\pm 3\text{ N}$ tension variation in the wire. Assume the effect of the weight of the arm on wire tension to be negligible.

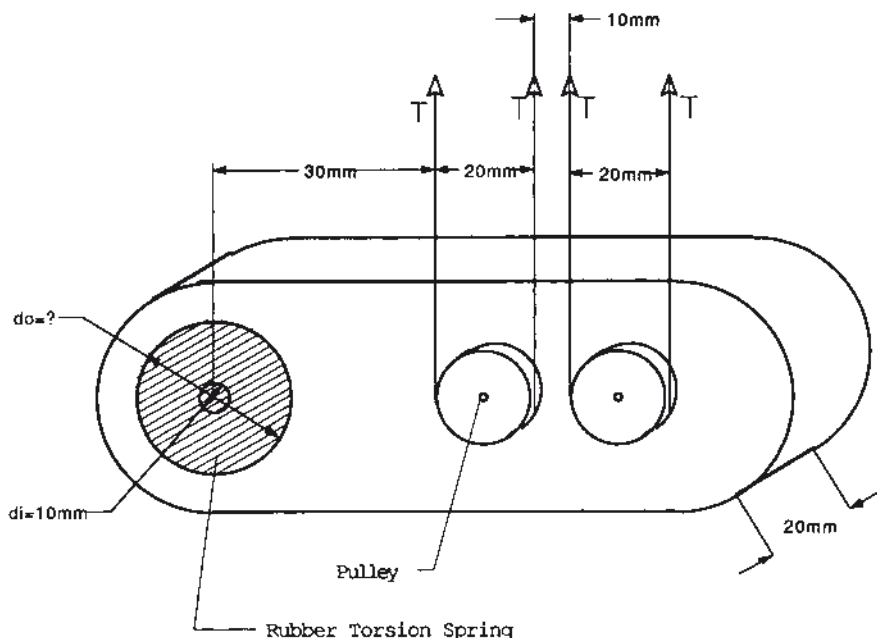


FIGURE 8.6 Wire tension arm

- What size of elastomeric bearing is required at the arm pivot point? (Assume an elastomer modulus of $G = 1034\text{ kPa}$, a bearing inside diameter of 10 mm, and an axial length of 20 mm.)

To find the bearing size, begin by summing torques on the arm about the pivot point due to 3 N of wire tension.

$$T_{\text{bearing}} = 3\text{ N} (0.030\text{ m}) + 3\text{ N} (0.050\text{ m}) + 3\text{ N} (0.060\text{ m}) + 3\text{ N} (0.080\text{ m})$$

$$T = 0.66\text{ N}\cdot\text{m}$$

Now calculate the desired torsion spring rate for the $\pm 5^\circ$ motion desired.

$$K_{\text{tor}} = \frac{T}{\theta} = \frac{0.66}{5} = 0.13\text{ N}\cdot\text{m}/\text{deg} = 7.6\text{ N}\cdot\text{m}/\text{rad}$$

Knowing the desired spring rate, solve Eq. (8.12) for d_o .

$$7.6 = \frac{\pi (1034 \times 10^3 \text{ Pa})(0.02 \text{ m})}{1/(0.01)^2 - 1/(d_o)^2}$$

$$\frac{1}{(d_o)^2} = \frac{1}{0.01^2} - 8590$$

$$d_o = 27 \text{ mm}$$

2. How much does the arm translate in the radial direction (vertical in Fig. 8.6) as a result of the imposed radial force caused by the wire tension?

A free body diagram on the arm shows a radial force F_r of 12 N at the bearing. Effective shape factor can be calculated as follows (see Section 8.2.4):

$$S = \frac{A_L}{A_B} = \frac{\text{load area}}{\text{bulge area}} \cong \frac{(d_o - d_i)L}{2\pi[(d_o)^2/4 - (d_i)^2/4]} \\ \cong 0.34$$

The radial direction in a tube form acts in the compression/tension direction on the rubber. Radial deflection can be calculated using the basic equation:

$$K_t = \frac{A E_c}{t} = \frac{F_r}{d_r}$$

or

$$d_r = \frac{F_r t}{A E_c}$$

Where

$$t = (d_o - d_i)/2 = 8.5 \text{ mm}$$

$$A \cong (d_o - d_i)L = 340 \text{ mm}^2$$

Knowing the elastomer modulus and shape factor, we can find E_c from Fig. 8.4.

$$E_c = 5000 \text{ kPa}$$

$$d_r = \frac{12 \text{ N}(0.0085 \text{ m})}{(340 \times 10^{-6} \text{ m}^2)(5.0 \times 10^6 \text{ Pa})} \\ = 0.06 \text{ mm for } 3 \text{ N of wire tension}$$

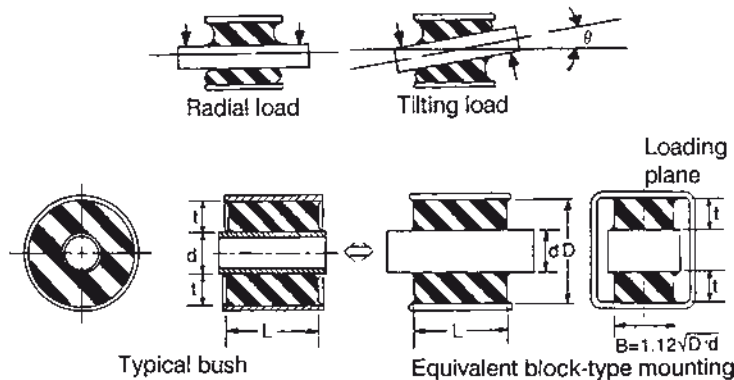


FIGURE 8.7 Bush and equivalent block

Another method of finding tube form mount or bearing shape factors accepted in the rubber industry is to convert the tube form to an equivalent block bonded with equivalent size parallel plates (see Fig. 8.7). The length is 20 mm and the width can be approximated by the following expression [5].

$$B = 1.12 \sqrt{d_0 \cdot d_i} = 0.018 \text{ m} \quad (8.13)$$

Now, shape factor

$$\begin{aligned} S &= A_L / B_L \\ &= \frac{0.020(0.018)}{2(0.020 + 0.018)[(0.027 - 0.010)/2]} \\ &= 0.56 \end{aligned}$$

The compression modulus \$E_c\$ is now 5900 kPa (Fig. 8.4 or Eq. (8.7)), and the radial deflection is:

$$\begin{aligned} d_r &= \frac{12 \text{ N} (0.0085 \text{ m})}{(340 \times 10^{-6} \text{ m}^2)(5.9 \times 10^6 \text{ Pa})} \\ &= 0.051 \text{ mm for 3 n of wire tension} \end{aligned}$$

This alternative method of calculation by replacing a tube form with an equivalent block can be used for more complicated combined radial and cocking loading conditions.

Problem 8.2.3.2

A wind tunnel diverter door (Fig. 8.8) needs to open 10° when an equivalent force of 300 N aerodynamic force is exerted as shown. How large in diameter does a full-length door hinge need to be if the hinge post is 20 mm in diameter? Assume that an elastomer with $G = 621 \text{ kPa}$ is used.

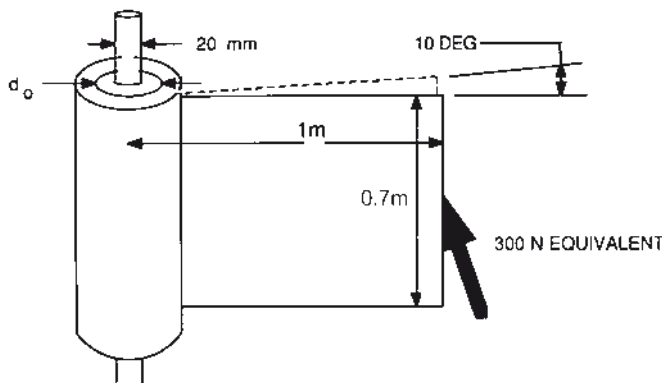


FIGURE 8.8 Wind tunnel hinged diverter door

From the known force and deflection, start by calculating the required spring rate.

$$K_{\text{tor}} = \frac{T}{\theta} = \frac{(300 \text{ N})(1 \text{ m})}{10} = 30 \text{ N} \cdot \text{m}/\text{deg}$$

$$= 1719 \text{ N} \cdot \text{m}/\text{rad}$$

Now, go back and determine the unknown geometry.

$$K_{\text{tor}} = \frac{\pi G L}{1/(d_i)^2 - 1/(d_o)^2}$$

Solve for d_o :

$$1719 \text{ N} \cdot \text{m}/\text{rad} = \frac{\pi(621 \text{ kPa})(0.7 \text{ m})}{1/(0.02 \text{ m})^2 - 1/(d_o)^2}$$

$$\frac{1}{(d_o)^2} = \frac{1}{(0.02 \text{ m})^2} - \frac{\pi(621 \text{ kPa})(0.7 \text{ m})}{1719 \text{ N} \cdot \text{M}/\text{rad}}$$

$$d_o = 24 \text{ mm}$$

8.2.4 Effective Shape Factors

The effective loaded area of tube form mountings described in Section 8.2.3 is dependent on the load or deflection of interest. Loaded areas in torsion or axial deflection are obvious, but the values used for effective loaded areas in radial or cocking deflections are only estimated approximately. In Problem 8.2.3.1 the radial load areas were taken as $(d_o - d_i) L$ and $1.12 L \sqrt{d_o d_i}$. It is not clear which of the various projected areas or effective areas should be used in radial and cocking stiffness calculations (see Fig. 8.9). To further complicate the calculation of stiffness for tube form mountings, secondary processing is often used to induce pre-compression in order to enhance performance and fatigue life. These secondary processes include:

- *Spudding* or enlarging the diameter of the inner member after bonding,
- *Swaging* or reducing the outer member diameter after bonding, and/or
- *Molding* at high pressure, high enough to cause residual pre-compression in the elastomer.

Figure 8.10 shows how swaging, spudding, and high pressure molding affect the elastomer behavior. In a tube form mounting without pre-compression, one side of the elastomer works in tension and the other side works in compression. Soft, low-modulus elastomers in tension can be damaged at relatively low loads due to internal cavitation. Elastomers in compression, on the other hand, particularly in high shape factor designs, have an effective modulus that can approach the modulus of bulk compression. Pre-compressing a tube form mounting effectively makes the “tension side” work in compression. This means that the radial and cocking

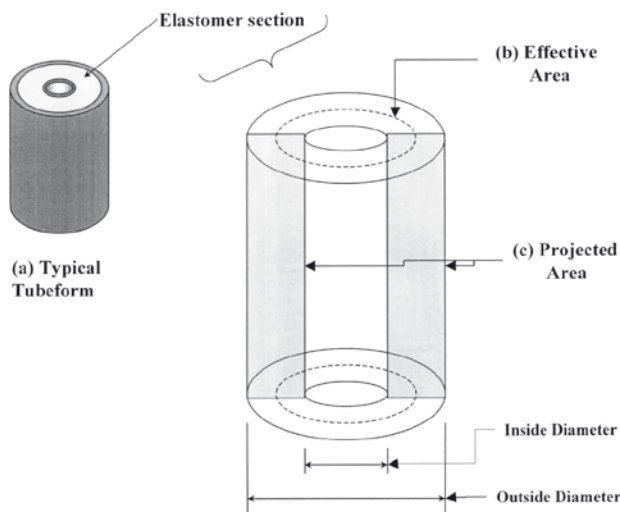


FIGURE 8.9 Radial and cocking load areas for a tube form

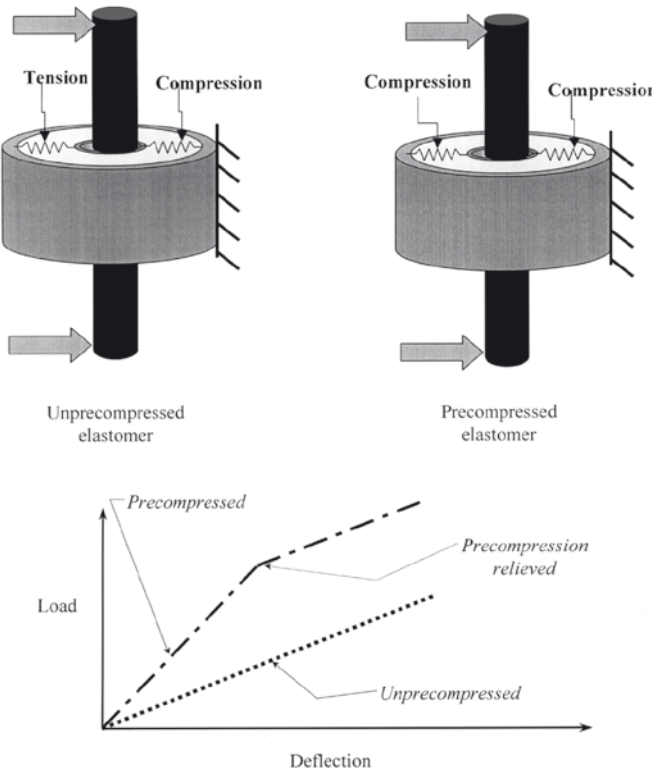


FIGURE 8.10 Tube form models for pre-compressed and unpre-compressed elastomer

stiffness can be nearly twice as high, at least until the deflection reaches a point where the initial pre-compression is relieved. When pre-compression is used, the effective shape factor increases as a result of an apparent increase in loaded area. It also could be said the shape factor does not change but the loaded area increases. In either case, some compensation is made to the numerator of the expression: $K_R = A E_c / t$ in calculating radial or cocking stiffness. For most engineering designs, the radial stiffness of a tube form mounting is calculated both with and without pre-compression to bound the expected performance.

■ 8.3 Vibration and Noise Control

The examples in this section show how to establish design requirements from a basic problem statement and then relate these requirements to the design of an appropriate elastomeric product.

8.3.1 Vibration Background Information

Solving vibration and noise control problems with elastomeric products requires understanding basic product design concepts and vibration theory. The basic equations from vibration theory are discussed in Chapter 4.

For the purposes of this section, all systems are assumed to be represented by a damped, linear, single degree of freedom system as shown in Fig. 8.11. The functions of the spring and damper in the mechanical system of Fig. 8.11a are replaced by a single elastomeric part in Fig. 8.11b, which works as both spring and damper.

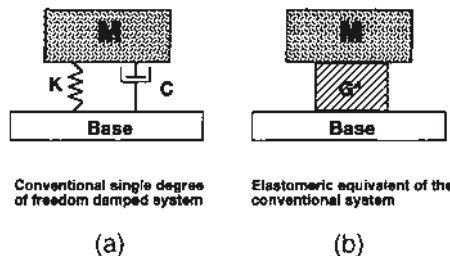


FIGURE 8.11 Damped linear single degree of freedom model

Two basic formulas are needed to work vibration isolation problems. The first defines the natural frequency of vibration for the isolation system and the second defines the transmissibility of the system as a function of frequency.

$$f_n = \frac{1}{(2\pi)} \left[(K' g) / W \right]^{1/2} \quad (8.14)$$

which reduces to

$$f_n = 15.76 \left(K' / W \right)^{1/2} \quad (8.15)$$

where

f_n = system natural frequency of vibration (Hz)

K' = dynamic spring rate (N/mm)

g = gravitational constant = 9800 mm/s²

W = weight of the system (N)

The second formula is

$$T_{ABS} = \left[\frac{1 + (\eta r)^2}{(1 - r^2)^2 + (\eta r)^2} \right]^{1/2} \quad (8.16)$$

which reduces to

$$T_{\text{ABS}} = \frac{1}{r^2 - 1} \text{ for } r > \sqrt{2} \text{ and } \eta \approx 0 \quad (8.17)$$

where

- T_{ABS} = transmissibility of input vibration at f
- r = frequency ratio $= f/f_n$ (dimensionless)
- f = vibration input frequency (Hz)
- η = dimensionless loss factor, defined in Eq. (8.19)

Equation (8.16) for transmissibility is shown in graphical form in Fig. 8.12. Note that isolation of input vibrations begins at a frequency of roughly $f / f_n = \sqrt{2}$, above which T_{ABS} is less than 1.0. Also note that isolation at high frequencies will be decreased as the damping in the system increases. Finally, for elastomeric products the actual isolation at high frequencies will be slightly less than predicted by the classical spring damper analysis used to create Fig. 8.12 as a result of deviation from a single degree of freedom model. The actual isolation depends on the type of elastomer, the type and magnitude of input, the temperature, and the amount of damping present.

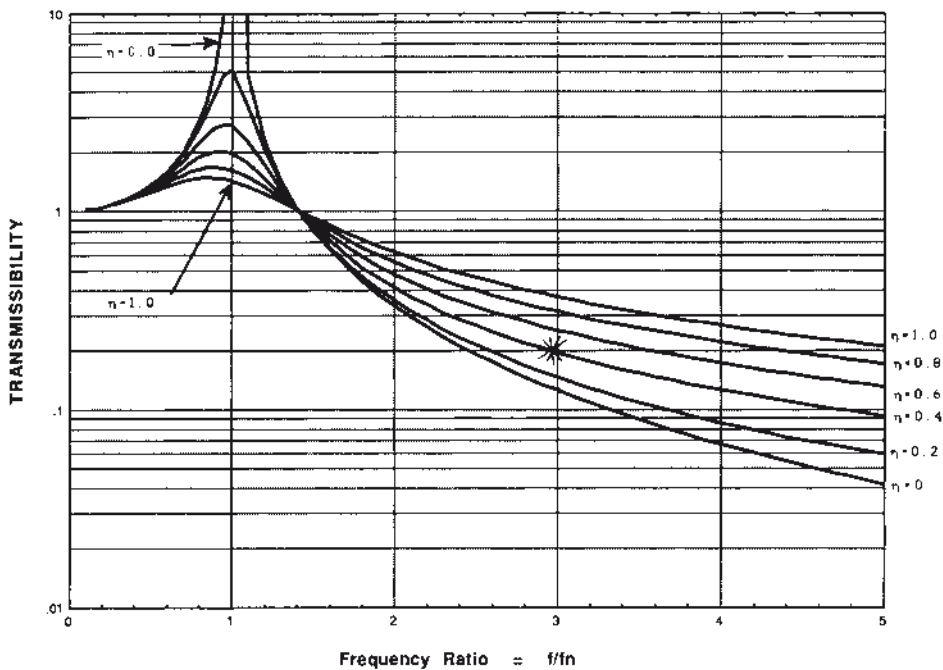


FIGURE 8.12 Transmissibility function

It is appropriate to note here that the elastomer shear modulus is actually a complex number G^* consisting of a real and complex part (see Chapter 4):

$$G^* = G' + i G'' \quad (8.18)$$

or

$$G^* = G' (1 + i \eta) \quad (8.19)$$

where η is called the loss factor ($\tan \delta$), given by $\eta = G''/G'$, G'' is the damping (loss) modulus (MPa), and G' is the dynamic elastic modulus (MPa).

8.3.2 Design Requirements

The basic equations from Section 8.1 and equations for vibration performance given above can be combined to solve product design problems. The starting point for any design is understanding the basic requirements. The most important factors are:

- Specifications for the equipment to be isolated (typically: weight, size, center of gravity, and inertias)
- Types of dynamic disturbance to be isolated (sinusoidal and random vibration, frequency and magnitude of inputs, shock inputs, etc.)
- Static loadings other than weight (e.g., a steady acceleration in many aircraft applications)
- Ambient environmental conditions (temperature ranges, humidity, ozone, exposure to oils and other fluids, etc.)
- Allowable system responses (what are the maximum forces the isolated equipment can withstand; what is the maximum system deflection allowed?)
- Desired service life

8.3.3 Sample Problems

Problem 8.3.3.1

A sensitive piece of electronic equipment is to be mounted on a platform that is subjected to a 0.4 mm SA sinusoidal vibration at 50 Hz. (SA means single amplitude, so the peak-to-peak motion will be 0.8 mm.) The input vibration (disturbance) is primarily in the vertical direction. The task is to design a vibration isolator that will provide 80% isolation while minimizing the clearances necessary to allow this level of isolation. The equipment has a mass of 5.5 kg and a weight of 53.9 N. Assume use of a very low damped elastomer with a loss factor $\eta = 0.02$ for this design.

To begin the design, solve Eq. (8.17) to find the system natural frequency that will provide $T_{\text{ABS}} = 0.2$, which is equivalent to 80% isolation. Equation (8.17) is acceptable because the material has a low loss factor and r exceeds $\sqrt{2}$ for isolation:

$$T_{\text{ABS}} = \frac{1}{f^2 / (f_n)^2 - 1} \quad (\text{solve for } f_n)$$

where

$$f = 50 \text{ Hz and } T_{\text{ABS}} = 0.2$$

$$(f_n)^2 = (50)^2 (0.2) / 1.2$$

$$f_n = 20.4 \text{ Hz}$$

Therefore, the isolation system must be designed to have a natural frequency of 20.4 Hz to isolate 80% of an input vibration of 50 Hz.

The isolation system dynamic spring rate can now be found using Eq. (8.15) and solving for K' :

$$K' = \frac{(f_n)^2 W}{248.4}$$

where

$$f_n = 20.4 \text{ Hz and } W = 53.9 \text{ N}$$

$$K' = (20.4)^2 (53.9) / 248.4$$

$$K' = 90.3 \text{ N/mm}$$

Now some assumptions and decisions about the isolation system need to be made to design the individual isolators. A key assumption is that the structural components of the system are infinitely rigid, so all deflections occur in the isolator. For stability, a four-isolator system will be used. Each isolator will be located symmetrically about the equipment center of gravity as shown in Fig. 8.13. Since the input is primarily in the vertical direction, the isolators will be oriented such that vertical deflections will cause shear deflections. To provide the desired isolation, a system dynamic spring rate of 90.3 N/mm is required. The dynamic spring rate for each isolator will then be 22.6 N/mm. The static load per isolator due to the equipment weight will be 13.5 N.

To find the appropriate isolator size, some design limits need to be applied. For a starting point, limit the static stress on the isolator to 0.069 N/mm². Knowing the static load of the equipment and applying a static stress limit, the minimum load area for the isolator can be determined using Eq. (8.3):

$$\sigma = \frac{F}{A}$$

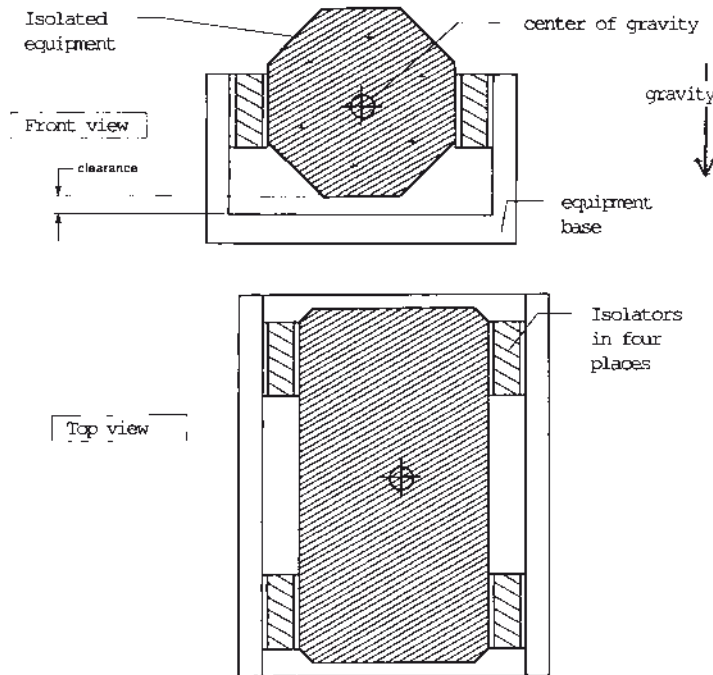


FIGURE 8.13 Four-mount system

where

$$\sigma = 0.069 \text{ N/mm}^2$$

$$F = 13.5 \text{ N}$$

so

$$A_{\min} = \frac{13.5}{0.069} = 196 \text{ mm}^2$$

From the specifications for the low-damping elastomer selected for this isolator, we find an available range of modulus from 0.345 to 1.38 N/mm^2 . From this range we select a modulus and use Eq. (8.2a) to determine the thickness of the elastomer required to get the desired dynamic spring rate:

$$K'_s = \frac{A G'}{t}$$

where $A = 196 \text{ mm}^2$, and we select $G' = 0.69 \text{ N/mm}^2$. Then

$$t = 196 \left(\frac{0.69}{22.6} \right) = 6 \text{ mm}$$

This completes the first iteration of the isolator design with the following results:

- Load area $A = 196 \text{ mm}$
- Thickness $t = 6 \text{ mm}$
- Dynamic shear modulus $G' = 0.69 \text{ N/mm}^2$
- Dynamic shear spring rate $K' = 22.6 \text{ N/mm}$

The isolation system uses four isolators in shear with a total system dynamic spring rate ($4 \times 22.6 = 90.3 \text{ N/mm}$). This provides a system natural frequency of 20.4 Hz for the specified weight of the isolated equipment. In turn, the equipment is isolated from 80% of the 50 Hz vertical sinusoidal disturbing vibration. Before the design is finalized, the static shear strain in the elastomer must be checked against design limits. This calls for the determination of the static spring rate of the isolator.

In general, the elastomer shear modulus is affected by frequency and strain. Therefore, the static spring rate K of an elastomeric isolator can be much softer than the dynamic spring rate K' . This difference tends to increase as the amount of damping in the elastomer increases. A dynamic-to-static ratio of 1.1 is reasonable for the low damped elastomer ($\eta = 0.02$) selected for this isolator.

Using the 1.1 factor, the static shear spring rate is given by:

$$\begin{aligned} K_s &= K'_s / 1.1 \text{ where } K'_s = 22.6 \text{ N/mm} \\ &= 20.5 \text{ N/mm} \end{aligned}$$

The static deflection is then given by Eq. (8.1):

$$K_s = \frac{F}{d}$$

where $K_s = 20.5 \text{ N/mm}$ and F (the static equipment weight) = 13.5 N. Thus:

$$d = \frac{13.5}{20.5} = 0.66 \text{ mm}$$

The static shear strain is then given by Eq. (8.4):

$$\varepsilon = \frac{d}{t}$$

where $d = 0.66 \text{ mm}$ and $t = 6 \text{ mm}$

$$\varepsilon = \frac{0.66}{6} = 0.11 = 11\%$$

A reasonable limit for static shear strain in this case is 20%, so the isolator design meets both static stress and strain criteria. The dynamic input vibration was given as 0.4 mm SA. The transmissibility of the isolation system at the disturbing frequency is 0.2 by design; therefore, the dynamic deflection transmitted to the equipment is

$$(0.2)(0.4) = 0.08 \text{ mm}$$

resulting in a dynamic strain of

$$\frac{0.08}{6} = 0.013 = 1.3\% \text{ at } 50 \text{ Hz}$$

The total clearance required to provide the desired isolation is:

$$0.66 \text{ mm static} + 0.08 \text{ dynamic} = 0.74 \text{ mm}$$

In practice, additional allowances need to be made for temperature, fatigue, and long-term drift effects when establishing adequate clearance.

A system with a natural frequency lower than 20.4 Hz would have provided even better isolation. However, the lower natural frequency means a lower spring rate, which results in increased static deflections, requiring additional clearance in the installation. Since one of the design goals was to minimize the required clearance, the 20.4 Hz system would be considered to be the best choice.

For the final step, assume that the isolator will be circular. The diameter required to provide 196 mm² load area is:

$$\left[\frac{(196)(4)}{\pi} \right]^{1/2} = 15.8 \text{ mm}$$

The resulting isolator design is shown in Fig. 8.14.

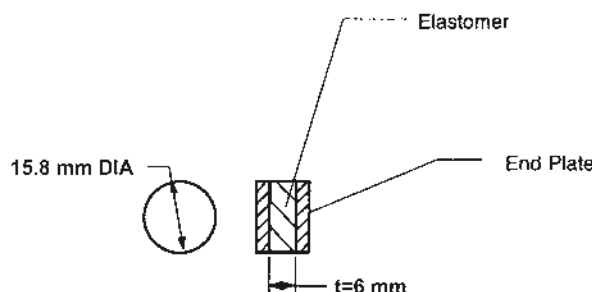


FIGURE 8.14 Final isolator design

Problem 8.3.3.2

Check the design of Problem 8.3.3.1 to see whether bending will impact the performance.

Section 8.2 demonstrates that bending may affect the shear spring rate, if the elastomer thickness-to-length ratio is greater than approx. 0.25. For the isolator of Problem 8.3.3.1, the length (= diameter) is 15.8 mm, and the thickness is 6 mm. Therefore the ratio is:

$$6 / 15.8 \approx 0.38$$

This means that bending may tend to reduce the actual spring rate of the isolator. From Eq. (8.5), the bending factor is calculated to be 0.96. Applying the bending correction factor has the following impact on the isolation system:

- Isolator dynamic spring rate becomes $(22.6)(0.96) = 21.7 \text{ N/mm}$
- System dynamic spring rate becomes $(4)(21.7) = 86.8 \text{ N/mm}$
- Solving Eq. (8.15) for the new system natural frequency yields

$$f_n = 15.8 \left(\frac{86.8}{53.9} \right)^{1/2} = 20 \text{ Hz}$$

The original design gave 20.4 Hz, so bending can be considered to have a negligible impact on performance, although some additional clearance space should be allowed.

Problem 8.3.3.3

For Problem 8.3.3.1, the only input was at 50 Hz. When the equipment and the isolation system were installed, it was found that vibrations in the 10–50 Hz range were also present and caused the equipment to malfunction. From additional measurements it was determined that the input vibration disturbance was 0.25 mm SA and that the equipment could withstand a maximum vibration disturbance of 0.9 mm in the 10–50 Hz frequency range. What design changes are needed to maintain 80% isolation of the 50 Hz disturbance while meeting the new requirements?

The original design used a very low damped elastomer with a high transmissibility at resonance. This was chosen to provide the desired isolation with the highest possible system natural frequency to limit the necessary clearance in the installation. Note in Fig. 8.12 that as the amount of damping increases (η increasing), the isolation at any given r value decreases. In other words, additional damping tends to decrease the isolation efficiency of the isolator. The trade-off is the transmissibility at resonance T_r . At resonance ($f = f_n$), Eq. (8.16) can be reduced to

$$T_r \approx \frac{G'}{G''} \quad (8.20)$$

For the material chosen in Problem 8.3.3.1, $\eta = 0.02 = G''/G'$, therefore

$$T_r = \frac{1}{0.02} = 50$$

The resulting vibration at the 20 Hz system natural frequency would be

$$(\text{input SA})(T_r) = (0.25 \text{ mm})(50) = 12.5 \text{ mm}$$

which is clearly much greater than the 0.9 mm the equipment can withstand. In fact, the 12.5 mm dynamic deflection produces 209% dynamic strain, which is much greater than the isolator designed in Problem 8.3.3.1 could withstand for an extended period of time. Typically, isolators are limited to less than 30–40% dynamic strain to minimize heat build-up and fatigue.

Given a 0.25 mm input and a 0.9 mm limit for transmitted vibration, the maximum allowable T_r becomes

$$T_{r \max} = \frac{0.9}{0.25} = 3.6$$

From a catalogue of available materials, an elastomer with $\eta = 0.4$ is chosen for the redesigned isolator, and

$$\eta = 0.4 \text{ is equivalent to } T_r = 2.5$$

The maximum transmitted vibration at resonance for this elastomer will be:

$$(\text{input SA})(T_r) = (0.25)(2.5) = 0.625 \text{ mm}$$

Having selected an elastomer with an appropriate loss factor to meet the requirement for maximum transmitted vibration at resonance, Fig. 8.12 can be used to find the frequency ratio required to provide 80% isolation of the 50 Hz disturbing vibration. The $\eta = 0.4$ curve intersects with the $T_{\text{ABS}} = 0.2$ line at $r = 2.95$:

$$r = 2.95 = \frac{f}{f_n}$$

where $f = 50 \text{ Hz}$

$$f_n = \frac{50}{2.95} = 16.9 \text{ Hz}$$

Repeating the same procedure used in Problem 8.3.3.1, the system dynamic spring rate, individual isolator spring rate, and isolator design parameters can be determined:

$$K' = \frac{(f_n)^2 W}{248.4}$$

where $f_n = 16.9$ Hz and $W = 53.9$ N

$$\begin{aligned} K' &= \frac{(16.9)^2 (53.9)}{248.4} \\ &= 62 \text{ N/mm} = \text{system dynamic spring rate} \\ \frac{62}{4} &= 15.5 \text{ N/mm} = \text{isolator dynamic spring rate} \end{aligned}$$

The static stress conditions are still the same, so

$$A_{\min} = 196 \text{ mm}^2 \text{ (from Problem 8.3.3.1)}$$

Assuming a dynamic modulus G' of 0.69 N/mm^2 ,

$$t = \frac{(196)(0.69)}{15.5} = 8.7 \text{ mm}$$

The dynamic strain at resonance is:

$$\begin{aligned} \varepsilon &= \frac{(\text{input SA})(T_r)}{t} \\ &= \frac{(0.25)(2.5)}{8.7} = 7\% \end{aligned}$$

which is acceptable.

The area has not changed, so the diameter of the isolator is 15.8 and the thickness-to-length ratio now becomes

$$\frac{8.7}{15.8} = 0.55$$

This factor can be reduced by maintaining the original thickness of 6 mm, to reduce any additional bending effects. In this case, the elastomer modulus must be changed to obtain the desired dynamic shear spring rate:

$$K' = \frac{A G'}{t}$$

where $t = 6 \text{ mm}$, $A = 196 \text{ mm}^2$, and $K'_s = 15.5 \text{ N/mm}$

$$G' = \frac{(15.5)(6)}{196}$$

$$= 0.47 \text{ N/mm}^2$$

A quick check of the materials specifications for the chosen elastomer shows that this modulus is available. The static shear deflection for the system will now be found as follows.

Assume:

$$\frac{K'}{K_s} \approx 1.4 \text{ for the elastomer chosen}$$

$$K_s \approx 15.5 / 1.4 = 11.1 \text{ N/mm}$$

$$d = \frac{F}{K_s} = \frac{13.5}{11.1} = 1.22 \text{ mm}$$

The resulting static shear strain on the elastomer will be

$$\varepsilon = \frac{1.22}{6} = 0.204 = 20.3\%$$

This is marginally acceptable for this application. Finally, the total deflection for the new system is

$$1.22 \text{ mm static} + 0.63 \text{ mm dynamic} = 1.85 \text{ mm}$$

Note that the dynamic deflection at 50 Hz (0.08 mm) is less than the dynamic deflection at resonance (0.63 mm). The larger of the two was used to determine the maximum clearance required.

In this case the new design requirements were able to be accommodated by changing the elastomer without changing any of the isolator geometry parameters. However, the installation had to be changed slightly to allow for the increased clearance required by the softer system. Had the system been softened any further, changes to the thickness and area would have been required to stay within reasonable static strain limits while keeping the necessary spring rate. Many further iterations of this problem could be performed by changing the input conditions or applying new temperature and/or environmental constraints. In the problem above, the size of the isolator was determined by the static design limits. In other cases, the size may be determined by the dynamic design limits on stress and strain. This is usually the case for isolators experiencing relatively high inputs and/or transmissibilities at resonance.

■ 8.4 Practical Design Guidelines

- Shear stress-strain performance can be assumed to be fairly linear up to 75 to 100% strain for rough sizing purposes.
- Tension and compression stress-strain performance can be assumed fairly linear up to 30% strain.
- Most product designs intentionally avoid using rubber in direct tension. Fatigue resistance and design safety requirements are usually best met by using rubber in compression and shear.
- A conservative starting point for isolator design is 0.069 N/mm^2 static stress. This minimizes potential creep for most lightly to moderately damped elastomers.
- Typical vibration isolators limit dynamic strains to 30 to 40% maximum to minimize fatigue wear and heat build-up.
- When designing within a range of available modulus for a given elastomer, it is best to stay away from both the softest and the stiffest available moduli. Approximations in the calculations and tolerances in the elastomer manufacturing process need to be allowed for. If a design uses the softest material available, and the part then turns out to be slightly too stiff, a costly design change is required to produce a softer part. If some room were allowed for changes in the original modulus selection, a softer part could be produced simply by using a lower modulus compound.
- To complete a design project involving dynamic conditions, you will need to know the dependence of modulus on frequency, strain amplitude, and temperature. In general, as damping in a material decreases, the dependence of modulus on frequency and strain amplitude also decreases.
- The relationship of dynamic to static modulus depends on the specific use conditions and the specific material's properties. Practically, static is assumed to mean a loading rate slower than one cycle per minute.
- For compression designs, stability generally becomes a concern when the overall elastomer thickness approaches the width or diameter of the component.

Tolerances:

In the calculations, assumptions and approximations are made about material properties, geometric factors, and loading. Examples include the effective loaded area for a tube form mounting, the effective compression modulus of the elastomer, and the assumption of infinitely rigid metal parts.

In manufacturing, tolerances in material properties and component geometry will cause variations in the actual performance of a design. Also, in testing a component, many variables exist that can significantly affect test results. Loading speed, test

fixture rigidity, deflection measurement, and operator/machine repeatability are some of the important factors.

Given the above causes of variability, it is not unusual to encounter differences between actual and calculated performance. However, as long as the assumptions in the calculation are not changed, empirical relationships can be developed between calculated performance and the results obtained using standardized tests. Most manufacturers have developed their own proprietary relationships of this kind and are able to predict actual product performance very closely using closed-form solutions like those presented in this book.

■ 8.5 Summary and Acknowledgments

This chapter presented a few specialized examples for designing elastomeric products. Resources containing additional examples and information are readily available from elastomeric product manufacturers. For example, [1] contains numerous examples and additional theory for vibration and shock isolation. For examples of seal design, hose design, and so on, the reader is referred to product catalogues for the major manufacturers in those industries.

For the problems presented herein, the design limits, procedures, and assumptions were based on the authors' practical design experience. The various values for elastomer modulus assumed in the problems were based on currently available materials.

Table 8.2 is presented to assist the reader in using both the SI and English systems of units.

TABLE 8.2 English to SI Conversion Factors

To convert from	To	Multiply by	Use for
psi	kPa or kN/m ²	6.895	Modulus
lb force	N	4.448	Force
in.	mm	25.4	Deflection
lb _f /in.	N/mm	0.175	Spring rate
$g = 9.8 \text{ m/s}^2 = 9800 \text{ mm/s}^2 = 386 \text{ in/s}^2$			

Thanks to three Lord Corporation colleagues, Jesse Depriest, Paul Bachmeyer and Don Prindle for their critical review of this chapter.

■ Nomenclature

A	= area
A_B	= bulge area
A_L	= load area
d	= deflection
d_c	= deflection, compression
d_s	= deflection, shear
E_b	= bulk modulus of elastomer
E_c	= compression modulus
E_t	= tension modulus
E_0	= Young's modulus
f	= input vibration frequency
f_n	= system natural frequency
F	= force
F_c	= force, compression
F_s	= force, shear
g	= acceleration due to gravity
G	= modulus (shear)
G^*	= complex modulus
G'	= dynamic modulus
G''	= damping modulus
I_b	= moment of inertia about bending material axis
K	= spring rate in general
K_c	= compression spring rate
K_s	= shear spring rate
K'_s	= dynamic spring shear rate
K_t	= tension spring rate
K_{tor}	= torsion spring rate
r	= frequency ratio
r_g	= radius of gyration
S	= shape factor

- t = thickness
 T_{ABS} = transmissibility
 W = weight
 ε = strain
 σ = stress
 ϕ = compression coefficient
 η = dynamic loss factor ($\tan \delta$)

■ References

- [1] P. R. Freakley and A. R. Payne, Theory and Practice of Engineering with Rubber, Applied Science Publishers, London, 1970.
- [2] A. N. Gent and E. A. Meinecke, "Compression, Bending and Shear of Bonded Rubber Blocks", *Polym. Eng. Sci.*, **10**(1), 48 (1970).
- [3] *Lord Kinematics Design Handbook*, Lord Corporation, Erie, PA, internal publication, 1971.
- [4] P. B. Lindley, "Engineering Design with Natural Rubber", Malayan Rubber Fund Board NR Technical Bulletin, Natural Rubber Producers' Research Association, London, 1974.
- [5] J. M. Horton, M. J. C. Glover and G. E. T upholme, *Rubber Chem. Technol.*, **73**, 69 (2000).
- [6] J. M. Horton, M. J. C. Glover and G. E. T upholme, *Rubber Chem. Technol.*, **73**, 253 (2000).
- [7] J. M. Horton, G. E. T upholme and M. J. C. Glover, *Rubber Chem. Technol.*, **79**, 233 (2006).
- [8] Lord Aerospace Products Design Catalog PC6116, Lord Corporation, Erie, PA, 1990.

■ Problems for Chapter 8

1. A tubeform mount is 50 mm long, has an elastomer outer radius of 10 mm and an inner radius of 3 mm. Assuming the part is as-molded, what is its shape factor? What is the radial stiffness if $G = 620$ kPa?
2. If the part described in Problem 1 is swaged 1 mm on a radius, what is the induced compression strain? What is the shape factor now? What is the radial stiffness?
3. A single-layer tube-form mount is required to deflect 10 degrees torsionally. To give the mount a long life, the shear strain is to be held below 30%. If 10 mm is available for the rubber outer diameter, how large can the inner diameter be?

4. A 500 mm diameter thrust bearing with a 20 mm elastomer wall thickness is compressed by a force of 10 kN. If the elastomer shear modulus is 1.03 MPa, what is the compression deflection?
5. If the bearing in Problem 4 consists of two rubber layers, each 10 mm thick, what is its deflection?
6. What feature is included in Fig. 8.5 to enhance the fatigue life of the component?
7. Estimate the static compression stiffness for the final design of the sample in Problem 8.3.3.3.
8. The elastomer used in Problem 8.3.3.3 had a shear modulus G' of 0.47 N/mm². The original material chosen has been taken off the market and the replacement material can only be had with G' in the range of 0.83 N/mm to 3.4 N/mm² and with a loss factor of 0.3 for $G' < 1.5$ N/mm².
 - (a) What is the impact on the performance, if the new material is substituted without changing the design?
 - (b) What design changes could be made to maintain the desired degree of isolation? For stability reasons and to limit rotational motion, the customer requires that we stay with the four-isolator system. Additionally, the customer does not want to change the installation but will allow some extra space for the isolators if needed.

■ Answers to Problems for Chapter 8

1. For this problem the as-molded tube-form will have the projected radial load area $A_L = 1.12 (d_o d_i)^{1/2} (L) = 613 \text{ mm}^2$.
Now $A_B = 2 \pi (d_o^2 - d_i^2)$. Thus, $A_B = 572 \text{ mm}^2$.
The shape factor $S = A_L / A_B = 1.07$ and the radial stiffness $K_R = A E_C / t$.
Thus, $K_R = 6.13 \times 10^{-4} (6000) / 0.007 = 525 \text{ N/m}$.
2. This problem deals with a higher performance version of Problem 1. The swaging induces pre-compression giving a higher radial stiffness up to a pre-compression relief point. Assume that the load area doubles.
Thus, $A = 1226 \text{ mm}^2$ and $K_R = 12.26 \times 10^{-4} (6000) / 0.006 = 1226 \text{ N/m}$.
(Note that the pre-compressed rubber wall thickness t of 6 mm is used.)
3. Shear strain = 0.3 = $\Delta / t = r_{\text{avg}} \theta / t = (5 + r_i) (10) (\pi / 180) / 2 (5 - r_i)$
Thus: $r_i = 2.75 \text{ mm}$; $d_i = 5.5 \text{ mm}$.

4. The shape factor $S = A_L / A_B = 0.196 / 0.031 = 6.32$

Thus, $E_c = 200 \text{ MPa}$.

Hence, $K_A = F / d = A E_c / t = 1.96 \text{ N/m}$, and:

$$d = F / K_A = 10000 / 1.96 \times 10^6 = 5.1 \text{ mm}.$$

5. In this case, the shape factor $S = 12.48$ and thus $E_c = 420 \text{ MPa}$.

Hence, $K_A = F / d = E A_c / t = 0.196 E_c = 8.23 \times 10^6 \text{ N/m}$ (for each layer).

K_A (total) = $4.12 \times 10^6 \text{ N/m}$, by adding the individual layers as two springs in series. Thus, $d = F / K_A$ (total) = 2.4 mm .

6. The edges of the elastomer have a radius. This radius reduces stress concentrations at the interface between the shims and elastomer. The trade-off is more difficult tool design and manufacturing procedures.

7. The final design was a round isolator with a thickness t of 6 mm, area A of 196 mm² and shear modulus G' of 0.47 N/mm.

The static shear modulus G , can be estimated using the dynamic to static ratio of 1.4. Hence, G (static) = $G' / 1.4 = 0.34 \text{ N/mm}^2$.

Then $K_c = E_c A / t$ from Eq.(8.6), and E_c can be estimated from Eq. (8.7) using $G = 340 \text{ kPa}$ and shape factor $S = 196 / \pi (15.8) = 3.95$.

$$\text{Thus, } E_c = 1060 [1 + (2)(0.9)(3.95)^2] = 30.83 \text{ MPa (or N/mm}^2\text{)}.$$

$$\text{Hence, } K_c = (30.83)(196) / 6 = 1.0 \text{ kN/mm}.$$

8. (a) Using the softest available modulus (0.83), f_n for the new system can be calculated using Eqs. (8.2a) and (8.15), or by using the square root of the ratio of new to old modulus:

$$f_n (\text{new}) = [f_n (\text{old})] [0.83 / 0.47]^{1/2} = 16.9 [1,33] = 22.5 \text{ Hz}$$

The transmitted vibration at resonance will be $(0.25 \text{ mm}) (1/0.3) = 0.83 \text{ mm}$, which meets the requirement to limit the amplitude of transmitted vibration to 0.9 mm maximum in the frequency range 10 to 50 Hz. The dynamic stress is $(27.1 \text{ N/mm}) (0.83 \text{ mm}) / (196 \text{ mm}^2) = 0.11 \text{ N/mm}^2$. This is within the acceptable range.

The isolation at 50 Hz is calculated using the new f_n of 22.5 Hz and Eq. (8.16). Figure 8.12 can also be used to find that the transmissibility at 50 Hz is 0.3. Therefore, the new material in the existing design provides only 70% isolation, not the 80% required.

- (b) Given that there is no softer material available and that the loss factor is fixed at 0.3, the r ratio must be increased to get more isolation. Recall from Eq. (8.16) $r = f/f_n$. From Fig. 8.12, r needs to be equal to or greater than 2.75.

This means f_n needs to be equal to or less than $50/2.75$ Hz, i.e., 18 Hz. To get to 18 Hz, the isolation system needs to be softened by a factor of $(18/22.5)^2 = 0.64$. The isolator stiffness in the present design is 27.1 N/mm and the four-isolator system has a stiffness of 108.4 N/mm. Therefore, the isolation system needs to be redesigned to have a stiffness no greater than $(0.64) (108.4) = 69$ N/mm.

For stability reasons and to limit rotational motion, the customer requires that we stay with the four-isolator system. Additionally, the customer does not want to change the installation, but will allow some extra space for the isolators if needed. Given this, the options are now limited to changing the isolator design. Based on Eq. (8.2a), the load area could be decreased and/or the thickness increased. Reducing the load area will increase the static stress above the design guideline of 0.069 N/mm. If we hold to this original limit, then the isolator thickness must become $6 \text{ mm}/0.64 = 9.4 \text{ mm}$ to reduce the system stiffness to 69 N/mm. The diameter of the isolator is still 15.8 mm, so the thickness to length ratio now becomes $9.4/15.8 = 0.59$. This indicates that a bending contribution to the deflection will further reduce the system stiffness, improving isolation. Given the low static and dynamic stresses and strains, a significant bending deflection will probably be acceptable in this design.

Perhaps the best design would be to increase the static stress in the isolator, redesign the shape to be rectangular and adjust the loaded area, rectangular dimensions and thickness to minimize the overall thickness increase without introducing additional bending. There are many possible combinations that would work.

Finally, the modulus typically changes with temperature, strain, and frequency. This requires that most designs be iterative in nature. Starting with an assumed value of modulus, the frequency f_n and strains are calculated and compared to the requirements. The assumptions are then refined and the process repeated until converging on a solution.

9a

Finite Element Analysis

Robert H. Finney

■ 9a.1 Introduction

A full discussion of finite element theory is available in many textbooks [1, 2] and will not be presented here. The basic concept of finite element analysis (FEA) will be presented, along with the terminology and examples, to provide the tools needed to determine if FEA can be applied and the confidence that the results are valid. There are many numerical methods for problem solving, but FEA is the most accurate, versatile, and comprehensive method for solving complex design problems. Most design handbooks contain equations for the solution of simple geometry problems. As the geometry becomes more complex, the techniques and assumptions used in an attempt to simplify the problem either produce an equation that is obviously inapplicable, or impossible for the design engineer to solve. FEA permits the analysis of these complex structures without the necessity of developing and applying complex equations. The primary aspect of FEA that must be understood and remembered is that FEA is a tool and only a tool. It is not magic and will only produce results that are as good as the input, including the skill of the analyst.

FEA of elastomers became a reality for the elastomer component design engineer in the early 1970's [3, 4] with commercial finite element programs such as MARC®. Since that time, additional FEA programs, such as ANSYS® and ABAQUS®, have incorporated the capability of analyzing elastomer-like materials. Verification of the FEA method has been done by the authors of the various finite element programs available. Personal verification may be accomplished by modelling and analyzing a problem to which one knows the answer from classical equations or from test results. Verification of linear analysis is usually easier than verification of non-linear analysis due to the limited availability of non-linear analytical solutions.

Key questions usually asked regarding finite element analysis of rubber components which will be addressed herein are:

1. How do I get the material properties and which material model do I use?
2. Should I do a linear or a non-linear analysis?
3. How do I evaluate the results?

4. Are the stress/strain values correct?
5. How do I apply the boundary conditions?
6. How much detail do I need in the model?
7. How do I generate the model?
8. Do I need a plane strain, plane stress, axi-symmetric, or a three dimensional model?
9. Do I need to model the complete component?
10. Can I determine the fatigue life of the rubber component directly from the finite element model?
11. Why are my finite element calculated spring rates not correlating with my measured data?
12. What element should I use?

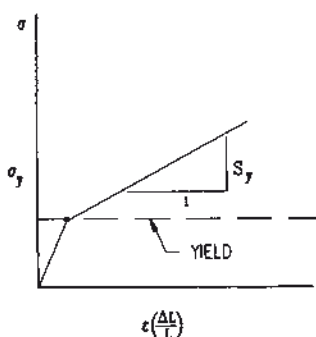
The symbols used in this chapter are:

- A = original area (mm^2)
 A_f = final area (mm^2)
 d = deflection (mm)
 E = Young's modulus (tensile) (MPa)
 E_c = apparent compression modulus (MPa)
 F = applied force (N)
 G = shear modulus (MPa)
 H_A = Shore A hardness
 K = bulk modulus (MPa)
 L = original length (mm)
 L_f = final length (mm)
 t = thickness (mm)
 w = width (mm)
 ΔL = change in original length (mm)
 ε = strain (mm/mm)
 ε_g = Green-Lagrange strain (mm/mm)
 ε_{\log} = logarithmic (true) strain (mm/mm)
 λ = stretch ratio ($1 + \Delta L/L$)
 λ_n = stretch ratio in "n" direction
 ν = Poisson's ratio
 σ = stress on original area - engineering stress (MPa)
 σ_n = engineering stress in "n" direction (MPa)
 σ_t = true stress (MPa)

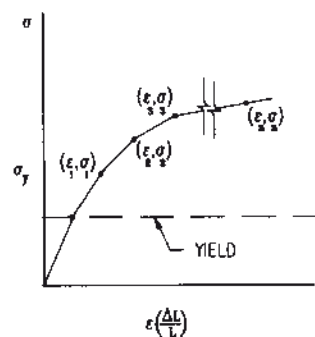
■ 9a.2 Material Specification

9a.2.1 Metal

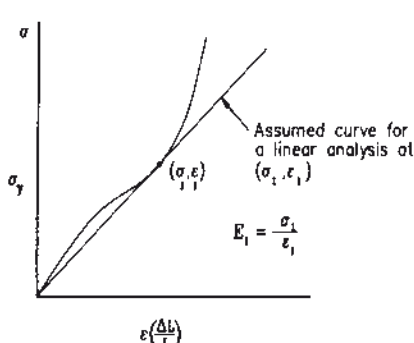
The key feature that sets FEA of elastomers apart from FEA of metal is the specification of material properties. Metal can generally be considered a Hookean material with a linear stress/strain relationship over its useable stress/strain range. Values for Young's modulus and Poisson's ratio for the metal are readily available in handbooks and are generally well-known by the analyst. They are common knowledge. If the loading on the metal is sufficient to cause yielding, a non-linear analysis of the metal component can generally be made by either specifying the stress-strain curve of the metal in terms of a bi-linear curve (Fig. 9a.1a) or using a nonlinear strain hardening rule (Fig. 9a.1b).



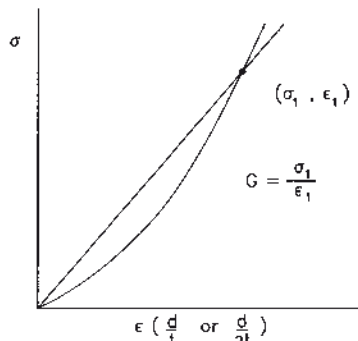
(a) Bi-Linear – Metal Tensile



(b) Non Linear Strain Hardening – Metal Tensile



(c) ASTM 412 Elastomer Tensile Curve



(d) Dual or Quad-lap Elastomer Shear Curve

FIGURE 9a.1 Typical stress-strain curves

9a.2.2 Elastomers

9a.2.2.1 Linear

Since Poisson's ratio for elastomers is between 0.499 and 0.5, the elements used in FEA need to be reformulated to accommodate this high value of Poisson's ratio. This is usually accomplished by utilizing an approach developed by Herrmann and Toms [5] and Herrmann [6], by introducing a new variational principle that includes another degree of freedom called the "mean pressure function". Reference [4] contains a discussion of its application to elastomer FEA programs.

The specification of material properties for the linear analysis of an elastomer component involves the same basic elasticity equations as for metal, therefore:

$$E = \frac{(9K + G)}{(3K + G)} \quad (9a.1)$$

$$\nu = \frac{(3K - 2G)}{[2(3K + G)]} \quad (9a.2)$$

$$K = \frac{(E)}{[3(1 - 2\nu)]} \quad (9a.3)$$

$$G = \frac{(E)}{[2(1 + \nu)]} \quad (9a.4)$$

Equations (9a.3) and (9a.4) are variations of Eqs. (9a.1) and (9a.2). It can be seen in Eq. (9a.3) that if Poisson's ratio is assumed to be 0.5, corresponding to an incompressible material, then the bulk modulus goes to infinity. This assumption also dictates that Young's modulus is 3 times the shear modulus $E = 3G$ (Eq. (9a.4)). Most handbooks make the assumption that Poisson's ratio is 0.5 and $E = 3G$. This is generally not exactly true for engineering elastomers, but it makes analytical solutions possible.

For steel, Young's modulus is generally 2×10^5 MPa, Poisson's ratio can be taken as 0.3, and there is usually a distinct linear stress-strain range. For elastomers, each formulation is different and generally there is only a small linear region. An ASTM 412 specimen tested in uni-axial tension will give a tensile stress-strain curve (Fig. 9a.1c) with an initial slope from which Young's modulus can be obtained. The two basic problems are that the data obtained from standard ASTM 412 testing

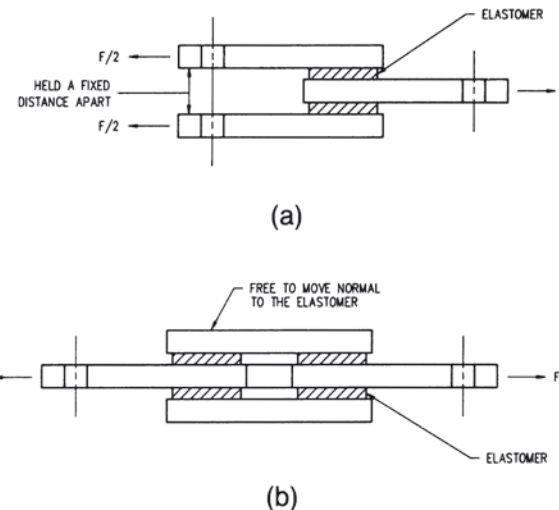


FIGURE 9a.2 (a) Dual-lap shear specimen, ASTM D 945, and (b) quad-lap shear specimen

generally are very inaccurate at lower strain levels, and it must be decided where to take the data on this non-linear curve. (NOTE: If a particular “modulus” is quoted by a supplier from an ASTM 412 test, question the use of the term. The “modulus” quoted will probably be the stress at a specified strain rather than Young’s modulus, which is the stress divided by the strain in the linear region, at small strains.)

The recommended approach is to test either a dual lap (Fig. 9a.2a) or a quad lap (Fig. 9a.2b) simple shear specimen. The dual lap specimen is easier to mold, but it tends to introduce some rotational strain that does not occur in the quad lap specimen, where the outer members are permitted to float. The resulting curve may be plotted as stress versus strain (Fig. 9a.1d), obtained from the measured load-deflection data as follows:

Dual-Lap Specimen

$$\epsilon = \frac{d}{t} \quad (9a.5a)$$

$$\sigma = \frac{F}{(2 L w)} \quad (9a.6a)$$

$$G = \frac{(F t)}{(2 L w d)} \quad (9a.7a)$$

Quad-Lap Specimen

$$\varepsilon = \frac{d}{(2t)} \quad (9a.5b)$$

$$\sigma = \frac{F}{(2Lw)} \quad (9a.6b)$$

$$G = \frac{(FT)}{(Lwd)} \quad (9a.7b)$$

The effective shear modulus at any point on the curve is the stress divided by the strain:

$$G = \frac{\text{stress}}{\text{strain}} \quad (9a.8)$$

If a linear FEA is to be performed, it is recommended that the shear modulus be taken in the strain region of interest and that the bulk modulus be assumed to be 1400 MPa, if the bulk modulus is unknown. This assumption will only be important, if the elastomer is highly constrained in the compression mode. If better correlation with the compression spring rate is desired, manufacture a compression disk and measure the compression spring rate. Then model the compression disk in FEA and adjust the bulk modulus until correlation is obtained in the desired region of the compression curve. This will be as close as can be obtained with a linear analysis.

Remember, when you select a point on the shear stress-strain curve to calculate the shear modulus, you are assuming during the linear analysis that the stress-strain curve is a straight line as shown in Fig. 9a.1d.

In the design of laminated bearings for use in helicopter blade retention systems, for example, the nominal steady-state design level of simple shear strain is generally 25–30%. Therefore, the shear modulus used was taken at 25% strain, with the assumption that the bulk modulus was 1400 MPa. These assumptions correlated well with measured shear and compression spring rate results.

The effect of the assumptions regarding bulk modulus and Poisson's ratio are illustrated in Table 9a.1 and Fig. 9a.3 [7]. Each of the materials listed in Table 9a.1 has basically the same shear and Young's modulus, with minor differences due to the bulk modulus or Poisson's ratio used. Material A (Lindley's curve) was obtained from [8] and is normally used in closed-form calculations. Material B is essentially the same material with the shear and bulk modulus assumed and the Poisson's ratio and Young's modulus calculated. Material C makes the favorite assumption that Poisson's ratio is 0.5 and Young's modulus is as shown. Material D makes

another favorite assumption that Poisson's ratio is 0.495 in an attempt to "trick" finite element programs not suitable for analyzing elastomers to accept the nearly incompressible material. The noted Young's modulus was also assumed.

TABLE 9a.1 Material Properties

Material	Young's modulus (MPa)	Shear modulus (MPa)	Bulk modulus (GPa)	Poisson's ratio
A	4.342 (u)	1.448	1.124 (u)	0.499356
B	4.342 (u)	1.448	1.064	0.49932 (u)
C	4.342 (u)	1.447	infinity	0.5 (u)
D	4.342 (u)	1.452	1.447	0.495 (u)

(u) = used in the calculations and/or input into finite element analysis

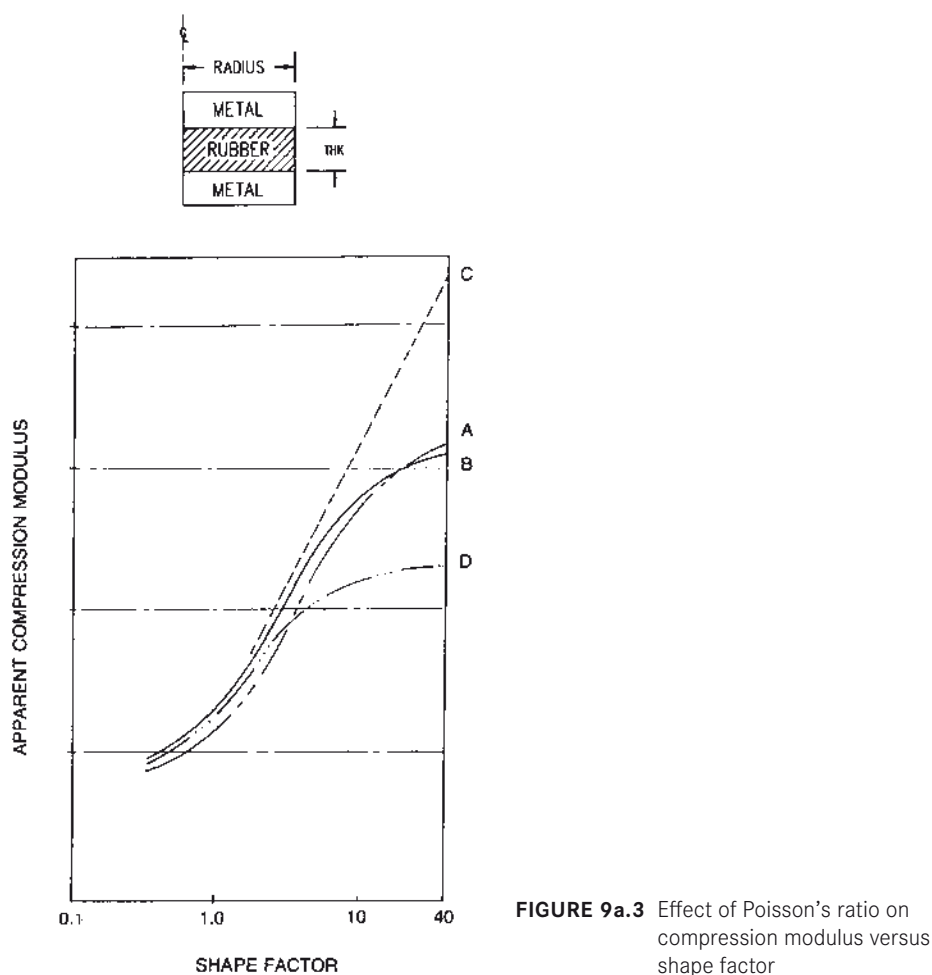


FIGURE 9a.3 Effect of Poisson's ratio on compression modulus versus shape factor

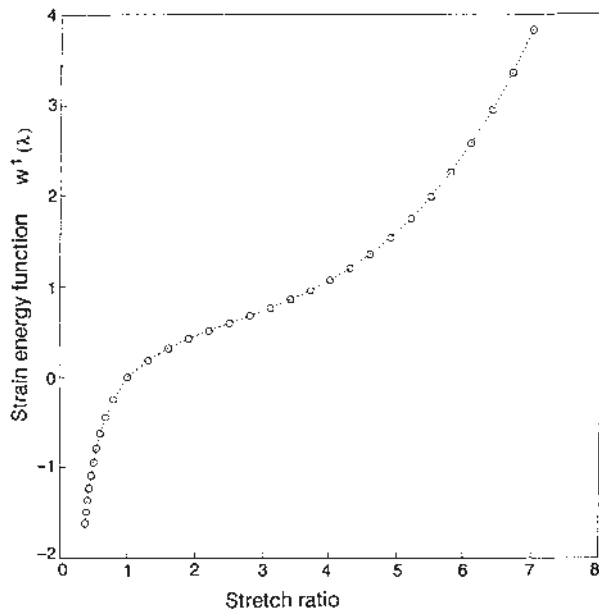


FIGURE 9a.4 Peng plot [$W'(\lambda)$ in MPa]

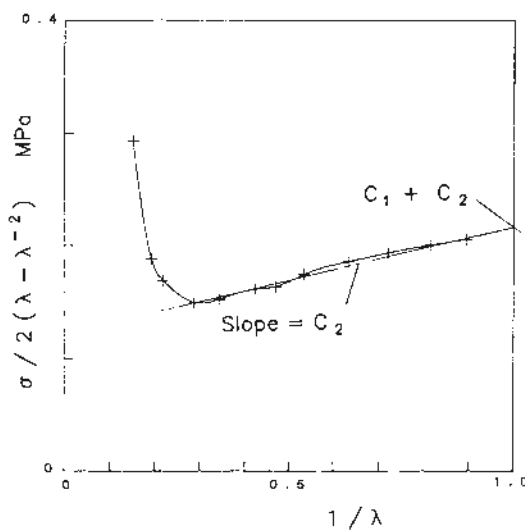


FIGURE 9a.5 Mooney-Rivlin plot

Figure 9a.3 shows that, if the shape factor is below 2.5, it does not matter what value is used for the bulk modulus or Poisson's ratio. Lindley's curve was developed from measured data and material B (normal FEA linear material properties) follows the curve very closely. Material C ($\nu = 0.5$) shows a significant increase in the apparent

compression modulus above a shape factor of 2.5 which will translate into lower strains for a given compression load. Material D ($\nu = 0.495$) shows a significantly lower apparent compression modulus above a shape factor of 2.5. This will translate into higher strains for a given compression load.

9a.2.2.2 Non-Linear

9a.2.2.2.1 Non-Linear Characteristics

“Force equals the spring rate times the deflection” is one of the first equations an engineer meets. This equation is valid as long as the object remains linearly elastic. If one deflects the component twice as much, the force increases twice as much. What if the structure yields, or if large displacements occur, or if the material for the spring has a non-linear stress-strain curve? You may have a non-linear problem and not even know it.

There are three major types of non-linearity:

1. A geometric non-linearity due to large deformations or snap-through buckling.
2. A material non-linearity due to large strains, plasticity, creep, or viscoelasticity.
3. A boundary non-linearity, such as the opening/closing of gaps, contact surfaces, and follower forces.

There are also combinations of any of these non-linear behaviors. To locate evidence of possible non-linear behavior, look for:

1. Permanent deformations and any gross changes in geometry;
2. Cracks, necking, or thinning;
3. Crippling, buckling;
4. Stress-strain values which exceed the elastic limits of the material.

9a.2.2.2.2 Non-Linear Material Models

The specification of non-linear material properties for elastomers is difficult. Several constitutive theories for large elastic deformations based on strain energy density functions have been developed for hyperelastic materials [9–17]. These theories, coupled with FEA, can be used effectively by design engineers to analyze and design elastomer products operating under highly deformed states. These constitutive equations are in two distinct categories. The first assumes that the strain energy density is a polynomial function of the principal strain invariants. In the case of incompressible materials, this material model is commonly referred to as a Rivlin material. If only first-order terms are used, the model is referred to as a Mooney-Rivlin material. In the second category it is assumed that the strain energy density is a separable function of the three principal stretches. Ogden, Peng and Peng-Landel material models are examples in this category.

The basic question is “Which material model should be used?” Both Gent [18] and Yeoh [19] have noted that high order strain energy functions are of little practical value because rubbery materials are not sufficiently reproducible to allow one to evaluate a large number of coefficients with any accuracy. Therefore, the extra terms only do a good job in fitting experimental errors. The Mooney-Rivlin model remains the most widely used strain energy function in FEA and should be the first choice due to its simplicity and robustness, even with its well-known inaccuracies. A Mooney-Rivlin model with a first coefficient equal to one-half of the shear modulus and a second coefficient equal to zero is called neo-Hookean. This material model exhibits a constant shear modulus and gives good correlation with experimental data up to 40% strain in uni-axial tension and up to 90% in simple shear.

A two-coefficient Mooney-Rivlin model shows good agreement with tensile test data up to 100% strain, but it has been found inadequate in describing the compression mode of deformation. It also fails to account for the stiffening of the material at large strains.

A three-term, or higher order, Mooney-Rivlin model accounts for a non-constant shear modulus. However, caution needs to be exercised on inclusion of higher order terms to fit the data, since this may result in unstable energy functions yielding non-physical results outside the range of the experimental data. The Yeoh model differs from other higher-order Rivlin models in that it depends on the first strain invariant only. This model has been demonstrated to fit various modes of deformation using data from a uniaxial tension test only. This leads to reduced requirements on material testing. Caution needs to be exercised when applying this model at low strains [20].

The Ogden material model gives good correlation with test data in simple tension up to 700%. It also accommodates non-constant shear modulus and slightly compressible material behavior. It has been successfully applied to the analysis of O-rings, seals, and other industrial products.

A comparison of the performance of various material models using the Treloar [21] material test data may be found in reference [22].

9a.2.2.2.3 Obtaining Material Data

The problem facing the analyst is how to obtain the data necessary to calculate the coefficients required for the material models [34]. The following tests will yield data that can be used to obtain the coefficients. Which tests are run will depend on what material model used, how “accurate” you want your material model to be and how much time and funding is available.

The simplest and most widely used test is a uni-axial tension test which utilizes an ASTM 412 Die C dumbbell specimen (Fig. 9a.6a) with a crosshead speed of approximately 5 mm/minute (0.2 in/min) to obtain an engineering stress-strain curve.

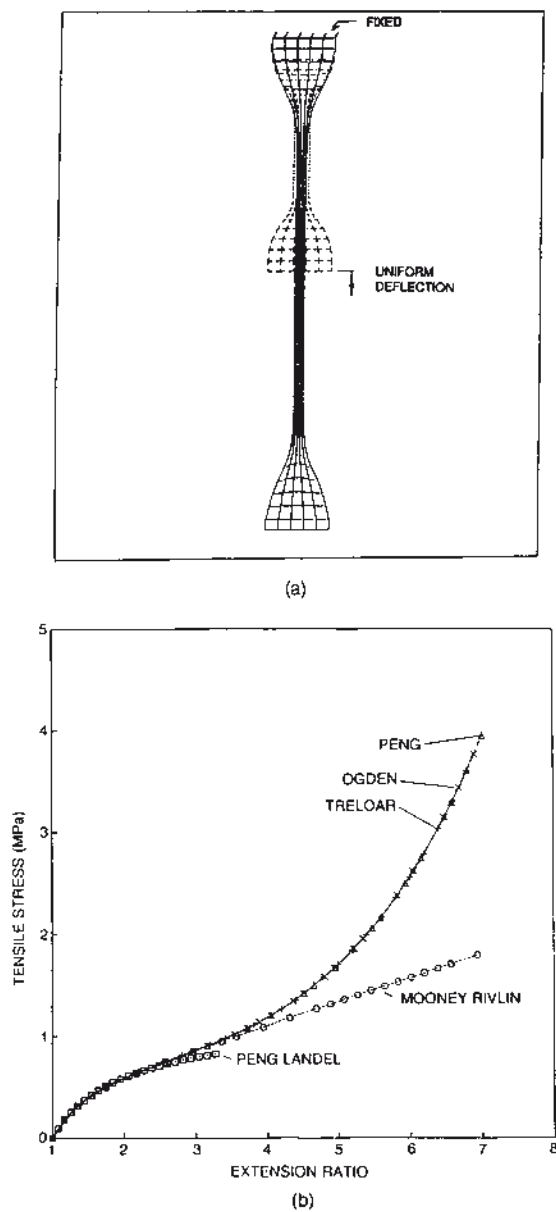


FIGURE 9a.6 Comparison of Treloar data with material models: uni-axial tensile.

The stress state is:

$$\sigma_1 = \sigma = \frac{F}{A} \quad \sigma_2 = \sigma_3 = 0 \quad (9a.9)$$

The deformation state is:

$$\lambda_1 = \lambda = \frac{L_f}{L} \quad \lambda_2 = \lambda_3 = \frac{1}{\lambda^{1/2}} \quad (9a.10)$$

A uni-axial compression test utilizes a specimen approximately 17.8 mm (0.7 in) diameter by 25.4 mm (1.0 in) thick with a cross-head speed of approximately 5 mm/minute (0.2 in/min) with the specimen contact surfaces lubricated.

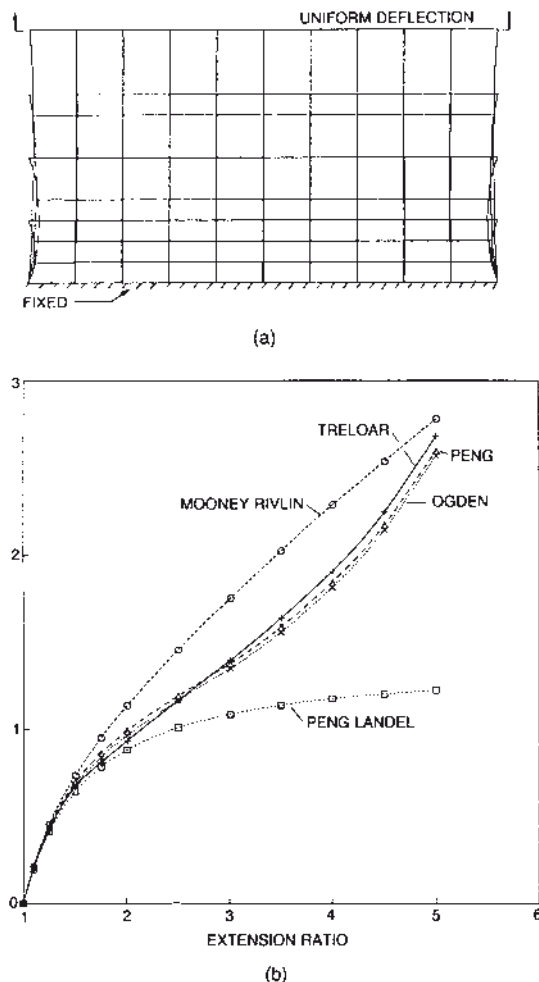


FIGURE 9a.7 Comparison of Treloar data with material models: pure shear

Obviously, this test cannot be taken to 100% compression strain. It is equivalent to the uni-axial tension test, i.e., the stress and deformation state is the same. No ASTM specimen is defined.

A bi-axial test utilizes a specimen approximately 122 mm (4.8 in) square by 1.25 mm (0.049 in) thick and a cross-head speed of approximately 5 mm/minute (0.2 in/mm). This test uses a special fixture which is capable of applying a uniform stretch in two perpendicular directions simultaneously. It is very difficult to run on a repeatable and consistent basis and is somewhat research oriented. One obtains an engineering stress-strain curve by measuring the strain within a defined center portion of the specimen and assuming that the measured force acts over the full cross section. A second method is to take a rubber tube with controlled thickness and inflate it while deflecting it axially at a rate that produces the same strain on the circumference as in the axial direction. The third method is to inflate a flat sheet of rubber (Fig. 9a.8a) and measure the strain along the spherical surface and calculate the stress based on the applied pressure.

The stress state is:

$$\sigma_1 = \sigma_2 = \sigma \quad \sigma_3 = 0 \quad (9a.11)$$

The deformation state is:

$$\lambda_1 = \lambda_2 = \lambda \quad \lambda_3 = \frac{1}{\lambda^2} \quad (9a.12)$$

A planar (pure) shear test utilizes a specimen (Fig. 9a.7a) approximately 76.2 mm (3.0 in) wide by 1.25 mm (0.05 in) thick by 12.7 mm high (0.5 in) using special grips at a cross head speed of approximately 5 mm/minute (0.2 in/min). In an absolutely pure shear test the free sides of this specimen would not neck inward as the restrained sides are pulled in tension.

A simple shear test utilizes either the dual-lap or the quad-lap shear specimens shown in Fig. 9a.2 with a cross-head speed of approximately 5 mm/minute (0.2 in/min). The dual lap specimen is used in the tire industry for low strain testing and the quad lap specimen is used in the bearing industry.

The deformation state is:

$$\lambda_1 = \lambda \quad \lambda_2 = \frac{1}{\lambda} \quad \lambda_3 = 1 \quad (9a.13)$$

Note that the procedures for conducting the above tests are quite general since there are no industry defined test procedures such as ASTM specifications. The analyst needs to know exactly how the test data was obtained since entirely different proce-

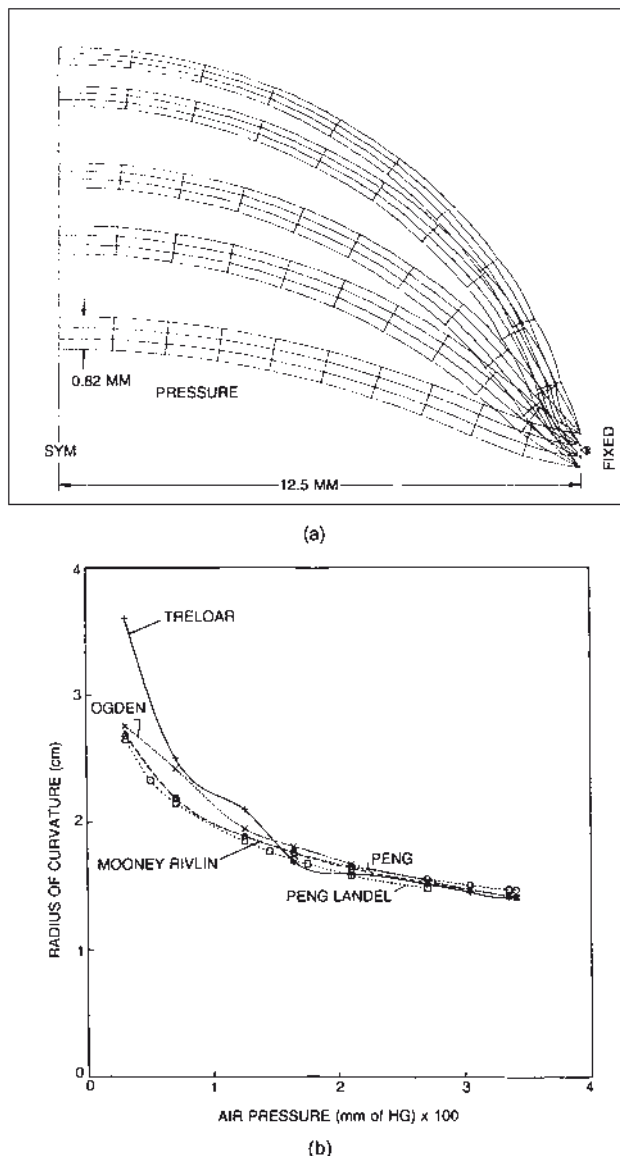


FIGURE 9a.8 Comparison of Treloar data with material models: bi-axial

dures may have been used for each of the tests. One test may have applied several cycles of maximum strain to the specimen before recording the data, the next test may have obtained data on the first cycle and a third may have recorded each data point after the specimen was permitted to relax. If the specimen was pre-strained prior to obtaining the data, be certain that the applied level of pre-strain was not sufficient to cause irreversible damage to the specimen.

The analyst cannot obtain test data in the same manner as the developer of the constitutive equation, because the majority of researchers have used material data published by Treloar [21] in 1944. Treloar describes his specimen and provides the data, but does not fully describe the test procedures used. Based on the high levels of strain for the reported data, it is probable that the data was obtained from the first cycle. It is well known that the stress-strain curve for elastomers does not stabilize until at least the 3rd cycle, with a significant change in the stress/strain curve from the initial cycle for most engineering compounds.

9a.2.2.4 Obtaining the Coefficients

The next problem facing the design engineer is how to develop the material coefficients (from the test data) needed in finite element programs that will accept them. Except for the Mooney-Rivlin material, the development of these constants is beyond the scope of this chapter. A methodology of how to develop the material input specifications for other material models can be found in [22]. Some of the non-linear examples presented in this chapter will use the following material specifications developed previously [22], based on test data published by Treloar [21]. The tests consisted of a two dimensional (bi-axial) extension test, a simple elongation test, and a pure shear test.

- Ogden: $C_1 = 0.6180 \text{ MPa}$ $B_1 = 1.3$
 $C_2 = 0.001177 \text{ MPa}$ $B_2 = 5.0$
 $C_3 = -0.009811 \text{ MPa}$ $B_3 = -2.0$
- Mooney-Rivlin: $C_1 = 0.1151 \text{ MPa}$ $C_2 = 0.1013 \text{ MPa}$
- Peng-Landel: 0.64 MPa at 116% strain ($E = 0.5517 \text{ MPa}$)
- Peng: Plot of strain energy function $W(\lambda)$ versus (λ) plot shown in Fig. 9a.4

If you have material test data, the easiest way to obtain the coefficients is to use the routines normally supplied by the commercially available FEA programs. These programs usually require the analyst to input the test data and the material coefficients are calculated and automatically placed in the material data segment of the FEA input data. The following precautions need to be taken:

1. If a two-coefficient Mooney-Rivlin model is going to be used, the second coefficient cannot be negative. Some programs do not check for this and will attempt to use a negative coefficient;
2. Use a FEA program that will provide curves (e.g., Fig. 9a.6b) which show how the material model using the calculated coefficients will act in each of the loading modes. Therefore, if only uni-axial tensile data was available and you want to use an Ogden material model, you can make sure that the material model does not exhibit unrealistic characteristics in bi-axial or pure shear loading before the FEA model is run.

3. If a high-order material model is used, check to make sure that it does not exhibit characteristics that are unrealistic beyond the limits of the inputted data.

9a.2.2.2.5 Mooney-Rivlin Material Coefficients

The Mooney-Rivlin strain energy function is the most widely used constitutive relationship for the non-linear stress analysis of elastomers. It is also widely misunderstood. For the special case of uni-axial tension of a Mooney-Rivlin material the stress-strain equation can be expressed as:

$$\sigma = 2(\lambda - \lambda^{-2})[C_1 + C_2(\lambda^{-1})] \quad (9a.14)$$

This equation can be plotted as $\sigma [2(\lambda - \lambda^{-2})]$ against $1/\lambda$, as shown in Fig. 9a.5. The intercept at $1/\lambda = 1$ gives $C_1 + C_2$ and C_2 = slope of the line. The data are from Treloar [21]. It is important to note that a true Mooney-Rivlin material will give a straight line, not the non-linear plot shown. Most elastomers do not give a straight line plot. Therefore, when you use Mooney-Rivlin coefficients in a finite element program, you are assuming that the data fall on a straight line as illustrated in Fig. 9a.5. The initial shear modulus is related to the material constants by: $G = 2(C_1 + C_2)$. If the material is assumed to be incompressible then the initial tensile modulus is given by: $E = 6(C_1 + C_2)$ or, for a compressible material, $E = (9KG)/(3K + G)$.

There are several “quick and dirty” ways to obtain Mooney-Rivlin coefficients without conducting expensive testing, or curve-fitting the data. In many instances, the application of one of these methods is just as good, if not better, than using a more “accurate” method. These methods are based on the fact that two times the sum of the two Mooney-Rivlin material coefficients [$2(C_1 + C_2)$] equals the initial shear modulus (G) and the value of Young’s modulus is approximately three times the shear modulus:

1. Record a durometer reading H_A and convert it to a Young’s modulus using $E(\text{MPa}) = (15.75 + 2.15 H_A)/(100 - H_A)$ and divide E by 6 to obtain C_1 . Specify $C_2 = 0$ to obtain a neo-Hookean material model [23].

Justification: The batch-to-batch variation for rubber compounds can be significant. If the acceptable hardness range of a typical elastomer is 70 ± 5 Shore A (H_A), the variation of Young’s modulus (E) is from 4.48 MPa to 7.03 MPa (650 psi to 1020 psi), i.e., 5.76 ± 1.28 MPa. This is a $\pm 22\%$ variation in the material modulus.

2. Record a simple shear stress/strain curve from a lap shear, or dual lap shear specimen and pick a point on the curve where the component operates to obtain a shear modulus. Divide the shear modulus by 2 to obtain C_1 and make $C_2 = 0$ to define a neo-Hookean material model [33].
3. Obtain data from a standard ASTM 412 uniaxial tension test, estimate the tensile modulus (E) from the curve. Calculate C_1 as noted in (1) above.

4. If the analyst only has a value for C_1 and wants to include a non-zero value for C_2 , the following can be used as a “best guess” method [20]. Set $C_2 = 0.25 C_1$ and solve the following equation for C_1 :

$$6(C_1 + C_2) = E, \text{ therefore, } 6(C_1 + 0.25 C_1) = E \text{ and } C_1 = E / (6 \times 1.25)$$

9a.2.3 Elastomer Material Model Correlation

The choice of material model is usually not critical for most applications as long as the rubber component is used within normal stress-strain levels. This is also true when FEA is being used as a comparative tool. If the strain level for the second model is 50% less than for the first model, the second model is obviously a better design. “How well do these material models work in finite element programs?” One way of illustrating this is to model the test specimen used to generate the test data. Analyze this model using the loading conditions applied during the test to obtain the load-deflection or stress-strain curve. Then compare the analytical results with test results. The following examples use the Treloar test specimens [21] with material coefficients obtained from Treloar’s data. Additional data concerning this comparison can be obtained from Hermann’s paper [6].

9a.2.3.1 ASTM 412 Tensile Correlation

An ASTM 412 uni-axial tensile specimen was modelled, as shown in Fig. 9a.6a, with the lower edge of the model fixed to simulate the lower grip in the test machine. The upper edge of the model was fixed in the direction parallel to the edge and deflected normal to the edge to simulate the upper grip moving. The analysis was done in plane stress in a non-linear mode. The resulting plots of stress versus extension ratio for the four material models are shown overlaid on the Treloar test data in Fig. 9a.6b. The Ogden and Peng material models match the experimental data, as they should, because the coefficients and the $W'(\lambda)$ terms were derived to match the Treloar data. The Mooney-Rivlin material model matches the experimental data up to approximately 225% tensile strain and then diverges. The Peng-Landel material model correlates with the experimental data up to approximately 150% tensile strain, where it starts to diverge. After this, it is difficult to maintain convergence.

The Mooney-Rivlin material model shows good correlation to as high as 225% primarily because of the large range of linearity in the plot shown in Fig. 9a.5. The material Treloar tested was a lightly loaded stock. Normal engineering elastomeric materials generally give a U-shaped plot. This usually means that only a few points on the test data curve will define the straight line drawn through the data to obtain C_1 and C_2 . The correlation will then only be good over a small portion of the test data curve.

9a.2.3.2 Pure Shear Correlation

A pure shear specimen identical to the specimen used by Treloar was modelled as shown in Fig. 9a.7a with the undeformed model overlaying the deformed model. If the specimen used was deformed exactly in pure shear, the sides would not curve inward when it was pulled, and lines drawn vertically before pulling would remain vertical and the same distance apart. Treloar's published data shows that the edges curved slightly inward as shown in the finite element model. Figure 9a.7b is a comparison of tensile stress versus extension ratio for the experimental data contained in Treloar's paper with finite element results for the four material models. The Ogden and Peng material models follow the experimental data well, within experimental error. The Mooney-Rivlin material model follows the experimental data up to 25% tensile strain and then deviates to the high side. The Peng-Landel material model shows correlation up to approximately 75% tensile strain, when the tensile stress becomes significantly less than the experimental values.

9a.2.3.3 Bi-Axial Correlation

To obtain two-dimensional extension, Treloar used a specimen 25 mm in diameter and 0.82 mm thick as shown in Figure 9a.8a. The circumference was clamped and air pressure was employed to inflate the sheet. Treloar determined the radius of curvature of the inflated sheet by taking measurements at set points on the sheet versus applied pressure. The potential for error at low extensions is relatively high, as is evident in Fig. 9a.8b. Figure 9a.8a shows the FEA model, the boundary conditions, and the deformed plot at four different pressures. Figure 9a.8b contains a plot of the experimental data from Treloar and the FEA results as radius of curvature versus air pressure. The Ogden material model shows the best correlation, with all of the material models showing good correlation at higher pressures.

9a.2.3.4 Simple Shear Correlation

Even though Treloar did not publish simple shear data for the material used in the previous examples, it is interesting to look at the shear stress-strain curves for the various material models. The finite element model used was a dual-lap shear specimen (Fig. 9a.2a). The resulting curves are presented in Fig. 9a.9. The Ogden material model provided a curve whose shape is consistent with normal test data. Peng-Landel (Peng-L) provided a lower shear modulus and Mooney-Rivlin provided a higher shear modulus. Neither of the two curves indicated that they would start to stiffen with strain. The isotropic reformulated element, which uses the same material property specification as the linear finite element model, was very close to the Mooney-Rivlin initial modulus.

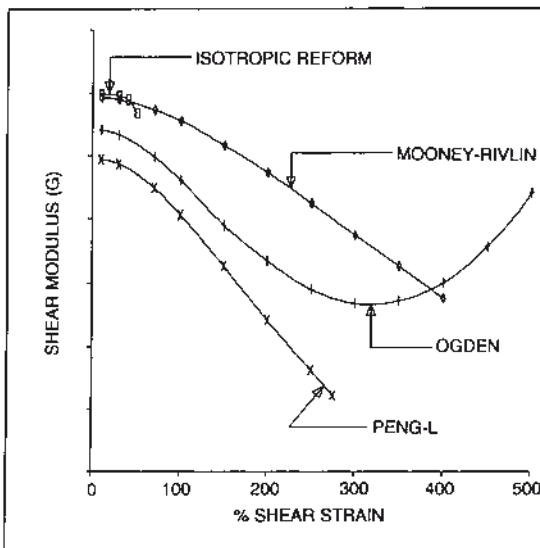


FIGURE 9a.9 Comparison of material models: simple shear

■ 9a.3 Terminology and Verification

9a.3.1 Terminology

In order to understand FEA, several terms need to be defined and understood:

1. Element: The structure to be analyzed is broken down into pieces called “elements”, which are usually triangles or quadrilaterals. When these elements are joined together they form a mesh which fully describes the geometry of the component to be analyzed (see Fig. 9a.10a).
2. Node: A “node” is a point where elements are joined. There is always a node at the corners of the elements and some elements also have mid-side nodes, which need to be specified (see Fig. 9a.10a). A mid-side node that is adjacent to an element without a mid-side node needs to be tied back to the corner node.
3. DOF: Each node has certain degrees of freedom (DOF). This means that the node is capable of moving in various directions, depending on the boundary conditions imposed on the node. The possible movements consist of displacements in three mutually perpendicular directions and rotation about these three axes for a total of six DOF (see Fig. 9a.10b).
4. Mesh or Grid: These two terms are generally used interchangeably and refer to the joined elements which look like a “grid” or “mesh”, (see Fig. 9a.10a).

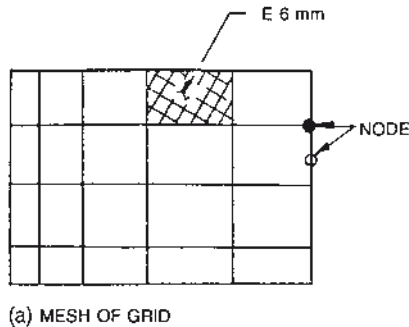


FIGURE 9a.10 FEA nomenclature

5. Boundary Conditions: The “boundary conditions” describe the loading to be applied to the component, and include deflections, pressures, forces, body forces, friction, and thermal loads.
6. Contact Surfaces: Contact surfaces are like boundary conditions, but they do not need to be in initial contact in the FEA model. It may be specified that the component can stick, can slide but not lift off, or can lift off, but not slide on the contact surface. Contact surfaces are rigid bodies. An FEA program for the analysis of elastomer components needs a robust contact surface capability [35].

9a.3.2 Types of FEA Models

Four types of FEA models can be constructed depending on the component that needs to be analyzed and the capabilities of the FEA program being used. The most common model is a two-dimensional (2-D) cross-section of the component with an axis of symmetry. This is also called an axi-symmetric model. The second type of model is a plane strain model, which is also a cross-section of the component. This model does not necessarily have a plane of symmetry. A generalized plane strain problem assumes that the out-of-plane displacement is constant over the entire model.

The third type of model is a plane stress model, which resembles the plane strain model, except it is assumed that the out-of-plane stress is constant. This model has some thickness to it. If you had a long strip of seal and wanted to evaluate how it

would react to a uniform compression deflection, then a plane stress model could be used.

The fourth type of FEA model and the most complex is a three-dimensional (3-D) model. This type of model does not usually have a plane of symmetry, or a continuous cross-section. A three-dimensional model is generally difficult to build and requires skill in interpreting the results. It should only be attempted after experience in using 2-D models. Sometimes a three-dimensional model does not need to be a full 3-D model, if a plane of symmetry is present, or if the component is cyclic symmetric. It is important to keep the number of elements to a minimum in a three-dimensional model.

9a.3.3 Model Building

The initial step in solving a problem using FEA is to take the geometry of the component and break it down into an element mesh which will accurately describe the geometry. This is accomplished by locating each node in a defined coordinate system and connecting the nodes to form the elements. During this connectivity operation, the element type and the element material type are usually specified. The element type needs to be compatible with the type of model, the material properties, and the type of analysis (linear or non-linear). Care must be taken to provide a sufficiently fine grid in regions that will have high strain gradients. These regions may be determined by experience, or by solving the FEA problem using an initial coarse mesh to locate the high gradient regions and refining the element mesh in these regions. Another method to obtain a finer mesh in local areas is to invoke “adaptive meshing” which is available in some FEA programs. This will automatically refine the mesh as specified criteria, such as strain energy level, or elements in contact, are encountered. These regions usually occur at discontinuities such as fillets, corners, at points of contact, and at the edge of the elastomer near a bond line. Every attempt should be made to construct the FEA model using quadrilaterals, avoiding triangular elements. Triangular elements are generally stiffer than quadrilaterals and usually exhibit constant strain across the element. It is true that if sufficient triangular elements are specified, the solution will approach the quadrilateral solution. The penalty is too many elements and high run times. Some programs on the market today will scan the elements and identify those with a poor aspect ratio, or are skewed too much. If triangular or poor quadrilaterals are unavoidable, locate them in non-critical regions of the model.

The elastomer portion of the component needs to have an element specified which is formulated to handle the near incompressibility of rubber. This is generally accomplished using a Herrmann “mixed method” solution for incompressible and

nearly incompressible isotropic materials which incorporates a “mean pressure” function as an independent variable. These elements need to be compatible with the elements specified for the non-elastomeric components.

Some FEA programs permit the geometry to be defined within the pre-processor, some require the geometry to be defined in some type of CAD package, and some permit both methods to be used. Most FEA programs will read as a minimum an IGS file, while some have translators for most popular CAD programs. It is generally significantly quicker to define the geometry in a CAD program and read an IGS file into the FEA program for meshing than to attempt to define the geometry within the FEA package which is normally not intended to be used as a full CAD package.

Modelling Hints for Non-Linear FEA

1. In non-linear FEA, you usually need a more refined model than in linear FEA. In other words, a given mesh is less accurate in predicting non-linear response than in predicting linear response, except in very special cases.
2. If the mesh distorts badly during a non-linear analysis, you need to re-zone the model, and change the mesh density in the deformed shape between load steps.
3. Keep the model as simple as possible.
4. A 3-D problem is always more complicated to analyze than a 2-D one. This is especially true in non-linear FEA. You should do your best to see if you can represent the problem in two dimensions, and see whether it makes sense to solve it as a plane strain, plane stress, or axi-symmetric problem. A simple model is much easier to develop, validate, execute, and evaluate.
5. Whenever possible, take advantage of symmetry in the structure and loading to reduce the size of your model. This is particularly true in non-linear FEA.
6. In non-linear FEA, lower-order elements are often preferred over higher-order elements, because of reasonable accuracy at reduced cost and their robustness for large deformation analysis and contact problems. Use a linear element in preference to quadratic and cubic elements.
7. When using lower-order elements, 4-node quadrilaterals are generally preferred over 3-node triangles in 2-D problems. Similarly, 8-node brick elements perform significantly better than 4-node tetrahedra in 3-D problems. In non-linear FEA, such as plasticity and rubber analysis, it is well known that the “linear” 3-node triangle and 4-node tetrahedron can give incorrect results because they are too stiff. The implication is that if you are using a pre-processor which generates such triangular and tetrahedral elements for a non-linear analysis, be careful of the results.
8. If you are using elements with different degrees of freedom, you need to provide appropriate constraints to account for the dissimilarity.

9. When constructing the mesh, place elements so that discontinuities in loads and material properties are located on the element boundaries, not inside elements. Three common discontinuities are: (1) interfaces between different materials or physical properties; (2) step changes in loads; (3) concentrated loads.
10. Be careful how a joint is modeled. Is it stiff, does it have some rotation, can it be smeared?
11. Be careful of how the support structure is modeled. If the stress-strain data around the support point are of interest, then there needs to be mesh refinement in that area and the support needs to be defined accurately.

9a.3.4 Boundary Conditions

After the mesh is generated, the boundary conditions are applied. For all types of FEA analysis, the boundary conditions need to be applied with caution. FEA of elastomers requires extreme caution due to the special nature of elastomeric materials. The most common boundary condition is when a surface of the component is firmly attached to another component or the ground. When the FEA surface (or node) is fixed, all of the DOFs are set equal to zero and the node cannot move in any direction. If the component is resting on a surface, but can move parallel to it, then only the DOF normal to the surface needs to be set to zero, leaving the component free to move parallel to the surface. This is like setting the surface on rollers.

The loading can be applied as a force or pressure. Forces are usually applied at the nodes, while a pressure is applied along a surface. In either event, it is essential to remember the type of model being used and specify the loading accordingly. A plane problem will usually require the loading to take into consideration the length and depth of the model. In an axi-symmetric problem, the modeled cross section is assumed to be a part of a 360° model. Therefore, the loading is either specified per radian, per arc length, or as force per unit area (pressure).

The loading can be applied as a deflection at the nodes, along a surface, or with a rigid body contact surface. If you know how a surface moves, this is the easiest and most appropriate method of loading an elastomeric component. To apply a force or a pressure over a surface, information about how it is distributed (which is usually unknown) is necessary.

Application of a pressure to an elastomer surface for a non-linear analysis introduces potential problems. The pressure has to be applied in steps to arrive at a solution. While this iterative procedure is attempting to arrive at an equilibrium point for each load step, significant changes in geometry may occur. This will require very small pressure increases in each step to attain convergence and the pressure needs to be specified as following the surface to which it is applied. The use of contact

surfaces is an excellent way to apply a deflection to a model. The characteristics of the contact surface can be specified to let the component stick, lift off, or slide, on the surface. Friction can also be specified.

9a.3.5 Solution

Modern non-linear FEA programs offer “automated” load stepping procedures to help users find the best solution at the least cost. These solution techniques should be more accurately called “semi-automatic”, because the engineer still needs to make decisions regarding the tolerance desired in the answers, convergence criteria, load/time step size selection, appropriateness of material properties, the need for adaptive meshing, mesh re-zoning, uniqueness or instability of the solutions, among others.

9a.3.5.1 Tangent Stiffness

In large deformation analysis, the relationship between incremental load and displacement is called a tangent stiffness. This stiffness has three components: the elastic stiffness, the initial stress stiffness, and the geometric stiffness. The elastic stiffness is the same as that used in linear FEA. The second term represents the resistance to load caused by realigning the current internal stresses when displacements occur. The third term represents the additional stiffness due to the non-linear strain-displacement relationship. In solving this type of problem, the load is increased in small increments, the incremental displacements are found, and the next value of the tangent stiffness is found, and so on. There are three approaches available to solve these types of problems:

1. Total Lagrangian Method – which refers everything to the original undeformed geometry. This is applicable to problems exhibiting large deflections and large rotations, but with small strains, such as thermal stress, creep, and civil engineering structures. It is also used in rubber analysis where large elastic strains are possible;
2. Updated Lagrangian Method – where the mesh coordinates are updated after each increment. This applies to problems featuring large inelastic strains such as metal forming;
3. Eulerian Method – where the mesh is fixed in space and the material flows through the mesh. This is suitable for steady-state problems such as extrusion and fluid mechanics problems.

9a.3.5.2 Newton-Raphson

Two popular incremental methods used to solve non-linear equilibrium equations are full Newton-Raphson and modified Newton-Raphson. The full Newton-Raphson (N-R) method assembles and solves the stiffness matrix at each iteration and is thus expensive for large 3-D problems. It has quadratic convergence problems, which means that in subsequent iterations the relative error decreases quadratically. It gives good results for most non-linear problems. The modified Newton-Raphson method does not reassemble the stiffness matrix during iteration. It costs less per iteration, but the number of iterations may increase substantially over that of the full N-R method. It is effective for mildly non-linear problems.

9a.3.5.3 Non-Linear Material Behavior

When stresses go beyond the linear elastic range, material behavior can be broadly divided into two classes:

1. Time-independent behavior (plasticity – applicable to most ductile metals; non-linear elasticity – applicable to rubber);
2. Time-dependent behavior (creep, viscoelasticity – applicable to high-temperature uses; viscoelasticity – applicable to elastomers and plastics).

Creep is continued deformation under constant load, and is a type of time-dependent inelastic behavior that can occur at any stress level. Creep is generally represented by a Maxwell model, which consists of a spring and a viscous dashpot in series. For materials that undergo creep, with the passing of time the load decreases for a constant deformation. This phenomenon is termed relaxation.

9a.3.5.4 Viscoelasticity (See Chapter 4)

Viscoelasticity, as its name implies, is a generalization of elasticity and viscosity. It is often represented by a Kelvin model, which assumes a spring and dashpot in parallel. Rubber exhibits a rate-dependent behavior and can be modelled as a viscoelastic material, with its properties depending on both temperature and time (creep, stress relaxation, hysteresis). Linear viscoelasticity refers to a material that follows the linear superposition principle, where the relaxation rate is proportional to the instantaneous stress. It is applicable at small strains. Non-linear viscoelasticity behavior may result when the strain is large. In practice, modified forms of the Mooney-Rivlin, Ogden, and other polynomial strain energy functions are implemented in non-linear FEA codes.

9a.3.5.5 Model Verification

After the mesh is generated, it should be plotted:

1. To verify that the mesh is defining the component correctly;
2. To verify that the nodes are correctly joined;
3. To verify that the correct boundary conditions are applied at the correct locations;
4. To verify that the correct material property is specified for each element;
5. To verify that the correct element types are specified at the correct locations.

9a.3.6 Results

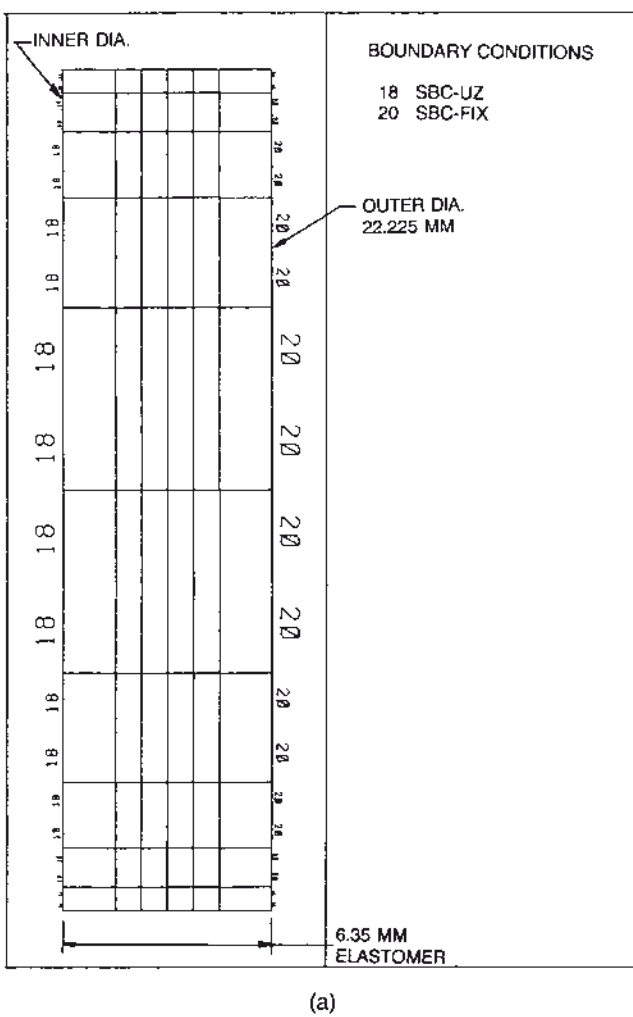
Normally, data extracted from FEA solutions for steel or aluminum components are in terms of stress. This is because the stress levels of one steel part can be readily compared with another steel part and most of the material property data is expressed in terms of stress. On the other hand, comparison and evaluation of FEA stress results from the analysis of elastomeric components can be made *ONLY* if the specified elastomer material properties are identical. Comparing the analysis of a component using a shear modulus $G = 1 \text{ MPa}$ (145 psi) with another using $G = 1.5 \text{ MPa}$ (217.5 psi) is not valid in terms of stress. Evaluation and comparison of elastomeric component analytical results need to be done in terms of strain energy, if different elastomers are to be considered. If the component with $G = 1 \text{ MPa}$ has a shear stress of 0.5 MN/m^2 , its shear strain is 50% strain, and its strain energy is 125 kJ/m^3 , while the component with $G = 1.5 \text{ MPa}$ under the same shear stress would have a shear strain of 33% and a shear strain energy of only 83 kJ/m^3 .

The interface between the elastomer and the metal to which it is bonded is a critical location to be checked during the analysis. A significant number of finite element programs will not distinguish between the two materials when the data along this interface is processed. The stress levels in the steel and the stress levels in the elastomer will be averaged at the nodes and reported. This is not valid. When carrying out FEA of an elastomer component with metal as part of your model, verify that the program is in fact reporting the actual stress-strain values in the elastomer and not “smearing” the data from the metal together with the elastomer results.

Various forms of plotted output can usually be obtained from FEA results. The use of plotted output is highly desirable due to the large volume of data that is generated. A mesh plot (Fig. 9a.11a) provides verification that the model has been properly constructed. This type of plot also can be used to verify the boundary conditions, show the element types, the location of the specified materials, and to check that the elements within the model are all properly connected. A deformed plot (Fig. 9a.11b) shows the manner in which the component is deforming. In the case of a non-linear analysis, the sequence of deformations may be over-laid, or placed in a “movie”.

Contour plots (Fig. 9a.17c) of all of the stress and strain components can be displayed on the model to show the locations of high values of stress and strain and the flow of the loading through the component. Profile plots (Fig. 9a.17d) can be obtained to show the stress and strain along a profile of the component. They are valuable in determining how the load is flowing. Plots of this type can also show the reactions along a surface, which will permit a more accurate analysis of the adjacent structure.

The movement of a particular point within a component, or the change in stress or strain during a non-linear analysis, is sometimes of particular interest. This may be done using a history plot. The better the plotting capability of the FEA program, the more usable is the analysis.



(a)

FIGURE 9a.11 (a) Linear analysis of an annular tube

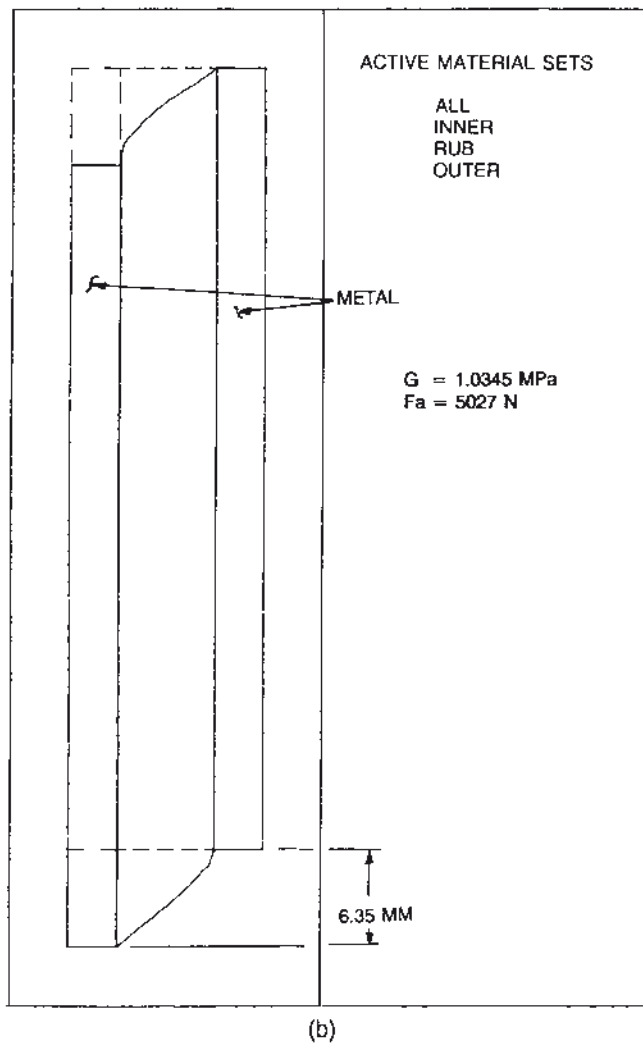


FIGURE 9a.11 (b) Deformed tube

9a.3.7 Linear Verification

The first problem is a 50.8 mm (2 in) long annular tube form (Fig. 9a.11). The elastomer layer is 6.35 mm thick (0.25 in) with a shear modulus of 1.034 MPa (150 psi). An inner metal tube with an outer diameter of 9.524 mm (0.375 in) and an outer metal tube with an inner diameter of 22.22 mm (10.875 in) are bonded to the elastomer. The outer tube is fixed, while the inner tube is deflected 6.35 mm (0.25 in).

The resulting axial force is 5027 N. This compares with 5150 N using Eq. (4.45) from Freakley and Payne [24]. This is within 2.4%. It may be noted in the deformed plot that the shape of the edge of the elastomer, when deformed, is not straight.

The second problem is the compression of a flat disk, shown in Figure 9a.3. The material properties were for material A in Table 9a.1. The thickness of the elastomer layer was changed to obtain various shape factors and the radius was held constant. The axial force was obtained for each shape factor.

Knowing the compression area and the thickness of the elastomer pads, the apparent compression modulus (E_c) was calculated [8] using:

$$E_c = \frac{F t}{\pi a^2 d} \quad (9a.15)$$

Figure 9a.3 shows a comparison between the FEA results and Lindley's E_c versus shape factor measured data from [8].

9a.3.8 Classical Verification – Non-Linear

There are few classical solutions of non-linear elastomeric problems. Two examples that FEA may be compared with are:

1. The problem of bending and inflation of a simply-supported circular flat elastomeric plate was solved by Oden [25]. The undeformed plate is 38.1 cm (15 in) in diameter and 1.27 cm (0.5 in) thick, using a Mooney-type material with material constants of $C_1 = 0.5517 \text{ MN/m}^2$ (80 psi) and $C_2 = 0.13793 \text{ MN/m}^2$ (20 psi) as shown in Fig. 9a.12a. The model is constrained only at the corner node between the two middle elements and is axi-symmetric. A quadratic isoparametric element with eight nodes using the 3×3 Gauss Integration Rule is specified. Note that the loads applied in this problem are non-conservative; therefore the element surface changes markedly in magnitude and orientation with applied pressure. Because of numerical instabilities encountered in the incremental loading process, as well as the incompressibility of the elements, Oden found it was impossible to predict the response beyond 0.2897 MN/m^2 (42 psi) without modifying the model. Using an element scheme similar to Oden, pressure was applied up to a maximum of 0.6414 MN/m^2 (93 psi). At 0.648 MN/m^2 (94 psi) it was impossible to continue due to poor conditioning of the Jacobian matrices. The deformed model is shown in Fig. 9a.12b at various increments of pressure. The straight line projecting out from the attachment point is the first element being stretched. Figure 9a.12c provides a comparison of the axial deflection at the center line obtained by Oden and the values from a commercial FEA program.

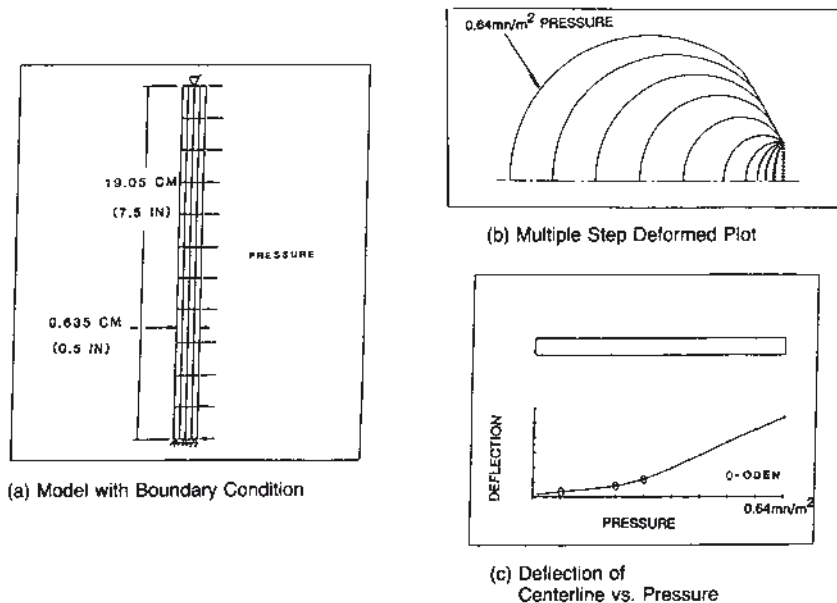


FIGURE 9a.12 Non-linear analysis of a simply supported circular flat elastomer plate

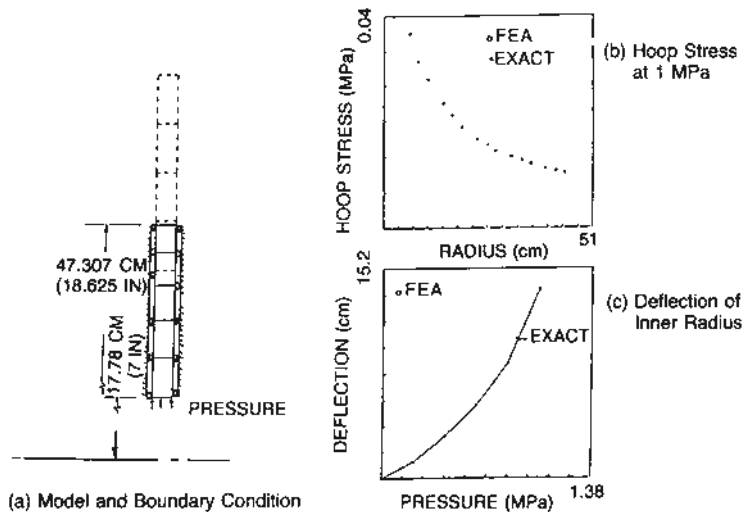


FIGURE 9a.13 Non-linear analysis of an infinitely long, thick-walled cylinder

2. For an “infinitely long, thick walled cylinder subjected to internal pressure”, the results may be compared with known solutions provided in [26] and [27]. This model has an inner radius of 47.307 cm (18.625 in) as shown in Fig. 9a.13a, along with the boundary conditions. The Mooney coefficients and the element used are the same as described in the preceding problem. The internal pressure was increased from 0 to 1.0345 MN/m² (150 psi), with the resulting radial deflection of the inner radius and the hoop stress through the cylinder shown to correlate with the exact solution in Fig. 9a.13b.

■ 9a.4 Example Applications

9a.4.1 Positive Drive Timing Belt

A positive drive timing belt [28] is normally composed of a cover of elastomer, a spiral wound cord layer, and a molded elastomer tooth as shown in Fig. 9a.14a. Each tooth is subjected to the same load history, which makes it possible to analyze one tooth to determine the location of the high strain regions. Figure 9a.14b illustrates the finite element model that was constructed for this analysis, with small elements placed in the tooth root region, because this is one obvious location of potential high strain. The Neoprene material was specified to have a bulk modulus of 2.687 GPa and a shear modulus of 12.5 MPa. The cord was specified to have a Young’s modulus of 206.9 MPa and a Poisson’s ratio of 0.35.

A plane stress analysis was performed because the belt is usually 25.4 mm in thickness. The metal gear tooth was defined as a rigid contact surface to simulate the meshing of the belt tooth into the gear and the model deflected radially on the cord elements. Figure 9a.14c shows the deformed plot overlayed on the undeformed shape. The tooth is pulled against one side and away from the opposing side, and the thin elastomer section between the cord and the tooth root is crushed. The highest strain in the elastomer occurs where the metallic gear and the tooth root initially meet. This indicates that the elastomer tooth will begin to shear at the high strain area in the tooth root and then separate along the cord-elastomer interface. This information can be used to redesign the tooth profile to reduce the level of strain. This is an example of using a non-linear analysis with linear material properties.

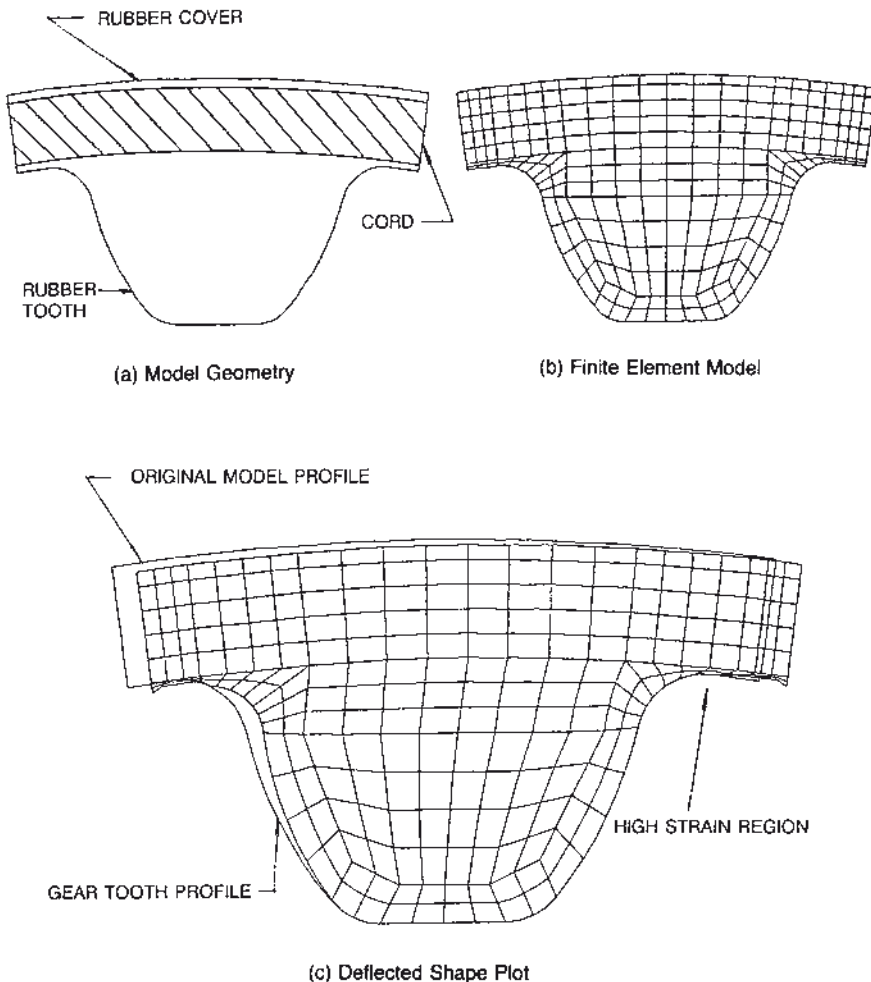


FIGURE 9a.14 Positive drive belt example

9a.4.2 Dock Fender

The modeling of a 71.12 cm thick cross-section of a dock fender in plane stress is another example of using a two-dimensional analysis to study a three-dimensional elastomeric component. This example is presented in detail in [29] with the model reproduced in Fig. 9a.15a. The function of the dock fender is to buckle when a vessel strikes the dock, thereby absorbing the energy of impact. The size of the component makes laboratory testing expensive, while the use of non-linear finite element analysis is a viable alternative.

Use of the generalized plane stress capability permits out-of-plane deflection of the model. The model also takes advantage of symmetry which reduces the size of the model by one-half. This is accounted for by specifying a slope (rollers) boundary condition on the plane of vertical symmetry. This assumes that what happens during the analysis of the upper half is a mirror image of what would happen to the lower half of the fender, if it were also included in the model. Care must be exercised when evaluating the spring rate from an analysis of this type. The spring rate is the load divided by the deflection. Since only one-half of the model is defined, the spring rate in this case would be the load divided by twice the deflection because, for the full model, the amount of deflection for the same load would have been twice as large. One result of this analysis that needs to be addressed is the formation of a cusp. Any further continuation of the analysis would show overlapping of the element boundary on itself in the region of the cusp. This effect was studied by Miller [29] who concluded that a restriction is needed on the motion of the elements to prevent boundary overlap and that a constitutive model, which is very accurate for very large values of strain and for possible inelastic behavior, is needed.

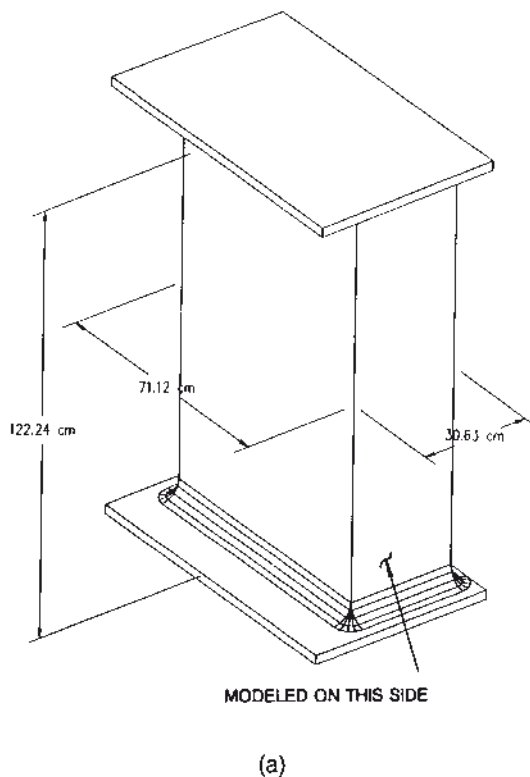


FIGURE 9a.15 (a) Dock fender example

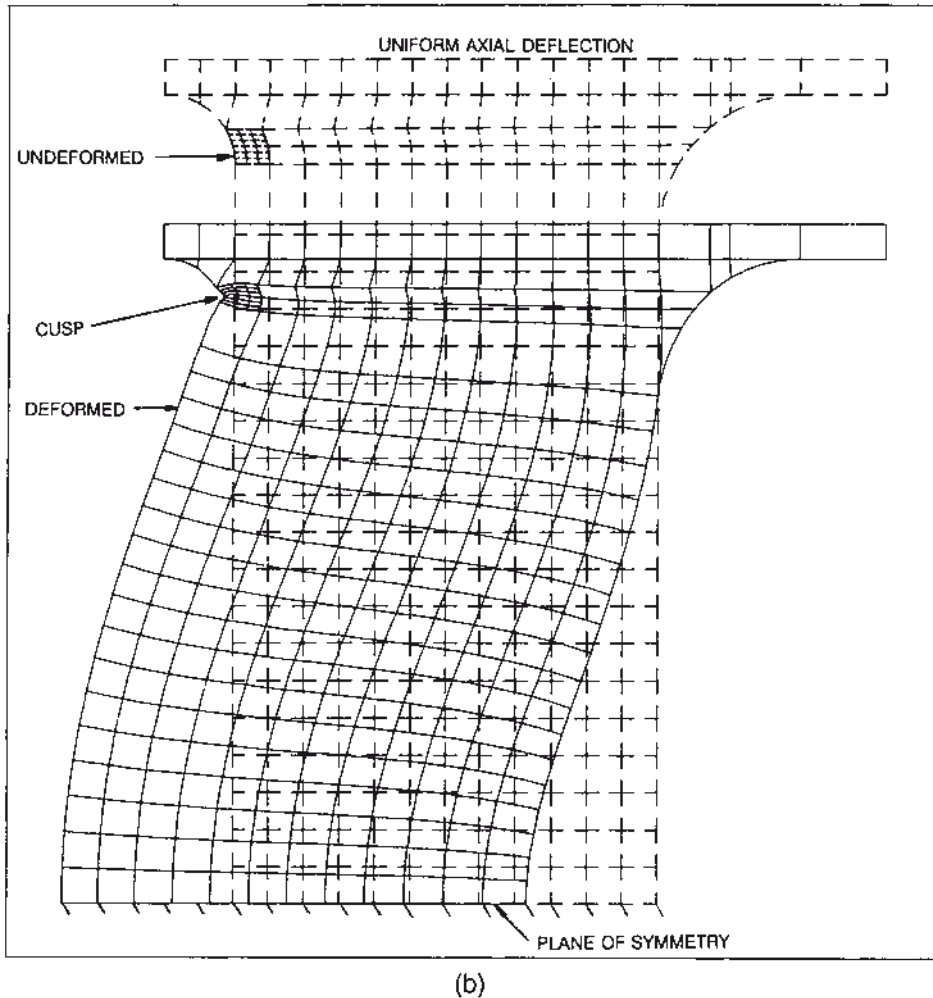


FIGURE 9a.15 (b) Deformed fender example

The resulting load-deflection characteristics of the model are shown in Fig. 9a.15c, where they are compared to single point test data. The test data were later determined to be tainted by the introduction of a side load to “help” the fender start to buckle. The finite element analysis helped to discover this invalid test procedure when questions arose as to why the test data did not follow the analysis in a local region of the curve, but both still reached the same limit load condition.

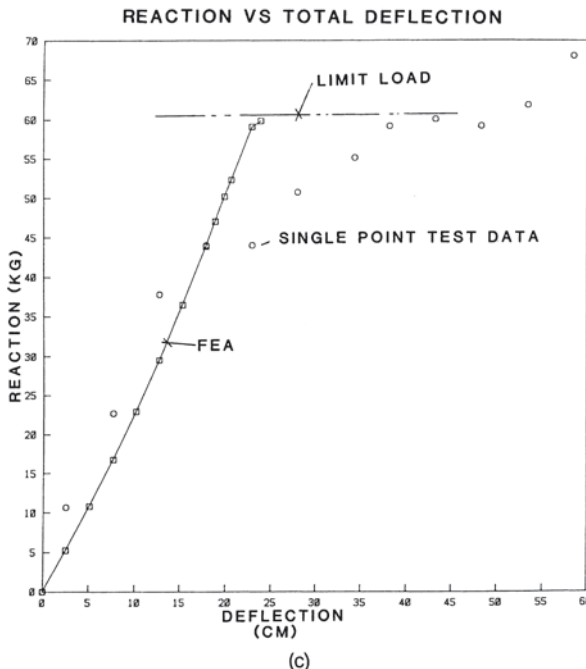


FIGURE 9a.15 (c) Load-deflection relation

9a.4.3 Rubber Boot

Elastomers are used to mold boots, used to protect joints from dirt and fluids. These boots need flexibility to move with the joint in all directions without impeding the motion, or unduly adding to the force needed to cause motion. An axi-symmetric model (top left plot in Fig. 9a.16) of a typical boot illustrates the need for self-contact and self-contact release capability in the FEA program on moving the boot in the axial direction. Obviously, this could be made into a three-dimensional model (partial view shown in the upper right plot in Fig. 9a.16) and rotation about and normal to the axis of rotation could be evaluated.

The two end diameters were assumed to be clamped rigidly to two cylinders which slide on the same axis. The middle and lower plots in Fig. 9a.16 show a sequence of deformations due to the applied axial deflection. Note the self-contact occurring and the lift off. Strain and strain energy contour plots can be obtained and the regions of high strain and strain energy identified and evaluated. The component can then be revised to obtain the desired deflection characteristics and to lower the strain levels prior to production.

The material model used in this example was a two coefficient Ogden, with the coefficients obtained using uni-axial tensile data within MARC.

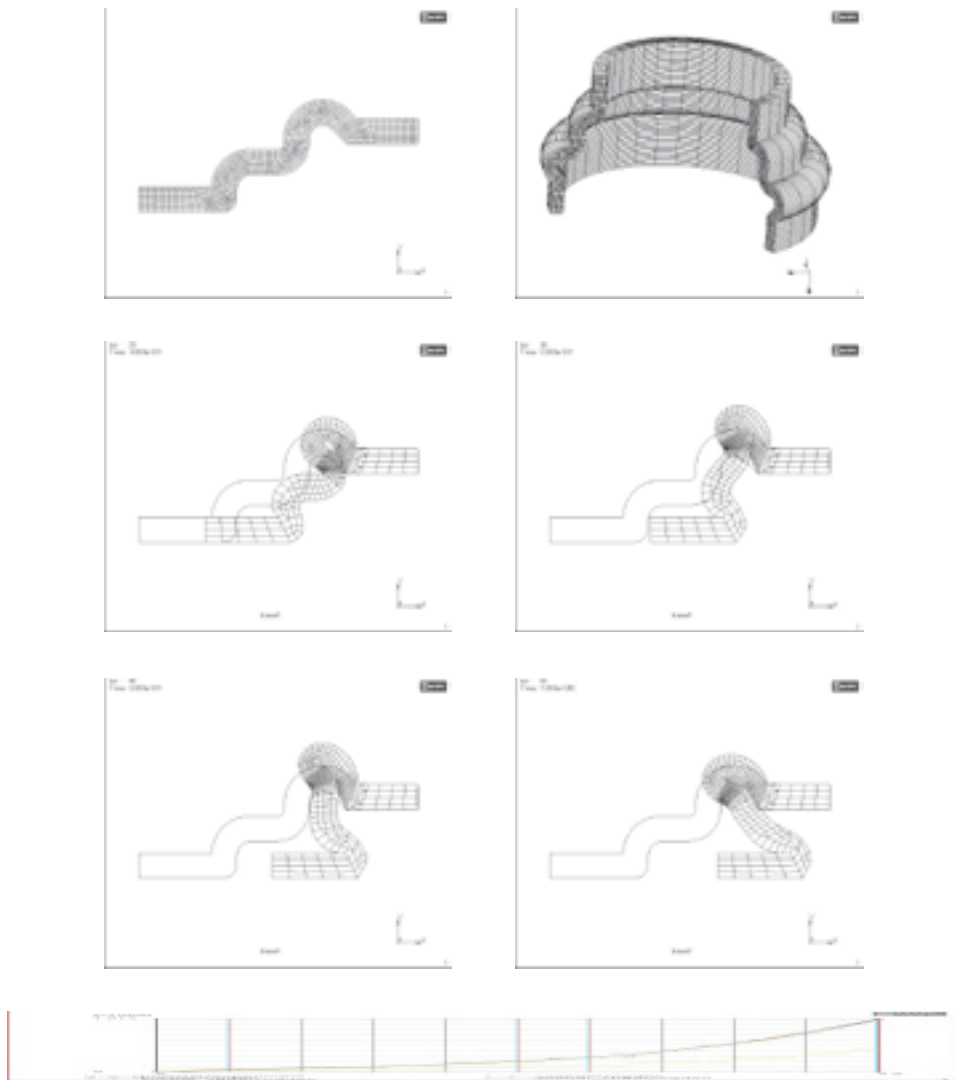


FIGURE 9a.16 Boot example

9a.4.4 Bumper Design

A good example of using FEA to develop a component configuration for a particular response, instead of developing the configuration and changing the compound or mold to obtain the response, is shown in Fig. 9a.17. The Ogden material coefficients listed earlier in this chapter were used and three different geometries defined as Bumper A, Bumper B, and Bumper C. A careful study of these three cross-sections will reveal that, except for the location of the upper surface, all of the significant characteristics are essentially the same. This includes the top contact area and the cross-sectional area. When the axial force versus axial deflection from FEA is plotted for each of the cross-sections it can be seen that Bumper B is approximately 50% stiffer than Bumper A. This effect would be difficult to determine using handbook equations.

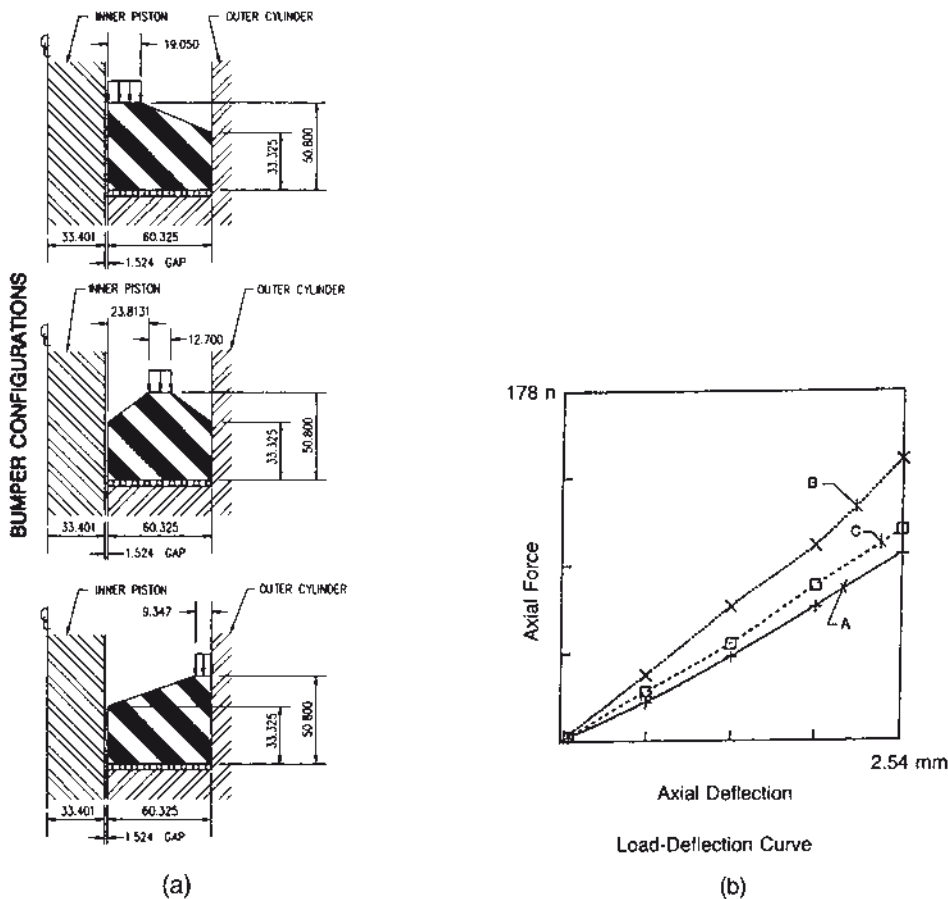


FIGURE 9a.17 (a) Bumper example; (b) determining stiffness of different bumper designs

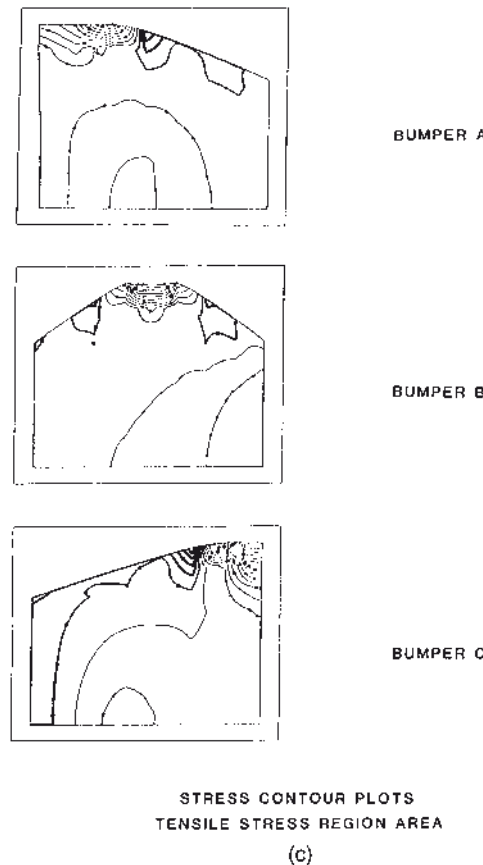
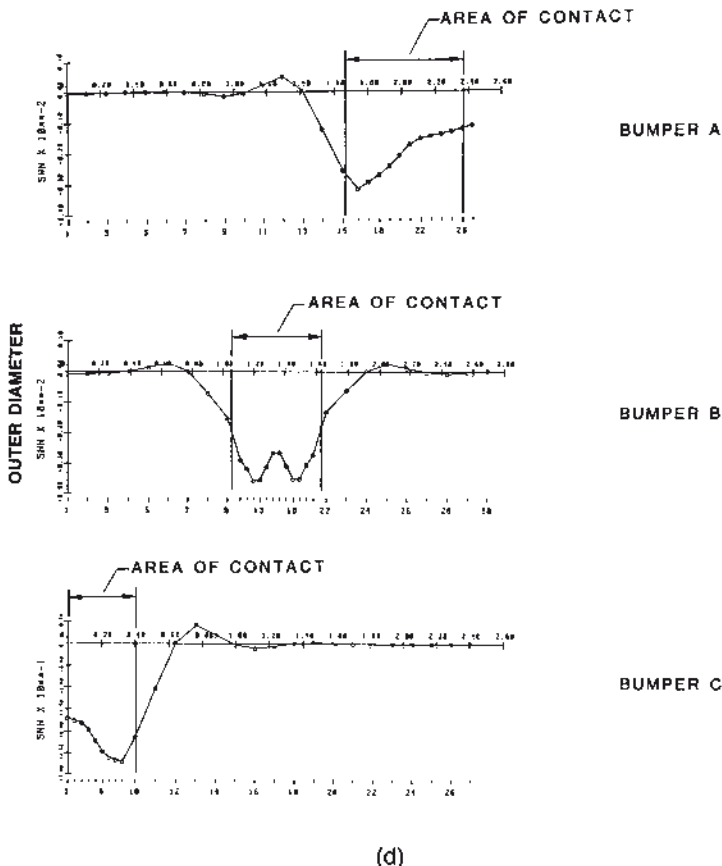


FIGURE 9a.17 (c) Maximum principle stress contours for different bumper designs

All of the load deflection curves are non-linear, with Curve B showing a “buckling” type mode around 1.9 mm and Curve C showing a slight drop off at 1.27 mm deflection. Without FEA, the configuration required to obtain a particular load-deflection curve would have been guessed at and molded. If the guess was not correct, the configuration would be changed, or the compounder would be blamed for the error and told to develop a different formulation to obtain the desired response.

The maximum principle stress contours are shown in Fig. 9a.17b and c, with the areas of tensile stress shaded on each of the three plots. This type of information is useful in locating potential areas of failure. These plots, along with all of the stress-strain components, may be obtained at any point in the loading process. This will enable the designer to understand not only the state of stress or strain that is occurring at each load level, but how it is changing. This also shows that any assumptions of uniform stress during loading are false. The normal stress (pressure) patterns on



(d)

FIGURE 9a.17 (d) Normal stress patterns on the upper surface of the different bumper designs

the upper surface for the three designs are anything but uniform, which is usually a basic assumption in closed form solutions.

9a.4.5 Laminated Bearing

An example from [3] is the redesign of a laminated elastomeric bearing for a helicopter blade retention system (Fig. 9a.18). The original cross-section was similar to previously designed and successfully tested bearings and was intended to give a stated torsional spring rate within a defined envelope. Using empirical data, the design was developed without the benefit of FEA. On testing, it exhibited unacceptable performance. The failure mode was rapid deterioration of the elastomer at the outer diameter near the top and at the inner diameter at the bottom. Closed-form equations would have predicted that each of the layers had an equal chance of failing because they were all identical.

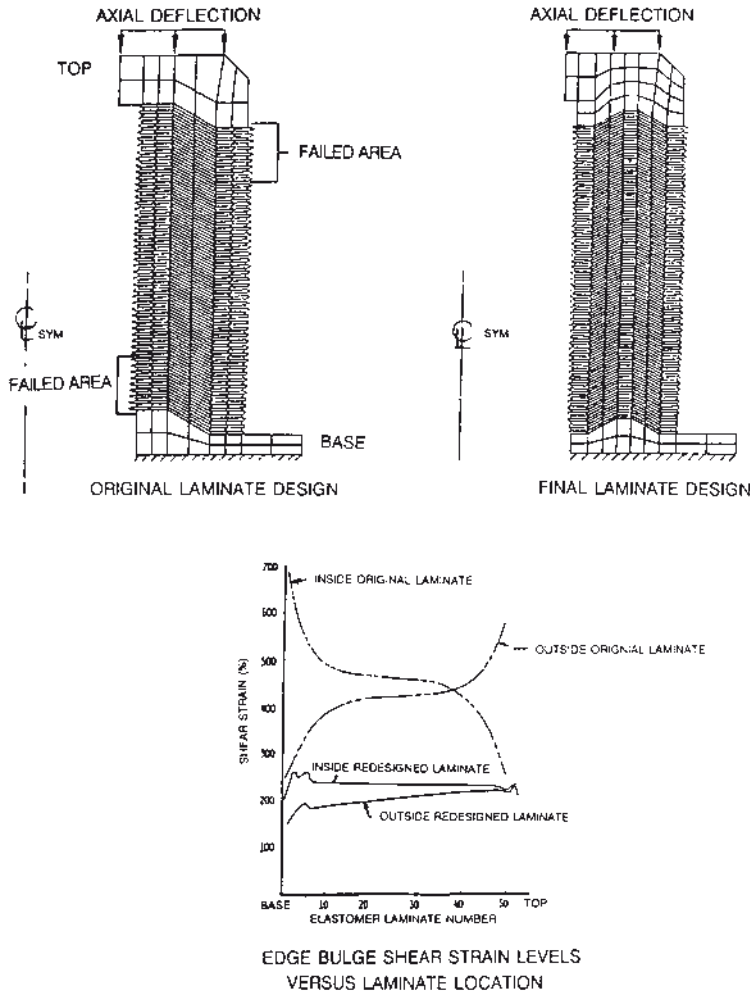


FIGURE 9a.18 Laminated bearing example

Post-test linear FEA revealed that the elastomer shear strain near the edge, in the region of rapid failure, increased significantly over the level of strain in the center of the stack height. A study of the pressure patterns on each of the layers also revealed that the load path was near the outer diameter at the top and near the inner diameter at the bottom. Several metal laminate configurations were modeled by FEA to arrive at the configuration shown as the final shim design. The FEA predicted a significant drop in the edge bulge shear strain and all of the layers became basically equal. This drop in edge bulge shear strain translated into a 3:1 increase in the fatigue life of the bearing.

This was an axi-symmetric analysis using a linear material model with reformulated elements. The compression strain levels of highly laminated bearings like these,

with shape factors above 10, are usually in the order of 5–7%. This means that a reformulated isotropic material model can usually be used with excellent results. The bulge shear patterns along the edge will generally match visual observations during compression testing.

It is important to note that the basic outside geometry of this bearing, including the height, was not changed. The torsional spring rate remained basically the same. The two designs could only be distinguished by cutting the bearing in two to reveal the metal laminate configuration, or by testing to reveal an early failure of the original design. This use of FEA to develop the design configuration eliminates the “cut and try” approach used in many elastomer designs. This translates into less mold rework (or redesign), earlier delivery to the end user due to less design iterations, and a component that satisfies the specifications the first time it is molded.

9a.4.6 Down Hole Packer

The oil industry uses packers to shut off the flow of oil in an emergency. One type of packer [36] is called an annular packer. This packer fits into a pipe and oil flows through the center. The packer is constructed of metal wedges spaced at intervals around the circumference and they are surrounded by rubber. The metal wedges have unique contours, which were determined by cut and try methods, to cause the packer to deflect toward the center and seal on itself when compressed radially. This sealing action is activated by mechanically pushing on the metal inserts and driving them into position. The rubber surrounding the metal components moves toward the center and “puckers up” on itself at the center. Therefore, there is significant self-contact.

This problem was defined as cyclic symmetric, which means that a radial plane can be passed through the center of one of the metal components for one side of the model and a second radial plane can be passed through the center of the rubber between two metal components for the second side of the model. Figure 9a.19 shows a 3-D model of the packer and the two radial cyclic symmetric planes. The upper right plot in Fig. 9a.19 shows all of the contact surfaces, including the cyclic symmetric planes. The outer diameter is restrained by the inner diameter of the pipe and the top is constrained with a flat surface. The long three-faced rigid body is the activation mechanism that pushes the packer inward to seal.

The middle two plots in Fig. 9a.19 show the undeformed packer in a top and side view. The lower two plots in Fig. 9a.19 show the deformed plots. Note that the lower left plot shows rubber in the apex of the two cyclic symmetric planes. The lower right deformed plot can be compared with the right plot to access the magnitude of the deformation. Note that rubber flows around the flat rigid surface opposite the actuation device. This is where the “puckering” of the rubber is occurring.

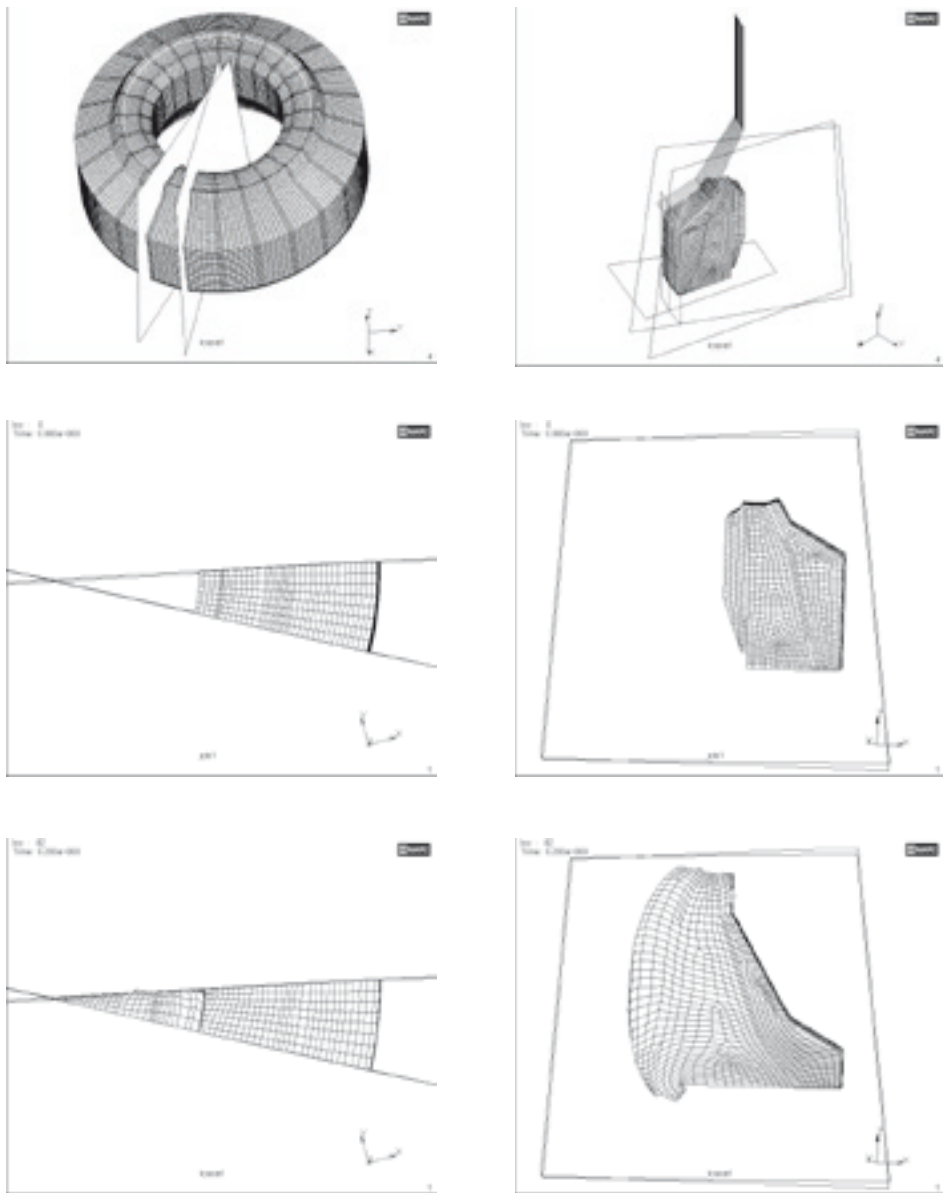


FIGURE 9a.19 Packer example

During the development of packers, the deformation pattern cannot be observed, except in the region where it “puckers” at the centerline on one side. The design is largely based on past experience. The use of FEA permits the deformed shape to be observed throughout the loading sequence.

9a.4.7 Bonded Sandwich Mount

A typical elastomeric product is a bonded sandwich mount [30] manufactured by Lord Corporation as shown in Fig. 9a.20. As simple as this part looks, it would require a very complex, if not impossible hand analysis. Incorporation of the insert affects the compression and shear response, while setting up unusual internal stress patterns. A non-linear analysis was performed for axial compression and a linear analysis for radial shear. A non-linear radial shear analysis could not be done because any analysis after the initial movement of the model would be on a model that was no longer symmetrical; therefore, a three-dimensional model would be necessary. The resulting compression and radial shear load-deflection characteristics from FEA are shown overlaying the published test results. The two additional compression curves were published in [31] and [32] using classical closed-form equations. The linear FEA radial shear load analysis predicted a “best fit” line through the slightly non-linear measured data.

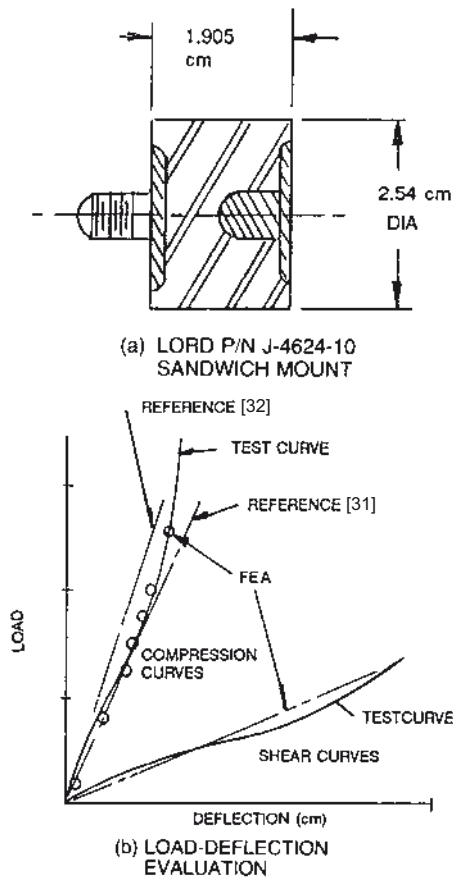


FIGURE 9a.20 Compression (sandwich) pad example

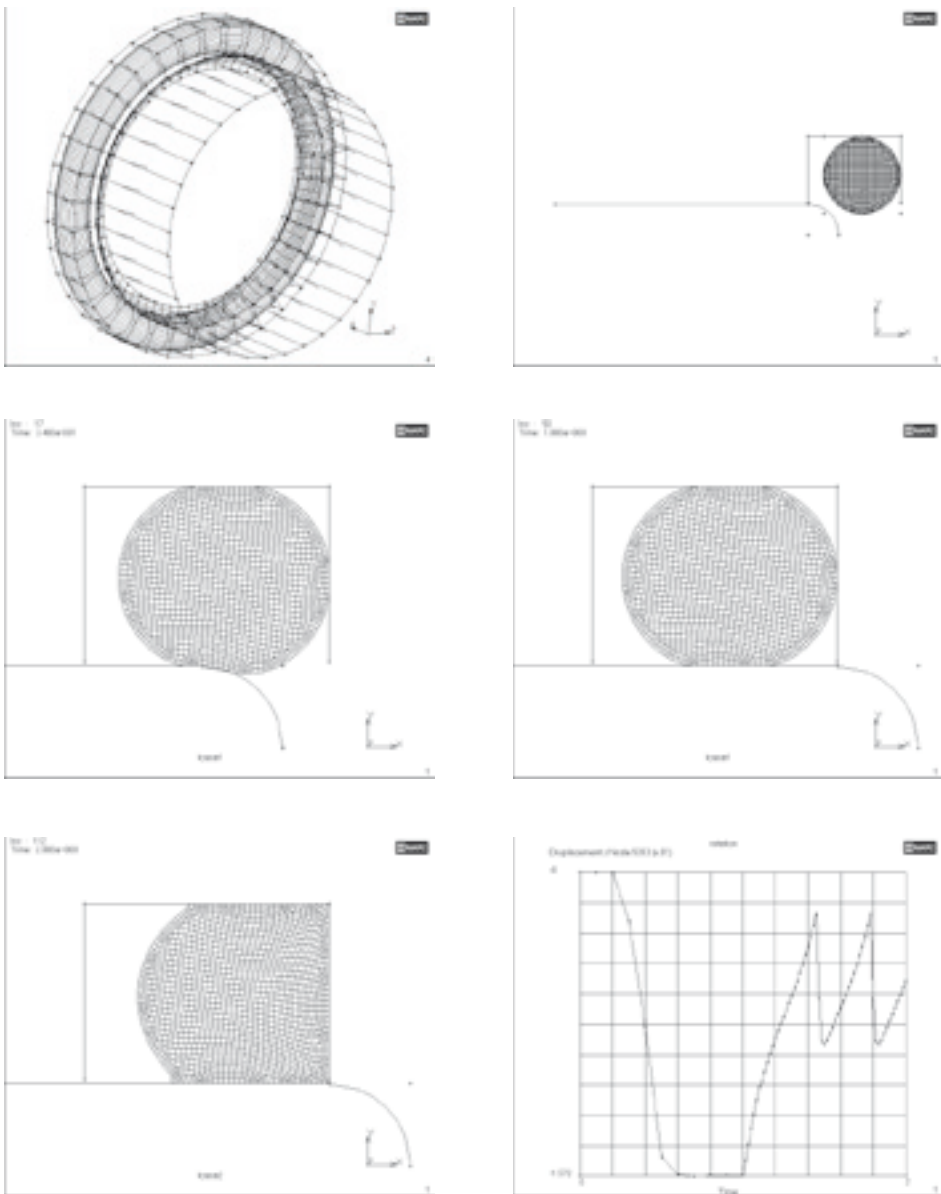


FIGURE 9a.21 O-ring example

9a.4.8 O-Ring

This sample O-ring 3-D problem illustrates the effect of friction on an O-ring due to torsional motion of the shaft after the shaft is inserted and pressure applied. The top left plot in Fig. 9a.21 shows the full model. The shaft was modeled as a rigid body with a rounded leading edge. The gland was modeled as a circular “U” channel using rigid body surfaces. Friction was specified between the shaft and the O-ring and the outer diameter of the gland and O-ring. The upper right plot in Fig. 9a.21 shows a cross-section through the shaft, gland, and O-ring.

The middle plots in Fig. 9a.21 show the insertion of the shaft into the O-ring and the lower left plot shows the deformation after the application of pressure. After pressure was applied, the shaft was rotated about its axis. The lower right graph in Fig. 9a.21 shows the movement of a node in contact with the shaft. The initial movement from Time = 0–1 is the insertion of the shaft. The movement between Time = 1–2 is due to rotation. The two “saw tooth” peaks on the right side of the graph show the O-ring slipping back as the friction force is overcome. The O-ring is twisting and un-twisting as the shaft is rotated.

This is an illustration of using FEA to review what is occurring to a component in a situation that cannot be observed during testing.

9a.4.9 Elastomer Hose Model

This problem illustrates the use of FEA to evaluate the crimping of a metal connection onto a hose with rubber and fabric construction. The problem is axi-symmetric, with the cross-section shown in the upper left plot in Fig. 9a.22 and the model rotated (upper right plot in Fig. 9a.22) into a partial 3-D plot to aid in visualizing the component. The metal was steel, the hose consisted of inner and outer layers of rubber defined by a 3-coefficient Rivlin material model and the material between the rubber layers was an impregnated fabric defined as an orthotropic material.

The hose assembly was inserted into the metal fitting (middle plots in Fig. 9a.22) and then the fitting was crimped on to the hose (lower plots in Fig. 9a.22). This type of analysis can study the material flow during the crimping operation, determine the crimping force, evaluate the retention ability of crimping by pulling the specimen after crimping, or review the stress-strain patterns set up to permit revising the components or the process. A 3-D model could have been made by rotating the 2-D model through 360 degrees and then the crimping action could have been applied at selected locations around the diameter instead of employing the full 360 degree crimping pattern utilized for this example.

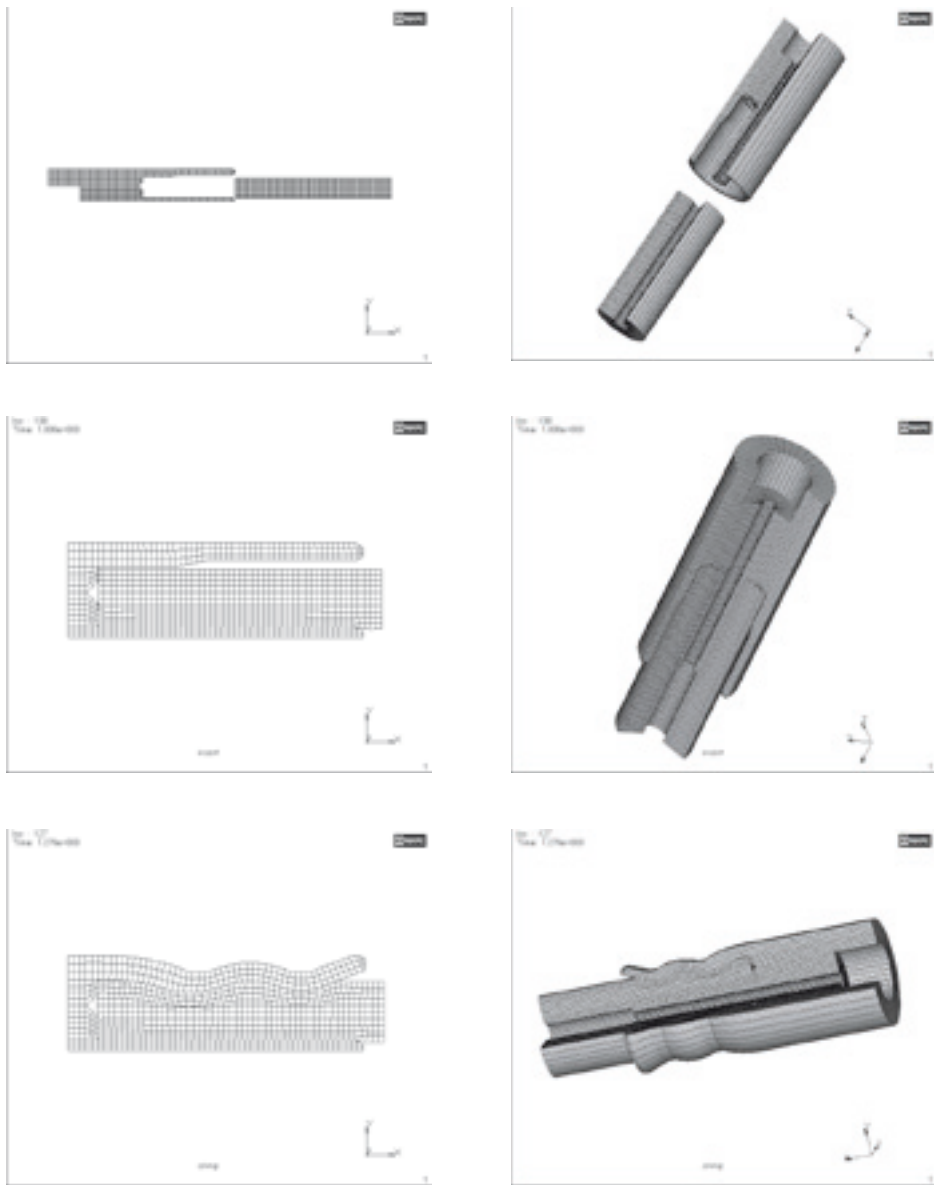


FIGURE 9a.22 Hose crimping example

9a.4.10 Sample Belt

One way of evaluating the robustness of a non-linear FEA program is to run an example like the one shown at the top of Fig. 9a.23 [36]. This model is a strip of rubber with a circular steel cable embedded in the center. One end of the model is

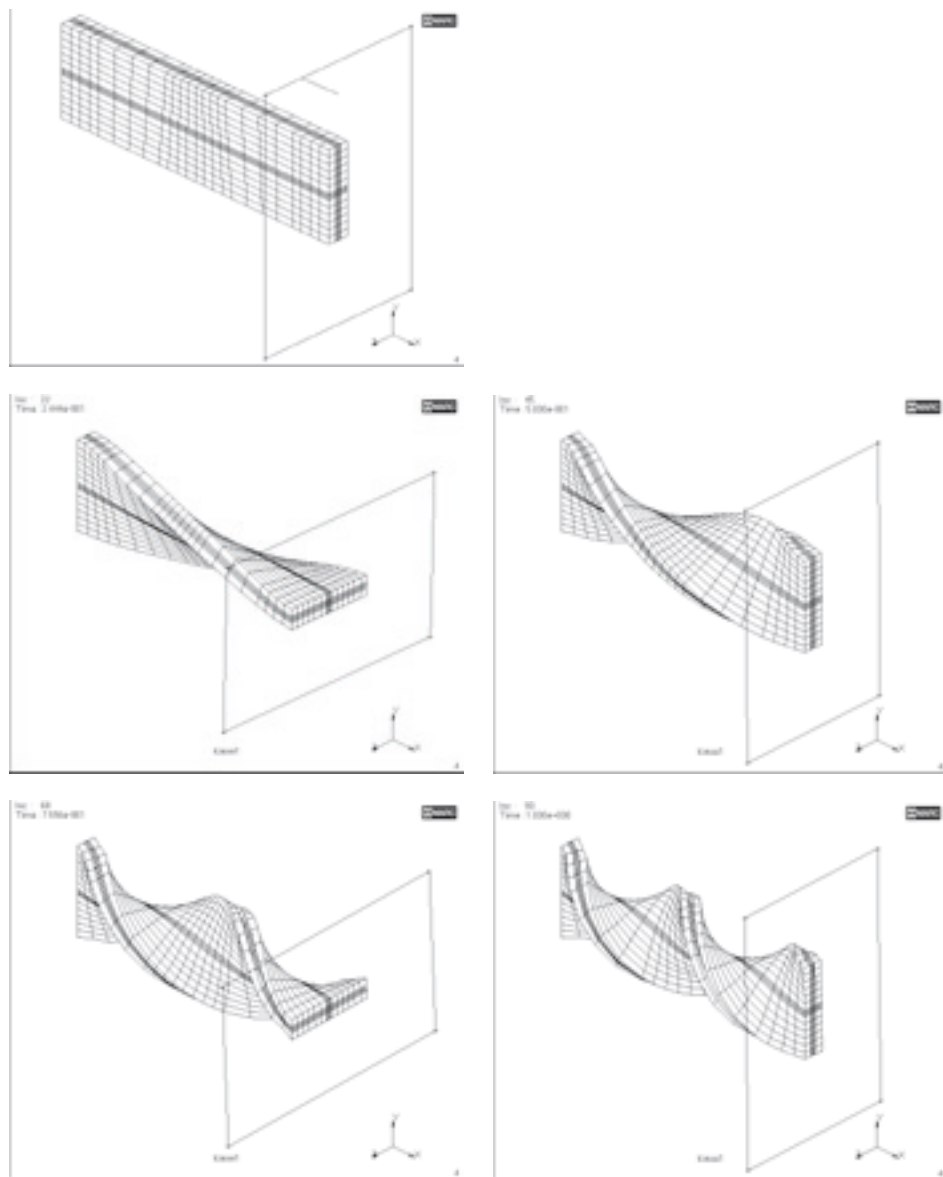


FIGURE 9a.23 Partial belt example

restrained in all three directions and the other end is attached to a rigid body which is rotated 360 degrees about the center of the steel cable. The elastomer material model was neo-Hookean with a specified bulk modulus of 1379 MPa. There are some commercial FEA programs that will not handle large deflections of this type. The middle left, middle right, lower left, and lower right deformed plots show the specimen twisted 90, 180, 270, and 360 degrees, respectively.

■ References

- [1] O. C. Zienkiewicz and R. L. Taylor, *The Finite Element Method*, 4th ed., McGraw-Hill, New York, 1989.
- [2] H. Kardestunger and D. H. Norie (Eds.), *Finite Element Handbook*, McGraw-Hill, New York, 1987.
- [3] Robert H. Finney and Bhagwati P. Gupta, *Design of Elastomeric Components by Using the Finite Element Technique*, Lord Corporation, Erie, Pennsylvania, 1977.
- [4] R. H. Finney and Bhagwati P. Gupta, in: *Application of Finite-Element Method to the Analysis of High-Capacity Laminated Elastomeric Parts*, *Experimental Mechanics Magazine*, pp. 103–108, 1980.
- [5] L. R. Hermann and R. M. Toms, “A Reformulation of the Elastic Field Equations in Terms of Displacements Valid for All Admissible Values of Poisson’s Ratio”, *Appl. Mech. Trans. ASME*, **85**, 140–141 (1964).
- [6] L. R. Hermann, “Elasticity Equations for Incompressible and Nearly Incompressible Materials”, *AIAA J.*, **3**(10), pp. 1896–1900 (1985).
- [7] Robert H. Finney, “Springy Finite Elements Model Elastomers”, *Machine Design Magazine*, pp. 87–92, May 22, 1986, Cleveland, Ohio.
- [8] P. B. Lindley, “Engineering Design with Natural Rubber”, Natural Rubber Technical Bulletin, 3rd ed. Natural Rubber Producers Research Association, Hertford, England, 1970.
- [9] R. S. Rivlin, *Phil. Trans. R. Soc. London, Ser. A*, **240**, 459 (1948).
- [10] M. Mooney, *J. Appl. Phys.*, **11**, 582 (1940).
- [11] R. W. Ogden, *Proc. R. Soc. London, Ser. A*, **328**, 567 (1972).
- [12] S. T. J. Peng, “Nonlinear Multiaxial Finite Deformation Investigation of Solid Propellants”, AFRPL TR-85-036, 1985.
- [13] S. T. J. Peng and R. F. Landel, *J. Appl. Phys.*, **43**, 3064 (1972).
- [14] S. T. J. Peng and R. F. Landel, *J. Appl. Phys.*, **46**, 2599 (1975).
- [15] K. C. Valanis and R. F. Landel, *J. Appl. Phys.*, **38**, 2997 (1967).
- [16] O. H. Yeoh, “Some forms of the Strain Energy Function”, *Rubber Chemistry & Technology*, **66**, 754–771 (1993).
- [17] E. M. Arruda and M. C. Boyce, *J. Mech. Phys. Solids*, **41**, 389 (1993).
- [18] A. N. Gent, “Fracture Mechanisms and Mechanics”, Elastomer – FEA Forum ’97, University of Akron.
- [19] O. H. Yeoh, “A Practical Guide to Rubber Constitutive Models”, Elastomer – FEA Forum ’97, University of Akron.
- [20] “Non-linear Finite Element Analysis of Elastomers”, MARC Analysis Research Corporation.
- [21] L. R. G. Treloar, “Stress-strain Data for Vulcanized Rubber Under Various Types of Deformations”, *Trans. Faraday Soc.*, **40**, 59 (1944).
- [22] Robert H. Finney and Alok Kumar, “Development of Material Constants for Non-Linear Finite Element Analysis”, 132nd Meeting, Rubber Division, American Chemical Society.
- [23] A. N. Gent, *Trans. Inst. Rubber Ind.*, **34**, 46 (1958).
- [24] P. R. Freakley and A. R. Payne, *Theory and Practice of Engineering with Rubber*, Applied Science Publishers, London, 1970.
- [25] J. T. Oden, *Finite Elements of Non-linear Continuum Mechanics*, McGraw-Hill, New York, 1972.

- [26] A. E. Green and W. Zerna, Theoretical Elasticity, Oxford University Press, London, 1969.
- [27] R. C. Vatra, "Finite Plane Strain Deformation of Rubberlike Materials", *Int. J. Numer. Methods Eng.*, **15**, 145–160 (1980).
- [28] A. D. Adams, "Finite Element Analysis of Rubber and Positive Drive Timing Belts", Goodyear Tire & Rubber Co., Akron, Ohio, Jan. 23, 1986.
- [29] R. H. Finney, Alok Kumar, and Trent Miller, "Applications of Finite Element Analysis to Large Stretch and Contact Problems in Elastomer Components", presented at the Rubber Division, American Chemical Society Meeting, 1987.
- [30] R. H. Finney, "Cut and Try? Closed Form Equations? Finite Element Analysis?" presented at the 129th Meeting, Rubber Division, American Chemical Society, Educational Symposium No. 16, 1986.
- [31] Paul T. Herbst, "Shock and Vibration Isolation, Transient Vibration and Transmissibility", presented at the 129th Meeting, Rubber Division, American Chemical Society, Educational Symposium No. 16, 1986.
- [32] Roy L. Orndorff, "Equilibrium Design Process", presented at the 129th Meeting, Rubber Division, American Chemical Society, Educational Symposium No. 16, 1986.
- [33] R. H. Finney, Dr. D. Shah, R. Cribbs, "Elastomer Have We Learned Anything Yet?", Elastomer - FEA Forum '97, publ. ARDL, Akron, Ohio, 1997.
- [34] R. H. Finney, "FEA of Elastomeric Components Questions and Observations", Elastomer - FEA Forum '98, publ. ARDL, Akron, Ohio, 1998.
- [35] R.H. Finney, "FEA of Rubber – Material Properties, Contact Surfaces and Output Data", Energy Rubber Group Educational Symposium, Dallas, Texas, 1997.
- [36] R. H. Finney, "A Look at Some Elastomer Products Analyzed Using MARC", Elastomer - FEA Forum '99, publ. ARDL, Akron, Ohio, 1999.

9b

Developments in Finite Element Analysis

Oon Hock Yeoh

■ 9b.1 Introduction

When non-linear finite element analysis (FEA) was first applied to rubber problems in the late 1960 s, only the largest universities and research institutes could afford the powerful computers needed. But significant advances in computer hardware and software have reduced the cost of computing so much that it is now available to almost everyone. Indeed, the playing field has been leveled to the extent that for moderately complex problems, the only significant difference between the capability of a large corporation and a small start-up company may lie in the skills of their analysts. The pace of development has been rapid and much has changed since Chapter 9 was first written and then revised for the second edition of this book. Yet, the fundamental principles have remained unchanged. Instead of revising Chapter 9 for this third edition, it was decided to write a second part to cover salient developments in the field.

This part is not intended to be comprehensive nor at the cutting edge of research. It is intended only to provide some practical guidance to engineers interested in using commercial FEA programs in the design of rubber components. Thus, the focus is on special FEA techniques specific to rubber and on interpretation of results. Those interested in the latest scholarly advances are directed to the Proceedings of the European Conference on Constitutive Models for Rubber which are available in book form [1–6]. This biennial conference series began in 1999 and continues to be the premier venue for discussion of the latest research.

■ 9b.2 Material Models

In the early days of rubber FEA, it was common to perform *linear* FEA as discussed in earlier sections of Chapter 9, even though rubber is inherently *non-linear*, because of the limited capability of even “super computers” of the day. However, modern

computers are now sufficiently powerful that non-linear FEA is the standard method employed for rubber.

FEA requires as input a mathematical description of the non-linear stress-strain properties of the rubber, i.e., a material model. Several reviews on the subject of rubber material models for FEA are available in the technical literature [7–11]. The present discussion is limited to basic principles and practical guidance for the novice user.

9b.2.1 Hyperelastic Models

It is useful to return to basics and recall that in general, deformation has two components:

- dilatational (or volumetric), which involves a change in volume without change in shape, and
- deviatoric (or shear), which involves a change in shape without change in volume.

Further, for rubbers, it is convenient to assume for most purposes that the material is incompressible. Therefore, much of the discussion about hyperelastic models revolves around how to model deviatoric behavior.

Hyperelastic models describe the stress-strain behavior of rubber in terms of strain energy functions. Models commonly used in commercial FEA programs fall into two main classes; they are expressed in terms of (a) strain invariants or (b) principal stretch ratios. For example the Rivlin form is

$$W = \sum_{i,j=1}^n C_{ij} (I_1 - 3)^i (I_2 - 3)^j \quad (9b.1)$$

where W is the strain energy density, I_1 and I_2 are the strain invariants, which may be expressed in terms of the principal stretch ratios, λ_1 , λ_2 and λ_3 , as

$$I_1 = \lambda_1^2 + \lambda_2^2 + \lambda_3^2$$

and

$$I_2 = \lambda_1^2 \lambda_2^2 + \lambda_2^2 \lambda_3^2 + \lambda_3^2 \lambda_1^2$$

and C_{ij} are the material coefficients, while the Ogden form is

$$W = \sum_{i=1}^n \frac{\mu_i}{\alpha_i} \left(\lambda_1^{\alpha_i} + \lambda_2^{\alpha_i} + \lambda_3^{\alpha_i} \right) \quad (9b.2)$$

where α_i and μ_i are the material coefficients.

In order to determine the material coefficients for Rivlin or Ogden models it is necessary to perform stress-strain measurements in several different modes of deformation; most commonly uniaxial extension, pure shear (also known as planar extension), and equi-biaxial extension of thin test specimens. Simple shear of bonded blocks and simultaneous extension, inflation, and torsion of tubular specimens have also been used. The material coefficients are determined from stress-strain data by regression analysis.

A common fallacy is to assume that the use of more terms in the strain energy function leads invariably to more accurate models. The fact is that the additional degrees of freedom associated with more adjustable parameters are often used by the regression analysis to provide a better fit to measurement errors inherent in any experiment! The result may be a model that is worse rather than better. There is no substitute for sound engineering judgment.

Commercial FEA codes provide utilities to perform the regression analysis. These are convenient but not necessarily the best tools for the job. Users may sometimes find it helpful to perform the data reduction using other computer software providing better control over the final model. Some advantages of applying additional constraints to the regression analysis while fitting the Ogden model to experimental data are discussed by Yeoh [12].

Unfortunately, the full experimental characterization of elastic behavior of rubbers *via* measurements in different modes of deformation is rather costly because of the effort and care required. Some simplification is possible, if *a priori* assumptions are made of the form of the strain energy function. For example, if W is assumed to be a function of I_1 alone (i.e., the contributions of I_2 are neglected) as advocated by Yeoh [13], then the Rivlin form reduces to

$$W = \sum_{i=1}^n C_{ij} (I_1 - 3)^i \quad (9b.3)$$

In this form, j is always zero but has been retained for consistency with the Rivlin form.

It is noteworthy that Rivlin arrived at his model from mathematical arguments involving symmetry and material incompressibility. Thus, there is little doubt about the need for I_2 terms. Indeed, the existence of I_2 terms is well documented by experimental data in the literature. It is merely the empirical observation that contributions of I_2 terms tend to be small relative to I_1 terms that justifies neglecting I_2 terms as an *approximation*. Neglecting I_2 terms greatly simplifies the problem of determining material coefficients, because it is no longer necessary to separate the respective contributions from I_1 and I_2 . The material coefficients in Eq. (9b.3) can now be determined from experimental stress-strain data from a *single* mode

of deformation. This advantage, albeit at the expense of mathematical rigor and accuracy, was appreciated and neglecting I_2 became fairly popular. Equation (9b.3), when truncated to the first three terms viz:

$$W = C_{10}(I_1 - 3) + C_{20}(I_1 - 3)^2 + C_{30}(I_1 - 3)^3 \quad (9b.4)$$

was originally described as the cubic model, but it is now more commonly known as the Yeoh model.

Yeoh is not the only proponent of hyper-elastic models involving just I_1 . From a consideration of a model network, Arruda and Boyce [14] proposed the hyperelastic model

$$W = G \left[\frac{1}{2}(I_1 - 3) + \frac{1}{20\lambda_m^2}(I_1^2 - 9) + \frac{11}{1054\lambda_m^4}(I_1^3 - 27) + \frac{19}{7000\lambda_m^6}(I_1^4 - 81) + \dots \right] \quad (9b.5)$$

and Gent [15] proposed the semi-empirical model

$$W = -\frac{G}{2}(I_m - 3) \ln \left[\frac{(I_m - I_1)}{(I_m - 3)} \right] \quad (9b.6)$$

where G is the shear modulus at small strains, while λ_m and I_m represent the limiting values of λ and I_1 associated with finite extensibility of molecular chains. These models are particularly attractive because of the use of just two adjustable parameters, which in addition have specific physical meanings.

There is also an important simplification in interpretation arising from the use of hyperelastic models that involve I_1 only. It is noteworthy that the relation between engineering shear strain, γ , and I_1 is

$$\gamma^2 = (I_1 - 3) \quad (9b.7)$$

and hence from Eq. (9b.4)

$$\tau = \frac{dW}{dy} = \frac{dW}{dI_1} 2\gamma = 2C_{10}\gamma + 4C_{20}\gamma^3 + 6C_{30}\gamma^5 \quad (9b.8)$$

or

$$\frac{\tau}{\gamma} = 2C_{10} + 4C_{20}\gamma^2 + 6C_{30}\gamma^4 \quad (9b.9)$$

So, in the cubic model, the secant shear modulus, τ/γ , has a second order (parabolic) relationship with γ^2 and $(I_1 - 3)$. The combination of a negative value of C_{20} and

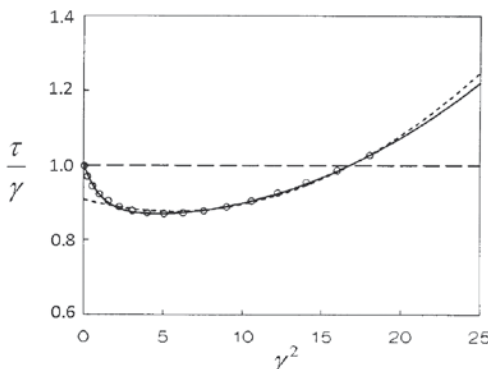


FIGURE 9b.1 Effect of deformation on shear modulus; the initial shear modulus $G = 2 C_{10}$ has been scaled to a nominal value of 1.0. Circular symbols show measured shear modulus data. Horizontal dashed line represents constant modulus (neo-Hookean model). Broken parabolic curve represents the cubic model (Eq. (9b.4)). Solid line represents improved fit with additional exponential term (Eq. (9b.10))

positive values of C_{10} and C_{30} captures the general form of the strain dependence of shear modulus as shown schematically in Fig. 9b.1. However, the cubic form is unable to provide an accurate fit to experimental data, especially in the case of rapid changes in modulus at small strains (strongly shear thinning) often found with practical engineering rubbers. Yeoh [16] has proposed adding an exponential term to Eq. (9b.5) to improve the fit, viz:

$$W = \frac{A}{B} \left\{ 1 - \exp \left[-B (I_1 - 3) \right] \right\} + \sum_{i=1}^n C_{ij} (I_1 - 3)^i \quad (9b.10)$$

Othman and Gregory [17] and Davies et al. [18] have proposed similar forms. Note that in the Arruda-Boyce or Gent models, the shear modulus increases monotonically and thus they do not capture the initial decrease discussed here.

Not all hyperelastic models discussed here are supported by commercial FEA codes. FEA code developers appear quite capricious in their choices. For example, the Arruda-Boyce model is supported by Abaqus but the Gent model (which is simpler) is not. Lack of direct support is inconvenient but not critical. There is usually provision in commercial FEA codes to invoke a user-defined subroutine in case the analyst wishes to use a strain energy function that is not supported.

Although the phenomenological theory of rubber elasticity has traditionally modeled hyperelastic behavior in terms of strain energy density functions as discussed above, it is not necessary to have explicit expressions for the purposes of finite element analysis. When I_2 is neglected, Marlow [19] has shown that the elastic response can be evaluated by interpolating directly from a single set of stress-strain data.

This method is supported within Abaqus as the Marlow model [20] or method. When I_2 is also taken into consideration, Lin [21] has succeeded in interpolating from three sets of stress-strain data obtained in simple, planar, and equi-biaxial extensions and implemented his method as a user-defined subroutine in commercial FEA software.

It should be pointed out that hyperelastic models assume that the material is isotropic. Some elastomers, notably natural rubber and polychloroprene, crystallize upon stretching and so become anisotropic and the stress-strain curves become irreversible. Hyperelastic models are incapable of capturing this behavior accurately. It is a limiting factor in the applicability of a strain energy density function [22] in FEA. Note that other mechanisms may also contribute to anisotropy or non-reversibility.

9b.2.2 Compressibility

Although it is common to think of rubber as incompressible, its bulk modulus is merely large (relative to its shear modulus) rather than infinite. For many applications the distinction is not important. However, when the rubber is highly constrained by rigid members as in steel laminated bearings used in helicopter blade mounts or under bridges and buildings, FEA results are significantly affected by bulk compressibility. Within commercial FEA software, the usual approach to modelling *nearly incompressible* rubber is to express the strain energy function in a form that decouples the deviatoric and dilatational contributions, for example

$$W = \sum_{i,j=1}^n C_{ij} (\bar{I}_1 - 3)^i (\bar{I}_2 - 3)^j + \sum_{k=1}^m \frac{1}{D_i} (J - 1)^{2k} \quad (9b.11)$$

where \bar{I}_1 and \bar{I}_2 are the first and second *deviatoric* strain invariants (i.e., after separating out the dilatational contribution), J is the ratio of compressed volume to uncompressed volume and D_i are the material coefficients. If $m = 1$, D_1 is recognized as twice the bulk compliance. Instead of D_1 some FEA programs may require the use of equivalent values for bulk modulus or Poisson's ratio as input. Equation (9b.11) allows the use of higher order terms although these are not often used. Indeed, for most applications, it is sufficient to use a rough estimate – for example, to assume that the bulk modulus is 1000 G which is equivalent to a Poisson's ratio of 0.4995. Analysts who are more fastidious may wish to measure bulk modulus or Poisson's ratio using experimental techniques, such as those described by Hollownia [23] and Kugler et al. [24]. It is noteworthy that some FEA programs default to a bulk modulus that may be considered unacceptably low; for example, Abaqus Explicit defaults to a Poisson's ratio of only 0.475 to reduce computation time.

The above considerations do not apply to highly compressible rubbers such as cellular or foam rubber. Storåkers [25] proposed a compressible version of Ogden's strain energy function and this is implemented in some commercial FEA codes. However, these materials are notoriously difficult to model.

9b.2.3 Deviations from Hyperelasticity

It should be noted that a hyperelastic material by definition exhibits no time- or rate-dependent behavior: it is *perfectly elastic* and responds instantaneously and recovers perfectly. While it is standard practice to model stress-strain behavior of rubber for FEA in terms of a hyperelastic model, and this approach is very useful, it must be recognized that in reality rubber deviates significantly from such idealized behavior. It is sometimes desirable to model deviations from hyperelasticity because they are in fact of great practical importance. However, the task of modeling more complex stress-strain behavior of rubber accurately is daunting. Muhr [26] has written an excellent review that includes a discussion of several modeling techniques beyond hyperelasticity. Only a couple of specific models are discussed in the following.

9b.2.3.1 Viscoelasticity

Time-dependent behavior may be simulated by assuming the material is viscoelastic. A common method is to assume that the material may be defined in terms of a generalized Maxwell model with n Maxwell elements *plus* an extra spring, as shown schematically in Figure 9b.2. It may be noted from Chapter 4 that the response of a Maxwell element involves an exponential function with a characteristic time, τ . Since the decomposition of a complex signal into a series of n exponential terms is called Prony's method, this method of representing viscoelastic behavior is commonly described as employing a Prony series.

More specifically, for linear viscoelastic materials, the time dependent shear modulus $G(t)$ is usually represented in FEA codes by

$$G(t) = G_0 \left[1 - \sum_{i=1}^n g_i \left(1 - e^{-t/\tau_i} \right) \right] \quad (9b.12)$$

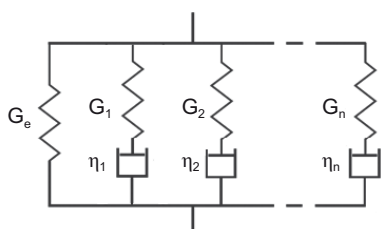


FIGURE 9b.2 Schematic representation of a viscoelastic model

where G_0 is the instantaneous (short term) shear modulus given by summing the moduli of all the spring elements, i.e.,

$$G_0 = G_e + \sum_{i=1}^n G_i \quad (9b.13)$$

The parameter g_i is the fractional contribution of the i th Maxwell unit to the initial modulus, i.e.,

$$g_i = \frac{G_i}{G_0} \quad (9b.14)$$

and the characteristic time (also called relaxation time) of the i th Maxwell unit is given by

$$\tau_i = \frac{\eta_i}{G_i} \quad (9b.15)$$

It is seen that the term within square brackets in Eq. (9b.12) is a dimensionless quantity that attenuates the instantaneous shear modulus. The contribution of the i th Maxwell element to the attenuation depends on g_i and it occurs in a time that depends exponentially on $-t/\tau_i$. Note that g_i and τ_i are assumed to be independent of strain (or stress) in this formulation. For finite strain viscoelasticity, a time domain generalization of the hyperelastic strain energy function is commonly implemented and the Prony series term acts similarly as a dimensionless scaling factor. For example, in the case of the Rivlin strain energy function, the effective Rivlin coefficients C_{ij} would be given by

$$C_{ij}(t) = C_{ij} \left[1 - \sum_{k=1}^n g_k \left(1 - e^{-t/\tau_k} \right) \right] \quad (9b.16)$$

The parameters of the Prony series may be determined from creep, stress relaxation or dynamic test data. An example of a stress relaxation experiment for such purposes is given by Dalrymple et al. [27].

9b.2.3.2 Stress-Softening

Practical rubber engineering compounds soften when deformed cyclically, i.e., the modulus of the rubber is reduced after experiencing deformation. The extent of softening depends on the previous deformation; the greater the strain, the greater the reduction in modulus. This phenomenon is called the Mullins effect and is

probably associated with disruption of weak filler-filler and rubber-filler bonds (see Chapter 3). The phenomenon is quite complex and for modeling purposes some idealization is necessary. In essence, the model invokes two components: first the response for monotonic straining from an undeformed state and a second associated with microscopic damage leading to a new unloading-reloading behavior. Thus, the stress-strain curve is described by a pseudo-strain energy density function that changes with subsequent loading cycles according to the maximum strain energy density experienced during the deformation history. This concept originally developed by Ogden and Roxburgh [28] was shown by Mars [29] to be effective for several benchmark cases. Users should refer to their FEA manual for specific details of how the Ogden-Roxburgh model is implemented and used in the code. It gets complicated quite quickly. For example, one commercial FEA program allows the combination of the Mullins stress-softening model with both viscoelasticity and permanent set [30].

■ 9b.3 FEA Modelling Techniques

9b.3.1 Pre- and Post-Processing

All major commercial FEA codes have strong native pre- and post-processors that allow users to create their models from scratch, submit the model to the solver for solution, and then view the results afterwards in a nearly seamless fashion. Much effort has been expended in creating slick graphical user interfaces (GUI) that facilitate many of the tasks involved in defining a model or reviewing results, often reducing several lines of commands to a single mouse click on a drop down menu. Indeed, there is a marketing push to try to make everything so user-friendly and automated that a designer with no special training can, in principle, launch an analysis from within a CAD program and view results without necessarily recognizing that he has performed FEA. Some of the commands that an advanced analyst needs might not be supported by the GUI but remain available by adding line commands. So, ultimately a user has to be comfortable with using both the GUI and text inputs. Support continues for the use of third party pre- and post-programs and some users prefer them to the native versions. Apparently, some tasks are easier to accomplish in some programs than in others. Often the choice is determined by the user's familiarity with a particular program; it takes considerable effort to learn and master another program, so the path of least resistance is usually to use the program that is most familiar. Another reason for choosing to use a third party program is when a customer requires an analysis of a part that has already been designed using a

CAD package. In this case, digital information about the part is already available and it is much more convenient to import this into the FEA package.

For most cases, it does not matter whether the analyst uses a third party or the native pre-processor to define the model; the results from the solver should be the same. However, there are also cases where the analyst will do well to plan ahead and choose accordingly. For example, after an analysis of the global stiffness of a part, the analyst might decide to do a fracture mechanics analysis to estimate the risk of fatigue failure. Now, a fracture mechanics analysis would involve insertion of cracks and estimation of the strain energy release rate (also known as tearing energy, see Chapters 5 and 6). This is most conveniently performed on the model geometry using special tools in the GUI. But this requires the model to have been created using the native pre-processor in the first place. A model created with a third party pre processor is typically defined in terms of the nodes only. It has no information of the associated geometry. So, the GUI tools available to facilitate crack insertion might not work on the third party model.

9b.3.2 Choice of Elements

Commercial FEA codes typically provide a rich element library to suit different types of analysis. 2D elements may be axi-symmetric, plane-stress or plane-strain, and triangular or quadrilateral in shape. 3D elements may be tetrahedral or hexahedral (brick).

Elements may use linear (first order) or quadratic (second order) interpolation. In addition, these elements may use full or reduced integration.

Conventional general purpose elements, formulated with displacements as variables, may be used for both linear and non-linear analyses. However, when incompressible or nearly incompressible materials are involved, hybrid or Hermann elements, which are formulated with displacements *and* pressure as variables, are strongly recommended.

Given the wide variety of element types available, it is important to select the correct element for a particular application. Choice of an element may be guided by the following considerations [30]:

1. Quadrilateral or hexahedral are generally preferred over triangular or tetrahedral elements. The latter tend to be too stiff. However, it might be difficult to mesh complex geometries entirely with quadrilateral or hexahedral elements. In such cases, a mesh consisting of mainly quadrilateral or hexahedral elements with some triangular or tetrahedral elements is recommended. Triangular or tetrahedral elements are preferably placed in locations where accurate results are not as important.

2. Second order elements are preferred for “smooth” problems as they are more accurate for a given mesh density. However, when problems involve extreme strain gradients or severe distortions, first order elements are preferred. Also, first order elements generally work better in problems involving contact. When first order elements are used, a higher mesh density is recommended. First order elements use less computational resources than second order elements, so a higher mesh density does not introduce a serious penalty. It is noteworthy that the computational resources required increase very rapidly with model size, especially in the case of 3D problems. Consequently, in large complex models, first order elements tend to be used.
3. Reduced integration elements reduce running time, especially in 3D problems. The combination of second order elements and reduced integration is typically recommended. For first order elements, reduced integration may be associated with a problem of uncontrolled distortion of the mesh termed “hour-glassing”, while full integration may be associated with a problem of excessive stiffness in bending termed “shear locking”. Full integration is also associated with a problem of excessive stiffening for deformations that should cause no volume changes termed “volume locking”. These problems do not always occur; they only occur under certain special conditions. Users are advised (as always with FEA) to check their results carefully.

9b.3.3 Convergence

Modern non-linear FEA programs offer automatic stepping procedures to help find solutions quickly. Default values for tolerance and convergence criteria are normally well chosen and reasonable solutions are usually obtained. However, it is not at all unusual to encounter situations where the solver has difficulty converging to a solution. Convergence problems are often associated with one of a few common causes:

1. errors in input, e.g., in the boundary conditions,
2. too large load/time steps,
3. severe distortion in a few elements.

Causes 2 and 3 can usually be identified by resubmitting the problem with a much smaller load step. If the solver converges, then the solution can be examined for clues. The process can be repeated with increasing loads to identify the point at which the solution stepping process fails and the reason for it. Relaxing the tolerance and convergence criteria sometimes helps. At other times modifications to the model and mesh are necessary. However, rubber problems sometimes involve such severe deformation that the process simply fails.

9b.3.4 Fracture Mechanics

Chapters 5 and 6 discussed the application of fracture mechanics to failure analysis of rubber. Failure is believed to be controlled by the strain energy release rate or tearing energy available. One of the difficulties that hindered the wider adoption of the fracture mechanics approach in rubber is the difficulty of estimating tearing energy when large deformations are involved. Finite element analysis has been a great help. Lindley [31] was a pioneer in showing that tearing energy can be simply estimated by taking the difference in total energy stored in the component before and after the growth of a crack, i.e.,

$$G = -\left(\frac{\partial U}{\partial A}\right)_l \approx -\frac{\Delta U}{\Delta A} = -\frac{U_1 - U_2}{A_1 - A_2} \quad (9b.17)$$

where G is the tearing energy, U is the total energy stored in the component, A is the area of one surface of the crack, and the subscripts 1 and 2 denote states corresponding to before and after the crack growth step. Although the technique involves the subtraction of one large quantity from another large quantity in order to estimate a small quantity, FEA calculations are sufficiently precise to yield satisfactory results.

The above approach requires running *two* FEAs, which is inconvenient. More recently, special techniques have been introduced to facilitate introduction of cracks in a model and to perform the tearing energy calculations by post-processing the stress and strain results in the vicinity of the crack. These calculations are usually based upon Rice's J -integral [32] or virtual crack extension [33].

■ 9b.4 Verification

To the user, a FEA package is a powerful computational engine inside a black box. The validity of results is rarely questioned. Indeed, results are sometimes used to calibrate an experiment in order to determine material properties. For example, Gurvich and Fleischman [34] proposed matching results of FEA to experimental measurements of radial deformations of axially loaded disks as a means of characterizing the finite compressibility of rubber. This, of course, assumes that the FEA results are correct in the first place. Although FEA programs are developed by teams of experts, they are not infallible and a reasonable attitude for users would be "trust but verify". If nothing else, solving a verification problem and comparing results with a known solution confirms that the user has understood how to pose

problems correctly. Verification problems provide a significant boost to the confidence of the user in his results.

It is important to remember that FEA provides approximate rather than exact solutions. Therefore, the verification exercise merely seeks to confirm that the FEA results and the known solution agree to an extent that is close enough for practical purposes. The criteria for agreement may vary. For example, it is quite reasonable to be satisfied with agreement of the *global* load-deflection results but less satisfied with the *local* stress-strain results. Indeed, the latter may present significant difficulties due to the presence of singularities. In spite of uncertainties about the detailed stress-strain distribution, the global load-deflection results may be quite satisfactory since it represents an average with local errors cancelling out.

9b.4.1 Stresses and Strains

When examining FEA results the novice user is reminded of the *different* non-linear measures of stress and strain that may be used. Most engineers are accustomed to thinking almost exclusively in terms of nominal (engineering) stresses and strains, which are referenced to the *undeformed* state. On the other hand, most non-linear FEA programs default to reporting results in terms of less familiar measures of stress and strain, which may be referenced to the *deformed* state. Commonly, but not invariably, the Cauchy (true) stress and the logarithmic (true, natural or Hencky) strain are used. The terms “stress” and “strain” are often used without qualification, potentially leading to confusion. Users are advised to seek clarification if in doubt of the specific measures of stress and strain used.

Among the early contributions to the literature on rubber FEA is a paper by Lindley [35]. Lindley wrote his FEA program himself and his computational techniques would certainly be considered quite primitive by modern standards. Yet his paper contains an example of the type of a verification test that lends credibility to the FEA technique. Lindley modeled the extension of a square sheet of rubber held by rigid clamps along two sides. There was a circular hole in the center of the rubber sheet, so there were significant strain gradients near the hole as well as near the four corners (the clamping positions). The finite element mesh was reproduced on the test piece before stretching using a pen. The FEA results for the deformed mesh were superimposed on photographs of the deformed test specimen for comparison. Lindley was able to show excellent agreement, including quantitative agreement for the strain distribution around the central hole, even though strains there exceeded 150%.

More recently, Ahmadi et al. [36] suggested torsion of a rubber cylinder as a benchmark problem for FEA. Yeoh [37] extended this benchmark test to include torsion

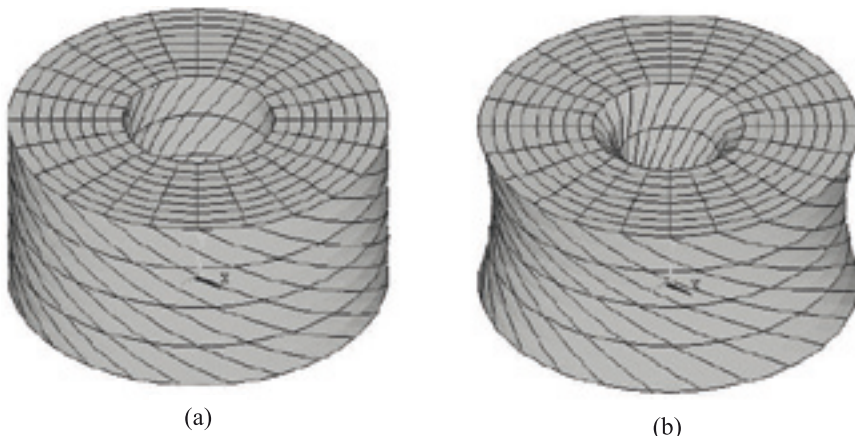


FIGURE 9b.3 Deformed shape of rubber annulus subjected to simultaneous torsion, axial constraint and (a) with or (b) without inflating pressure

of a rubber annulus (tube), using Rivlin's theoretical solutions [38, 39] as the basis for comparison with FEA results. Torsion of an annulus is especially useful since it provides the opportunity to compare simultaneously the tangential (shear) stresses, the axial (compressive) stresses, and the internal pressure required to maintain the specified combination of torsion, axial constraint and inflation (Fig. 9b.3a). When all these check out, as found by Yeoh [37], then the analyst has good reason to be confident of the results for more complex problems such as shown in Fig. 9b.3b. Yeoh [40] has also used a benchmark involving torsion of a cylinder to check the proper implementation of the Marlow model when applied to a material that displays strongly shear thinning behavior.

The importance of verification is seen in a recent study by Ciambella et al. [41] of the finite viscoelastic model of a popular commercial FEA program. In this case, an established implementation of the non-linear viscoelastic model was found to produce spurious relaxation stresses in the normal direction when a rubber block is subjected to simple shear. This FEA program has since been changed.

9b.4.2 Tearing Energy

Similarly, it is useful to compare the results of estimates of tearing energy by FEA with established solutions since agreement reinforces the validity of both methods. Examples of such studies include those by Lindley [35], Chang et al. [42], and Yeoh [43, 44]. Estimates of tearing energy by the classical method of taking the difference in total energy stored in the component before and after the growth of a crack and

by the newer techniques involving J -integral or virtual crack extension have been found to be satisfactory. In a few instances, some minor discrepancies were found, but these could be rationalized [43, 44].

■ 9b.5 Applications

There are numerous studies involving the application of FEA to rubber engineering. Within the limitations of this chapter only a few selected studies are discussed to give an idea of the variety of successful applications. These are divided into studies primarily interested in (a) the global load-deflection behavior and (b) predicting failure.

9b.5.1 Load Deflection

A nominal simple shear arrangement (i.e., a block of rubber bonded between parallel metal plates which are displaced laterally) is widely used in the laboratory for testing rubber, as well as in practical engineering designs. However, true simple shear is not achieved because of contributions from bending and the absence of required stresses at the free surfaces. Gregory and Muhr [45] studied this problem and found that warping at the edges contribute to a slightly larger compliance relative to that obtained using common engineering design equations.

Another important configuration is the compression of a thin rubber blocks between rigid plates. Small-strain solutions for global load-deflection relations as well as local stress-strain distributions are available from linear elasticity analyses (see Chapter 3). Yeoh et al. [46], using linear FEA, confirmed the validity of these solutions for long strips (plane strain), cylindrical disks, and annular blocks (axisymmetric) as well as for rectangular blocks (3-D) bonded to rigid plates. Gent et al. [47] studied the compression of cylindrical disks between two rigid frictional surfaces including the effect of local slippage.

Cylindrical rubber bush mountings are very important in automotive engineering as they permit motion in axial, radial, torsional, and tilting (cocking) modes simultaneously. Controlling stiffness in the various directions is important and available design equations are somewhat inadequate. Both linear and non-linear FEA have been employed in these studies [48, 49].

Indentation hardness testing is the most widely used physical test in the rubber industry. Both the International Hardness Tester and the Shore Durometer have been studied by FEA [50, 51].

9b.5.2 Failure

FEA provides stress, strain and strain energy density results at every node in the model. These are commonly shown as colourful contour plots and used to assess the risk of failure. The question is which failure criterion to use. Maximum principal strain or strain energy density are commonly used as a fatigue life predictor. Maximum principal stress has also been used [52] but according to a literature survey [53] this is less common. Empirical correlations of fatigue life with the chosen parameter (Wöhler curves) have been used for design purposes.

Alternatively, the location of maximum principal strain, principal stress, or strain energy density may be taken as the likely site for crack initiation. Recently, Mars [54] introduced the concept of “cracking energy density”, which represents the portion of the strain energy density that is available to be released by crack growth in a specified plane. Some success in fatigue analysis of rubber components subjected to multi-axial loading conditions has been achieved with this approach [55, 56]. A small crack may be inserted at the chosen location and the tearing energy calculated. The calculation is then repeated with cracks of increasing length and in this way, a relation between tearing energy and crack length is established for the assumed locus of crack propagation under the specified loading conditions. If the crack growth characteristics of the material are known, the fatigue life may be estimated by integrating the tearing energy/crack length curve, as discussed in Chapter 6.

An example of the use of FEA and fracture mechanics to predict failure is found in the analysis by Yeoh [57] of adhesion test geometries. He performed FEA of cylindrical rubber test pieces bonded to flat, spherical, or conical end-pieces subjected to the same tensile force. It was difficult, if not impossible, to compare the test pieces on the basis of traditional “at-a-point” parameters, such as stress, strain, or energy density because of the presence of singularities at the rubber-substrate interface. Figure 9b.4 shows that the strain energy density rose sharply in the vicinity of the expected singularities and the peak values depended strongly on the mesh density.

When cracks were inserted at the rubber-substrate interface to simulate failure at these locations, the tearing energies were easily calculated. An important advantage of the tearing energy approach is the fact that it is obtained from global energy considerations or, in the case of estimation via J -integral, from contours located away from the immediate vicinity of the crack tip. Consequently, the tearing energy is not as sensitive to mesh density as “at-a-point” parameters and hence the results are easier to interpret. The relative ranking of risk of failure is quite apparent in Fig. 9b.5.

Cracks do not always propagate in a straight line along the expected path. A seminal study [58] of why cracks turn sideways was performed by Gent et al. They studied

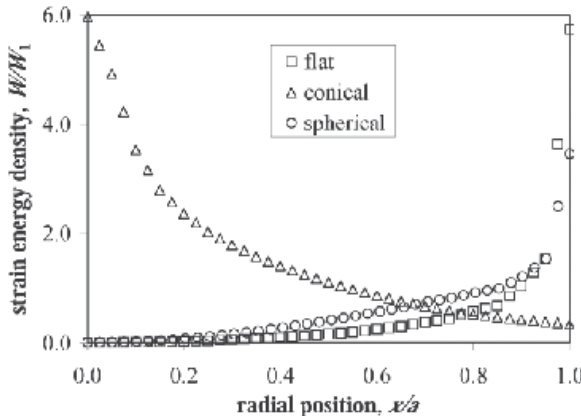


FIGURE 9b.4 Strain energy distribution at the rubber-substrate interface; results shown are for nominal stresses equal to $0.35 G$, similar results were obtained at other load steps

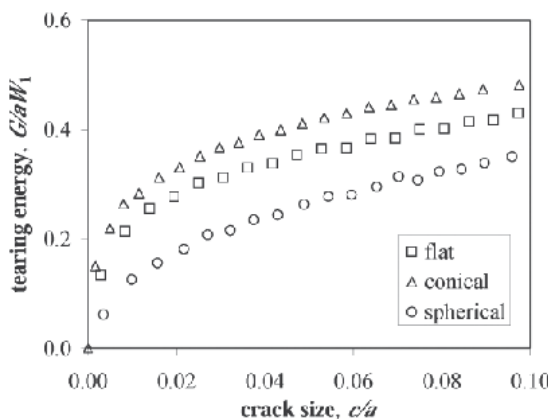


FIGURE 9b.5 Tearing energy for crack growth at the rubber-substrate interface; results for conical end-pieces assume crack initiation at the cone tip in the interior; results for flat and spherical end-pieces assume crack initiation at the perimeter

the apparently simple case of a crack in a test piece subjected to simple extension. It was found that the strain energy release rate for growth of a crack in a direction parallel to the direction of the applied strain is a substantial fraction, about 60%, of that for continued propagation across the test piece. Thus, crack splitting or turning can occur when there is only a relatively minor anisotropy in strength properties. However, the strain energy release rate for a sideways crack decreases rapidly as the crack grows. This explains why the crack path is often irregular.

Fracture mechanics studies relevant to practical engineering components have also been performed with FEA. Gregory and Muhr [45] studied crack propagation

from the leading and trailing edges of a bonded rubber block in simple shear. Gent and Wang [59] studied the tearing energy for crack growth in an elastic cylinder subjected to axial shear. This is important for understanding failure in bushings. Gent et al. studied crack propagation in twisted rubber disks [60–62] and in a tilted rubber block [63]. Özüpek and Becker [64] developed a computational procedure to predict the initiation and growth of belt layer separation in tires.

Other significant FEA studies not involving fracture mechanics include an experimental and finite element study of heat build-up in rubber components by Kerchman and Shaw [65] and modelling of Schallamach waves found in abrasive wear by Gabriel et al. [66].

■ References

- [1] A. Dorfmann and A. Muhr, Constitutive Models for Rubber (Eds.), Taylor & Francis, 1999.
- [2] D. Besdo, R. H. Schuster, and J. Ihlemann (Eds.), Constitutive Models for Rubber II, Taylor & Francis, 2001.
- [3] J. Busfield and A. Muhr (Eds.), Constitutive Models for Rubber III, Taylor & Francis, 2003.
- [4] P.-E. Austrell and L. Kari (Eds.), Constitutive Models for Rubber IV, Taylor & Francis, 2005.
- [5] A. Boukamel, L. Laiariandrasama, S. Meo, and E. Verron (Eds.), Constitutive Models for Rubber V, Taylor & Francis, 2007.
- [6] G. Heinrich, M. Kaliske, A. Lion and S. Reese (Eds.), Constitutive Models for Rubber VI, CRC Press, 2009.
- [7] D. J. Charlton, J. Yang and K. K. Teh, *Rubber Chem. Technol.*, **67**, 481–503, (1994).
- [8] O. H. Yeoh, “Phenomenological Theory of Rubber Elasticity”, Chap. 12, in “Comprehensive Polymer Science”, Supplement 2, ed. by G. Allen, Elsevier, Oxford, 1996.
- [9] V. Vahapoglu and S. Karadeniz, *Rubber Chem. Technol.*, **79**, 489–499, (2006).
- [10] G. Marckmann and E. Verron, *Rubber Chem. Technol.*, **79**, 835–858, (2006).
- [11] A. Ali, M. Hosseini and B.B. Sahari, *American J. of Engineering and Applied Sciences*, **3**, 232–239, (2010).
- [12] O. H. Yeoh, *Rubber Chem. Technol.*, **70**, 175–182, (1997).
- [13] O. H. Yeoh, *Rubber Chem. Technol.*, **63**, 792–805, (1990).
- [14] E. M. Arruda and M. C. Boyce, *J. Mech. and Phys. Solids*, **41**, 389–412, (1993).
- [15] A. N. Gent, *Rubber Chem. Technol.*, **69**, 59–61, (1996).
- [16] O. H. Yeoh, *Rubber Chem. Technol.*, **66**, 754–771, (1993).
- [17] A. Othman and M. J. Gregory, *J. Nat. Rubber Research*, **5**, 144, (1990).
- [18] K. L. Davies, D. K. De and A. G. Thomas, *Rubber Chem. Technol.*, **67**, 716–728, (1994).
- [19] R. S. Marlow, “A General First-Invariant Hyperelastic Constitutive Model”, in “Constitutive Models for Rubber III”, ed. by J. Busfield and A. Muhr, Taylor & Francis, 2003.
- [20] Abaqus Analysis User’s Manual, version 6.10, Dassault Systèmes Simulia Corp., Providence, RI, USA, 2010.

- [21] B. Lin, *Acta Mechanica*, **208**, 39–53, (2009).
- [22] A. N. Gent, G.-B. Lee, J. Y. Lim, Y. H. Kim, R. SenGupta, and C. Nah, *Internat. J. Non-Linear Mech.*, **45**, 232–235 (2010).
- [23] B. P. Holownia, *Rubber Chem. Technol.*, **48**, 246–253, (1975).
- [24] H. P. Kugler, R. G. Stacer and C. Steimle, *Rubber Chem. Technol.*, **63**, 473–487, 1990.
- [25] B. Storåkers, *J. Mech. Phys. Solids*, **34**, 125–145, (1986).
- [26] A. Muhr, *Rubber Chem. Technol.*, **78**, 391–425, (2005).
- [27] T. Dalrymple, J. Choi and K. Miller, “Elastomer rate-dependence: A testing and material modeling methodology”, Paper 11, Fall Meeting of the Rubber Division, ACS, Cleveland, Oct. 16–18, 2007.
- [28] R. W. Ogden and D. Roxburgh, *Proc. Roy. Soc., Lond.*, **A455**, 2861–2877, (1999).
- [29] W. V. Mars, *Tire Sci. Tech.*, **32**, 120–146, (2004).
- [30] Abaqus Analysis User’s Manual, version 6.10, Dassault Systèmes Simulia Corp., Providence, RI, USA., 2010.
- [31] P. B. Lindley, *J. Strain Analysis*, **7**, 132–140, (1972).
- [32] J. R. Rice, *J. Appl. Mech.*, **35**, 379–386, (1968).
- [33] R. M. V. Pidaparti, T. Y. Yang, and W. Soedel, *Int. J. Fracture*, **39**, 255–268, (1989).
- [34] M. R. Gurvich and T. S. Fleischman, *Rubber Chem. Technol.*, **76**, 912–922, (2003).
- [35] P. B. Lindley, *J. Strain Analysis*, **6**, 45–52, (1971).
- [36] H. R. Ahmadi, K. G. N. Fuller, J. Gough, and A. Dusi, “Torsional Behaviour of an Elastomeric Cylinder – a Benchmark Problem”, in “Finite Element Analysis of Elastomers”, D. Boast and V. A. Coveney (Eds.), Professional Engineering Publishing Ltd., London, 1999.
- [37] O. H. Yeoh, *Rubber Chem. Technol.*, **76**, 1212–1227, (2003).
- [38] R. S. Rivlin, *Philos. Trans. R. Soc. London*, **A242**, 173–195 (1949).
- [39] A. N. Gent and R. S. Rivlin, *Proc. Phys. Soc. B*, **65**, 487–501 (1952).
- [40] O. H. Yeoh, “Modeling strongly shear-thinning materials in Abaqus”, Paper 23, Fall Meeting of the Rubber Division, ACS, Milwaukee, Oct. 12–14, 2010.
- [41] J. Ciambella, M. Destrade and R. W. Ogden, *Rubber Chem. Technol.*, **82**, 184–192, (2009).
- [42] Y.-W. Chang, A. N. Gent and J. Padovan, *Intl. J. Fracture*, **60**, 363–371, (1993).
- [43] O. H. Yeoh, “Strain energy release rates for some classical rubber test pieces by finite element analysis”, Paper 2, Fall Meeting of the Rubber Division, ACS, Nashville, Sept. 29 – Oct. 2, (1998).
- [44] O. H. Yeoh, *Mechanics of Materials*, **34**, 459–474, (2002).
- [45] I. H. Gregory and A. H. Muhr, “Stiffness and Fracture Analysis of Bonded Rubber Blocks in Simple Shear”, in “Finite Element Analysis of Elastomers”, D. Boast and V. A. Coveney (Eds.), Professional Engineering Publishing Ltd., London, 1999.
- [46] O. H. Yeoh, G. A. Pinter, and H. T. Banks, *Rubber Chem. Technol.*, **75**, 549–561, (2002).
- [47] A. N. Gent, F. M. Discenzo, and J. B. Suh, *Rubber Chem. Technol.*, **82**, 1–17, (2009).
- [48] J. J. C. Busfield and C. K. L. Davies, *Plast. Rubb. and Comp.*, **30**, 243–257, (2001).
- [49] J.-S. Chen and C.-T. Wu, *Mech., Struct. & Mach.*, **25**, 287–309, (1997).
- [50] J. J. C. Busfield and A. G. Thomas, *Rubber Chem. Technol.*, **72**, 876–894, (1999).
- [51] H. J. Qi, K. Joyce, and M. C. Boyce, *Rubber Chem. Technol.*, **76**, 419–435, (2003).
- [52] N. Andre, G. Cailletaud, R. Piques, *Kautsch. Gummi Kunstst.*, **52**, 120, (1999)
- [53] W. V. Mars and A. Fatemi, *Intl. J. Fatigue*, **24**, 949–961, (2002).
- [54] W. V. Mars, *Rubber Chem. Technol.*, **75**, 1–18, (2002).
- [55] W. V. Mars and A. Fatemi, *Rubber Chem. Technol.*, **80**, 169–182, (2007)

- [56] W. V. Mars, J. G. R. Kingston, A. Muhr, S. Martin and K. W. Wong, "Fatigue life analysis of an exhaust mount", in "Constitutive Models for Rubber IV", ed. by Per-Erik Austrell and L. Kari, Taylor & Francis, 2005.
- [57] O. H. Yeoh, *Rubber Chem. Technol.*, **79**, 320–337, (2006).
- [58] A. N. Gent, M. Razzaghi-Kashani, and G. R. Hamed, *Rubber Chem. Technol.*, **76**, 122–131, (2003).
- [59] A. N. Gent and C. Wang, *Rubber Chem. Technol.*, **66**, 712–732, (1993).
- [60] H. Aboutorabi, T. Ebbott, A. N. Gent and O. H. Yeoh, *Rubber Chem. Technol.*, **71**, 76–83, (1998).
- [61] D. K. De and A. N. Gent, *Rubber Chem. Technol.*, **71**, 84–95, (1998).
- [62] A. N. Gent and O. H. Yeoh, *Rubber Chem. Technol.*, **76**, 1276–1290, (2003).
- [63] A. N. Gent and M. Razzaghi-Kashani, *Rubber Chem. Technol.*, **73**, 818–829, (2000).
- [64] Ş. Özüpek and E. B. Becker, *Rubber Chem. Technol.*, **78**, 557–571, (2005).
- [65] V. Kerchman and C. Shaw, *Rubber Chem. Technol.*, **76**, 386–406, (2003).
- [66] P. Gabriel, Y. Fukahori, A. G. Thomas and J. J. C. Busfield, *Rubber Chem. Technol.*, **83**, 358–366, (2010).

10

Tests and Specifications

John G. Sommer, Oon Hock Yeoh

■ 10.1 Introduction

Rubber is unique among engineering materials in the diversity of physical properties that can be readily achieved by the manufacturer through judicious choice of polymers, compounding ingredients, and processing methods. Because the physical properties of the rubber material are crucial to the service performance of a component, the rubber industry has devoted significant efforts to the development of physical testing methods.

10.1.1 Standard Test Methods

The most widely used tests in America are the methods published by the American Society for Testing and Materials (ASTM) [1]. Other important organizations publishing standard test methods include the Society of Automotive Engineers (SAE) [2] and foreign standards bodies such as the British Standards Institution [3]. International standardization of rubber test methods is undertaken by Technical Committee 45 of the International Organization for Standardization (ISO/TC 45). Although ISO standards are not yet widely used, it is reasonable to expect them to become of increasing importance in a global economy. Several countries have already started to adopt ISO standards as their national standards whenever possible, while other countries at least try to align their national standards with ISO. ISO standards are available from the American National Standards Institute (ANSI) and other national standards organizations.

Standards are not permanent documents. They are drawn up by consensus among leading experts of the day and are revised periodically as necessary. Some standards organizations require review and revision (or reapproval if no revision is necessary) every 5 years to ensure that the information reflects current consensus. When referring to standards, it is good practice to include the year of publication.

10.1.2 Purpose of Testing

It is pertinent to distinguish between tests that yield data for engineering design and quality control tests, which merely verify that one batch of material has the same properties as the preceding batch. In an ideal world, such a distinction would be unnecessary; the tests used to generate design data would also be used for quality control purposes. Unfortunately, this is not so in the real world. Tests useful for generating design data (e.g., shear modulus measurements) are often regarded as too difficult or tedious and consequently are rarely used on a routine basis. Indeed, most of the standard test methods adopted by the rubber industry are quality control tests, which yield data that cannot be directly related to performance. While quality control tests are very important, they are not adequate substitutes for tests that yield design data.

Physical tests are important in specifications for rubber components. The designer needs to communicate to the component manufacturer the nature of the rubber material to be used and the expected properties of the finished component. This takes the form of a technical specification, which normally defines acceptance criteria based on a number of standard physical tests. In establishing the specification, the designer should bear in mind the precision, or more often the lack of precision, of the physical tests being used [4, 5]. ASTM has made a policy of including in its standard test methods statements giving guidance on the normal within-laboratory and between-laboratory variation of test results.

10.1.3 Test Piece Preparation

A distinction should be made between results obtained from test pieces taken from special test slabs prepared in the laboratory and those from test pieces cut from a finished component. Both preparation procedures [6, 7] are allowed in standard test methods and specifications, and it is sometimes assumed that the results are equivalent. It is seldom possible to exactly duplicate factory processing conditions in a small-scale laboratory trial, for example, it is more difficult to achieve good dispersion of fillers with large factory mixers than with small laboratory mixers, and the heat history of a production part is difficult to define and match in a laboratory. Therefore, it is prudent to verify experimentally that results from test pieces of two different types are indeed comparable when quantitative comparisons are needed. Tensile strength and elongation at break results obtained from test pieces cut from a finished component are often about 10% lower than results from specially prepared test slabs. Some specifications provide for lower test requirements when test pieces are cut from finished components.

10.1.4 Time Between Vulcanization and Testing

Users of physical tests should also be aware of the variation of test results as a function of time. Crosslinking does not stop precisely at the time the rubber is taken from the mold. It continues as the rubber cools to room temperature (this can be several hours in the case of a bulky component) and even proceeds slowly at room temperature. Changes are most rapid initially, and it is standard practice [6] not to test rubber within 16 hours of vulcanization. The time between vulcanization and testing is usually less than 96 hours for laboratory-molded test slabs. For finished products [7] it may be necessary to allow longer time periods, but usually testing should be completed within 60 days of delivery to a purchaser. It is preferable to standardize the time between vulcanization and testing in critical experiments.

10.1.5 Scope of This Chapter

Within the space limitations of this chapter, it is not possible to discuss all rubber test methods even superficially. Instead, we shall highlight some of the more important and popular tests. The purpose is to acquaint the reader with the strengths and limitations of these selected tests. For more complete treatments of rubber testing, the reader is referred to the book by Brown [8] and book chapters by Conant [9] and Sommer [10].

Specifications for rubber products are illustrated by critical discussions of selected products. Full specifications are not included here. For these, the reader is referred to the original documentation.

■ 10.2 Measurement of Design Parameters

Although the design engineer may use Young's modulus or shear modulus in his calculations, these are not common parameters in the rubber industry. Instead, hardness is traditionally used as a substitute for modulus and as a convenient means of classifying rubber vulcanizates. This practice is so entrenched that there is no ASTM method for the determination of shear modulus, even though its value to the engineer is unquestioned. This supports our earlier statement that industrial standards are more concerned with quality control tests than tests that yield usable design data. Similarly, although creep and stress relaxation are important phenomena that may affect the service life of a component, these variables are not measured and used as often as they should be.

10.2.1 Young's Modulus

One may argue that rubber does not have a Young's modulus, since the stress-strain properties of rubber are known to be nonlinear and, strictly speaking, no portion of the stress-strain curve obeys Hooke's law. However, the more common view is that the stress-strain relation for rubber is approximately linear over small strains hence, for practical purposes, Young's modulus may be taken as the slope of the stress-strain curve over small tensile or compressive strains. Unfortunately, there is no agreement as to how small the "small" strains may be. It has been pointed out [11] that for a material obeying the statistical theory of rubber elasticity, fitting the best straight line to experimental stress-strain data will yield a Young's modulus that differs from the "true" modulus at infinitesimal strain by an amount of the order of $\varepsilon \%$, where ε is the maximum strain in the experiment (Fig. 10.1). Also, Young's modulus estimated from compressive data will tend to be higher than that estimated from tensile data.

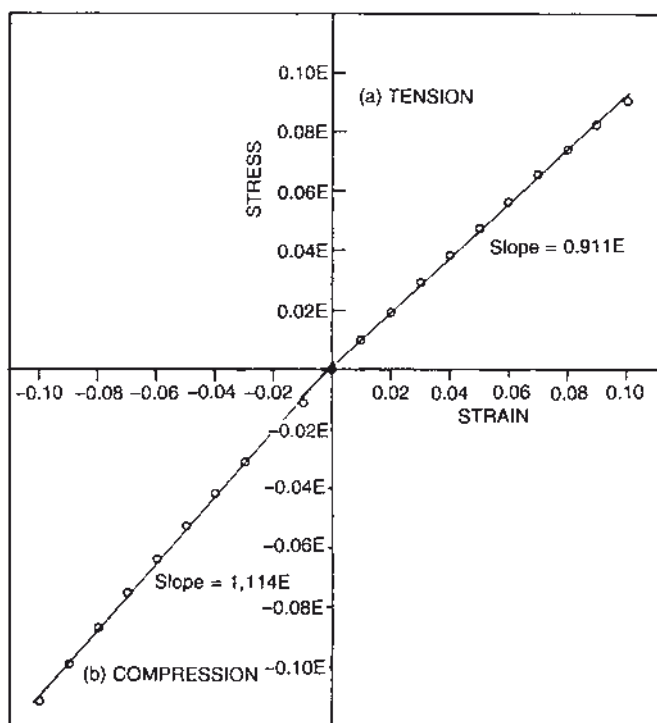


FIGURE 10.1 Fitting straight lines to stress-strain data over the ranges (a) 0–10% tension and (b) 0 to –10% compression yields estimates of Young's modulus that differ from the "true" modulus by about 10%. Hypothetical data calculated for a rubber obeying the statistical theory of rubber elasticity with a "true" modulus of E (© The Plastics and Rubber Institute. Reprinted with permission from [11])

Young's modulus may be estimated by hanging weights on a long strip of rubber and measuring elongation with a cathetometer. This classical method is tedious but gives satisfactory results. Young's modulus should not be estimated by pulling a dumbbell test piece in a conventional tensile test as described in ASTM D 412-06a [12]. Extensometers usually used with rubber are designed to measure large strains and cannot measure small strains with sufficient accuracy.

Alternatively, Young's modulus may be obtained by compressing a cylindrical test piece between flat, parallel platens lubricated with an inert fluid such as silicone oil. The general procedure described in ASTM D 575-91 [13] may be used, with lubrication to facilitate slippage of the rubber at the contact faces rather than with sandpaper to resist slippage. Constraining slippage will lead to a high apparent Young's modulus resulting from shape factor effects [14] (see Chapter 3). A simple device has been described [15] for rapid measurement of compression modulus for routine quality control purposes.

An important consideration in compression measurements is accurate measurement of the original and deformed heights of the test piece. A 10% deformation on the Standard ASTM test piece [13] measuring 28.6 mm in diameter and 12.5 mm in height requires a deflection of 1.25 mm. An error of 0.01 mm in the estimate of deflection means an error of 0.8% in the modulus. One way of improving the test precision is to use a taller sample. A sample measuring 25 mm in diameter and 25 mm in height is convenient. It may not be advisable to take the crosshead travel as a measure of deflection, because the compliance of the load cell and/or the machine itself may be large enough to be a source of error in some machines. It is preferable to measure the separation between the platens directly.

One of the major difficulties in measuring Young's modulus in either tension or compression is its sensitivity to previous deformation. Rubber, especially when filled with reinforcing carbon black, softens when deformed. This phenomenon is often called the Mullins effect [16] after its principal investigator. Most of the change occurs during the first deformation, but small changes may still be detectable after many cycles. Part of the change in modulus is recovered upon prolonged storage. To arrive at a quasi-equilibrium state, it is often suggested that the test piece be subjected to several conditioning cycles before taking stress-strain measurements. ASTM D 575-91 [13] suggests only two conditioning cycles. This is probably inadequate for most rubbers. Since the amount of softening is a function of the magnitude of the conditioning deformation (see Table 10.1), the deformation should be at a level that is consistent with expected service deformation, if design data are sought. Strain-induced softening is discussed further in Chapters 3 and 4.

TABLE 10.1 Effect of Conditioning on Young's Modulus Estimated from Tensile Measurements on an NR Vulcanizate Containing 40 phr Carbon Black

Strain cycle during conditioning (%)	Young's modulus (MPa) ^a
0–15	3.91
0–30	3.71
0–70	3.51
0–100	3.38
0–150	3.13

^a Estimated from the slope of the least-squares line through stress-strain data over the strain range 1–5%

10.2.2 Shear Modulus

Rubber engineering components are commonly deformed in shear. Shear stress-strain data are usually obtained by deforming rectangular blocks or cylinders of rubber bonded to metal plates. One of the bonded plates is held fixed while load is applied to the other plate such that it is displaced in its own plane (Fig. 10.2).

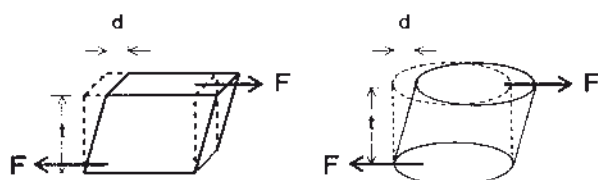


FIGURE 10.2 Simple shear

Shear stress, τ , is defined as

$$\tau = \frac{F}{A} \quad (10.1)$$

where F is the applied load and A is the cross-sectional area of the rubber block. Shear strain γ is defined as

$$\gamma = \frac{d}{t} \quad (10.2)$$

where d is the linear displacement and t is the thickness of the rubber block.

In practice, it is more convenient to use a double-sandwich construction, which tests a pair of such rubber samples together (Fig. 10.3a). Alternatively, the quadruple-shear test piece (Fig. 10.3b) may be used. The use of four replicate rubber samples

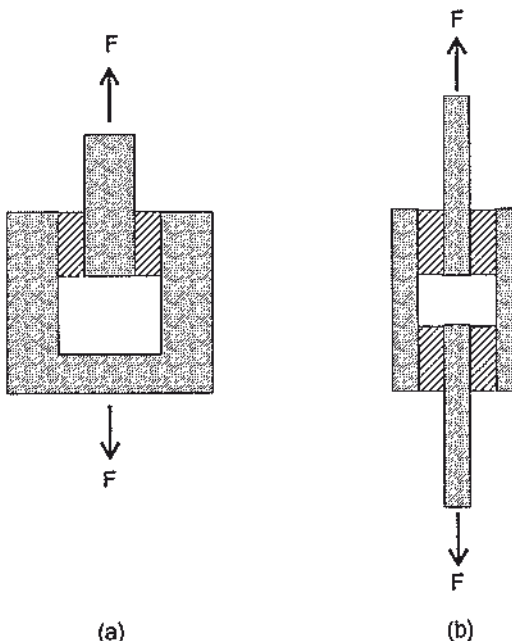


FIGURE 10.3 (a) Double-sandwich shear test piece and (b) quadruple-shear test piece:
hatched area, rubber; shaded area, metal

compensates for the turning couples internally and thus avoids the need for rigid, restraining fixtures. The outer plates keep the bonded faces of the rubber blocks parallel, but the plates are free to move toward one another. This deviation from the definition of simple shear deformation is usually ignored because it has only a minor effect on the test results.

Strictly speaking, the deformation of the rubber is not simple shear in any case. To produce simple shear, it would be necessary to apply suitable forces to the free surfaces [17]. Because there is no means to apply such forces, the true deformation in the rubber is complex. Fortunately, the deviation from simple shear is small, provided the thickness of the rubber block is small relative to its other dimensions. The usual recommendation is to keep the ratio of thickness to side dimension at less than 1:4. The apparent shear modulus obtained using a test piece of this aspect ratio is about 94% of the true shear modulus [18].

As in the case of tensile and compressive measurements, it is necessary to subject the rubber test piece to several conditioning cycles so that a representative stress-strain curve may be obtained. Again it is important not to overstress the test piece. The shear stress-strain curve for rubber is often described as being nearly linear. This is true for unfilled rubber vulcanizates; for practical engineering compounds, which usually contain carbon black filler, however, the shear stress-strain curve has

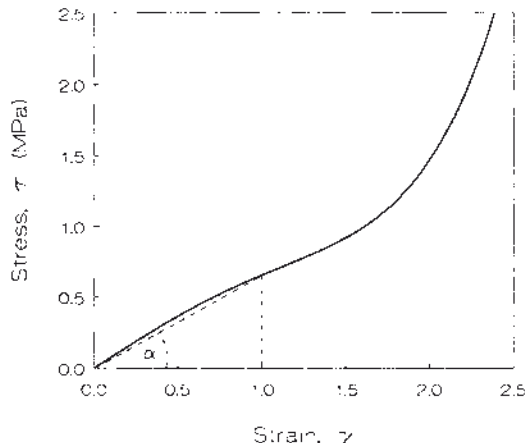


FIGURE 10.4 Typical shear stress-strain curve for NR vulcanizate containing 40 phr carbon black.
Secant modulus at 100% strain = $\tan \alpha$

an S-shape as shown in Fig. 10.4. Such nonlinear behavior requires clarification of the concept of shear modulus. The simple ratio of stress to strain is the slope of the line joining the origin to a point on the stress-strain curve. This ratio is called the “secant modulus” or “chord modulus”. It should be distinguished from the slope of the stress-strain curve at a particular strain, which gives the “tangent modulus” at that strain. The secant modulus, being more easily calculated, is the more popular measure. It is noteworthy that both measures of shear modulus are functions of applied strain. Initially, as the strain increases, the modulus decreases. This may be ascribed to changes in filler-filler or rubber-filler interaction [16]. The modulus eventually rises again at larger strains. This is attributed to the finite extensibility of rubber chains, aggravated by the strain-amplifying effect of the filler [16].

Notwithstanding the conditions above, design engineers commonly use a constant shear modulus in their calculations. The assumption of linearity significantly simplifies calculations. Moreover, this approximation is sufficiently accurate for most practical purposes, provided the shear modulus chosen is appropriate for the average state of strain in the component [19].

10.2.3 Creep and Stress Relaxation

Creep is an increase in deformation with time under conditions of constant stress. It is important in rubber mounting applications such as engine mounts and structural bearings. Stress relaxation is a decay in stress with time under conditions of constant strain. It is important in rubber sealing products such as O-rings and gaskets. Both creep and stress relaxation are important because they often play a

role in the failure of rubber components. Both involve physical and chemical relaxation processes as discussed in Chapter 7.

The physical process is due to the viscoelastic nature of rubber and occurs as an approximately linear function of log time. Typical values for physical relaxation of an engineering rubber in tension are of the order of a few percent per decade of time at ambient temperatures.

The chemical process is caused by chain scission or modification of crosslinks and usually occurs as a linear function of time. Typical chemical relaxation rates for thin strips of rubber are of the order of a few percent per year at ambient temperatures.

Both processes occur simultaneously. Physical relaxation predominates at short times, while chemical effects are more significant at long times. Chemical effects are more obvious under conditions that favor oxidation, such as high temperatures and absence of chemical antioxidants in the rubber.

10.2.3.1 Creep

Buildings are sometimes mounted on composite rubber bearings (similar to bridge bearings), to isolate them from vibration caused by railroads and subways. This base isolation concept has been extended to the protection of buildings from earthquakes. Obviously, settling of a building caused by creep must be controlled in this application.

Creep is sometimes measured in tension in the laboratory by hanging a weight on a dumbbell test piece and following the elongation with a cathetometer as a function of time. Alternatively, creep may be measured in compression or simple shear by placing a weight on a suitable test piece and following the change in deflection over time. For tests in compression, a rubber cylinder bonded to metal is usually used to avoid ambiguity due to slippage at the interface. For tests in shear, a double sandwich test piece as shown in Fig. 10.3a may be used. The weight may be applied via a system of levers. The leverage keeps the weights manageable while facilitating measurement of the small deflection. It is important to minimize friction in the apparatus and to apply the load smoothly. Also, it is important to keep the temperature constant during the test, particularly if leverage is employed; otherwise, expansion and contraction of the test piece may mask the effects due to creep.

There is always some doubt in extrapolating laboratory data to service performance. This is of greatest concern in the case of phenomena such as creep, where measurements are by necessity made over time scales much shorter than the service life. It is therefore reassuring to find an example [20] (Chapter 7 also) of excellent correlation between predictions based on laboratory measurements and site measurements. In this case, a building mounted since 1964 on rubber bearings for the

purpose of vibration isolation has been inspected from time to time, and the rate of creep has been found to be close to that predicted (about 6 mm over 100 years) on the basis of laboratory measurements.

10.2.3.2 Stress Relaxation

Stress relaxation is most often measured on rubber specimens or components in the compressive mode. In this test, measurement is made of the back or residual stress exerted by the rubber after compressing it at constant deformation for prolonged time periods.

In this test, the plates, between which the test specimen is compressed, are made of steel thick enough to withstand the imposed compressive stress without bending. The surfaces against which the specimen is held have a highly polished, chromium-plated finish; they are thoroughly cleaned and wiped dry before each test.

Typically, a cylindrical test piece measuring 28.6 mm in diameter and 12.5 mm high is held compressed at 25% for 2 days at 100 °C. The reaction force exerted by the rubber at the end of the aging period is measured and compared to the initial reaction force. The reaction force may be measured using a special test device which exerts and records the force needed to compress the rubber further by a small amount. Test results should only be compared among specimens of similar sizes and shapes tested under the same conditions.

Tests for stress relaxation are intended to measure residual stress after the rubber specimen has been held deformed for prolonged time periods. On the other hand, compression set tests are intended to measure residual deformation after recovery following release of the rubber from deformation. The two tests are not equivalent. For sealing products, such as O-rings and gaskets, stress relaxation is the more relevant property.

■ 10.3 Quality Control Tests

Physical tests are commonly used in specifications and quality control. In the case of specifications, the purchaser conveys to the manufacturer the qualities expected in the material to be used in the manufacture of the product. In the case of quality control, the main purpose is to verify that production materials and processes are under control and that the present batch is for all intents and purposes identical to previous batches that were acceptable to the customer. In either case, it is customary to use widely accepted test methods. The more common test methods are described here.

10.3.1 Hardness

Perhaps the most widely used test in the rubber industry is the measurement of hardness. Hardness is defined by ASTM as the resistance to indentation as measured under specified conditions. Rubber technologists use hardness as a convenient means of classifying rubber materials.

There are two different hardness tests that claim near universal acceptance. These are the durometer [22] and the International Rubber Hardness tester [23].

10.3.1.1 Durometer

The durometer is commonly referred to as the Shore durometer after its original maker, although equivalent instruments are now available from several other companies.

Different durometers are designed to cover the wide range of hardness encountered in rubbers. These give results on scales designated as A, B, C, D, DO, O, and OO. Care should be taken to distinguish among the various durometer scales when reporting hardness results. The A scale is the most appropriate for rubber compounds commonly used in engineering. The D scale is appropriate for harder rubber compounds such as ebonite. The D scale is also used for plastics.

The original A durometer was designed as a portable, handheld instrument; a truncated cone indenter of precisely controlled dimensions protrudes from its case. In use, the durometer is pressed firmly against a flat rubber sample so as to force the indenter back into the case. A calibrated steel spring resists the force exerted on the indenter by the rubber. The deflection of the indenter is displayed on a dial gauge giving a measure of the rubber hardness on the arbitrary A scale of 0 to 100. Rubber compounds commonly used in engineered components are typically in the range of 45–75 A.

The durometer owes its popularity to its simplicity and portability, making it very useful and convenient as a quality control tool. However, it is not particularly accurate. The hardness result depends on the manner in which the operator applies the durometer to the test piece. Also, the truncated cone indenter is easily damaged, and the steel spring requires calibration.

Attempts have been made to improve the accuracy of the durometer by mounting it on a stand and applying it to the test piece with a constant force and at a constant rate. Also, modern digital readout and an automatic timing device to standardize the elapsed time before taking the hardness reading may be used to reduce operator error. These modifications lead to significant improvements in repeatability and reproducibility [24]. They have become increasingly popular in recent years. However, they eliminate the important advantage of portability.

Care should be taken to test only a flat test piece and to support it on a flat, firm surface. Also, the plane dimensions of the test piece should be large enough to permit measurements at least 12 mm from any edge. The test piece should be at least 6 mm thick, to minimize errors arising from penetration of the indenter to a significant proportion of the depth of the test piece. Failure to comply with these precautions will yield an “apparent” hardness value. This is sometimes done deliberately, as in quality control testing of O-rings [25]. “Apparent” hardness values cannot be easily related to measurements made in the standard manner but may still be useful for comparison purposes.

Recently, microhardness testers that read approximately on the A scale have been marketed. These devices use different indenters under reduced loads to limit the penetration of the indenter into the test piece; thus samples thinner than the recommended 6 mm can be tested. Microhardness testers of this type are standardized by ASTM as Type M durometers. Samples as thin as 1.25 mm may be tested with Type M durometers.

ASTM [22] states that

“The geometry of the indentor and the applied force influence the measurements such that no simple relationship exists between the measurements obtained with one type of durometer and those obtained with another type of durometer or other instruments used for measuring hardness. This test method is an empirical test intended primarily for control purposes. No simple relationship exists between indentation hardness determined by this test method and any fundamental property of the material tested.”

This strongly negative statement requires some qualification. Classical linear elasticity theory can be used to relate the indentation hardness to the Young’s modulus of the material and hence provide a theoretical pathway to convert between hardness scales [26]. Even though local deformations during indentation may be sufficiently large as to exceed the small deformation limitations of linear elasticity, non-linear finite element analysis has been used successfully to provide a mapping of A and D durometer values to the stress-strain behavior of elastomers [27]. So, relationships do exist between the different types of durometers and stress-strain behavior. The relationships will of course be less than exact for rubber materials which display significant viscous (time-dependent) behavior but nevertheless some approximate, semi-quantitative correlation may be expected.

10.3.1.2 International Rubber Hardness Tester

The International Rubber Hardness tester [23] differs from the durometer in several important aspects. It is a small benchtop instrument that uses dead weights to apply defined loads to a spherical indenter, while the penetration is measured with a

dial gauge. The dial gauge is commonly calibrated directly in International Rubber Hardness degrees (IRHD). The IRHD scale was chosen to have readings numerically equivalent to the popular A scale over the range normally encountered in practical engineering compounds. While the approximate equivalence of the IRHD and the A scales is valid for highly elastic materials, significant differences may be expected for materials that show marked time-dependent behavior.

According to the ASTM [23], the penetration of the indenter bears a known relation to the Young's modulus of the rubber. This relation is an empirical relation obtained by Scott [30]:

$$\frac{F}{E} = 1.9 p^{1.35} r^{0.65} \quad (10.3)$$

where F is the indenting force (N), E is Young's modulus (MPa), p is the depth of penetration (mm), and r is the radius of the indenter (mm).

Gent [31] showed that a theoretical relation may be derived from the classical theory of elasticity in the form

$$\frac{F}{E} = 1.78 p^{1.5} r^{0.5} \quad (10.4)$$

with no arbitrary fitting constants. His experimental data indicate that this relation is as good as, if not better than Scott's. Finite element analysis [28] has confirmed that Eq. (10.4) is a better representation of elastic behavior than Eq. (10.3). If we take Young's modulus to be equal to three times the shear modulus G , we may write

$$\frac{F}{G} = 5.33 p^{1.5} r^{0.5} \quad (10.5)$$

These relations between hardness and Young's or shear modulus, whether empirical or theoretical, should be regarded as only approximate. Significant discrepancies may occur simply from the way Young's modulus is defined and measured [11]. Local deformation in the immediate vicinity of the indenter is not infinitesimal, so some consideration of the strain dependence of modulus may be needed [28]. Discrepancies are also expected when the material deviates markedly from perfectly elastic behavior. Although the International Rubber Hardness test [23] is an established ASTM method and well recognized internationally, it is not as widely used in the U.S. as the durometer. In principle, it is an absolute method requiring no calibration, and should therefore be more reliable than the durometer.

Test pieces should be flat and at least 4 mm thick, preferably 8–10 mm thick. Measurements should be made at least 10 mm from any edge. Otherwise, the results should be reported as an “apparent” hardness. The effect of specimen thickness on

indentation hardness has been studied experimentally [29] and by finite element analysis [28]. For thinner samples, a micro version of the test may be used. This method, which is also described in ASTM D 1415-88 [23], involves the use of reduced loads and a smaller diameter spherical indenter. The indentation must be multiplied by a scale factor of 6 before comparison with the indentation in the Standard International Rubber Hardness test. In one commercial instrument, instead of measuring the indentation directly, the test piece table is raised by means of a 6:1 sliding wedge to return the indenter to its original position. The horizontal movement of the wedge gives a measure of the vertical movement of the test piece table, hence the indentation.

10.3.2 Tensile Properties

Although rubber is rarely used in simple extension, tensile properties are the most measured parameters after hardness. This is in part attributable to the use of tensile strength as a general measure of quality. This, in turn, is because attempts to produce a cheap rubber compound by significantly increasing the content of inexpensive fillers usually result in a decrease in tensile strength. Similarly, tensile properties are sensitive to such errors in processing as inadequate dispersion of fillers during mixing and incorrect vulcanization conditions. Tensile set is particularly useful for checking rubber vulcanizates for adequate cure.

An important advantage of the tensile test is that in one relatively simple test procedure, several useful parameters may be obtained. The stresses at several selected elongations (typically 100 and 300%) and at break are determined. By convention, tensile stresses are calculated by reference to the original (unstrained) cross-section. In addition, the elongation at break is usually reported. The uninitiated reader should note that the rubber industry sometimes refers to the stress at 300% strain as the tensile modulus or 300% modulus. This incorrect use of the term modulus is strongly discouraged. "Modulus" should be used only when referring to the ratio of stress to strain.

Tensile properties are usually measured in accordance with ASTM D 412-06a, which provides for the use of dumbbells, parallel-sided strips, or rings [12].

Dumbbell specimens are the most popular. ASTM D 412-06a specifies several dies to be used for cutting specimens from a flat sheet, between 1.3 and 3.3 mm thick. Die C is the preferred die. Sheets of the correct thickness are usually molded directly, but may be prepared by cutting and buffing from finished articles. Before testing, the thickness is measured at three points along the center straight portion of the dumbbell and averaged. The width of the test piece is not measured; by convention, it is taken as the width of the die.

Parallel-sided strip specimens are used when it is impractical to cut dumbbell or ring specimens, as in the case of a narrow rubber strip or small-diameter tubing. Dumbbell and strip specimens should be held in the tensile testing machine by means of self-tightening grips, which distribute the clamping pressure evenly over the width of the tab. Pneumatic action grips are popular, but properly designed roller grips are also suitable.

Extension of the test piece is usually measured by means of a clip-on extensometer attached to the central portion of the specimen. The extensometer must be carefully designed to grip the specimen with sufficient force to prevent slippage but not with so much force that failure results. It also requires a counterbalance mechanism to avoid imposing its weight on a soft specimen. Of course, it must be capable of accommodating the large extensions commonly encountered in testing rubber. Non-contact extensometers using optical followers are sometimes used. These avoid some of the problems associated with clip-on extensometers but they are expensive. Also, on some materials, it may be difficult to mark the gauge length with sufficient contrast for the optical followers to work flawlessly.

Ring specimens are usually cut from a flat sheet by a rotating cutter mounted on a drill press. Alternatively, they may be cut from tubes on a lathe. A dilute soap solution may be used to lubricate the blades during cutting.

Ring specimens are held in the tensile testing machine by means of a pair of fixtures each consisting of a 4.75 mm spindle mounted on bearings treated with a suitable lubricant. The purpose of the lubricant is to facilitate slip, helping to equalize the stress in the rubber on either side of the spindle.

A significant disadvantage of the ring specimen is that the state of strain in the specimen is not uniform; the inside circumference is more highly strained than the outside, and the state of strain in the portion of the ring in contact with the spindle is quite complex. As a result, the tensile strength observed with ring specimens is usually lower than with dumbbells. On the other hand, the use of the ring specimen is favored in some countries for the simplicity of test operation, which facilitates automation. Installation of the test specimen in the grips can hardly be simpler, and there is no need for an extensometer because the extension can be calculated approximately from the grip separation. The latter is advantageous when testing at nonambient temperatures, since some extensometers are not designed for use with environmental chambers.

In testing of O-rings, provided the O-ring is of suitable size, the entire ring may be used as the test specimen [25].

Care should be taken to ensure that all dies and cutters used to prepare test specimens are kept sharp. Rubber fails in tension by the propagation of flaws (see Chapter 5). A poorly maintained die or cutter is likely to introduce relatively large edge flaws that initiate failure prematurely, leading to much lower strength values.

10.3.3 Compression Set

ASTM D 395-03 [32] describes methods for testing compression set. A short cylindrical test piece is held in a compression device either under a constant force or at a constant deflection for a fixed period of time at a specified temperature. The residual deformation of the test piece is measured 30 minutes after removal from the compression device.

Measurement under constant deflection (method B) is much more common than under constant force (method A), probably because it requires a much simpler device. It should be noted that there is no simple general relationship between compression set results by the two methods. Indeed, the results are not even expressed in the same way. For the more common compression set test under constant deflection, the residual deformation is expressed as a percentage of the imposed deflection. For compression set under constant force, the residual deformation is expressed as a percentage of the original thickness of the test piece.

ASTM D 395-03 allows a multitude of options, which include:

1. A choice of two standard sizes of test piece
2. Preparing test pieces by direct molding, by cutting from a larger slab, or by plying up a limited number of cylindrical disks
3. Use of a lubricant between the test piece and the compression plates. All these options affect the test results.

Even without these options, which make interlaboratory comparisons very difficult, a compression set test is rather imprecise and irreproducible. Much of the difficulty lies in the task of making reliable thickness measurements after recovery. This apparently simple task is made difficult because recovery is time dependent and is by no means complete after the standard 30 minutes allowed for recovery. Moreover, the top and bottom surfaces of the test piece are often no longer parallel as a result of different recovery rates at the edges compared to the center. Stiehler [33] commented that the poor repeatability and reproducibility of the test must be improved if the test is to be useful. Unfortunately, there is little evidence of improvement in the intervening years.

The compression set test is intended to reflect the ability of the rubber to recover after prolonged periods under compression. A common misconception is that the lower the compression set, the better the rubber, and there is a tendency to write specifications that permit very little set. Figure 10.5 shows the effect of cure time on compression set. It can be seen that compression set decreases with increasing cure time. Indeed, compression set is quite a good indicator of the state of cure. It is possible to achieve quite low values of compression set by overcuring the rubber.

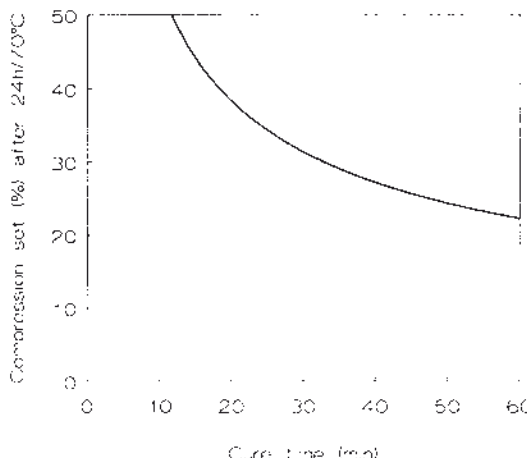


FIGURE 10.5 Effect of cure time on compression set of a typical NR compound

With overcure, other physical properties such as strength, flex resistance, and aging resistance tend to be impaired. Hence, a low compression set rubber is not necessarily a better material. The rubber technologist must balance these different properties to obtain the most acceptable combination.

The compression set test is usually performed at elevated temperatures, but the test has also been used at subzero temperatures [34], particularly to study crystallization behavior.

10.3.4 Accelerated Aging

One of the concerns of the design engineer is the expected life of a component (see Chapter 7). Properties of rubber vulcanizates change during service, especially in a hostile environment. In an effort to study these phenomena in the laboratory, a number of accelerated aging tests have been devised.

10.3.4.1 Aging in an Air Oven

ASTM D 573-04 [35] describes the standard test method for deterioration of rubber in an air oven due to the combined effects of oxidative and thermal aging. The basic principle of the test is to expose rubber test pieces to air at an elevated temperature for specified periods of time. After aging, their physical properties are determined and compared to properties determined on the original test pieces. Usually tensile properties are measured, but other properties, such as hardness, may also be tested. Properties both before and after aging are normally measured at room temperature.

TABLE 10.2 Preferred Elevated Temperatures for Aging Tests Selected from ASTM D 1349

Temperature (degrees)		Remarks
Celsius	Fahrenheit	
40	104	Commonly used in ozone cracking tests
55	131	
70	158	Commonly used
85	185	
100	212	Commonly used
125	257	
150	302	
160	320	Not an ISO preferred temperature
175	347	
200	392	
225	437	
250	482	

Source: [36]

The preferred temperatures for aging are given in Table 10.2. These have been taken from a previous (1987) edition of ASTM D 1349. The current (2009) edition [36] has an expanded list of test temperatures. For comparison with existing data bases, use of temperatures in Table 10.2 is recommended, unless technical reasons dictate selection from the expanded list. Intervals of time that are commonly used are 3, 7, and 14 days.

It is important to avoid the simultaneous aging of materials that are markedly different; for example, rubbers containing no antidegradants should not be aged in the same oven as rubbers heavily protected with antidegradants, because chemicals migrate from one material to another in an aging oven, invalidating the results. An oven design that divides the available capacity into a number of aging cells is recommended to segregate the test pieces [37]. The importance of other aspects of oven design, particularly spatial temperature variation and air velocity within the oven, is discussed by Spetz [38].

There are significant difficulties in predicting service life from accelerated oven aging tests. Use of test temperatures much above anticipated service temperatures is not advisable, because the correlation between such tests and service performance becomes increasingly tenuous.

10.3.4.2 Ozone Cracking

Unsaturated rubbery polymers, such as natural rubber, polybutadiene, styrene-butadiene rubber, and polychloroprene, are susceptible to ozone attack. When

vulcanizates are held stretched in the presence of ozone, cracks can develop on the surface. They grow at right angles to the direction of principal strain. The severity of ozone attack is proportional to the partial pressure of ozone in the test environment [39]. Cracking occurs in air, even though the amount of ozone in the normal atmosphere is only of the order of a few mPa partial pressure. Under standard atmospheric conditions, 1 mPa ozone partial pressure is approximately equal to an ozone concentration of one part per hundred million parts (pphm) by volume.

Ozone cracking occurs only in rubber subjected to tensile stresses. Rubber components used in compression will crack only in the regions of the surface where tensile stresses are induced. These cracks are unable to penetrate very far because they soon encounter compressive rather than tensile stresses. Thus, ozone cracking is not a serious problem for large rubber components, such as bridge bearings, which are used in compression. Nevertheless, ozone cracks are unsightly and may initiate fatigue crack growth, which ultimately leads to failure; thus it is good practice to avoid ozone cracking by the use of protective waxes and antiozonants in the rubber compound.

ASTM D 1149-07 [40] describes procedures for evaluating the deterioration of rubber subjected to dynamic (Method A) and static loads (Method B) while in an ozone environment. Static tests, which are more common than dynamic tests, use test pieces cut from flat sheets of rubber 1.9–2.5 mm thick. In Method B1, a rectangular strip, typically measuring 150 mm × 25 mm, is held stretched in a frame. A typical tensile test strain is 20%. In Method B2, a rectangular strip measuring about 95 mm × 25 mm, is bent into a loop and clamped. The material on the outside of the loop is in tension. Method B3 uses a tapered strip whose width decreases from 25 mm to 12 mm over a length of 131 mm. This test piece is held extended by a nominal 10, 15, or 20% during the test; the actual strain increases from the wide to the narrow end. The advantage of Methods B2 and B3 is that in each single test piece a range of strains is covered. However, the precise strain is not known unless it is separately measured.

ASTM D 1171-99 [41] describes a test piece with a triangular cross section that is bent over a mandrel. Testing consists of exposing the stretched test pieces in an ozone-rich atmosphere at a fixed temperature (usually 40 °C) and inspecting the surfaces for cracks with the aid of a magnifying glass at intervals of time. The standard ozone partial pressures for testing are 25, 50, 100, and 200 mPa with a ±10% tolerance. Part of the difficulty in ozone testing is the determination of the amount of ozone in the test chamber. The most accurate and experimentally convenient way of determining the amount of ozone is by the use of a rather expensive instrument working on the principle of attenuation of UV light [42].

Many rubber vulcanizates depend on the migration of waxes to the surface to form a physical protective layer. Compounds that rely primarily on chemical antiozon-

ants also require the migration of these chemicals to the surface. It is necessary to allow time for these diffusion-controlled processes to take place before testing. ASTM recommends that rubber sheets intended for ozone testing be molded between sheets of aluminium foil or polyester film, which are removed before the test pieces are mounted in their frames. This procedure provides fresh surfaces. The mounted test pieces are then conditioned for 24 hours in an ozone-free atmosphere prior to exposure in the ozone chamber. It is important to avoid touching the test surfaces.

10.3.5 Liquid Resistance

Some rubber components are exposed to liquids, and it is important that these liquids not shorten component service life or adversely affect component performance. Exposure might result in liquid absorption by rubber, extraction of soluble constituents (especially plasticizers and antidegradants) from rubber, and chemical reaction with rubber. Chemical reaction is a significant factor with some rubber components (e.g., the attack of aggressive fuels on rubber seals used in liquid rockets). The physical effects of absorption are more commonly encountered. Hence the following discussion is limited to physical effects, with emphasis on liquid absorption and associated swelling of rubber. Proper matching of rubber and liquid is especially important to control swelling in components such as rubber O-rings.

10.3.5.1 Factors in Swelling

The absorption of liquids by rubber is a diffusion-controlled process, and the effect of the liquid therefore depends on both the time of immersion and the thickness of the rubber (see Chapter 7). With adequate exposure time to a liquid, rubber swells to an equilibrium. The amount of swelling is used as a measure of resistance of a rubber to a liquid, such as oil. Oil-resistant rubbers, of course, do not swell significantly in oil but they may swell substantially in other liquids. Nitrile-butadiene rubber (NBR) is an example of an oil-resistant rubber that finds wide use in seals and other components that call for this property.

Natural rubber (NR), in contrast, is non-oil-resistant, but this feature does not necessarily preclude its use in components subjected to intermittent or limited oil exposure. It is the rate at which oil is absorbed that determines whether a component will fail prematurely. A thin NR sheet will swell rapidly because of its large surface area and small volume and can be expected to fail prematurely when exposed to oil. On the other hand, inherent in the design of many components, rubber volume is relatively large while exposed surface area of rubber is small. In such cases, swelling is likely to be less significant. NR engine mounts are well known to operate successfully in an oily environment for long time periods. The reason for this is

that the depth of penetration of the oil depends roughly on the square root of time. For example [43], an SAE 40 oil will penetrate 1 mm in 4 weeks, but it will take 100 years to penetrate 40 mm. Hence, thick components such as engine mounts are effectively protected by their bulk.

Swelling causes loss in mechanical strength in rubber as well as the obvious volume and dimensional changes. Tests are widely used to measure these changes.

10.3.5.2 Swelling Tests

The ASTM standard for measuring resistance of rubber to liquids is ASTM D 471-06 [44]. The preferred method for volume change measurements is the gravimetric method, in which the test piece is weighed in air and in a liquid (usually water) before and after immersion. The volume change is then calculated on the basis that volume is proportional to the weight in air minus the weight in water.

As an alternative, volume change can be calculated from dimensional changes after fluid immersion. This procedure is considered [46] to be less desirable than the gravimetric method because of the poorer accuracy of making dimensional measurements. For comparative purposes, a 5% linear increase in swelling corresponds approximately to a 15% increase in volume swell.

The effect of liquids on tensile and hardness properties can be measured by two procedures specified in ASTM D 471-06 [44]. In one procedure, properties are measured immediately after removal from immersion; in the other, measurement takes place after removal from immersion and subsequent drying.

10.3.6 Adhesion to Substrates

Rubber is bonded to many different types of substrates such as fabrics, plastics, and metal for service in a range of applications. Here we consider rubber bonded to metal, in suitable shapes and forms such as plates and tubes, to provide a secure means of attachment. Another important reason is to modify the stiffness of the rubber by means of the shape factor effect (see Chapter 3). Indeed, rubber would not have found such wide spread use in engineering without the development of suitable methods for bonding rubber to metals. Today, there are numerous chemical bonding agents available commercially.

The wide variety of rubber formulations, bonding agents, and metal types mean that there are innumerable permutations. Some combinations are better than others in any particular application, so it is necessary to evaluate and choose carefully. Another important reason for testing adhesion of rubber to metal substrates is quality control of materials and processes.

Several methods for adhesion testing are described in ASTM D 429-08 [45]. In Method A, a test piece, consisting of a disc of rubber 39.9 mm in diameter and 3.2 mm thick bonded on its flat sides to metal plates of the same diameter, is broken in tension. Although intended as a test of adhesion, Method A is not very discriminating. One reason is that cohesive failure occurs in the rubber at relatively low stresses from triaxial tension (see Chapters 3 and 5).

Cohesive failure is caused by a small cavity that forms in the central region of the disc that expands under negative pressure [46]. The negative pressure results from stresses caused by outwardly directed tension. These stresses cause an elastic instability in the specimens similar to those observed when an ordinary balloon is inflated. The need to limit triaxial stress was demonstrated by laminated, bonded steel-rubber bearings used in a solid rocket. One end of the bearing is attached to the lower portion of a rocket case; the other end is attached to the rocket nozzle. Pressurized gases from burning propellant places the bearing under considerable compressive stress. Extremely low modulus rubber of about 0.12 MPa or 18 psi is used in the bearing to minimize the force necessary to move the nozzle. This low modulus rubber is especially prone to triaxial failure. Compressive strain in the rubber is low because of the very high shape factor ($SF = 15-20$) used in the nozzle. A nozzle bearing was tested in shear and compression, its normal stress modes in service; additionally, it was tested in tension to give assurance that it was satisfactory. The tensile test caused failure and a number of voids were observed in the failed regions.

These voids could result from gasses trapped during molding or from cavitation during tensile testing. To establish the cause, the same rubber used in the bearing was used in method A specimens; half of those were sliced through with a sharp knife while the other half were tested to failure in tension. The ruptured surfaces of the failed specimens were covered with pock marks or voids while the cut surfaces were free of blemishes. Hence, the blemishes were caused by testing in triaxial tension and this shows the importance of test selection and interpretation of results.

Method B consists of measuring the force needed to peel a 25 mm wide strip of rubber from the metal substrate at an angle of 90° . It was used to measure the adhesion of NBR rocket insulation to a steel rocket chamber [47]. Generally, the upper usable temperature limit for the steel in this application is considered to be about 300°F . Hence, it is desirable to know the adhesion values of the NBR to steel over a temperature range. Peel values were established over a test temperature range of 73 to 400°F as shown in Table 10.3.

The test results in Table 10.3 show that the adhesion values were acceptable at the higher test temperatures.

TABLE 10.3 Adhesion Strength for NBR to Steel

Test temperature (°F)	90° Peel value (lbs/in)
73	140
200	52
300	32
400	12

An additional attraction of this test geometry is the fact that it is amenable to a simple fracture mechanics analysis. According to this analysis, failure occurs at a characteristic strain energy release rate, G , which is related to the peel force per unit width, F , and the peel angle, θ , by

$$G = F(\lambda - \cos \theta) - W h \quad (10.6)$$

where λ is the extension ratio, W the strain energy density, and h the undeformed thickness, all referring to the rubber strip that has been peeled off [49]. However, the problem is complicated by significant bending stresses in the rubber [50]. For strong rubber-metal bonds, failure often occurs by tearing in the rubber. While such failure away from the bond-line is often welcomed as a sign that the bond is stronger than the rubber, it may be misleading. The same test piece may fail at the interface when tested at a peel angle that is less than 90°. The locus of failure is apparently dependent on the detailed stress distribution in the vicinity of the peel front. It may also depend on the method of loading and whether cavitation occurs [51].

In Method C, a standard test specimen, consisting of a rubber cylinder bonded to two conical metal end pieces, is broken in tension. The half-angle of the cone vertex is 45° and the base of the cone is 25 mm in diameter. Stress concentrations at the embedded tips of the cones cause failure to initiate at the bond interface. However, the locus of failure soon deviates from the interface as the debond grows, and the test piece eventually fails by rubber tearing. Visual inspection of the failure surface to assess the percentage of interfacial failure compared to rubber tearing is recorded, in addition to the load at break.

In recent years, ASTM has added even more test pieces. In Method F, the rubber cylinder, bonded to two convex-shaped (spherical) metal end pieces is broken in tension. In Methods G (double shear) and H (quadruple lap shear), the bond is loaded in simple shear but the shapes of the specimens are different, being cylindrical in Method G and cuboid in Method H. The diversity of specimen geometry and methods of loading mean that the results cannot easily be compared and interpreted. Unfortunately, there appear to be relatively few attempts at analysis and rationalization. A recent comparison of Methods A, C, and F by finite element analysis and fracture mechanics highlights the opportunities for research in this area [48].

It is noteworthy that adhesion testing is mostly done on special test specimens prepared in the laboratory. While this gives some indication of likely performance of bonds made from the same rubber and adhesive systems, it does not provide adequate assurance of the bonds achieved in a real world manufacturing process. Taking specimens from finished components is destructive, expensive, and rarely possible because the geometry of the component does not usually permit the extraction of standard adhesion samples. Because of this, it is common practice to apply a tensile “proof” load on finished components as a quality control test for adequate bonding. However, such a tensile “proof” test should be used with care. Rubber components subjected to tension may fail by internal cavitation (see Chapters 3 and 5). This occurs at relatively low tensile loads. Internal damage is difficult to detect by visual inspection, so it is quite possible for a tensile “proof” test to cause damage of the component that passes undetected. It would be ironic to specify a tensile “proof” test of 100% of production to assure adequate bonding only to damage the entire output by performing the test!

It is also noteworthy that short term pull-to-failure tests of adhesion as described in ASTM D 429 reveals little about the long term durability of adhesive bonds. Long term failure of adhesive bonds in severe environments is known. Examples of severe environments known to be detrimental to certain adhesive systems include high temperatures [52], ozone [49], solvents [52], and sea water [52]. The long term durability of adhesive bonds is a subject worthy of further study (see Chapter 7).

10.3.7 Processability

A number of factors are involved in the manufacture of rubber products. These include materials selection, the combining of these materials to form compounds, and finally the conversion of these compounds into rubber products. This conversion can involve a number of processing procedures, such as mixing, milling, extrusion, molding, bonding, and crosslinking. It is important that these procedures be appropriate to the product and that they be properly controlled.

Viscosity, a measure of resistance to flow of a rubber material, significantly affects processing behavior. The ingredients added during mixing further affect viscosity and therefore processing behavior. Added fillers, especially those having a small particle size, rapidly increase compound viscosity and make the compound non-processable at too high a filler content. Appropriate amounts of filler, plasticizer, and other ingredients in the proper rubber material can result in a compound with desirable processing behavior along with the requisite properties for the intended service application.

The Mooney test described in ASTM D 1646 is widely used to measure the viscosity of a rubber compound [53]. In this test, a roughened disc rotates at a shear rate of about 1 s^{-1} in a mass of compound at a temperature of $100\text{ }^{\circ}\text{C}$ ($212\text{ }^{\circ}\text{F}$); the resulting viscosity value indicates the processability of a compound. The test can be run in about five minutes. A disadvantage is that it determines viscosity at a single deformation rate.

Rubber compounds experience a multitude of deformation rates during processing operations such as mixing, extrusion, and molding. For a better assessment of processing behavior over a range of deformation rates, a capillary rheometer can be used. This test is significantly more complicated and costly than the Mooney test and is therefore used more for research and development.

A compound must remain flowable during processing operations. After too long a period of time at high temperature during processing, a thermosetting compound will crosslink (scorch) and stop flowing. If this happens, the scorched compound must be removed from the equipment and fresh compound introduced. A test is needed that will predict whether a compound has sufficient resistance to scorch during processing.

The Mooney scorch test described in ASTM D 1646 is run using a smaller rotor at a higher temperature, typically $121\text{ }^{\circ}\text{C}$ ($250\text{ }^{\circ}\text{F}$), than that used for determining Mooney viscosity. The scorch test measures the onset of crosslinking and the resulting scorch value indicates whether there is sufficient time to complete the necessary processing operations before crosslinking starts and impedes flow. Because the rotor rotates continuously, this test can measure only the very early stages of crosslinking. This is not a problem with the oscillating disc rheometer (ODR).

The ODR incorporates a biconical rotor that oscillates at a small angle, typically $\pm 1^{\circ}$, as described in ASTM D 2084. These conditions permit determination of properties for uncrosslinked, partially-crosslinked, and *fully-crosslinked* compounds. A subsequent development is the moving die rheometer (MDR, standardized in ASTM D 5289), which eliminates the rotor and uses a lower biconical die oscillating with respect to a stationary upper biconical die [54]. Better temperature control results from this arrangement compared to instruments containing a rotor.

The rubber process analyzer (RPA, standardized in ASTM D 6204, 6601, and 7605) has further improved the testing capabilities of the MDR [55]. Like the MDR, the RPA is a rotorless rheometer that measures rubber properties before, during, and after crosslinking and it retains the operating characteristics of the MDR. These characteristics include easy loading and unloading of rubber specimens for testing, a significant advantage compared to the capillary rheometer. The RPA can measure properties over ranges of temperature, frequency, and strain and then compile the resulting data in a straightforward manner. It is said to detect most processability variations [56].

Dynamic properties of EPDM elastomers and their compounds were measured with the RPA to assess its value as a quality control tool [57]. The dynamic data permitted detection of variations in compounding ingredients and mixing time. It was concluded that the data could be very useful as a quality measuring tool. Dynamic mechanical measurements of crosslinked compounds on the RPA provide useful information on engineering properties [58].

Another device can sinusoidally deform crosslinked compounds in additional deformation modes [59]: tension, compression, shear, and bending. It has a force capability of 200 N and a frequency range of 0.5 to 50 Hz. A number of factors can be varied during testing, such as static displacement and temperature.

■ 10.4 Dynamic Properties

Dynamic properties are important in numerous engineering applications. These applications include the use of components to improve man's comfort and to protect equipment. We first review some of the terms used in connection with dynamic properties, as well as some of the differences in dynamic behavior between rubber and other materials, for example, steel. This subject is discussed more fully in Chapter 4.

A steel spring stores energy when deformed and will release nearly all this energy when the deforming force is removed. Its behavior is like that of a Hookean solid. The deformation is instantaneous and linearly related to the deforming force. Hence, a Hookean solid shows no rate or time dependence.

Contrasting sharply with Hookean behavior is that of a Newtonian liquid. The response is time and rate dependent. A Newtonian liquid has no memory and does not recover when the deforming force is removed.

Rubber response to dynamic excitation is quite complex in that it includes elements of both Hookean and Newtonian behavior [46]. Rubber behavior can be approximated by a model that consists of a Hookean spring and a Newtonian dashpot as shown in Fig. 10.6. The spring represents the element in rubber that is associated with elastic or instantaneous response; the dashpot is the element associated with time- or rate-dependent (loss) response. A major objective of dynamic testing is to separate and measure the response associated with the spring (in-phase or elastic response) and that associated with the dashpot (out-of-phase or loss response). Dynamic response is generally measured in terms of a complex modulus or spring rate.

Rubber dynamic behavior is considerably more complicated than indicated by this simplified model. In addition to the rubber material, a number of other factors affect dynamic properties [60]. These include the type and level of ingredients added to

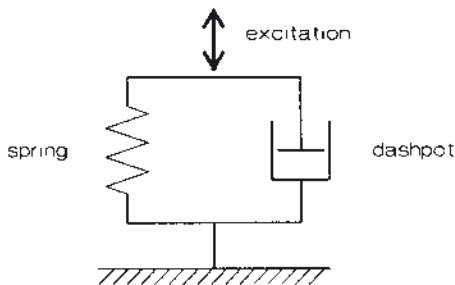


FIGURE 10.6 Simplified model for rubber behavior

form compounds (discussed in Chapter 2), the type of test specimen, specimen conditioning, the test method, and others. Factors like these were included in an extensive examination of dynamic properties using an experimental design [61]. It was concluded that a wide variety of instruments in combination with several types of test specimens can provide better measurement of dynamic modulus than of dynamic loss factor. The latter is subject to greater scatter as well as to greater sensitivity to the test method. Another worker concluded that test artifacts can be separated from material properties and that dynamic properties can be used to predict performance in processing and final applications [62].

The modulus of a rubber composition is an intrinsic property; that is, it is independent of the geometry of the specimen. In contrast, spring rate depends on both rubber composition and specimen geometry. These terms [60] are considered further in Fig. 10.7.

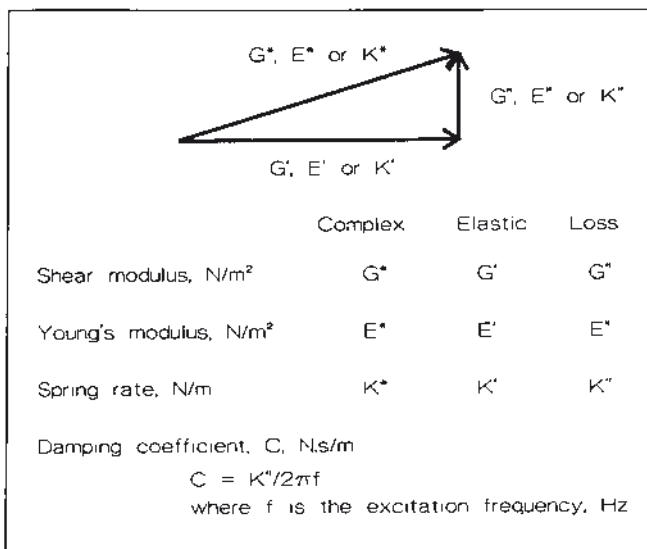


FIGURE 10.7 Definition of terms ([60], with permission; © 1973 Society of Automotive Engineers, Inc.)

The complex modulus G^* or E^* is the vector sum of the elastic and loss moduli; the complex spring rate K^* is the vector sum of the elastic and loss spring rates. For engineered structures or components, the damping coefficient C is often specified, given by

$$C = \frac{K''}{2\pi f} \quad (10.7)$$

where f is the test frequency in Hertz.

Engineered structures frequently combine rubber with metal to form a composite structure, for example, a rubber mount. Boundary conditions between metal and rubber can significantly affect the dynamic properties of such a mount or bearing. Dynamic modulus in compression will be lower and losses higher if slippage occurs between rubber and metal. Chemical bonding of rubber to metal is the preferred method of avoiding slippage during dynamic testing. Minimizing slippage by the use of sandpaper between platens and rubber specimens is permitted as an alternative.

Dynamic properties of rubber can be determined with the help of a variety of instruments. Some of these are simple and inexpensive, while others are complex and quite expensive. ASTM D 5992 gives valuable guidance on dynamic testing of rubber.

10.4.1 Resilience

Resilience is the ratio of the energy returned upon recovery from deformation to the energy required to produce the deformation. With the Bashore resiliometer [51], the rebound of a dropped mass impacting a solid rubber specimen is measured as a percentage of the drop height on a scale marked in 100 equally spaced divisions. The mass weighs 28 ± 0.5 g and is guided by a vertical rod during its free fall onto the test specimen and its subsequent rebound from the specimen.

Other rebound tests are based on a pendulum impacting a specimen. The angle of rebound is measured and resilience is calculated by Eq. (10.8).

$$R = \frac{1 - \cos(\text{angle of rebound}) \times 100}{1 - \cos(\text{angle of fall})} \quad (10.8)$$

The rebound value is usually stabilized after the specimen has been preconditioned with about six impacts. Two pendulum instruments are the Goodyear-Healy [64] and the Lüpke [65]. High correlation should not be expected between results from different rebound tests such as these because the results are affected by pendulum weight, drop height, and energy absorbed by the apparatus. Less energy absorption is expected with the Lüpke apparatus because the mass that strikes the rubber is suspended by flexible wires.

While resilience measurements provide an assessment of the dynamic behavior of rubber, measurements for engineering applications are more usually determined by free or forced vibration methods. A common free vibration instrument is the Yerzley oscillograph [66].

10.4.2 Yerzley Oscillograph

The Yerzley oscillograph, which is strictly mechanical, is shown schematically in Fig. 10.8 [67]. It consists of a horizontal rocking arm that deforms a rubber sample either in compression or in shear. A pen attached to the arm records the rocking motion as a damped sinusoidal curve to yield an oscillogram.

The test is applicable primarily to materials that have static moduli at the test temperature such that stresses below 2 MPa in compression or 1 MPa in shear will produce about 20% deformation. Also, resilience should be high enough to permit recording of at least three complete cycles of oscillation. Materials may be compared under either comparable mean stress or mean strain conditions.

The Yerzley oscillograph is relatively easy to operate and inexpensive; in addition, it provides a fair understanding of the relative dynamic stiffness and damping properties of different rubber compositions. Limitations of the Yerzley are that it employs a decreasing force input rather than a steady one, and testing occurs at low frequencies, usually between 3 and 6 Hz. Also, test data are generated on standard rubber cylinders or shear specimens, not on an engineered component such as a rubber mount. Rubber mounts can be tested directly on other equipment.

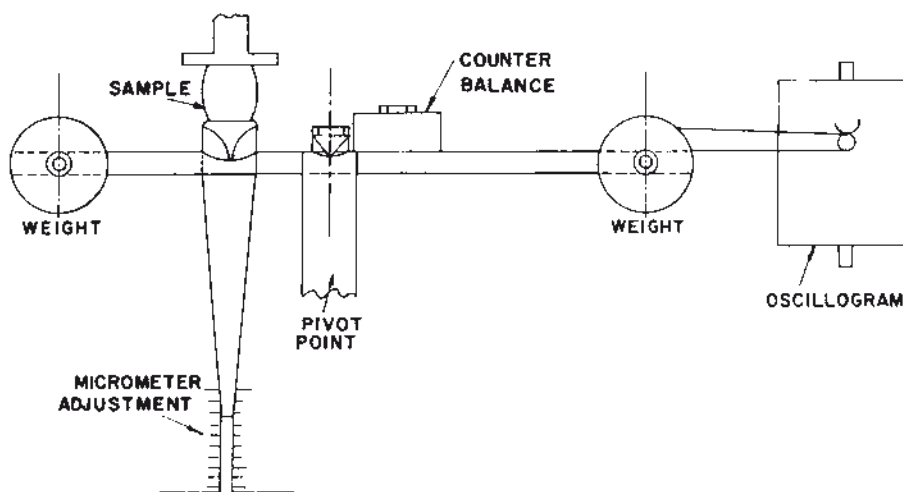


FIGURE 10.8 Yerzley oscillograph (© ASTM. Reprinted with permission from [67])

10.4.3 Resonant Beam

A schematic of a resonant beam device with a sample in place is shown in Fig. 10.9. The sample for testing (e.g., a mount) is installed between a stiff beam and its base. The beam is pivoted at one end, and an exciter vibrates the beam in rotation about the pivot. Power and frequency are adjusted to give the desired displacement at resonance. The value of K' is calculated from frequency and machine constants, while C is calculated from power requirements and machine constants. Frequencies are higher than for the Yerzley, generally in the 10–30 Hz range.

The resonant beam device operates on the principle that a known mass (the beam) supported on a spring (the sample) will oscillate freely at a natural frequency f_n given by

$$f_n = \frac{1}{2\pi} \left(\frac{K'}{m} \right)^{1/2} \quad (10.9)$$

where K' is spring rate and m is mass.

The force used to excite the specimen is a minimum when the force and displacement are 90° out of phase (resonance); under these conditions, the magnitude of the force is a measure of damping in the system. Operating at resonance permits testing large specimens with high spring rates at desirable amplitudes without requiring large and expensive vibration exciters. Peak-to-peak amplitudes of 0.25 to 0.64 mm are commonly used [68].

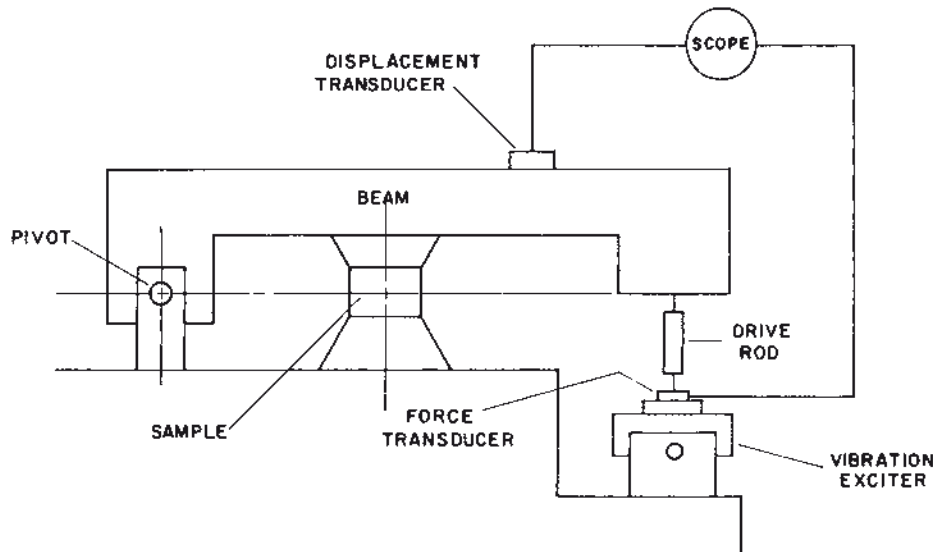


FIGURE 10.9 Resonant beam (© ASTM. Reprinted with permission from [67])

There are several limitations. The beam weight and shape limit the range of possible static loads. This precludes the use of conventional resonant beam systems for testing large engineered structures such as earthquake mounts. Also, since the test frequency depends on the spring rate of the part being tested, the frequency cannot be independently selected.

Modified resonant beam testers permit operation under nonresonant conditions. They require more powerful vibration excitors and a different calculation method, since equations applicable to resonance conditions do not apply. Typical mounts with K' values of 875–1050 N/mm have been tested in this way at amplitudes of 0.10 mm [68].

10.4.4 Servohydraulic Testers

More versatility is available with servohydraulic testers. Figure 10.10 shows a typical arrangement, with a specimen in place. This specimen might consist of rubber only, a tire, or an engineered composite, such as a bonded rubber mount in compression or in shear. A displacement transducer senses motion imparted to the moving side of the specimen; a load cell on the stationary side measures force. Although servohydraulic testers are expensive, they provide in a single device the capability for high force, large displacement, and typical frequencies to several hundred Hz. A number of errors can occur when testing compounds at high frequencies [69]. The errors can be induced by both the test machine and the fixtures used to secure a test specimen to the machine. Machine induced errors include non-linearities in the servo-loop and those associated with transducers; fixture induced errors include

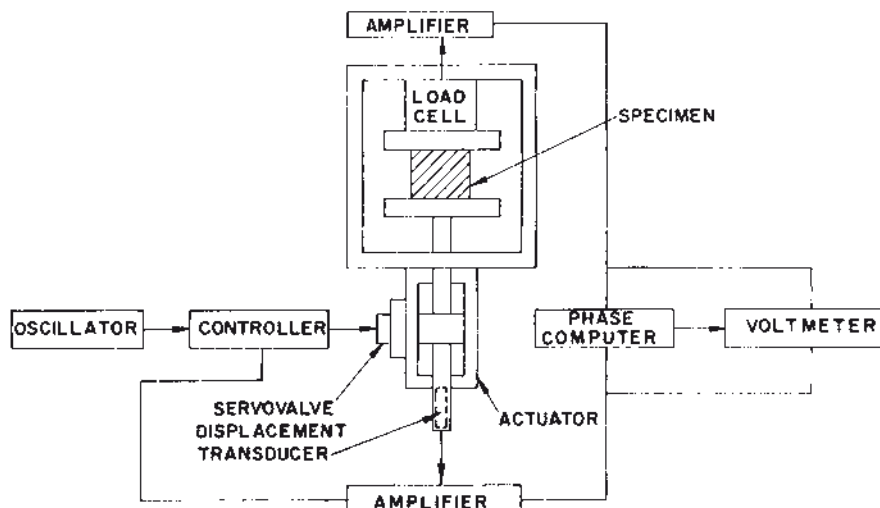


FIGURE 10.10 Servohydraulic tester (© ASTM. Reprinted with permission from [67])

changes in data caused by specimen end effects and superimposed loads due to the mass of the fixture and specimen.

While most testing is commonly done in the uniaxial mode, the use of dynamic testing in the multiaxial mode is increasing [70]. Multiaxial modes include orthogonal axial-torsion and orthogonal biaxial. The multiaxial modes place special requirements on the reaction frame and control system.

As an example, a multi-axis machine can test engine and suspension mounts [71]. The vertical axis can provide up to 30 kN for static loads and 20 kN for dynamic loads, and displacement capability is up to 50 mm. A horizontal actuator can provide up to 15 kN for static loads and 10 kN for dynamic loads, with displacements up to 100 mm. A five ton bed plate gives the weight needed for testing to frequencies up to 220 Hz.

10.4.5 Electrodynmaic Testers

A number of test machines rely on an electrodynmaic actuator to provide cyclic excitation for dynamic testing. Such testers are usually used with small test pieces rather than full-sized components because of the limited force and displacement capacities of the electrodynmaic actuator. These testers are often easy to use and well suited to the characterization of dynamic properties of rubber materials over a wide range of variables, including temperature, frequency, and strain.

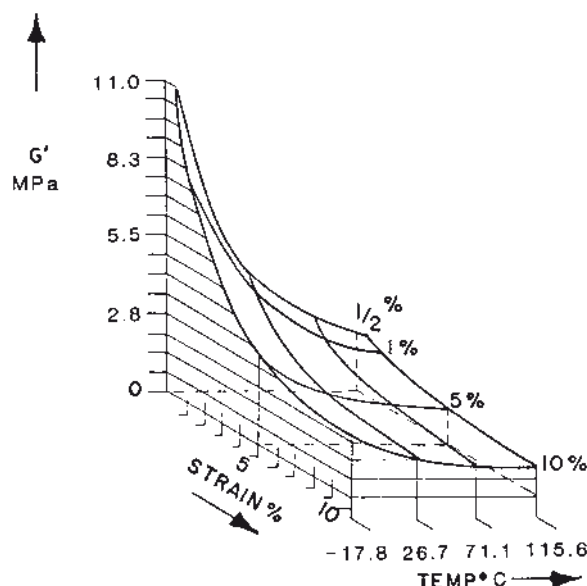


FIGURE 10.11 Effect of strain and temperature on G' at 20 Hz ([60] with permission; © 1973, Society of Automotive Engineers, Inc.)

Using a tester like this, dynamic properties were determined for a high damping compound based on natural rubber that contained 75 parts per hundred rubber (phr) HAF carbon black and 37.5 phr paraffinic oil. Figure 10.11 shows G' as function of strain and temperature in a three-dimensional graph [60].

10.4.6 Preferred Test Conditions

Selection of test conditions for dynamic testing should be guided by expected service conditions for the article being tested. For the purposes of developing a general database for comparison of materials, it would be logical to choose from some preferred conditions. The now obsolete ASTM D 2231-87 [72] suggested the use of a sinusoidal waveform at one or more of the following frequencies: 0.1, 1, 10, 60, 100, or 200 Hz, at one of the temperatures shown in ASTM D 1349-09 [36]. Strain values recommended are listed in Table 10.4. Surprisingly, ASTM D 5992, which replaced ASTM D 2231, omitted providing guidance on preferred test conditions. Some additional guidance for dynamic testing are given in ISO 2856 [73], ISO 4664 [74], and SAE J1085a [75].

TABLE 10.4 ASTM Recommendations for Strain During Dynamic Testing

Stress	Mean strain (%)	Strain amplitude (%)
Compression or tension	0.5, 10, 15, 20	0.1, 0.3, 1.0, 2.5, 5
Shear	0, 10, 20, 30, 40, 50	0.3, 1.0, 2.5, 10, 20

Source: [72]

■ 10.5 Tests for Tires

Tires are complex mechanical structures comprised of various rubber compositions and other components (beads, reinforcement, etc.). These compositions and components, each of which makes some particular contribution to overall performance, are usually tested individually before they are incorporated into tires. The tests include several of those mentioned above, such as hardness, tensile strength, and breaking elongation. Passing these tests indicates that the components are of sufficiently high quality to be fabricated into tires. But it does not give assurance that the fabricated tires will perform satisfactorily in service.

A tire needs to be ultimately evaluated as a system. As an example, a rubber composition might be selected because tests show it to have improved flex resistance.

But if the improved composition does not adhere properly to an adjacent layer in the tire, tire performance will be compromised. For this reason, a number of tests have evolved for testing finished tires.

Both nondestructive and destructive tests are used. Nondestructive tests [76] include ultrasonic, holographic, X-ray, and force variation methods. Force variation, a measure of tire uniformity, is determined by pressing a tire against a steel drum that is then rotated. Radial force variation (force perpendicular to the road) and lateral force variation (force parallel to the axis of rotation) are measured and recorded. A regular, low amplitude waveform is a desired characteristic of a good tire, while a large amplitude, irregular waveform is undesirable. Automobile manufacturers specify permissible force variation for original equipment tires because large force variations adversely affect vehicle dynamics.

Thermographic scanners permit another useful test to be conducted on tires and other rubber structures that generate heat while in service. In this test, a scanner monitors images generated by infrared radiation from a tire during operation either on a test wheel or on a vehicle. The monitoring system continuously records temperature gradients on the tire surface and identifies regions of high temperature. These measurements [76] show the effects of tire construction and service conditions on rates of heat generation and modes of heat dissipation.

There are a large number of tests and specifications (standards) applicable to passenger, truck, bus, and motorcycle tires. The information here is abstracted from federal standard 109 for new pneumatic tires for passenger cars [77]. Portions of this specification include test requirements for bead unseating resistance, strength, endurance, and high speed performance. In addition, load ratings are defined.

10.5.1 Bead Unseating Resistance

The tire-wheel assembly is prepared by washing the tire, drying it at the beads, and mounting it without lubrication or adhesives on a clean, painted test rim. The tire is inflated using inflation pressures at ambient temperature as shown in Table 10.5.

TABLE 10.5 Test Inflation Pressures Established by U.S. Department of Transportation

Ply rating of tire	4	6	8
Maximum permissible inflation pressure (kPa)	240	280	300
Pressure to be used in tests for bead unseating, tire strength, and tire endurance (kPa)	180	220	180
Pressure to be used in tests for high speed performance	220	260	220

Source: [77]

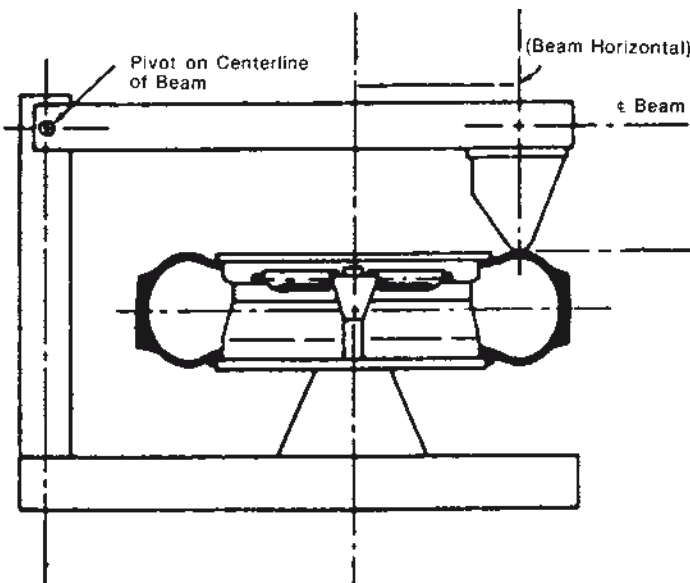


FIGURE 10.12 Bead unseating fixture [77]

The wheel and tire assembly is then mounted in the fixture shown in Fig. 10.12, and the appropriate bead unseating block is placed against the tire sidewall as required by the geometry of the fixture. A displacement is applied through the block to the tire sidewall at a rate of 50.8 mm/min. The load arm is maintained substantially parallel to the tire and rim assembly at the time of engagement. The load is then increased until the bead unseats or the applicable value is reached.

For tubeless tires having a designated section width of less than 152.4 mm and a maximum inflation pressure other than 410 kPa, the applied force required to unseat the tire bead at the point of contact shall be not less than 337.1 N. For tires with a designated section width of 152.4 mm or more, but less than 203.2 mm, the bead unseating force shall be no less than 449.4 N. The test is repeated at four places, equally spaced around the tire circumference.

10.5.2 Tire Strength

The tire is mounted on a test rim and inflated to the applicable pressure specified in Table 10.5 and then conditioned at room temperature for at least 3 hours. The pressure is readjusted to the applicable pressure specified in Table 10.5. A 19 mm diameter cylindrical steel plunger with a hemispherical end is then forced perpendicularly into the tread rib as near to the centerline as possible. The tread rib is penetrated at a rate of 50.8 mm/min, avoiding penetration into a tread groove.

The force and penetration are recorded at five test points spaced equally around the circumference of the tire. If the tire fails to break before the plunger is stopped by reaching the rim, the force and penetration is recorded as the rim is reached. The breaking energy for each test point is determined by means of Eq. (10.10):

$$W = \frac{F P}{2} \quad (10.10)$$

where W is energy (N·mm), F is force (N), and P is penetration (mm).

The breaking energy value for the tire is determined by computing the average of the five values obtained in accordance with Eq. (10.10).

10.5.3 Tire Endurance

A new tire is mounted on the test rim and inflated to the applicable pressure specified in Table 10.5. The tire assembly is conditioned as before, at 37.8 °C, and then mounted on a test axis and pressed against a flat-faced steel wheel 1.71 m in diameter and at least as wide as the section width of the tire to be tested, or an approved equivalent test wheel. The test is conducted at 80 km/h without pressure adjustment or other interruptions. The applicable times and test load ratings are shown in Table 10.6.

TABLE 10.6 Test Times and Percent of Maximum Load Rating Established by U.S. Department of Transportation

Test period (h)	Maximum load rating (%)
4	85
6	90
24	100

Source: [77]

Immediately after the tire has been run for the required time, inflation pressure is measured. The tire is allowed to cool for an hour, deflated, and then removed from the test rim. Upon inspection of the tire, there shall be no visual evidence of tread, sidewall, ply, cord, inner liner, or bead separation, and nor any chunking, broken cords, cracking, or open splices.

10.5.4 High Speed Performance

The tire is prepared and mounted as for the tire endurance test. The mounted tire is forced against the test wheel with a load of 88% of the tire's maximum

load rating as marked on the tire sidewall. The tire is conditioned by running it for 2 hours at 80 km/h. The tire is allowed to cool to 37.8 °C and the air pressure is readjusted to the applicable value specified in Table 10.5. Without further readjustment of inflation pressure, the tire is tested at 120 km/h for 30 minutes, followed by 136 km/h for 30 minutes. Immediately after the tire has been run for the required time, its inflation pressure is measured and the tire is allowed to cool for an hour. Then the tire is deflated, removed from the test rim, and inspected. Upon inspection, the tire shall show none of the defects described at the end of Section 10.5.3.

■ 10.6 Specifications

A technical specification is an important means of communication between the design engineer, the rubber manufacturer, and the purchaser of rubber components. In laying down requirements for a component, the designer has to steer a course between underspecifying, which is likely to compromise the suitability or quality of the component, and overspecifying, which almost inevitably leads to increased cost and delivery time.

In Sections 10.6.1–10.6.4, two topics important to specifications are discussed. These are the ASTM classification system for rubber materials for automotive applications [78] and the recommendations of the Rubber Manufacturers Association (RMA) on dimensional tolerances [79]. The ASTM classification system is commonly used for the selection of rubber materials, while the RMA recommendations are a valuable guide to production tolerances and design.

The designer may also make use of standard specifications for particular products. While standard specifications do not contain all the information needed for a complete specification, they usually cover most of the important points. Two products, bridge bearings and pipe sealing rings, are discussed to illustrate considerations important in specifications.

10.6.1 Classification System

ASTM D 2000-98 [78] is the standard classification system for rubber materials used in, but not limited to, automotive applications. ASTM D 2000-98 has been approved by the Society of Automotive Engineers as SAE Recommended Practice J200 [80], and the standard is often listed as ASTM D 2000/SAE J200.

This standard was developed in a manner that permitted modification without the need for complete reorganization. Furthermore, its organization facilitates the incorporation of new test methods to keep pace with changing requirements. The Standard assists engineers and other personnel in the selection of practical rubber compositions that are commercially available. However, if the provisions of the standard conflict with the detailed specifications for a particular product, product specifications take precedence.

Sometimes tests are run on rubber specimens prepared from finished products. The act of preparing these specimens can affect their properties. For example, buffing specimens might reduce tensile strength and elongation values relative to properties determined on molded specimens. Hence, when standard test specimens are cut from finished parts in accordance with ASTM D 3183-84 [7], a deviation to the extent of 10% (on tensile strength and elongation values only) is permissible when agreed on by the purchaser and the supplier.

Typically, engineers will be dealing with ASTM D 2000-98 when specifying rubber materials. Values stated in SI units are designated by the letter M. ASTM D 2000-98 designates rubber materials on the basis of type (heat resistance) and class (oil resistance). Basic values for type and class, together with additional requirements, permit a complete description of the quality of elastomeric materials.

10.6.1.1 Type

Type is based on changes in tensile strength of not more than 30%, elongation of not more than 50%, and hardness of not more than ± 15 points, after aging for 70 hours at an appropriate temperature. Table 10.7 shows the temperatures at which these materials shall be tested in order to determine type.

TABLE 10.7 Basic ASTM Requirements for Establishing Type by Temperature

Type	Test temperature (°C)
A	70
B	100
C	125
D	150
E	175
F	200
G	225
H	250
J	275
K	300

Source: © ASTM. Reprinted with permission [78]

10.6.1.2 Class

Class is based on the resistance of the material to swelling in oil by measuring the amount of swell after immersion for 70 hours at a temperature determined from Table 10.7, except that a maximum temperature of 150 °C (the upper temperature limit of oil stability) shall be used. Traditionally, ASTM Oil No. 3 was used in the swelling test. However, it has recently been replaced by another oil, IRM 903, because ASTM Oil No. 3 is no longer manufactured [44]. Table 10.8 lists the limits of swelling for each class.

As an example, the letter designation BC specifies a test temperature of 100 °C (Table 10.7) and a maximum volume swell of 120% after 70 hours (Table 10.8). Letter designations are always followed by a three-digit number that specifies hardness and tensile strength: for example, in 507, the 5 signifies 50 ± 5 durometer hardness on the A scale, and the next two digits, 07, indicate a minimum tensile strength of 7 MPa.

TABLE 10.8 Basic ASTM Requirements for Establishing Class by Volume Swell

Class	Volume swell, max. (%)
A	No requirement
B	140
C	120
D	100
E	80
F	60
G	40
H	30
J	20
K	10

Source: © ASTM. Reprinted with permission [78]

10.6.1.3 Further Description

The basic requirements do not always sufficiently describe the qualities desired for a rubber material. Hence, deviations or additional requirements are made through a system of prefix *grade* numbers. Grade No. 1 indicates that only the basic requirements are compulsory. For expressing deviations or additional requirements, grade numbers other than Grade No. 1 are used. These are listed in Table 6 of ASTM D 2000-98 (this rather lengthy table is not included here). For identification purposes, a grade number is written as a material prefix to the letter designation for type and class.

TABLE 10.9 Meaning of ASTM Suffix Letters

Suffix letter	Test required
A	Heat resistance
B	Compression set
C	Ozone or weather resistance
D	Compression-deflection resistance
EA	Fluid resistance (aqueous)
EF	Fluid resistance (fuels)
EO	Fluid resistance (oils and lubricants)
F	Low temperature resistance
G	Tear resistance
H	Flex resistance
J	Abrasion resistance
K	Adhesion
M	Flammability resistance
N	Impact resistance
P	Staining resistance
R	Resilience
Z	Any special requirement, which shall be specified in detail

Source: © ASTM. Reprinted with permission [78]

In addition to grade numbers, suffix letters and numbers describe further requirements. Table 10.9 describes the meaning of suffix letters. Each suffix letter should preferably be followed by two suffix numbers, the first of which (given in Table 5 of ASTM D 2000-98, not included here) indicates the test method. The second suffix number, if used, indicates test temperature (Table 10.10). Suffix letters and suffix numbers may be used singly or in combination.

Examples of suffix number and letter combinations are A14 and EO34. Suffix A stands for heat resistance (Table 10.9). Suffix 1 specifies testing by ASTM D 573 for 70 hours (Table 4 of ASTM D 2000-98, not included here); suffix 4 specifies a test temperature of 100 °C (Table 10.10). EO signifies fluid resistance (Table 10.9). Suffix 3 specifies testing according to ASTM D 471 in IRM 903 oil for 70 hours (Table 4 of ASTM D 2000-98); the second suffix number, 4, specifies a test temperature of 100 °C.

It should be noted that basic requirements are always in effect unless they are superseded by specific suffix requirements. In the examples above, suffixes A14 and EO34 supersede basic requirements for heat resistance and fluid resistance, respectively, but the basic requirement of 80% maximum compression set for BC materials (in Table 6 of ASTM D 2000-98) is not superseded.

TABLE 10.10 ASTM Suffix Numbers to Indicate Temperature of Test

Applicable suffix requirements	Second suffix number	Test temperature (°C) ^a
A, B, C, EA, EF, EO, G, K	11	275
	10	250
	9	225
	8	200
	7	175
	6	150
	5	125
	4	100
	3	70
	2	38
	1	23
	0	^b
Suffix F	1	23
	2	0
	3	-10
	4	-18
	5	-25
	6	-35
	7	-40
	8	-50
	9	-55
	10	-65
	11	-75
	12	-80

^a These test temperatures are based on ASTM Practice D 1349.

^b Ambient temperature in the case of outdoor testing.

Source: © ASTM. Reprinted with permission [78]

A “line callout” identifies a specification in a much abbreviated form and is used for effective communication between materials producers and others. For the rubber material described above, the “line callout” would appear as ASTM D 2000 M2BC 507 A14EO34. The basic and suffix requirements of this “line callout” are defined and summarized as follows.

Requirements of ASTM D 2000 M2BC 507 A14EO34

Basic Requirements

- M Classification based on SI units
- 2 Grade number (provides for deviations or additional requirements)
- B Type (based on resistance to heat aging)
- C Class (based on resistance to swelling in oil)
- 5 Hardness (50 ± 5 durometer hardness)
- 07 Tensile strength (minimum of 7 MPa)

Suffix Requirements

- A Heat resistance
- 1 Test method (ASTM D 573, 70 h)
- 4 Test temperature (100 °C)
- EO Fluid resistance
- 3 Test method (ASTM D 471, 70 h in IRM 903 oil)
- 4 Test temperature (100 °C)

Adding requirements generally increases the cost of rubber materials. Hence, only those needed to meet service requirements should be specified. This discussion of ASTM D 2000-98 is limited by space restrictions. The complete standard is very thorough and occupies some 29 pages. The reader is referred to it for further information.

10.6.2 Tolerances

It is important that the designer be generally familiar with the many factors that affect the dimensional tolerance of rubber products, since these tolerances influence both product performance and cost. Among important factors are the method of production (molding, extrusion, or lathe-cutting), whether the product is cellular or dense, and the compound hardness and shrinkage. The effects of these factors on tolerance, along with other considerations, have been described [79, 81].

The Rubber Manufacturers Association [79] provides tolerance recommendations for rubber products as a function of part size, method of manufacture, compound type, and other factors. The following discussion is for dense products, with emphasis on the effect of the manufacturing method.

10.6.2.1 Molded Products

The three major molding methods used in rubber product manufacture are compression, transfer, and injection molding. In compression molding, rubber enters

an open mold, which closes to shape the molded part. For compression molding, the tolerance for the part dimension in the mold closure direction must be greater than in other dimensions. Flash, the excess rubber on a molded product, accounts for this variation. For transfer and injection molding, in contrast, rubber enters a closed mold; comparable tolerance values can be expected in all three dimensions for parts molded by these methods.

A molded rubber component will have nearly the same dimensions as its mold at the molding temperature. However, owing to differences in the coefficients of thermal expansion of rubber and the metal mold, the rubber component will be smaller than its mold at ambient temperature. The amount of mold shrinkage (usually about 1.5–2%) is a function of the rubber compound and the molding temperature and must be taken into consideration in mold design, if the desired dimensions are to be achieved.

If a rubber compound is bonded to another material (e.g., a steel insert), or if it contains oriented fiber, non-uniformity in shrinkage must be taken into account in specifying dimensions and tolerances for a product. For example, nearly all the shrinkage in laminated and bonded steel-rubber bridge bearings occurs in a direction normal to the plane of the steel plates in the bearing [81].

Standard dimensional tolerances are specified by RMA [79]. They depend on factors such as the level of tolerance required, whether a fixed or a closure dimension is involved, and the product size. Four levels of tolerance are given: high precision, precision, commercial, and basic. Respective drawing designations are “A1”, “A2”, “A3”, and “A4”. For example, a drawing designation “A3” specifies a commercial product that could be used for most products. Tolerances are associated with product sizes increasing from dimensions in the range of 0–10 mm, to dimensions greater than 160 mm. Table 10.11 compares dimensional tolerances for products in the size range of 16–25 mm, for molded products with different drawing designations (tolerances for products in this size range will be compared later to dimensional tolerances for extruded products).

TABLE 10.11 RMA Standard Dimensional Tolerance Table for Molded Rubber Products (16–25 mm)

Drawing designation	Tolerance (mm)	
	Fixed	Closure
A1, High precision	±0.16	±0.20
A2, Precision	±0.25	±0.32
A3, Commercial	±0.32	±0.50
A4, Basic	±0.50	±1.00

Source: [79]

Dimensional tolerances increase of course as part size increases. Note in Table 10.11 that "A4" tolerances apply to products in which dimensional control is non-critical. For these products, reduced cost is expected. In addition to these tolerances, RMA also describes [79] relative dimensions for molded rubber products, including concentricity, squareness, flatness, and parallelism.

10.6.2.2 Extruded Products

The tolerances for extruded products are more liberal than for molded products, because more variables are encountered in the extrusion process. During extrusion, rubber is forced under pressure through a die of the desired cross section. Variables such as compound viscosity, elastic recovery (or die swell), complexity of the extrudate cross section, temperature, pressure, and need for subsequent curing (often without support of the extrudate) affect extrudate dimensions and therefore tolerance range.

Comparison of tolerances for extruded products (Table 10.12) with those for molded products (Table 10.11) shows that extruded products have wider tolerances, especially extruded products designated as high precision. This comparison illustrates the effect of the manufacturing process, extrusion versus molding, on tolerances. The RMA standards permit design engineers, product manufacturers, and purchasers to establish tolerances that are reasonable and cost-effective.

TABLE 10.12 RMA Cross-Sectional Tolerances for Group 1 Compounds for Extruded Products (16–25 mm)

RMA Drawing designation	Tolerance (mm)
E1, High precision	±0.70
E2, Precision	±1.00
E3, Commercial	±1.60

Source: [79]

This section is limited to consideration of tolerances for molded and extruded products with a narrow range of dimensions. The RMA handbook [79] describes many other standards, including cut length tolerances for extrusions, angle cuts, and splices.

10.6.2.3 Load-Deflection Characteristics

Load-deflection characteristics might be specified in products such as mountings, vibration isolators, and dampers, where they are of primary importance. RMA specifies [79] tolerances for load-deflection as a function of rubber hardness, rubber wall thickness, and the drawing designation (viz., D1, very high precision; D2, precision; and D3, commercial).

As examples, tolerance range for load-deflection for D3 commercial products with A hardness of 65 or lower is $\pm 15\%$ when wall thickness is 6 mm or more; for a wall thickness of less than 6 mm, the tolerance range is $\pm 20\%$. These ranges increase to ± 20 and $\pm 25\%$, respectively, for hardness above 65 A.

10.6.3 Rubber Bridge Bearings

10.6.3.1 Function

A bridge bearing, placed between a bridge deck and its fixed supports, has three main functions:

1. It supports the dead weight of the bridge deck and live loads due to passing traffic.
2. It accommodates changes in length of the deck resulting from temperature variations without transferring excessive lateral loads to the bridge supports.
3. It accommodates the slope and changes in slope of the deck caused by bending.

These functions require, in essence, a bearing that is very stiff in the vertical direction, and soft in the lateral directions and in rotation. A rubber pad loaded on its major surfaces can provide this demanding combination of directional stiffness. This is obtained by deforming the pad in compression in the vertical direction and in shear in horizontal directions. The stiffness in compression may be made many times larger than the shear stiffness by using a pad of high shape factor (see Chapter 8). Rotational stiffness may be kept small by limiting the lateral dimensions.

Simple rubber pads have been used as bridge bearings for a hundred years, but their capacity is limited because the maximum shear strain possible without the pad slipping or curling at the leading and trailing edges is about 0.5. Thick pads cannot be used because they would be too soft in the vertical direction. The introduction in the late 1950 s of steel-laminated rubber bearings enabled the widespread replacement of traditional mechanical bearings. The sandwich construction of the steel-laminated bearing (Fig. 10.13) provides high stiffness and load-carrying capacity in the vertical direction because the shape factor of each rubber layer is high. At the same time, the deformation capacity of the bearing in shear is not affected.

Plain rubber pads and steel-laminated rubber pads are cost effective as bridge bearings. They are easy to install and require no maintenance. In contrast, mechanical bearings that roll or slide are expensive and difficult to install. Usually made of steel, they require lubrication, if corrosion and wear is to be minimized. Even with the best maintenance, wear is inevitable owing to the small and repeated movements the bearings are required to perform.

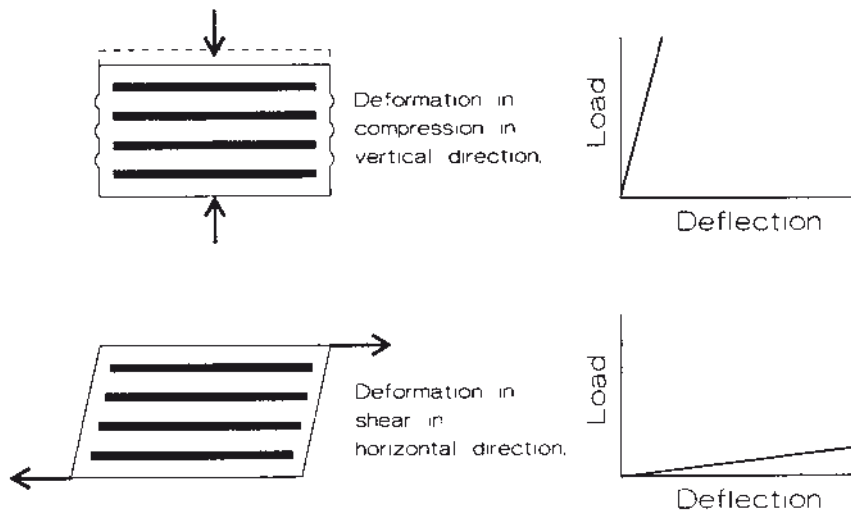


FIGURE 10.13 Deformation of steel-laminated rubber bearings in compression and shear

10.6.3.2 Design Code

There are two rather empirical basic philosophies behind the various design codes in use around the world, namely:

- Limiting strains
- Limiting stresses

The British standard [82] is based on the first approach of limiting the maximum strain in the bearing. The engineer is required to calculate from established theory the shear strains in the rubber induced by the highest compression, shear, and rotation deformations that the bearing is expected to encounter in service. These individual shear strains are then added together to estimate the maximum strain, which must be less than the limits specified in the standard.

The second approach of limiting the stress is the prevalent method adopted in North America. The average compressive stress limit adopted at one time appeared to be related to the permissible bearing stresses for concrete rather than to properties of the rubber.

In a comprehensive monograph, Stanton and Roeder [83] reviewed and compared the principal design codes in use around the world. The monograph included several recommendations, for specifications.

10.6.3.3 Materials Specification

Although a number of different elastomers have been used, only two, natural rubber and polychloroprene, are widely used in bridge bearings. This is reflected in the major standard specifications for bridge bearings [82, 84, 85], which exclude the use of other elastomers. Both materials have excellent records in engineering applications requiring high load-carrying ability and long fatigue life. Therefore, there is little doubt that either material is suitable if properly used.

However, there is considerable controversy over which of these two materials is preferred. Advocates for polychloroprene often point to natural rubber's greater susceptibility to ozone attack and oxidation and imply that the service life of polychloroprene would be longer. But there is no evidence that polychloroprene's superior aging resistance would matter in service. Studies described in Chapter 7 of bridge bearings and similar rubber components that have been in service for periods of up to a hundred years have shown that oxidation and ozone degradation tend to be confined to the first few millimeters of rubber at the surface. The properties of a large, bulky component such as a bridge bearing are not much affected by such surface degradation. It appears, therefore, that the aging resistance of natural rubber bearings, when properly made, is adequate to ensure long service life. Many such bearings have been installed around the world and continue to perform satisfactorily.

On the other hand, advocates for natural rubber point to the greater tendency of polychloroprene to stiffen at low temperatures. It must be remembered that one of the primary functions of a bridge bearing is to accommodate changes in length of the bridge deck without transmitting excessive lateral forces to the bridge supports. This is accomplished by relying on the low shear modulus of rubber. As the temperature falls, the shear modulus increases. Exposure to low temperatures can lead to a considerable increase in shear modulus, resulting in an unacceptable increase in the forces transmitted to the supporting structures.

Stiffening that results from exposure to low temperatures arises from two quite separate mechanisms. First, certain rubber molecules (including natural rubber and polychloroprene) tend to align themselves, forming a partially crystalline structure. This process is time and temperature dependent. There is some evidence that mechanical movements will inhibit the process and that the extent of stiffening in service may be somewhat less than that observed in the laboratory. But more research is needed to establish whether this is sufficient to relax requirements in current specifications.

Second, the mobility of the rubber molecules is reduced at low temperatures, resulting in a loss of rubber-like characteristics. If the temperature falls to the glass transition temperature, rubber becomes hard and glassy and even brittle under impact. But it is not necessary for the temperature to fall as low as the glass

transition temperature for the shear modulus to increase significantly; the increase is measurable even at temperatures well above the glass transition (see Chapter 4).

The engineer designing bearings for use in cold climates is advised to give careful consideration to the low temperature properties of the rubber intended for use. Natural rubber has less tendency than polychloroprene to stiffen at low temperatures. Hence, there is reason to prefer natural rubber for low temperature applications.

The ASTM specification for bridge bearings [84] divides rubber bearings into four grades depending on the typical operating temperature conditions. Low temperature performance requirements of the different grades are assessed by a low temperature brittleness test performed on five test strips at the specified temperature in accordance with method A of ASTM D 2137-94 [86]. None of the test pieces may fail. It is not obvious that this short term brittleness test alone provides sufficient safeguards against low temperature stiffening discussed above. A previous version of ASTM D 4014 included limits on hardness change and compression set after several days of exposure to low temperatures. These additional requirements appear reasonable, but they have been dropped during a revision exercise presumably because the standards committee was satisfied that they were unnecessary. But it is noteworthy that the AASHTO specifications retained long-term low temperature stiffening tests.

A particularly important consideration in bridge bearings is achieving good rubber-to-metal bonds. It must be remembered that the high load-carrying capacity of the bearing depends on the ability of the steel laminate to restrict lateral deformation of the rubber. Bearing failures are often related to poor manufacturing practices that failed to ensure adequate bond strengths. Bond strength may be determined by dissecting a bearing and taking test specimens for standard rubber-metal bond tests. Unfortunately, this approach destroys the bearing, hence can be applied to only a small number of randomly chosen samples. For quality control purposes, most specifications recommend a compression test at 1.5 times the design load, while the bearing is visually inspected for faults such as abnormal bulges, cracks, and unusual displacement of the steel plates. This test is relatively inexpensive and practical to perform on a 100% sampling basis. Some specifications require in addition a shear test at 1.5 times the design shear deflection. This test requires a special test fixture to avoid transferring large lateral loads to the testing machine.

10.6.4 Pipe Sealing Rings

10.6.4.1 Function

Underground pipelines are usually constructed by joining together a large number of short pipes. The joints are often made by means of rubber rings. In addition to providing leak-proof seals, the rubber rings lend some flexibility to the pipeline, enabling it to accommodate small movements caused, for example, by differential settling of the ground.

Sealing is achieved by deforming the rubber ring in radial or axial compression. In certain joint designs, deformation of the rubber may be assisted by the fluid pressure in the pipe. Reaction stresses developed in the rubber ring must be high enough to form an effective seal, yet low enough to ensure that the pipe does not fracture.

As an example of specifications for rubber components in general, and of pipe sealing rings in particular, we now discuss ASTM D 1869-95 [87], which is ASTM's standard specification for rubber rings for asbestos-cement pipes.

10.6.4.2 Materials

The specification [87] permits the use of natural rubber, synthetic rubber, or a blend. However, only virgin rubber containing no scrap, reclaim, or rubber substitutes may be used. Avoiding the use of recycled scrap, reclaim, and like material is prudent, because such materials tend to be ill defined and their long-term performance is uncertain. The cost of rubber rings is insignificant compared to the cost of digging up underground pipes in the event of leakage.

10.6.4.3 Tensile Properties

Among the requirements of the specification are tests for tensile strength and elongation at break. It may appear strange that a product used in compression is tested in tension. During installation, it may be necessary to stretch the rubber ring over the pipe, but this is unlikely to be near the breaking elongation of most rubbers. Tensile strength and elongation at break tests are not directly relevant to service performance. Their inclusion in the specification is justified because they serve as general indicators of quality. Rubber compounds containing high levels of diluent fillers, scrap, or reclaim rubber are significantly weaker than higher quality compounds. Hence, their use will be excluded by stringent tensile strength requirements.

Requirements for tensile strength and elongation at break for oil-resistant rings are less stringent than for non-oil-resistant rings, because the latter are traditionally made from natural rubber, which is intrinsically stronger than synthetic rubbers used for oil-resistant rings. Tensile strength and elongation at break levels typical

of a good quality natural rubber ring are usually very difficult to achieve with most synthetic rubbers.

Even though pipe rings are not subject to tensile elongations of the order of 300% in service, the stress at 300% elongation is a test requirement. It is a traditional measure used by the rubber industry as a substitute for modulus.

10.6.4.4 Compression Set

The elastic reaction in the rubber ring arising from its deformation provides the sealing pressure. Leakage will occur if the fluid in the pipe exerts a pressure difference across the seal in excess of the sealing pressure. Clearly, the rubber must maintain the sealing pressure if the seal is to function properly. As discussed in Section 10.2.3, the stress in a rubber held under fixed deformation relaxes with time. The rate of stress relaxation would be a logical parameter to specify. Unfortunately, stress relaxation tests are seldom performed. Instead, there is a tendency to rely on a compression set test, even though the correlation between the two tests is poor. The popularity of the compression set test lies in its simplicity.

It is noteworthy that ASTM D 1869-95 [87] has adopted a nonstandard variation of the compression set test. A section of the ring is tested at a compressive strain of 50% rather than the standard cylindrical test piece at a strain of 25%. Such a variation in test procedure is common in product specifications, and the user is advised to pay attention to the small print.

The test temperatures for oil-resistant and non-oil-resistant rings differ. Similarly, the expected test results differ. This does not reflect on differences in severity of service conditions for the two types of ring, but rather on differences in quality control test procedures for different materials. It must be remembered that the primary function of the compression set test is to exclude rubber rings that have not been adequately cured. The synthetic rubbers that are used for oil-resistant rings are generally less susceptible to high temperature degradation than natural rubber, the traditional rubber for non-oil-resistant rings. For this reason, synthetic rubbers are usually tested at higher temperatures to obtain an easily measurable compression set. The test results needed for acceptance are established at levels that are intended to exclude undercured rings of the respective types.

10.6.4.5 Low Temperature Flexibility

Temperature affects the elastic properties of rubber. At low temperatures, rubber stiffens significantly. At temperatures below the glass transition temperature, rubber becomes extremely stiff and brittle. The low temperature flexibility test at -25 °C does not provide a guarantee that the rubber will be serviceable at any particular temperature, but it is better than no test at all.

10.6.4.6 Oven Aging

The correlation between oven aging tests and service performance is poor, and the test requirements in the specification do not pretend to correspond to any designed service life. For a product such as a pipe sealing ring, which should last for many decades, it is conventional to incorporate chemical antidegradants to provide a good level of protection. The main purpose of oven aging tests is to exclude improperly formulated rings (e.g., those from which chemical antidegradants have been omitted inadvertently).

The differences in test time, temperature, and required test results for oven aging of non-oil-resistant and oil-resistant rubber rings arise because of differences in conventional quality control test procedures for natural and synthetic rubbers.

10.6.4.7 Oil Resistance

For oil-resistant rings, tests after immersion in ASTM Oil No. 3 are required. ASTM Oil No. 3 tends to swell most rubbers to a high degree and it is commonly used in specifications. This is an arbitrary choice, however, and it is not safe to assume that passing the test means that the ring is resistant to all oils. For example, the presence of alcohol in gasoline may have deleterious effects on some rubbers conventionally thought of as oil-resistant. Indeed, since ASTM Oil No. 3 is no longer manufactured, it is necessary to replace it with the similar but not identical IRM 903 oil. This substitution may affect results because the swelling characteristics of the two oils are different.

10.6.4.8 Closing Remarks

The foregoing rather critical analysis of ASTM D 1869-95 is intended to illustrate the difficulties and limitations of rubber product specifications in general rather than to highlight inadequacies in this document in particular. It should be emphasized that specifications such as ASTM D 1869-95, supplemented as necessary by additional requirements in purchase agreements, do serve users quite well. Thus, judicious use of tests and specifications assists the design engineer and manufacturer in producing quality rubber components at economic prices.

■ References

- [1] Annual Book of ASTM Standards, Vols. 09.01 and 09.02, American Society for Testing and Materials, Philadelphia, published annually.
- [2] SAE Handbook, Vol. 1, Society of Automotive Engineers, Warrendale. PA, published annually.
- [3] BS 903, Methods of Testing Vulcanized Rubbers (published in numerous parts at different times), British Standards Institution, London.
- [4] A. G. Veith, *Polym. Test.*, **7**, 237–267, (1987).
- [5] R. Brown, *Eur. Rubb. J.*, **25–26**, (Jan./Feb. 1989).
- [6] ASTM D 3182-07, Standard Practice for Rubber: Materials, Equipment, and Procedures for Mixing Standard Compounds and Preparing Standard Vulcanized Sheets.
- [7] ASTM D 3183-09, Standard Practice for Rubber: Preparation of Pieces for Test Purposes from Products.
- [8] R. P. Brown, Physical Testing of Rubber, 3rd. ed. Chapman & Hall, 1996.
- [9] F. S. Conant, “Physical Testing of Vulcanizates”, in M. Morton (Ed.), Rubber Technology, 3rd ed. Van Nostrand Reinhold, New York, 1987, Chapter 5.
- [10] J. G. Sommer, “Physical Properties and Their Meaning”, in K. C. Baranwal and H. L. Stephens, (Eds). Textbook for Intermediate Correspondence Course, Rubber Division, American Chemical Society Akron, OH, 2000, ch. 10.
- [11] O. H. Yeoh, *Plast. Rubber: Process. Appl.*, **4**, 141–144 (1984).
- [12] ASTM D 412-06a, Standard Test Methods for Rubber Properties in Tension.
- [13] ASTM D 575-91, Standard Test Methods for Rubber Properties in Compression.
- [14] J. G. Sommer, *Rubber World*, **201**(3), 29 (1989).
- [15] O. H. Yeoh, *Polym. Test.*, **7**, 121–136 (1987).
- [16] L. Mullins, *Rubber Chem. Technol.*, **42**, 339–362, (1969).
- [17] R. S. Rivlin and D. W. Saunders, *Trans. IRI*, **24**, 296–306 (1949).
- [18] I. H. Gregory and A. H. Muhr, “Stiffness and Fracture Analysis of Bonded Rubber Blocks in Simple Shear” in “Finite Element Analysis of Elastomers” ed. by D. Boast and V. A. Coveney, Professional Engineering Publishing, Suffolk IP32 6BW, England.
- [19] A. H. Muhr, G. H. Tan, and A. G. Thomas, *J. Nat. Rubber Res.*, **3**, 261 (1988)
- [20] V. A. Coveney, C. J. Derham, K. N. G. Fuller, and A. G. Thomas, “Vibration Isolation and Earthquake Protection of Buildings”, in A. D. Roberts (Ed.), Natural Rubber Science and Technology, Oxford Science Publications, Oxford, 1988.
- [21] ASTM D 1390-76, Standard Test Method for Rubber Property: Stress Relaxation in Compression.
- [22] ASTM D 2240-05, Standard Test Method for Rubber Property: Durometer Hardness.
- [23] ASTM D 1415-88 (94), Standard Test Method for Rubber Property: International Hardness.
- [24] G. Spetz, *Polym. Test.*, **12**, 351–378, (1993).
- [25] ASTM D 1414-94. Standard Test Methods for Rubber O-Rings.
- [26] A. W. Mix and A. J. Giacomin, ANTEC 2009, 2878.
- [27] H. J. Qi, K. Joyce and M. C. Boyce, *Rubber Chem. Technol.*, **76**, 419, (2003)
- [28] J. J. C. Busfield and A. G. Thomas, *Rubber Chem. Technol.*, **72**, 876, (1999)
- [29] N. E. Waters, *Br. J. Appl. Phys.*, **16**, 557, (1965)

- [30] J. R. Scott, *J. Rubber Res.*, **17**, 145 (1948).
- [31] A. N. Gent, *Trans. IRI*, **34**, 46 (1958).
- [32] ASTM D 395-03, Standard Test Methods for Rubber Property: Compression Set.
- [33] R. D. Stiehler, in *Rubber and Related Products: New Method for Testing and Analyzing*, ASTM STP 553, American Society for Testing and Materials, Philadelphia, 1974, pp. 87–103.
- [34] ASTM D 1229-03(97). Standard Test Method for Rubber Property: Compression Set at Low Temperatures.
- [35] ASTM D 573-04(94), Standard Test Method for Rubber: Deterioration in an Air Oven.
- [36] ASTM D 1349-09(93), Standard Practice for Rubber: Standard Temperatures for Testing.
- [37] ASTM D 865-99 Standard Test Method for Rubber: Deterioration by Heating in Air (Test Tube Enclosure).
- [38] G. Spetz, *Polym. Test.*, **15**, 381–395, (1996).
- [39] A. G. Veith and R. L. Evans, *Polym. Test.*, **1**, 27–38, (1980).
- [40] ASTM D 1149-07, Standard Test Method for Rubber Deterioration: Surface Ozone Cracking in a Chamber.
- [41] ASTM D 1171-99, Standard Test Method for Rubber Deterioration: Surface Ozone Cracking Outdoors or in a Chamber (Triangular Specimens)
- [42] ASTM D 4575-09, Standard Test Methods for Rubber Deterioration- Reference and Alternative Method(s) for Determining Ozone Level in Laboratory Test Chambers.
- [43] E. Southern, *Rubber Dev.*, **18**, 51 (1965).
- [44] ASTM D 471-06, Standard Test Method for Rubber Property: Effect of Liquids.
- [45] ASTM D 429-08, Standard Test Methods for Rubber Property – Adhesion to Rigid Substrates.
- [46] J. G. Sommer, Elastomer Technology-Special Topics, Chapter 8, K. Baranwal and H Stevens (Eds.), Rubber Division, American Chemical Society, Akron, OH, 2003, p. 269.
- [47] J. H. Daly, W.A. Hartz, D. A. Meyer, and J. G. Sommer, *Applied Polymer Symposium No. 25*, p. 261 (1974).
- [48] O. H. Yeoh, *Rubb. Chem. Tech.*, **79**, 320, (2006)
- [49] P. B. Lindley, *J. I. R. I.*, **5**, 243–248, (1971).
- [50] A. N. Gent and G. R. Hamed, *J. Adhesion*, **7**, 91, (1975).
- [51] M. A. Ansarifar and G. J. Lake, *J. Adhesion*, **53**, 183–199, (1995).
- [52] A. Stevenson and A. M. Priest, *Rubb. Chem. Tech.*, **64**, 545–558, (1991).
- [53] J. G. Sommer, *Rubber World*, **214**(3) 16 (1996).
- [54] J. S. Dick, *Rubber World*, **209**(4) 19 (1994).
- [55] John Sezna, *Rubber and Plastics News*, **28**(9) 12 (1998).
- [56] John Sezna, *Rubber and Plastics News*, **28**(10) 12 (1998).
- [57] K. P. Beardsley and W. A. Wortman, *Rubber World*, **219**(4) 38 (1999).
- [58] C. Stevens and H. Burhin, *European Rubber Journal*, **180**(12) 24 (1998).
- [59] R. A. Heinrich, *Measurements and Control*, **19**(4) 203 (1985).
- [60] J. G. Sommer and D. A. Meyer, in B. M. Hillberry (Ed.): *The Measurement of the Dynamic Properties of Elastomers*, SAE SP-375, Society of Automotive Engineers, Warrendale, PA, 1973, pp. 109–117.
- [61] R. J. Del Vecchio, “Comparison of Dynamic Test Methods and Machines for Elastomers”, paper No. 35, presented to the Rubber Division of the American Chemical Society, Orlando, FL, October 26, 1993.

- [62] J. M. Funt, *Rubber World*, **194**(3) 25 (1986).
- [63] ASTM D 2632-96, Standard Test Method for Rubber Property: Resilience by Vertical Rebound.
- [64] ASTM D 1054-92(97), Standard Test Method for Rubber Property: Resilience by a Rebound Pendulum.
- [65] ISO 1767-1971, Vulcanized Rubbers: Determination of Rebound Resilience-Lüpke Pendulum Method.
- [66] ASTM D 945-87, Standard Test Methods for Rubber Properties in Compression or Shear (Mechanical Oscillograph).
- [67] W. C. Warner, in *Rubber and Related Products: New Methods for Testing and Analyzing*, ASTM STP 553, American Society for Testing and Materials, Philadelphia, 1974, pp. 31–55.
- [68] R. C. Puydak, *Automot. Elastomers Design*, **2**(4), 8–21 (1983).
- [69] W. C. Diamond and G. E. Henderson, *Rubber World*, **203**(4) 22 (1991).
- [70] K. K. Biegler, *Rubber and Plastics News*, **21**(15) 25 (1992).
- [71] L. White, *European Rubber Journal*, **175**(1) 22 (1993).
- [72] ASTM D 2231-87, Standard Practice for Rubber Properties in Forced Vibration.
- [73] ISO 2856-1981, Elastomers: General Requirements for Dynamic Testing.
- [74] ISO 4664-1978, Rubber Determination of Dynamic Properties of Vulcanizates for Classification Purposes (by Forced Sinusoidal Shear Strain).
- [75] SAE J1085, Recommended Practice, Test for Dynamic Properties of Elastomeric Isolators, Society of Automotive Engineers, Warrendale, PA, 1995.
- [76] F. J. Kovac, *Tire Technology*, 5th ed., Goodyear Tire and Rubber Company, Akron, Ohio, 1978.
- [77] *Code of Federal Regulations*, National Highway Traffic Safety Administration, U.S. Department of Transportation, Oct. 1, 1986, Vol. 49, Chapter V, Regulation 571.109.
- [78] ASTM D 2000-08, Standard Classification System for Rubber Products in Automotive Applications.
- [79] Rubber Manufacturers Association, *Rubber Handbook of Molded, Extruded, Lathe-Cut and Cellular Products*, 5th ed., RMA, Washington, DC, 1992.
- [80] SAE J200, Classification System for Rubber Materials for Automotive Applications, 1998.
- [81] J. G. Sommer, “Rubber Parts”, in J. G. Bralla (Ed.), *Handbook of Product Design for Manufacturing*, McGraw Hill, New York, 1986, pp. 6–131 through 6–153.
- [82] BS 5400:1983, British Standard Steel, Concrete and Composite Bridges, Part 9, Bridge Bearings, Section 9.1 (Code of Practice for Design of Bridge Bearings) and Section 9.2 (Specifications for Materials, Manufacture and Installation of Bridge Bearings).
- [83] J. F. Stanton and C. W. Roeder, Report 248: Elastomeric Bearings Design, Construction, and Materials, Transportation Research Board, Washington, DC, 1982.
- [84] ASTM D 4014-89(95), Standard Specification for Plain and Steel-Laminated Elastomeric Bearings for Bridges.
- [85] Standard Specifications for Highway Bridges, 14th ed., American Association of State Highway and Transportation Officials, Washington, DC, 1989.
- [86] ASTM D 2137-94, Standard Test Methods for Rubber Property: Brittleness Point of Flexible Polymers and Coated Fabrics.
- [87] ASTM D 1869-95, Standard Specification for Rubber Rings for Asbestos-Cement Pipe.

■ Problems for Chapter 10

1. An engineer required a rubber spring to operate in compression under strains of about 25%. He assumed that the material has a Young's modulus of 3.0 MPa and designed the spring using equations given in Chapter 8. How should he write the technical specifications to control the quality of the rubber material so that the spring has the desired load/deflection characteristics?
2. A rubber manufacturer was asked to provide the shear modulus of his rubber. He used a standard Yerzley shear specimen made from his material in accordance with ASTM D 945, which specifies that the specimen has rubber blocks with a ratio of length-to-thickness of 1.9. He mounted it on a universal testing machine, performed three loading and unloading cycles to 100% shear strain and reported the maximum shear stress on the third cycle as the shear modulus. Using this shear modulus, an engineer designed a tube-form rubber bushing to operate under small torsional strains. Later, he was surprised to find that the prototype part produced by the manufacturer was much stiffer than he had expected from his design calculations. What may have contributed to the observed discrepancy between design and experiment?
3. Simple rubber bands or rings are often used as drive belts for vacuum cleaners. Because of electrical discharges from the motor, the operating environment is rich in ozone. Seeking to improve his product, a rubber manufacturer evaluated the ozone resistance of compounds containing different anti-degradant systems by exposing bent-loop specimens to high concentrations of ozone in accordance with ASTM D 1149. Based upon results from this experiment he changed the anti-degradant system in his product, only to find that his "improved" product failed much sooner than before. What is a possible reason and what should he have done instead?
4. Does the lack of swelling resistance of natural rubber to oil necessarily preclude its use in some engineering applications?
5. What are some of the factors that cause poor correlation among different dynamic test results?
6. Is it desirable to specify "high precision, A1" on the drawing specification as the dimensional tolerance for all molded rubber articles?

■ Answers to Problems for Chapter 10

1. A Young's modulus of 3.0 MPa corresponds to a rubber of medium hardness. So, it is tempting to simply write in the material specifications the requirement that the hardness shall be 50 ± 5 IRHD (or A durometer). However, this is not advisable. The relation between Young's modulus and hardness is only approximate. Further, design equations (such as those in Chapter 8) assume linear elastic behaviour, whereas load/deflection behavior under strains of the order of 25% compression is undoubtedly non-linear and the values predicted by design equations are only approximate. These approximations mean that the designed spring may not have the desired load/deflection characteristics even though the material used met the specified hardness requirement. The preferred way is for the engineer to consult the rubber manufacturer at an early stage and communicate the performance requirements. They should develop the material specifications together.
2. First, the length-to-thickness ratio of the Yerzley shear specimen is too low for simple shear to be a good approximation. Additional contributions to the deflection from bending and warping will be significant, resulting in an under-estimate of the shear modulus if they are neglected. Second, the amount of stress-softening due to previous loading cycles (Mullins effect) depends on the magnitude of the strain. Preconditioning the specimen to 100% strain in the test is inappropriate when the part only operates at small strains. Again, we expect the test result to be an under-estimate. Third, shear stress-strain curves of filled rubber compounds are non-linear. The shear modulus at small strains tends to be significantly higher than at large strains. By reporting the shear stress at 100% shear as the shear modulus, the manufacturer is not measuring at relevant (small) strains and so underestimates the shear modulus still further.
3. Practical rubber compounds usually rely on a combination of waxes and chemical antiozonants for protection against ozone. These anti-degradants bloom to the surface to form a protective layer. Flexing may disrupt this protective layer. Thus, a protective system may appear excellent when evaluated in a static test (such as the bent loop exposure method in ASTM D 1149), but be quite inadequate under dynamic loading conditions. Because the application calls for repeated flexing of the rubber, it would be better to evaluate materials in ozone under dynamic strain conditions such as described in ASTM D 3395.
4. Not necessarily. If the rubber volume is relatively large and the volume of oil is small, swelling may be insignificant. As an example, NR automotive engine mounts operate in an oily environment for long time periods. This occurs because the depth of penetration depends upon approximately the square root of time (see Chapter 7). Moreover, only a few drops of oil are likely to contact the mount and swell it.

5. Some of these tests, e.g., the Yerzley oscillograph, are run at the natural frequency and the strain amplitude decreases with each cycle. The dynamic elastic modulus decreases significantly with increasing strain, especially for highly-filled compounds. Other dynamic testers are run under forced vibration conditions and use different waveforms, different levels of static pre-stress, and vibration amplitudes, all of which can affect test results.
6. No, specifying rubber products with an AI tolerance may result in unnecessary costs. Molds for such products are more expensive and will contain fewer cavities than those with less demanding tolerances. Also, an AI tolerance implies more costly in-process controls and inspection procedures. Remember that rubber stretches easily and this should be considered in establishing tolerances. A3 tolerances are normally applied to most commercial products. Also, remember that allowable tolerances are scaled to the product size.

Appendix: Tables of Physical Constants

Alan N. Gent, Tomoaki Sueyasu, and Chi Wang

TABLE 1 Properties of Raw and Unfilled Vulcanized Rubber

Property	Material (data in parentheses are for vulcanized rubber)										Ref.
	NR	IR	SBR	CR	NBR	IIR	BR	EPDM	FKM	Silicone	
Density, kg/m ³	913 (970)	930	940 (980)	1230 (1320)	1000	920	910	860	1850	980	1
T _g , °C	-72 (-68)		-60 (-55)	-50 (-45)	-40 ^a to -10	-72	-100 ^b	-55	-20 to -10	-123	2,3

^a Acrylonitrile contents: 20–50%.

^b High *cis* BR

1. R. O. Babbit, *Rubber Handbook*, R. T. Vanderbilt, Norwalk, CT, 1978.

2. M. C. Shen and A. Eisenberg, *Rubber Chem. Technol.*, **43**, 95 (1970).

3. D. W. Brazier, *Rubber Chem. Technol.*, **53**, 437 (1980).

TABLE 2 Mechanical Properties of Typical Filled Rubber Compounds

Property	Material										
	NR	IR	SBR	CR	NBR ^a	IIR	BR	EPDM	FKM	Silicone	
Density, ^b kg/m ³	1130 (50)	1130 (50)	1140 (50)	1430 (50)	1210 (60)	1130 (50)	1150 (60)	1070 (50)	1960 (15)		
Engineering stress (MPa) at 300 % strain	15.4	16.8	17.9	20.3	16.2	5.5	8.4	7.6 ^c	2.8 ^d		
Breaking stress, MPa	28.1	30.7	22.1	22.9	22.1	15.7	18.6	18.1	16.5	2–10	
Ultimate strain, %	490	510	330	350	440	650	610	420	310	80–500	

^a Acrylonitrile content: 35 %.

^b Calculated values from recipes.

Numbers in parentheses indicate carbon black content in parts by weight per 100 parts of rubber

^c Stress at 200 % strain.

^d Stress at 100 % strain.

Source: R. O. Babbit, *Rubber Handbook*, R. T. Vanderbilt, Norwalk, CT, 1978.

TABLE 3 Electrical Properties of Raw and Unfilled Vulcanized Rubber

	Material (data in parentheses are for vulcanized rubber)				
	NR	SBR	CR	IIR	BR
Resistivity, $\Omega\cdot\text{cm}$	$5 \cdot 10^{15}$			$10^{10}\text{--}10^{11}$	
Dielectric constant, 1 kHz	2.43 (2.51)	2.50 (2.66)	6.5 (8.1)	2.38 (2.42)	(3.06)
Dissipation factor, 1 kHz	0.0015 (0.002 to 0.043)	0.001 (0.001)	0.086 (0.031)	0.003 (0.005)	(0.062)

Source: A. T. McPherson, *Rubber Chem. Technol.*, **36**, 1230 (1963).

TABLE 4 Thermal Properties of Rubber

Material	Thermal conductivity (W/m·K)	Heat capacity (J/kg·K)	Coefficient of linear thermal expansion (10^{-6} m/m·K)
Polyisoprene (NR)	0.14	1900	220
Polybutadiene (BR)	0.23	1960	180
Polychloroprene (CR)	0.19	2180	200
Poly(butadiene-co-styrene) (SBR)	0.25	1900	250
Poly(isobutene-co-isoprene) (IIR)	0.13	1950	
Poly(butadiene-co-acrylonitrile) (NBR)	0.28	1970	260
Ethylene-propylene diene monomer (EPDM)	0.20	2060	250

Sources:

- Mark, H. F., Bikales, N. M., Overberger, C. G., and Menges, G. *Encyclopedia of Polymer Science and Engineering*, Vol. 16, Wiley, New York, 1989.
 Sircar, A. K., and Wells, J. L., *Rubber Chem. Technol.*, **55**, 191 (1982).
 Van Krevelen, D. W., and Hoflyzer, P. J., *Properties of Polymers*, Elsevier, Amsterdam, 1976.
 Wood, L. A., *Rubber Chem. Technol.*, **49**, 189 (1976).
 Wood, L. A., and Bekkedahl, N., *Rubber Chem. Technol.*, **41**, 564 (1968).

TABLE 5 Permeation Coefficients P ($\times 10^{10}$) [gas volume cm^3 (STP)/ cm^2 of area/ $\text{s}/\text{cm Hg}$ pressure per cm of thickness]

Material	Gas			
	N_2	O_2	CO_2	H_2
Polyisoprene (NR)	9.43	23.3	153	50.3
Polybutadiene (BR)	6.42	19.0	138	41.9
Polychloroprene (CR)	1.20	4.0	25.8	13.6
Poly(butadiene-co-styrene) (SBR)	1.71	17.5	122.7	40.9
Poly(isobutene-co-isoprene) (IIR)	0.324	1.3	5.16	7.2
Poly(butadiene-co-acrylonitrile) 61/39 (NBR)	0.234	0.961	7.43	7.1
Dimethylsilicone rubber	280	600	3250	650
Poly(isoprene-co-acrylonitrile)	0.181	0.852	4.32	7.41
Polyurethane rubber	0.47	1.54	18.0	6.24

Sources:

Brandrup, J., and Immergut, E. H., *Polymer Handbook*, 2nd ed., Wiley, New York, 1975.

Van Krevelen, D. W. and Hoflyzer, P. J., *Properties of Polymers*, Elsevier, Amsterdam, 1976.

TABLE 6 Rubber-Solvent Interaction Parameters χ

Material	Solvent			
	Benzene	Toluene	Pentane	Dioxane
Polyisoprene (NR)	0.421	0.393	0.598	0.60
Polybutadiene (BR)	0.314			
Polychloroprene (CR)	0.263		1.129	0.497
Poly(butadiene-co-styrene) (SBR)	0.398		0.729	0.538
Poly(isobutene-co-isoprene) (IIR)	0.578	0.557	0.627	1.55
Poly(butadiene-co-acrylonitrile) 82/18 (NBR)	0.390		1.078	0.454
Ethylene-propylene rubber (EPR)	0.58	0.49	0.53	

Sources:

Brandrup, J., and Immergut, E. H., *Polymer Handbook*, 2nd ed., Wiley, New York, 1975.

Orwoll, R. A., *Rubber Chem. Technol.*, **50**, 451 (1977).

Sheehan, C. J., and Bisio, A. L., *Rubber Chem. Technol.*, **39**, 149 (1966).

Index

Symbol

2D elements 354
3D elements 354

A

abrasion resistance 8
accelerated aging tests 27
accelerators 19
acrylic rubber 17
acrylonitrile 15, 17
acrylonitrile-butadiene rubber 15
adaptive meshing 315
additives 11, 28
adhesion 385
adhesion strength 387
agglomerates 24
aging 381, 415
air oven 381
aliphatic petroleum resins 29
allylic chlorines 23
allylic hydrogens 18
alum solution 12
ambient temperatures 214
amine antioxidants 27
amplitude of strain 109
anisotropic 350
anti-flex-cracking agent 136
antioxidants 25, 26, 136, 229
antiozonants 25, 141, 215
approximate relations 94
aspect ratio 49
axi-symmetric model 314

B

balloon 74
bead unseating resistance 398
bearings 217, 267
bending strains 77
beta-pinene 30

biaxial stresses 182
biocompatibility 16
blowing agents 11
bond durability 245
bonded rubber units 190
bond failure rates 247
bond strength 243
boundary conditions 314, 317
bound rubber 24
breaking elongation 13, 196
breaking force 133
bridge bearings 217, 409
brittle fracture 22, 160
Brownian motion 37, 110
buckling 78
bulk compression 38
bulk compression modulus 39
bulk modulus 3, 298, 350
burst of pressure 5
butadiene-styrene copolymer 42
butyl acrylate 17
butyl lithium 12
butyl rubber 15, 23, 111

C

cable 14
cable coverings 16
CAD 353
calcium carbonate 29
calendering 24
cantilever 98
carbon black 23, 38, 42, 114
carbon gel 24
catastrophic tearing energy 180
catastrophic tear strength 163, 178
cavitation 77, 147, 386
cavity 76
chain-breaking antioxidants 26
chain scissions 14, 20, 26, 27, 28

- chemical aging 240
 chemical relaxation rate 211
 chlorinated polyethylene 16
 chlorosulfonated polyethylene 16
 clay 29
 coagulation 12
 coal 29
 coefficient of friction 8
 coefficient of thermal conduction 108
 colorants 11
 compatibility 30, 259
 complex dynamic modulus 100
 component design 261
 compounding 18
 compounds 11
 compressibility 350
 compression 52, 77, 106, 108, 127, 146, 189, 260, 261
 compression modulus 265, 266, 272, 301
 compression molding 406
 compression of blocks 50
 compression set 211, 380, 414
 compression stiffness 217
 compressive strain 264
 conduction of heat 108
 confinement 4
 constrained 350
 constrained compression 77
 constrained tension 61, 62
 contact surfaces 314
 continuous stress relaxation 27
 convergence 355
 conversion factors 288
 conveyor belts 17
 cord-rubber composites 184
 corrosive liquids 224
 coumarone-indene resins 29
 coupling agents 24
 crack 77
 crack growth 119, 120, 121, 131, 135, 144, 171, 189, 361
 crack growth characteristic 166
 crack growth constant 167
 crack growth rate 146, 166, 191
 crack growth resistance 178
 cracking energy density 360
 cracking stress 147
 crack length 122
 crack propagation 181
 creases 77
 creep 96, 207, 208, 214, 259, 372, 373
 creep compliance 5, 94
 creeping cure 20
 crosslink density 21
 crosslinking 18, 19, 26, 27, 37, 41, 210
 crosslinking agents 11
 crosslinks 212
 crystallization 72, 129, 137, 221
 curatives 11
 cure systems 23
 curing 18
 cyclic crack growth 139, 145
 cyclic loading 138
- D**
- damping 3, 109, 259
 damping coefficients 105
 dashpot 93
 deflection 260, 359
 deformation 211, 349, 371
 deformed shape 358
 degradation 249
 degrees of freedom 313, 316
 delayed elasticity 99
 design 3, 260
 design guidelines 287
 design parameters 367
 dichloroethane 16
 diene elastomers 23
 diffusion 232
 disruption 353
 dissociation energy 134
 dithiocarbamates 19
 durability 195, 205, 243, 250
 durometer 375
 dynamic mechanical properties 89
 dynamic modulus 94, 98, 111, 112, 113, 114
 dynamic properties 106, 390
 dynamic shear modulus 101
 dynamic shear viscosity 101
- E**
- edge crack 122
 effective density 81
 elastic behavior 38, 78
 elastic constants 38
 elastic instability 72
 elastic modulus 3, 40, 108
 elastic properties 38
 electrical resistivity 12

electrodynamic testers 396
 embrittlement 222, 224
 emulsion polymerization 12
 energy dissipation 89
 engineering stress 60
 engine oil temperatures 8
 entanglements 28, 41, 82, 209
 enthalpy 227
 entropy 227
 epichlorohydrin rubber 17
 equibiaxial compression 77
 equibiaxial extension 61, 182, 183
 equibiaxial stretching 61, 64, 182
 equilibrium stress 28
 ethyl acrylate 17
 ethylene 15
 ethylene-methyl acrylate rubber 17
 ethylene-propylene copolymer 42
 ethylene-propylene rubber 15
 Eulerian method 318
 explosive decompression 76
 extenders 11, 29
 extension 47, 59, 60, 61, 63, 64, 65, 73, 108
 extension ratio 28, 66
 extrusion 24, 408

F

failure 119, 134, 135, 246, 356, 360
 fatigue 159, 259
 fatigue behavior 181
 fatigue crack growth 170, 191
 fatigue crack growth rate 179, 183, 186, 195
 fatigue cracking 189
 fatigue crack propagation 170, 172, 185
 fatigue failure 142
 fatigue life 164, 169, 170, 182, 261
 fatigue limit 132
 fatigue resistance 179
 fatty acid 12
 FEA 295, 345
 FEA models 314
 Fick's laws of diffusion 232
 filled rubber vulcanizates 65
 filler aggregates 23
 flame resistance 16
 flaws 193
 flexibility 414
 Flory-Rehner equation 21
 fluorocarbon rubbers 17

forced nonresonance vibration 106
 forced resonance vibration 106
 fracture 119
 fracture energy 120, 125
 fracture mechanics 119, 144, 356
 free-radical polymerization 12
 free vibration 104
 free vibration methods 107
 frictional effects 146
 frictional forces 78
 frictional surfaces 50
 fuel resistance 15
 fuel tank sealants 16

G

gaskets 15, 16
 gas permeability 17
 gas permeation 239
 Gaussian elasticity 79
 gel point 22
 general purpose elastomers 12
 glass transition 106, 220
 glass transition temperature 110, 111, 125, 127, 210
 graphite 8
 graphitization 24
 green strength 13
 grid 313
 guanidines 19
 GUI 353

H

hardness 375
 heat aging 8
 heat build-up 8
 heat generation 108
 Hevea brasiliensis 13
 Hookean behavior 390
 hose 14, 15
 hydrocarbon 232
 hydrocarbon liquid diffusion 234
 hydrodynamic film 8
 hydrogen abstraction 26
 hydrogenated nitrile rubber 15
 hydrolytic stability 17
 hydrolyzing agents 17
 hydrophilic fillers 230
 hydrostatic pressure 38
 hyperelasticity 351
 hyperelastic models 346, 350

I

- imaginary dynamic compliance 101
- imaginary dynamic shear modulus 101
- imaginary modulus 94
- implants 16
- incompressibility 3
- incremental modulus 91
- indentation 53
- indentation hardness 41
- inflating pressure 73
- inflation 73, 76
- injection molding 407
- intermittent stress measurement 27
- internal energy dissipation 89
- internal fractures 52
- International Rubber Hardness 376
- interply shear cracking 188
- isobutylene 15
- isomerization 13

K

- knotty tearing 129

L

- laminate bearing 267
- large elastic deformations 56
- lateral contraction strain 39
- lateral displacement 99
- latex 13
- life prediction 248
- linear verification 322
- liquid resistance 384
- load-deflection 408
- longevity 214
- longitudinal tension strain 39
- loss factor 114
- loss modulus 127
- low temperature stiffening 222

M

- mastication 12, 136
- material coefficients 309
- material models 345
- material specification 297
- Maxwell model 94, 95
- Maxwell representation 93
- mean pressure function 298
- mechanical fatigue 193
- melt elasticity 24
- mercaptan 12

mesh

- 313
- metal oxides 23
- microcrystalline waxes 25
- microhardness 376
- model building 315
- model verification 320
- modulus of elasticity 37
- molding 274
- molecular scission 167
- molecular strand 80
- molecular weight 82
- molecular weight distribution 12
- Mooney-Rivlin equation 21, 57
- Mooney-Rivlin material coefficients 310
- Mooney-Rivlin model 304
- Mooney-Rivlin relation 81
- mountings 269
- moving-die rheometer 20
- Mullins effect 352
- multiaxial loading 182

N

- natural defects 163
- natural rubber 13, 42
- network chain density 28
- Newtonian behavior 390
- Newton-Raphson method 319
- nitrile rubber 8, 15
- node 313, 317
- noise control 275
- nonaqueous liquids 232
- non-crystallizing elastomers 120, 125
- non-linear analysis 324
- non-linear FEA 316
- non-linearity 303
- nonrelaxing conditions 174
- nonrelaxing effects 137
- nonrelaxing tests 175
- nonresonance vibration 103
- nucleation 164

O

- Ogden material model 304
- oil extension 29, 42
- oil resistance 16, 415
- onset of vulcanization 19
- organic liquids 224
- orientation 129
- O-rings 5, 16
- oscillating disc rheometer 20

oscillation 5, 103, 109
 oscillatory deformation 90
 oxidation 26
 oxidative degradation 223
 oxygen 13, 26, 135, 160, 193, 207, 223
 ozone 26, 132, 138, 160, 163, 193
 ozone cracking 140, 215, 382
 ozone resistance 17

P

para-phenylenediamines 26
 partial solubility 4
 peel test 245
 pentachlorothiophenol 28
 peptizers 28
 permeability 15
 permeation 234
 peroxides 23
 peroxy radicals 26
 phase angle 97, 99, 102
 phenolic resin 29
 physical properties 30
 physical relaxation rate 211
 pine tar 29
 pipe sealing rings 413
 plane strain model 314
 plane stress model 314
 plasticization 42
 plasticizers 28
 Poisson's ratio 3, 39, 98, 298
 polybutadiene 14
 polychloroprene 14, 23, 177
 polydimethyl siloxane 16
 polyisobutylene 111
 polyisoprene 13
 polysulfide rubber 16
 polysulfidic crosslinks 221
 polyurethane elastomer 113
 polyvinyl chloride 15
 power steering hose 17
 preventive antioxidants 26
 primary bond strength 134
 processability 388
 process aids 28
 propylene 15
 prostheses 16
 protective agents 160
 protrusion 55
 pure shear 61

R

radiation stability 242
 rate of crack growth 215
 rate of tearing 121
 real dynamic compliance 101
 rebound resilience 101, 107
 reinforcement 23
 reinforcing fillers 176
 relaxation 96, 209
 reorientation 209
 repeatability 288
 resilience 15, 392
 resistance 27, 259
 resonance 109
 resonance frequency 103
 resonance vibration 103
 resonant beam 394
 response time 7
 retardation 95
 retraction 44, 65, 90, 91, 134
 retraction velocity 90
 reversion 20
 rigidity modulus 3
 roofing 15
 rosin 29
 rosin acid 12
 rosin derivatives 29
 rubber-metal bonds 243
 rubber process analyzer 389
 rubber-wire composites 188
 running friction 8

S

salt 12
 salt water 246
 saturated elastomers 23
 Schallamach waves 77
 scorch 19
 seal 5, 15, 16
 seal deformation 7
 seal friction 8
 seal life 8
 servohydraulic tester 395
 set 207, 211
 shaft seals 5
 shape factor 264, 265, 301
 shear 260, 261
 shear deformation 45, 105, 146, 192
 shear modulus 39, 41, 68, 298, 348, 349,
 370

- shear stress-strain 372
 shear stress-strain curve 371
 shock absorbers 109
 shock absorption 5
 shoe soles 17
 shrinkage 38
 silica 23, 114
 silicone rubber 8, 16
 siloxane 16
 simple extension 38
 simple shear 38
 simple shear test 307
 single crack growth 139
 sinusoidal oscillation 105
 skim rubber 13
 S-N curve 164, 168, 187
 socketing 188
 solubility parameter 229
 solvent 11
 specialty elastomers 14
 spring rate 260
 spudding 274
 static deformations 108
 steady state flow viscosity 94
 stearic acid 12, 20
 stiffness 27, 44, 220, 260
 storage shear modulus 5
 strain-crystallizing elastomer 120
 strain-crystallizing rubber 183
 strain energy 123, 124
 strain energy density 124, 161, 169, 346
 strain energy distribution 361
 strain energy function 59, 63, 67, 82
 strain energy release rate 121, 145
 strain-hardening 58
 strain-induced crystallization 13, 180
 strain invariants 346
 strain ratio 58
 strength 119
 strength anisotropy 129
 stress at constant rate of strain 94
 stress-induced crystallization 185
 stress relaxation 13, 96, 207, 372, 374
 stress relaxation modulus 94
 stress softening 43, 352
 stress-strain curve 177, 297, 353
 stress-strain relations 59, 66, 72
 stress waves 90
 styrene-butadiene rubber (SBR) 12
 sulfonic acids 28
 sulfur 16
 sulfur blooming 18
 sulfur curing 18
 sulfuric acid 12
 sunlight 215
 surface area 23
 surface cracks 160, 248
 surface creasing 77
 surface energy 125
 swaging 274
 swelling 14, 207, 249, 384
 swelling tests 385
 synthetic polyisoprene 13
- T**
- tack 13, 18, 29
 tackifiers 29
 tangent stiffness 318
 tear 22
 tear energy 120
 tearing energy 356, 358, 361
 tearing energy surfaces 126
 tear strength 125, 129
 temperature-resistant elastomers 8
 tensile elongation 39
 tensile modulus 39
 tensile properties 378, 413
 tensile strength 22, 119, 142, 196
 tensile stress 66
 tension 260
 terpene oligomers 30
 test conditions 397
 test piece preparation 366
 thermal degradation 224
 thermal expansion 4
 thermal pressure 4
 thermoplastic elastomers 194
 thermoplastics 11
 thermosets 11
 thiazoles 19
 thin-walled tube 73
 thiurams 19
 thixotropic 42
 thixotropic effects 108, 114
 time-dependent behavior 319
 time-dependent failure 138
 time-dependent tearing 163
 time-independent behavior 319
 tire 109, 397
 tire endurance 400

- tire innerliners 15
 tire strength 399
 tolerance 287, 406
 torque 20, 70
 torsion 70, 274, 347, 357
 torsional stiffness 269
 transient stress 7
 transit times 90
 transmissibility 277
 transmission seals 17
 tube 73
 tube form 275
 tube form mountings 274
- U**
 ultra-accelerators 19
 ultraviolet light 26
 ultraviolet radiation 160, 215
 uni-axial compression 306
 uni-axial tension test 304, 307
 unstable deformation 77
 urethane rubber 17
- V**
 van der Waals forces 42
 vibration 5, 275
 vibration isolation 109
 viscoelastic behavior 92
- viscoelastic elements 93
 viscoelasticity 92, 319, 351
 viscoelastic losses 89
 viscoelastic relaxation 43
 viscous damping coefficient 93
 voids 386
 Voigt element 102
 Voigt model 95
 Voigt representation 93
 vulcanization 18, 37
 vulcanizing agent 21
- W**
 weatherability 16
 weathering 215
 wire 14
 WLF equation 125
- X**
 xanthates 19
- Y**
 Yerzley oscillograph 393
 Young's modulus 3, 49, 301, 310, 368
- Z**
 Ziegler-Natta polymerization 13
 zinc oxide 20

Alan N. Gent

Engineering with Rubber

This book provides the principles of rubber science and technology: what rubber is, how it behaves, and how to design engineering components with rubber. It introduces the reader to the principles on which successful use of rubber depends and offers solutions to the questions engineers in rubber engineering face every day:

- How is an elastomer chosen and a formulation developed
- Why is rubber highly-elastic and relatively strong
- How to estimate the stiffness and strength of a product
- How to guarantee high quality and durability

The authors describe current practices in rubber engineering. At the end of each chapter, sample questions and problems (together with solutions) are provided, allowing the reader to gauge how well he/she has mastered the material.

Contents:

- Materials and Compounds
- Elasticity
- Dynamic Mechanical Properties
- Strength
- Mechanical Fatigue
- Durability
- Design of Components
- Finite Element Analysis
- Developments in Finite Element Analysis
- Tests and Specifications

www.hanserpublications.com
Hanser Publications
ISBN 978-1-56990-508-1

www.hanser.de
Carl Hanser Verlag
ISBN 978-3-446-42764-8



HANSER

@seismicisolation